DEVELOPMENT OF A SMALL ENVELOPE PRECISION MILLING MACHINE

D. F. KIRK

A thesis submitted for the degree of
Doctor of Philosophy
at the Department of Mechanical Engineering University of Canterbury
Christchurch
New Zealand

2006

Abstract

The credit card industry is huge with over two and a half billion cards shipped annually. A local card manufacturer, with a production volume in excess of forty million cards annually, approached the University of Canterbury to design and develop advanced card manufacturing technology. The motivation behind this development was the desire of the sponsoring company to keep abreast of new technologies and to have the ability to manufacture and supply cards with this new and emerging technology into a highly competitive world market.

This thesis reports the research surrounding the development of a dedicated new machine tool explicitly designed to implement the emerging technologies found in the international credit card industry. The machine tool, a dedicated milling machine, was not developed in its entirety within these pages; however, three major constituents of the machine were researched and developed to a point where they could be implemented or become the subject of further research.

The three areas of interest were;

- A machine table system that avoided the increased zonal wear to which linear bearings are subject, typically due to short high frequency traversals, and also the high friction and mass generally found in dovetail slides.
- Design requirements demanded the use of a single commercially available carbide cutter to produce 1500 components per hour. Therefore, a purpose built high (revs per minute) rpm spindle and drive system specifically for use with polymeric materials, (R-PVC in particular) was deemed necessary.
- Tracking the cutter depth in relation to an RFID aerial track embedded within the credit card core. The aerial tracking was to be dynamic and occur during the machining process with the machine "remembering" the depth of cut at contact with the aerial.

Each of the three areas was researched via an in-depth literature review to determine what and if any material had been published in these fields.

For the development of the machine table a novel flexure hinge idea was considered.

Considerable material was discovered about flexures, but very little was found to be relevant to the application of high displacement metal flexures necessary to meet the required levels of table movement. In effect the proposed machine table system and research in this field would be novel.

The high performance spindle investigation became directed into a much narrower focus as it progressed; that of determining the power consumption required to machine the integrated circuit pockets in an R-PVC work piece. This was due to the lack of information pertaining to the physical properties of polymeric materials, in particular the specific cutting pressure.

The depth following sensor array was configured using capacitance detection methods to determine the distance between the cutter's end and the aerial tracks. Capacitance sensing methods, whilst not new, were developed into a novel arrangement to meet the specific cutter tracking requirements of the proposed new machine tool.

Each of the respective development areas had concept designs completed and were prototyped before being tested to determine the effectiveness of the respective designs.

The outcomes from the testing are reported herein, and show each constituent part to be basically feasible, in the application. The results were sufficient to indicate that each development showed distinct potential but further development and integration into the machine tool should ensue.

Acknowledgements

My sincerest gratitude to my overall supervisor, Dr David Aitchison, without whose trust, direction, advice, support and guidance, this project would never have been commenced and concluded.

I am indebted to Dr Shayne Gooch for his assistance and advice during the course of the research, especially in the areas of materials selection and the use of modern design tools and philosophies.

I wish to thank Professor Harry McCallion for his willing advice and continued interest in this venture.

Thank you to Dr Andrew Shaw for his assistance in editing and review of the writing style and thesis structure.

Dr S Ilanko and Dr E van Houten are to be gratefully thanked for the time given in discussions regarding the solid mechanics questions that arose, particularly with regard to the flexure hinges.

My thanks to Dr John Smail for his continued encouragement and interest in this project and his assistance and advice with regards to a number of materials science questions.

Thank you to Dr John Pearse who assisted with administrative duties during any absences of Dr Aitchison.

Thank you to Mr Eric Cox for his assistance in many ways, not just with metrological and CMM assistance, but also for continued encouragement, advice and support.

Many thanks Mr Julian Phillips and Mr Julian Murphy of the department's electronics workshop for their input and assistance in all things electrical and electronic, particularly the drive unit for the high speed spindle and the aerial detection system.

Mr Scott Amies, Mr Ken Brown and Mr Paul Wells are to be thanked for their invaluable help in the manufacture of the various apparatus and equipment required throughout the project

I am very grateful to the many others in the Department of Mechanical Engineering for their constant interest and encouragement.

Many thanks to Mr Rolf Junkers and Mr David Brewster who instigated the initial project and developed the outline for the project design specification requirements.

Last but not least, by any means, Stephanie, my wife, and my four wonderful girls, Annaliese, Ashleah, Whitney, Devon, and my many friends, without whose support and encouragement this project may never have been completed.

Research papers and contributions

Published papers:

1. Sherwood M.J, Devane P.A, Horne J.G., Leslie H.J; Aitchison D.R, Kirk D.F (2000). *A comparison of the measurement of wear in UHMWPE acetabular implants using the Polywear™ three-dimensional method and direct Coordinate Measuring Machine measurement of retrieved cups*. NZ orthopedic Association – 49th Scientific Meeting. Watangi, New Zealand. October 2000.

2. Aitchison D. R., Shaw A. I., Kirk D. (2002). *High level CAD automation through API programming - an engineering education case study*. 6th International Conference on Engineering Design and Automation. Maui, Hawaii. CD ROM. August 2002.

Table of Contents

Table of Figures

Chapter 5

Appendices

Table of Tables

Appendices

Nomenclature

Chapter One

Symbol	Definition	Units
X, Y and Z	machine axis labels	
μm	microns or micrometers	

Chapter Two

Symbol	Definition	Units
hr	hours	
m	metres	
min	minutes	
mm	millimetres	
s	seconds	

Chapter Three

Symbol	Definition	Units
A	cross sectional area	m^2
a’	Abbe offset	mm or m
b	thickness	m or mm
b’	fatigue strength constant (number of cycles)	
c	distance from neutral axis to outer fibres	m or mm
C	fatigue strength constant	
D	diameter	m or mm
D*	measured diameter	m or mm
d_r	real position relative to measurement probe	m or mm
E	modulus of elasticity	GPa
e	eccentricity or offset	m or mm
$f[\ ]$ or $g[\ ]$	function of	
F	resultant feed force	N
F_a	axial feed force	N
F_c	force component in direction of relative tool travel (feed force)	N
F_t	force component perpendicular to direction of cut (tangential force)	N
F_i	Functional parameters	

F_x, F_y or F_z	load applied along an axis direction	N
g	gravitational acceleration	m/s^2
G_i	geometrical parameters	
h	width	mm
I_{zz}	second moment of area along Z axis	mm^4
K	geometric constant	
k	stiffness constant	
K_{1c}	fracture toughness	$MPa\text{-}m^{1/2}$
k_a	surface factor	
k_b	size factor	
k_c	reliability factor	
k_d	temperature factor	
K_{tS}	fatigue strength reduction factor (Shigley)	
k_f	miscellaneous fatigue factor (Shigley)	
K_f	theoretical stress concentration factor (Smith)	
K_t	stress concentration factor	
l	working length of flexure blade	mm
l_A or l_B	length of A or B flexure	mm
l_{eff}	effective length of flexure blade	mm
m	mass	kg
M_B	bending moment	Nm
M_i	material parameter	
N	factor of safety	
p	performance	
P	applied load	N
P'	linear translation	mm
P_{cr}	critical buckling load	N
P_{crx} of P_{cry}	critical buckling load in the X or Y direction	N
Pt_i	point number i	
q	notch sensitivity (Shigley)	
R	notch radius	mm
r	bending radius	mm
R^2	trend line fit	
R_a	roughness average	

r_n	radius of gyration	mm
R_{sx}	rotation angle about X axis due to span length variation (pitch)	deg
R_X	rotation angle about the X axis (pitch)	deg
R_{xi}	rotation angle about the X axis inner pair of blades (pitch)	deg
R_{xo}	rotation angle about the X outer pair of blades axis(pitch)	deg
R_Y	rotation angle about the Y axis (roll)	deg
R_{yi}	rotation angle about the Y axis inner pair of blades(roll)	deg
R_{yo}	rotation angle about the Y axis outer pair of blades axis (roll)	deg
R_Z	rotation angle about the Z axis (yaw)	deg
r_z	radius of blade end translation for small displacements	mm
s	measurement scale length	mm
S	distance between adjacent blades in a pair in the displacement direction	mm
s′	apparent measurement scale length	mm
S_i	distance between adjacent inner blades in a pair in the displacement direction	mm
S_o	distance between adjacent outer blades in a pair in the displacement direction	mm
s_θ	apparent travel	mm
t	thickness of flexure hinge or blade	mm
T	time	seconds
T_X	translation in X direction	mm
T_{Ax}	lateral translation in X direction of platform at end A	mm
T_{Bx}	lateral translation X direction of platform at end B	mm
T_Y	Platform translation in Y axis direction	mm
U_i	stored energy	Ws/mm^3
V	shear force	N
x	distance from reference point to applied load	mm
z_A	vertical displacement of platform at blade A	mm
z_B	vertical displacement of platform at blade B	mm
Δx_o	horizontal offset at zero table displacement	mm
T_z	vertical displacement of the working platform	mm
Δz_o	vertical offset at zero table displacement	mm
Π	group symbol – dimensionless equation	
Ψ_i	flexure property group symbol	
α	angle between neutral axis in vertical XY plane	deg

β	angle between principle axes of inertia in horizontal ZX plane	deg
δ	displacement or deflection	mm
$\delta\theta$	angle of misalignment between measurement axes	radians
ε	strain	
ϕ_d	horizontal component of the stage drive's angle of incidence to the drive surface	deg
γ	angle between planes through the instantaneous centres of the flexures	deg
θ	rotational angle of hinge	radians
θ'	angle between measurement axes	radians
θ_o	line of action of measurement	radians
σ_a	stress amplitude	MPa
σ_B	bending stress	MPa
σ_E	endurance strength	MPa
σ'_e	endurance limit	MPa
σ_f	failure stress or fatigue strength	MPa
σ'_f	mean fatigue strength	MPa
σ_m	mean stress	MPa
σ_{max}	max applied stress	MPa
σ_{ut}	tensile strength	MPa
σ_y	yield stress	MPa
ω	natural frequency	Hz
ψ_i	equations remaining relevant to materials selection	
ζ	vertical component of drives angle of incidence to the drive surface	deg

Chapter Four

A comparative list of specific nomenclature relating to the cutting theory comparison is cited on page 233ff.

Symbol	Definition	Units
$\overline{F_x}$, $\overline{F_y}$, $\overline{F_z}$	average orthogonal feed force	N
a	axial depth of cut (Altintas term)	mm
A_s	shear plane area	m^2
b	width of cut	mm
c	feed per tooth	mm

c_s	specific coefficient of heat (Altintas term)	Nm/kg^{o}C
c_t	thermal conductivity of the work material (Altintas term)	W/(m^{o}C)
d	differential	
D	cutter diameter	mm
d	depth of cut (Kobayashi term)	mm
d_c	deformed chip thickness (Kobayashi term)	mm
F	resultant force (Altintas term)	N
f	feed/tooth/rev	mm
F_a	axial feed force	N
f_c	tool feed velocity	m/s
F_c	force component in direction of relative tool travel (feed force)	N
F_f	frictional force between chip & rake face (Kobayashi term)	N
F_{ft}	feed cutting force – perpendicular to tool travel (Altintas term)	N
F_{fm}	normal force on rake face	N
F_n	normal force on shear plane (Altintas term)	N
F_{ns}	force perpendicular to shear plane (Kobayashi term)	N
F_r	radial cutting force – perpendicular to the cutting edge direction of travel (Altintas term)	N
F_s	force component along shear plane	N
F_t	force perpendicular to tool travel (Kobayashi term)	N
F_{tt}	tangential cutting force – in direction of tool travel (Altintas term)	N
F_u	friction force (Altintas term)	N
F_v	normal force (Altintas term)	N
F_x, F_y, F_z	orthogonal feed force	N
h	depth of cut (Altintas term)	mm
h_a	average chip thickness	mm
h_c	deformed depth of cut	mm
h_j	cutting depth for flute j	mm
hp	power consumption	W
i	oblique cutting angle	deg
j	flute designation number	
K	specific cutting force (constant)	kg/mm^2
K_{ac}	cutting constant - axial	N/mm^2
K_{ae}	edge cutting constant - axial	N/mm^2
K_F	Feed specific cutting pressure	N/mm^2

K_f	cutting force ratio	
K_{fc}	cutting constant - feed	N/mm^2
K_{fe}	edge cutting constant - feed	N/mm^2
K_{rc}	cutting constant - radial	N/mm^2
K_{re}	edge cutting constant - radial	N/mm^2
K_T	tangential specific cutting pressure	N/mm^2
K_t	tangential specific cutting pressure	N/mm^2
K_{tc}	cutting constant - tangential	N/mm^2
K_{te}	edge cutting constant – tangential	N/mm^2
l	length of cut	mm
l_c	extend of cutter's initial contact	mm
L_c	shear plane length (Altintas term)	mm
l_t	chip contact length (Altintas term)	mm
m_c	metal removal rate (Altintas term)	kg/sec
N	no. of flutes on cutter	
n	rotation speed	rpm
p, q	experimental cutting force constants	kg/mm^2
P_p, Q_p, R_p, S_p	substitute variables in weighting calculations	
P_s	shear power (Altintas term)	W
P_t	total power (Altintas term)	W
P_u	friction power (Altintas term)	W
Q_c	metal removal rate [m^3/sec] (Altintas term)	m^3/sec
R	resultant cutting force	N
r	chip thickness (or compression) ratio	
r_c	cutter radius	mm
R_c	chip compression ratio (Altintas term)	
rpm	revolutions per minute	min^{-1}
R_T	non dimensional thermal number (Altintas term)	
S_f	roughness of cut surface	
s_t	feed per tooth per rev	mm
T	torque	Nmm
t	cutting time	seconds
t_c	approx undeformed chip thickness	mm
T_{int}	average temp change at rake face – chip interface (Altintas term)	^oC

T_r	ambient temperature (Altintas term)	^oC
T_s	shear plane temperature (Altintas term)	^oC
u	specific cutting force (Kobayashi term)	Ws/mm^3
u_f	friction energy/unit volume (Kobayashi term)	Ws/mm^3
u_s	shear energy/unit volume (Kobayashi term)	Ws/mm^3
V	velocity of tool parallel to F_c	m/s
v	feed rate	mm/min
V_c	chip velocity	m/s
V_m	cut volume per unit time	m^3/s
V_p	peripheral cutting speed	m/min
V_s	shear velocity	m/s
V_w	volume of tool wear/unit time	m^3/s
w	width of cut	mm
z	axial depth of cut	mm
Δd	undeformed shear plane (Altintas term)	
Δs_K	change in chip length parallel to shear plane (Kobayashi term)	mm
Δs_A	deformation in shear plane (Altintas term)	mm
Δt	time increment (Altintas term)	s
ΔT_c	average temperature change in chip (Altintas term)	^oC
ΔT_m	max temp rise of the chip at rake face – chip interface (Altintas term)	^oC
Δy	change in chip thickness perpendicular to shear plane (Kobayashi term)	mm
K_{fe}	average edge force coefficient (Altintas term)	N
K_{te}	average edge force coefficient (Altintas term)	N
α	rake angle (Kobayashi term)	deg
α_n	oblique cutting rake angle	deg
α_r	rake angle (Altintas term)	deg
β	friction angle (Kobayashi term)	deg
β_a	average friction angle between rake face and moving chip (Altintas term)	deg
β_h	helix angle of cutter (Altintas term)	deg
β_n	Normal friction angle in oblique cutting	deg
δ	ratio of plastic layer over deformed chip thickness (Altintas term)	deg
ϕ_i	instantaneous immersion angle	deg
ϕ	shear angle (Kobayashi term)	deg

ϕ_c	shear angle (Altintas term)	deg
ϕ_{ex}	cutter exit angle	deg
ϕ_j	immersion angle for flute j	deg
ϕ_n	normal shear angle (oblique cutting)	deg
ϕ_p	tooth spacing (cutter flute pitch)	deg
ϕ_{st}	cutter start angle	deg
γ	shear strain on shear plane (Kobayashi term)	
γ_s	shear strain (Altintas term)	
γ'_s	shear strain rate (Altintas term)	/s
η	chip flow angle	deg
η^1_c	machinability factor (Kobayashi term)	
η^2_c	machinability factor (surface finish neglected) (Kobayashi term)	
η^3_c	machinability factor (tool wear neglected) (Kobayashi term)	
η_c	machinability index	
η_s	machinability (orthogonal cutting) (Kobayashi term)	
η_t	machinability (turning) (Kobayashi term)	
λ_h	factor to consider plastic work done in the thin shear zone (Altintas term)	
λ_s	proportion of heat conducted into work material (Altintas term)	
μ	coefficient of friction (Kobayashi term)	
μ_a	coefficient of friction (Altintas term)	
ρ	specific density (Altintas term)	kg/m^3
σ_c	Specific cutting force (Kobayashi term)	kg/mm^2
σ_s	normal stress (Kobayashi uses kg/mm^2)	MPa
τ_s	shear stress (Kobayashi uses kg/mm^2)	MPa
ω	rotational speed	rads/sec
ψ	flute lag angle	deg

Chapter Five

Symbol	Definition	Units
A	area of plates	m^2
C	capacitance	pF
C_i	capacitor number	
d	distance between plates	m
DC	direct current	amp

f_a	actual feed speed	mm/s
f_c	feed speed	mm/s
F_p	measured cutting force	N
F_r	reference force	N
P_D	residual signal strength	pF
R_i	resistor number	
S	sensitivity	pF/mm
V_{ac}	alternating voltage	V
V_{out}	output voltage	mV
x	change in distance between plates	mm
%	percentage	
α	distance between cutter and aerial	mm
β	distance between platen and aerial	mm
δV_{out}	change in output voltage	mV
ε	permittivity of the dielectric material	F/m
γ	distance between platen and cutter	mm
μm	micron or micrometer	

Chapter Six

Symbol	Definition	Units
rpm	revolutions per minute	min^{-1}

Table of Contents

Table of Figures

Table of Tables

Nomenclature

Chapter One

Symbol	Definition	Units
X, Y and Z	machine axis labels	
μm	microns or micrometers	

Chapter Two

Symbol	Definition	Units
hr	hours	
m	metres	
min	minutes	
mm	millimetres	
s	seconds	

Chapter 1

DEVELOPMENT OF A SMALL ENVELOPE PRECISION MILLING MACHINE

1.1. Introduction

The notion of developing a small envelope "High Speed" Computer Numerically Controlled Milling Machine was initially driven by a request from a 'bank' card manufacturer with a specific need for such a machine tool. The sponsoring company markets its "World Class" quality products globally and therefore demanded a machining facility to match. The combination of features for this design project was unique and unusual: a milling machine with a small working envelope, high spindle speed and laminated plastic with embedded electrical copper wire tracks (an aerial) as a workpiece material (Figure 1.1). Thus, it was apparent from the outset that a research and development based project was required.

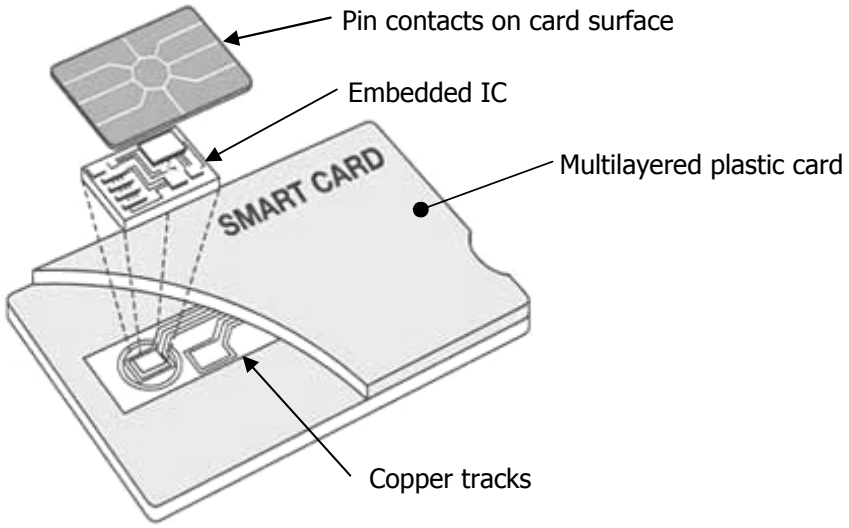

Figure 1.1: Representation of a typical 'new generation' bank card

At this point brief statistical information provided by the sponsoring company from the International Credit Card Manufacturers Association (ICMA) website is presented to furnish the reader with an appreciation of the size of the global smart card industry.

The use of smart cards globally for 2004 was as follows:

- 2.3 billion Smart cards shipped in 2004 – an increase of 28% over the previous year.

- Telecom was the largest market sector with 1.71 billion cards.
- Financial markets were the second largest sector with 315 million cards.
- Other markets: Government/Healthcare 65 million, Transport 75 million, Pay TV 55 million, Security 22 million, Other 22 million.[1]

Table 1.1 presents a further view of the volume of cards circulating globally. The table shows the top fifteen countries and the number of VISA/MasterCard (credit/debit) cards in circulation[2].

Table 1.1: Cards in circulation (millions)

Rank	Country	Cards
1	USA	795 500
2	China	206 093
3	Brazil	192 252
4	UK	139 667
5	Japan	126 847
6	Germany	108 846
7	S. Korea	93 228
8	Taiwan	70 867
9	Turkey	63 648
10	Spain	60 813
11	Canada	54 100
12	India	49 063
13	Mexico	47 042
14	Italy	45 649
15	France	43 260
Top 15	Total	2 096 875
Global	Total	2 549 700

The information presented above indicates that the magnitude of the global smart card industry is huge. The ever increasing demand for secure high technology cards (see statistics above) places the card manufacturers in the enviable position of ever having to increase their production capacity. It was the requirement for this increasing production capacity and the need to incorporate new technologies and processes that drove the sponsoring company to investigate a new machining facility. In line with the statistical information above and the sponsoring company's perceived need, it is significant to provide further background information to the project, which is introduced in the following section.

Much of the general information about bank cards presented in this and subsequent chapters is anecdotal. Therefore, the lack of referenced material is due to the fact that it is commercially sensitive in many cases and manufacturers obviously do not publish technical information about their processes and products.

1.2. Background

Society is increasingly reliant on many everyday products being 'intelligent' in some way; as a consequence, the use of embedded integrated circuits (IC's) or microprocessors is becoming commonplace. This increasing use of intelligent devices in consumer goods is providing exciting opportunities for research in the design and development realms of the associated high volume manufacturing facilities, amongst others. To this end, these new and more reliable technologies are being introduced and included into electronic transaction card designs on a continuing basis. What's more, the necessary higher level of sophistication and technology that is being cost effectively integrated into today's manufacturing capabilities is enabling the manufacture of products and parts that were once thought impossible.

A major factor in this evolution is the increase in electronic financial transaction fraud, which has forced the banking industry to demand an increase in the level of security attached to the cards. This heightened security requirement has driven the card manufacturers into new spheres of advanced technology, which to be cost effective, must be produced in high volumes. Cost effective manufacturing must be fully considered during the development phase, in any good product design solutions. In support of efforts by the sponsoring company to develop a new generation of bank card, researchers from the University of Canterbury were engaged. The University of Canterbury staff were employed to investigate, design and develop the associated commercially viable high volume manufacturing facility.

The reference term 'sponsoring company' is used interchangeably with the term 'card manufacturer' throughout this work.

1.2.1. Overview of bank card configurations

Bank cards are typically used in the banking industry for financial transactions. There are a wide array of cards used in a huge variety of these and other applications. Other card functions include security access, library borrower transactions, club membership identification, air travel points and grocery shopping purchase points access, and finally but by no means last, as formal identification. This list is by no means exhaustive, but represents some of the more commonly recognisable applications where these cards are implemented. The numerous types of card are generally grouped by the

technology and materials used in their manufacture. They are also further subdivided by the different card producers and the manufacturing processes peculiar to them.

This monograph considers two specific groups of card, only one of which is the focus of the project. These groups will be referred to throughout this work as 'Conventional' and 'Smart' cards or for generic purposes, 'Cards.' Some explanation of the groups is now presented as further background for the reader.

Conventional cards (Figure 1.2a & b) are the industry standard laminated cards that are used for any purpose whereby the information carried on them may be accessed by a magnetic strip reader (Figure 1.2b).

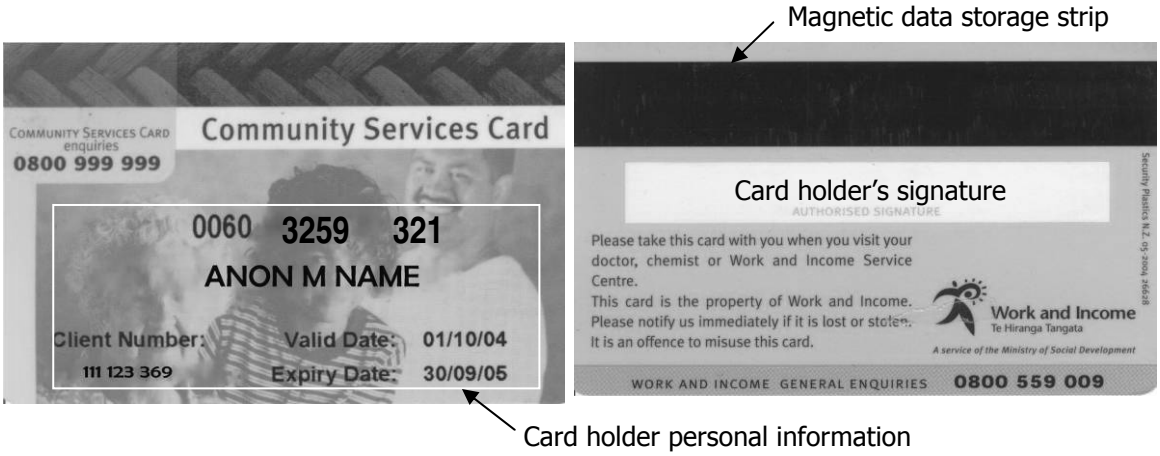

Figure 1.2: Typical conventional card front (a) (left) and rear (b) (right)

In contrast, Smart cards store information in an embedded IC. This particular group of cards may be further subdivided into two categories: Those with an on-board IC that requires a contact reader (an array of pins, which make contact with terminals grouped together on the card's surface), to access stored information (Figure 1.3a), and those that contain an embedded aerial for use with non contact proximity readers. The pin reader style of card is also known as a contact card, whilst the proximity card is often called a contactless card. Furthermore, these types of cards are known as 'frame relay access device' (FRAD) cards (Figure 1.3a) or 'radio frequency identification device' (RFID) cards. A typical aerial layout within the RFID card is shown in Figure 1.3b below. Note that the contacts for the IC connection are shown here, but the IC is not.

The basis of this work revolves around the development of a machine tool to partially manufacture a new generation of card that goes beyond the existing contact and proximity card systems by combining both types in the one card; designated a Dual

Interface Card. However, this technological development spawned far reaching consequences for the associated downstream manufacturing processes used in the production of these new laminated card products.

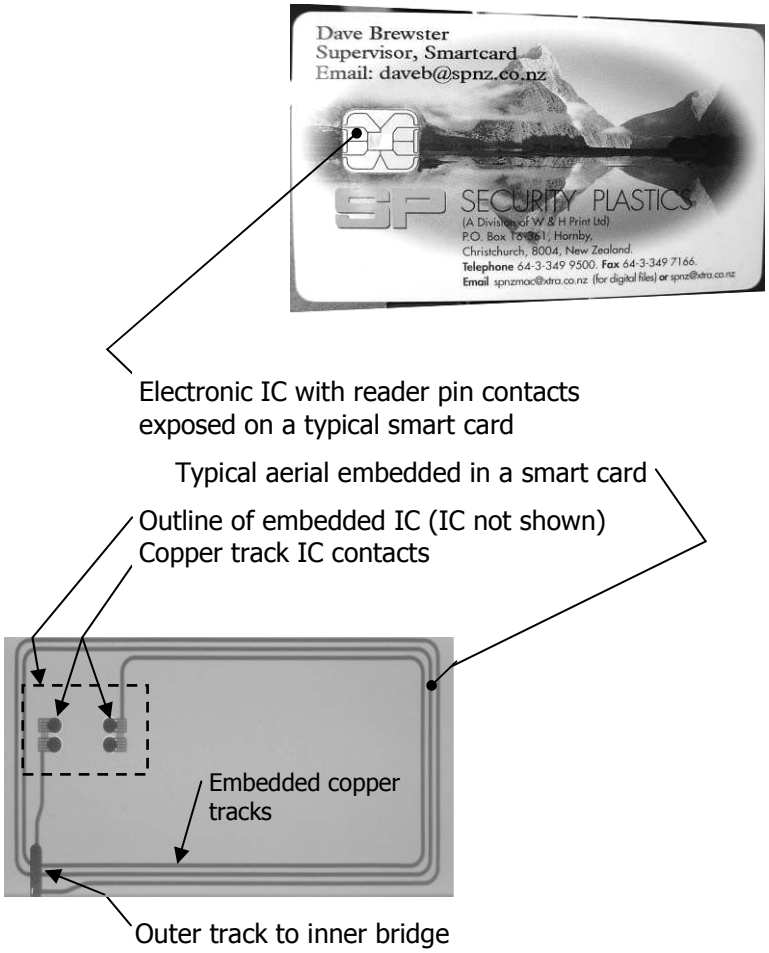

Figure 1.3a: (top) the front of a smart card, (pin reader contacts shown), & b: (lower) embedded aerial with contact

The reason for the term 'partial manufacture' above is that the proposed facility will only be concerned with one operation of the many processes that are used in the production of a complete card. To help clarify this statement, in the following paragraphs, is a brief description of the general composition of the laminated cards.

These cards are manufactured from a sandwich of layers comprising of white and transparent sheets of rigid polyvinyl chloride (R-PVC) plastic. The method of manufacture is such that the card remains tamperproof. In this regard, the white layers form an inner core and the transparent outer layers are applied to the exterior to provide a protective cover. The graphical content of the cards is printed on the underside of the transparent layers before they are applied to the white core. A magnetic strip is also secured beneath the transparent layer on the back of the card. In

the FRAD cards, the embedded copper tracks constitute an aerial, which must be electrically connected via contacts to the aerial end-points (Figure 1.3b) to terminals on the underside of the IC. Currently, card core manufacturing processes are costly to operate when exposed IC contacts are required on the face of the card, as they are in the previously mentioned smart card arrangement. These cards take on two forms, one where the IC is fully embedded in the core with the attached aerial and the other where the IC is embedded in a machined pocket on the cards' surface with exposed pin reader contacts and no aerial.

The dual interface cards will continue to be manufactured as per the conventional laminating processes but the pocket opening for the IC cavity production will be met by the nominated production process: milling. Furthermore, the dual interface card blank will be manufactured with the copper tracks already sandwiched between two white R-PVC core sheets.

Figure 1.4 demonstrates the sequence of operations necessary to manufacture smart cards. There are fourteen or sixteen steps in the process. Some steps are excluded depending on the final form of the card. For example, the contact card will not have step six, as it does not require an aerial. Whereas the contactless card will not have a pocket milled into it (skip steps thirteen and fourteen) but will require testing (step fifteen) before being designated as finished (step sixteen).

The cards must all be manufactured to a standard thickness, 0.78 mm for a standard card and 0.45 mm for a standard 'thin' card. These requirements are specified by the ISO standards applicable to the manufacture of the cards: typically ISO 7810-2003, Identification cards - Physical characteristics and ISO 7813-2001, Identification cards - Financial transaction cards. Obviously, the cards with three thicknesses making up the core (steps two, three and four – Figure 1.4) must have appropriately thin material so that the three layers combine to form a thickness that is similar to a card without an aerial (steps two and four only – Figure 1.4), thus producing both types of card at the standard thickness. It is important to note here that the layers are very thin. The transparent layers are approximately 0.08 – 0.1 mm thick and the two or three core layers then make up the balance of approximately 0.58mm.

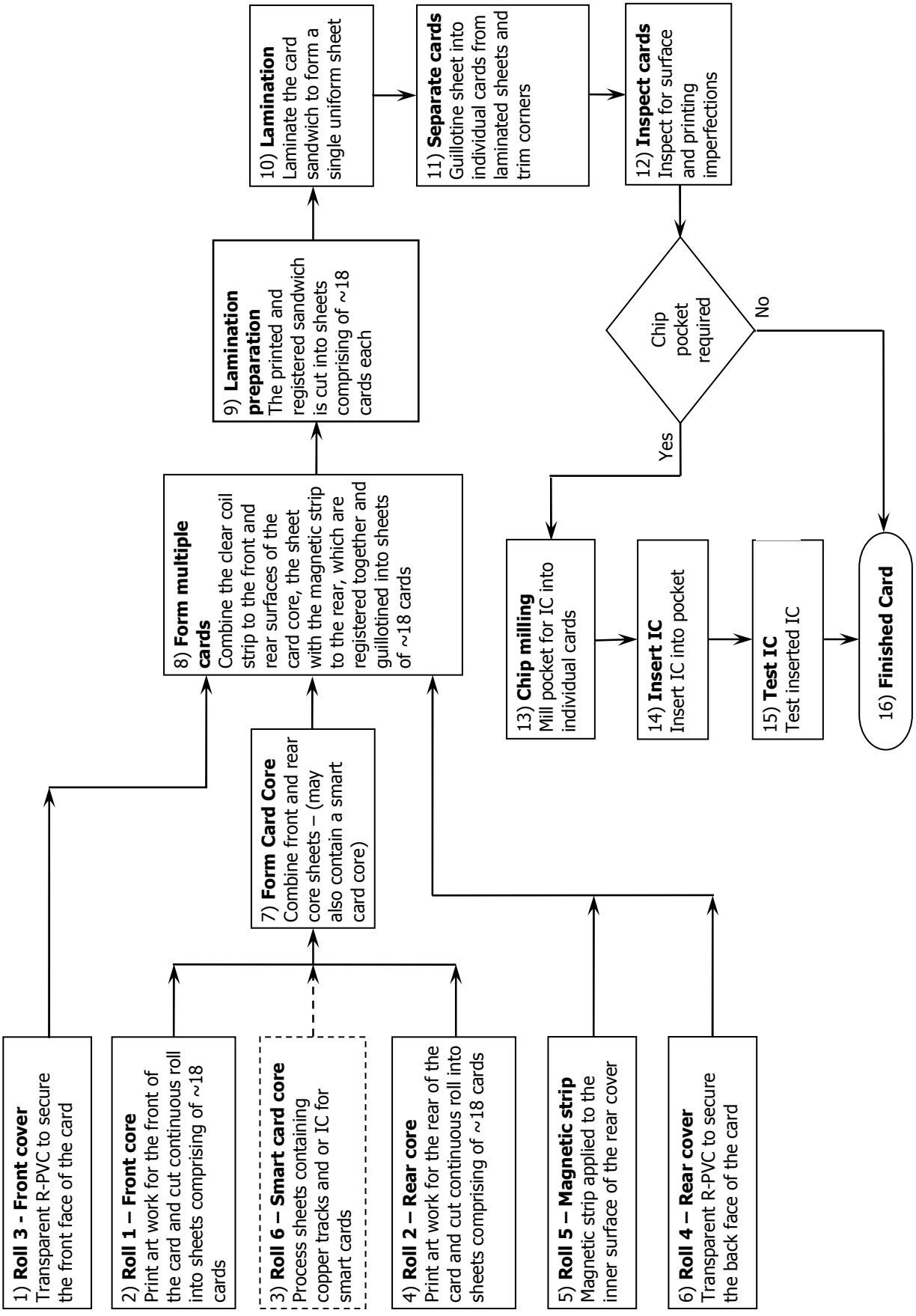

Figure 1.4: Steps in the manufacture of a smart card

1.2.2 The reasons behind the investigation

This design and development oriented project was initiated due to the bank card manufacturer's explicit requirement for a specialised Computer Numerically Controlled (CNC) high spindle speed machining facility to meet a specific manufacturing requirement. The primary function for this equipment was for use in the IC pocket production of laminated R-PVC bank cards.

This new requirement for the IC pockets necessarily complicates the machining process when compared to the previous card design in that the aerial tracks must be exposed by the machining process. Firstly, the machine must remove sufficient material to a level where it exposes the IC contact points of the embedded copper tracks. Therefore, the pocket depth is a critical factor in the manufacture of the cards. If it is too deep, excess copper will be removed, if too shallow insufficient plastic will be removed, both causing defective connections between the IC and aerial contacts. It is therefore essential that the copper is only just exposed. At this stage, it is important to note that the tracks are very thin (approximately 100 μm).

As requested by the sponsoring company, the proposed machine tool, a milling machine, was to produce shallow stepped pockets into which low profile IC's were to be fitted. The depth machining process demanded very precise control to prevent over-machining. This prerequisite meant that the proposed machine tool required a measure of onboard intelligence and the associated sensory system to detect the presence of the copper contacts on the tracks and thus to prevent over-cutting the depth of the pockets.

Machines capable of machining a basic pocket are readily available for the pocketing function and generally fall into two categories.

1. Those re-engineered from existing equipment and modified to suit the purpose[3]

   These machines often begin life as wood routers, electrical circuit board milling machines or drilling machines. Unfortunately, these beginnings present inherent limitations with respect to the downstream machining accuracy and performance: The original design never intended these machines would be developed into high speed, accurate, volume production equipment.

Anecdotal evidence suggests that these machines are often re-engineered in-house or by an engineering contractor and are not provided by card industry recognised manufacturers.

2. Purpose built facilities[4] [5]. These are a group of machines purpose manufactured to produce pockets in cards. However, these machines do not always meet the specific needs of manufacturers and retain some of the inherent difficulties in requiring skilled CNC operators to use them. The sponsoring company has such a machine in service and reports that initial accuracy problems caused by operator inexperience have been resolved. The machine, however, is too difficult to set up, operate and maintain.

An in depth search of the internet with regard to manufacturers that produce milling machines for card manufacture revealed very little information. The sponsoring company was able to indicate that the number of certified card manufacturers was between 100 and 120. A search for additional leads through the International Credit Card Manufacturers Association (ICMA) website provided confirmation of 103 card manufacturers. Further to this, the number of companies listed on ICMA website as suppliers of products or services to card manufacturers was seventy. Of these, fourteen contacts were associated with card milling and only two actually related specifically to machine manufacturers. A subsequent search, again of the ICMA website, relating directly to dual interface card production equipment only produced the same two companies as it had previously.

As indicated previously only two companies consistently appeared in the results as being companies that manufacture chip pocket milling equipment relating to smart cards and/or dual interface cards. There may be others, but due to the lack of information available about them, they are not represented here. The very low number of machine tool manufacturers in this field would indicate that the market for this specialised production equipment is very small due to it being an emerging technology.

Anecdotal evidence from the sponsoring company and the consistent appearance in the ICMA searches suggests that Mühlbauer AG is one of the most advanced machining technology suppliers in the card industry.

Both of the companies represented in the results of the ICMA website search are world leaders in the manufacture of the most advanced card production systems available. As such, they do produce machinery that will execute the pocketing process required for dual interface cards. However, they are unable to produce the milled pocket for the sponsoring company's dual interface card design, as they do not dynamically sense the aerial during milling.

Mühlbauer is represented by two factories that manufacture and sell their specialist equipment, one in Germany and the other in the USA. A brief outline of Mühlbauer AG is included below.

The second company that was also consistently returned by the ICMA search engine was MELZER Maschinenbau GmbH. The information regarding this company's existence in the market was shallow but sufficient to include a brief outline of their presence in it.

The Mühlbauer AG website, www.mühlbauer.de provided the following company information.

> Mühlbauer AG[6]
>
> Mühlbauer is a global, independent consultant and manufacturer of turnkey automation solutions for the Smart Card, Smart Label, Semiconductor Backend and Vision industries. Headquartered in Roding, Germany, the company currently has about 1,500 employees in 26 locations on five continents.
>
> Mühlbauer solutions enable clients to manufacture any type of Chip Cards, including ID Cards, ePassports, eVisa, Contact and Contactless Cards, Dual Interface as well as Multimedia Cards and Smart Labels for access control, supply chain management, tracking of textiles and applications for the retail industry.
>
> With more than 3,000 systems installed worldwide, Mühlbauer is the leading supplier of production equipment for the Smart Card and Smart Label industry, and is currently the only company in the world that offers a full range of turnkey manufacturing solutions – from die bonding over card production and card personalization to enrolment and verification of personal data. Mühlbauer is the market leader of the Smart Card and Smart Label

manufacturing equipment market and can count on an in-house research & development centre with over 300 engineers and technicians.

Milling

Cavities for IC modules are milled into the card bodies. The cavities are dimensioned according to the module size to be implanted. Depending on the application Mühlbauer milling systems offer a wide range of process and quality control features (e.g. for dual interface card production).

SCM 515 / SCM 525
The Milling systems SCM 515 and SCM 525 are used for automatic milling of cavities for IC modules in plastic cards. The systems represent a very economic way of card milling for small to medium sized production tasks with a throughput of up to 2,500 cards per hour.

Figure 1.5: Chip milling machine available from Mühlbauer AG

Mühlbauer AG has a subsidiary company in the USA. However, the information available on the website was a repetition of that found on the German website. The sites appeared to be linked together. There was however, more machine tool information with the US site offering four machines designated as combined milling and implanting equipment compared with two on the German site. The two German machines appear to be milling machines only. Figure 1.5 shows a typical example of one of the German milling machines. Figure 1.6 presents a mill/inserter machine tool typical of those available from the US subsidiary[7].

Mühlbauer USA[8]

Mühlbauer solutions enable to manufacture any type of chip card, including ID cards, contact and contactless cards, dual interface as well as multimedia cards and smart labels for access control, supply chain management, tracking of textiles and applications for the retail industry.

CMI 3010plus
The fully automated Smart Card Milling & Implanting system CMI 3010plus combines the standard Card Milling & Implanting system CMI 3000/05 with an integrated lamination unit and an in-line plug punching unit. The system throughput is up to 3,000 cards per hour.

Figure 1.6: Milling/IC implanting machinery available from Mühlbauer USA

Further to this, the MELZER maschinenbau GmbH website, www.melzergmbh.com, was less informative but provided the following information allowing some insight into their business in the card machine supplier industry.

> MELZER, as a special machine producer, was founded in 1956, beginning business as a price tag manufacturer. Since 1966, machines have been supplied in a unique modular concept worldwide. More than 80 modules are available to be combined into an absolutely unique and tailor-made machine tool, which, at the same time, is highly flexible for the future.
>
> The products made on MELZER machines are extremely widespread; from (smart) tickets, tags and labels made of cardboard or other materials, to ISO plastic cards of any kind (credit cards, contactless or dual interface cards).
>
> Production of Dual Interface Cards
>
> We have modified and specialised our machinery for producing this card type. In step one, an antenna with contact points, placed on a PVC carrier, are produced. Thereafter the different layers (front/reverse side print, PVC carrier and top/bottom overlay) are laminated into one card body in a hot lamination process. As a last step, the individual card is punched out.
>
> In a separate milling and implanting process (effected on the MI-6000 mill/inserter), the cavities are milled out and a second milling tower makes contact to the copper wire (contact point) where the modules are then fixed by hot melt glue after the antenna contact and IC module have been connected by conductive glue. All processes in the MI-6000 are controlled by sensors, camera inspection system and RFID tester[9].

Nonetheless, all of the commercially available machine tools fall short in the provision of the sensory equipment required to meet the process demands for correctly exposing the copper tracks/contacts, whilst machining the pocket to an exact depth in the correct position on the card. This required adaptive and intelligent machine tool control to facilitate location of the aerial tracks, at an unknown depth in the card's core through a plunge milling operation. Novel sensing techniques had to be developed and implemented along with a software based adaptive control capability to achieve the levels of automation demanded by the client. Knowledge based software technology

was also required to provide a degree of flexible machine programming intelligence. Through the implementation of a suitable user interface, the operator would be isolated from the inner mechanics of the control system functionality and this advanced, applied technology. This said, the sponsoring company's dual interface card design is sufficiently different in process requirement to necessitate their own newly designed purpose built facility.

At this point, it is significant to include some description of the existing plant and its apparent limitations to explain the reasons behind the need of the new facility. The

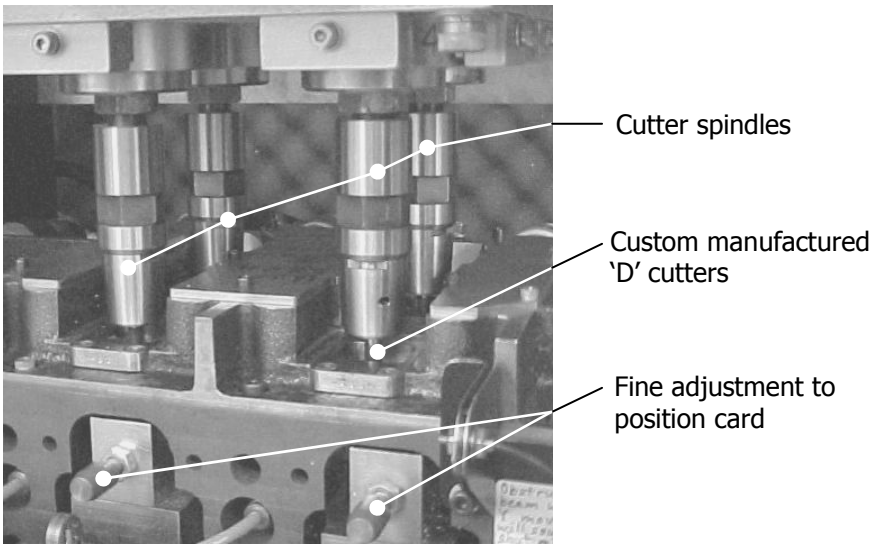

Figure 1.7: Existing four spindle configuration

existing card machining plant was a specially adapted wood router to process four cards simultaneously (Figure 1.7). This four spindle arrangement presented inherent shortfalls that are recognised throughout the machining industry as problematic. The major issues associated with multi-spindle machines:

- consistent and accurate feeding of two simultaneous streams of cards
- moving and positioning the cutter head such that each spindle machined consistent depth pockets relative to each other.
- aligning four cards accurately in relation to the spindle positions
- a lack of consistency in the tool offset lengths
- uneven tool wear across the four cutters.

The above bullet points outlining the major shortfalls of the existing plant have been presented in detail in the following text.

The existing machine tool used a card transport system with two streams of cards passing through simultaneous machining processes. This created a number of issues that the sponsoring company did not want repeated in any new facility. The two streams of cards required indexing simultaneously such that there were four cards positioned and clamped ready for machining. Figure 1.7 shows the two fine adjustment micrometers fitted to the machine. These allow fine movement in the x axis or perpendicular to the card flow direction. Each card holder has its own micrometer, which by necessity is adjusted independently, creating further provision for positional tolerance problems. A single card machining station would not present the same difficulties. A second issue arises from the two stream system. A principal requirement was for the milling component in the card manufacturing process to be one station in a fully automated multi-station machine. The two stream card output from the existing machine was considered ill-arranged due to the perceived problems in card handling when combining the two streams into a single flow for further automated downstream processing. Thus, for this reason, modifying the existing plant was considered unrealistic. Alongside the card handling there were other major shortcomings to be considered.

One of these was moving and positioning the cutters, whilst maintaining card alignment. Achieving the accuracy requirement in these circumstances was a major problem. Firstly, this came about due to the nature of the machine design and secondly, setting four individual tool offset lengths. The machine design had four vertical linear bearings that guided the spindle carrier platform in the Z-Axis direction (vertical to the card surface) and a single leadscrew to position it. The relationship of the leadscrew to the cutters inherently caused the spindle platform to 'droop' on one side as it was placed outside the square formed by the linear bearings. Some attempt had been made to correct the 'droop' due to the leadscrew offset with added balancing springs. In practise, the system operated reasonably well for short periods before requiring further maintenance to realign the perpendicularity of the spindles with the card holders.

A third issue that arose from the existing machine design was that of the small machining process envelope. All axes were fitted with ball type linear bearings. The X and Y axes were fitted with recirculating ball type bearings and the Z axis with fixed ball

tubular rails (see Figure 1.8). Unfortunately, due to the very short throws in each direction these types of bearings tend to wear excessively and erratically. This wear pattern is generated because the balls don't move far enough along the rails to allow a full rotation or exchange of the balls. This constant fretting type motion tends to wear the balls and rails in very confined and specific areas causing the machine to lose

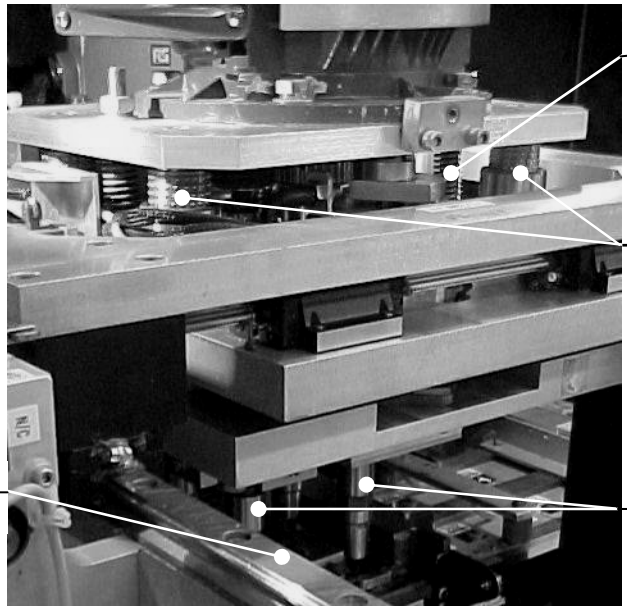

Figure 1.8: Existing four spindle mill

accuracy. This type of wear is slow and insidious in terms of the machine process cycle, but was of major concern to the card manufacturer because the existing machine had seen a long service life. A cause for worn bearings and machine slides was the elevated number of cycles the machine had performed. This was seen as a major contributing factor to some of the ongoing accuracy problems. It was the reason alternative machine bed designs were sought as part of the manufacturer's requirements. Figure 1.8 is a partial presentation of the existing four spindle machine slide configuration. Part of the desire of the sponsoring company was to limit the effects of the short machine slide travel by seeking a system that would minimise it and/or reduce the friction and mass of the existing available systems.

The second concern raised previously was perhaps the more difficult task to execute when configuring the machine, that of ensuring consistent tool offsets across all four cutters. The cutters required fitting into the spindle chucks with the offset all equally set relative to the known machine datum. It was necessary to set the offset distance

across all four cutters within the process tolerances to ensure the pockets were all machined within the given tolerance band.

Allied with the problems associated with four spindles was the design of milling cutter itself. It was a single edged carbide cutter, commonly referred to as a 'D' cutter (Figure 1.7 above), custom designed and manufactured, specifically for the sponsoring company, to machine the pockets in the R-PVC material. Experience and intuition largely formed the basis of the cutter design. Sharp, rag free edges are required in the pockets and the form of the cutter was generally able to provide this requirement. However, due to the custom manufacturing nature of the cutters, consistent performance was difficult to maintain.

Cutters of this kind present major drawbacks in terms of not only cost but also availability. These cutters were very high cost items to have initially manufactured. They were then resharpened on a regular basis until new ones were required. In terms of availability, it was necessary to have a number of these cutters in process at any one time to ensure continuity of supply, which added considerably to the overall expense of using custom manufactured cutters. When consideration was being given to the cutters, the possibility of using alternative commercially available carbide cutters was broached.

Commercial carbide cutters would be multi-fluted (multiple cutting edges) and would possibly be subject to finer feed rates at higher rates of rotation. A major unknown in machining R-PVC at fine feeds and high cutter rotations was the possibility of the cutter rubbing and either burning or melting the workpiece material. A fear unfounded as later results showed.

From here though, the question arose as to the magnitude of the actual power being absorbed by the spindle drive and cutter. The existing machine had a 3 kW electric motor fitted: a legacy from the machine as a wood router. Whilst this size motor would provide an unlimited life due to the light load, the duty cycle was considered reasonably severe. The motor was required to run continuously for 8 hour shifts. This only being interrupted to perform maintenance. Determining how much power was actually absorbed during the milling process was an efficiency parameter to be minimised.

A desired production rate of 1500 cards per hour was the target set by the card manufacturer. This was approximately 20 - 30% higher than their existing capability but not considered impossible.

Another area of concern to the sponsoring company was the style of programming employed on the existing machine. It was a pseudo "G" code, G code being the traditional programming language for CNC equipment. This meant that any changes required significant programming skills to manually write the necessary coded commands to operate the machine tool. A task that was extremely difficult to any but the most skilled operators. Also should there be any requirement for a new pocket, composing the necessary code to generate it was almost impossible and excessively time consuming. Added to the programming difficulty was the fact that the existing plant had no means of testing the code effectively without the possibility of incurring major damage to the machine at the command of any possible incorrect code: a high likelihood even with a competent programmer. A more user friendly system or method of programming was sought in a further attempt to streamline their production.

The combination of awkward machine design, difficulty in setting consistent tool offsets across the four cutter spindles, inconsistent machine accuracy, lack of commonly available cutters, and CNC programming difficulties, amongst others, all lead to the decision to produce a new facility that minimised these issues. Modification to the existing plant was considered impractical because the machine was large and cumbersome with respect to its task. Having considered these key points, amongst others, concluded the preliminary phase of the investigation. At this point, the sponsoring company sought a milling machine as one processing component in a multi process fully automated single stream card processing facility.

Thus, the sponsoring company required a new machining capability to meet an advanced technology manufacturing requirements and was able to specify that it required a new milling facility. This position, taken by the card manufacturer, defined the starting point of the project, which was to develop the unique underlying concepts for the new machine tool with the specific purpose of minimising the inherited limitations, outlined above.

At this point, some additional information with regard to the sponsoring company's aptitude to produce a design specification requirement for a new machining facility

would be helpful to the reader. The following paragraphs present a brief synopsis of the sponsoring company's industry qualifications.

1.3 Brief background information about the project sponsor

Established in 1983, Security Plastics (a division of W & H Print Ltd) specialises in the manufacture and processing of all types of plastic cards. As a leading supplier of credit cards to the Banking industry Security Plastics has earned widely acclaimed international reputation for excellence. The company fully meets international security and quality standards and manufactures in excess of 40 million cards per annum. Security Plastics (SP) is one of the most sophisticated plastic card and credit card manufacturing facilities in the world. They currently manufacture credit and debit cards for 130 banks in 30 countries[10].

Smartcard technology is of growing international interest where IC's are incorporated onto cards to enable multi purpose use. SP pioneered the introduction of these cards and in 1993 established the first chip card manufacturing facility in Australasia. Since that time, they have been awarded a number of contracts to produce chip cards for trials worldwide. SP is the only Smartcard manufacturer in New Zealand.

At the heart of Security Plastics is a sophisticated 'state of the art' card manufacturing facility, employing a wide range of processes and production techniques. The variety of production techniques allows clients to choose the type of card that best suits their needs[11].

Quality is central to everything the company does. This commitment to quality is clearly illustrated by the fact that approximately 25% of the production staff are employed solely on quality inspection while the remaining staff are performing quality checks at each stage of the production process. Security Plastics has invested considerable resources into implementing ongoing process improvement as evidenced by gaining ISO 9002 accreditation[12].

---

[1] Eurosmart via ICMA website – www.icma.com
[2] Nilson Reports via the ICMA website – www.icma.com
[3] Kobayashi, Akira. *Machining of Plastics*. 1967 McGraw-Hill Inc. 35266 New York. Library of Congress Catalogue Card Number 66-16772 Page 1
[4] Muehlbauer AG – www.muehlbauer.de
[5] MELZER maschinenbau GmbH·Ruhrstr. 51-55·58332 Schwelm·Germany - www.melzermaschinenbau.de

[6] Muehlbauer AG – www.muehlbauer.de
[7] ibid
[8] Muehlbauer USA – www.muehlbauer.com
[9] MELZER maschinenbau GmbH·Ruhrstr. 51-55·58332 Schwelm·Germany
http://www.melzermaschinenbau.de/html/prodconcept_en.html
[10] http://www.securityplastics.net
[11] ibid
[12] Ibid

Chapter 2

PROJECT OVERVIEW

2.1 Approach to the problem

To aid in the investigation of this project, a design tool or methodology, of which there are many available to today's design engineers, was sought. A brief review of the project in light of a suitable design tool pointed to a method capable of being clearly understood in its initial stages by the manufacturer's engineering staff. It also had to expand into a process that would provide in depth viable solutions and results that met the requirements of the project. This methodology is further discussed below.

2.1.1 Design requirement specification

The Design Requirement Specification methodology as presented by Hales and Gooch[1] was chosen to aide in management of the design. This method was derived from a checklist, first presented by Pahl and Beitz[2] in a 1984 publication and further formalised and developed by Hales et al (1993), whereby the designer examines the project in terms of its requirements and any contributing factors. These are configured into chart form and assigned a precedence of either demand or wish. A demand is a non negotiable requirement from within the machine's design. A wish is as it says; something desirable that may improve the value or quality[3] of the manufactured component but is not necessary. The wishes should ideally be arranged in order of relative importance[4]. The design requirement specification is sometimes referred to as a 'Demands and Wishes' list. A full representation of Hales' 'design requirement specification' worksheet can be found in Appendix A1.

During the early phases of the project, this design methodology was used to clarify and solidify the design requirement specification between the laminated card manufacturer and the machine designers. In order to achieve this and in an attempt to systematically record the requirements of the project, a set of 'design requirement specification' worksheets or checklists were made available and the relevant staff at the sponsoring company were asked to complete them. This specification was driven by the requirements of the project, the laminated cards being manufactured, the material from

which the cards are manufactured and the environment into which the machine would be commissioned.

The design requirement worksheets were prepared by the author, prior to being completed for the project by the sponsoring company. Once staff at the sponsoring company had completed the lists of demands and wishes, they were analysed by the author, who used them as a guide throughout the project.

These worksheets were based on the broader requirements of the design requirement specification checklists[5]. The major worksheet groupings were correlated directly to the following major categories, with these being further divided into the relevant topics (indented below) within the main groupings. The design requirement specification checklist extends to more than thirty entities, thus in the interest of conciseness only the most relevant are presented here.

These are listed below as an overview to the reader:

- *Functional*
    - *Overall geometry*
    - *Energy requirements*
    - *Material specifications*
- *Safety*
    - *Operational safety*
    - *Human interaction*
    - *Environmental*
- *Quality*
    - *ISO standards*
- *Manufacturing*
- *Economic*
- *Ergonomic*
- *Life-cycle*

The above labels were then applied as table headings in the machine design requirement specifications and the completed worksheets are presented in Appendix A2 (Tables 1 – 7).

From the completed worksheets, the 'design requirement specification' was developed for this specialist machine. A number of dominant requirements were compiled during formulation of the complete design and these are summarised in the following text:

- The usual requirements for a machine tool are for the largest working envelope in the smallest machine packet or footprint.
- The tool working envelope was to be limited to a rectangular cube measuring approximately 20 x 20 x 15 mm: a small envelope by conventional standards.
- The target product was to be predominantly manufactured from laminated Rigid Poly-Vinyl Chloride (R-PVC) sheet.
- The milling machine was to be capable of machining a variety of pocket shapes and sizes within the nominated material to the ISO tolerances applicable to the particular associated integrated circuit (IC) components. In accordance with this, the depth of the cavities was to have a repeatability tolerance band of 3 – 5 μm (microns) as specified by the IC reader manufacturer, instead of the more usual repeatability found in today's quality CNC technologies of 7 – 10 μm[6].
- The productivity of the machine was to be approximately 1500 standard cavities per hour, which required the laminated cards to be infed, machined and then outfed at the rate of 2.4 seconds per card. Despite the volume of material removal being low, the high productivity meant a high material removal rate was necessary. This in turn dictated a high spindle speed. In the realm of this work a spindle speed in excess of 20 000 rpm is considered high though it is acknowledged that milling machines can support speeds of up to 100 000 rpm nowadays.

These were the basic functional requirements of the machine design, (see Table 1, Appendix A2) and were fundamental points of consideration. They, therefore, represent the main reasons as to why the project exists.

It is pertinent here to present some basic information about vertical spindle milling machines, the type of machine tool proposed for the project. From here the research goals will be identified and presented.

2.1.2 Identification of research goals

Figure 2.1 shows the functional features and the axis triad of a typical vertical spindle milling machine of the type to be used in the project. The axis triad forms the reference basis used throughout this work to represent the table travel axes, the direction of process based applied accelerations and the cutter forces. The directions shown on the triad indicate the particular machine axis: Y – long travel axis, X – short travel axis and Z – vertical axis. Other areas of the machine have been highlighted and labelled as major components that make up a conventional machine of this nature.

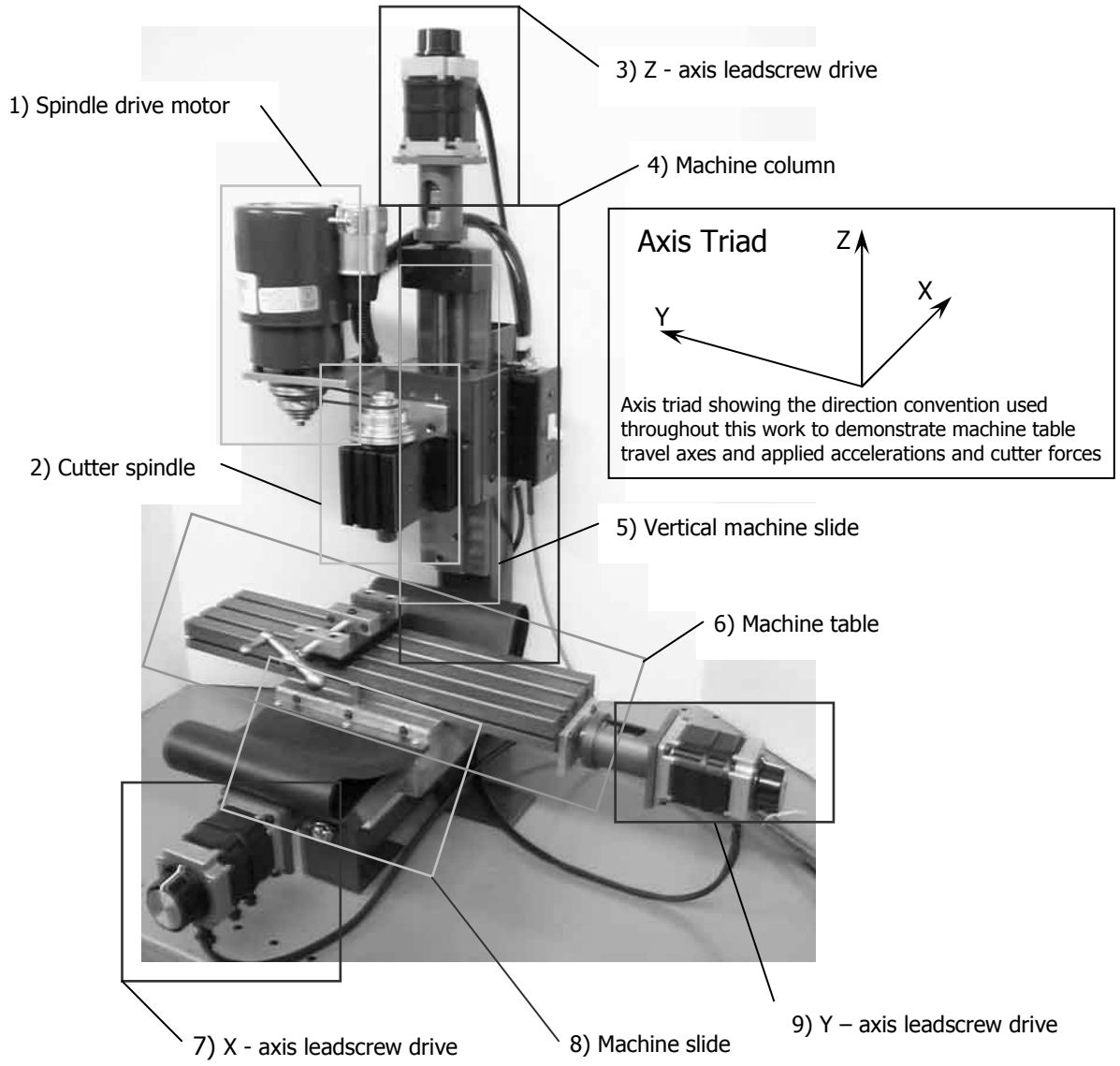

Figure 2.1: Typical vertical spindle milling machine

The highlighted features in Figure 2.1 have been tabulated in Table 2.1 below. Those features indicated in Table 2.1 as having sufficient current technology were sub-systems known to be suitable for direct transfer to the proposed new milling facility.

However, those features indicated as requiring further research consideration were the subject of the undertaken investigation. As such, they were developed to meet the design specification requirement for the new facility. The adaptive control system however, was an area of new technology yet to be applied to this type of machine control structure and as such is represented as a non existent feature in the table below.

Table 2.1: Typical features found on a vertical spindle milling machine

	Machine feature	Existing technology sufficient	Requires research consideration
1	Spindle drive motor	no	yes
2	Cutter spindle	no	yes
3	Z – axis leadscrew drive	yes	
4	Machine column	yes	
5	Vertical machine slide	no	yes
6	Machine table	yes	yes – in conjunction with new slide configuration
7	X – axis leadscrew drive	yes	
8	Machine slide	no	yes
9	Y – axis leadscrew drive	yes	
10	Adaptive control on the axes	non existant feature	yes

The features requiring research consideration pointed toward new and unique technology or applications of existing technology in a new way to meet the facility requirements. These features combined with the design requirement specification indicated the following points as those requiring in-depth research.

- a machine table to minimise the problem of localised wear and high frictional drag encountered in current designs
- a single energy efficient high rpm spindle drive
- a high rpm spindle speed using conventional commercially available carbide tooling but working in plastic with embedded copper as a workpiece material
- an adaptive CNC control system to allow fast accurately machined pockets and exposure of the embedded copper aerial contacts
- an interface to allow pocket programming without the need of skilled CNC operators or programmers

In the context of this thesis, the author has examined in detail, three specialised individual areas making up the research topics presented herein. The "interface" was not considered in any detail and is only reported as the thesis context may require.

The initial approach to the topics raised by the project requirements was to determine the level of published technological and research material available for review.

2.1.3 Preliminary literature survey

An in depth literature review allowed the critical design issues to be assessed and reported. The preliminary project investigation showed there were two major areas to be reviewed in depth with a third to a lesser extent. These areas were:

a.) the utilisation of flexure hinges with a travel of greater than plus or minus ten millimetres for a machine table. (Conventional machine slides have been discounted due to localised wearing and high friction in section 1.2.2)

The use of flexure hinges was found to be well represented with published data in the fields of 'sub-micron[7]' and 'micro[8] [9]' movements and to a lesser extent multi-millimetre (<10 mm) movement[10]. However, the documented use of metal based flexures, where the movement was greater than 10 mm or a hinge arc of greater than a few degrees was severely lacking[11] [12].

b.) the analytical determination of the cutter power required to machine rigid polymeric materials (R-PVC in particular) at high spindle speeds using conventional metal cutting tooling and the repeatable machining accuracy whilst working on these products.

The available published research material was limited in regard to the proposed topics. There were a myriad of publications with regard to the machining of plastics[13] [14] [15] but not the material of primary focus, (R-PVC) nor the core topic: that of cutting power determination[16] [17].

c.) adaptive control for the depth detection of the thin copper tracks embedded in an R-PVC smart card. The requirement was for the tracks' IC contacts to be exposed at a precise depth, by a milling cutter, for subsequent connection to an IC. This was to be performed at the maximum requested production rate, set at approximately 1500 cards/hour.

The published literature with regard to this system of sensory adaptive machining depth control was again very deficient with no directly relevant literature found. This required that a robust sensory detection method be tailored into a system using a custom solution designed to meet the constraints of the proposed facility.

For further information and a more comprehensive literature survey, see chapter three for the flexure hinge report, chapter four for the plastics cutting research and chapter five for the adaptive control design study.

2.2 Overview of the work conducted

In the undertaken work, there were a number of significant features, which made the new machine unique. Two of these core developments monopolised the research effort of the project work. These were:

- The elimination or further reduction of backlash and slide error in the bedways by developing a suitably rigid, high displacement compliant hinge assembly. This was primarily an investigation into the suitability of using high displacement compliant hinges and the problems associated with them. The initial investigation concerned monolithic structures, which later progressed to composite flexures. The words *compliant hinge* and *flexure* are used interchangeably throughout this thesis. The term *compliant* will be used to denote and encompass those mechanisms that produce an output through elastic deformation. Also, *compliance* is defined as the inverse of a flexure's spring rate or stiffness[18].
- The second was the power requirement during high spindle speed machining of plastic using proprietary conventional metal cutting cutters. Also included was a brief investigation into the nature of the cutting, such as burning or ragging on the cut edges.

Two further topics of lesser interest that were explored were;

- A method of detecting the position of a wire aerial array embedded within the laminated plastic thus enabling adaptive control functionality for the machine tool. The control system is adaptive in the sense that it is able to detect and record the embedded depth of the array within the laminates. From there the recorded data is used as a reference point for the embedded array depth when machining the subsequent card.

- A new operator interface environment to eliminate the need for CNC trained programmers.

Of the last two topics, only the detection method is developed to any depth. The operator interface is included as it forms a novel feature of the proposed facility and also integrates the subsystems.

These four topics, cutter power, compliant hinges, adaptive control and the operator interface are introduced in more detail in the following sections.

2.3 Compliant hinge configuration and design

2.3.1 Compliant hinge research

The research dedicated to assessing the specific issues surrounding the use of high displacement flexure blades to produce rectilinear movement was investigated. The results were applied to a machine table of suitable design to meet the criteria as it was outlined in the design specification tables. The initial investigation researched the use of notched beams to form the hinges. The application of circular notches to create very thin sections of high flexibility was considered in depth. Early investigations showed that the notches provided a suitable pivot, but the applied stress concentrated at the notches exceeded allowable limits for most materials. As the notch diameter was increased, the applied stress values were reduced but the manufacturability of the notches also decreased.

2.3.2 Design evolution

As they arose, the technical challenges in the flexure design were met with further research and investigation to find creative solutions that continued to meet the specification. As stated previously the original intent was to use beams with circular notches in them to provide a hinge or flexure mechanism. An evolution from notched monolithic construction to a flat blade unnotched monolithic design came about when it was determined that a dramatic increase in notch radius gave rise to a more acceptable stress concentration. Evidence mounted through analysis that a notch of infinite radius would be the most suitable proposal. This naturally tended toward a flat thin blade that was more easily analysed using the well known and robust beam theories[19]. The problems encountered with manufacturing the long thin blades became an issue in the design.

The most suitable methods in terms of manufacturability, being EDM-based processes, were ruled out due to the poor response in fatigue life from components manufactured with these processes. However, in saying that, the prototype monolithic structures were in fact manufactured using EDM wire-cut machining. This was done, as it was a means of quickly producing the prototype test pieces, where the fatigue life was not a major consideration. These EDM manufactured structures were used as proof of concept only.

To avoid the fatigue issues surrounding the EDM processes, the proposed solution was to design a composite system. This was not without some considerable rethinking of the original concept, thus making a well founded and viable transition from a monolithic structure to the composite system. The composite system adopted individual flat blades as flexure hinges. The terms 'blade' and 'flexure' are used somewhat interchangeably within this work.

2.3.3 Materials selection

The design of the flexures and the selection of a suitable material from which to manufacture them were concurrent processes. This was less obvious when the design was focused on the monolithic structure, but became vitally important as the composite systems were considered. At all times a suitable material was required to meet the flexibility demands. When the notion of a composite structure was conceived, the material selection process became crucial for the blades but less so for the supporting frame structure in terms of meeting the elastic property requirements. This then gave the opening to use one material for the blades and another for the supports.

A method of determining a suitable material for the blades was developed. This was loosely based around material selection parameters as published by Johnson et al[20] and further developed by Ashby[21].

A new means of material selection was developed from both Johnson's and Ashby's work with the addition of a form of dimensional analysis. This work involved non-dimensionalising the standard equations as they relate to beams and then separating the variables into three types. These were geometrical, functional and material related requirements. With the isolation of the three groups, the material related parameters were taken and applied as ratios to extract the various materials that met the property criteria for the flexure blades.

To aid with the process of eliminating unsuitable materials a computer software package was used. The selected package was the Cambridge Materials Selector software called CES™ materials selector[22]. The use of the software package and the results obtained is discussed in a later section of this work. The above determined material parameter ratios were applied to the CES™ materials selector software to eliminate those materials that failed to meet the desired property requirements. The resulting 'Ashby diagrams' were used and manipulated until the most suitable materials were short listed. This method of selection very easily and quickly produced a range of materials with properties that suitably met the design requirement. The original list of materials in the CES database was approximately 1800, which was reduced to approximately 20 choices exhibiting suitable characteristics. The task of selecting the material of choice was very much simplified with the shortened list to analyse. The final material of choice was a stabilised and aged titanium alloy.

2.3.4 Accuracy and repeatability

A prime requirement for the flexure table design was its accuracy and repeatability. The design brief was to improve on the accuracy and repeatability of the existing table system by getting better results either from a slide system or by replacing the slide system with an alternative. The notion of rectilinear translation using flexure hinges arose from a desire to eliminate the zonal wear that is precipitated in linear bearings where the normal range of travel is very short. The short translations are often not enough to give a full revolution or circulation of the supporting ball bearings found in precision linear bearings. The slides found in common bedways were an option in the choice of translation systems open to the designer. These however were very expensive to produce at the accuracies being sought. They also tend to be heavy and bulky and rely on these features to maintain any degree of rigidity. Slide type bedways also suffer from high frictional resistance and wear. The high frictional resistance and bulk has a detrimental effect on the drive systems, which are required to be large to produce the accelerations required. These are the main issues that were sought to be overcome using flexure blades.

Progressing the design from a monolithic system to a composite system was in some ways a backward step when the accuracy capability of the composite system is compared to the monolithic structure. However, there were definite manufacturing

advantages to be exploited, even if the manufacturing tolerances required significant tightening to regain the accuracy. Hatheway[23] et al published an excellent paper describing the mathematical relationships between the errors in rectilinearity and the manufacturing and assembly errors.

The use of Hatheway's equations allowed a greater understanding of the potential errors and misalignments likely to be encountered. They also revealed how best to treat the errors in order to reverse the negative effects produced. These effects are generally related to the manufacturing errors in the structure's components. It is well known that as the tolerance bands reduce and precision requirements increase, the cost of manufacture also increases. This phenomenon is made more complex by the use of multiple 'identical' components which add a further dimension, that of repeatability, to the already increased accuracy requirements. A comment on the effect of repeatability and accuracy is included from a publication by Slocum et al. "The accuracy and repeatability have a direct bearing on the cost of the system to manufacture and thus affect the manufacturability. Superficially, by meeting the increased precision requirements, the manufacturability of the system necessarily reduces"[24] and the cost naturally rises. Hence, the manufacturability of the composite system came under closer scrutiny.

2.3.5 Manufacturability

One of the prime points of consideration in the design and development of the flexure platform table was its manufacturability. With the development of any prototype, the manufacturability should be of prime concern. For although the prototype costs are usually many times that of the final production machine, the ultimate shape of the prototype is influenced by the process methods and layout of the machine manufacturing facility[25]. Aside from the influence on the design by the manufacturing facility, there is a critical requirement in the production machine part component design to ensure it meets a 'design for manufacture' condition. This will ensure that the design is of minimal complexity and still fully meets the machine design requirement specifications.

During the design process, whilst maintaining a hold on the notion of design for manufacture, an additional constraint became apparent as the design progressed towards a composite structure. The composite system would require consideration in

the realms of 'design for assembly' as well as 'design for manufacture'. To this end, processes and forms were considered that would simplify the manufacturing of the components. Also, the combinations of machining processes were intended to give the best overall result in terms of simplicity, precision and repeatability.

Designing and manufacturing the composite structure raised an additional issue with regard to manufacturability due to the five fold increase in the number of component parts when compared to the monolithic structure. The issue was the increase in component numbers. This necessarily narrowed the threshold on the manufacturing tolerances and thus increased the costs in both manufacturing and assembly. One of the features of the composite design was the use of 'identical' parts throughout the assembly. For example, all sixteen of the titanium blades were of identical design. Although this simplified design and assembly, it necessitated the need to manufacture identical components, to minimise the effects of the Hathaway errors[26]. The repeatability and accuracy in the manufacture of the components then became an issue to which a suitable solution was found that was within the capability of the available manufacturing resources.

The final prototype rectilinear flexure table design was manufactured using the common processes, traditional and non-traditional, available in the Mechanical Engineering Departments' workshop. These were designed and manufactured to a geometrical and dimensional tolerance attainable by the same equipment. Following the manufacture and assembly of the composite platform, testing for rectilinearity was performed in the Metrology Laboratory on a coordinate measuring machine (CMM). The engineering drawings are presented in Appendix C.

2.3.6 Testing

In many ways, the testing was the most crucial part of the project. The testing procedure for the composite system is described in the relevant section of this work. The results were tabulated and discussed and conclusions drawn as to how they compared to the expected theoretical values. Discussions are also presented with regard to the assembly of the system and particular issues that arose due to manufacturing inconsistencies.

2.4 The card machining process

2.4.1 Card machining process requirements

With reference to the design specification tables (Appendix A2), an investigation to design and manufacture a high performance precision machine tool was initiated.

The product specification called for a micro-machining capable process to be developed to produce pockets in laminated rigid polyvinyl chloride (R-PVC) sheet. The precision capability of the facility demanded repeatable results in the micron rather than tens of microns range which is commonly associated with machining. The accuracy requirement was demanded by the need to ensure that the surface contacts of the IC were as close to coincident with the card's surface as was possible. This is because R-PVC is well known as an abrasive material and the pin contacts of the card reader would wear very quickly as they pass over the sharp edges of the pocket if the IC was too deep. Should the IC be proud of the surface, the contact edges of the IC will wear quickly. In both cases, the low or high position of the IC detracts from the aesthetic value of the card. To minimise both of these issues the machine by necessity had to perform to the above accuracy levels.

A desired production rate of 1500 cards per hour, using a single cutter spindle and commercially available multi-edge cutters, was the chief aim of the machining process. The single cutter spindle requirement was an attempt to keep the machine relatively uncomplicated in design and construction compared with other equipment currently in use and to reduce production inaccuracies and inconsistencies. The precision requirement was a particularly arduous one given the nature of the specified work piece material and card design.

The card material was laminated R-PVC, a rigid plastic supplied in sheet form for which the published data is comprehensive in many respects. R-PVC was specified as it is an industry standard for the particular consumer product being manufactured. However, the usual material properties published are of significance to component designers invariably utilising moulding processes and not generally relevant to machining processes. A search of available machining resources appeared to reveal no machining 'bible' for polymers, as there is for metals. The Machining Data handbook[27] is the commonly referred to resource when investigating metal properties with regard to machining, but is does not contain corresponding plastics data.

As there were no readily available published references for the machining characteristics of R-PVC or plastics generally, the investigation turned to journal publications as a source of possible information. This research provided two characteristics for R-PVC that were not commonly found in metal cutting processes. They were; 1) R-PVC can be cut relatively easily, except when the depth of cut, cutting speed or positive rake angle of the tool is too large[28]. 2) R-PVC is highly abrasive and causes flank edge and cutting edge wear simultaneously, to round off the cutting edge, which is a phenomenon, not found in metal cutting[29] to the same extent.

The machining considerations of the card pocket necessarily dictated the type of operation that would be most suitable. To that end, the machining operation considered appropriate for the project was milling and specifically end milling/slot drilling. This process was selected to meet both the component design specification and the desired production rates at the required dimensional accuracy.

The factors that affected the production process are outlined in the following sub-sections as they relate to end milling/slot drilling operations.

- Material removal rate

The material removal rate, which is proportional to the tool/workpiece power requirement, was determined by the card manufacturing production rate. The production rate was set at 1500 cards per hour or 2.4 seconds per unit. The standard pocket had a material removal volume of approximately 80 mm^3 giving a material removal rate of 40 mm^3/s. This rate allowed for a product transfer and clamping time in the order of 0.4 seconds through the infeed and outfeed sections of the process cycle.

- Cutter type

The cutter type was selected from a readily available standard solid carbide range suitable for machining aluminium and known to work well with R-PVC. These cutters were selected on the basis that they would have a relatively high rake angle, consistent with tool design for machining plastic. The commercially available requirement was essential to keep the cost of the cutters minimised. The use of solid carbide was specified in order to reduce the abrasive effect of the R-PVC material on the tools' cutting edge.

- Cutter style and size

The standard rectangular pocket being machined had a designated 2.0 mm radius in the corners to give clearance to the IC component (see Figure 2.2). As a consequence, a 4.0 mm diameter cutter was the obvious choice for the machining task. However, due to workpiece relaxation this may have produced over-cut corners as the machine changed directions in the pocket. A 3.0 mm cutter was therefore chosen which allowed the corners to be interpolated, rather than a stop start change as would have been used with the 4.0 mm cutter. This strategy would also help to maintain axis velocities

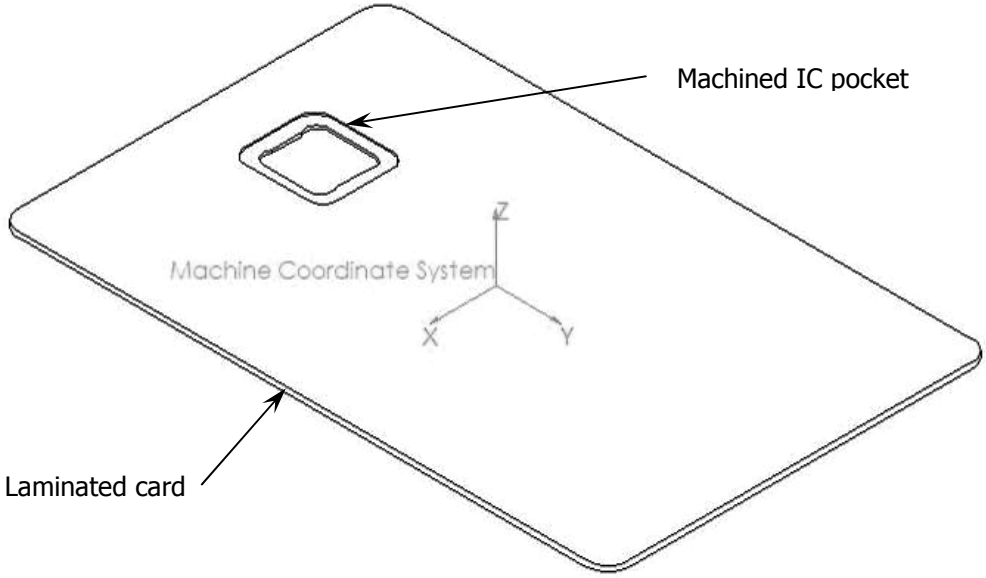

Figure 2.2: Smart card showing a standard pocket

due to smooth acceleration and deceleration as the corner was negotiated.

A three fluted cutter was chosen rather than a two fluted cutter or a single edged 'D' cutter, as is currently used. One of the issues that was a problem with current manufacturing methods was the rag being left attached to the machined edges. A multi fluted cutter taking smaller cuts at shorter intervals was considered a method of reducing the ragging on the edges. This was proven during cutting and spindle commissioning trials, although it appeared again with badly worn cutters as was expected.

- Speeds and feeds

The speeds and feeds are dependent on the material removal rate, which in turn is dependent on the cutter size and style. The cutter feed and rotational speeds were determined by the overall length of cut and the time taken to form the pocket. The

rotational speed of the cutter was also dependent on the allowable feed rate for the particular chosen cutter, the feed/tooth/rev.

- Cutter forces and cutter selection

The forces generated by the cutter are dependent on the depth of cut feeds and speeds in use during the machining operation. The actual forces generated are a function of the work done during the pocket formation process, and the tool geometry.

As the pocket parameters and process conditions set the size and type of cutter, it remained only to select a suitable cutter from a particular manufacturer. Cutter availability proved to be limited with only two and four fluted cutters suitable for machining aluminium being readily available. The use of aluminium suitable cutters was initially considered due to their more suitable cutting edge geometry: a high rake angle. However, due to the limited availability of aluminium cutting cutters, the decision was made to test more commonly available cutters; those being suitable for machining steel. The cutter eventually selected was a three fluted slotting drill. The choice of the three fluted cutter was driven primarily by its availability and maximum feed rate per tooth, also called its choking feed rate. Trials using a four fluted cutter were performed and compared to the three fluted one. The results were so similar that the choice of the three fluted cutter was confirmed. This is discussed more fully in the relevant sections of the following text.

2.5 Spindle power and cutting research

2.5.1 Determination of the spindle power

The determination of the cutter power was one of the primary factors that prompted this investigation. The previous machine in use had been a modified wood router using the 3 kW legacy motor from the original machine. Therefore, the desire to determine the power requirement and apply a correctly sized electric motor to the cutter spindle was vitally important to the optimised design solution. This was to minimise the mass of the spindle drive and to provide a responsible solution with regard to its energy requirements. The information obligatory to determining the power requirements were the force values developed by the working cutter. There were two approaches, which could be made to determine these forces, an analytical or an experimental approach. A complex and time consuming experimental approach was deemed to be very cost

ineffective with regard to the overall project value, and so an analytical solution was sought.

The use of an analytical solution was held to be the most appropriate means of determining the cutting power. This decision was made on the basis that the cutter forces could be calculated by using the specific cutting force data, a freely published property for metals in metal machining handbooks. With this information available and knowledge of the cutter specification, the cutter torque and power would be easily determined. Herein lay a problem. The specific cutting force information was not readily available with regard to polymeric materials as it is with metallic materials. Thus an investigation was begun to determine what work had been published with regard to machining plastics.

2.5.2 Determination of the specific cutting force

The determination of the specific cutting force or specific cutting pressure, or the specific energy of cutting is a complex process relating to the material properties and the tool geometry. It is dependent on both of these parameters and as such is unique for each variation of the tool geometry and work piece parameters. The value of the specific cutting force is usually found by experimental orthogonal cutting trials. The experimental work is required to determine the cutting forces and in some cases to observe the shape of the chip and its geometry. From these factors, it is possible to find the shear plane angle, if one is formed, and hence the specific cutting force. However, not all plastics form shear planes during cutting[30]. For those materials that do, determination for the specific cutting force is possible and once known may be used to determine the orthogonal cutting power.

The limitation to this was the fact that the host component was being processed with helical end mills or slot drills, which placed a severe discrepancy between the orthogonal characteristic information and the specific cutting force relevant to the chosen cutters. Further investigation was required to determine the relationships that existed between orthogonal cutters and helical cutters, if indeed there was one in regard to polymeric materials. This investigation forms a major part of the following study to research and report on such a relationship if it exists, particularly in regard to R-PVC. The following relevant chapter is an account of the literature review and research undertaken to find a method of determining the theoretical cutter power for a

helical milling cutter machining plastic. This was sought to avoid the expense, time and complication of determining the missing data experimentally as would be necessary without an analytical method.

The analytical results were tested experimentally using a high rpm spindle and measuring the power absorbed during cutting, rather than attempting to measure the forces directly in a force dynamometer.

2.6 Adaptive control research

The banking and security card industry is moving towards cards that are capable of more than just being cash, debit or credit cards or an access key. This increased sophistication has occurred at a time when new technology is being incorporated into the card systems. Specifically there is a move towards "smart" cards. These have a capability of interacting with a parent system in a variety of ways. For such developments, the parent system may be the security system in a building, an ATM, or even the lock system in a vehicle that sends out a pulse of radio frequency that can be sensed by the card. As a consequence of this electro-magnetic interaction, the card is 'powered up' and able to respond to allow the carrier to gain access to the building, vehicle, or service. To make the interaction possible the card must have its own tuned aerial that will absorb and use the broadcast radio frequency. Due to manufacturing restrictions, cards are produced with the aerials embedded in their core. However, there are difficulties in exposing the connectors on the aerial whilst allowing the Integrated Circuit (IC) chip to be inserted into a suitably machined pocket and make connection with the aerial. As the card blanks are manufactured from laminated sheet material, the aerial has a tendency to be deposited within a specific zone of the card structure.

The object of this study was to discover a method of locating the aerial terminals within the PVC core during conventional milling operations where the X and Y location of the terminal is known, but the Z location is not (see Figure above for the axis directions).

Chapter Four describes a method that was developed to enable the dynamic detection of the aerial terminals during the milling operation. As the pockets are machined the information as to the position of the aerial array contacts in the card is recorded. This data is stored in the machines computer and used as the basis for the anticipated position of the aerial contacts in the next card. As each card is processed through,

these parameters are updated to allow precise control of the machine axes and thus the cutters' approach to the target depth and contact with the terminals.

The machine axes were required to move at the maximum controllable velocity at all times because the pocket machining time was very short in the overall context of the production time allocated to each card. Hitherto sensing and axis control technologies would not allow the terminals to be exposed without fear of the cutter overshooting and machining them away. The above system allowed the aerials' location to be sensed and the cutters' trajectory to be dynamically controlled to minimise the possibility of overshoot and damage to the terminals.

2.7 Conclusions and recommendations

The final chapter, chapter six, summarises the work described in chapters three, four and five and adds concluding remarks. The chapter also presents the recommendations for future work and system integration.

---

[1] Hales, C., Gooch, SD. *Managing engineering design.* 2nd Edition 2004. Springer-Verlag London Limited, London, England. ISBN 1-85233-803-2 Pages 110 -115.
[2] Pahl & Beitz, *Engineering design.* Springer-Verlag, New York 1984. Page 110
[3] Ibid Page 110
[4] Ibid Page 111
[5] Ibid Pages 114 - 115
[6] Kalpakjian, S., Schmid, SR. *Manufacturing engineering and technology.* 4th edition 2001 Prentice Hall Inc. New Jersey USA. ISBN 0-13-017440-8 Page 962
[7] Smith, ST. Chetwynd, DG. *Foundations of Ultraprecision mechanism design. Developments in nanotechnology volume 2*. 1st Edition 3rd printing 1997. Overseas publishers association, Amsterdam, The Netherlands.
[8] Jones, RV. *Instruments and experiences, Papers on measurement and design.* 1988 edition John Wiley & Sons Ltd Chichester England. ISBN 0 471 91763 X
[9] Smith, ST. Flexures, Elements of Elastic Mechanisms. 2000 Ed, Gordon & Breach Science Publishers. The Netherlands. ISBN: 90-5699-261-9
[10] Jones, RV. *Instruments and experiences, Papers on measurement and design.* 1988 edition John Wiley & Sons Ltd Chichester England. ISBN 0 471 91763 X
[11] Jones, RV. *Instruments and experiences, Papers on measurement and design.* 1988 edition John Wiley & Sons Ltd Chichester England. ISBN 0 471 91763 X
[12] Lobontiu, N. *Compliant mechanisms – Design of flexure hinges.* 2003 CRC Press LLC. Boca Raton Florida USA. ISBN 0-8493-1367-8.
[13] Rohlfs, T. Understanding the art of machining plastics. White paper published on internet by Connecticut Plastics Inc. Sales/Technical Support/Quoting Tom Rohlfs tom@connecticutplastics.com http://www.connecticutplastics.com/resour/articles.htm Publish date 22/07/02
[14] Kobayashi, Akira. Machining of Plastics. 1967 McGraw-Hill Inc. 35266 New York. Library of Congress Catalogue Card Number 66-16772
[15] Ward, IM., Sweeney, J. *An introduction to the mechanical properties of solid polymers* 2nd edition John Wiley & Sons, Ltd, West Sussex, England, UK ISBN 0471 49626 X
[16] Alauddin, M., Choudhury, I.A., Baradie, M.A., Hashmi, M.S.J. *Plastics and their machining: a review.* Journal of Materials Processing Technology 54 (1995) pages 40 – 46 Elsevier Science Publishers

[17] Kobayashi, Akira. Machining of Plastics. 1967 McGraw-Hill Inc. 35266 New York. Library of Congress Catalogue Card Number 66-16772
[18] Lobontiu, N. *Compliant mechanisms – Design of flexure hinges.* 2003 CRC Press LLC. Boca Raton Florida USA. ISBN 0-8493-1367-8. Pages 5 -7
[19] Smith ST. *Flexures, elements of elastic mechanisms* 2003 Taylor & Francis, London UK ISBN 90-5699-261-9 Page 153 ff
[20] Johnson, RC. *Optimum design of mechanical elements.* 1980 John Wiley & Sons Inc. Toronto Canada. ISBN 0-471-03894-6
[21] Ashby, MF. *Materials selection in mechanical design*. 1st edition 1992. Pergamon Press Ltd. Oxford UK ISBN 0-08-041907-0
[22] CES Selector Version 4.5 Copyright© Granta Design Ltd. Build 2004, 3, 16, 1. Granta Design Limited. Rustat House, 62 Clifton Rd., Cambridge, CB1 7EG, United Kingdom
[23] Hatheway, AE. *Alignment of flexure stages for best rectilinear performance.* Proceedings of SPIE – The International Society for Optical Engineering. V2542, 1995, pages 70 – 80. ISBN 0-8194-1901-X
[24] Slocum, AH. *Precision machine design.* 1992 Prentice Hall Inc. Englewood Cliffs, New Jersey USA. ISBN 0-13-690918-3 Page 58ff
[25] Kalpakjian, S., Schmid, SR. *Manufacturing engineering and technology.* 4th edition 2001 Prentice Hall Inc. New Jersey USA. ISBN 0-13-017440-8 Page 512
[26] Hatheway, AE. *Alignment of flexure stages for best rectilinear performance.* Proceedings of SPIE – The International Society for Optical Engineering. V2542, 1995, pages 70 – 80. ISBN 0-8194-1901-X
[27] Machining Data Handbook. Metcut Research Associates Inc., Cincinnati, Oh. USA. 3rd Edition
[28] Kobayashi, A. Machining of Plastics. Page 50
[29] Ibid Page 54
[30] Ibid Page 38

Table of Contents

Table of Tables

Chapter 3

Nomenclature

Chapter Three

Symbol	Definition	Units
A	cross sectional area	m^2
a′	Abbe offset	mm or m
b	thickness	m or mm
b′	fatigue strength constant (number of cycles)	
c	distance from neutral axis to outer fibres	m or mm

C	fatigue strength constant	
D	diameter	m or mm
D*	measured diameter	m or mm
d_r	real position relative to measurement probe	m or mm
E	modulus of elasticity	GPa
e	eccentricity or offset	m or mm
$f[\ ]$ or $g[\ ]$	function of	
F	resultant feed force	N
F_a	axial feed force	N
F_c	force component in direction of relative tool travel (feed force)	N
F_t	force component perpendicular to direction of cut (tangential force)	N
F_i	Functional parameters	
F_x, F_y or F_z	load applied along an axis direction	N
g	gravitational acceleration	m/s^2
G_i	geometrical parameters	
h	width	mm
I_{zz}	second moment of area along Z axis	mm^4
K	geometric constant	
k	stiffness constant	
K_{1c}	fracture toughness	$MPa-m^{1/2}$
k_a	surface factor	
k_b	size factor	
k_c	reliability factor	
k_d	temperature factor	
K_{tS}	fatigue strength reduction factor (Shigley)	
k_f	miscellaneous fatigue factor (Shigley)	
K_f	theoretical stress concentration factor (Smith)	
K_t	stress concentration factor	

l	working length of flexure blade	mm
l_A or l_B	length of A or B flexure	mm
l_{eff}	effective length of flexure blade	mm
m	mass	kg
M_B	bending moment	Nm
M_i	material parameter	
N	factor of safety	
p	performance	
P	applied load	N
P'	linear translation	mm
P_{cr}	critical buckling load	N
P_{crx} of P_{cry}	critical buckling load in the X or Y direction	N
Pt_i	point number i	
q	notch sensitivity (Shigley)	
R	notch radius	mm
r	bending radius	mm
R^2	trend line fit	
R_a	roughness average	
r_n	radius of gyration	mm
R_{sx}	rotation angle about X axis due to span length variation (pitch)	deg
R_X	rotation angle about the X axis (pitch)	deg
R_{xi}	rotation angle about the X axis inner pair of blades (pitch)	deg
R_{xo}	rotation angle about the X outer pair of blades axis(pitch)	deg
R_Y	rotation angle about the Y axis (roll)	deg
R_{yi}	rotation angle about the Y axis inner pair of blades(roll)	deg
R_{yo}	rotation angle about the Y axis outer pair of blades axis (roll)	deg
R_Z	rotation angle about the Z axis (yaw)	deg
r_z	radius of blade end translation for small displacements	mm
s	measurement scale length	mm
S	distance between adjacent blades in a pair in the displacement direction	mm
s’	apparent measurement scale length	mm

S_i	distance between adjacent inner blades in a pair in the displacement direction	mm
S_o	distance between adjacent outer blades in a pair in the displacement direction	mm
s_θ	apparent travel	mm
t	thickness of flexure hinge or blade	mm
T	time	seconds
T_X	translation in X direction	mm
T_{Ax}	lateral translation in X direction of platform at end A	mm
T_{Bx}	lateral translation X direction of platform at end B	mm
T_Y	Platform translation in Y axis direction	mm
U_i	stored energy	Ws/mm^3
V	shear force	N
x	distance from reference point to applied load	mm
z_A	vertical displacement of platform at blade A	mm
z_B	vertical displacement of platform at blade B	mm
Δx_o	horizontal offset at zero table displacement	mm
T_z	vertical displacement of the working platform	mm
Δz_o	vertical offset at zero table displacement	mm
Π	group symbol – dimensionless equation	
Ψ_i	flexure property group symbol	
α	angle between neutral axis in vertical XY plane	deg
β	angle between principle axes of inertia in horizontal ZX plane	deg
δ	displacement or deflection	mm
$\delta\theta$	angle of misalignment between measurement axes	radians
ε	strain	
ϕ_d	horizontal component of the stage drive's angle of incidence to the drive surface	deg
γ	angle between planes through the instantaneous centres of the flexures	deg
θ	rotational angle of hinge	radians
θ'	angle between measurement axes	radians
θ_o	line of action of measurement	radians
σ_a	stress amplitude	MPa
σ_B	bending stress	MPa

σ_E	endurance strength	MPa
σ'_e	endurance limit	MPa
σ_f	failure stress or fatigue strength	MPa
σ'_f	mean fatigue strength	MPa
σ_m	mean stress	MPa
σ_{max}	max applied stress	MPa
σ_{ut}	tensile strength	MPa
σ_y	yield stress	MPa
ω	natural frequency	Hz
ψ_i	equations remaining relevant to materials selection	
ζ	vertical component of drives angle of incidence to the drive surface	deg

Chapter 3

INVESTIGATION AND DESIGN OF A FLEXURE HINGE AXIS

3.1 Introduction

A manufacturing process developed for the production of smart cards required a repeatable machining accuracy of two to three microns. Pockets being machined into the cards, into which an IC (integrated circuit) was to be embedded, required this exceptionally narrow tolerance band.

- This was to ensure the IC top surface was as close as practicable to the top surface of the card. Electrical contacts on the IC's exposed face are used via a card reader to gain access to the stored data. By having the two faces coplanar (upper card surface and embedded chip face), excessive wear on the electrical contacts is minimised as they pass over any sharp or abrasive edges during insertion into the card reader.
- A second issue relating to the coplanar nature of the surfaces was the aesthetic appeal of the chip/card combination. Any visible inconsistency between the surfaces would result in the card appearing to be poorly made and therefore not have the look or feel of the world class product it was designed to be.
- A third consideration was the thickness of material remaining below the IC pocket; ideally in the region of 100 μm. A major cause of these rejects stemmed from the difficulty in accurately controlling the depth of the pockets.

The tolerance band requirement was exceedingly tight and as such, machines with conventional slide ways or linear bearings were unable to meet a consistent and sustainable standard, resulting in a high number of products (4 – 15%) being rejected as out of tolerance. For a considerable period, some specialist machine tools have had a capability to meet this tolerance requirement with slides having sub-micrometer repeatability and recent advances in tribology giving slides a repeatability of better than 1 nm over a 50 mm range[5]. These systems were in the ultra precision realm and deemed to be cost ineffective and unsuitable for the high production rates this project called for. As stated earlier in Chapter 2 the required repeatable tolerance band was to be 3 – 5 μm. Research by Kalpakijian[1] et al indicates that conventional milling

machines have accuracies of approximately 7.5μm and that this will improve to 1μm in the next 5 to 10 years. This then indicates that even the slides available in current modern machine tools fail to meet the design requirement specification of 3 – 5 μm.

A preliminary examination into the causes and sources of the erroneous effects in the existing three axis machine tool, used to manufacture the cards, prompted a search for technologies or methods to minimise these effects. The findings from this investigation are presented in the following sub section.

3.1.1 Investigation of the machine axis problem

Initial thoughts in seeking the causes and sources of the erroneous effects came from observing the existing machine in operation and knowledge of the process requirements. It became evident quite quickly that part of the problem came from the process requirements in that the axis traversal ranges were very short and needed to be repeated at high cycle rates and speeds for the high manufacturing volumes. The short traversals meant that the linear bearings, on the existing machine, were always working in the same zones and often the rolling elements were not completing a full revolution. This situation is known to be undesirable for linear bearings as it leads to excessive and accelerated wear in the working zones and almost no wear elsewhere. The alternative to linear bearings was a system of traditional dove tail slides, which are commonly used in many modern and current machine tools. The very nature of their rigid design makes them large, heavy and ill-suited to short stroke high speed traversals with a very light product payload. The inertial loads due to the high traversal speeds and acceleration rates created by the slide's dynamic mass are thus very high. This problem is exacerbated by the workpiece mass to dynamic mass ratio: the workpiece being very light, and the machine structure very heavy. What's more, they are well known to have high frictional resistance when adjusted to meet the tight tolerance bands. This is mainly due to the lack of adequate lubrication and high shear loads when these high cycle short traversals are used. The lack of adequate consistent lubrication not only increases the frictional power requirement but is also a source of high wear, as it fails to flush away dirt particles, which will cause binding, and further wear.

If the goal of having an axis with accuracy or repeatability of two to three microns and a relatively low drive power was to be achieved these issues had to be eliminated or at

the least reduced significantly. Minimising the number of parts that had sliding relationships with other parts was paramount to reducing the frictional and wear concerns. A proposed design to achieve this was to eliminate the axis slides and replace them with a flexible structure. Systems such as these, without slides, have been successfully developed for very small displacements in precision measuring equipment by the use of compliant or flexure elements[2] (Figure 3.1). There are some

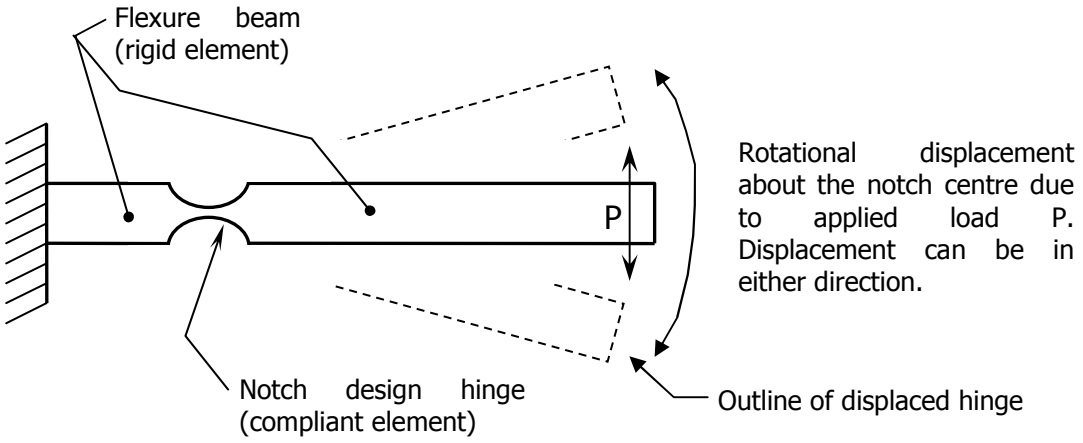

Figure 3.1: Flexure or compliant hinge concept

excellent monographs with regard to the topic of precision movements and instrumentation, Jones, RV.[3], Smith, ST.[4], Smith, ST. and Chetwynd, DG.[5], Howell, LL[6]. A further publication written by Lobontiu, N.[7], covers the design and mathematical relationships for the compliances of various flexure configurations. A review of published material indicated that a great deal of research has been published with regard the use of small displacement flexures in instrumentation and measurement movements where the displacement traversal is on a micrometric or nanometric scale. Only a small number of publications with any relevance with regard to flexures that can traverse tens of millimetres were found, Jones[3] et al being one of these. There appeared to be minimal published material regarding the notion of large displacement metallic flexures and their usage outside the widely adapted realms of instrumentation. From this point, the notion of developing a precision machine tool work platform using flexure hinges was investigated for use in the manufacture of smart cards. The main reasons for initially pursuing the investigation were that flexure hinges have no sliding, therefore no wearing surfaces and configurations that would theoretically give near perfect linear displacement whilst accommodating inherent manufacturing deviations in the flexures themselves[8].

However, developing the flexures to give the working life, travel and linear accuracy to meet the requirements of a small working envelope precision machine tool created some challenging design issues, which form the basis of this work. The linear displacement of the machine axes and the fatigue life of the hinges were only two of these issues.

To ensure that all readers have a common understanding of the concepts or terms used herein, it is pertinent to present a background and a brief history to the term, 'flexure'.

3.1.2 Description and history of flexure mechanisms

Flexure is the term used to describe a mechanism consisting of a combination of rigid components interconnected with flexible or compliant elements. The device is generally designed to produce a well defined motion upon the application of a force[9].

For more than three hundred years, elastic mechanisms have been utilised in fine instrument design and precision machines. If one considers a hunter's bow as a precision machine then the period of use goes well beyond three hundred years. Hooke (1635-1703) and Marriot (1620-1684) were the fathers of linear elasticity, although the seeds were sown by Galileo (1564-1642) in his work with built-in beams and their response to an applied force. Perhaps the marked point in history of the first use of precision flexures was when John Harrison (1693-1776) developed a clock of unsurpassed precision that enabled accurate determination of longitude. Harrison spent the bulk of his eighty three years attempting to produce a mechanism of temporal accuracy to encompass the new Newtonian description of the universe[10].

A further surge in the use of flexures in measuring devices came with the development of the galvanometric instruments by electrical researchers including, Helmholtz, Joule, Kelvin, Maxwell and Weber. Today's flexure uses are found in a raft of applications at the cutting edge of precision technology, but also may be found in everyday consumer products. Some of the precision applications where flexures are found include fine positioning platforms, mass balances, probe microscopes and x-ray interferometers. Commercial products using these devices include hard disk drives, CD players, coordinate measuring machines and dial indicators to name a few. The main reason for the success in the use of flexural devices may be derived from their ease of manufacture and ability to provide smooth motion that is both friction and wear free.

In a marked contrast, friction induced errors often account for a major proportion of the precision motion errors of conventional mechanisms[11].

3.1.3 Advantages and disadvantages of flexure hinges

The following quotation illustrates well the difficulty in citing a comprehensive catalogue of the advantages and disadvantages of flexures.

> "In outlining and listing the benefits and drawbacks of flexure hinges one leaves open the door to criticism from other designers. The notion of listing the merits and demerits of flexures generally is a purely subjective process, which is open to contention. What may be a major benefit to one design may have serious negative implications for another."[12]

These would generally relate only to the application to which they are being applied and it is on this basis that the ensuing discussion outlines some of the basic issues surrounding these devices.

Perhaps the greatest benefit to all designers of flexures is that they are wear free[13]. This is one of the properties of these mechanisms that has prompted this investigation into the design and use of flexures on a machine axis. As there are no sliding parts, the only wear is likely to be some corroding or fretting between any assembled parts[14], though this is not thought to be an issue for this development. Other advantageous properties along similar lines are friction free, lubrication free, ease of manufacture and low maintenance[15].

Flexures can be manufactured as a monolithic structure using a single piece of material. This effectively removes all issues associated with assemblies and the manufacturing of the component parts[16].

The displacements are very smooth and continuous at all levels, essentially without backlash. Additional to this they can be designed to be tolerant of bulk temperature variation and even to temperature gradients in some planes[17]. Additionally symmetric designs are naturally compensated and balanced.[18]

Depending on the stress levels within the flexure, some degree of hysteresis will exist due to dislocation movements within the materials. The level of movement also depends on temperature, grain structure and atomic bonding[19].

For the flexure mechanism, displacement characteristics produce predictable forces, which are based on the design and known material properties. Furthermore, the flexure may require calibration after manufacture[20]. Careful design allows these performance characteristics to be positioned within the linear elastic range of the flexure material[21]. However, in saying this, it is notoriously difficult to accurately predict values for the elastic modulus closer than 1%[20]. To ensure the success of a particular design the flexure material must remain in the linear elastic region with regard to induced stresses. Consequently the displacements must generally be kept relatively small for any given flexure size and stiffness[22].

Even so, for elastic distortions, the linear relationship will be independent of any manufacturing tolerances applied[24]. This is somewhat due to the tolerant nature of flexure designs toward the inevitable manufacturing errors that may cause deviations from the ideal translation path but translation will remain linear[23]. However, the wider the manufacturing tolerance band the less well defined will be the direction of motion[24].

An elastic plastic material used as the hinge provides a slow degradation of the hinge due to fatigue or perhaps overloading. This may be a useful property in that it will avoid catastrophic failures that tend to occur in elastic brittle materials[25]. The use of multiple hinges would eliminate damage to the workpiece or machine tool in the same way that manufacturing errors are 'automatically' compensated.

System stiffness is often of concern, as the drive plane stiffness tends to be quite high and the out of plane stiffness relatively low. This is contrary to other bearing systems. For this reason, it is imperative that the drive axis remain collinear to the direction of desired motion[26].

Two key disadvantages that may have a major effect on the outcome of this project are; flexures cannot tolerate large loads and secondly overloads can change the flexural characteristics, though they may still operate as a linear mechanism. These devices are unable to tolerate large and fluctuating loads and this may be the main reason for not having seen such devices used previously in machine tools[27]. With the application of large loads, it may be possible for more than one state of equilibrium to exist, possibly leading to instabilities such as buckling or 'tin-canning'[28]. The investigation into the use of flexures for this project is on the basis that the work

pieces only weigh a few grams each and the major loadings will come from the machine bed/table accelerations during the machining cycle. The effects of this may be minimised by optimising the design in the way the flexures are applied and dynamically loaded. This is more fully discussed in section "3.5.5, Optimisation of flexure design."

Lobontiu[7], in his monograph regarding compliant mechanisms also points out that there are some further drawbacks in the application of flexure hinges. The hinges are only capable of relatively low levels of rotation, the rotation is not pure and the in situ deformation is complex. The rotation centre is not fixed and will displace under the action of combined loads. Temperature variation can lead to changes in the original compliance values[29]. These issues are not considered problematic with the project described forthwith, as the mechanism is to be a wholly rectilinear device where the influence of the varying rotational centres is symmetrically counterbalanced and does not directly influence the linearity performance.

As stated in Chapter 2, a design requirement specification was created for this project. It was with this specification in mind, that flexure hinges were chosen over slides as they theoretically provided a more suitable basis than conventional slides. The design specification requirement for the machine's working platform is reported in the following subsection.

3.1.4 Machine design intent and axes/direction definition

The design intent was to develop a machine table to minimise or negate issues relating to high cycle short traversal applications of linear bearings or conventional machine slides whilst maintaining or improving the linear accuracy of a machine table. The primary reason this section of the project was initiated was to develop multiple flexure assemblies into a novel configuration for a machine table. This table was to be integrated into a new, small working envelope milling machine design to provide the requisite three degrees of freedom necessary for the relative movement between the tool and workpiece. Figure 3.2 presents the three axis designation used throughout this work.

Although there are two horizontal axes in the proposed machine tool, the development work for only one axis is presented within this report. However, the second axis can be provided by mounting another near identical axis assembly atop

the first axis and recognising that the additional axis would be rotated 90°. The overall effect would be to give the system equal travel in both horizontal axis directions. The fact remains that the long travel and the bending direction of the flexures, for any axis is always parallel to the leadscrew for that axis.

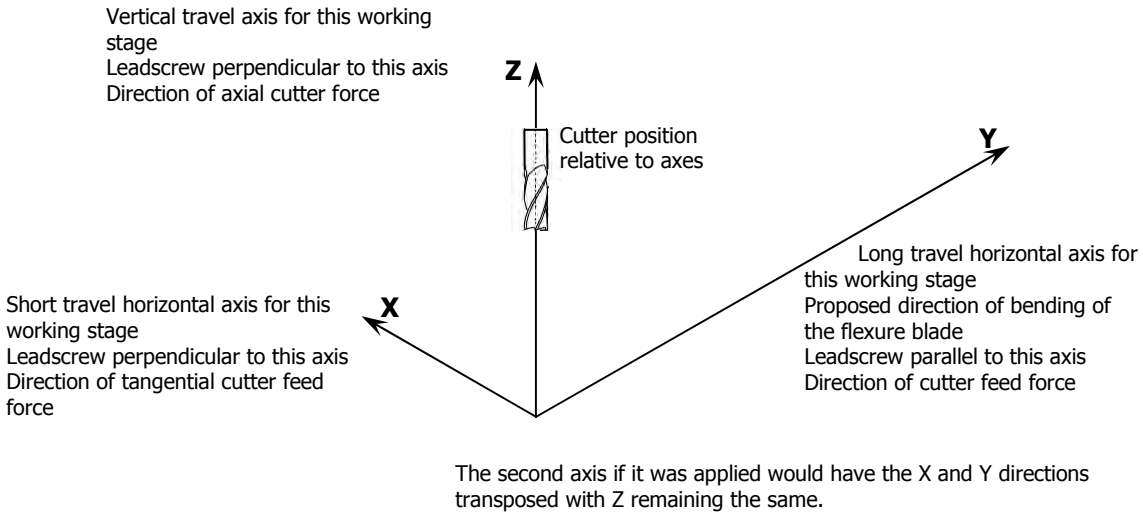

Figure 3.2: Relationship of direction and forces to the machine axis

- Directions of motion

The directions of motion were determined for the table using a naming convention similar to that generally used in CNC milling machines (Figure 3.2). The Y axis direction of travel is the long horizontal axis and it's leadscrew is parallel to the Y axis travel direction. Travel in the X axis direction is parallel to X axis leadscrew and forms the short horizontal axis. The Z axis travel direction is perpendicular to both the X and Y axes.

In the case of the single axis flexure system being discussed throughout this work, the same convention will be applied. Translational motion will be along the Y axis, parallel to the degree of freedom allowed by the flexing or bending of the blades. The flexures will be required to resist motion in the direction of both the X and Z axes.

- Forces

As such the applied forces F_X, F_Y and F_Z acting on the single travel direction axis are discussed in terms of the X, Y and Z axes directions. In so saying, the force, F_Y, is the force applied to the table in the direction of the working stage table travel. Force applied in the direction perpendicular to Y and in the same horizontal plane is designated by F_X. Forces perpendicular to both F_X and F_Y are represented by the Z direction and the force is designated F_Z.

The forces on the machine table are derived from two sources. The first source is the cutter, from which the cutter feed force, F_c, the tangential feed force, F_t, and the axial feed force, F_a, are developed due to the cutting action. The cutter feed force is the force developed as the work piece travels against the cutter in the particular axis feed direction. This force is applied along the Y axis, for example, when the feed direction is along the same axis. The tangential cutter feed force is perpendicular to the direction of feed and the axial force is applied along the cutter axis, in this case the Z axis. These forces are also referred to as orthogonal feed forces and reported in Table 4.19. Relevant values from Table 4.19 are reported in Table 3.1 to give the reader an appreciation of the magnitude of the cutter induced forces. The negative sign in the F_t and F_a values relate to the rotational direction of the cutter (conventional or climb milling) and the axis directions presented in Figure 3.2.

Table 3.1: Cutter (orthogonal) feed forces from Table 4.19

Description	**Magnitude** at 10^o rake angle	**Type**
F_t	-1.27 N*	tangential
F_c	2.59 N	feed
F_a	-0.21 N	axial
F	2.90 N	resultant

The second source of system forces stems from the table structure itself. Accelerating the table assembly and workpiece fixture mass, in the table traverse direction, Y, will cause a force, F_Y, to be developed in the direction of the leadscrew. Generally, the leadscrew would be configured to resist the travel direction force,

however the flexures will be required to support the table structure when forces perpendicular, F_X, to the Y axis travel direction are applied. In the tandem axes system, one axis's flexures will be required to support the combined weight of the second axis, the workpiece fixture and the workpiece, resulting in a vertical force, F_Z, being applied to the table system. The second axis will be required to carry only the workpiece fixture and workpiece, resulting in a lesser force being applied to the second axis flexures. Careful and discrete design for each of the flexure arrays will be required to accommodate the differing loads, under which each flexure array would be expected to function.

The total magnitude of the forces, F_X, F_Y and F_Z, (which include the cutter induced forces) on the flexure table system are at this point undetermined as they are dependent on the final construction mass and process driven accelerations in the machine axis directions (Figure 3.2). Developing a design solution will require a number of iterations to balance the table mass against its design strength to ensure the design requirement specification is met by the final design.

3.1.5 Design specification requirement:

A design specification table was created to summarise and highlight the design requirements for the flexure axis design. Table 3.2 presents the design specification table for this section of the project.

Table 3.2: Design specification requirements for the Flexure Axis Design

Demand	Wish
Repeatable accuracy limits – 2 - 3 μm	
5 mm travel minimum on Z-axis	±10 mm axis travel (20mm total)
Minimal parasitic deviations	Min stress for max displacement
Accuracy levels better than slides	Able to support a horizontal axis
Max stress below the endurance limit	Compact design
Good manufacturability	Ideally monolithic construction
	Able to support the spindle assembly

The above table gives a summary of the design requirements for the axis design. These were the demands and wishes for the project as specified by the initial industry partner in an effort to retain their product to a 'world class' standard.

3.2 Machine tool metrology

3.2.1 Principles of accuracy

In his excellent monograph called Precision Machine Design[30], Alexander Slocum discusses the principles of accuracy, repeatability and resolution in some depth. Some of his comments are worth noting with regard to the design of a flexure blade supported machine table. A number of references are made here pertaining to Slocum's discussion concerning accuracy, reliability and resolution and their effect on the machine design.

The design engineer must have a good understanding of the basic physics that represent the design of the component or system. This is fundamental to the development of functional designs and the proper selection of components[31]. The ability to predict the performance of machine tools by the designing and manufacturing engineers gives rise to high quality precision machines. Many of the general factors affecting the quality of design are difficult to predict but are well understood in the design context. That said, then perhaps, the three most critical factors affecting the machine's performance are accuracy, repeatability and resolution of the components and the means by which they are integrated together. This is a critical point, as it will affect the components, the machine tool is designed to manufacture. To that end, minimising the machine cost and maximising its performance necessarily requires in-depth consideration of these three factors. Awareness of these factors allows the specification of optimum components and manufacturing tolerances to be specified[32].

Designing precision machine tools with good accuracy, repeatability and resolution has historically been regarded as a black art helped along by scientific principles[33]. Perhaps this statement quoted by Slocum best sums up the process of precision machine design: "A basic finding from our experience in dealing with machining accuracy is that machine tools are deterministic. By this we mean that machine tool errors obey cause and effect relationships, and do not vary randomly for any reason[34]." Thus, the design of any component or system, will only appear as a black art, when the designer lacks the resources to gain a full and complete understanding of a particular phenomenon[35].

In order to develop a better appreciation of these critical issues the following definitions are cited:

- Accuracy is the ability to tell the truth. It is the maximum translational or rotational error between any two points in the machine's working volume[36].
- Repeatability (precision) is the ability to advise the same information repeatedly. It is the error encountered between successive attempts to position the machine at the same point[37].
- Resolution is a measure of the detail in the information. It is the larger of the smallest programmable step or the smallest mechanical step the machine is capable of when making a point to point movement. Resolution is important as it offers a lower bound to the machines absolute capability[38].

These statements are almost simplistic in their definition, but how the measurements are made to quantify them is often a source of debate[39]. The design of machine tools by necessity uses the science of these three aspects to produce equipment that will perform to a specific design requirement specification. Subsequent to the machine tools' manufacture, metrology must be used to validate that the machine tool falls within that required specification.

The following discussion attempts to quantify the errant factors considered major in terms of the flexure design and their effect on it.

3.2.2 Principles of alignment

- Measurement errors

This section comprises discussion of the various components that create havoc with the perfect alignment of machine tools and mechanical instrumentation of various types. These points are pertinent to the design development of the flexure table system and must be considered during the design process, hence their inclusion.

- Cosine error

An example of a typical error is the 'Cosine error' presented in Figure 3.3, which shows the measurement and measurand axis displaced by the angle θ. For this reason, it is extremely important that measurements are made parallel to the axis of any displacements requiring measurement. Variations of this problem occur commonly, and can never be completely eliminated[40].

In this example where the measurement is not made parallel to the axis of displacement, then the measurement becomes a projection of the measured value of the actual displacement. This misalignment of the measurement and displacement axes exaggerates the true value. This type of error frequently occurs in the world of manufacturing and metrology. Figure 3.3 illustrates this basic form of alignment error, where a diameter measurement is being taken using external callipers. The angle θ in the figure indicates the relationship between the axes of the callipers and the shaft. The difference between the actual length D and the measured length D* is a fundamental trigonometric relationship given in equation [1]:

$$D^* - D = D^*\left(1 - \cos\theta'\right) \qquad [1]$$

where

D = actual length
D* = measured length
θ' = the angle between measurement axes

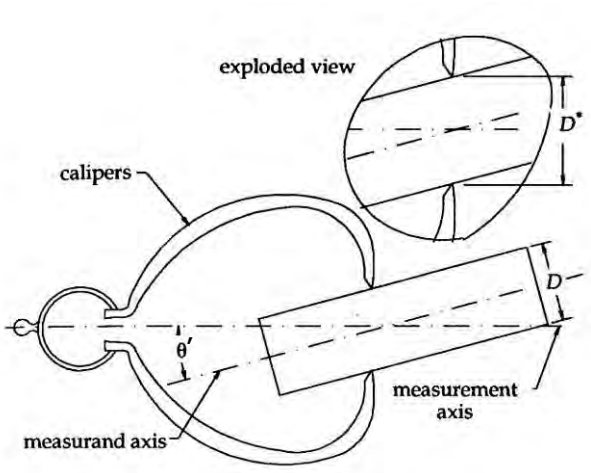

Figure 3.3: Alignment error in diameter measurement

The cosine variation from unity changes very slowly with small angles and as such, there is a tendency to ignore or dismiss it. This however is not wise as the small variations may become significant in high range to resolution applications. Table 3.3 presents the values of the cosine error for small angular misalignments[41].

Table 3.3: Magnitude of misalignment errors

Misalignment angle [deg]	**Error** [%]
1	0.015
5	0.4
10	1.5

These errors may be well approximated by equation [2] when $\theta << 1$[42].

$$D^* - D = D^* \theta'^2 / 2 \qquad [2]$$

The expectation that the misalignment will be constant during a real operation is unreasonable. Therefore a corollary to equation [1] would be, it is best to measure the shortest length possible between the datum and point of interest in a short range high precision measurement.

- Abbe offset

A second error that builds on the notion of the cosine error is the Abbe offset error; this is accounted for by Abbe's alignment principle. The principle was first stated by Abbe, the founder of the Carl Zeiss Foundation. It is simple by nature but its implications are profound and it is of great practical importance:

> *When measuring the displacement of a specified point, it is not sufficient to have the axis of the probe parallel to the direction of motion, the axis should also be aligned with (pass through) the point*[43].

Figure 3.2 and Figure 3.5 illustrate the reasoning behind Abbe's comment. The scales x and s are interchangeable in the two figures.

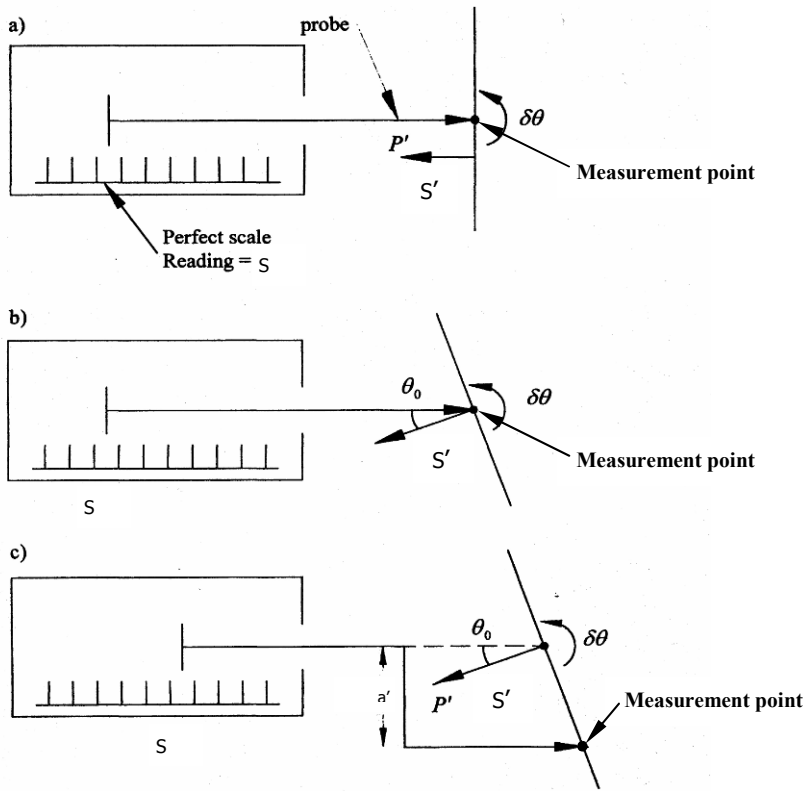

Figure 3.4: Abbe Error - diagram of alignment errors that can occur with linear displacement, a) perfect measurement, b) probe aligned but with axis initially passing through point to be measured, c) misalignment error with Abbe offset

The variables in these figures are as follows;

s = measurement scale length

s' = apparent measurement scale length

P' = linear translation including parasitic translation

d_r = real position relative to the probe

$\delta\theta$ = rotation or misalignment of the P' axis

θ_o = line of action of the measurement[44]

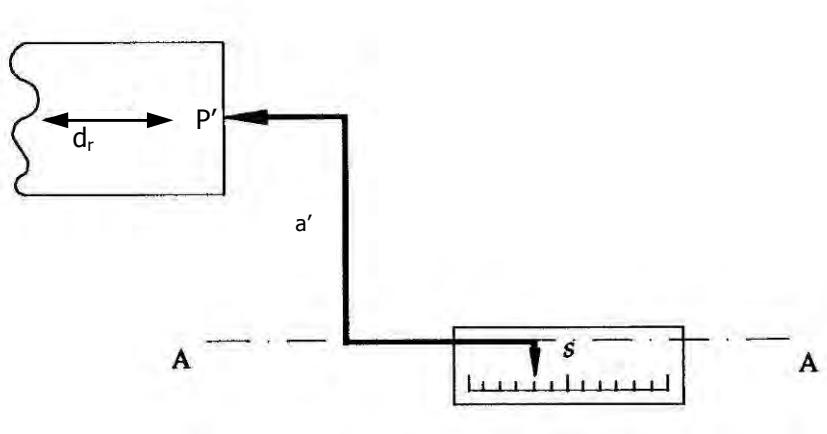

Figure 3.5: Measuring displacement with an Abbe offset 'a'

A measurement scale, 's', monitors the position of point, 'P". The measurement probe is carried on its own axis AA in Figure 3.5 which runs exactly parallel to an axis through 'P", but is offset by distance 'a' (the Abbe offset). Providing the parallelism criteria is preserved then the scale, 's", will exactly record the movement of 'P" along the direction 'd_r'. If the two axes become misaligned by an angle 'θ_o' (Figure 3.4), an apparent change in position at 's" will be recorded even though 'P" has not been displaced. Setting the real position relative to the probe as 'd_r' then the apparent movement 's_θ' will be:

$$s_\theta = \frac{d_r(1-\cos\theta)}{\cos\theta} - a'\sin\theta \qquad [3]$$

where

s_θ = the apparent movement

a' = perpendicular distance between the measurement and measurand axes (Abbe offset)

The first term in equation [3] is a typical cosine error $\left(\frac{d_r(1-\cos\theta)}{\cos\theta}\right)$, which may well be negligible. However, the second term is the Abbe error ($a\sin\theta$) , which is likely to be much more significant as it is proportional to the misalignment at small angles. The Abbe principle asserts that 'a' should be equal to zero to minimise s_θ in equation [3]. If the misalignment angle between the scale and the slide axis is finite, and fixed, the error in the scale value 's' is a positional change 'd_r' and simply becomes dependant on the cosine error term. It would appear that there is no incremental effect on the Abbe error on a machine axis, therefore in theory; it could be removed by calibration processes. The notion of calibrating out the error falls into error itself because as the pointer mimics the position of 'P'' it will move relative to its own bearings along axis AA (Figure 3.3) thus creating a small variation in the angular alignment for the system. A large Abbe offset will amplify this misalignment error more so than the cosine term in equation [3]. A more comprehensive description of the Abbe error is given by Smith[45].

As Abbe originally stated his principle in terms of displacement, the principle can be applied to the positional errors experienced by an extending actuator. It is for this reason that the drive axis should be aligned collinear with the slide axis and coincident with the measurement datum point[46].

- Null point measurement reference

Smith et al consider that the characteristics of measurement devices are sufficiently linear and repeatable to allow direct interpretation of an output in terms of a measurand such as displacement[47]. A prime concern is the maintenance of springs, transducers and other components of a system. This is to ensure they remain sufficiently constant through environmental changes, over time, and so that the measuring process itself does not affect the accuracy.

Achieving high accuracy becomes increasingly more difficult as measuring sensitivity increases and alternative methods are sought. Feed-back systems are commonly used to achieve a higher precision; a special case of feed back that may be used is called nulling. In this case, the system is referenced to a null or neutral point and a measured input signal is used to keep the system at the chosen reference point[48].

Smith et al note that for somewhat variable and other non linear devices, their high sensitivities makes them useful as sensors in systems that are driven to maintain a

constant output value compared to a chosen reference. The drive signal applied to maintain the system at the null point can be used as the output measurement value. The detailed characteristics of the sensor are unimportant, as it is only a solitary point in its operating range that is employed. The authors give an example of the assay balance, where a mass to be measured is balanced against a known mass. This balance functions by only returning the measurement when the balance arm has returned to its balanced position. This effectively eliminates potential errors from the non-linearities of the knife point about which the arm rotates[49].

3.2.3 Machine performance defect compensation

The need to correct errors in mechanical equipment has long been considered essential. For example, thermal movement in materials has been documented since the time of Galileo, who recognised its effect on timing mechanisms due to changes in the pendulum geometry. The correction applied to mechanical equipment to correct the transformations caused by thermal effects, manufacturing deficiencies etc. is called compensation[50]. The more significant compensation types applicable to this project are discussed below.

- Mechanical compensation

By considering the example of a leadscrew, an understanding of the machine errors associated with this project can be appreciated. A lead screw and its associated nut will have manufacturing errors incorporated into them at the time of their manufacture. This is inevitable due to the effects of cosine error and Abbe offsets amongst others. A long screw will have a slow variation in its pitch, which arises from its manufacture and its mounting and so will be systematic. If the nut was perfect then these screw errors would be transmitted into the machine motion. In an attempt to minimise the effects of the error transmission the nut may be rotated. This makes the feed screw/nut assembly a differential device. If the nut is rotated about its nominal position, then it may be used to compensate for the screw error.

However, a problem arises when using this method of compensation as it does not correct for the short range irregularities. These short range anomalies come about, as it is not possible to manufacture the nut to perfectly fit the screw without some clearance in the thread. Therefore, the possibility of producing a precision, high stiffness drive eludes the manufacturer, as it is not practicable to manufacture a

screw/nut combination that is perfectly made, rigid, and with a fully conforming thread, such that clearance is neither provided nor required.

Since there is a constant presence of errors, the necessity of a compliant nut to minimise these effects becomes essential. One method of reducing errors uses elastic averaging to increase the effective system stiffness to compensate and improve the definition for the screw/nut motion. Smith et al write that this method was first recognised and used in the 1870's by Henry Rowlands, and that it has subsequently been utilised by some modern manufacturers to minimise errors.

The authors reported that the use of PTFE reduced errors in the linear relationships to better than 1 part in 10^6 between the rotation of the screw and the motion of the nut. These reduced errors included the longer range compensation[51].

In extending the notion of the lead screw as an actuator, other devices provide similar linear displacements; hydraulic and pneumatic cylinders or electric linear drives etc. These devices must be used across their entire stroke range and so any nonlinearity must be compensated for actively. For this process, various feedback sensors that encompass an adequate range of linearity are often used on large machine tools and micro-actuators alike[52]. For many applications, positional uncertainty may be a serious limitation and recent work done in this area has revealed the use of laser measuring systems in an attempt at compensation on each axis[53].

- Computer compensation

The repetition of systematic errors means that they can be compensated. However, there is a tendency to say that they can be corrected, which would be tempting an over optimistic view. Devices that collect and store the error information and their corrective actions are expensive to manufacture. The obvious method of collecting, storing and processing error information so that it may be reproduced is via a computer. The installation of an online computer to improve the working precision may be the most economic solution, as many machines and instruments already incorporate the use of computers for analysis and control. This being the case, the cost of digital compensation may only be marginal[54].

For the situation where upon an unpredictable systematic error can occur in a new design, computer controlled compensation would be ideal. Once the new design is

commissioned, the data measured from the error can be processed directly and stored digitally. The classic case of this is CNC controllers, where the errors in the positional control system are minimised by interpolating between a set of points set up during the machines commissioning and calibration. These points are usually defined using a laser interferometer. The main issue with this method is the size of the data library when the whole working volume is mapped. In practice, the size of the data package is minimised by mapping less points and sacrificing some accuracy. As an example, a simple three axis machine tool has 21 independent error profiles that are combined to give the overall combined volumetric uncertainty[55].

3.2.4 Machine errors

Other errors that must be considered in the development of the work platform are those that are inherent in the carrier system and guideways. The guideway systems in machine tools are generally statically indeterminate[56], making a suitable functional analysis difficult to perform. Those components of the cutting forces normal to the machining surface strongly influence the machine accuracy. However, these normal forces are often balanced by the frictional forces in the guideways and other elements, the feed drives and the carrier system support structure. Thus as a rule the guideway systems are internally loaded by the frictional forces which are balanced by the drive element forces. Should these frictional forces be varied in any way then variation in the translational motion will occur due to the elastic nature of the feed drive[57].

The influence of the clearances in the guideways, when the machine tool is under load, is unfavourable when the reaction on one face is close to or equal to zero. This allows the carriage to float about depending on the direction of the cutting forces. If the clearances are filled with liquid lubricant, this creates a dashpot effect, which will damp the movement but not stop it. Where there is insufficient lubricant the clearance can operate as an absorber of the vibrations and shock loads up to the magnitude of the clearance. The overall effect is to create a skewed position of the carriage on the bed[58].

A further significant detrimental effect, particularly on machines with knee type configurations, where the table hangs over the guideways, is rocking. The overall condition caused by this is the distortion of the orthogonal axes. For example the axis of a hole may not be perpendicular to the bearing surface. Therefore, parallelism

between consecutive hole axes may be adversely affected. On machine tools where plane surfaces are being machined these surfaces may not be flat or parallel with their base[59].

The foregoing paragraphs consider some of the issues that must be regarded with the design of a conventional table and guideways. The application of flexure hinges to the design will overcome all errors relating to guideway clearances, as they do not inherently require any sliding or rolling clearance. Careful placement of the supporting flexures will also minimise the compliance effects of the materials from which the work platform is manufactured.

Due to the interacting nature of the metrological errors mentioned above, creative solutions were required to eliminate or minimise these effects. A possible method of eliminating these errors may be through the application of strain gauges to the flexure blades to estimate table displacement. This approach reduces the need to fit any sort of measuring scale parallel to the displacement axis, thus reducing or negating the cosine or Abbe errors. However, an issue with strain gauges operating in this situation may be over-strain. This strain may be able to be minimised by careful design and application of the strain gauges. Also in question with regard to strain gauges is their traditional bonding method and their ability to survive the 10^8 cycle fatigue life requirement. These issues may form the basis of future research. For the purposes of this research these errors do not need to be considered in this light as conventional methods can be adapted.

3.3 Flexure hinge design

-Areas of investigation

Table 3.4 lists the major areas of investigation that were considered mandatory to contribute towards the successful design of the proposed flexure hinge system. These areas were the functional hinge design itself, the manufacturability of the design, and use of current manufacturing process technologies. For example, if the final hinge design was suitable for monolithic construction, what would be the most suitable method of production? In this situation, Electro-discharge machining (EDM) wire-cut machining may be considered a suitable manufacturing process to machine any monolithic designs. However, the condition of the cut surface created by the cutting action is detrimental to a long fatigue life.

In the course of the investigation that follows this process was considered to be suitable to manufacture the initial prototype flexures. However, as the fatigue life was not under consideration at this point this process would be suitable for a prototype but not for a production model.

Table 3.4 additionally lists the proposed methods of approach for each of the major areas of investigation. In areas such as beam and notch design, and stress regimes, conventional methods of analysis and design can be used. However, the manufacturability of the proposed design required consideration, as the flexures are inherently difficult to manufacture[60].

Table 3.4: Major Areas of Investigation for the compliant hinge design

Areas of Investigation	Method of approach
Beam & notch designs	Analytical/design
Stress regimes in the compliant hinges	Analytical
Manufacturability	Assess machining processes
Acceleration effects on the primary platform	Analytical/design
Acceleration effects on the secondary platform	Analytical/design
Fatigue stress & fatigue life	Analytical
Vibration and vibration damping	Analytical

Flexure type structures have previously been used in many instrumentation designs[61] but have not been successfully incorporated previously into the axes of machine tools[62]. Smith et al consider the main reason for this is the fact that the movement available from the flexures is comparably small and not suitable for the long travel requirements of large machine tools[63]. The application investigated in this thesis however, only requires relatively small displacements of the axis (up to 20 mm maximum) when compared with the larger more general purpose machines. With this goal in mind, a compliant element design was researched and a prototype produced.

Table 3.4 presents the major areas of the design to be considered before a production model may be developed and commissioned.

This thesis considers the first three entries in Table 3.4 in detail, as they are requisite in the development of a viable design. Acceleration effects are considered in terms of their affect on the design, but their magnitudes have still to be considered in light of the process cycle times. As the outcome from the research was to produce a

prototype, investigations into the fatigue stress and vibration, entries six and seven in Table 3.4, were considered important but minor issues that would not effect the resulting prototype and are therefore not fully considered in the context of this thesis.

3.3.1 Investigation and flexure design for rectilinear motion

- Introduction to Beam & Notch Design Concepts

An initial review of current technology for notched hinge designs and their uses was undertaken, which included published research into the design of flexures. Mathematically, the design of the flexures is extremely difficult; however, several engineers in the past have developed robust approximations for the mathematics that enables them to be designed in relatively simple terms. See, for example Lobontiu[7] and Howell[6].

The current design was also verified using established analytical techniques and furthermore by solid modelling and finite element techniques. The drawback with this type of modelling was the inability of the modelling packages to introduce working tolerance bands to the modelled parts and then have the assembly demonstrate the geometrical errors that will occur because of the manufacturing processes.

The configuration in compliant hinge design for rectilinear movement was quickly ascertained to require at least a double or tandem compound flexure design, to remove the parasitic errors[64]. However, using conventional materials such as bronze alloy or steel meant that the flexure beam lengths were relatively long when using flexures created with circular notches. An extensive mathematical optimisation analysis was performed to minimise the beam length, stress concentration and maximise the bending angle to achieve the greatest movement in the most compact configuration. It proved to be extremely difficult to design a compact configuration using a tandem beam design (See Figure 3.8 below).

To improve the travel and at the same time utilise the maximum bending allowable, a triple movement flexure design was investigated. After an extensive search the author was unable to source any previously published information relating to the parasitic errors that manifest from the use of a triple compound flexure hinge design. Furthermore, a wider review of literature relating to a triple compound movement flexure design found no published research relating to this topic.

Due to the lack of published information into the characteristics of a triple movement flexure design a full investigation was made. The triple flexure was modelled in a solid modelling software package. It quickly became apparent that the software package was not able to model the assembly movement accurately. For the model, the dimensional accuracy was able to be retained, but the moving assembly quickly became unstable and 'locked up', which required all the mating relationships to be deleted and re-established. Alternative approaches and methods of modelling the monolithic flexure were then subsequently investigated in an attempt to quantify the parasitic errors induced by the movement of the relative parts of the structure.

An extensive technology and literature review of CAD (computer aided design) software packages and their ability to model manufacturing errors was completed prior to the commencement of this project. In part, the review sought to discover the capability of 3D CAD modelling systems to accurately model manufacturing tolerances beyond the usual means of merely presenting the desired tolerance range, both dimensional and geometric, on the appropriate engineering drawings. The object was to seek out a CAD system that would allow the 'perfect' CAD representations to be distorted in a manner such that they would more accurately represent the component as it had been manufactured. This representation would allow the addition of dimensional or geometric errors and their variations in the 'as built' configuration. The search proved fruitless and it was found that current CAD systems were unable to allow these manufacturing distortions to be simply and easily modelled[65]. On the basis of this review, the decision was taken that an analytical design would be thoroughly researched and prototyped rather than attempt to CAD model the design in its deviant form. The design of the flexure system was continued and concluded on the basis of conventional and iterative design practises as detailed in the following sections.

The design concept progressed from the initial short beam (~60 mm) triple movement monolith concept to a longer beam (~95 mm) style of a tandem monolith. This redesign saw the overall width of the monolith reduce to less than 200 mm but the height increased to ~250 mm. The flexure thickness was in the region of 0.35 mm – 1.00 mm dependent on the beam length to give acceptably low stress values and still maintain the ±10 mm of movement on the primary platform. This initial flexure design concept was used to gain knowledge of possible working dimensions for the

machine tool bed. This initial concept was further refined by investigating the stress regime in the thin flexure working zone.

3.3.2 Stress regimes within the flexure

The optimisation analysis noted in section 3.3.1 was further developed to examine the relationships between the flexure thickness and the notch radius. The equations developed by Smith[66] in his thesis used a relationship of R/t of between 1 and 5, where R is the circular notch radius and t is the flexure thickness between the notches (Figure 3.6). This configuration appeared to give very high stress levels for the required displacements. However, these calculations did not provide results consistent with the larger displacements required for this project. The relationships were initially developed by Smith for use with very small displacements[67]. Therefore the spreadsheet results were further developed to investigate the relationship between stress and displacement for the circular notch. Although more difficult to analyse, a notch design other than circular, elliptical, hyperbolic or parabolic, was thought to

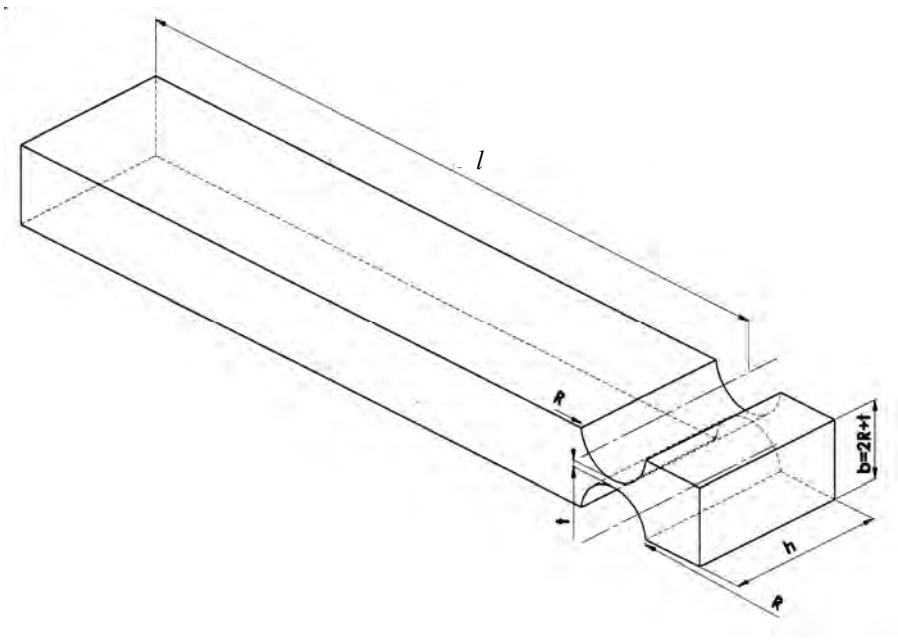

Figure 3.6: Circular notch flexure design

produce a more desirable and practical stress level in the flexure. The spreadsheet was developed to model a range of variables to represent possible configurations of the circular notch style of hinge to investigate the stress concentration factors and their effects on the maximum stress levels experienced by the flexure. The formulae for the mathematical analysis were used as Smith derived them and are presented in Equations [4] – [7][68].

The notch type of rectilinear spring was chosen for analysis in the spreadsheet as it has a proven record in minimising the parasitic errors intrinsic to manufacturing complex assemblies[69]. The monolithic construction has a self-compensating capability by the very nature of its construction. Relevant formulae were used to determine the functional design requirements of the notched spring type axis in terms of the achievable rotation angle.

$$\theta = \frac{2KM_BR}{EI_{zz}} \qquad [4][70]$$

where

θ = rotational angle of the hinge (rads)

M_B = applied bending moment (Nm)

R = notch radius (m)

E = modulus of elasticity (Young's modulus) (GPa)

$I_{zz} = t^3h/12$ = Second moment of area (m^4)

K = geometric constant as given in equation [5]

$$K = 0.565\frac{t}{R}+0.166 \qquad [5]$$

where

t = hinge minimum thickness [m]

The correlation of the K values with regard to increased displacements was tested. The system had to remain in the elastic range of the chosen material so that the fatigue life in bending was not reduced due to any plastic deformation with each switch in displacement direction or cycle change. Smith[71] was only looking for micro-movement in the displacement values: with the larger displacement called for by the machine axis design specification, new values of K were calculated using equation [5]. Then equation [4] was rearranged to give the equivalent value of K based on a theoretical force applied to a sample beam and hinge (Figure 3.6).

The maximum stress occurs in the thinnest part of the hinge and is given by equation [6] which was used as shown below

$$\sigma_{max} = \frac{6M_B K_t}{t^2 h} \quad [6]$$

where

σ_{max} = max applied stress in the hinge (MPa)

K_t = stress concentration factor[72]

$$K_t = \frac{2.7t+5.4R}{8R+t}+0.325 \quad [7]$$

The stress concentration factor, K_t is given in equation [7]. This factor is used for a uniform circular notch and is a well defined value that has been tabulated in previous work by Smith[73].

The analytical results for a steel beam length, L = 135 mm, and end displacement δ = 5 mm, are shown in Table 3.5. This shows values that were less than 550 MPa and a notch radius, R <=12 mm for various minimum flexure thicknesses. A maximum stress level 550 MPa was chosen to be representative of a nominal maximum design stress. The use of the 135 mm long beam significantly increased the overall width of the monolithic structure, therefore careful and innovative design was required to maximise the use of minimal material and ensure the desire for a compact design in order to fulfil the design requirement specification.

Table 3.5: Theoretical analytical results for 135 mm beam length and 5 mm displacement with steel as the flexure material

Hinge Stress [MPa]						
	Notch Radius [mm]					
Flexure min thickness [mm]	**7**	**8**	**9**	**10**	**11**	**12**
0.35	506.912	451.063	406.313	369.649	339.060	313.149
0.40		506.912	457.360	416.646	382.595	353.694
0.45			506.912	462.381	425.053	393.308
0.50				506.912	466.479	432.028
0.55					506.912	469.853
0.60					546.391	506.912

Table 3.5 presents the refined results from the spreadsheet optimisation analysis. The hinge thickness "t" and notch radius "R," are shown in the table. These represent suitable values from which a notch type flexure hinge may be manufactured. The stress values of less than 550 MPa are given in the body of the table. These stress levels were chosen in combination with the notch radius and hinge thickness values. Under consideration of manufacturing processes, the combinations shown were the most practicable. However, it was recognised at the time that the high level of alternating stress was unsuitable when fatigue conditions were applied.

At this point, for the sake of completeness the fatigue stress and fatigue life is discussed. It is acknowledged that a major fatigue investigation will be required before the flexure hinge table design is complete. However, it is also pertinent to point out to the reader that the manufacturability and compactness of the blades along with a feasible rectilinear system are the main focus, ahead of fatigue, at this point in the progression of the design.

A high grade alloy steel was selected as a suitable candidate for a high cycle fatigue check. Three possible candidate alloys are given in Table 3.6, along with their properties and typical applications. AISI 5160 was selected as a recognised material from which leaf springs were manufactured. Although spring materials were at this point being considered, a comprehensive materials selection process was used to define and select a material more suited to flexure hinges, which ideally should store as little strain energy as possible in the deflected state; the opposite requirement for a well designed spring.

Table 3.6: Typical mechanical properties and applications of alloy steels[74]

Alloy AISI-SAE number	Condition	Tensile strength (MPa)	Yield strength (MPa)	Typical applications
4140	Annealed tempered	655 1550	421 1433	Aircraft gears & transmissions
5140	Annealed tempered	573 1580	297 1449	Automobile gears & transmissions
5160	Annealed tempered	725 2000	276 1773	Automobile coil & leaf springs

Using the values from data given in Table 3.6 for the 5160 alloy in a tempered state, a theoretical high cycle fatigue analysis was performed. Ideally, this analysis should be performed using experimental data acquired from laboratory testing of a rotating beam sample of the material to be used to find the endurance or fatigue limit, σ'_e. In

the absence of such laboratory data the theoretical approach was considered adequate. The primary consideration with fatigue calculations was the endurance strength, σ_E and the use of empirical fatigue calculation formulae[75] was rigorously used as the basis from which to form a useful design beginning.

The factors that affected the results in such calculations were somewhat arbitrary, and should be validated by actual fatigue test information from real design samples once they are known. The endurance strength was assumed to be $\sigma_E = 0.65\sigma_{ut}$ and also the endurance limit, σ'_e, was assumed to be between $0.4 – 0.5\sigma_{ut}$[76], where σ_{ut} was the ultimate tensile strength of the selected material. Widely published evidence suggests that the maximum endurance limit value of 700 MPa[77] is used when considering classical high cycle high stress fatigue problems.

The endurance or fatigue limit σ'_e is given by

$$\sigma'_e = 0.45\sigma_{ut} \text{ or } 700 \text{ MPa} \qquad [8]$$

Where the value of 0.45 in equation [8] was initially chosen as a mid range value in the absence of any sample laboratory data. The value for σ'_e is normally determined by making a sample rotating-beam specimen from the material to be tested. To assess the value σ_E, for the component part as designed into a machine, the endurance limit, σ'_e must be modified by a series of modifying factors. The modifying factors are shown in equation [9].

$$\sigma_E = k_a k_b k_c k_d K_e k_f \sigma'_e \qquad [9]$$

where

σ_E = endurance limit

σ'_e = endurance limit for rotating beam specimen, (equation [8])

k_a = surface factor

k_b = size factor

k_c = reliability factor

k_d = temperature factor (not applicable as temperature < 300^oC

K_e = stress concentration factor

k_f = miscellaneous-effects factor (no parameters applicable)

Each of the above factors was determined using tables from Peterson[78] and Shigley[79]. Some were not applicable to this study and therefore had their values set to one.

The stress concentration factor k_e, was approached from two points of view, one proposed by Smith[80] whose work covered circular notches, but with small bending displacements and the other, Shigley[81], whose work was more generalised. Smith's work was considered above [5] and Shigley's stress concentration formulation is considered below, equation [7].

$$K_f = 1+q(K_{tS}-1) \quad [10]$$

and putting

$$k_e = K_f^{-1} \quad [11]$$

where

K_f = theoretical stress concentration factor[82]

q = notch sensitivity[83]

K_{tS} = fatigue strength reduction factor

When K_t, the stress concentration factor derived by Smith, above, is used in fatigue calculations as it is below then its inverse should be used giving:

$$k_e = K_t^{-1} \quad [12]$$

This gives the same designation and value range as Shigley. Values for the fatigue calculation stress modification factors are presented in Table 3.7.

Table 3.7: Fatigue stress modification factors

Factor	Value	Comment
K_{tS}	1.4	interpolated from Shigley[84]
q	0.9	interpolated from Shigley[85]
k_a	0.9	surface factor – shot peined and/or polished
k_b	1	size factor $8 < d \leq 250$ where $d = 0.808(hb)^{½}$
k_c	0.897	reliability factor equating to 90%
k_d	1	temperature facture (not applicable)
k_e	0.735	stress concentration factor determined from equation [10] Shigley

k_e	0.99	stress concentration factor determined from equation [7] Smith
k_f	1	no parameters applicable

Generally these values are determined from various well reported publications and applied to situations as necessary. The two k_e, factors, are given as a comparison and the Shigley value was used as it gave the more conservative approach.

Table 3.8: Endurance limit for 5160 low alloy steel – analytical result

Alloy AISI-SAE number	**Tensile strength σ_{ut}**	**Yield strength σ_y**	**Endurance limit $\sigma'_e = 0.45\sigma_{ut}$ or 700 MPa max**	**Modified endurance limit σ_E**
	MPa	MPa	MPa	MPa
5160	2000	1773	900	
			700	415.5

By applying the factors from Table 3.7 and the yield and tensile strength values from Table 3.6 for the 5160 steel to the above equations [5] – [9], a value for the endurance limit σ_E was determined. This value was considerably higher than maximum value of 700 MPa[86] for the endurance limit, so 700 MPa was substituted into the analysis and the value for the endurance limit, σ'_e.

Inspection of Table 3.8 shows the allowable or modified endurance limit stress (415.5 MPa) to be significantly below the yield stress when the 5160 steel is used in a fatigue prone application. A further factor, the mean fatigue strength σ'_f was also determined using the following relationship.

$$\sigma'_f = 10^C N^{b'} \qquad [13]$$

where

$$b' = \frac{1}{3}\log\left[\frac{0.8\sigma_{ut}}{\sigma'_e}\right] \qquad [14]$$

and

$$C = \log\left[\frac{(0.8\sigma_{ut})^2}{\sigma'_e}\right] \qquad [15]$$

where

σ'_f = mean fatigue strength

N = number of cycles to failure

Using equations [13]-[15] and the additional variables given in Table 3.9 the fatigue strength, σ'_f, of the 5160 was determined.

Table 3.9: Fatigue strength

Factor	Value	
N	10^7	cycles
b'	-0.1003	
C	3.505	

Table 3.10 presents the results of the fatigue analysis showing the allowable stress amplitude and the mean stress for the material selected.

Table 3.10: Stress analysis results

Stress type	Value	
σ'_f	540.3	MPa (fatigue strength)
σ_E	415.5	MPa (endurance limit)
σ_a	415.5	MPa (stress amplitude)
σ_m	207.76	MPa (mean stress)

Review of Table 3.5 and comparing the values with those given in Table 3.10 reveals the hinge thicknesses and notch radii that would function satisfactorily with the proposed design. That is, those values that are below 415.5 MPa as indicated to the left of the heavy line bordering the applicable cell values.

Figure 3.7 below, presents the Goodman diagram demonstrating graphically the relationships between the various stress components. As can be seen the fatigue limit (415.5 MPa) is positioned just below the fatigue strength – tensile strength line, and as such falls into the safe region of the diagram.

The stress applied to the notches is a fluctuating stress, oscillating between zero and maximum giving a mean value of 207.76 MPa. It is important to note that the fatigue limit will only be attained at maximum displacement, which in the application of the machine table will not occur with every movement.

Observation of Table 3.5 will point the reader to the 313.149 MPa value as the lowest, but attempting to manufacture a hinge with a 0.35 mm thickness would prove to be

very difficult and as such expensive. Even at 0.5 mm, the methods of producing a hinge of such a thickness consistently are limited.

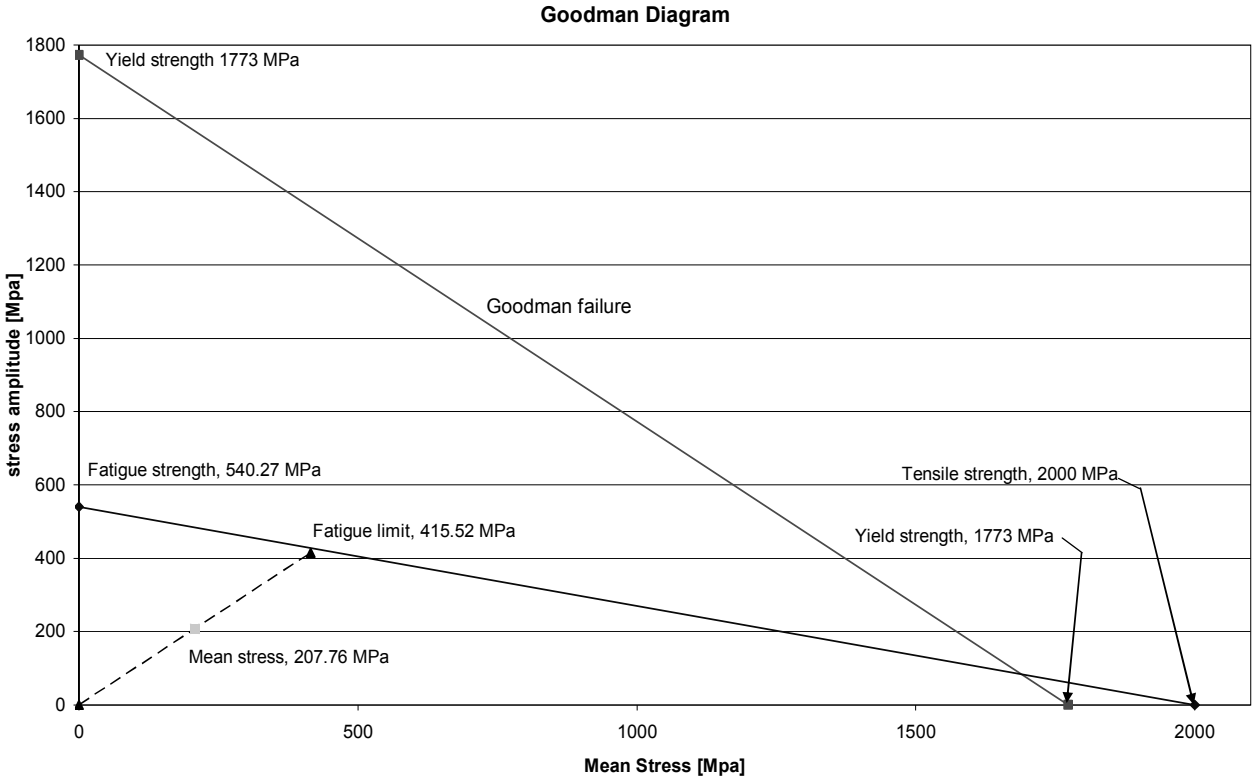

Figure 3.7: Goodman diagram

This is important, as the design of the tandem flexure hinge system requires that all of the hinges are identical in thickness and shape as well as being accurately positioned to minimise the inherent parasitic errors[87]. Another issue considered was the increase in spring stiffness of the flexure system, as the hinges were thickened. A stiffer spring would increase the force required to displace the machine table, thus requiring a more massive structure to counteract the increased force effects. Ultimately, this would affect the sizing of the leadscrew drives, all the while making the structure heavier.

So as can be seen from the above discussion, the selection of an appropriate set of parameters had a far reaching effect on the final design. It was the uncertainty of the preciseness of suitable manufacturing processes combined with the factors mentioned above that caused the design to evolve in the direction described in the following sections.

However to enable the reader to grasp an understanding of the start point of the development, a hinge thickness of between 0.5 mm and 0.6 mm was selected combined with a working radius of 11 mm – 12 mm. When used in conjunction with

the arbitrarily selected beam length and thickness of 135 mm x 5 mm, the stress levels were considered acceptable. From this combination of parameters, an apparent resolution had been established. The effect of the stress levels and a fatigue life analysis is given and further discussed in section 3.7.2.

However, the chosen dimensions were to prove impractical to incorporate into a successful overall design solution as the design requirement specification demand for a compact design was compromised. Further analysis and optimisation ensued before practical and workable geometry was identified. This required evolution of the guideway's through several iterations. The final design evolved from the various iterations and configurations examined in the course of meeting the design specification requirement. The design evolution is presented in the following sections.

3.3.3 Impact of material grain sizes on very thin hinges

Another issue that affects flexure based structures is the very thin minimum hinge thickness. These very thin sections between the notches were briefly considered here in terms of the material grain size and heat treatment processes.

The correct selection of the material for the manufacture of the monolithic structure was critical to ensure good fatigue life and minimise hysteresis losses in the proposed hinges. It is known that material grain structure will be a factor in the fatigue life of the hinges. However, if pre-heat-treated and tempered material was used for the hinges the grain size would not adversely effect the fatigue properties of the hinges. Early design implications pointed to an alloy steel for the hinges (eg 4140 or 5160 grade). If selected, these materials would require heat treatment prior to manufacture of the individual flexure blades to ensure machinability and then post machining to ensure a fine grain structure. However, the heat treatment process would cause significant uniformity issues due to the huge variation in the thicknesses contained in the blades.

3.3.4 Notched beam design solution

As an initial starting point for investigating monolithic solutions in rectilinear movements notched beam design solutions were considered. The first concept was a large monolithic construction with the flexures positioned between the base stage and the working stage (Figure 3.8). The base stage formed the basis of the design to

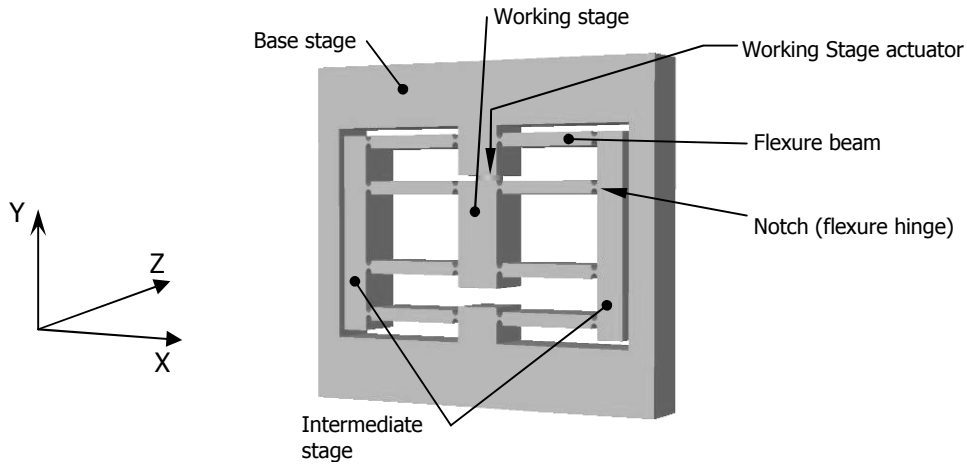

Figure 3.8: Initial flexure concept showing both working and intermediate stages

which the intermediate and working stages were attached. The rectilinear translation of the working stage is generated by displacing the working stage in the Y direction relative to the base stage (Figure 3.8). As the working stage translates the hinges attached to the intermediate stage bend forming double encastra beams (a pair of parallelograms) between the two stages. A second set of parallelograms is formed in the same manner between the intermediate stage and the base stage. As the dimensions of the beam lengths, hinge thickness and notch radius are all similar across the mechanism, the expectation is that the parallelograms will all deform at the same rates. A single pair of flexures will give parallel, but not rectilinear translation. The additional pair positioned in the reverse direction also provides the same motion. This being the case, the pairs of flexures will balance each other. The intermediate stage will move parallel to the working stage due to the affect of the radius arms formed by the notches. At the same time the equivalent effect will occur between the intermediate stage and the base stage. The two pairs will neutralise the effects of the radius arms on each other, thus theoretically forming rectilinear translation. (The described mechanism function forms the basis of the flexure research reported herein, however the configuration of the system changes as the design evolves to find suitable solutions to the various issues that arise in meeting the design specification requirement.)

The initial flexure concept (Figure 3.8) was designed with the above explanation of the mechanism in mind and as such the working stage shaped as a rectangular block with the hinge attachments placed at the four corners as shown in the centre of the figure. The base stage was connected to the working stage via the intermediate stage and short flexure beams formed parallelograms between the stages as shown. The

notches can be seen on the ends of the flexure beams. If this arrangement, which was developed directly from the work of Smith,[88] was to be useful, the length of the flexure beams required reducing or rearranging into a more compact design. However, reducing the beam length only exacerbated the flexure overstress problem; it was crucial to avoid the overstress if the use of this type of movement was to be functional as the guideway in the machine tool. For a given material, the main issue of reducing the bending stress in the flexures could only be achieved in two ways, either by decreasing the thickness of the hinges or by increasing the length of the beams between the notch centres. As can be seen in Figure 3.8, which is not to scale, increasing the length of the notch centres would prove impractical, as the width of the structure would have quickly become unmanageable in the context of a machine tool guideway. The practical manufacturability of the hinges also precluded the minimum flexure thickness from being reduced to less than 0.5 mm.

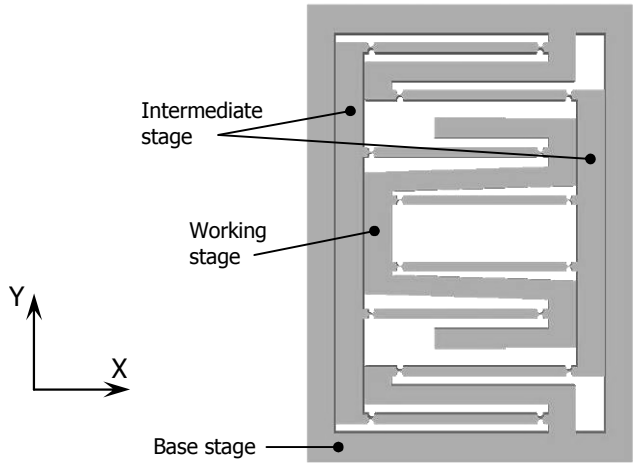

Figure 3.9: 2nd Evolution with 'Top Hat' working stage.

The second configuration considered and shown in Figure 3.9 was still a monolithic structure, but the working stage was shaped like a 'Top Hat' lying on its side. This inter-leaved configuration significantly reduced the width of the monolithic structure, but the height was notably increased and thus was still a concern. An interesting point was that the thickness of the structure had a minimal effect on its performance. One exception was an increase in the force required to displace the working stage: the flexure stiffness. The displacement force required consideration as it affected the choice of displacement method; e.g. the size and load rating of a leadscrew.

The structure thickness also influenced the spring constant of the system, which may have a downstream effect on the overall vibration damping when the loss coefficients are considered during the materials selection processes. Both the spring constant value and the level of displacement force are a function of the Second Moment of Area of the hinge section. Calculating the displacement force and the spring constant were difficult to achieve mathematically due to the complicated nature of determining the working second moment of area. Establishing the working second moment of area requires integration over a section of the notch where the thickness "t" varies continuously but symmetrically with the distance from the notch centre in the direction along the beam length. This variation is caused by the circular nature of the notch formation. Particular difficulty occurs due to an unknown integration range. This is the range over which the actual flexure strains elastically. Should the range extend beyond the straining zone then the Second Moment of Area value will be larger than it should be. The converse applies if the range is too short. Due to the difficult nature of calculating the displacement force, experimental measurements would be required to determine its magnitude. This would be concluded once a final design had been completed and as such presented no negative impact on progressing the design at this stage in the development.

Due to the dimensional constraints discussed in the preceding section, the concept was modified in an attempt to minimise their effect. The next variant, an overlapping structure, was used to reduce the height made by putting the flexure blades parallel to, and above each other. This was done because consideration of the manufacturability of the flexures in this style of structure was a major concern. As a consequence of these changes, the solid model showed impossibly complex components that would prove to be very difficult to manufacture in a truly monolithic construction. Furthermore, there were major difficulties encountered in achieving a design of this nature that would meet both the displacement criteria and at the same time stay within a practical size envelope that was in proportion to the achievable travel. Shorter beam lengths could be used to minimise the overall size, but this change raised the hinge stress levels above acceptable limits. Conversely, any added beam length had a negative impact on the structure's overall size. On this basis, the notion of a unit construction monolith was discarded and the second stage of evolution (Figure 3.9) was reworked to include the separate flexures as a fabricated structure.

3.3.5 Fabricated notched beam design solution

A multi-component assembly concept was developed (Figure 3.10). This concept allowed superior materials to be independently selected for both the flexure blades, and the main frame components. However, there are known difficulties associated

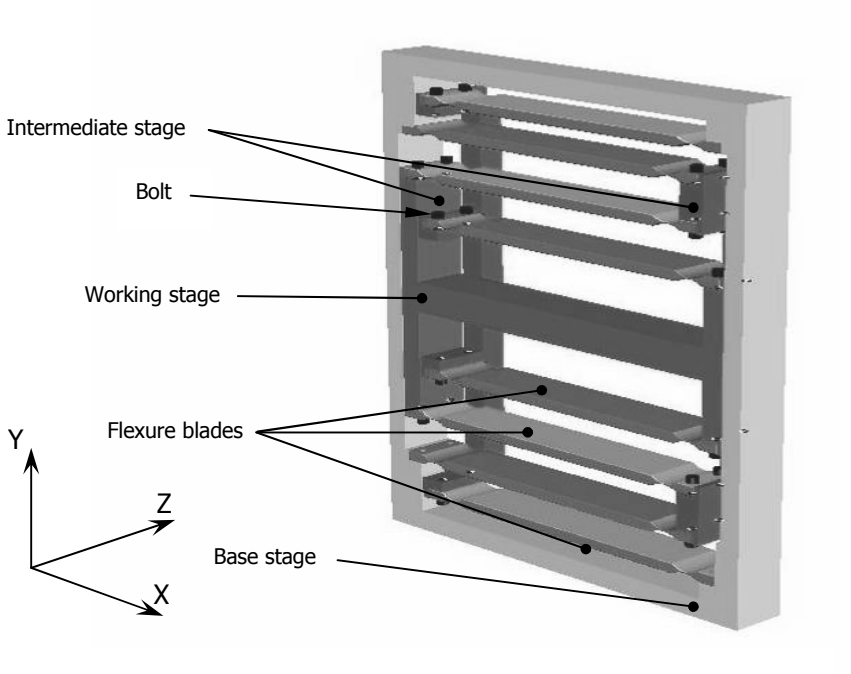

Figure 3.10: First concept of a fabricated flexure structure

with fabricated flexure systems. Specifically, rectilinear spring systems traditionally fabricated from individual components inevitably give rise to a multitude of parasitic errors that are cumulative in the mechanical action. These errors traditionally come from machining tolerances, mechanical interfaces, and stress concentrations in the vicinity of the fixtures, construction inaccuracies and mismatched thermal expansions[89]. This was the main reason for initially steering away from the fabricated construction and is why a monolithic construction is normally used in its place.

The multi-component assembly design was essentially the same layout as for the monolith described in Figure 3.9 except that it was modified to accommodate the 'bolted' flexure blades. This new concept (Figure 3.10) was used to investigate the mechanics of the bolted connections before proceeding with further configuration development. Using this model the forces, and thus the stresses concerned, relating to the flexure/support structure joints proved insignificant in a static analyses. However, the fatigue analysis of the same system required further investigation, which is beyond the scope of this thesis. (See future work)

The fixings in the new concept added further complications to the structure in that provision was required to accommodate the bolt heads and the manufacturing inaccuracies in the flexure blades and the mounting seats. A design that would seat the flexure completely and precisely was required to ensure that there was no movement between the body of the various platforms and the flexures themselves. The flexure blades were also required to be aligned accurately and simply during assembly. So although the separately manufactured flexures simplified the manufacturability to some extent, this configuration added other complications. The design failed to reduce the envelope of the overall structure and apart from the simplified manufacturing of the flexures, very little overall improvement to the design was gained.

The next step in the concept development was to rearrange and redesign the flexures to reduce the overall envelope of the structure whilst maintaining the integrity of the parallel action of the platforms. Placing the flexures parallel and adjacent to each other was an obvious solution, however this approach would introduce severe eccentric loading into the flexure components of the structure. This loading would have been difficult to remove or minimise and could lead to buckling in the hinge sections of the beams. To avoid this dilemma, half of the blades were divided lengthwise. This reduced the width of the blades to 12.5 mm from the original 25 mm. The narrow blades were assembled to either side of a full width flexure blade.

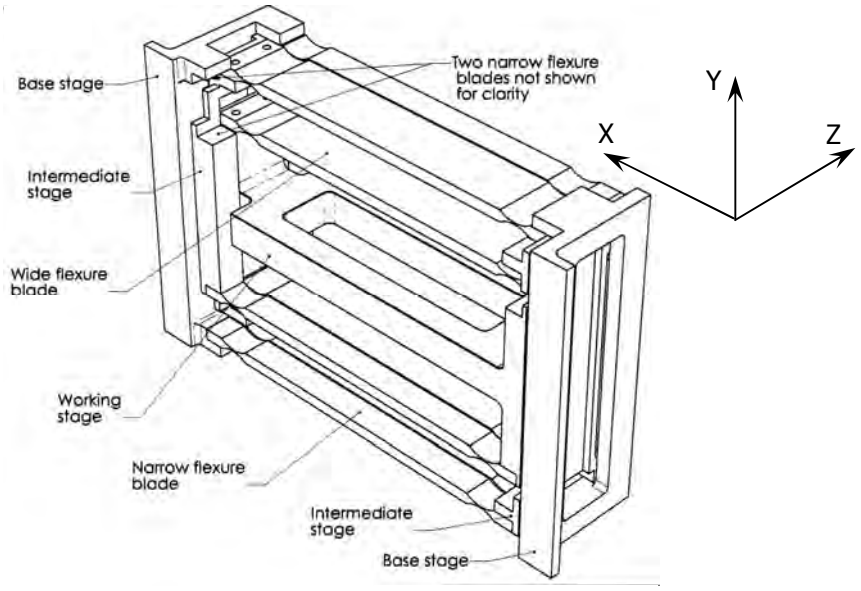

Figure 3.11: Fourth iteration of the flexure

Figure 3.11 shows this fourth iteration concept with the two top left narrow flexure beams removed to enhance the visual clarity. The proposed XYZ machine axes are also shown in the figure.

To further increase the compactness of the structure, the vertical distances between the various 'levels' of flexure were reduced to a minimum. The down side of placing the beams adjacent to each other was the increase in the structure's thickness or depth. That is, the depth was effectively doubled and also required was a small clearance between the beams (0.25 – 0.5 mm). Several issues in terms of the manufacturability arise from this configuration, which were solvable but with the penalty that the size of the structure increased as interferences were discovered and corrected with additional small clearances.

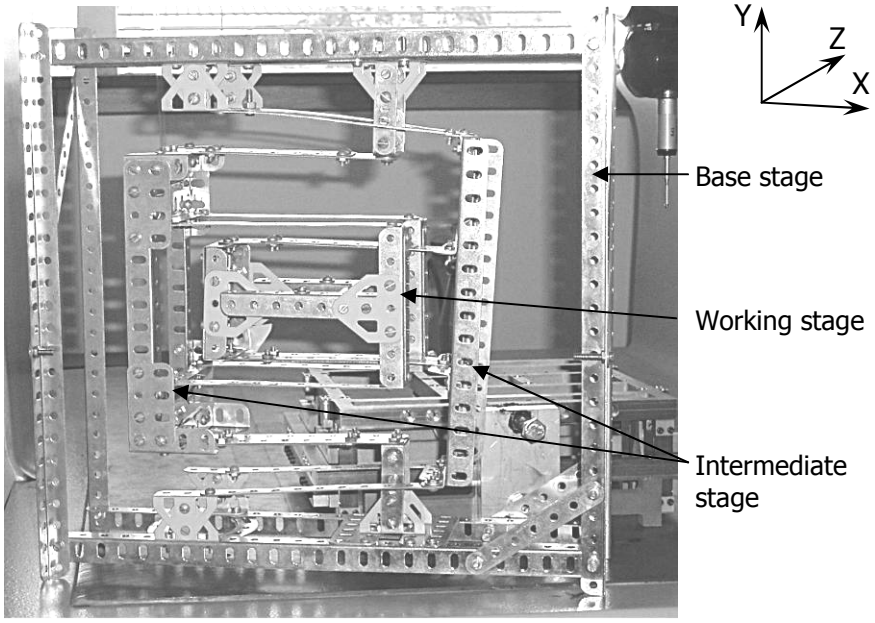

Figure 3.12: Trial concept flexure assembly modelled in Meccano™

At this point, a crude model was constructed from "Meccano"™ (Figure 3.12) to better visualise the action of the assembly of the parallel beams. The model appeared to mimic the required action very closely. It did not deflect as accurately as the notched flexures were expected too, as it had long thin beams that allowed bending and torsional deflection over their full lengths (~140 mm). As expected, it clearly showed the beams bending into a flattened 'S' shape with an obvious point of inflexion. To some extent, the slender blades allowed the primary platform to roll, as they were able to twist notionally under eccentric loading. Therefore, an appropriate blade design

with notched hinges would need to be designed that were substantial enough to resist the torsional effect caused by any eccentric or out of plane loading.

Other issues likely to be encountered with this design were considered. For the notched beams to deflect torsionally, the hinge zones themselves would have had to buckle which was found to be impossible with the intended design loads. The reason for this was that the notches were circular and separated by a distance (hinge thickness, t) of approximately 0.5 mm. By referring to Figure 3.6, the shape of the hinge waist and the rapid section change on either side of the tangent points can be seen. This section change is preventative of buckling displacements. The blades however have length, l; enough to allow a nominal rotation about an imaginary axis parallel to the notch axes, but through the thinnest part of the waist. Again referring to Figure 3.6 it can be seen that by increasing the magnitudes of dimensions 'b' and 'h' any tendency to displace laterally or torsionally can be reduced. However, increasing dimension 'R', thus lengthening the waist section, will have the opposite effect and increase the risk of buckling failure or torsional over-strain through the hinge if any torsional loads are applied. This mechanism is discussed in more detail in a subsequent section regarding the application of forces on the blades.

3.4 Blade design

As the design progressed, it became obvious that the circular notched hinges would fail to meet the design requirement criteria. To achieve the desired deflection the overall length of the blades (>135 mm) made them unwieldy to apply in a compact guideway design.

Other notch shapes were briefly considered, eg parabolic, hyperbolic and elliptical etc,[90] before the leaf type was selected. The main reason for not selecting one of these other notch types was that manufacturing them would pose the same or more complex problems than the circular notch type. Circular notches can be manufactured using an appropriate combination of drills and reamers or boring tools. These tools are able to produce round holes in the near correct positions prior to removing the balance of unwanted material using other metal removal methods. However, this luxury cannot be afforded in the manufacture of notches other than circular. The leaf flexures can be formed in two different ways: EDM wire cutting or fabricate them from sheet material. As discussed earlier the EDM process was suitable for any prototypical

models but highly unsuitable for a production flexure system. It is with the above comments in mind that the design progressed to leaf blades and that progression is discussed in the following section.

3.4.1 Leaf flexure design solution

The selection of the leaf type blade brought with it a set of design issues, that required careful consideration as to how the blades were to be applied one of which was the torsion concern noted above. Some insight as to the behaviour of the long slender flexures was gained from the previous crude Meccano™ model earlier mentioned. This showed that short leaf blades would be optimal.

Other problems were associated with loading; the resulting axial and transverse forces were two main contentious design concerns[91]. These forces came about due to the change from the comparatively thick flexure elements with notch hinges, to the relatively long slender configuration of the leaf flexures. That is, when the leaf flexure is loaded axially or transversely, the characteristics of the flexures response will change accordingly. By referring to Figure 3.13, the X-axis flexure blades can be seen

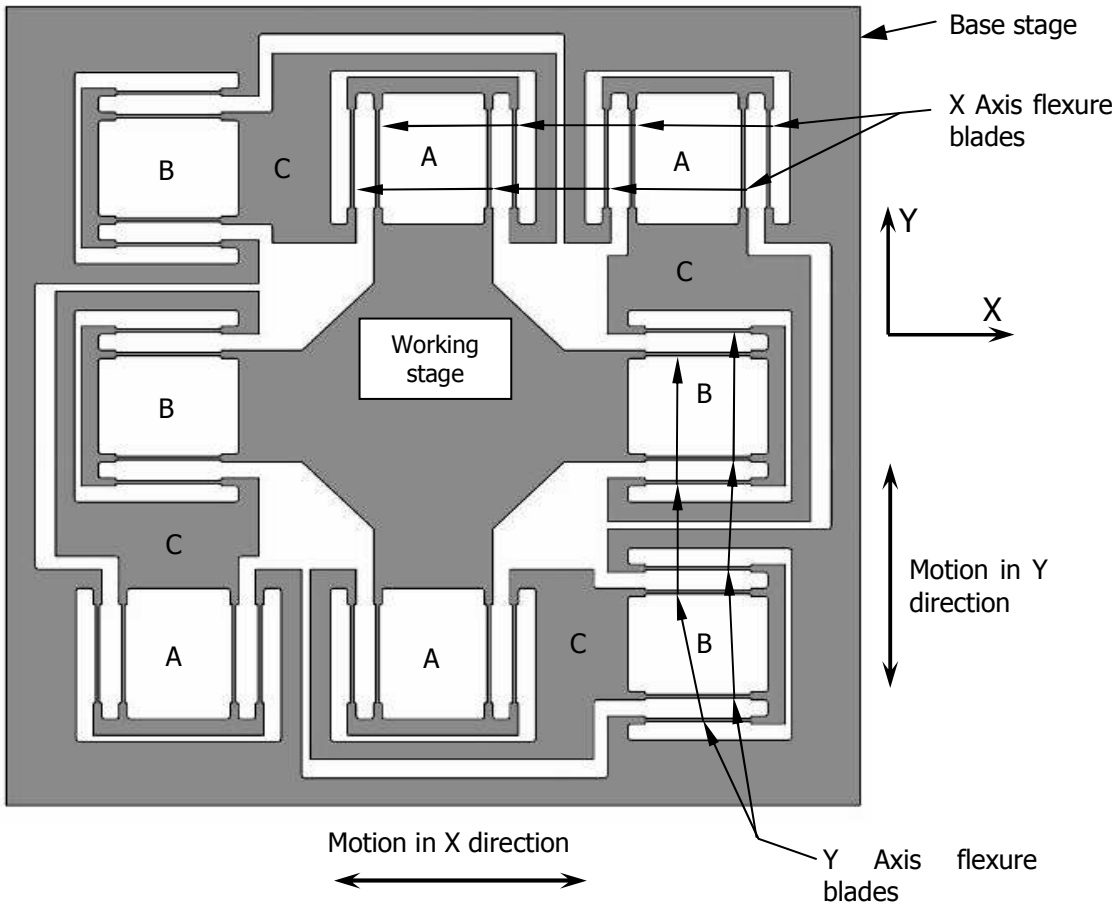

Figure 3.13: Two axis monolithic flexure system

to be loaded axially by forces applied in the Y-axis direction. A similar loading scenario occurs with the Y-axis blades when loads are applied in the x-axis direction. A compressive axial load will typically cause buckling whilst a tensile load will cause the flexure to stiffen. Often the compressive load presents an unwanted instability, whilst the stiffening is tolerable in most instances[92]. The influence of the compressive and tensile loads on the flexure, whilst present for both types, the notch and the leaf, has a more detrimental affect on the leaf flexures. Considerable design effort was applied to minimise these negative affects on the flexures for the final design solution. A design strategy using the application of tensile axial loads was sought in an attempt to move away from the torsional and compressive axial forces known to cause structural instability.

With the decision made to pursue the leaf style hinges, a two axis monolithic design was created (Figure 3.13). This original configuration was based on the micro-precision 'Pentaflex'[93] design presented in a proposal published by Shorya Awtar et al[94] (with the third axis excluded). However, it was originally designed to give a deflection of microns rather than millimetres as now required by this project. Its function is relatively simple in that the leadscrews must connect the working and base platforms, perpendicular to each other, thus giving motion in both directions as indicated (Figure 3.13). To achieve motion in the X direction, a force is applied to the working platform in that direction and the 'A' blades will deflect. The working platform and the intermediate platforms, 'C' will displace relative to the base in the direction of the applied force. At this point the 'B' blades remain undeflected and therefore no displacement occurs in the Y direction. Since this design is a two axis system, a force may be applied in direction Y. This will cause the 'B' blades to deflect in relation to the working platform, the intermediate platform, 'C' and the base giving translation in the Y direction.

The two axis design, though successful in that it provided a reasonably compact guideway system (250 x 250 x 10 mm thick), was found to be not without a problem. That is, the design was such that it allowed cross coupling between the two axes. This occurs because both directions of travel use the common intermediate platform, C, to transfer displacements into the respective blades. A computer controlled axis drive system may have been applied successfully to adequately compensate for the cross

coupling, however it would have been difficult to improve the performance found in existing available guideway technologies.

A new single axis monolithic structure was designed using the knowledge gained from the two axis structure, but with the intent of removing the cross coupling effects and reducing the bending stress. The result was the dual stage design presented in Figure 3.13. A major characteristic of this design (Figure 3.13) enabled twice the displacement in the direction of motion when hinges of the same dimensions as the two axis design (Figure 3.13) were used. This was the main reason for pursuing the second prototype. This prototype also provided a similar compact design envelope (270 x 250 x 10 mm) that was comparable to the two axis system.

The function of the single axis design was similar to the two axis system. The major difference between the two was the single axis system had all the flexures oriented in the same direction. This meant that the displacement per hinge was the same as the two axis system, but the displacement between the base and working platform was twice, due to having double the number of flexures.

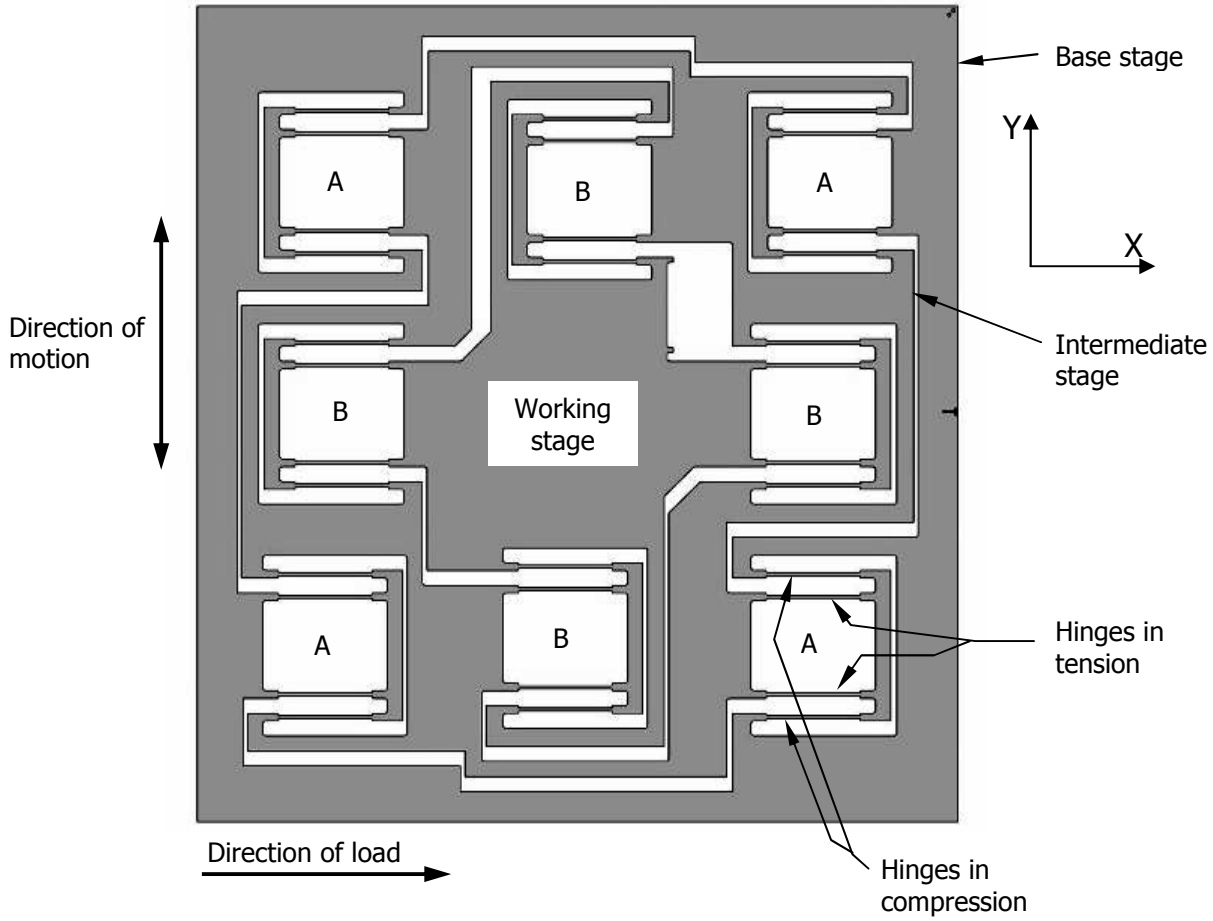

Figure 3.14: Flexure table as a monolithic dual stage single axis configuration

Figure 3.14 is a schematic drawing of a single degree of freedom (1 DoF) monolithic flexure hinge table with a two stage tandem leaf flexure configuration. A prototype was manufactured in the department's workshop using the Wire EDM process to machine it from a single plate of 5083 aluminium alloy. It was recognised that the fatigue life of a machine part manufactured with this process would be severely compromised[95], however in this instance the part served to satisfactorily demonstrate the principles involved in deflecting the working platform.

Proving the design concept was the reason behind having these prototypes machined. Although not ideal, the thicker hinges (nominally 1.00 mm instead of the preferred 0.5 mm thick) caused severe limitations to the range of working platform travel and increased the displacement force substantially. The travel was restricted to ± 2 mm per hinge, giving a total range, without risking plastic deformation, of ± 4.0mm. The double tandem single axis system did give twice the deflection when compared to the two axis system, but appeared to be more susceptible to errant movements (twisting). Some basic linearity tests were performed and due to problems with poor results ensuing from an unsuitable drive configuration were discarded without being reported. Difficulty with the drive mechanisms is known and discussed at a later point. The poor performance issue was not further discussed as it became moot with the decision to change away from a monolithic structure.

It was evident from the constructed monolithic prototype that this concept was functional and delivered the required displacement capability. However, EDM Wire Cut machining was also the manufacturing process used to construct this prototype and as already mentioned is unsuitable as a production process. Therefore, an alternative method of manufacture that embodied this design required consideration. For this reason and the duty cycle of the hinge blades, the simplistic monolithic style of design was given over to a more complex fabricated design.

With the decision to use leaf springs and a fabricated design, the blades' strength was considered with regard to its load carrying capacity in the possible design configurations. The following section presents a general analysis of the flexure blade strength was considered and presented as reader background information.

3.4.2 Flexure Blade Strength

In previous sections, consideration has been given to the bending stress and the minimum length of the hinge design so that it will meet the displacement criteria of the design specification. However, up to this point, the column strength of the flexures has all but been ignored. Table 3.11 gives a summary of assumed geometric values used in subsequent design development by the author. These geometric parameters were selected as they met the physical size constraints outlined in the design specification requirement.

Table 3.11: Flexure hinge geometric parameters

Parameter	Value
Length	~ 30 mm
Width	Nominally 12 mm (yet to be finalised)
Thickness	0.5 – 1.0 mm
Eccentricity	2.5 mm (max)

A typical flexure blade may be analysed as a special case of cantilever beam called a sinking support beam. The sinking support[96] configuration of the flexure hinge is shown in Figure 3.15, which represents a single flexure blade, subjected to the columnar loading that will be discussed in the subsequent sections.

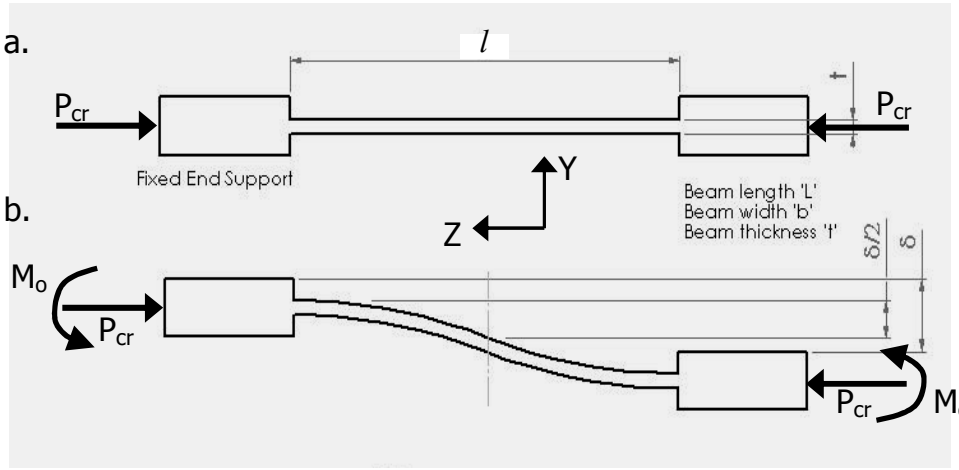

Figure 3.15: Sinking support beam with end loading (a. undeflected, b. deflected)

These loadings are due to the nature of the milling cutter action and machine table movements during manufacture of the pockets. Other major forces will be applied to the hinges, the most significant of these will be the forces induced by the high operational accelerations of the table parallel to the directions of the orthogonal axes. The analysis adopted the Euler and Secant equations and these assessments are

presented below. Based on the parameters in Table 3.11 the critical columnar loads (P_{cr}) of the flexure blades were then determined to enable calculation of the maximum machine table mass.

3.4.3 Column strength analysis

Under normal operational conditions the flexure could adopt one of two forms as shown in Figure 3.15a and b above. The axial load bearing capacity (critical buckling load P_{cr}) of a straight flexure without any eccentricity can be calculated using the well known Euler equation (Equation [16]). This particular arrangement is represented in Figure 3.15a. The beam is capable of carrying a much greater load in this situation than in the one shown in Figure 3.15b.

The general Euler equation is useful only with in-plane axial loading as shown in Figure 3.15a.

$$P_{cr} = \frac{\pi^2 EI}{l_{eff}^2} \qquad [16]$$

where

P_{cr} = the critical buckling load

E = modulus of elasticity

I = 2nd moment of area

l_{eff} = the effective length of the flexure blade

For the straight flexure the effective length, l_{eff}, of the flexure is the working length of the flexure multiplied by a factor calculated to account for the flexure's end fixing conditions (pin jointed or fixed). For the case of the undeflected sinking support beam, the fixed/fixed end conditions were obviously applied. This effectively reduced the working length of the flexure to half its actual length as l_{eff} = beam working length, $l/2$[97]. The Euler equation assumes the flexure is perfectly aligned along the neutral axis, and as such promotes a large load bearing capacity. There were two critical values for a rectangular section: P_{crx}, with the bending as shown in Figure 3.15, and P_{cry}, perpendicular to P_{crx}.

The use of the Euler equation required that nominal geometrical parameters be chosen such that the load bearing capacity of the flexure could be ascertained.

Using the parameters from Table 3.11, the Euler load capacities P_{crx} and P_{cry} for the straight flexure are presented in Table 3.12. The subscripts x and y represent the axes direction in which the buckling loads were calculated.

To aid in the readability of this thesis, the result of the material selection constituent of the design solution is introduced here, to enable a comparison of the loading capability of each of the structures shown in Figure 3.15. The use of titanium alloy as a flexure material (Table 3.12) and the rationale for its selection is described in section 3.5.

Table 3.12: Euler column capacities for a straight flexure

Property	**Value**	**Unit**
Material	Titanium Alloy Ti6Al4V STA	
Modulus of elasticity, E	1.135e11	Pa
Working length, l	30	mm
Thickness, t	0.5	mm
Width, b	12	mm
2nd moment of area, I_x	1.25e-13	m^4
2nd moment of area, I_y	7.2e-11	m^4
Factor of safety, N	1	
Critical load (column) P_{crx}	622.333	N (per hinge)
Critical load (column) P_{cry}	358464.03	N (per hinge)

Note the reduced load capacity, P_{crx}, through the thickness, t of the hinge compared with the load capacity, P_{cry}, through the width, b. However, when the flexure hinge was displaced, as shown in Figure 3.15b, the Euler equation cannot be used to calculate the critical buckling load capacity, as it does not permit out of plane loading. Therefore, an estimate of the reduction in load capability must be determined using the Secant formula.

3.4.4 Eccentrically loaded column analysis

On application of the displacement, the horizontal end load no longer acts along the neutral axis of the beam. For the purposes of quantifying the allowable flexure load capacity the Secant formula,[98] (equation [17]), for eccentrically loaded columns was applied.

$$\sigma_y = \frac{NP}{A}\left[1 + \frac{ce}{r_n^2}\sec\frac{l}{r_n}\sqrt{\frac{NP}{4AE}}\right] \qquad [17]$$

where;

σ_y = yield stress

N = factor of safety

P = allowable load

A = cross sectional area

c = distance from the neutral axis to the outer fibres of the section

e = eccentricity

r_n = radius of gyration

l = working length of the column

E = modulus of elasticity

The radius of gyration is given in equation [18].

$$r_n = \sqrt{\frac{I}{A}} \qquad [18]$$

where

r_n = radius of gyration
I = 2nd moment of area
A = cross sectional area

Using equations [9] and [10] and the material properties for titanium alloy the allowable load P was estimated. The results are presented in Table 3.11. However, the allowable load, which is based on the yield stress σ_y, is difficult to find and the equation must be solved using a solver function in a computer or performed iteratively by a manual means. For the purpose of this exercise, the solution was determined using a spreadsheet and its solver function.

Table 3.13: Eccentrically loaded beam performance – Secant formula results

Property	**Value**	**Units**
Material - Titanium Alloy Ti6Al4V STA		
Modulus of elasticity, E	1.135e11	Pa
Yield strength, σ_y	948e6	Pa
Working length, l	30	mm
Thickness, t	0.5	mm
Width, b	12	mm
2nd moment of area I_x	1.25e-13	m^4
2nd moment of area I_y	7.2e-11	m^4
Area of section, A	0.000006	m^2
Radius of gyration r_{nx}	0.0001443	m
Radius of gyration r_{ny}	0.0034641	m
Distance from neutral axis to outer fibres, c	0.25	mm

Eccentricity, e	2.5	mm
Factor of safety, N	1	
Critical load (column), P_{crx}	80.168	N (per hinge)
Critical load (column), P_{cry}	5385.351	N (per hinge)

From Table 3.13 it can be seen that the critical load is 80.168 N per hinge. However, the design of the flexure table has two such hinges in parallel (shown schematically in Figure 3.16), giving a critical load of approximately 160 N.

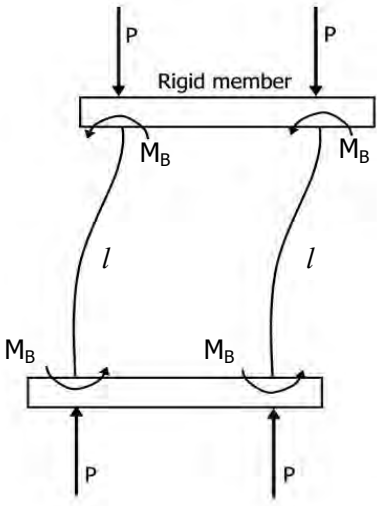

Figure 3.16: Tandem slender columns with lateral displacement

3.4.5 Flexure strength based on a tandem blade configuration

The following method for calculating the maximum load considers the flexures in tandem pairs, whereas the previous two methods analysed a single blade at a time.

Consideration of the tandem slender column arrangement was considered here as it is representative of the configuration of flexure blades found in the proposed concept design solution. Figure 3.16 is a diagram of tandem slender columns supporting a vertical load and shown with lateral displacement. Deutschman, Michels and Wilson[99] offer an equation for use in calculating the loading capability of a pair of slender columns arranged in tandem and in compression such as they are in the proposed flexure arrangement. Equation [19][100] gives a modified Euler equation with which to determine the load, P. It is the same as the previous version of the equation as given in [16], but has the effective length modified to reflect the change in configuration of the columns and their supporting structure.

$$P_{cr} = \frac{\pi^2 EI}{l^2} \quad [19]$$

where;

P_{cr} = critical load

E = modulus of elasticity

I = second moment of area

l = column length

Taking the flexure material and geometric dimensions for the tandem pair arrangement as the same as for the previous single flexure analysis (Table 3.5 and Table 3.6) and using equation [19] to determine the allowable load, the critical load P can be estimated.

Table 3.14 presents the results, which show that the load was calculated at approximately 155 N. This is similar to the Secant formula, which gave approximately 160 N (approximately 80N per column).

Table 3.14: Tandem columns critical load

Property	**Value**	**Unit**
Material	Titanium Alloy Ti6Al4V STA	
Modulus of elasticity, E	1.135e11	Pa
Working length, l	30	mm
Thickness, t	0.5	mm
Width, b	12	mm
2nd moment of area, I_x	1.25e-13	m^4
Critical load (tandem columns) P_{cry}	155.583	N (per hinge pair)

The maximum theoretical load capacity of the deflected struts in compression is shown in Table 3.15. This effect will not be able to be ignored and therefore the axial acceleration forces must be minimised or applied in directions where the magnitude has the least detrimental effect on the blades.

Table 3.15: Critical compression strut load comparison

	P_{cr} Load/flexure [N]	**No. of flexures**	**Total load [N]**
Euler formula (no eccentricity)	622.33	8	4978.6
Secant formula	80.168 (per hinge)	8	641.34
Modified Euler	155.583 (per pair)	4	622.33

For the displaced load configurations, the modified Euler method for the estimated total load was shown to be marginally more conservative than the Secant formula method. Hence, either could be used in estimating the compression performance of the proposed flexure blade configuration.

3.4.6 Alternative loading strategies of the flexures

The use of the secant and Euler formulas gives an approximation of the loading capacity of the blades when an axial load is applied. As shown in Table 3.15 the eccentricity significantly reduces the load carrying capacity of the columns, or in this case, the flexure elements. Further to this effect, the application of these external loads will reduce the stiffness of the flexure system[101]. This reduction is cause for serious concern, as the speed of the machining operation will create significant forces on the flexures due to the expected high acceleration and the resultant loads being carried by each flexure assembly respectively. Figure 3.17[102] shows the loading of the

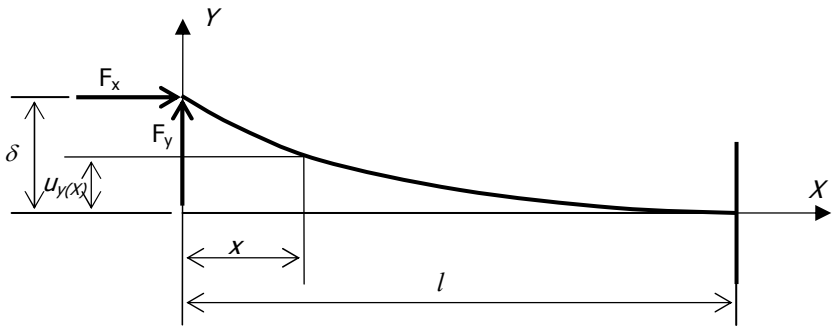

Figure 3.17: Diagram of buckling for a fixed/free column

flexure beams when they are in columnar loaded mode and the reduction of the stiffness due to the eccentricity (δ) of the loading can be seen.

Again referring to Figure 3.17, an alternate design configuring the major loading of the flexure elements in the Z direction (perpendicular to the page) can be conceived. It is possible that this alternate design can only be achieved by reverting to a fabricated or modular flexure assembly (See Figure 3.19).

The use of monolithic designs appears to favour axial loading of the flexures to give compact configurations. Nevertheless, a fabricated design may be oriented to favour the major loading (process cycle forces) through the flexure element in the direction of its width (across the blade, force P in Figure 3.18a). In this loading configuration, axial loading of the flexures would remain due to the mass (working stage, workpiece

fixture and workpiece) carried by the machine table; however, the large forces due to the acceleration of the table to meet the machining process cycle times would be applied only to those axes transverse to the flexure. Axial loading of the flexures due to the machine table and workpiece mass will be significantly less than the forces created by the high acceleration requirements of the machining process cycle. With

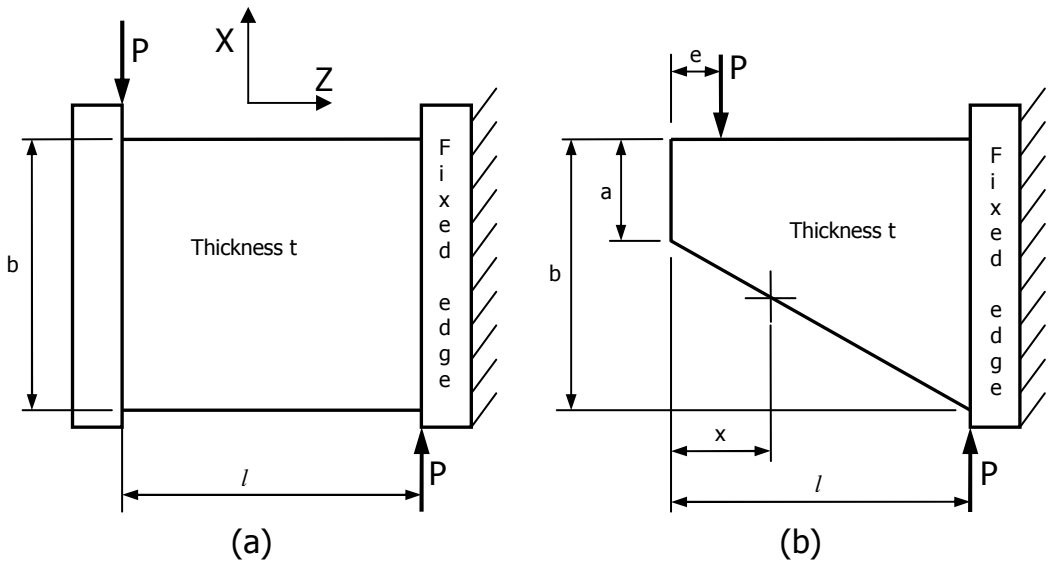

Figure 3.18: (a) Diagram of flexure with shear loading
(b) Typical plate bracket model with shear loading

the loading applied through the width (X direction) of the flexure, (shear), and the notion of local buckling or twisting may become the predominant method of likely failure. The bending stress must also be considered.

The shift from a columnar design in which the major flexure loading is axial, compressive or tensile, to a shear design where the flexure elements are subjected to shear forces gives rise to a new set of design considerations. Figure 3.18b shows a typical plate bracket model (similar configuration to a flexure blade) subjected to shear loading. When the plate length *l*, is relatively long, the plate must be designed to resist bending, shear and local buckling[103]. The short tapered cantilever shown in Figure 3.18b is loaded on its top edge with load, P. A section through the plate at distance x, must be stressed such that the stress varies from tensile to compressive vertically through the section. The maximum bending stress, σ_B, which varies with the taper, can be calculated using equation [20][104].

$$\sigma_B = \frac{6Pl^2(x-e)}{t[al+x(b-a)]^2} \quad [20]$$

where

σ_B = bending stress (N/m^2)

P = applied load (N)

l = working length of the plate (m)

t = plate thickness

b = plate width – maximum (m)

a = plate width – minimum (m)

e = distance of applied load from the free end (m)

x = point at which stress is to be calculated (m)

The highest stress developed in the cantilever at distance x, is found by setting the slope of the beam to zero and solving for x. Therefore, with the boundary condition as given in equation [21], the distance x is given by equation [22] and may be substituted back into equation [20] to determine the maximum stress value.

$$\frac{d\sigma_b}{dx} = 0 \quad [21]$$

$$x = e + \left(e^2 + c\right)^{\frac{1}{2}} \quad [22]$$

where c is a value that relates to the geometry of the supporting system and can be calculated using equation [15] [105].

$$c = \frac{al[2e(b-a)+al]}{(b-a)^2} \quad [23]$$

Figure 3.18a shows the bracket modified from Figure 3.18b by making lengths 'a' and 'b' equal. Figure 3.18a also illustrates the shear loading system as it could be applied to the flexure blades with the load in the X direction. The maximum bending stress, σ_B, was limited to the yield stress, σ_y, a known value.

By rearranging equation [12] for the load, P, the bending force in the X direction was determined, and then compared with the allowable loads for the axially loaded system by substituting σ_y for σ_B. The parameters in Table 3.11 and Table 3.13 were used to calculate the bending load and the results are listed in Table 3.16. This shows that the bending load as applied in Figure 3.18a gives an advantage to the load carrying capacity when compared with the axial capacity, F_z vs. F_x in Figure 3.17.

Table 3.16: Comparison of axial to bending load capability of the fabricated flexure system

	P Load/strut [N]	No. of struts	Total load P [N]
Modified Euler (axial load)	155.583 (per pair)	4	622.33
Bending load	380	8	3040

The proposed design of the complete single system will have eight blades in compression and eight in tension (loaded in the Z direction) at any one time (Figure 3.22). This configuration has the effect that the axial load compressing the blades will reduce the nominal load capacity of the compression struts[106]. By dividing the load carried by the flexures evenly across the eight blades, the reducing effect will be minimised. This solution was considered most favourable as it fulfilled the majority of the design specification requirement.

However, there were still two additional concerns to be considered. What is the effect of the load on the flexure blade when displaced out of plane and secondly, how was the system going to be affected by possible twisting or buckling of the blades? These questions will be addressed in the section 6.4.1, future work.

3.4.7 Fabricated leaf flexure design solution

Having considered the direction and maximum magnitude of the applied loads and the induced stresses, a design solution was established. The proposed design (Figure 3.19 below), offered more scope and variation to any previous design configurations considered. This design, often referred to as 'Jones' springs[107], allowed the blades, to be oriented to each axis such that they were positioned to carry the highest loads in the most advantageous directions. The benefits and shortfalls of the fabricated style of hinge are largely the same as for the monolithic style. However, the unique benefit of the fabricated flexure design is the ability to arrange the flexures in the most gainful way to minimise the adverse effects of the machine and process induced loads.

However, the choice of a fabricated design introduces several issues that required addressing. These issues mainly relate to the manufacture and assembly of the components of the flexures and the compliances of the various components that make up the whole. However, to mitigate this effect the characteristics of the flexure can be changed depending on the direction and type of loading[92].

The switch in the design approach to a fabricated design allowed careful consideration of the machine and process induced loads to be applied to the work platform such that the lightest loads were applied to the blades in the axial (Z) direction. The loads from the process cycle, the acceleration and deceleration forces were applied in directions that were parallel to the leadscrews (Y). This put the forces either parallel or perpendicular to the primary bending direction of the flexure blade, which was in the Y axis direction. At this point in the investigation the influence of the second axis has been ignored, but it is acknowledged that the flexure system will be required to carry the second horizontal table axis to give a full XY configuration.

Figure 3.19b illustrates the direction of the applied acceleration forces, P and F on the fabricated design. The forces generated in the 'F,' or feed direction are controlled by

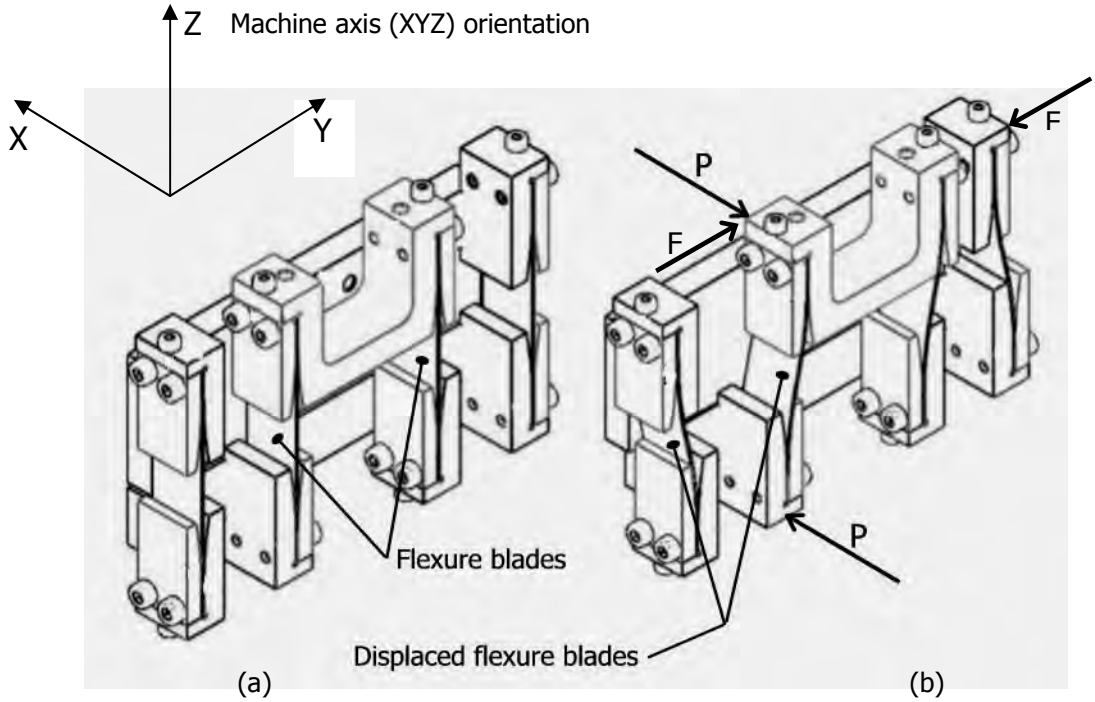

Figure 3.19: Fabricated flexure hinge assemblies, a) neutral, b) displaced

the feed screw and are perpendicular to 'P' and in the same horizontal plane. P induces lateral deflection in the flexure assembly and F produces the desired working deflection as shown in Figure 3.19b.

As the embodiment design shown in Figure 3.19 progressed, the details of the individual components were considered at two levels. That is, how the components interacted with any adjacent parts and the effect of these interactions on the final configuration of the design. Manufacturability of the proposed design was also

considered as a part of the design exercise. One of the critical areas of the fabricated design was the method of connecting the blades to the stages to minimise any of the inevitable manufacturing and unconstrained deflection discrepancies. This connection mechanism, which involved clamping the blades, was of particular interest as it was influenced by the compliances of the component parts making up the specific assembly. In his monograph, Smith discusses the clamping mechanism[108] in some detail, which is summarised in the following paragraph. Smith considers that important features in the assembly are; the clamping blocks, the blades and the upper, mid and lower platforms.

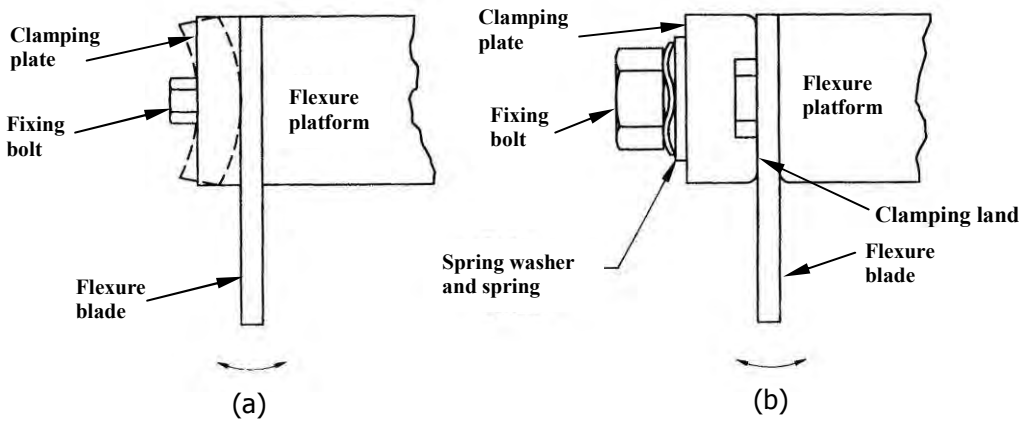

Figure 3.20: Typical clamping arrangements[109]

Figure 3.20[109] presents two sketches typical of a clamp plate assembly. The diagram on the left (a), shows the clamping plate being too thin with an undersized bolt. The interface geometry is also shown as incorrect as the sharp edges give rise to large stress concentrations in the blade element. Figure 3.20b on the other hand is a more acceptable method of clamping the flexure blades as it minimises stress concentrations at the clamping zones. The clamp is shown with a shallow groove recessed into the clamping face, configurations such as this present the clamping force as two lines across the width of the clamp face as opposed to a concentrated zone around the fixing bolt as in Figure 3.20a. The clamp was required to provide the resistance necessary to induce a bending moment into the end of the flexure blade. The clamping force may be resolved into two equal and opposite forces acting at equivalent distances from the fixing bolt's centre. For a given bending moment, the forces will reduce with increasing separation within the practical limits of the design. To ensure that the applied clamping forces are a minimum on the blade, the contact points will ideally be lines at the outer edges of the clamp. This configuration

however, would be unsuitable as it results in large stresses along the contact lines. Therefore, to minimise the stress concentrations, a narrow land is used either side of the bolts.

The clamp screws will also impose a compression stress on the blades as they are tightened; clamps are often tightened to a stress level close to their yield stress to minimise material compliance effects. To minimise this effect, the bearing area of the clamp is required to be larger than the combined cross sectional area of the clamping bolts. The compressive stresses developed by the clamps and the stresses developed in bending must be applied by superposition giving the total stress as the sum of the two[110]. Thus, the overall effect of the clamp/blade assembly stresses, then depend entirely on the compliances of the materials selected for the design and of the size of the components.

Other discussion regarding fabricated parallel and rectilinear movements was published by Jones in 1951[111]. In particular, he stresses the importance of maintaining the parallelism between the working platforms by the clamping system during operation[112]. Jones states, "The performance of the system depends greatly on the

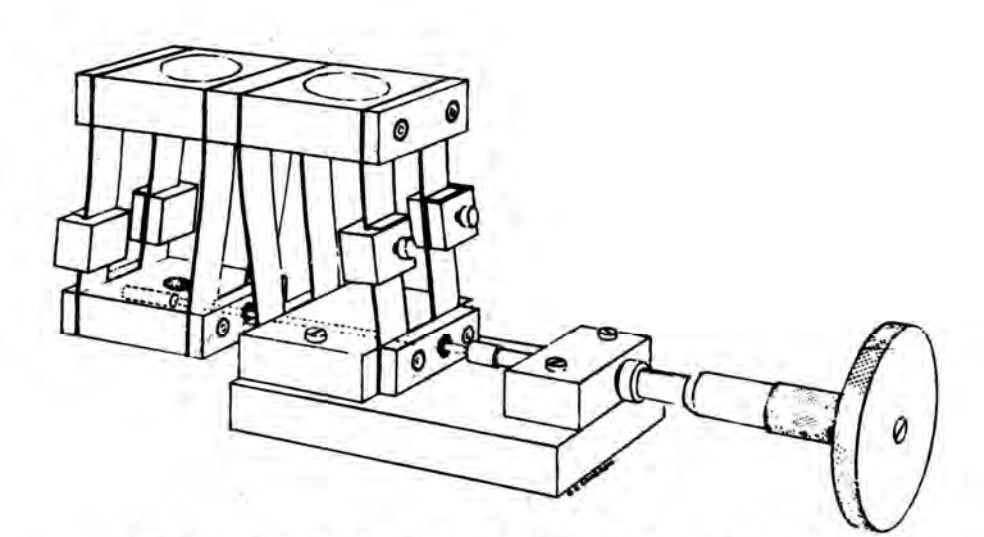

Compound parallel spring movement. Dimensions of specimen tested: spring length between blocks, 42 mm; spring width, 2 × 10 mm, separated by 10 mm; spring thickness, 0.56 mm; block length between springs, 25 mm

Figure 3.21: Compound parallel flexure assembly[114]

design and positioning of the blades relative to each other within the structure. The shear length/deflection strength should be maximised to gain the best performance. This can be done by minimising the thickness compared to the width of the spring. The limits are set by the tendency of the thin springs to buckle or fail to return to their

undeflected shape whilst still supporting the working platform." [113] Figure 3.21[114] presents a typical compound parallel flexure assembly. It shows the separation of the springs to improve stability, both the transverse tilt (roll) and the sideways shift (drift). In practice, when the split springs are used it is better to fabricate them from a single piece and remove the centre portion. This will avoid using separate leaves, which are difficult to uniformly manufacture and install so that they are kept parallel to one another[101].

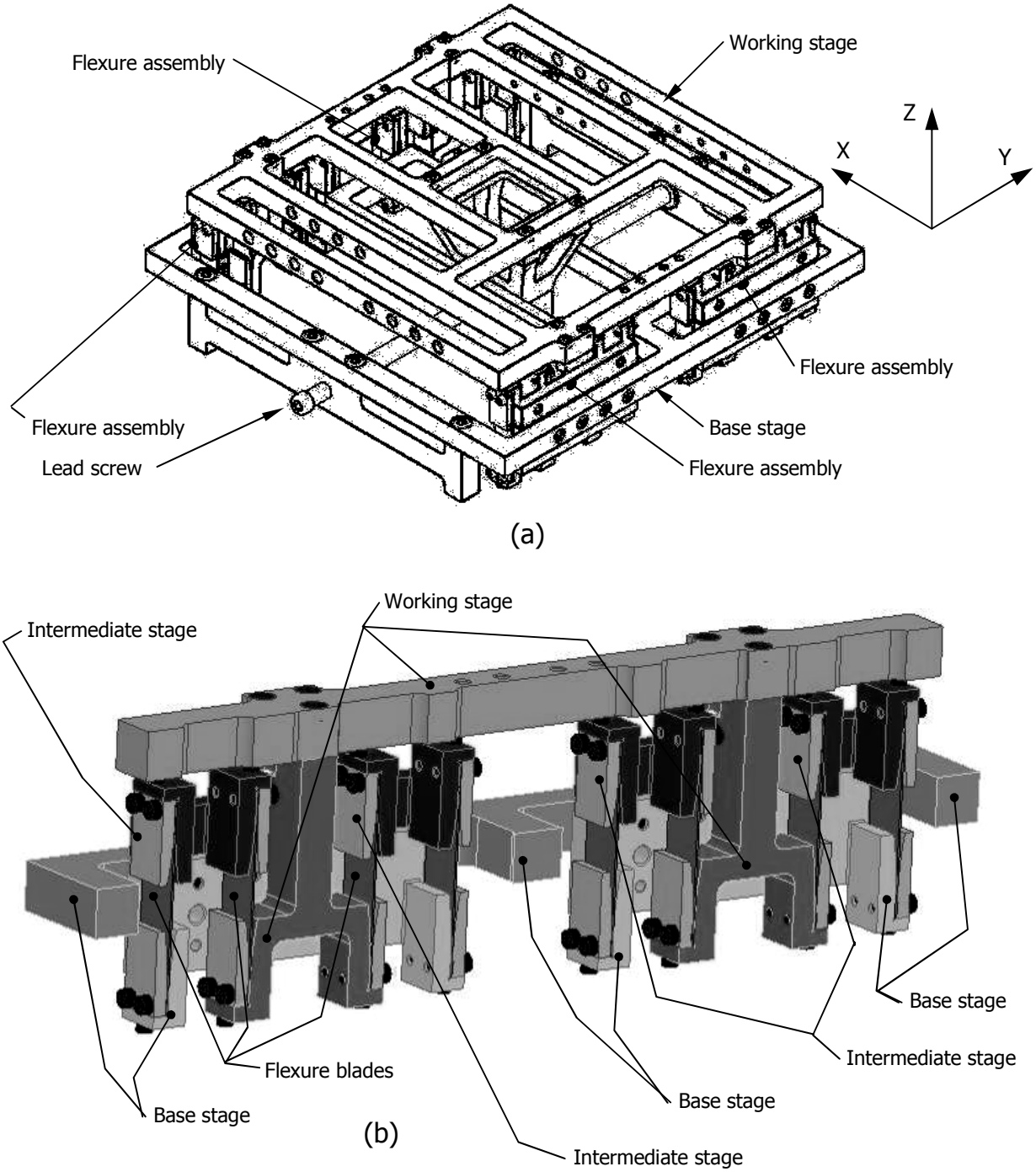

Figure 3.22: Final test design – (a) complete structure, (b) Section through complete structure showing two flexure assemblies in situ

Figure 3.22a presents a final design of a single axis fabricated flexure assembly as manufactured for test purposes. This incorporates the design and system recommendations proposed by Smith and Jones and as discussed in the preceding text.

Figure 3.22b presents a section through the tested flexure table system showing two of the four flexure assemblies used in its construction. The flexure blades are indicated (three only) and allow relative movement in the ±Y direction between the base stage, the intermediate stage and the working stage. Refer to Figure 3.19b for a figure of a typically displaced flexure assembly.

Having established a workable flexural concept and before the expanded embodiment and detailed design could be completed, the correct choice of material from which the flexure blades should be manufactured required consideration. This material consideration was necessary to minimise the physical dimensions of the flexure structure as demanded by the design specification requirements. The following section is a discussion of the process and consideration of the design constraints and factors that lead to a suitable materials selection.

3.5 Materials Selection for the flexure hinges

The design of flexures with a 5 mm deflection in any axis called for a very severe cyclic demand on the material. The original thought with regard to the material was to use a low alloy steel, possibly one of the SAE 5160 steels, heat treated and annealed to produce the required tensile strength and fatigue life. Due to the heat treatment problems foreseen in the manufacture of the blades, other materials were considered and investigated. This was completed using a similar approach to that presented by Gooch[115] in his design of a vertical cantilever vibrating blade. The materials analysis done by Gooch and presented in his work was based on published work by MF Ashby, Materials Selection in Mechanical Design[116]. Ashby's philosophies and methods have been used as a basis for this material search and design optimisation. Design optimisation and flexure performance leading to material selection is discussed in the following sections.

3.5.1 Design optimisation

When determining an optimum design for a mechanical element a study of the relationships between functions is required to determine the performance of the element under study. These functions however, generally consist of a great number of variables. An explicit solution may be complex in its forming due to the large number of variables involved. It is necessary to study not only the variations within an individual function, but the range of variations within several limited functions as determined by the designer. The study of such domains of variation with respect to all feasible designs will produce evidence of the feasible designs, from which an explicit solution can be selected. The problem of optimum design will benefit greatly from an ordered and organised method of solution[117]. To this end, Johnson's Method of Optimum Design is outlined following.

3.5.2 Johnson's method of optimal design

The method of optimal design, as presented by Johnson[118] as a design tool, can greatly facilitate the convergence on an explicit solution to a mechanical design problem. A general method is published, but it is disclaimed as a "cook book" solution, which must be rigidly followed by rote for all specific design problems. In this approach, the basic underlying theoretical concepts must be rigidly adhered to, but the designer is free to apply these concepts as necessary to generate a solution[119]. Optimum design most often requires a complex study of the functional variations and functional relationships contained within the design objective. This approach generally constitutes several very limited functions, each of many variables[120] and these functions generally relate mathematical relationships or numerical values to each other within the problem definition. Perhaps the clearest means of demonstrating this optimising process will be to use the example published by Johnson[121], which has been reproduced below. In this typical example, Q may be the quantity upon which the optimum design is based. In a generalised form, an optimisation problem may be defined by the following parameters. In this case, Q is the optimum design measure and is related to the problem via the following set of equations

$$Q = f_1(u, v, w, x, y, z) \quad [24]$$

$$A = f_2(u, v, w, x, y, z) \quad [25]$$

$$B_1 = f_3(u, v, w, x, y, z) \quad [26]$$

$$u = f_4(M_i) \quad [27]$$

$$v = f_5(M_i) \quad [28]$$

$$A_{max} = f_6(M_i) \quad [29]$$

where i = 1, 2, 3, …, n;

$$A \leq A_{max} \quad [30]$$

$$w \leq w_{max} \quad [31]$$

$$x \geq x_{min} \quad [32]$$

$$y_{min} \leq y \leq y_{max} \quad [33]$$

$$z = z_j \quad [34]$$

where j = 1, 2, 3, ..., m

Equations [24] – [34] above are representative of a possible optimisation problem. The functions shown [24] – [29] designate the specific functions relating to the design issue. A and B_1 represent specific values and the symbols with min or max beside them are the limiting values of the feasible ranges. In Johnson's monograph[122], the letter M designates materials, with the subscript 'i' indicating a specific material from a discrete list. The z term is representative of specific standard available sizes, which is a typical constraint for real design problems.

The equation, which expresses the optimisation quantity, is the most important design equation. The result of this equation, called the primary design equation, (PDE), in this case equation [24], directs the outcome of the optimisation and the direction in which the design will proceed. For any particular mechanical element design, this equation will be determined by the most significant functional requirement or the most significant undesirable effect.

The subsidiary design equations (SDE) are all the equations other than the primary design equation, (in the above example, equations [25] – [29].) These equations express functional requirements or significant undesirable effects, either directly or by implication. It is important not to neglect a subsidiary design equation even if it is only implied. An example would be stress equations, which are often only implied, but never the less are extremely important[123].

Constraints are applied to the optimisation method by simple limit equations (see equations [30] – [34]. These equations express the acceptable range of values mathematically. Constraints may be categorised into one of two types; regional

constraints and discrete value constraints. The regional types are those which express acceptable ranges for a particular set of variables by means of the limit equations. The discrete value constraints are those that are expressed via a list of values for a variable. For example, discrete constraints could be introduced to satisfy a manufacturing size range. All constraints must be considered, and none should be neglected, even those that are constraints by implication to ensure a fully optimised design. Any existence of similar or repeated constraints (eg geometric constraints), must be balanced against each other to ensure all are encompassed in the overall solution. Johnston says that balancing of the constraints is based on the experience of the designer[114].

In summary then, the equation system ([24] – [34]) in the initial formulation includes the optimisation quantity, the subsidiary design equations, and the various types of constraints applicable to the design problem. The equation set will be the first system of equations that relates all the components of the optimisation mathematically. From

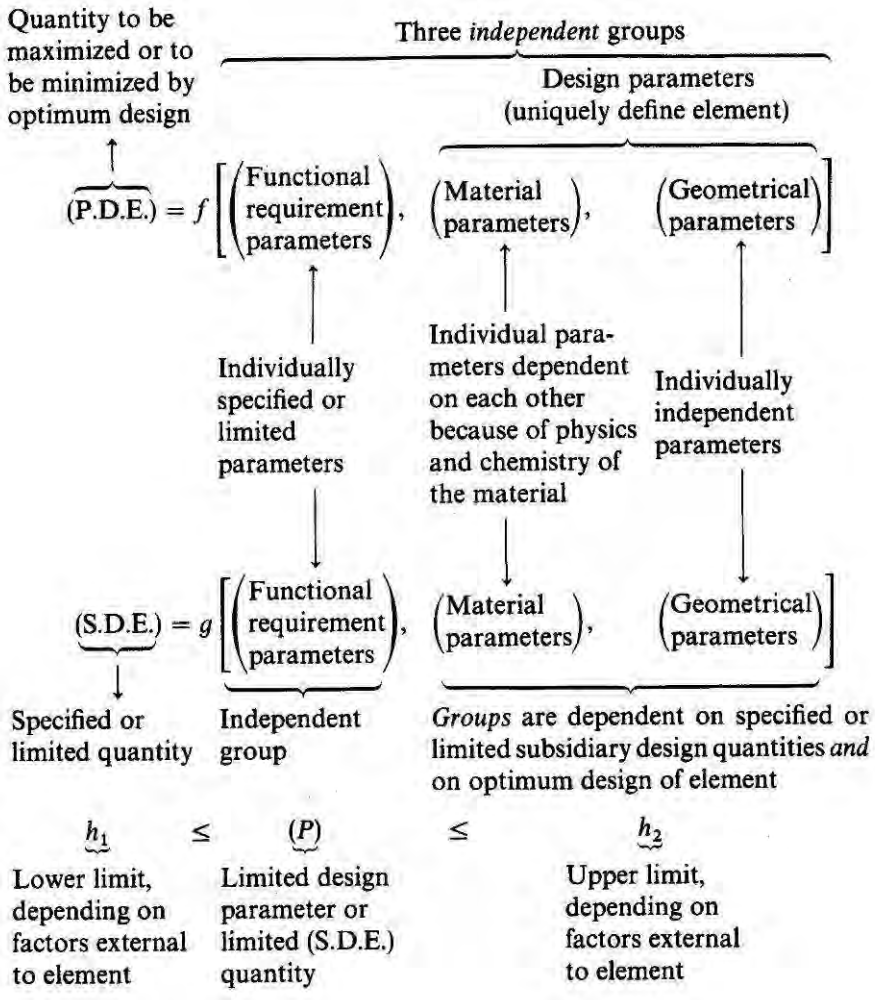

Figure 3.23: Schematic representation of Method of Optimum Design[125]

this system of equations, the judgement of the design engineer must be applied to some extent to determine the significance of each of the formulated equations[124].

The initial formulation should be as simple as possible and should have included only those items that are of definite significance. The inclusion of these items will ensure that the optimisation process will give a solution to the design problem and that this solution has been thoroughly analysed and includes no marginal items. If no marginal items are found in the initial formulation then the optimum design has been found. If any violations of the system were found then reformulation is required to ensure compliance. The reformulation would then allow a new attempt at optimisation.

Figure 3.23[125] is a diagram of the method of optimum design in schematic form. For the case in hand, the range of material possibilities was vast, this method was applied to the design of the flexure element.

The bounds of the compliant hinges were definable in terms of system equations and variables. However, the one major component for consideration within the design specification regime that was not discernibly definable was the manufacturability of the design. This component was defined outside the Method of Optimum Design as it was based on knowledge of machine and manufacturing processes rather than a mathematical basis. This issue is discussed later in Section 3.7. First, the outcome of the optimisation was determined and is reported below.

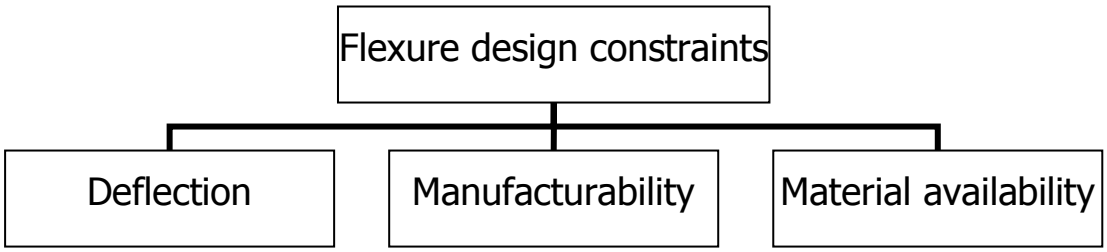

Figure 3.24: Design constraints for the flexures

3.5.3 Optimisation of the flexure hinges

The flexures may be optimised by determining the system variables. Gooch's[126] variables were determined on the basis of the equality and inequality constraints as defined by Johnson[127]. The equality constraints are those that are fixed in terms of the design requirement table. The inequality constraints are those factors that present lower and upper limits within the design[129]. Figure 3.24 presents in diagrammatic form, the constraints that relate to the successful design of flexure hinges.

Using Johnson's definition, a list of the equality and inequality constraints as they relate to the flexure blades is given in Table 3.17.

Table 3.17: The equality and inequality constraints that relate to the design

Equalities (fixed)	**Inequalities** (limits)
Beam deflection (δ)	Bending stress (σ_B)
Manufacturability	Fatigue strength (σ_E)
	Material properties
	Modulus of elasticity [E]
	Yield stress (σ_y)
	Stiffness (l/EI)
	Beam thickness (t) – dependent on thicknesses of available materials
	Beam width (b) accounted for in by 2nd moment of area I
	Strain energy (U_i)

The equalities and inequalities listed here were used in the optimisation of the hinge design, and thus, ultimately defined a suitable material.

3.5.4 Flexure performance indices

The initial step in the design optimisation of the flexure was to determine the variables and constraints that would allow the construction of the various system performance equations. Ashby had taken the notion of Johnson's primary design equation and extended it to give the performance indices[130] as they relate to the object under consideration. Ashby further states that the design or performance, *p*, of a structural element is specified by three things; these are functional requirements, the geometry, and the material properties with which the design must comply. These functional requirements can be described as the performance, p of the element, where

$$p = f\left[\begin{bmatrix} Functional \\ requirments,\ F_i \end{bmatrix}, [Geometry,\ G_i], \begin{bmatrix} Material \\ properties,\ M_i \end{bmatrix}\right] \qquad [35]$$

The performance equation as given in equation [35] shows the material parameter as *M*. The design of the hinge was driven by the equalities and inequalities listed above. Each of the components contained in that list are in turn affected by the particular material and its properties under consideration. From a review of each of the components, the material properties are the dominant parameters that affect the final functional design. It was with this consideration in mind that the research into an

appropriate material concentrated on the material property *M*, which was defined in the context of various performance equations.

The material property was then isolated and used to limit the selection of materials available via the use of the Ashby diagrams[131]. Table 3.18 and Table 3.19 present the equality and inequality constraints for the design in terms of the free variables and the various constraints such that they can be utilised in developing the performance index equations.

Table 3.18: Free variables for a compliant hinge and their influence or effect on the hinge

	Description	**Influence or effect**
t	thickness of hinge	manufactured material property but limited to t < 1.0mm
b	width of the hinge	influences the displacement force
l	length of the hinge	to be minimised
r	bending radius	to be minimised
K_{1c}	fracture toughness	material property
U_i	Energy	stored in bending

The thickness t is constrained to particular values via the available manufactured material thicknesses. Therefore, by adding a physical requirement to keep the value of the thickness, $t \leq 1.00$ mm, the bending stress can be minimised. The bending stress is dependant on the thickness of the hinge. The force P, required to displace the hinge is also dependant on the hinge thickness and is a consideration as it will effect the design and size of the driving leadscrew. The stiffness of the hinge k, is effected not only by the thickness but also by the width. This consideration is accounted for by the inclusion of the 2nd moment of area in the equations.

Table 3.19: Hinge constraints

	Description
δ	Displacement (fixed to give hinge system the required displacement)
$\sigma_B < \sigma_f$	Bending stress less than failure stress
$\sigma_E < \sigma_f$	Endurance stress less than failure stress
$\frac{\sigma_E}{\sigma_B} \Rightarrow$ maximised	Endurance stress/bending stress maximised
P	Displacement force applied to hinge (dependent on displacement specification. hinge section dimensions and material properties
k	Beam stiffness

By using the information contained in the tables above, a method of optimisation was implemented to determine the performance indices and thus gain enough information to establish the most suitable material and geometric properties for the final hinge design.

3.5.5 Optimisation of the flexure design

The optimisation of the flexure was critical to the intended application. The parameters that were significant to the characterisation of the design were the maximum displacement and the maximum bending stress. The displacement was demanded by the design specification whilst the maximum stress was a significant factor in the fatigue life of the mechanism and resulted from the specified maximum deflection requirement.

The range of variation in the parameters that quantify the stress based on the displacement was vast, particularly when a range of materials was included in the consideration. As a beginning to the optimisation process of the flexure design, and based on Buckingham's 'Π' theory, the Π groups formed from the system of equations[132] that described the flexure were minimised. This approach was based on the concept of dimensional analysis as presented by Massey[133].

The notion to use dimensional analysis as a tool for optimisation was inspired by work presented by Gooch[134] in the dimensional scaling of a kinetic sculpture. Consequently, some of the common variables and dimensional processes were incorporated into this work. However, it must be noted that Gooch was looking for scaling factors whereas this work is primarily concerned with material optimisation. The dimensional analysis process being followed is well documented by Massey, [135] but to this authors knowledge has not hitherto been directly applied to the process of material selection. The analysis that follows is an innovative adaptation of this method to materials selection.

This dimensional analysis method though did not yield analytical solutions; it did however show the relevant mathematical connections between the various and germane variables. Also, this process suggested a most effective technique for grouping the system variables[136]. Using this method, the combined results of this analysis allowed the identification of the appropriate material properties, M_i, as a

clearly defined group of parameters that could be isolated from the equations used to describe the flexure[137 138 139].

The variables of interest are given and tabulated below in Table 3.20. These variables were correlated from the well known and robust equations used to describe bending, vibration and energy as they relate to solid mechanics in beams. They are shown in the table and represented by the appropriate combination of mass, M, length, L and time, T.

Table 3.20: Properties concerned with dimensionally optimising the flexures

Item no.	Properties	Equation or Symbol	Dimensional formula		
			[M] (kg)	[L] (m)	[T] (s)
1	length	l		1	
2	width	b		1	
3	thickness	t		1	
4	radius of curvature	r		1	
5	lateral displacement	δ (x/l)		1	
6	mass per unit length	m	1	-1	
7	second moment of area	I		4	
8	elastic modulus	E	1	-1	-2
9	combined variable	EI	1	3	-2
10	displacement force	P	1	1	-2
11	spring constant	k	1		-2
12	bending moment	M_B (x/l)	1	2	-2
13	shear force	V (x/l)	1	1	-2
14	gravitational acceleration	g		1	-2
15	natural frequency	ω			-1
16	bending stress	σ_B	1	-1	-2
17	endurance stress	σ_E	1	-1	-2
18	strain energy	U_i	1	2	-2
19	fracture toughness	K_{1c}	1	$1^{-½}$	-2

As a first step, the items listed in the table were then rendered into near dimensionless terms as follows. Items 1 - 5 in Table 3.20 were divided by l (length) to make them into dimensionless terms. Items 7 & 8 were combined to form a single variable Item 9. Items 6, 14 & 15 were considered irrelevant to this element of the investigation, because their inclusion would add no value to the outcome. Thus, Item 6 was ignored because mass per unit length is not required in the equations describing beam

mechanics and in this instance nor is item 14, gravitational acceleration. Item 15, natural frequency was excluded at this point as it related to the vibration analysis, which is outside the scope of this work. Items 9, 12 - 17 were divided by EI. Item 18 was divided by the displacement force, P and 2nd moment of area, I. Item 19 was divided by endurance stress. The results of the first step are presented in Table 3.21.

Table 3.21: Results from the first step in the dimensional analysis

Item no.	Properties	Equation or Symbol	Dimensional formula		
			[M] (kg)	[L] (m)	[T] (s)
1	length (l)	l/l			
2	width (b)	included in 2nd Moment of area			
3	thickness (t)	t/l			
4	radius of curvature (r)	r(x/l)/l			
5	lateral displacement (δ)	δ (x/l)/l			
9	combined variable	EI/EI			
10	displacement force	P/P			
11	spring constant	kI/P		2	
12	bending moment	M_B (x/l)/EI		-1	
13	shear force	V (x/l)/EI		-2	
14	bending stress	σ_B/EI		-4	
17	endurance stress	σ_E/EI		-4	
18	strain energy	U_i/PI		-3	
19	fracture toughness	K_{1c}/σ_E		½	

A second step was required to further non-dimensionalise the remaining equations. These equations are shown as items 11, 14 - 18 in Table 3.21, which were multiplied through by the appropriate powers of l (length) to give the dimensionless parameters shown in Table 3.22. At this point an additional parameter, Ψ was added into Table 3.22 to denote those equations, items 5, 11, 12 and 14 – 19 that remain relevant to this investigation.

Table 3.22: Results from the second step in the dimensional analysis

Item no.	Properties	Ψ Group	Equation or Symbol	Dimensional formula		
				[M] (kg)	[L] (m)	[T] (s)
1	length		l/l			
2	width		b/l			
3	thickness		t/l			
4	radius of curvature		r(x/l)/l			

5	lateral displacement	Ψ_7	δ (x/l)/l
9	combined variable		EI/EI
11	spring constant	ψ_6	kI/Pl^2
12	bending moment	ψ_1	M_B (x/l)l/EI
13	shear force		V (x/l)l^2/EI
14	bending stress	ψ_2	$\sigma_B l^4/EI$
17	endurance stress	ψ_3	$\sigma_E l^4/EI$
18	strain energy	ψ_4	$U_i l^3/PI$
19	fracture toughness	ψ_5	$K_{1c}/\sigma_E l^{½}$

The developed ψ groups (as opposed to Π groups as designated by Massey[140] and other users of this methodology) presented in Table 3.22 were defined using dimensional analysis of the flexure hinge with the intention of using them to define a suitable flexure element material. By taking each ψ group equation and rearranging it by applying the performance equation [27] method, the various material properties were extracted. The rearranged ψ group equations are presented below, where the variables are defined in the previous tables, 3.5 – 3.9.

$$\psi_1 = \frac{M_B l}{EI} = \frac{l\sigma_B}{yE} \Rightarrow M_0 = \frac{\sigma_B}{E} \qquad \text{(from 12)} \qquad [36]$$

where the bending moment: $M_B = \frac{\sigma_B I}{y}$

and putting $\sigma_B \le \sigma_f$ (from Table 3.19)

gives $M_0 = \frac{\sigma_f}{E}$ [37]

Similarly

$$\psi_2 = \frac{\sigma_B l^4}{EI} \Rightarrow M_1 = \frac{\sigma_B}{E} \le \frac{\sigma_f}{E} \qquad \text{(from 14)} \qquad [38]$$

$$\psi_3 = \frac{\sigma_E l^4}{EI} \Rightarrow M = \frac{\sigma_E}{E} \le \frac{\sigma_f}{E} \therefore M = M_1 = \frac{\sigma_f}{E} \qquad \text{(from 17)} \qquad [39]$$

$$\psi_4 = \frac{U_i l^3}{PI} = \left(\frac{M^2 l}{2EI}\right)\left(\frac{l^3}{PI}\right) = \left(\frac{\sigma_f^2 I^2}{y^2}\right)\left(\frac{l}{2EI}\right)\left(\frac{l^3}{PI}\right) = \left(\frac{\sigma_f^2 l^4}{2y^2 PE}\right) \qquad \text{(from 18)}$$

$$\Rightarrow \psi_4 = \frac{1}{2P}\frac{l^4}{y^2}\frac{\sigma_f^2}{E} \qquad \therefore M_2 = \frac{\sigma_f^2}{E} \qquad [40]$$

$$\psi_5 = \frac{K_{1c}}{\sigma_E l^{\frac{1}{2}}} = \frac{1}{l^{\frac{1}{2}}}\frac{K_{1c}}{\sigma_E} \quad \therefore M_3 = \frac{K_{1c}}{\sigma_E} \qquad \text{(from 19)} \qquad [41]$$

$$\psi_6 = \frac{kI}{Pl^2} = \left(\frac{l^3}{EI}\right)\left(\frac{I}{Pl^2}\right) \Rightarrow \psi_6 = \frac{1}{P} l \frac{1}{E} \qquad \text{(from 11)} \qquad [42]$$

$$\therefore M_4 = \frac{1}{E}$$

$$\psi_7 = \frac{\delta}{l} \qquad [43]$$

Substituting $\delta = Pl^3/12EI$ into equation [43] gives

$$\psi_7 = \frac{\delta}{l} = \frac{Pl^2}{12EI} \qquad \text{(from 5)} \qquad [44]$$

Substituting the bending moment equation into equation [44] and rearranging gives

$$\psi_7 = l^2 = \frac{6\delta E y}{\sigma_f} = 6\delta y \frac{E}{\sigma_f}$$

$$l = \sqrt{(6\delta y)}\left(\frac{E}{\sigma_f}\right)^{\frac{1}{2}} \quad \therefore M_5 = \frac{E^{\frac{1}{2}}}{\sigma_f{}^{\frac{1}{2}}} \qquad [45]$$

The material parameters M_i, have now been isolated and extracted from the performance equations using the new methodology presented above. As can be seen by inspection, $M_0 = M_1$, giving the five material parameters presented below (Table 3.23). Although M_5 and M_1 are also equal, the M_5 parameter is derived from the displacement approach, whereas M_1 was derived from the bending equations. There is little apparent gain to be had from the M_5 parameter being included at this point. However, as maximum displacement capability is a highly sought after property, M_5 is retained and presented here to be used later to optimise the minimum blade length for a suitable material.

Table 3.23: Flexure hinge material parameter equations and line slope values

Material parameter	Equation	Line slope value	Comment
M_1	σ_f/E	1	Largest value most suitable
M_2	σ^2_f/E	0.5	Smallest value most suitable
M_3	K_{1c}/σ_E	1	Smallest value most suitable
M_4	$1/E$	1	Largest value most suitable
M_5	$\sigma_f^{1/2}/E^{1/2}$	1	Largest value most suitable

These material parameters may be plotted as lines on the log/log axes in an Ashby diagram to assist in the selection of appropriate materials. The lines of various slopes (see Table 3.23) were plotted on Ashby diagrams at positions where they eliminated materials that were unsuitable. However, due to the number of materials included in the selection diagram this method only gives a broad indication of those materials that are suitable, those along the slope lines where they intersect with the material bubbles.

Where the largest values are required those materials above the line are considered suitable and similarly where the minimum value is required those below the line are retained. Table 3.23 presents the relationship between the material parameters and their variables as they relate to one another on a log/log graph, e.g., in the case of M_2 the relationship creates a line with a slope of 0.5. The application and results of using these line slope values on an Ashby diagram is shown (Figure 3.28 - Figure 3.31) and discussed in the section regarding quantifying the material parameters.

The line slope values given in Table 3.23 are presented here to give conclusion to the results obtained from the dimensional analysis process. The next section confirms the results of this method by calculating the same parameters by a more traditional method.

3.5.6 Confirmation of the dimensional analysis approach

The metallic flexure hinge is based on the notion of remaining within the elastic limit of the hinge material and as such, Hooke's law must be maintained. Equation [46] gives Hooke's law.

$$\sigma = \varepsilon E \qquad [46]$$

where

σ = stress (N/m^2)
ε = strain
E = elastic modulus (N/m^2)

The compliant hinge, shown in Figure 3.25, is elastic and, as such, the bending stresses σ_B must stay at a level below the elastic limit and the modulus of rupture or failure stress σ_f. When the hinge is subjected to frequent reversals of stress then a further consideration must also be made. That is, the endurance stress σ_E, as it becomes a significant factor in determining the life of the hinge[141]. When considering

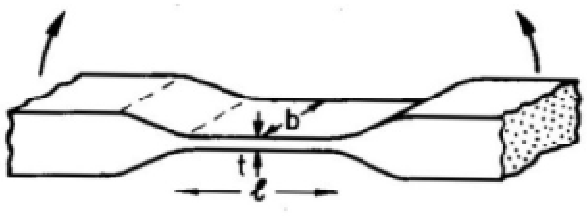

Figure 3.25: Diagram of compliant hinge

the stress induced into the hinge due to its design function, the hinge must meet the design specification in terms of its displacement or angle of rotation due to bending. In achieving this requirement, the radius of curvature, the working length and the displacement δ, must all be considered closely.

Of these parameters, the radius of curvature is perhaps the most crucial. The radius of curvature is the property that relates the hinge length to the displacement via the material properties. For example, a stiff rigid material will require a significantly longer beam to achieve a specific displacement than will a soft pliable one.

In the context of verifying the dimensional analysis method of material selection above, the radius of curvature was investigated first.

- Radius of curvature

Equation [47], the general bending equation gives the relationships between the various parameters of a beam in pure bending as they relate to each other[142].

$$\frac{\sigma_B}{c} = \frac{M_B}{I} = \frac{E}{r} \qquad [47]$$

where
σ_B = bending stress (N/m^2)
c = distance from neutral axis to outer fibres (m)
M_B = bending moment (Nm)
I = 2nd moment of area (m^4)
E = modulus of elasticity (N/m^2)
r = radius of curvature (m)
As the strain, ε is then:

$$\varepsilon = \frac{c}{r} \qquad [48]$$

By considering equation [48] and rearranging equation [47], the bending stress in terms of the beam depth or hinge thickness and the radius of curvature can be derived.

$$\sigma_B = \frac{Ec}{r} \quad [49]$$

where the variables are shown above for equation [47].

The distance from the hinge's neutral axis to its outer fibres, c, can be equated to the hinge thickness (t) by equation [50]

$$t = 2c \quad [50]$$

Thus giving the maximum bending stress, σ_B in the hinge as[143]

$$\sigma_B = \frac{Et}{2r} \quad [51]$$

To ensure the hinge will not rupture due to stress

$$\sigma_B \leq \sigma_f \quad [52]$$

where

σ_f = failure stress or modulus of rupture (N/m^2).

Substituting [51] into [52] and rearrange the result gives:

$$r \leq \frac{t}{2}\frac{E}{\sigma_f} \quad [53]$$

Consideration of equation [53] in terms of the optimisation schema shown in Figure 3.23 and grouping the terms into the three factors gives a materials parameter of:

$$M_1 = \frac{E}{\sigma_f} \quad [54]$$

where

M_1 = material parameter.

This material parameter will give the smallest radius of curvature for the smallest value of index M_1. Alternatively, expressing $M_1 = \sigma_f/E$ would give the smallest radius of curvature for the largest value of the index, M_1.

The above set of equations [46] to [54] give a materials parameter in relation to the radius of curvature in terms of the fatigue life. However, the length of the hinge requires consideration and this will be investigated in the strain energy calculations.

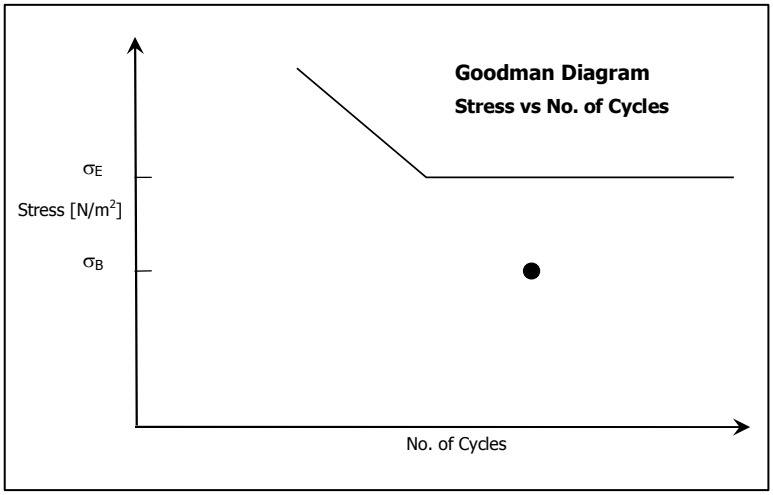

Figure 3.26: Goodman Schematic Diagram for a typical ferrous material

Figure 3.26 illustrates the Goodman diagram for a typical curve for a ferrous material. The Goodman diagram shows the relative position of the bending stress and the endurance limit on the y-axis. For a typical ferrous material, the stress at which the component may fail will 'flatten' off in relation to the number of cycles it may well endure: the endurance limit σ_E. Beyond this point, the number of stress cycles the component can endure becomes infinite.

The specification of the hinge requires that it be of compact design, therefore the optimisation process calls for a material that has material properties that will maximise σ_E/σ_B. Substituting equation [51] into σ_E/σ_B gives:

$$\frac{\sigma_E}{\sigma_B} = \frac{2\sigma_E r}{Et} = 2r\frac{1}{t}\frac{\sigma_E}{E} \qquad [55]$$

By putting $\sigma_E \leq \sigma_f$, where σ_f = the modulus of rupture[144], the material parameter from equation [55] becomes

$$M_1 = \frac{\sigma_f}{E} \qquad [56]$$

Therefore, the material with the greatest index M_1 will give the greatest fatigue life for the hinge. This is a similar ratio to that found for the hinge radius of curvature and it follows that the material that will give the minimum radius of curvature will also give the maximum fatigue life.

- Strain energy

The elastic strain energy due to bending is a second consideration for use to define a material parameter. The strain energy is to be related to the stress if it is to be used to define the material parameter, M_2.

$$\sigma_B = \frac{-M_B c}{I} \quad [57]$$

where

M_B = Bending moment (Nm)

c = distance from neutral axis to outer fibres (m)

I = 2nd Moment of area (m^4)

and

$$U_i = \frac{M_B^2 l}{2EI} \quad [58]$$

where

U_i = strain energy

l = length of beam (m)

E = modulus of elasticity (N/m^2)

The equation relating strain energy to stress is given in equation [59][145]

$$U_i = M_B{}^2\left[\frac{l}{2EI}\right] = \left(\frac{\sigma_B I}{c}\right)^2\left(\frac{l}{2EI}\right) = \frac{\sigma_B^2 I^2 l}{2c^2 IE} \quad [59]$$

$$\Rightarrow U_i = \frac{\sigma_B^2 Il}{2c^2 E} \quad [60]$$

where

U_i = strain energy for a constant bending moment

but

$$I = \frac{bt^3}{12} \quad [61]$$

and

$$c = \frac{t}{2} \quad [62]$$

Combining equations [52], [61] and [62], and substituting into equation [60] gives:

$$U_i = \frac{2bl\sigma_f^2}{tE} = \left[\frac{2bl}{t}\right]\left[\frac{\sigma_f^2}{E}\right] \quad [63]$$

Now again by separating the resulting equation [63] into the material, functional and geometric parameters, the material parameter, M_2, can be isolated:

$$M_2 = \frac{\sigma_f^2}{E} \quad [64]$$

Where

M_2 = material parameter

Thus, the material that will store the greatest quantity of energy and therefore be the most suitable material for springs will be that which has the greatest value for M_2.

- Fracture Toughness

A third material parameter M_3, can be determined from the fracture toughness of the material, though in this particular case the process to determine the appropriate ratio is not markedly different from the dimensional analysis method. The stress at which crack propagation is expected of occur is given by equation [65][146]:

$$\sigma = \frac{K_{1c}}{\sqrt{\pi a}} \qquad [65]$$

where

K_{1c} = material toughness value (MPa –$m^{1/2}$)

a = half the crack length (m)

σ = yield stress (N/m^2)

By substituting the modulus of rupture σ_f, into equation [65] and rearranging, the material parameter may be determined as presented in equation [66]:

$$\begin{aligned} (\pi a)^{\frac{1}{2}} &= \frac{K_{1c}}{\sigma_f} \\ \therefore M_3 &= \frac{K_{1c}}{\sigma_f} \end{aligned} \qquad [66]$$

The parameter M_3 will give the best material for the smallest value of the ratio K_{1c}/σ_f.

- Deflection of the beam

The shape and function of the flexure hinge can be described as a sinking support beam. Figure 3.27 presents a diagram of the notion of the sinking beam. This simplified sketch shows the load P, applied to the right hand end, which is supported in such a way as to have a moment M_o, generated at the sinking end as well as the supported end - Figure 3.27b. As such, the beam may be treated as a double ended cantilever and may be analysed as a single cantilever beam divided at mid span as shown in Figure 3.27c. where the working length is $l/2$. A set of equations describing the bending and deflection of the beam were developed in terms of l and δ, the

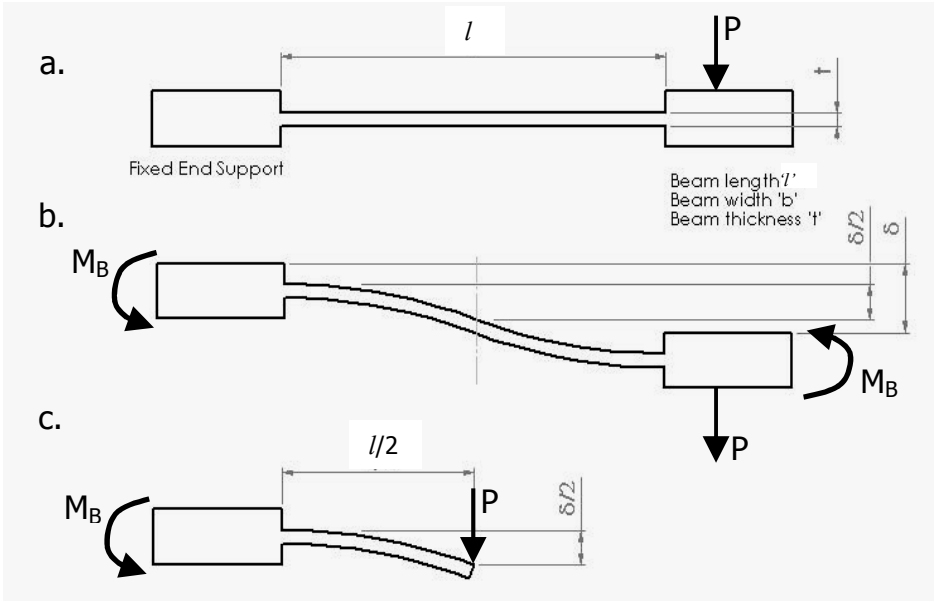

Figure 3.27: Sinking support beam (a. undeflected, b. deflected, c. symmetry of the system shown)

deflection, for the full working length of the beam rather than for just half of it as shown in Figure 3.27c.

The deflection equation for the beam in bending with a sinking support is given by [67][147]:

$$\delta = \frac{Pl^3}{12EI} \qquad [67]$$

where;
δ = displacement of the beam endpoint (m)
P = applied load at the sinking support (N)
l = beam length (m)
E = modulus of elasticity (N/m^2)
I = 2nd moment of area (m^4)
The reaction or end fixing moment at the ends of the beam is given in equation [68]:

$$M_B = \frac{Pl}{2} \qquad [68]$$

where;
M_B = end fixing moment
l = beam length
P = applied load
Substituting [68] into [67] gives:

$$\delta = \left(\frac{Pl}{2}\right)\left(\frac{l^2}{6EI}\right) = \frac{M_B l^2}{6EI} \qquad [69]$$

Rearrange equation [57] and substitute into [69] gives:

$$\delta = \left(\frac{\sigma_f I}{c}\right)\left(\frac{l^2}{6EI}\right) = \frac{\sigma_f l^2}{6Ec} \qquad [70]$$

Rearrange equation [50] and substitute into [70] to find δ in terms of the failure strength or modulus of rupture, σ_f[148]:

$$\delta = \frac{\sigma_f l^2}{3tE} \qquad [71]$$

Finally rearrange equation [71] to give a working beam length, l:

$$l = \sqrt{\left(\frac{3\delta tE}{\sigma_f}\right)} \qquad [72]$$

Equation [72] may be solved easily as all the parameters it contains are identifiable from the material or physical properties of the hinge, which in turn are defined by the design specification. A fifth material parameter M_5 may be defined from equation [72] also. This equation can be separated to give the geometrical and material parameters as before. This is presented in equation [73] from which M_5 can be extracted and is shown in equation [74]:

$$l = (3\delta t)^{\frac{1}{2}}\left(\frac{E}{\sigma_f}\right)^{\frac{1}{2}} \qquad [73]$$

$$M_5 = \left(\frac{E}{\sigma_f}\right)^{\frac{1}{2}} \qquad [74]$$

The fourth material parameter also comes from the deflection equation, equation [67]. By rearranging the equation and grouping the components accordingly, M_4 may be established as shown in equation [75]:

$$\delta = \frac{P}{12}\frac{l^3}{I}\frac{1}{E} \Rightarrow M_4 = \frac{1}{E} \qquad [75]$$

Table 3.24 presents a comparison of the result from the derivation of the material parameters from the dimensional analysis as compared to those derived using the confirmation analysis. Inspection of the table shows confirmation of the results from each method. Once again $M_0 = M_1$ giving five material parameters, M_5 is included for the reasons previous stated.

Table 3.24: Comparison of material parameters

Material parameter	Result (Dimensional analysis)	Result (Confirmation analysis)	Design guide line slope value[149]
M_1	σ_f/E	σ_f/E	1
M_2	σ_f^2/E	σ_f^2/E	½
M_3	K_{1c}/σ_E	K_{1c}/σ_f	1
M_4	$1/E$	$1/E$	Not applicable
M_5	$E^{1/2}/\sigma_f^{1/2}$	$E^{1/2}/\sigma_f^{1/2}$	1

The line slope value has been presented in the table and will be applied to the Ashby diagrams presented in Figure 3.28 – Figure 3.31.

3.5.7 Quantifying the material parameters

Table 3.25 presents a list of materials that are traditionally considered as suitable for spring materials and as such are rated against their associated σ_f^2/E value. Ashby's comments have been included to briefly describes each material.

Table 3.25: Comparison of traditional spring materials for efficient springs of low volume[150]

Material	σ_f^2/E	Comment
Spring steel	15-25	The traditional choice: easily formed and heat treated
Titanium alloys	15-20	Expensive, corrosion resistant
Carbon fibre reinforced plastic (CFRP)	15-20	Comparable in performance with steel, expensive
Glass fibre reinforced plastic	10-12	Almost as good as CFRP and less expensive
Glass fibre	30-60	Brittle in tension, but excellent if protected against damage, very low loss factor
Nylon	1.5-2.5	The least usable, cheap easily shaped, but high loss factor
Rubber	20-60	Better than steel but high loss factor

Table 3.20 gives some basic material properties considered important for flexural components[151]. The flexure hinge can be described as a type of low energy spring, and the traditional requirements of a spring are similar to those required for an efficient flexural hinge. Therefore, a material with a low hysteresis was sought. As an example, the greatest values of M_1 and M_5 will give the material for shortest beam working length with the greatest flexibility.

Table 3.26: Important properties of flexures relating to the project[152]

Application requirement	Desired material property
Small size	High max permissible stress equal to yield stress unless fatigue is of concern then max stress = fatigue strength
Maximum movement for a given size	High max permissible stress/Young's modulus
Minimum stiffness	High inverse Young's modulus value ($1/E$)

Gaining an understanding of the properties that affected the hinges was an important part of designing the hinges to meet their specific requirements. Also, the establishment of the material properties that defined the most suitable material was essential. The choice of material ultimately affects the flexures dimensional parameters and thus the overall size of the components. An appropriate material that is practicable to meet the design specification will have the most flexibility, bend with the shortest radius of curvature, and have the shortest length. Once an appropriate material selection was made, the choice of overall dimensions could be defined: this includes the working length, thickness, and width.

The first step in the selection process was however to use the material parameters to isolate a set of suitable materials.

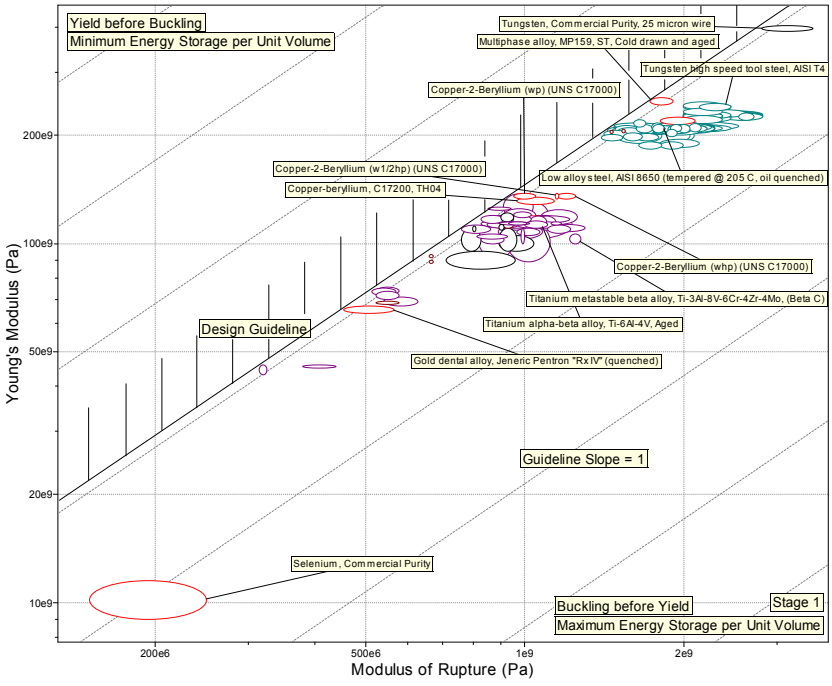

Figure 3.28: First step, eliminating unsuitable materials from above the design guide line.

The ratios, M_1, M_2, M_3 and M_5 were plotted as design guidelines on the Ashby diagrams[153] (Figure 3.28 – Figure 3.31) using the CES Materials Selector v4.5[154]. It is worth noting here that the parameter M_4 has no particular importance when plotting the Ashby diagrams. Therefore, as stated in Table 3.24, it has no application in this particular materials selection process.

Table 3.26 shows that a material suitable for a high performance flexure represents the minimum stiffness value of a material where the value $1/E$ would maximised. It was therefore only used as a further parameter once a list of possible candidates had been selected. The use of the Ashby diagrams procedure was an iterative process that was commenced by placing the design guidelines to select materials that were known to be suitable materials for springs.

Please note that polymeric materials have been discounted due to known various unsuitable characteristics (eg creep) thus reducing the set of suitable materials to metals only. The material parameters, M_i, were represented in the Ashby diagrams with design guidelines of appropriate slopes as shown in Figures 3.26 – 3.29.

These figures show the material selection steps from the CES Materials Selector v4.5[155]. There were six steps using the M_i material parameters developed earlier in

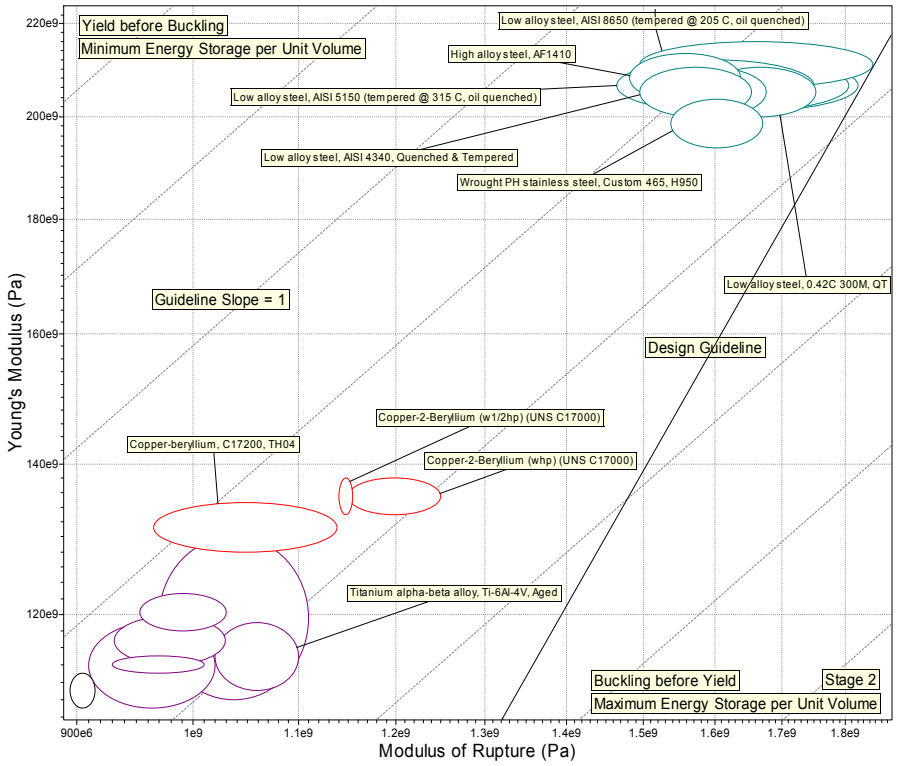

Figure 3.29: Second step, eliminated unsuitable materials from below the design guide line.

this section. (Only the steps with significant observable change are presented.)

Figure 3.28 shows the first step using the Modulus of Rupture/Modulus of Elasticity, $M_1 = \sigma_f/E$, as the axis with a line slope = 1. The selection was set so only those materials with the complete bubble below the design guide line were accepted and the line positioned to ensure materials of known spring suitability were included. This reduced the number of materials from 1842 listed materials to approximately 150.

Figure 3.29 presents the second step of selection using M_2 as the selection parameter. This step was set to select materials that were above the design guide line. Additionally, the window was 'zoomed' to focus on the materials being investigated and to remove the extreme ends of the range selected in Figure 3.28. For example, the materials at the extreme ends were tungsten at the upper end and selenium and gold at the lower end. These materials were considered too exotic for use in the flexure blades. The total number of materials that passed this step was 1755 from the 1842 materials available. The software allows an intersection collection of the first step with the second step selections, which further eliminated the choices to less than 150.

The third and fourth steps showed very little change in the number of selected materials and as such, the figures have been omitted. The axes scales remained the

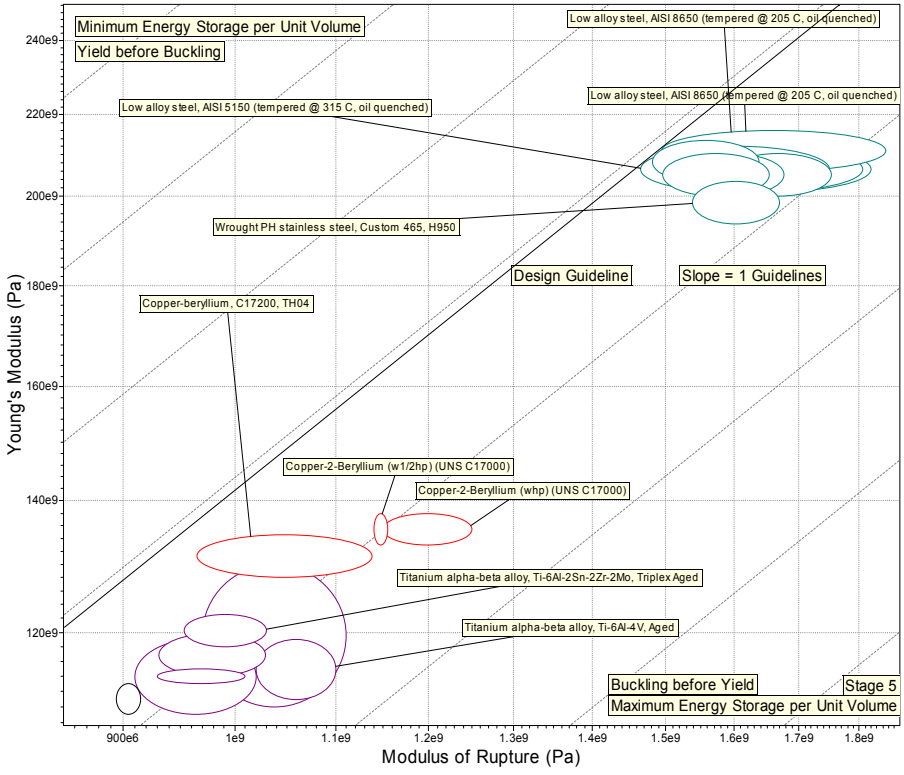

Figure 3.30: Fifth step of selection

same for the second to fifth iterations with only the design guidelines being added and positioned to achieve the greatest reduction effect.

Figure 3.30 represents the fifth step, which is a selection group again based on the elastic modulus E and plotted against the modulus of rupture σ_f. The plotted design guideline line slope was 1, and positioned and set once again to remove materials above it. The presented result was achieved by positioning the design guideline at a point where the material bubbles below were considered suitable candidates.

Figure 3.31 shows step six, the final selection of suitable possibilities. The axes of the charts were changed at this step to represent fracture toughness, K_{1c}, on the vertical axis and endurance stress, σ_E, along the horizontal axis. Recall that in equation [47]

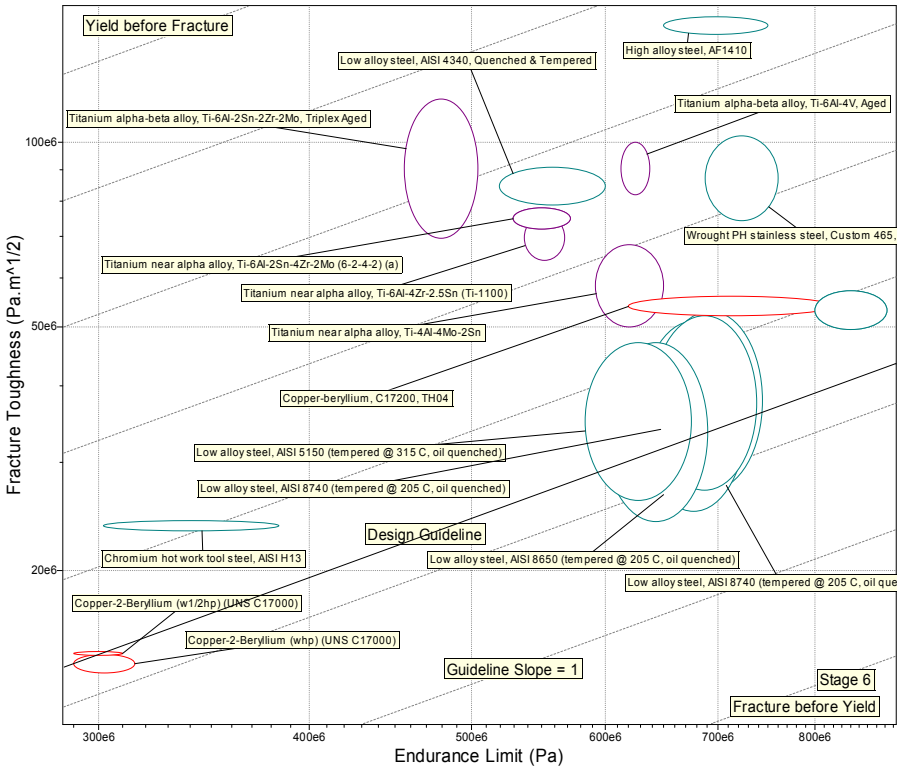

Figure 3.31: Sixth step of selection

the substitution $\sigma_E \leq \sigma_f$ was made. Following trials with both the rupture stress and the endurance stress applied to the horizontal axis, the endurance stress was chosen as it presented a more definitive result.

The materials remaining at the conclusion of step six numbered twenty one. This number of material options was considered a manageable result, and should have

Table 3.27: Final selection of suitable flexure materials

	Material Description	Young's Modulus	Rupture Modulus	Endurance Limit	Fracture Toughness	M_1	$1/M_2$	$1/M_3$	M_4	M_5	Sum of M_i values
		E GPa	σ_f MPa	σ_E MPa	K_{1c} MPa.m$^{1/2}$	σ_f/E	E/σ_f^2	σ_E/K_{1c}	1/E	$\sigma_\phi^{1/2}/E^{1/2}$	ΣM_i
	Value most relevant to analysis					High	High	High	High	High	High
1	Copper-18% Niobium Composite (wire)	111	905	447.5	19	0.88	0.03	***1.00***	0.65	0.94	***3.50***
2	Copper-2-Beryllium (whp) (UNS C17000)	135.5	1200	302.5	*14.1*	0.96	0.02	0.91	0.53	0.98	3.40
3	Copper-2-Beryllium (w1/2hp) (UNS C17000)	135.5	1147.5	300	14.65	0.92	0.02	0.87	0.53	0.96	3.30
4	Titanium near alpha alloy, Ti-4Al-4Mo-2Sn	120	1040	621	59	0.94	0.02	0.45	0.60	0.97	2.98
5	Copper-beryllium, C17200, TH04	131.3	1051.5	720	54	0.87	0.03	0.57	0.55	0.93	2.94
6	**Titanium alpha-beta alloy, Ti-6Al-4V, Aged**	115	1060	625.5	91	***1.00***	0.02	0.29	0.62	***1.00***	2.94
7	Low alloy steel, AISI 8740 (tempered @ 205 C, oil quenched)	206.5	1655	694.5	40	0.87	0.02	0.74	0.35	0.93	2.90
8	Low alloy steel, AISI 8650 (tempered @ 205 C, oil quenched)	211	***1670***	679	38	0.86	0.02	0.76	0.34	0.93	2.90
9	Low alloy steel, AISI 86B45 (tempered @ 205 C, oil quenched)	206.5	1645	689.5	39.5	0.86	0.02	0.74	0.35	0.93	2.90
10	Titanium near alpha alloy, Ti-6Al-4Zr-2.5Sn (Ti-1100)	114	970	552.5	70	0.92	0.03	0.34	0.63	0.96	2.88
11	Titanium alpha-beta alloy, Ti-6Al-4V, STA	113.5	984.5	625.5	91	0.94	0.03	0.29	0.63	0.97	2.86
12	Low alloy steel, AISI 5150 (tempered @ 315 C, oil quenched)	206.5	1607.5	629.5	36.5	0.84	0.02	0.73	0.35	0.92	2.86
13	Low alloy steel, 0.42C 300M, QT	205.15	1669.5	***841.15***	53.295	0.88	**0.02**	0.67	0.35	0.94	2.86
14	Titanium near alpha alloy, Ti-6Al-2Sn-4Zr-2Mo (6-2-4-2) (a)	114	965	550.5	75	0.92	0.03	0.31	0.63	0.96	2.84
15	Titanium alpha alloy, Ti-6Al-2Sn-4Zr-2Mo, Triplex annealed	116.9	980	550.5	75	0.91	0.03	0.31	0.61	0.95	2.82
16	Low alloy steel, 0.40C 300M, QT	205.15	1597	***841.15***	53.295	0.84	0.02	0.67	0.35	0.92	2.80
17	Chromium hot work tool steel, AISI H13	***216***	1650	343	23.65	0.83	0.02	0.62	**0.33**	0.91	2.70
18	Titanium alpha-beta alloy, Ti-6Al-2Sn-2Zr-2Mo, Triplex Aged	120.3	991.5	480	93.575	0.89	0.03	0.22	0.60	0.95	2.68
19	Wrought PH stainless steel, Custom 465, H950	198.55	1604	723.95	88.435	0.88	0.02	0.35	0.36	0.94	2.54
20	Wrought aluminium alloy, 5083, H343	*71.79*	283.15	*111.8*	32	0.43	0.02	0.15	***1.00***	0.65	2.43
21	Unalloyed titanium Grade 1	102.5	*150*	199.5	57.5	**0.16**	***1.00***	**0.15**	0.70	**0.40**	*2.40*
22	Low alloy steel, AISI 4340, Quenched & Tempered	205.15	1574.5	559.5	85	0.83	0.02	0.28	0.35	0.91	2.39
23	High alloy steel, AF1410	208.2	1560	700	***155***	0.81	0.02	0.19	0.34	0.90	**2.27**
	Maximum value	216	1,670	841.15	155	1.00	1.00	1.00	1.00	1.00	3.50
	Minimum value	71.79	150	111.8	14.1	0.16	0.02	0.15	0.33	0.40	2.27

been the most suitable materials to meet the design requirements for the compliant hinge system, based on the selection process using the M_i parameters.

Table 3.27 below presents the final list of selected materials with appropriate mechanical properties, these properties were used to quantify the material parameters M_i. With the M_i parameters quantified, a numerical comparison could be performed, thus allowing a suitable material to be selected.

The M_i parameter values, as listed in Table 3.27, were calculated and are appropriate values for the flexure. Depending on the parameter in question, either the greatest or the smallest value for a particular parameter would be selected. However, so as to be consistent, the parameters utilising the smallest value (M_2 and M_3) were inverted so that their values were inline with the other M_i values. This allowed all the parameters to be summed, thus giving the material that was most suitable.

The optimisation values (Table 3.27) are highlighted and are the maximum values in each column. Due to the normalisation of the M_i values, all the maximums appear as one's Both maximum and minimum values are given at the bottom of each column respectively.

The wrought aluminium and unalloyed titanium grade 1 (rows 20 and 21) are included in Table 3.27 as comparisons with the other more suitable materials. Both the aluminium and titanium demonstrate via their M_i parameters that they are most unsuitable materials, as do the two alloy steels (rows 22 and 23) at the bottom of the table.

At first glance, the copper-niobium emerges as though it would be an apt material, as it shows in Table 3.27 to have the highest value for the sum of the $_{\mathrm{Mi}}$ parameters putting it at the top of the table. However, the material parameter M_5 that used the deflection as one of its factors actually puts the copper- niobium lower down the table and one of the titanium alloys is seen to score a higher value. Secondly, the copper niobium is only commercial available as wire. This example serves to demonstrate that the most appropriate material is not immediately evident from the tabulated data.

From the table of values (Table 3.27) it is still difficult to conclude which material will give the longest life, the most compact hinge, or the smallest radius of curvature.

In review, and as indicated earlier, the M_1 ratio (equation [56]) is a major determining factor for the flexure hinge. The M_2 parameter as given above and by equation [64] determines that the material most suitable for a spring would be the material with the highest M_2 value. This material will store the greatest measure of strain energy. However, in the case of the flexure hinge, high strain energy is not required. Perhaps more importantly, a low hysteresis is a more useful property to attain. A material with high strain energy will have a higher bending resistance and therefore is more likely to fail at the repeated maximum displacement required by the design specification. A high M_4 value is considered one of the ideal properties for a flexure as it represents a material with minimum stiffness. M_5 is considered highly influential as its approach through the displacement rather than the radius of curvature criterion is required to develop the shortest flexure length.

From Table 3.27 a material that scored highly in more than one M_i parameter was the Titanium alpha-beta alloy, Ti-6Al-4V, Aged, which gained the best score for two of the five parameters. This would lead to the conclusion that it was the material most suitable for the purpose. Closer investigation showed that the parameters may be ranked in order of significance, expressed by the features they represent. Table 3.28 presents the material parameters in order of their importance in meeting the design specification. The most significant property is listed first and the others follow in descending order. Aged titanium Ti-6Al-4V is given as the most appropriate material to meet the design specification requirements of the flexure hinge.

Table 3.28: Material parameters ranked in order of significance

		M_i	**Material**
1st	Minimum radius of curvature	M_1	Titanium Ti-6Al-4V, Aged
2nd	Minimum length	M_5	Titanium Ti-6Al-4V, Aged
3rd	Minimum stiffness	M_4	Aluminium alloy, 5083
4th	Minimum stored energy	M_2	Unalloyed titanium, Grade 1
5th	Fracture toughness	M_3	Copper-18% Niobium Composite (wire)

The final choice of a material however, depended on the total adherence of the preferred material to the design specification. To that end, the displacement equation (equation [67]) must also be used to determine the minimum length of the hinge. This can be done by rearranging equation [57] and substituting into equation [70] to

include a stress component in the calculation. Equation [76] presents the length in terms of the appropriate values. It does however use the modulus of rupture, σ_f, as its stress value.

$$l = \sqrt{\left[\frac{3\delta tE}{\sigma_f}\right]} \qquad [76]$$

The values for minimum flexure length, l, were calculated for all of the materials listed; the most relevant from each material group is presented in Table 3.29. The table compares the working length values for the blade when calculated using either the rupture stress or the endurance stress. Also shown is the variation in length by hinge thickness for each stress regime. Table 3.29 confirms the choice of Titanium Ti-6Al-4V Aged as the primary choice of material for the flexure when the modulus of rupture, σ_f is applied as the maximum stress value. On the other hand, when the endurance limit, σ_E was substituted as the maximum stress value the most suitable material was the Titanium Ti-6Al-4V STA. These values are presented here (Table 3.29) as they formed the basis for the shortest possible blade used in subsequent prototype design and manufacture.

Table 3.29: Calculated beam lengths with regard to stress type and hinge thickness

Stress type		***Rupture stress***		***Endurance stress***	
		Length of hinge (t=1.0 mm)	**Length of hinge** (t=0.5 mm)	**Length of hinge** (t=1.0 mm)	**Length of hinge** (t=0.5 mm)
Material description			*L* [mm]		
Beam displacement	δ [mm]	5	2.5	5	2.5
Titanium alpha-beta alloy Ti-6Al-4V STA		29.965	21.188	*36.890*	*26.085*
Titanium alpha-beta alloy Ti-6Al-4V Aged		*28.525*	*20.170*	37.133	26.257
Low alloy steel AISI 4150 (tempered @ 425 C oil quenched)		33.500	23.688	52.011	36.778
Low alloy steel AISI 4340 (tempered @ 425 C oil quenched)		33.887	23.962	52.930	37.427
Carbon steel AISI 1095 (tempered @ 425 C H2O quenched)		40.315	28.507	54.009	38.190
Carbon steel AISI 1095 (tempered @ 425 C oil quenched)		44.883	31.737	54.009	38.190
Carbon steel AISI 1340 (tempered @ 425 C oil quenched)		36.746	25.983	55.595	39.312
7% Phosphor bronze extra hard (wrought) (UNS C51900)		36.613	25.889	57.608	40.735
Copper-2-Beryllium (whp) (UNS C17000)		29.101	20.577	57.961	40.984
Copper-2-Beryllium (w1/2hp) (UNS C17000)		29.759	21.043	58.202	41.155

Unalloyed titanium, Grade 1	71.589	50.621	62.075	43.894
Wrought aluminium alloy, 5083, H343	43.608	30.835	69.399	49.072
Minimum Length	*28.525*	*20.170*	*36.890*	*26.085*

As the hinge section thickness was one of the primary defining characteristics and controlled the minimum flexure working length, the availability of appropriate sheet thickness was of the utmost importance. This was also an important consideration from a design for manufacture viewpoint. A brief perusal of suppliers and their products indicated that 1.00 and 0.5 mm thick material was readily available. On this basis, the minimum lengths shown in Table 3.29 are those attainable with these two material thicknesses. Although the 1.0mm thickness does not satisfy the design requirement for minimum flexure length, it is included here so that a comparison can be made as to the effect a small change in thickness has on the flexure length.

3.6 Additional flexure blade considerations

3.6.1 Blade loads in the fabricated system

The ends of each of the flexure blades were fixed and unable to be freely displaced, giving the only degree of freedom effectively in the direction of the applied force. The blades were also designed in parallel pairs with each pair being in series. The two

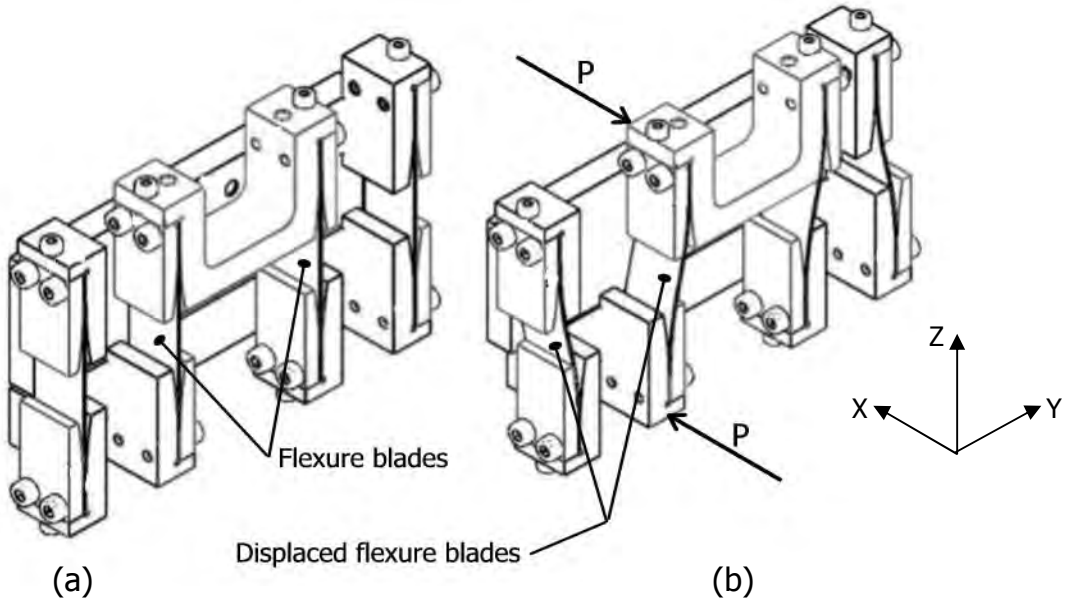

Figure 3.32: Fabricated flexure arrangement

inner blades were in parallel as were the two outer ones as shown in Figure 3.32. This effectively negated or prevented any tendency for the ends of the blades to twist relative to each other. Figure 3.32 shows two diagrams of the working section of the

fabricated flexure system in both its rest (a) and maximum travel positions (b). It also shows a schematic representation of the applied load direction due to the acceleration in the Y direction of the machine table. The load, P, is shown as a couple in one direction (Y) only however, other forces will apply perpendicular (X) to P for the second axis, and vertically (Z) for any axial loads imparted by the cutting tool and mass carried by the table. The forces (P) will result in a displacement in the Y plane parallel to P. The following section will investigate the effects of this loading on the displaced hinge (Figure 3.33b).

Elastic instability causing buckling of the displaced flexure was considered in light of work by authors such as Timoshenko[156], Gere[157] and Pilkey, in his compendium of Formulas for stress and strain[158]. It appears as though this type of loading model has not been investigated in any depth. However, these publications indicated that the

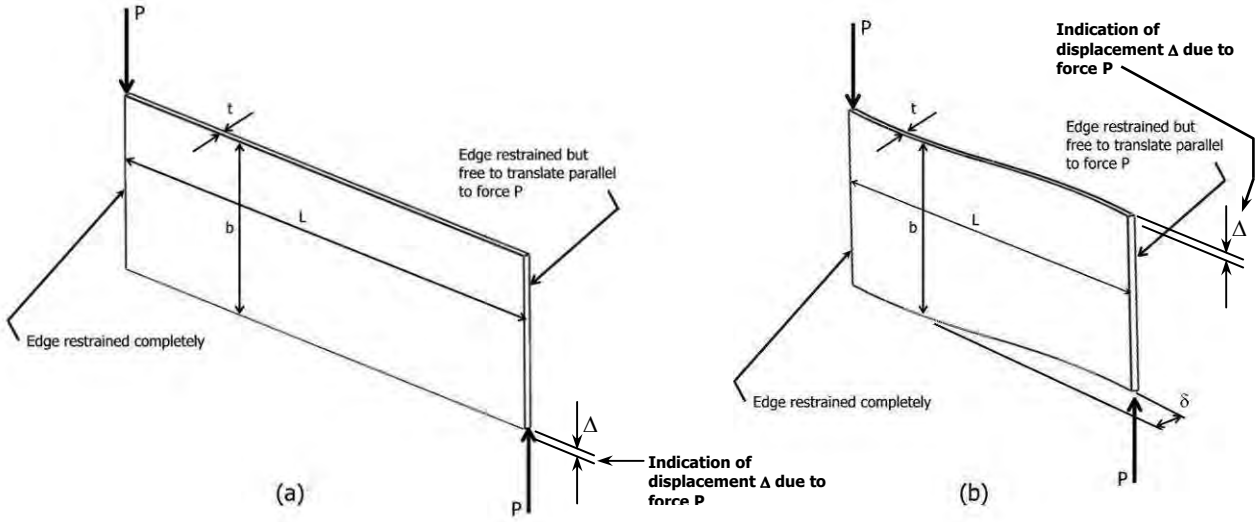

Figure 3.33: Schematic diagram of the straight (a) and displaced flexure blade (b)

structure could be considered as a deep thin unsupported beam. The configuration was similar to the sinking support arrangement considered earlier. The major difference was that the earlier consideration was with the 2nd Moment of Area through the weak axis whereas this structure has the loading and therefore deflection in the direction of the strong axis.

Figure 3.33 shows an individual blade with the force configuration applied. Figure 3.33a represents the straight blade and Figure 3.33b represents the blade at full table displacement along one axis. The value δ is the table's working displacement and can be plus or minus relative to the neutral position. The value Δ is the blade deflection due to the applied load P and can be calculated for the configuration in Figure 3.33a

using the beam theory equation [59] (where δ is replaced with Δ) that relates to a sinking support style of constraint and boundary conditions. The configuration shown in Figure 3.33b poses a more serious problem to analyse and thus is addressed in the following paragraphs.

The displacement in the blade creates an out of plane loading that is very difficult to define in the terms of beam theory. Finite element analysis (FEA) software was used to determine the loading ratio between the straight blade and the displaced one. The blade model (Figure 3.33) was constrained in the FEA software to represent the configuration used in the fabricated flexures assembly shown in Figure 3.32. This configuration had one end constrained completely and the other end restrained but free to translate in the direction of the applied force, P. A nominal load of 1 kN was applied as shown in Figure 3.33a and the deflection Δ, in the direction of the load, was noted. The same nominal load was applied to the displaced blade as shown in Figure 3.33b and the subsequent resulting deflection was noted. The ratio between the two results was calculated at approximately 0.25, indicating that the load capacity of the displaced blade was only 25% of that of the straight beam. This load value could then be used in determining the maximum acceleration of the work table for the deflected blades once the mass of the worktable system was known. As can be seen in Figure 3.32 there are four blades in each flexure assembly. Figure 3.22 shows the four flexure assemblies in place supporting the intermediate stage above the base platform. This in turn equates to sixteen blades supporting the intermediate stage. Based on the ratio calculated above the proposed design can be used with a maximum load that can be calculated by determining the maximum safe load with the displacement set to zero. Once this safe load is known and the maximum mass of the worktable system established, the maximum acceleration can be calculated.

Table 3.30: Comparison of load capacity of the flexures systems

Description	Type	Load capacity per blade [N]	No of blades/stage
Column loading	Modified Euler	80.178	8
	Secant	77.792	8
Beam loading	Non displaced	490.4	16
	Displaced	122.6	16

Table 3.30 gives a comparison of the expected load capacity of the blades in the various configurations. For the beam loading analysis, the endurance stress was applied as the limiting factor. It must be noted that the data in the comparison table is relative and remains unmodified. There have been no factors of safety or fatigue modification factors applied at this point.

The comparison in Table 3.30 shows that the beam loading style of design gives a significant advantage with regard to the load capacity. It must also be noted that the modified design brings the loads on the blades to bear in two very different configurations. The axial or columnar loading is valid only for those blades that are in compression, the blades in tension will stiffen under the tensile load[159], but they are not in any danger of failing compared with the blades functioning as struts. To this end, there are twice the number of blades being loaded as beams compared to the blades being loaded as struts. Therefore, the fabricated configuration will provide a larger acceleration capability during the process cycle. Compare the direction of loading in Figure 3.15 and P in Figure 3.32, which represents the same load, to gain an appreciation of the changes made to the orientation of the hinges. These configuration differences between the two designs indicate how the fabricated flexure assembly is better able to withstand the expected loads by repositioning the blades.

Table 3.31 presents a summary of the feed forces from chapter 4, considered likely to occur during the pocket milling operation. The forces in the X and Y directions (refer to section 3.1.4 for direction explanation) are presented here along with the resultant value for a 10^{o} rake angle cutter. The values given include the cutter edge coefficients in both the horizontal directions, however no data was available for the axial force, F_Z and so has been omitted. By observation the forces generated by the cutter are seen to be very small with their influence being equally small in the overall design. A full explanation of this is given in section 4.4.7 in chapter 4.

Table 3.31: Summary of feed forces from Chapter 4

Feed force	Direction	value [N]
Orthogonal feed force	F_x	-0.44
	F_y	3.00
Resultant feed force	F	3.02

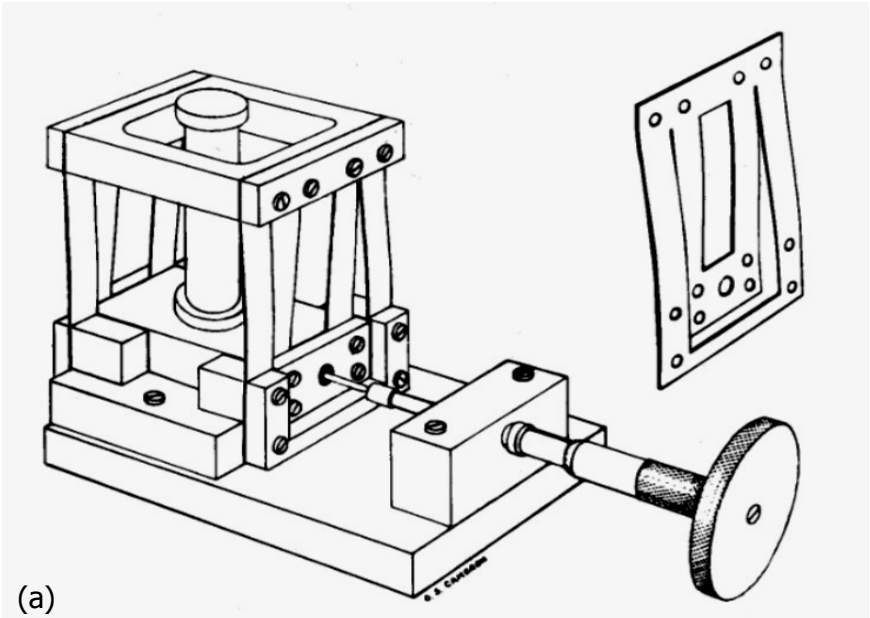

(a)

Folded compound movement. Dimensions of specimen tested: spring length between blocks, 41 mm; spring width (outer set), 2 × 10 mm, separated by 30 mm; spring width (inner set), 2 × 10 mm, separated by 10 mm; spring thickness, 0.56 mm; block length between springs, 50 mm

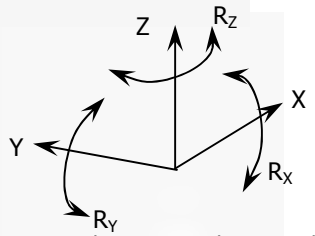

Axes diagram applies to the three flexure figures - a, b, c

(b)

Compound parallel spring movement. Dimensions of specimen tested: spring length between blocks, 42 mm; spring width, 2 × 10 mm, separated by 10 mm; spring thickness, 0.56 mm; block length between springs, 25 mm

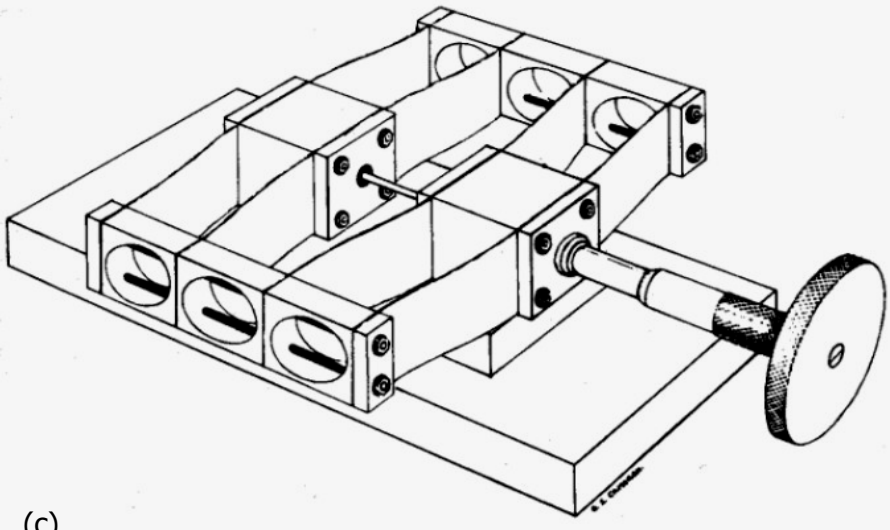

(c)

Balanced compound movement. Dimensions of specimens tested: spring length between blocks, 40 mm; spring width, 25 mm; spring thickness, 0.36 mm; block length between springs, 25 mm

Figure 3.34: Compound parallel flexure assemblies[114]

3.6.2 Alignment issues with fabricated flexures

The manufacturability of the flexure system remains one of the critical issues in the success of the design and implementation of the system as a machine tool working platform. The superior trajectory accuracy of traditional machine tool slides moving through long distances remains undisputed and their attainable precision has been well researched[1]. However, there remains the issue of friction and wear within the slide system. Friction absorbs power and wear compromises the accuracy over measurable periods of use. The instigation of the flexure system is completely dependant on achieving accuracy values that are the same or better than the slide system in terms of definable linearity. To that end, an investigation into the difficulties likely to be experienced in the fabrication and assembly of a suitably designed flexure based machine tool worktable were reviewed. Jones[160] and Hatheway[161] discuss these issues and consider the construction of rectilinear designs, such as those proposed for the design concept. They both recognise the difficulty in manufacturing these devices.

Figure 3.32, shows the proposed configuration of the blades in the design concept assembly, based on this design a rectilinear translation should occur. This translation is based on the premise that all of the blades are manufactured identically and are assembled perfectly parallel to each other. In practice, perfect parallelism is unable to be achieved, because of the variation in the spring strength, and the spring and block dimensions[162].

In order to investigate the manufacture of the proposed design, the method used by Jones will be examined. Jones investigated the properties of composite rectilinear movements, specifically the variability of pitch in the output stage. Jones's design (Figure 3.34a - c) measured the travel (T_Y), pitch (R_X) and height (z) variations of the rectilinear movement produced by the mechanisms. He further used compensation blocks (Figure 3.34b) on the flexures to correct for the manufacturing errors/misalignments. Table 3.32 presents performance data for both compensated (c) and uncompensated (u) blades. The compensation blocks can be seen in Figure 3.34b on the two nearest and two distant blades. Jones found that the compensation blocks improved the performance of the system from ±112 to ±3.5 sec of arc with a 6.0 mm displacement, when using a simple two spring parallel mechanism[163]. When

applying the system as shown in Figure 3.34b the error in departure from the pitch angle (R_X) was ±7.5 sec and from the mean straight line ±0.9μm.

Table 3.32[164]: Performance results for the system shown in Figure 3.34b

Travel	0	1	2	3	4	5	6	7	8	mm
Pitch [u] (R_X)	0	28	55	83	110	139	185	224	263	sec
Pitch [c](R_X)	0	14	35	43	49	58	58	58	58	sec
Height [u] (z)	0.0	4.0	8.5	14.0	19.0	28.0	29.1	34.9	39.8	μm
Height [c] (z)	0.0	2.3	3.8	5.1	6.8	6.6	6.8	6.0	6.3	μm

Jones made no attempt to minimise the roll (R_Y) or yaw (R_Z) errors, which were measured at approximately ±30 sec[165].

A second set of test data presented in Table 3.33 using the configuration shown in Figure 3.34a[166]. This model was used by Jones to minimise the unwanted effects generated by the model in Figure 3.34b. These effects were the prising action created by the drive mechanism, and the undesirable torques due to the blade variations[167]. Although not shown by Jones in the diagram, the mechanism in Figure 3.34a required compensation to achieve the results given in Table 3.33. For the 5.0 mm of travel (T_Y) between 3 and 8 mm, Jones reported deviations from a straight line of ±0.45μm in height (z), ±0.4 μm in sideways drift (T_X), ±9.5 sec in pitch (R_X), ±0.5 sec in roll (R_Y) and ±9.0 sec in yaw (R_Z). Jones concluded that this was a useful improvement over the results achieved by the mechanism in Figure 3.34b.

Table 3.33[168]: Performance results for the system shown in Figure 3.34a

Travel [mm]	0	1	2	3	4	5	6	7	8	9	10
Pitch [sec] (R_X)	0	6	12	16	25	26	31	32	35	34	35
Roll [sec] (R_Y)	0	12	14	30	30	31	31	31	31	26	14
Yaw [sec] (R_Z)	0	10	20	28	38	40	45	44	46	50	53
Height [μm] (z)	0.0	1.5	1.8	2.1	2.3	2.6	2.6	1.9	1.7	0.3	-0.6
Drift [μm] (T_X)	0.0	1.0	2.0	2.8	3.4	3.4	2.5	2.5	2.6	2.6	2.0

In order to achieve still better balancing of the assembled blades the configuration presented in Figure 3.34c[169] was constructed by Jones. This mechanism represented a further simplification in the construction[170]. Due to the improved balance of the flexures, this system required less compensation.

Table 3.34[171]: Performance data for configuration shown in Figure 3.34c

Travel [mm]	0	1	2	3	4	5	6	7	8	9	10
Pitch [sec] (R_X)	0	4	7	7	7	7	7	5	5	5	-6
Roll [sec] (R_Y)	0	0	3	7	12	17	24	24	30	30	37
Yaw [sec] (R_Z)	0	0	0	8	9	12	24	24	24	24	24
Height [μm] (z)	0.0	0.5	0.8	1.0	1.1	1.3	1.5	1.5	1.5	1.3	1.0
Drift [μm] (T_X)	0.0	0.1	0.0	0.5	2.1	1.7	1.6	1.8	1.0	0.6	-0.7

A final set of data for Figure 3.34c is presented in Table 3.34. The 5.0 mm of travel (T_Y) from 4.0 – 9.0 mm showed the deviations to be much reduced over those obtained from the previous configurations. These deviations were ±0.2μm in height (z), ±0.75μm in drift (T_X), ±1 sec in pitch (R_X), ±9 sec in roll (R_Y) and ±6.5 sec in yaw (R_Z). Over the full range of travel, this was the best system tested, and when specially compensated for rectilinearity, the deviations were further reduced[172].

This style of design depicted in Figure 3.34c represented the least deviations from rectilinearity. However, there were issues relating to the configuration that were detrimental to its application as a machine tool table. The primary concern was the lack of compactness embodied in the configuration. As compactness was a primary design requirement for the machine table, the configurations developed by Jones were unsuitable. Consequently, the concept developed in Figure 3.32 was adopted as it better represented the design requirement.

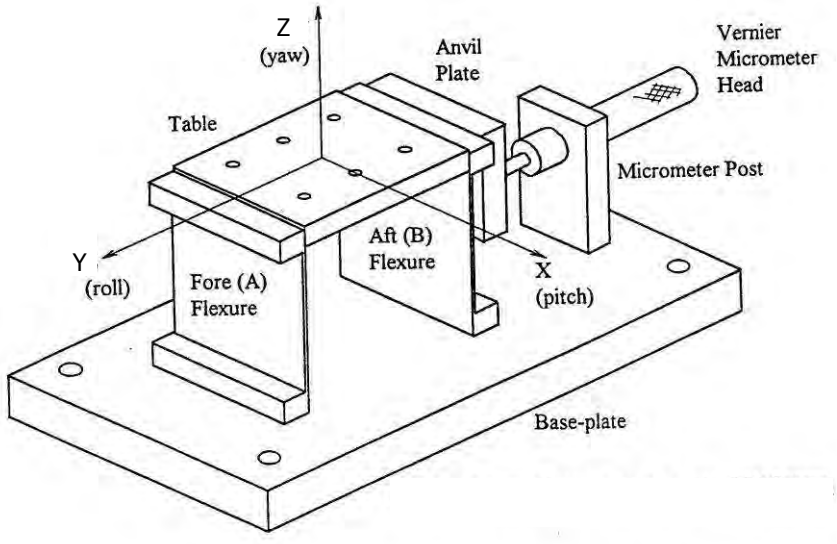

Figure 3.35: Hatheway's simple flexure stage

Jones's publication presented no definitive analysis of the errors that occurred in terms of a mathematical description. However, in 1995, Hatheway[173] published a paper in which equations were developed that described the parasitic motions and the deviations from the ideal trajectory. In this paper, Hatheway compared the precision behaviour of a simple flexure stage constructed from monolithic blade flexures and a similar stage using a composite (five components per blade) assembly. Hatheway's publication is based upon a simple single flexure stage, that is, a base, two blades, and a work platform, (Figure 3.35). This type of mechanism gives parallel but not rectilinear displacement. Hatheway's equations will be utilised in the following section to analyse the kinetics of the design concept.

3.6.3 The kinetics of a simple flexure stage

The notion of a double cantilever or sinking support beam (Figure 3.16) forms the basis of Hatheway's exposition wherein the beam forms the flexure blade. Hatheway's assumptions are presented and include the notion of assembling exact length blades into a simple flexure with an identically equal span on both the base and work platform (Figure 3.35). A further assumption puts the neutral axes and the principle axes of the blades exactly parallel. These assumptions identify the variables that require controlling to achieve the kinetics of a well aligned simple flexure stage[174]. These variables are;

l = flexure blade length

S = span or distance between flexure blades

α = angular misalignment in the vertical, XZ, plane of the fore and aft neutral axes

β = angular misalignment in the horizontal, XY, plane of the principle axes of inertia[175].

Hatheway also considers the effect of the drive system and coins the phrase "properly driven" to describe a system that was technically error free. A "properly driven" stage is driven by a force that acts on a line through the kinetic centre, wherever it may be. The kinetic centre is that point which is ideally at the geometric centre of the flexure blades; that is, half the span, half the length and half the breadth. In reality, the kinetic centre will only be in close proximity to the geometric centre, due to manufacturing differences in the flexures and misalignments between them[176].

A well aligned and properly driven flexure stage will displace through a trajectory as defined by the kinetics of the blades. A circular arc in a vertical plane will trace the locus of the trajectory, with no discernable out of plane motion. The loads on the blades will be near identical and the motion of both ends of the table for and aft will be similar. The table will not rotate with respect to the base but will remain parallel to it. The last property stated is important because angular motion of the table, the parasitic motion, may be easily measured over large displacements using an autocollimator. These angular deviations may then be used to assess parasitic or other misalignments that otherwise may be unobservable and indeterminate[177].

The misalignments are all dimensional. In order for them to be evaluated, individual dimensions are selected so that their influence on the system can be determined. The misalignment variables are,

- unequal blade lengths
- unequal span lengths
- non-parallel neutral axes
- non-parallel principle axes of inertia.

The influence of each of these parameters as reported by Hatheway[178] will be considered analytically in section 3.6.4 – 3.6.8.

3.6.4 Unequal blade lengths

When the flexure work table(Figure 3.35) was assembled with unequal length blades, there was a tendency for the platform to rotate (pitch) about the X axis, R_x. The difference in the blade lengths is defined as Δl and this dimension allows the calculation of the pitch motion relative to the displacement.

Using an assumption of small displacements (travel in the Y direction), T_Y, the kinetics of the blades may be represented by circular arcs of radius r_Z, and angular displacement θ. Hence,

$$r_Y = \frac{2l}{3} \qquad [77]$$

where,

r_Z ~ radius of the blade end translation for small displacements

l = blade length

and

$$\theta_A = \frac{3T_Y}{2(l_A - \Delta l)} \quad [78]$$

where,

θ_A = the angle the instantaneous centre of flexure A will translate through

T_Y = platform displacement

l_A = Length of flexure blade A

Δl = blade length difference

Due to the variation in the blade lengths, the platform end adjacent to blade A will be displaced vertically (z_A) given by equation [79][179].

$$z_A = \frac{-3T_Y^2}{4(l_A - \Delta l)} \quad [79]$$

where,

z_A = vertical displacement

The parameters relating to blade B, θ_B and z_B, are found using a similar analysis.

The pitch rotation, R_x, for the table of span S, is given by equation [80][180]

$$R_x = \frac{\Delta y}{S} = \frac{z_A - z_B}{S} = \frac{-3\Delta l T_Y^2}{4l^2 S} \quad [80]$$

where,

R_x = pitch rotation about the X axis (horizontal axis perpendicular to the platform displacement)

S = the span, the horizontal distance between the blades in the displacement direction (Figure 3.35)

and assumes that Δl is small with respect to l_A and l_B so that,

$$l \approx \frac{(l_A + l_B)}{2} \quad [81]$$

The pitch rotation R_x, is shown by equation [80] is shown to be proportional to the platform displacement T_Y[181].

3.6.5 Unequal span lengths

When the span lengths vary between the platform and base there will again be a pitch rotation R_{sx}, present in the translation. By assuming small displacements, again represented by equation [77], the angle between planes through the instantaneous centres of the flexures can be quantified by equation

$$\gamma = \frac{3\Delta S}{2l} \quad [82]$$

where,

γ = the angle between the planes through the instantaneous centres of rotation of the blades

ΔS = the difference in the span lengths of the platform and base

The pitch rotation, R_{sx}, relative to the difference in the span lengths is given by equation [83], which shows that R_{sx} is proportional to the displacement of the table T_Y[182].

$$R_{sx} = \frac{-3\Delta S T_Y}{2Sl} \qquad [83]$$

where,

R_{sx} = the pitch rotation about the X axis due to the difference in the span lengths

All other variables are as given above.

3.6.6 Non-parallel neutral axes

The influence of non-parallel neutral axis is to cause the ends of the table to displace in opposite directions in the horizontal XY plane. The motion will manifest as a rotation about the Z axis R_Z when the table is translated parallel to the Y axis. The translations are represented by equations [84][183].

$$T_{Ax} = \frac{-3T_Y^2\alpha}{8l}$$
$$T_{Bx} = \frac{3T_Y^2\alpha}{8l} \qquad [84]$$

where,

T_{Ax} = lateral translation of the platform at end A

T_{Bx} = lateral translation of the platform at end B

α = the angle between the neutral axes in the XZ plane

The net yaw rotation R_Z of the table is given by equation [85], which shows the yaw caused by non-parallel neutral axes to be proportional to the square of the stroke T_Y[184].

$$R_Z = \frac{(T_{Ax} - T_{Bx})}{S} = \frac{-3\alpha T_Y^2}{4Sl} \qquad [85]$$

where,

R_Z = net yaw of the platform about the Z axis

3.6.7 Non-parallel principal axes of inertia

In the case where the principal axes of inertia of the blades are not parallel, a yaw rotation about the Z axis will generated. The effect of these axes not being parallel is given by equation [86], which shows the yaw to be proportional to the displacement of the table[185].

$$R_Z = \frac{\beta T_Y}{S} \qquad [86]$$

where,

R_Z = Yaw rotation about the y axis in the XY plane

3.6.8 Driver influences

The drive mechanism, by the nature of manufacturing process, places eccentric loads on the flexure stage (indicated by the micrometer drive in Figure 3.35). The effect of these eccentric loads cannot be determined from the kinetics of the flexure alone. To determine the equilibrium position of the system an elastic equilibrium analysis must be completed for the eccentrically applied loads and drive mechanism. The analysis must contain the influences of both the shear and bending forces, especially in the stiff direction of the blades[186].

When the drive is designed to impart a force directly in the direction of the translation T_Y, this force will be through the kinetic centre of the stage and will likely occur at only one point during the translation. At all other points along the translation the force will only act through the kinetic centre with an additional application of a moment equal to the product of the force and the distance that the force is offset from the kinetic point. This transfer is consistent with the principles of static equilibrium[187].

When the axis of the drive is normal to the drive surface of the platform it will act through a specific point. This force and any moments generated by deflecting the blades, will be linearly proportional to the displacement and the product of the force and offset respectively. Alternately, if the axis of the drive is not normal to the drive surface, the offset from the point of action to the kinetic centre will be dependent on the magnitude of the translation, T_Y. In this case, the offset may vary linearly while the moment varies as a product of the force and the offset. This product will vary the moment proportionally with the square of the translation T_Y[188].

The drive installation has both a linear term and a second degree term for the moments as functions of the table translation, T_Y. These effects may be quantitatively described by equations[189]

$$\begin{aligned} R_X &= T_Y\left[\Delta z_o + \zeta T_Y\right]\left[\frac{dR_x}{dT_Y}\right] \\ R_Z &= T_Y\left[\Delta x_o + \phi_d T_Y\right]\left[\frac{dR_Z}{dT_Y}\right] \end{aligned} \qquad [87]$$

where,

R_X = pitch angle of the table

R_Z = yaw angle of the table

T_Y = table translation in the z direction

Δx_o = horizontal offset at zero table displacement

Δz_o = vertical offset at zero table displacement

ζ = vertical component of the drives angle of incidence to the drive surface

ϕ_d = horizontal component of the drive's angle of incidence to the drive surface

dR_X/dT_Y = elastic coupling coefficient determined by analysis for a fixed offset

dR_Z/dT_Y = elastic coupling coefficient determined by analysis for a fixed offset

From the above equations, the influences of the component manufacture, the assembly precision and the drive installation all affect the translational accuracy.

3.6.9 Influence of Hatheway's equations

The use of the Hatheway equations in the context of this design is limited, as the equations were developed for a single pair of flexures giving parallel but not rectilinear movement (Figure 3.35). Hatheway had not extended the equations to a double/tandem pair giving rectilinear movement, nor in the wider context, multiple tandem pairs of flexures. During the course of this reported research the author intended to broaden and determine the robustness of the Hatheway equations for the new configuration from the prototypical results. However, limited time and other influences were dominant (discussed in a later section) and precluded the extension to a tandem pair flexure assembly. Further to this, the effects predicted by Hatheway were disrupted by not only using the flexures in the tandem pair configuration, but also by having four tandem pair assemblies interacting through the main framework of the machine table.

The major gain from investigating Hatheway's equations in relation to this project was to understand and determine the nature and consequence of unavoidable manufacturing and assembly errors likely to occur in the flexure assemblies. Hatheway's work and the resulting equations were confined to small displacement single pair flexures (Figure 3.35) where the displacement allowed the well known and robust beam bending equations to be applied. Hatheway had considered a number of issues that relate to flexure assemblies and it was logical to attempt to

incorporate his work where possible, whilst also recognising the limitations in applying it outside his original intent. The final design prototype incorporated four double pairs of flexures, being displaced beyond the small displacement limits of the recognised beam bending theories.

The robustness of using the single pair equations in a tandem pair configuration may be questionable as the equations fail to relate the interaction between the sets of flexures within each assembly, or the relationships between the four flexure assemblies. Some attempt was made to develop an overall understanding of the influences noted by Hatheway in the context of the tandem design. Under the influence of Hatheway's work and a job shop machining capability, the manufacturing tolerance values for the tandem system were specified and adopted. The effects of these tolerance values are further discussed in section 3.7.3.

A much more difficult implication was that of the stage drive (leadscrew) arrangement. The influence of moments and forces applied due to the leadscrew action and the bending flexures in the pair assemblies will cause a measure of deflection in the system support frame. This influence was exacerbated by much stiffer flexures than was originally anticipated. In the prototype flexure assemblies, a commercial grade of titanium was used in place of the selected titanium alloy, due to its availability. However, this material proved to have wholly unsuitable material properties, particularly stiffness. Spring steel, which was almost twice as stiff, was substituted for the commercial grade titanium in the final prototype. This material change had a greater negative impact on the structure than was first anticipated, subjecting the system, including the leadscrew drive system to higher loads during working stage translation.

During the design of the prototype an attempt was made to position the leadscrew attachment points such that they adhered to Hatheway's recommendations. The leadscrew was attached to the working stage at its geometric centre in the XY plane but offset in the Z direction imposing a moment equal to the product of the force of the 16 displaced bladed and the Z direction offset. To counteract this moment, there were four reaction moments, one at each corner of the working stage Figure 3.22. This combination of moments and forces was resisted by the supporting frame for

the stage which was originally designed for the less stiff titanium blades and with a design intent of saving weight.

Retrospectively, the change to spring steel blades nearly doubled the expected loads on the structure, thus increasing the deflection in the working stage. The effects of increased deflection became clearly apparent during testing as the areas chosen for data capture were all at the extremities of the working stage (Figure 3.37). This trend is further discussed in the test result discussion section, 3.10.

Metrological results from the testing showed an unexpected outcome; the errors were more severe than expected or predicted by the Hatheway equations. As cited earlier the errors predicted by Hatheway's equations were extremely small (Table 3.36 - Table 3.38), therefore it was obvious that other influences were affecting the resulting output. This adverse output is also the subject of discussion in section 3.10.

In conclusion, the use of the Hatheway equations in their original context is restricted and therefore use in the final table design is limited without them being extended to incorporate the additional components. The work required to extend Hatheway's research into a context useful to this project did not go beyond a basic analysis to determine the effect the maximum values of the manufacturing tolerance bands would have on single blade pairs. Efforts to encompass the design intent saw these single blade pair results summated to attempt to find the worse case. Combining the individual effects was considered to be a satisfactory conclusion to draw regarding the individual tandem pair assemblies. However, the influence attributed to the interaction of the other blade assemblies on each other could not be reconciled as simply.

Future work is required to examine the possibility of extending Hatheway's equations to include wider influences of multiple tandem assemblies assembled into a single structure. This extension will also consider the assembly issues with regard to the individual tandem pairs, their alignment with the overall structure and their alignment with each other.

The next consideration was the effect of the applied manufacturing and assembly tolerances.

3.7 Manufacturability considerations

Another important parameter considered during the course of this project and in the design of the final flexure working table was 'design for manufacture' (DFM). In addition, the final design concept was intended to be cost conservative in terms of the manufacturing processes and the number of components in the assembly. Perhaps the greatest drawback in switching from a conventional guideway system to the compliant hinge system concept is the penalty paid due to the increase in complexity and the number of parts. A conventional guideway has only three major components, the base, the slide and the gib, plus an assortment of screws and bolts etc. The fabricated flexure on the other hand has a large number of parts mainly used to achieve the chief advantage of the system that of being frictionless and wear free.

The design of a guideway system using multiple flexural hinges was chosen as it inherently works to minimise the discrepancies that are resident in all manufacturing processes[190], however the additional number of parts statistically works against this premise. The initial notion of the monolithic structure showed some promise as a workable design and only contained a single part, whereas the final design contains multiple parts. Therefore, it was to be expected that there was to be a negative compromise in the manufacturing accuracy, however the system was manufacturable, as opposed to the monolith, which was not.

As the design for the flexure system and the monolithic structure progressed, it became increasingly evident that machining the thin flexures would be a difficult problem to solve. In the early stages of development, initial thoughts gave rise to machining and polishing the notch holes in a CNC milling machine and then removing the unwanted material with an EDM Wire Cut or similar process. With the very thin hinge thickness at values of ≤0.5 mm, this process may have proven to be very challenging in trying to achieve the desired results. The notch solution was not heat treatable due to the very thin and very thick adjacent sections in the monolithic design. This situation would have necessitated its manufacture from a pre-heat-treated and tempered material. However, the resultant hardened material is very difficult to machine other than by EDM wire-cut which, as previously indicated, is not a suitable process for enhancing fatigue life. Furthermore, the flexure blades would prove extremely difficult to machine by other material removal processes due to their

slenderness. The possibility existed to shot peen and/or polish the blade surfaces after wire cutting, but this would be a very expensive and time consuming process. There was also the possibility of compromising the accuracy by altering the thickness of the flexures inconsistently. These considerations drove the following manufacturing changes.

3.7.1 Notch manufacture considerations

The design requirement specification in section 3.1.5 called for 'infinite' life in the flexure blades if possible. This requirement was desirable; as it would ensure that the flexure would stay well within the elastic deformation range at the maximum displacement and thus avoid critical limiting stresses. However, in designing the monolithic flexure system to withstand the imposed bending regime for an infinite life, the demand on the fatigue strength of the chosen material may have been beyond reach as it was not possible to heat treat the monolith, post manufacture due to the extremes in section thicknesses.

A further design consideration was the relationship between the maximum flexural stress and the beam length whilst maintaining the required displacement. As can be readily seen the stress will reduce as the effective beam length increases. A problem arises when the beam length gets very long as it increases the overall size of the monolith and tends towards negating the wish for a compact structure. In an effort to minimise the maximum calculated flexural stress and maintain the desire for compactness the effective beam length was set to 135 mm. This value was chosen as the maximum possible acceptable beam length that gave a machine table envelope of dimension acceptable to the design specification.

Using the 'W' design (Figure 3.9) primary platform was considered the best starting point for the monolith design. This configuration allowed for the longest possible notched beams within the narrowest envelope. A second and not so minor consideration was the effect of the notch radius on the stress or stress concentration. The calculations showed clearly that increasing the notch radius reduced the expected stress levels in the flexural bending. Again, this conflicted with the design requirements. Increasing the notch radius had the effect of increasing the overall dimensions of the monolith and complicating the manufacturing process.

Ideally drilling and boring, or drilling and reaming the notch holes using a CNC machining centre would have been the chosen process to manufacture the notches. This method would have required enough space to allow the maximum sized 24 mm diameter holes (Figure 3.36) to be machined at each end on both sides of the blades. Therefore, the use of this method was not initially considered viable for the monolithic construction.

Notches with radius of ~7 mm (14 mm diameter) were investigated, as this was considered the maximum viable size in terms of the tables overall dimensions. The stress levels arising from these sized notches proved unacceptable, and therefore methods of increasing the effective notch radius whilst maintaining or reducing the

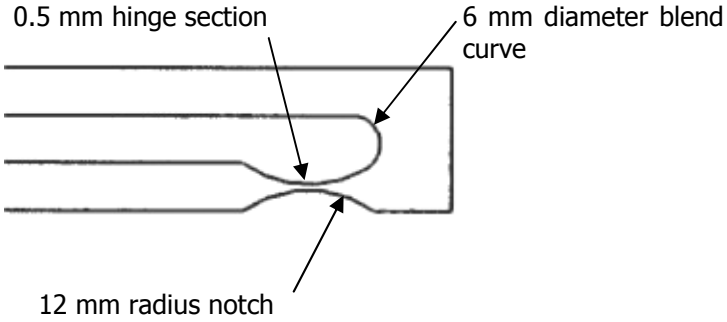

Figure 3.36: Example of blended flexure configuration

overall size of the monolith were investigated. The result was a 12 mm radius on either side of the beam to form the notch. A 6mm diameter fillet was then used to blend the flexures into the main body of the supporting structure in those areas where a blended connection was required (Figure 3.36). The figure is a representative sketch only and fails to show clearly the increase in member spacing required when using the 24 mm diameter machined holes. This lack of compactness was a primary reason the monolithic style was abandoned, with high stress concentrations in the notches with smaller radii confirming the decision. However, it was the 'W' design concept that gave the proposed parameters (Table 3.35), in terms of the dimensions and calculated stress at the required beam displacement, rather than any analytical process. See Table 3.35 below for a summary of the concept design stricture introduced in section 3.3.2.

Table 3.35: Design parameters to produce a notch with a theoretical infinite (>10^8) life

Parameter	Value
Max displacement	5.0 mm
Max beam Length	135 mm
Hinge thickness	0.6 mm
Notch radius	12 mm
Max allowable stress (Calculated)	415.5 MPa

Much of the early work done in this project centred on the determination of the maximum stresses developed in the notch when the required displacement was reached. When all the contributing factors were considered and it became apparent that a circular notch design would not be suitable for the application, other types of notches were considered briefly. The shape that was finally considered suitable was the leaf type blade as the stress distribution was less concentrated due to the absence of stress risers. Once the design proceeded with the leaf spring style flexure, the dependency on the material type became much more apparent. Also at this stage in the development, a fabricated style of design was in process.

When all the above factors were considered, it was necessary to choose a material with appropriate properties to meet the fatigue life and strength concerns. The change in design simplified the material selection to something that was commercially available in thin sheet form that would not require any further heat treatment. This led to the detailed material selection process described previously in which a dimensional analysis scheme was used to isolate materials into groups that were suitable for the flexure blades. The material selection became a much smaller problem in light of the now five fold increase in componentry required for the fabricated design.

3.7.2 Manufacturing changes from notched hinges to leaf hinges

A major factor that determined the shape of the final design was the manufacturing process chosen to machine the flexure components. The monolithic construction required a hinge of suitable width to minimise the out of plane rotation. The selected material, from which these structures were manufactured, was 5000 series aluminium alloy. The choice of this material was due to the excellent properties that allowed high quality EDM wire-cut machining of the thin sections. Even so, the minimum thickness of the hinges was limited to 1.00 mm to ensure there was no 'burn through' during the

cutting process. In the prototype units, 10 mm thick aluminium plate was used and the range of hinge lengths initially investigated was 25 – 32 mm. These dimensions were chosen to maintain the compact design constraint.

From the developed equations [35], it can be seen that the hinge length has no direct analytical bearing on the maximum stress experienced by the hinge except by association with the bending moment and thus the length. Therefore, longer blades required less force to bend them to the required displacement, but the longer the blade, the more difficult it was to produce accurately. The hinge width was driven in the first instance by the requirement for minimal or nil out of plane rotation and secondly by the machining processes available to manufacture the thin slender component sections. As the investigation and embodiment design of the flexures progressed, it became increasingly evident that to gain a displacement of 5 mm with an acceptable beam length, the notch radii were going to be larger than could be comfortably drilled and then polished. Also, based on the above discussion, leaf type blades could not be inexpensively and successfully machined to provide the component fatigue life required.

Due to these manufacturing considerations, investigations commenced into exploring a non-monolithic or fabricated construction design. This new approach meant that the flexure blades could be manufactured from a suitable sheet material of commercially available thickness. It also meant that the shape of the flexure components was considerably less involved, being of a flat leaf type. With this type of design philosophy now being followed, the length of the hinges and the lack of a notch design meant there was much less of a machining process concern. However, the accuracy of individual components required tighter tolerance bands to ensure that the parasitic errors apparent in sliding type bedways were not introduced into the flexure bedways by poor tolerance design and subsequent manufacture. In addition, the assembled component flexures were prone to assembly errors and tolerance stacking errors that would not have occurred in the monolithic flexure design[191]. The final blade design called for a working length of 40 mm x 12 mm wide, and the blades were to be manufactured from 0.5 mm thick titanium alloy sheet. These hinges were stack machined in one setting to the required profile using an EDM wire cut process.

3.7.3 Manufacturing and assembly tolerances

The design of the components for the assembly required careful consideration during the embodiment design phase to avoid creating parts that were compromised by manufacturing processes. Manufacturing and assembly tolerances were sources of error that were to be minimised to maximise the performance of the assembly in terms of rectilinearity, as it is known that manufacturing and assembly tolerances represent the principal cause of errors in fabricated rectilinear mechanisms. Matching the springs plays the single biggest role in affecting the performance of these devices[192]. The design for this project addressed the spring/flexure manufacture and assembly positioning by creating a clamping system that provided stops that accurately located the end of the blades. These stops can clearly be seen in Figure 3.19 at the end of each of the blades.

On the basis, that all manufacturing must be contained within a tolerance band the influence of the manufacturing capability must be considered. A relatively loose tolerance regime (lower manufacturing costs) may defeat the precision capability of the assembly. Then again, a tighter tolerance (higher manufacturing costs) band may defeat the design on the basis of its failure to be cost effective. By considering the sizes and the tolerances as applied to the flexure system (Figure 3.19), an analysis of the expected errors was carried out. The basic dimensions and the applied tolerances are given in Table 3.36. The manufacturing tolerance ranges for each of the manufactured components were applied to the individual Hatheway equations in order to determine their effect on rectilinearity. That is, the resulting Y_A, Y_B (vertical displacement) and R_{xi}, R_{xo} (pitch rotation) due to manufacturing tolerances of the blades.

Table 3.36: Dimension and tolerance values for the composite flexure assembly

	Nominal value [mm]	**Tolerance values**		
		Upper limit	Lower limit	Difference
Blade length, L	52	0.0	0.05	0.05
Span length, S_i [inner]	35	0.10	0.0	0.1
Span length, S_o [outer]	80	0.08	0.08	0.16
Blade width, b	12	0.0	0.1	0.1
Blade perpendicularity	52	0.03	0.0	0.03
Blade parallelism	12	0.03	0.0	0.03
Translation, T_z	5	0.0	0.0	0.0

The nominal dimension and tolerance values presented in Table 3.36 were the values as they were applied to the prototype fabricated flexure component manufacturing drawings (appendix C). The blade component was manufactured to the above tolerances or better, in which case Table 3.37 represents a worst case scenario.

Table 3.37: Numerical results from Hatheway equations based on the designated manufacturing tolerances

	y_A [mm]	y_B [mm]	y_A-y_B [mm]	R_{xi} [deg]	R_{xo} [deg]
Unequal blade lengths	-0.3609	-0.3606	-0.00035	-0.00057	-0.00025
Unequal span lengths	ΔS_i	0.1	L-ΔL	-0.02363	-0.01654
	ΔS_o	0.16	L+ΔL	-0.02361	-0.01653
Non parallel neutral axis		Geo tolerance	Angle α^o		
Perpendicularity	width	0.03	0.1432		
	length	0.03	0.0331		
	Total angle		0.1763		
	T_{xA}	T_{xB}	T_{xA}-T_{xB}	R_{yi}	R_{yo}
	-0.00055	0.00055	-0.00111	-0.00182	-0.00079
Non-parallel principal axes of inertia			Angle β^o	R_{yi}	R_{yo}
			0.039	0.000097	0.000043

The included angle between the non-parallel principal axes of inertia was calculated using the section property tool of a CAD system. The values for R_x and R_y offered in Table 3.38 result from combining the above equations. The equations with similar results are listed in the parasitic motion column and the values for each blade pair are tabulated in the flexure influence column. The maximum and minimum values shown in the total influence column were determined by adding and subtracting the inner and outer values respectively.

Based on the values presented in Table 3.29 and Table 3.30, Table 3.31 show the influence of the design tolerances on the flexure response. It can be seen that this influence is very small. As they are the worst case values for a single flexure set as shown in Figure 3.19, the expected rectilinearity is within the design requirements stated in section 3.1.4. However, this case used only the manufacturing tolerance values as deviations for a single flexure assembly (Figure 3.17) and have not

considered any of the possible stacked tolerance errors that may occur when the table system is assembled.

Table 3.38: Total influence of parasitic motion

Parasitic motion	Flexure influence	Total influence per flexure assembly	
R_{xi} [deg]	-0.0240	-0.0409	max
$R_{xo\ [deg]}$	-0.0168	-0.0074	min
R_{yi}	0.0038	0.0054	max
R_{yo}	0.0017	0.0021	min

The influence of the stacking effect of the assembly tolerances is somewhat more difficult to define in an analytical sense because there was more than one blade assembly set in the working platform. In fact, there are four individual flexure assemblies in the final table concept design. The cumulative assembly errors of the four sets must be considered in the final error considerations of the table concept. In this error analysis, the influence of the axis drive has not been considered because the design has multiple kinetic points relating to each included flexure assembly. As such, this error will be determined experimentally.

To reduce assembly costs on the work platform, components were arbitrarily selected and randomly assembled to give a final work platform configuration. Hatheway's equations, [77]-[87], allow insight into the influence and underlying effects of blade manufacturing tolerances on a single flexure assembly. It is extremely difficult to visualise and quantify the overall effect on the platform when the influences from the four assembly sets were considered. When all four flexure assemblies are considered as a whole, three potential results were possible. Firstly, the misalignments, pitching and rotation of the platform would be exacerbated. Secondly, the misalignments, pitching and rotation of the platform would be minimised by the random assembly cancelling the errors out. Thirdly, the errors would be somewhere in between the two extremes. This notion was based on the capability of the support structure being able to resist the distorting influences when the working platform was translated.

3.7.4 Assembly influences

The misassembly of the blades and their supporting structure will have an effect on the resulting rectilinear precision and this error will be similar to the manufacturing tolerances. Equations [77]-[87] can also be used to determine the expected parasitic

influence, pitch and yaw errors, on the translation of the platform. These errors will effectively be the same as the values given in Table 3.30 and Table 3.31. However, further influence from the assembled joints must be considered as well. The joints will not be perfect, as they will be affected by the geometric tolerances applicable to the mounting faces. Inaccuracies will occur in the torque values of the assembly bolts and due to the cleanliness of the joints[193].

These errors will be significantly reduced if a controlled assembly is adhered too. However, controlled assembly is an area of huge cost and, in the light of the 'design for manufacture' design requirement, it should be avoided or at least minimised to reduce costs. The design intent using the four, four blade assemblies was devised in an attempt to force the assemblies to work against each other, and thus reduce the parasitic pitch and yaw and therefore the cost of assembly.

Although the components were selected randomly, two of the three above influences were carefully controlled. These were cleanliness and consistency in the torque value of the mounting bolts. The cleanliness issue mainly concerned lint, dust, swarf and other contaminants on the mating surfaces, as a small misalignment could easily be incorporated by the inclusion of dust or fibres in the joints[194]. The precision of the structure will be affected by the elastic distortion around the blade mounting areas caused by the bolts[195]. The effect was minimised by using a consistent torque value on the mounting bolts.

The use of Hatheway's equations extends beyond the prediction of the parasitic influences. They are able to be used to determine the corrective actions required of an assembled system. Using precision measuring methods, the data about the parasitic pitch and yaw may be captured. From this data, the equations can be used to solve the variables that cause the misalignments. For example, when the pitch R_x is known for a particular combination of span, blade length and translation, the span differential ΔS can be calculated. Once the ΔS value has been determined, the blade may be shimmed or lapped to bring about the required correction to the assembly[196]. The equations can be used to determine any variations required to correct the parasitic influences, however repeatability and cleanliness should be checked thoroughly before and metalworking corrective action occurs. In a similar way, the drive influences may be adjusted and corrected[197].

Although the equations successfully predict the parasitic motions for simple flexures, their capability to predict the same motions in more complex structures such as the concept table design remains to be seen. The notion of using random assembly to negate some of the parasitic motion relies heavily on the adherence to the applied manufacturing tolerances to minimise the parasitic effects early in the manufacture. These parasitic motions will necessarily displace the platform when each of the four blade assemblies is considered separately. When combined together out of plane forces will be generated. This tendency to load the assemblies with 'out of plane' forces caused by these parasitic movements were to be counteracted by the stiffness of the connecting frames. This theory was tested by selecting components randomly for assembly and the resulting structure was tested for rectilinearity with the departmental coordinate measuring machine. The results are presented in section 3.9

3.7.5 Assembly of a single axis flexure structure

The production of the prototype identified aspects of the design that proved difficult to manufacture. In particular, the interface between using the EDM wirecut process to rough out the basic shapes or 'blanks' of the blade supporting structure, and the CNC milling machine processes required to finish the items. The main difficulty was found when setting the blanks up in the mill and gaining the precision required in locating particular features accurately. The original design was executed with greater use of the wirecut process with the mill being used to remove that material not able to be machined by wire cutting. A redirection of the design switched from this manufacturing philosophy to one whereby the mill was used to remove all material to finished cut precision instead of using the wirecut for a portion of it. This change in machining philosophy was able to produce components of sufficient quality to remain within the designated manufacturing tolerances.

The final concept design was executed with the use of CNC machinery in mind, where only minimal manual input was required. The use of human manual manufacturing input on a large scale would introduce errors similar to those found in the more traditional 'jobbing' style of manufacture. These types of errors were to be avoided to minimise the effects they would have on the outcome of the table assembly. Therefore, CNC methods and processes were adopted. Consideration of the manufacturing methods indicated there were sufficient numbers of similar components

to warrant the time to manufacture jigs and fixtures for the CNC mill. These jigs and fixtures were necessary to ensure that all the same components were similar. That is, they were all within the specified tolerance bands.

With the completion of the components, the fabricated flexure table was assembled as shown in Figure 3.37. The whole assembly was set up on a coordinate measuring machine (CMM) to test its rectilinearity. Testing was performed by measuring the vertical and horizontal position of the displaced platform relative to its neutral point. The displacement of the platform was performed with an integrated manual leadscrew (see Figure 3.37), in the first instance and secondly by additional adjusting screws after having disengaged the leadscrew. As testing progressed, the emphasis was placed on measuring the vertical displacement error rather than the horizontal errors. It became evident during initial testing just how important the position of the drive axis relative to the flexures was. Hence the second series of tests with the drive axis in a different position was performed.

The flexure set up on the CMM and the method of testing the flexure assembly is described in the next section.

3.8 Method of testing and set up on the CMM

The test procedure measured the displacement characteristics of the working stage with respect to horizontal travel in a direction parallel to the leadscrew axis. The vertical displacement and horizontal yaw of the working stage were of particular interest, as these characteristics will affect the integrity of the machines ability to machine at constant depth in straight lines. The procedure was also chosen, as it would mimic the machining functions required of a milling machine. By investigating these characteristics, the concept design's suitability for a machine table could be determined. That is, it will be possible to gauge the system's rectilinearity, which was the primary goal of the research.

The completed assembly was positioned on the CMM with the base platform (Figure 3.37) fixed in place. This was done to prevent loosing the reference point position in 3D space on the CMM whilst adjusting the working stage through a displacement cycle. The assembly was placed with the leadscrew aligned with the 'Y' axis of the CMM and the drive towards the front of the CMM in a place on its bed that

conveniently allowed the operator to work all round the assembly. A 3.0 mm diameter ball x 30 mm long stylus probe was fitted to the CMM touch probe. This combination was selected as a medium sized probe that would tend to minimise any small surface aberrations and yet remain small enough to achieve all the desired contact points.

The reference point was chosen as the front left hand corner on the upper surface of the base platform (Figure 3.37). All data captured by the CMM was referenced to this point. Points *Pt1 – Pt4* were further 'live' reference points taken on the top corners of the base platform as shown in Figure 3.37. These points were measured with every cycle and were used to ensure there was no distortion or movement in the base platform during the course of a displacement cycle.

The displacement cycle was the travel moved through by the working stage as positional data was recorded. This position of the table was incremented as the leadscrew was rotated through an approximate half turn for each data set. This cycled the working platform from the neutral position to one extremity of its stroke, back to the other extremity before returning to the neutral position or starting point. No attempt was made to increment the position at which the probe contacted the working stage as it was displaced. The contact point on the working stage was always in the same 3D position relative to the reference point. In effect, this meant the probe was contacting a new surface point on the working stage and was therefore subject to

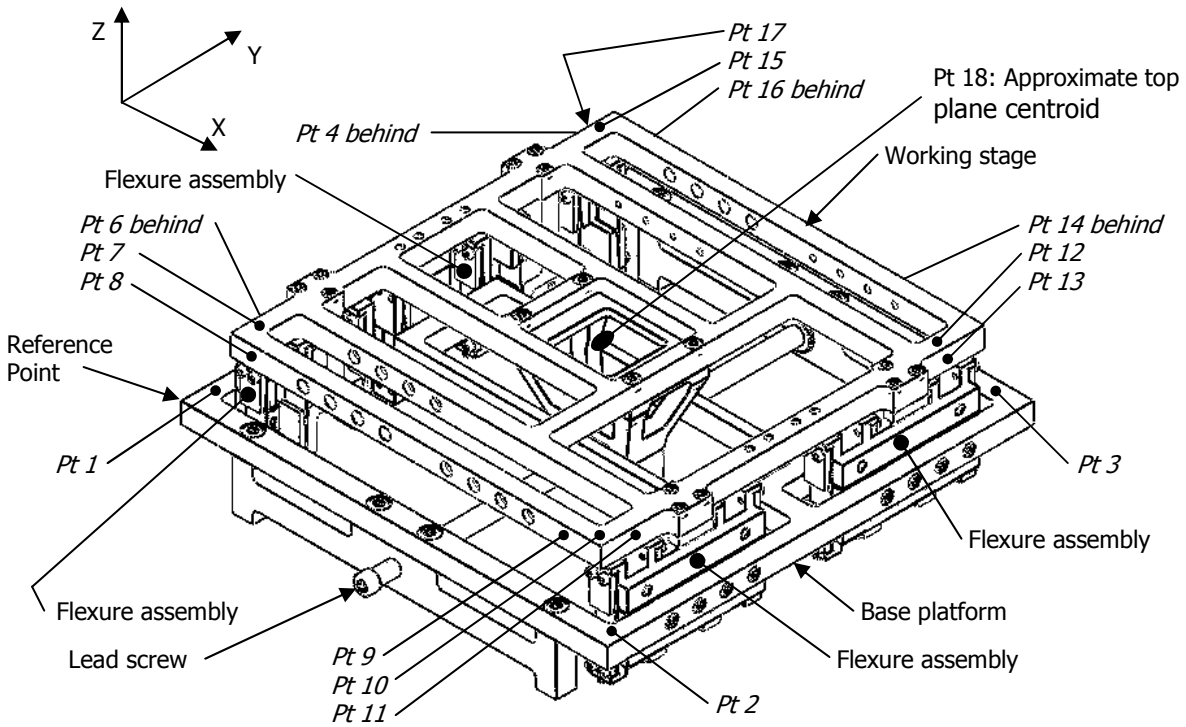

Figure 3.37: Final test flexure table design – single axis only

being influenced by and surface aberrations on the working stage contact surfaces.

As the working stage was incremented, all the points, *Pt1 – Pt4* and *Pt6 – Pt16*, shown in Figure 3.37 were probed and their position recorded as a continuous comma delimited CSV file. The incremental movement provided approximately 45 - 50 data sets per cycle. The CSV files were then imported into a spreadsheet where the results were analysed and charted. The analysis took the form of comparing the data sets common to each axis. For example, all the data points that related to the Z axis in all data sets were considered together to give an overall picture of their loci in the YZ

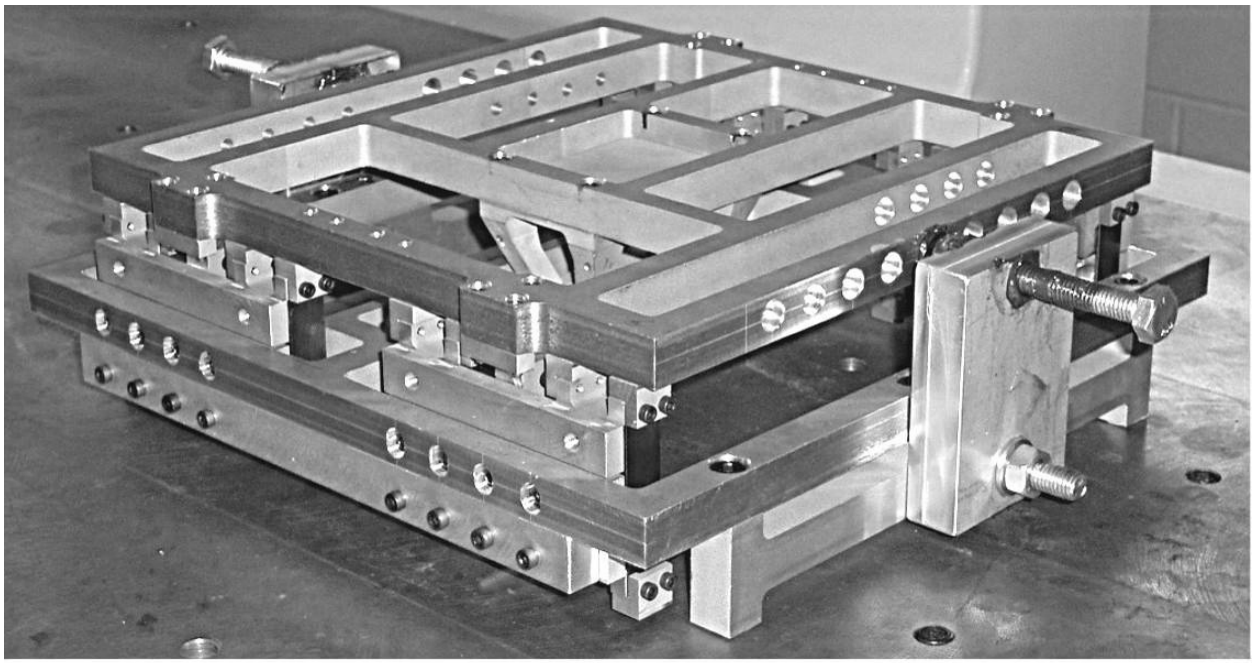

Figure 3.38: Flexure assembly as built showing with the leadscrew removed and the direct acting displacement screws fitted.

plane. The coordinate system directions are shown in Figure 3.37. The same approach was used to analyse the data for the other two axes in the XY and XZ planes. The results from the analysis are presented below in the section entitled experimental test results.

As indicated previously, the drive location on the table assembly has a significant effect on the capability of the flexure assembly to produce rectilinear movement. To provide an indication as to the sensitivity of the system to the drive axis location, the original leadscrew was removed and replaced with two direct acting screws (Figure 3.38). These screws acted directly onto the end of the working stage vertically above the centreline of the original leadscrew. A dome nut with a hemispherical end was fitted to the end of the displacement screws, to act as a smooth bearing surface

against the working stage. Grease was applied as lubricant between the nut's dome and the working stage's contact face to minimise the drag and frictional influences the drive may have on the flexures performance.

Given Hatheway's comment about the drive passing through the kinetic centre of the system, moving the stage drive to the face of the working stage, a considerable offset from its original position, should not have provided any improvement in the systems rectilinearity. However, the test results did show an improvement over those achieved with the drive in its original location. The relocation of the stage drive and the results attained are further discussed in section 3.10 – Hatheway effects.

A final measurement series was performed to investigate the relationship between the working stage top surface and the data capture zones. This relationship was important in determining what influence, if any, the flatness of the working stage top surface may have had on the results. The final examination was performed in a similar manner to the previous tests, except that the working stage was not displaced. A series of 10 points along the previous linear probe path were measured at each of the four corners and these were compared to a datum plane to show the geometric form of the working stage in the data capture zones at each of the four corners.

Table 3.39: Measurement zone naming convention

Zone designation	Point number
Left front top	Pt 7
Right front top	Pt 10
Right rear top	Pt 12
Left rear top	Pt 15
Top plane centroid	Pt 18

The points of interest were the same points that the CMM probe traversed when the working stage was being displaced. These points have been designated; Left front top, Left rear top, Right rear top and Right front top. This designation will be used throughout the following discussion to indicate the particular zone being discussed. Figure 3.34 may be used to reference the location of the zones and Table 3.39 presents the relationships between the points on Figure 3.34 and the zone titles, which have come about from the position of the flexure assembly on the CMM table.

3.9 Experimental test results

The flexure assembly was tested using the above outlined procedure and representative charts are presented below to demonstrate the vertical displacement and repeatability of the flexure assembly system. These charts also show error bars representing the published CMM error in the vertical or z axis direction. The majority of the testing was performed using a 0.6mm table increment per measurement cycle over the range of the desired flexure travel along the Y axis direction (Figure 3.37). To test for aliasing in the results, a more accurate test was performed at 0.1mm increments over the same range of travel as for the other tests.

Typical charts from each of the measurement zones are presented and discussed in the following section.

In all, eight series of data were captured during the investigation. The first four series were taken with the leadscrew used to drive the working stage as it was originally designed. For those test results, an undesirable influence from the leadscrew was found to be affecting the vertical displacement values. As a consequence the leadscrew was changed to the alternative drive method (Figure 3.35). Data subsequently taken was noted to be significantly less influenced by the drive; thus confirming the choice to change the drive method. The full effect of the new drive influence, at the time of this report remains untested. With the improvement to the system performance (resulting in less vertical displacement), the final four data test series (4 – 8) were assessed and utilised to present the performance results.

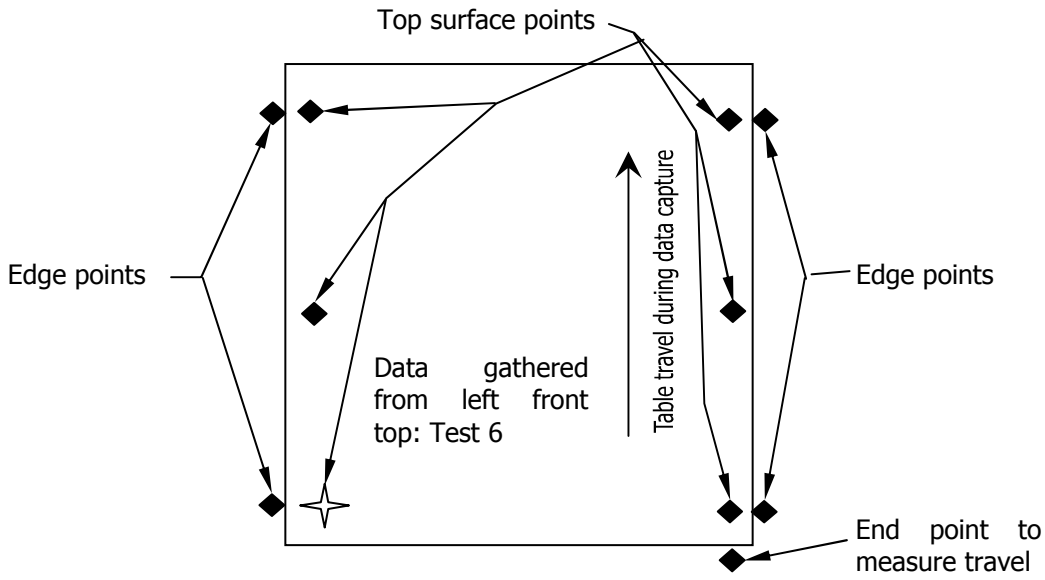

Figure 3.39: Plan view of flexure working stage

To gain a measure of reasonable comparison between the data test series, all the vertical displacement data were normalised. This was achieved by subtracting the smallest value in each set from all the other values in the related sets, a data set being that data captured in any one CMM session. This normalising method allowed presentation of the all the data as positive above the x axis.

Error bars were applied to the charts, where appropriate to represent the limit of the CMM repeatability in relation to the results presented herein.

Figure 3.39 represents a plan view of the flexure working stage showing the eleven data collection points. The star in the lower left corner is labelled "Data gathered from Left Front Top" and represents the point of interest on the current chart. The black diamonds (◆) represent data points where data was captured with each capture cycle. These diamonds will be omitted on the chart pictograms, but are shown here to give the reader an appreciation of the position and quantity of data taken in each working stage travel position.

The four edge points were used to gather data that was relevant to testing for system yaw. Travel position data was gathered via the end point shown in the lower right corner of Figure 3.39. The six top surface points were employed to gather data used to determine the vertical displacement of the working stage relative to the travel position. The arrow is representative of the direction the working stage was travelling relative to the data position when the charted data was captured.

For ease of reference, similar representations will be placed on the various charts used to plot the vertical displacement at each point or zone under consideration.

3.9.1 Presentation of results

The results presented in this section are from test series 4 – 8, and were used as they fairly represented the results achieved. In addition, multiple data series were gathered for the purposes of testing the data repeatability.

As the test process progressed, and further understanding was gained, the need for more positional information was required. The understanding gained by the removal of the leadscrew was the primary reason for the extra data requirement. The improvement in working stage performance with the change from the leadscrew precluded going back to it. So, as a result, only data from the last three test series

contained sufficient information to allow a clear presentation of the overall results. From this information, test series 6 was used to present the performance of the four capture zones. These results are presented in Figure 3.40 to Figure 3.44.

The realisation of the need to present data relating to the centroid of a plane through the working stage did not arise until test 7 had been performed. With this in mind, test 8 was executed and the CMM calculated the vertical displacement of the working stage plane centroid position.

- Left front capture zone

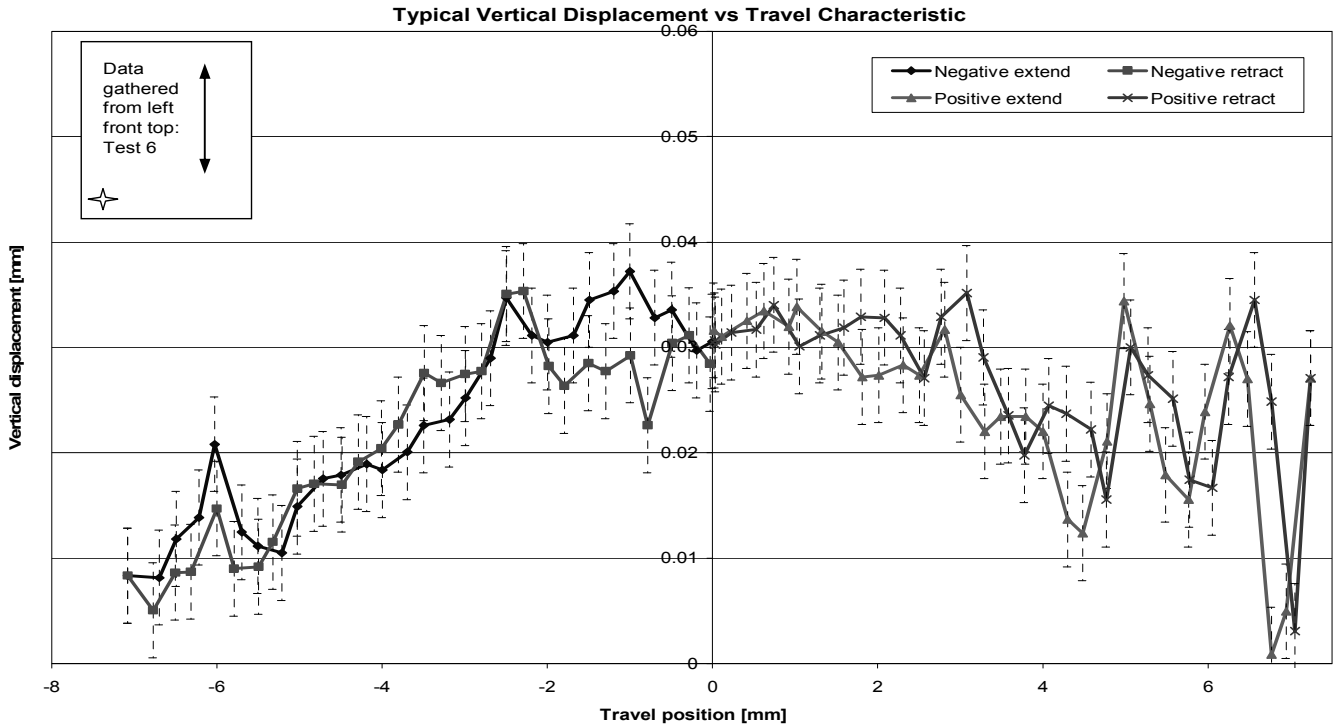

Figure 3.40: Charted results for the Left front capture zone

Figure 3.40 presents the charted data gathered from the left front capture zone. The data was divided and plotted according to the direction the table was moving relative to a reference point set by the CMM. The four lines representing each component of the data series are indicative of the direction the table was being moved during data capture. Each of the four represented measuring zone charts are presented in this way as information to the reader as to the direction of travel for each section of the plotted data.

Perhaps the first observation from Figure 3.40 is the apparent evidence of a measure of hysteresis as the table traverses a full cycle or travel and the curving general trend,

perhaps suggesting a geometric error in the working stage. The plot shows the extend and retract data crossing which suggests that this 'hysteresis' may only be a result of the CMM working very close to its published accuracy limits.

The rippled appearance of the plot in the 'Y' direction is likely caused by influences from the surface finish at the measurement location of the working stage platform. This was shown not to be the case when further test data was processed and a surface roughness test (Figure 3.47) was performed on the upper surface of the working stage (Figure 3.37).

A review of the data showed the maximum displacement value from the working stage neutral position as 37μm. However, the high frequency data spread is contained within a curved band of approximately 10 - 15μm in width.

The general form of the chart is much more difficult to explain in that it is influenced by the construction of the flexure, the travel drive mechanism and by the factors already mentioned above, for example, the surface roughness and the geometric flatness of the working stage platform. These influences will be discussed in section 3.10.

- Left front capture zone – General trend of data

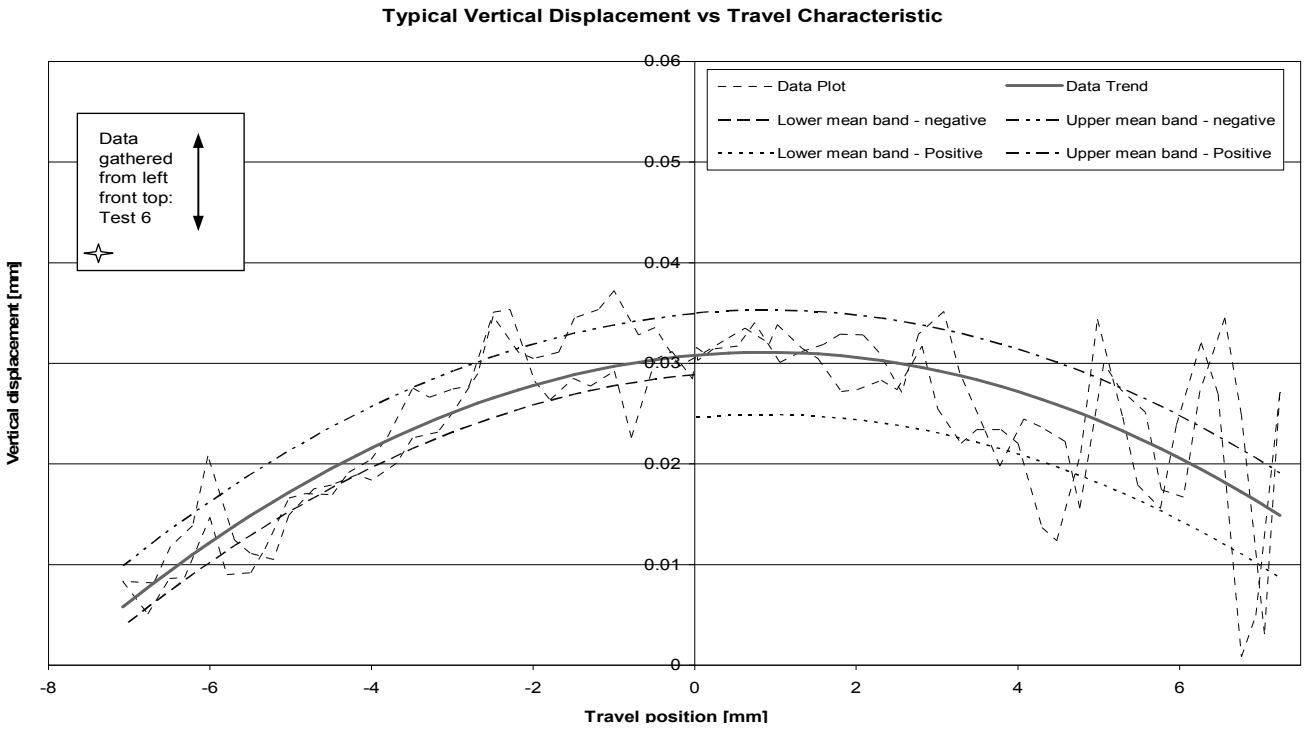

Figure 3.41: Travel characteristic shown as a general trend with upper and lower mean bands

In an attempt to gain an appreciation of the action of the flexure assemblies, a second chart of the data from the left front capture zone was plotted. This chart, Figure 3.41, differed however, from Figure 3.40. Figure 3.40 showed the data from each of the four separate series; extend and retract in both positive and negative directions. Whereas Figure 3.41, showed the data as a single series, represented by the fine dashed line, henceforth identified as the data plot. A trend line was plotted through the data to give an appreciation of the general trend or form of the path travelled by the capture zone as it was probed. This general trend is graphically represented by the curved heavy dark line, described as the data trend.

Table 3.40: Mean band separation distances from the data trend line

Chart line	**Mean band separation value from the data trend line [μm]**
Upper mean band – positive	4
Lower mean band – positive	6
Upper mean band – negative	4
Lower mean band - negative	2

The upper mean band lines were derived and plotted by averaging the data above the data trend line. In the case of the lower mean band line, the data below the data

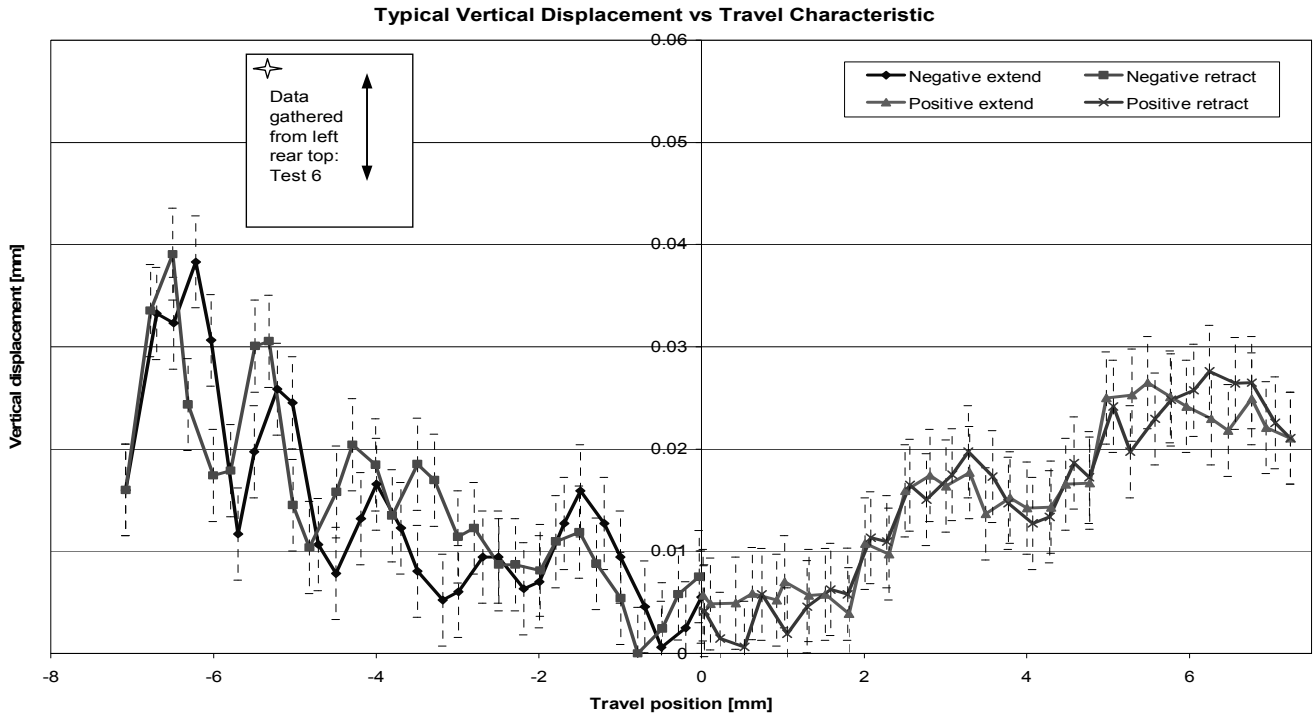

Figure 3.42: Charted results for the Left rear measurement zone

trend line was averaged and plotted. These lines were separated from the data trend line by the differing values presented in Table 3.40. The mean bands were introduced to provide a better appreciation of the general trend or movement of the working stage at the data capture zones by eliminating some of the apparent noise from the data.

Figure 3.41 is presented here showing the trend and the average spread of data on either side of the data trend line. Similar charts have not been presented for the other capture zones, as the general form was similar for all four zones.

- Left rear capture zone

Figure 3.42, the left rear zone, exhibits a plot shape similar to that shown in Figure 3.40 except it is an inverted mirrored image. The maximum range extends to 38μm and the data can be seen to be spread over a wider band. In this particular plot, this dispersion of data points suggests that the range spread is caused by more than the CMM error band (±4.5μm).

- Right rear capture zone

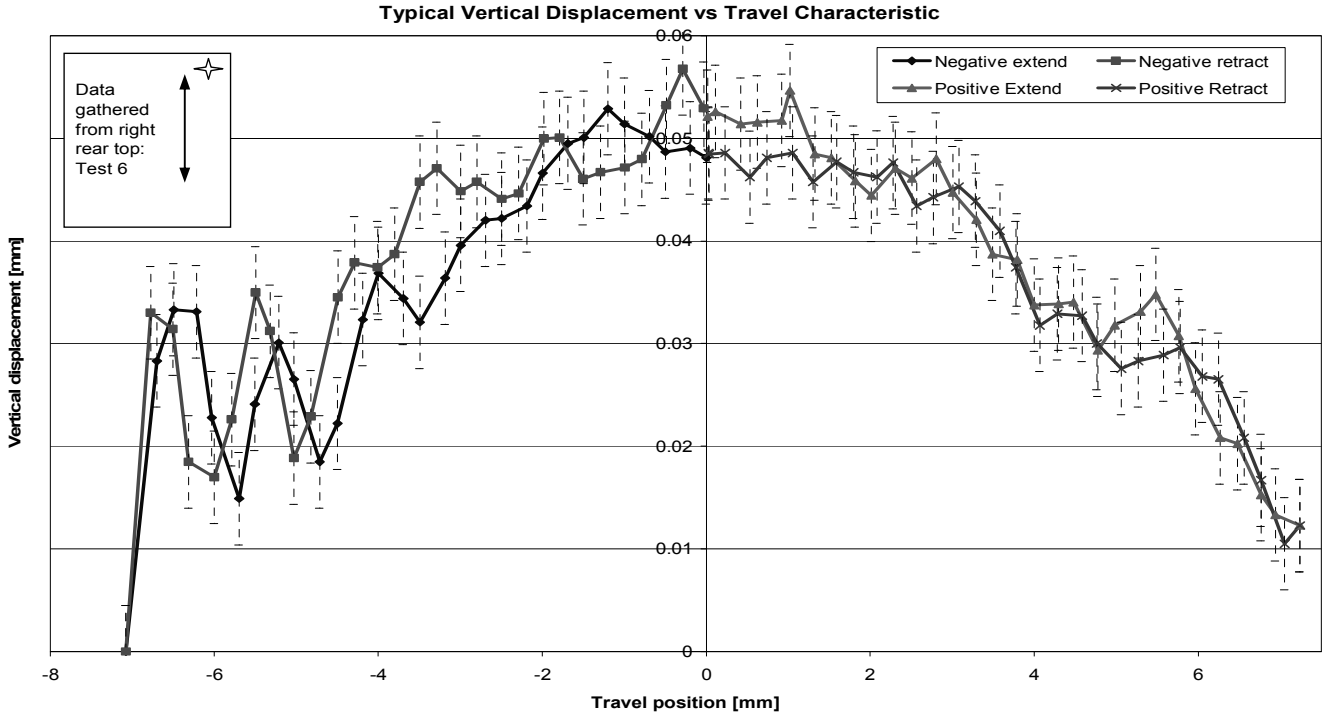

Figure 3.43: Charted results form Right rear measurement zone

Figure 3.43, the right rear zone, exhibits a similar characteristic to Figure 3.40. However, the range is greater, reaching 58μm. Again, there is an apparent hysteresis

shown in the chart. However, the data paths cross over, which would discount the notion that there is hysteresis present. The variation in the data series is within the published range of the CMM as shown by the error bars. The positive travel data appears less dispersed than the negative side data and to this end is possibly reflective of the surface roughness along the probe path. It is difficult to accept that surface roughness is the factor causing this difference as the probe traversed the same path in both directions. The surface roughness effects will be more fully discussed in a subsequent following section.

- Right front capture zone

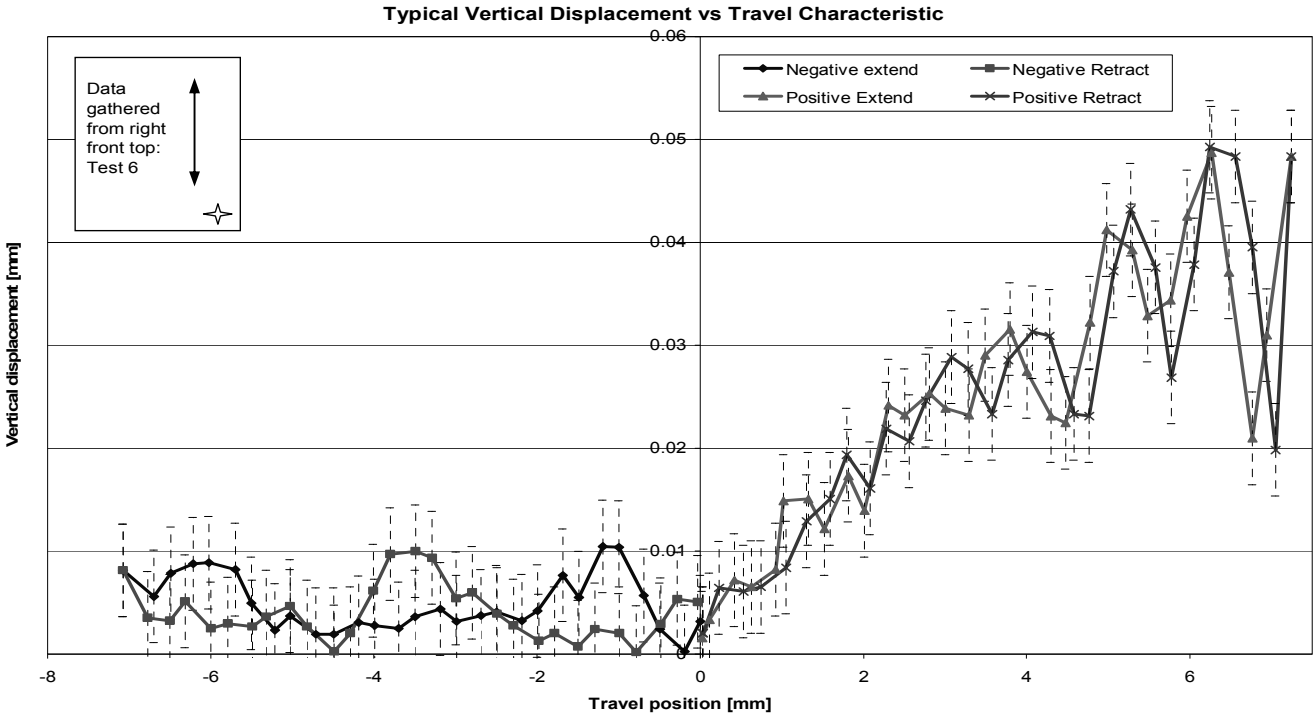

Figure 3.44: Charted results for the Right front measurement zone

Figure 3.44, the right front zone, exhibits characteristic similar to that shown in Figure 3.42. The positive travel data in Figure 3.44 mirrors the negative travel data shown in Figure 3.42. However, the maximum vertical displacement in Figure 3.44 is 49μm compared with the 38μm shown previously in Figure 3.42. The negative travel characteristic is very different from any of the other data series. Here, observation shows that the characteristic is almost flat with a data range spread of approximately 10μm. Although a result such as this was the intended outcome of this project, in this case it is out of character with the other results.

The same apparent hysteresis and characteristic crossing of the data series is still observed in Figure 3.44, although it is less evident when compared to the previous charts.

- Additional results

Test 8 was also performed using a working stage travel position increment of 0.1mm to test for any aliasing in the charted results. This high density data was not used in all the charts presented as the addition of error bars to the plots gave them an extremely overcrowded appearance.

- Working plane centroid – derived result

The data presented for the centroid displacement was calculated by the CMM. Due to the method used by the CMM to determine the centroid position, the results will be influenced by the errors accumulated from each of the capture zones. Four points were probed on the top of the working stage platform from which the CMM formed a plane and hence determined the vertical position of the centroid of the plane. This computation then, was subject to the constraints of the machine's repeatability as well the accuracy capability to measure the plane in 3D space. A reduction in repeatability will influence the derived centroid result, due to the fact that four individual measurements are used to derive the centroid. Each of these four measurements are themselves subject to the repeatability of the CMM. Using a combination of errors

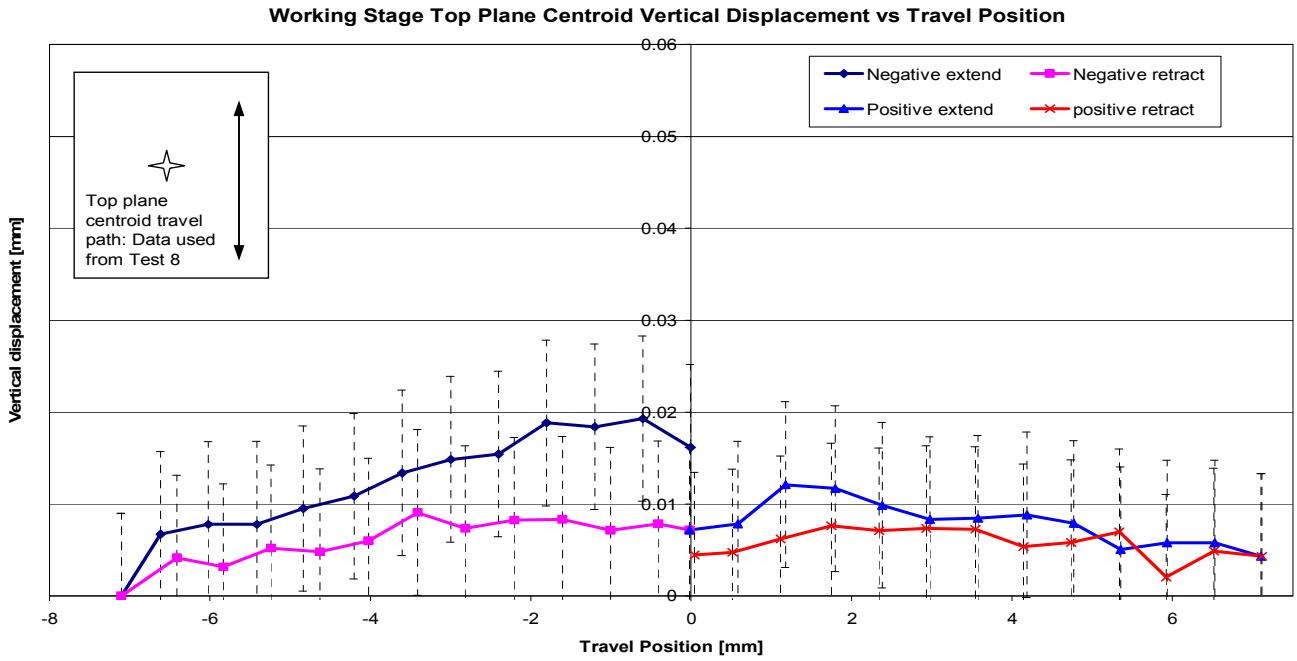

Figure 3.45: Charted results for the top plane centroid

product rule to predict the likely influence of the errors, a value of ±9μm was determined and shown as error bars in Figure 3.45. This result is further discussed in the section 3.10 below.

The results from the working stage top plane centroid shown in Figure 3.45 show the vertical displacement has been held to within an overall range of 19μm. There continues to be a trend characteristic of having 'sagging' ends more in line with the characteristic shown in Figure 3.40 and Figure 3.43. In this plot (Figure 3.45), the tendency for the data series to cross over is not characterised on the negative side and the data is spread in a wider band, falling outside the error bars for approximately half the travel. The positive side continues to follow the trends shown in the previous charts with the data series crossing over and remaining close together, within the limits of the CMM repeatability.

- Testing for aliasing of results

The tests plotted in the previous six figures were captured from the working stage platform by manually incrementing the working stage travel position by 0.4 – 0.6mm per data capture cycle. Initial inspection of the data as it was plotted raised concerns as to the possibility of aliasing being present in the plots. A high density data set was subsequently captured where the travel position was again manually incremented by 0.1 mm per cycle. A dial gauge was used to ensure the manually applied increments

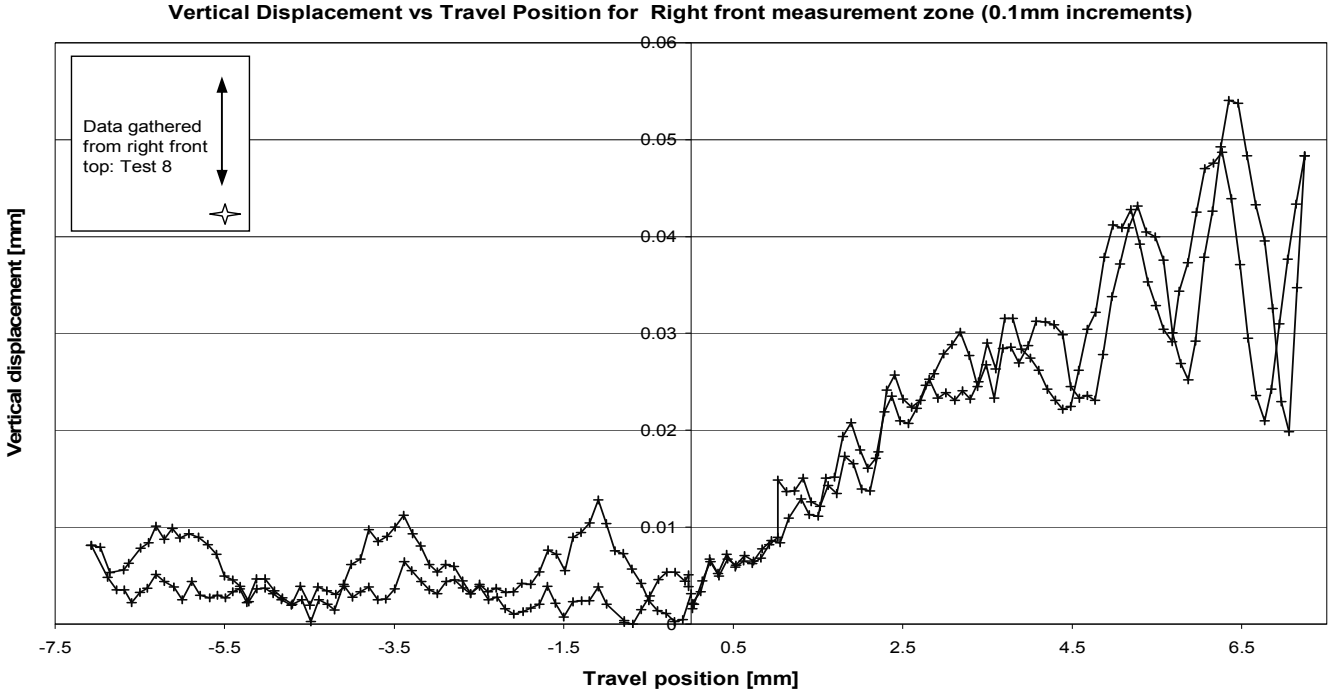

Figure 3.46: Right front displacement result using a travel position increment of 0.1mm

were a consistent 0.1 mm per cycle. These closer increments were applied to ensure the data being captured at the larger increment values was a true representation of the flexure system's vertical displacement (ie no aliasing was influencing the results). Figure 3.46 presents the plotted data from the 0.1mm test cycle. Observation and comparison of the plots in Figure 3.46 and Figure 3.44 confirms there was minimal aliasing. Figure 3.44 therefore, was a reasonable representation of the probe's travel path, and so it was assumed the other charts, Figure 3.40 to Figure 3.43, are also reasonable representations of the results.

Error bars were not added to Figure 3.46 due to the high density of the data points. The addition of error bars would have added significant confusion to the plot rather than any useful information. The error bars can be seen on Figure 3.44, a plot of other data from the same capture zone.

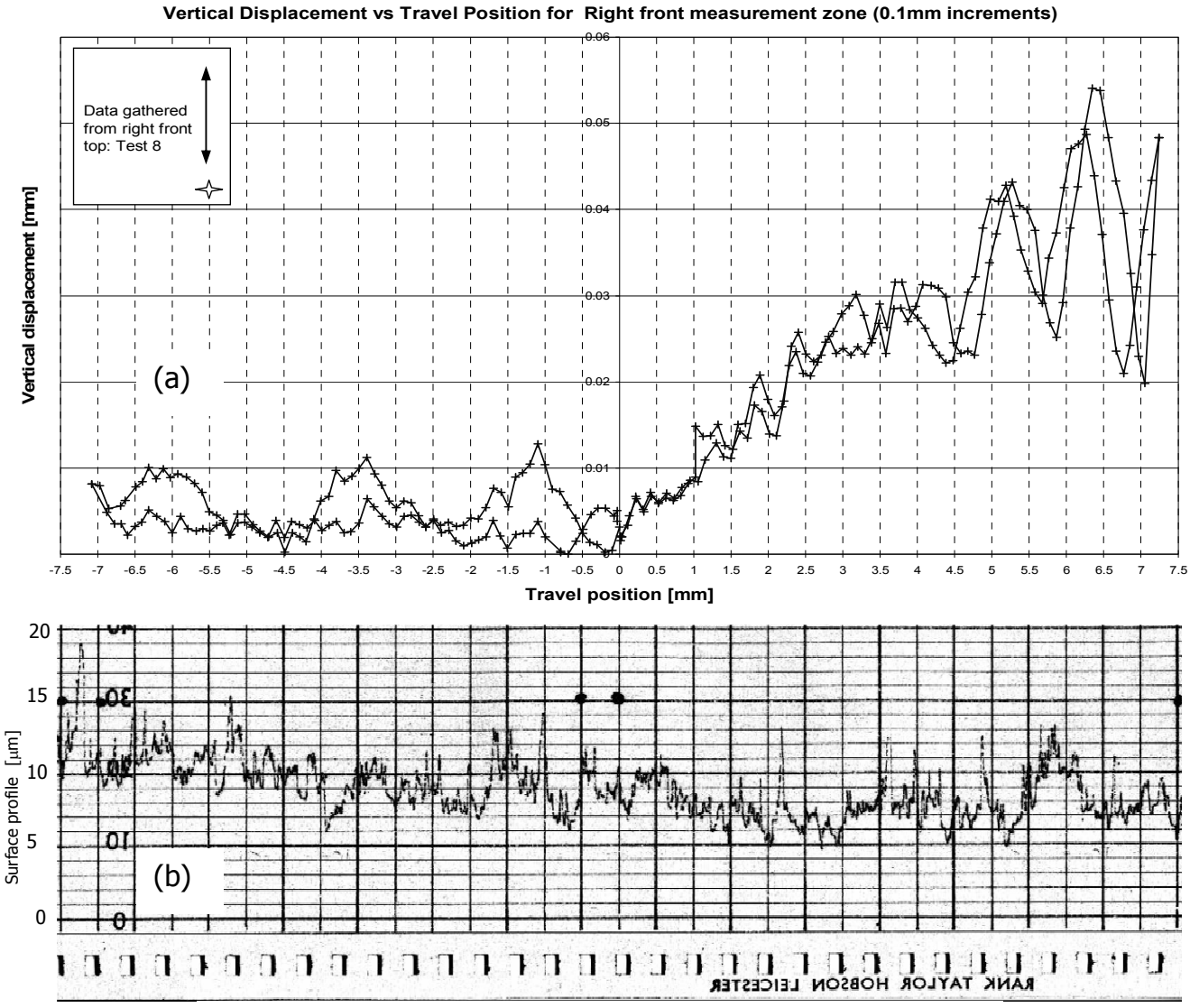

Figure 3.47: Comparison of CMM vertical displacement data (a) with the surface roughness (b) taken from the data capture zone

- Influence from the surface roughness

Figure 3.47 is a comparison of two sets of data captured from the right front top data capture zone of the working stage. Figure 3.47(a) presents the same data as Figure 3.46 with additional x-axis gridlines. These were added to the chart to help clarify the position of data series peaks. Figure 3.47(b) is a copy of the surface roughness chart produced by measuring the surface roughness in the right front top data capture zone using a Taylor Hobson Tallysurf 10 (Manufactured by Rank Taylor Hobson, Leicester, England).

The standard output from the instrument is Roughness Average though a surface profile is output on a tape, which is what has been reproduced in Figure 3.47(b). "Roughness Average (R_a) is defined as the arithmetical average of the departures of the profile above and below the reference line (centre or electrical mean line) throughout the prescribed sampling length[198]." To arrive at the R_a value, a continuous surface profile is measured over a cut off length and a single value is calculated. The single value is not of any significant value here, but the surface profile is of interest as it can be crudely compared with the CMM data for any similarities in the surface profile.

Comparing the two plots reveals that there are peaks and troughs that align reasonably well, but more so, the bulk of the profile plots do not align well. The magnitudes are different but the form remains similar. The main reason for the magnitude difference could very well be attributed to the fact that the CMM is measuring values that are very close to its limit and that there is an inverse effect from the 3.0mm diameter ball end on the CMM probe. This along with the dynamic influences found to affect the results, is further discussed in the discussion section following.

Figure 3.47(b) is reversed to align the charts above (Figure 3.47(a)) and the vertical gridlines are spaced to represent 0.5mm, which also aligns with the chart above. The horizontal gridlines are spaced such that they represent 1.0μm. Both figures represent the total travel of the working stage, which was limited to approximately ±7.0mm.

The travel limitation was placed on the flexure system when the decision was made to switch the flexure material from the designated titanium blades to a more commonly

available material, 1095 H&T spring steel. The spring steel was able to provide almost the same flexibility as the titanium. However, there was some risk of overstrain occurring in the blades and so the total displacement was reduced to minimise any overstraining risk.

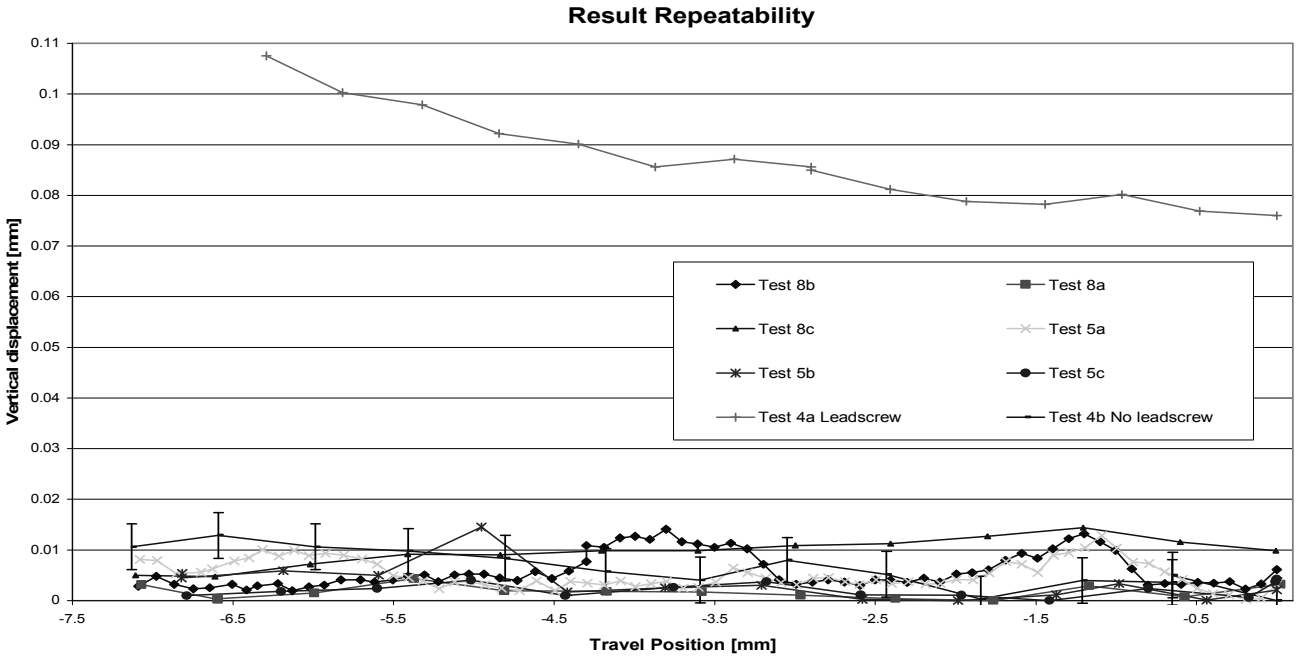

Figure 3.48: Repeatability of test data

- Repeatability of results

The chart presented in Figure 3.48, shows each data series partially, and where applicable, the multiple runs from each, are plotted on a single axis. The presented data series have been truncated with only the negative component of their travel plotted. This form of presentation provides the finest detail on the x axis. Comparison of the data, as it was captured, and plotted in Figure 3.48 demonstrated a fair facsimile of the data spread generally and so is included here to demonstrate the repeatability of the test procedure and flexure system itself.

From observation of the chart, it can be seen that there was slight variation in the data captured. The data was contained in a band spread to a maximum of 16μm. The spread in the data series appears to have been caused, to some extent, by the use or non use of lubrication on the displacement screws. Test 4b was performed with no lubrication between the head of the dome nut and the edge of the working stage upon which it was bearing. Subsequent tests were lubricated with grease applied to the contact patch between the head of the dome nut and the working stage contact point.

Test 8 also suffered from diminished lubrication during the test, which has caused a slight spread in the data series. This demonstrates to some extent the system's sensitivity to the position of the drive point on the working stage; however, the data was still bunched tightly. The data spread also requires consideration in terms of the CMM accuracy and to this end, error bars have been applied to a single data series. However, error bars on all series were omitted from the chart, as it made the chart very busy and confusing to interpret.

The data series, Test 4a Leadscrew was included with these results to give the reader an appreciation of the gains made with the relocation of the leadscrew drive point, and hence its influence on the vertical displacement outcome.

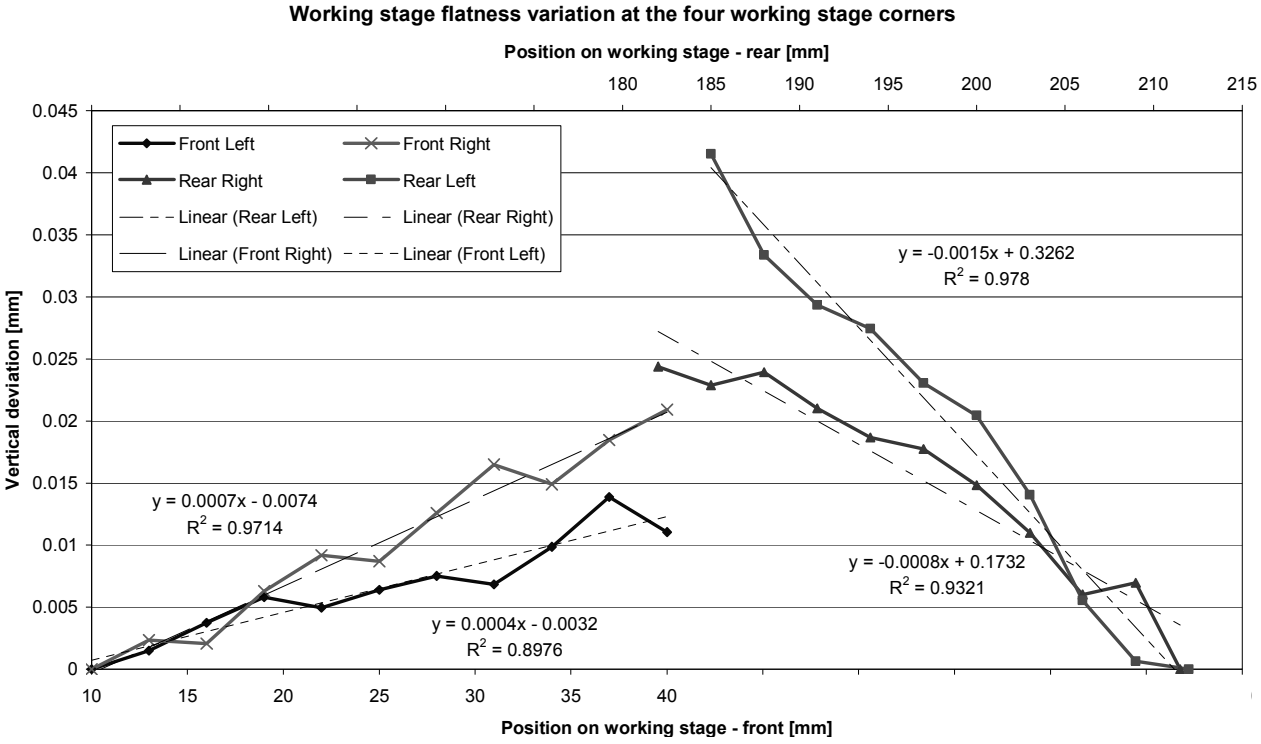

Figure 3.49: Working stage flatness assessment in the data capture zones

- Working stage capture zone flatness

A final check was made to the working stage flatness at the data capture zones. Using the CMM, a plane was set up through the corners of the working stage at the capture zones. Using this plane as a reference, the probe path followed during the displacement sequences was again tracked. Normalised data was plotted in Figure 3.49 to give an indication of the data capture zones' flatness relative to each other whilst using the reference plane as an absolute position. The chart shows that the corners all "hang down" by varying degrees. The rear left zone shows the greatest

variation (42μm) over a 30 mm travel length from the flexure assembly attachment point towards the rear end of the working stage. The front right data capture zone shows a variation of 21μm over a 30mm cut-off length from the flexure assembly attachment point towards the front edge of the working stage. These sloping surfaces will have an effect on the vertical displacement results. As the working stage was traversed in the original test procedure, the probe position remained fixed in an 'x' and 'y' location. Determining the effectiveness of the flexure table system may have been somewhat compromised when the flatness profiles were considered. In this case, the probe would appear to be moving 'virtually' up or down the slope as the working stage was traversed through a travel cycle.

The trend lines were added to each of the curves in the chart (Figure 3.49) in an attempt to quantify the influence the zone slopes will have had on the overall result. The trend line equations were used to assess the vertical influence magnitude at each probe position and thus add to or subtract from the values in the data retrieved in the main data capture series.

3.10 Discussion of results

The results presented in the above section demonstrate that there is some further work in the design of the flexure system to be completed to bring the performance into the range required by the design specification requirement. This said, the presented results represent only the flexure system performance in the vertical direction. The yaw characteristics of the table have yet to be considered and tested which will be the subject of a future project. At this stage in the development, only the vertical displacement characteristics are reported and discussed below.

An important entry point into this discussion is the CMM and its repeatability. As mentioned earlier the published repeatability of the CMM is ±4.5μm. The manufacturer of the machine does not publish any accuracy figures only the repeatability. The design requirement specification for the machine tool called for a repeatability tolerance band of 3 -5μm, which was specified by the IC manufacturer. A comparison of the design specification requirement and the CMM's published repeatability shows the CMM to be operating very close to its limit. Usual high precision metrology applications call for equipment with a capability of measuring ten times higher precision than the smallest tolerance being measured. Unfortunately, in

this case, the higher precision equipment was not available, therefore the Mechanical Engineering department's CMM was used, with its limitations being noted and accepted. All of the data capture zone charts have had error bars applied and in many cases, this shows the overlap of the CMM's output. These results initially indicate the relative success of the mechanism. However, there are components of the results that require discussion and this will be reported in the following arguments.

Table 3.41: Summary of data from the charts presented in Figure 3.40 - Figure 3.45

Figure	Approx. Curve shape	Maximum value [mm]	Average data band width [mm]	
			Negative travel	Positive travel
Figure 3.40	Inverted parabolic	0.037	0.006	0.010
Figure 3.42	parabolic	0.038	0.006	0.013
Figure 3.43	Inverted parabolic	0.058	0.007	0.020
Figure 3.44	Flattened parabolic	0.049	0.003	0.019
Figure 3.45	Flat	0.019	0.006	0.003

Table 3.41 is a summary of the pertinent values and features on the charts presented in Figure 3.40 to Figure 3.45. Although the curved trend shape implied by the data in the charts may be just that, curved, the word parabolic is used to give the reader a better perception of the shape portrayed. The parabolic nature was a most disconcerting aspect of the charted flexure system performance results in that a flatter response was expected.

These parabolic results were somewhat offset by the flattened nature of the combined centroid data shown in Figure 3.45. The centroid data outcome is more representative of the desired project result. However, the spread of the data is somewhat larger in magnitude than expected. This may be attributed to either, firstly, the additional effects of the CMM derived result or secondly, multiple influences acting on the flexure system during its displacement cycle or during manufacture and assembly. These two items are discussed below:

Firstly, the published repeatability of the CMM is ±4.5μm as discussed earlier and is applicable to each probe touch in the z axis of the CMM. The derived centroid result is

determined from four probe contacts and as such, each is subject to the ±4.5μm tolerance. A combination of errors product rule was used to determine the overall effect on the derived result.

The centroid was found to be affected by a product error of magnitude ±9μm. This product error, when applied to the derived results, shows the data to be predominately within the error band generated. Given the data has maximum band width of 19μm and that the measurement scope is close to the limit of the CMM, this result requires further investigation with a more accurate means of measurement.

Secondly, the multiple influences affecting the output performance of the flexure system are likely to be:

- manufacturing inconsistencies/variances
- material inconsistencies/variances
- manufacturing induced assembly variations
- the working stage drive design and position
- the final shape of the surfaces upon which the CMM probe was acting; surface roughness and flatness
- the accuracy of the CMM itself

Initial review of the data showed an oscillation present (with wavelength of order 1.0mm) in the data plots. The oscillations can be seen in Figure 3.40 to Figure 3.44. There are portions of the data lines in each of the figures where the oscillations are less severe. Hence, a possible explanation as to the cause for these high frequency oscillations may have been the CMM responding to the surface texture of the working stage along the probe path.

To this end, a surface profile test was performed along each data capture zone probe path, using a cut-off length of 30mm. A result showing the surface profile of one such test (right front data capture zone) was included in Figure 3.47(b). These results show a high frequency component in the surface roughness machine's output. Careful observation shows this high frequency surface profile not to be consistent with the CMM produced profile. There are two portions, which appear to coincide; however, over the balance of the data it is difficult to correlate any other significant features.

Data from the CMM shows the wavelength of the high frequency component to be reasonably widely spaced (of the order of 1.0mm). In observing this spacing, a misalignment of the Tallysurf data with the CMM data would distort the comparative analysis considerably, making any possible correlation subject to suspicion with regard to its accuracy. Any such relative axial shifting of the plots reveals no improvement in direct correlation of the data forms: No significant correlation is evident.

The surface roughness profile data captured by the CMM is subject to the intermittent contact of the probe and thus aliasing will occur in the results. This aliasing is absent from the surface roughness test as the probe is in continuous contact over the cut-off length. A further softening of the CMM data is caused by the use of a 3.0mm diameter ball on the end of the probe and hence it was not able to demonstrate similar surface roughness characteristics.

A major difference between the surface roughness testing and the CMM data capture was the method in which the tests were performed. The surface roughness test was performed by the Tallysurf, which dynamically passes a probe over the surface being measured. Hence, the working stage was static and the measuring device was moving. With the CMM process, the working stage was displaced by a prescribed increment between each CMM probe point touch. Consequently, that data was subject to the kinematic influences applied to the working stage during each increment in its travel position.

Though given the narrow band (approximately 8μm) of the surface roughness profile (Figure 3.47(b)) it is highly unlikely that the surface roughness has caused the high frequency oscillations seen in the CMM results when using a 3.0mm stylus (ball end), Figure 3.40 - Figure 3.44.

It is worth noting that due to the sag on the ends of the working stage, the Tallysurf probe was slope corrected to ensure it stayed within its range capability. This correction has caused an apparent near linear trend in the output data. A characteristic of data recorded by such a device.

Given all the variations and influences, discussed above, there was not any practical or majorly useful information or understanding of the surface roughness effect on the rectilinear result to be gained.

With the failure of the surface roughness examination to elucidate the reason for the high frequency oscillations, an alternate explanation was sought. Closer examination of the plotted charts showed a distinct pattern in the oscillations. For example, the two front capture zones had oscillations in the positive travel zone, whilst the two rear zones were in the negative travel zone. Also, inspection of the oscillation's pitch indicated a value of approximately 1.25mm; coincidently the pitch of the thread on the M8 screw actuators.

Table 3.42: Position of large magnitude oscillation with respect to screw actuator position

Figure	Large magnitude oscillation position relative to x axis	Working table direction of travel	Screw actuator position on flexure assembly
Figure 3.40	positive	positive	front
Figure 3.42	negative	negative	rear
Figure 3.43	negative	negative	rear
Figure 3.44	positive	positive	front

Table 3.42 summarises the position of the higher magnitude oscillations with respect to the x axis, the working table direction of travel and the location of the screw actuator used to displace the working stage through a travel cycle. From the table one may observe that the oscillations are adjacent to the screw actuators, depending on the direction of travel. Using Figure 3.40 as an example, the large magnitude oscillations are above the positive x axis, the working table travel direction is positive (front to rear) and the actuator is operating on the front working stage cross member (Figure 3.38), which is very slender.

The influence from the actuating screw and dome nut acting on the cross member was sufficient to distort the working stage both in plane (in the direction of the screw actuator axis) and out of plane (vertically, perpendicular to the screw actuator axis). It is believed that the out of plane distortion is causing the working stage output oscillations. This is evidenced by the increasing magnitude of the oscillations with increasing spring force from the flexure blades as the travel position increases. It has

been assumed that the dome nut contact point is not concentric with the centreline of the thread on the actuator (normal mass production tolerances in effect). This will cause the contact point on the dome nut to 'gyrate' on its axis influencing the working stage output at the thread pitch frequency. With increasing spring force, the contact point load is higher, and thus the tendency to influence the working stage surface position vertically, increases.

Again using Figure 3.40 as the example, there is none of the characteristic oscillation seen for the negative travel. This occurs because there is no influence from the screw actuator on the front end of the working stage during this part of the travel cycle. In fact, the actuation screw is operating on the rear end cross member, influencing the output in both the left and right rear capture zones as observed in Figure 3.42 and Figure 3.43. So where there is no drive actuator contact there is no influence and the data appears much smoother.

The structural stiffness of the working stage appears to play a major role in the actuation screw's influence by allowing it to displace vertically under the affect of the drive's eccentricity.

- Structural stiffness

A major influence on the output was the lack of structural stiffness in both the working stage and the supporting structure. This was exacerbated by the extra stiffness of the latterly adopted spring steel flexure blades, which were considerably stiffer than the titanium blades. The higher modulus of elasticity of the spring steel, which is approximately twice that of the titanium, was responsible for increased forces being applied to the structure during the displacement cycle, as the physical dimensions remained unchanged from the original design. These increased forces caused the working stage to distort, particularly when the leadscrew drive was in its original offset position.

The chart (Figure 3.48) showing repeatability has one data series included from the tests performed with the leadscrew in its originally designed position (Test 4a). The negative effect of the leadscrew on the rectilinearity of the flexure table system was profound, as evidenced by the outlying curve. The original location had the leadscrew offset from the working stage by approximately 40mm, which produced a moment

load on the working stage. As already discussed, the flexure structure was less rigid than it should have been and as such, this applied moment induced considerable bending forces in the structure. These forces were compounded by the stiffer steel blades. Observation of Figure 3.48 shows that data series 4a starting almost 60μm above the non leadscrew drive data. This apparent step in the starting point has occurred due to the normalisation process: The extreme end of the positive side of the chart (not shown) is where the zero point occurs (travel position +7.5mm). So taking the curve as it is presented a continued rise in vertical shift may be observed with further displacement; increasing to nearly 110μm at the -7.5mm end of the travel. Hence, (in the full chart -7.5mm to +7.5mm) the observed change in the data trend magnitude, between the leadscrew drive and the alternate drive, was justification enough to make the change away from the eccentric leadscrew position.

Analysis of earlier data indicated the moment from the leadscrew was most likely causing a problem and the need to move it became paramount. Changing the drive position removed the bending moment caused by the offset leadscrew, but replaced it with direct bending of the working stage edge members (Figure 3.35). There was a remaining influence caused by the working stage displacement drive, which was shown by a lack of lubrication on the screw drive/working stage contact point when testing. Data recorded using the new drive, showed a marked improvement in the performance of the system and so the results achieved with this drive configuration were retained. The influence of the drive and finding a solution negating any of its effects has been left to a future project.

- Working stage geometric flatness

The influence on the output results of the working stage geometric flatness was considered by measuring the form of the working stage at the data capture zones. Figure 3.49 shows the plotted profile of the capture zones and the magnitude of the variation from flat. Consideration of the figure shows that all the zones tend to "hang down" towards their extremities. The normalised data, which is presented in Figure 3.49, was extracted from each of the capture zones individually along the lines that the probe traced when travel position data was being measured. The geometric flatness range covered 30mm from a point approximately 10mm from the front and rear edges of the working stage.

A further consideration relating to the geometric flatness was the method by which the working stage was measured and how this influenced the results. The working stage was static in this case and the probe traversed the cut-off length. When the displacement data was being captured, the working stage was moving and the probe was static. This gave the effect of the probe "moving" vertically as it traversed the data capture zone. As the working stage was displaced horizontally, the 'sagging' ends would cause the probe to travel further to make contact with the working stage surface.

Table 3.43 summarises the data from Figure 3.49 showing the maximum deviation and direction of the slope in each capture zone. With the normalised data plotted, a trend line was added to each data series in an attempt to quantify the influence on the rectilinear travel. Trend line equations, relating to each line slope, were then used to calculate the sloping corner influence on the working stage rectilinear performance.

Although the flatness data was retrieved from a 30mm range, the actual platform travel movement was confined to approximately 14mm (or approximately ±7.0mm) within this range.

Table 3.43: Maximum flatness deviation of the working stage

Zone designation	Maximum vertical form deviation [mm]	Influence of form deviation [μm/mm]	Slope direction
Left front top	0.014	0.4	positive
Right front top	0.021	0.7	positive
Right rear top	0.024	-0.8	negative
Left rear top	0.042	-1.5	negative

The influence of the slope on each respective corner is shown in Table 3.43 in the column labelled, "Influence of form deviation." Trend line representation values are presented showing the magnitude of influence each corner slope had in terms of vertical shift per mm of cut-off length (Trend line gradients). These values equated (using the trend line equations) to a maximum value of approximately 10μm vertical variation over the travel range of 14 mm (or ±5μm for ±7.0mm of travel) in the case of the right front capture zone (Figure 3.46). Observation showed little significant difference was made when any correction values were applied to the plotted data

shape or spread. With these correction values applied, their effect was minimal. However, if they were considered their effect was somewhat positive.

From the above discussion, the assumption was drawn that the use of the 'static' position probe with the CMM was little influenced by the sloping end zones on the working stage. In isolation, the error of approximately 5μm per 7mm of travel was considered insignificant in the overall magnitude of the vertical deviations at right front capture zone. Errors of similar magnitude were found for each of the capture zones.

- Flexure assembly alignment

Another influence on the response of the flexure system was the alignment of the individual flexure assemblies relative to the direction of travel. The rectilinear properties of the flexure assemblies require that they are aligned 'perfectly' with the direction of travel. If the directions of travel of the table assembly and the flexure assemblies are not all parallel to each other then the working stage will distort as each of the flexure assemblies attempts to move the table in its own aligned direction. This will create a vertical drift at each corner of the working stage. To this end, the system was assembled with care to ensure the required parallelism was achieved within the practical limits of the manufacturing and assembly facilities at hand.

Up to this point in the discussion, only those issues that were noted to have a minor influence on the output have been discussed. The following paragraphs discuss those influences that were noted to have a major effect on the system output in terms of data spread and the curve shapes of the charts previously presented.

- Blade balance

Perhaps the most probable explanation of the parabolic variation in the movement of the working stage is the imbalance in the deflection of the blade pairs relative to each other within each of the tandem flexure assemblies. Rectilinear displacement relies on the harmony between the two blade pairs within each flexure assembly, balancing each other as the curve in the blades form, and their effective lengths reduce. An equalising effect ensues as the reduction in length occurs in opposite vertical directions (relative to the working stage top) for each stage blade pair, in each of the four flexure assemblies. Such a configuration neutralises the blade reduction effect, theoretically giving true rectilinear movement. There are known to be influences that

affect this output negatively. Jones[93] published research on the compound flexure assembly, (used as one per corner of the working stage in this work) whereby he applied small clamps to the flexures (Figure 3.32(b) to correct the bending rate (maladjusted by various influences) and thus improve the flexure system's performance. Although this adjustment method was known for single flexure assemblies, the influence of multiple assemblies used in the configuration here was not known. It is recognised that the ideal system requires balance, consistency and harmony across quad compound flexure assemblies to perform rectilinearly. It is pertinent here to discuss the output results in light of the obvious influences and set aside those less well known as later discussion. This effect is brought about by the distinct influences, discussed below.

- Hinge thickness and stiffness

Possibly the most obvious influence would be the variations in the physical characteristics of the hinges themselves. If for example, hinge thickness varies due to the allowable material manufacturing tolerance from pair to pair, then the pairs (intermediate stage and working stage) will displace at different rates (Referring back to Figure 3.34 will refresh the reader's memory with regard to the naming convention for the flexure assembly components.) As the system requires equal displacement rates of each stage to provide the required performance, any imbalance that occurs between tandem flexure assembly blade pairs (stages) will cause the working stage to raise or lower vertically, dependent on which pair has the reduced displacement. This action will give a parabolic like shape to the output data.

In a similar manner, the hinge stiffness is dependent on the consistency of the heat treatment process, which will give impaired results comparable to those caused by variations in hinge thickness. The heat treatment process is used to alter the characteristics of the steel sheet to meet the spring specification requirements of the desired grade of spring steel. This process, although finely controlled will have small variations in the temper distributed across the sheet (exacerbated by thinner sheet sections).

Whilst, these thickness or heat treatment variations are very small, only minimal disparity in the hinges is required to cause the tandem flexure arrangement to be unbalanced in its travel. For example, using one of Hatheway's equations [71] to

calculate the vertical shift in the intermediate stage; a difference of 0.1mm in the travel direction displacement between the stage pairs will make a vertical displacement difference of 14μm; a difference of 0.5mm will cause a variance of approximately 70μm.

- Hatheway effects

As discussed in an earlier section above Hatheway's equations relate to beams being displaced with small displacements where the locus of the end of the blade appears to rotate about a centre point approximately two thirds of the way from the free end towards the fixed end[199]. This is a fundamental assumption relating to beam bending theory. The use of Hatheway's equations becomes limited when the displacement exceeds the 'small displacement' assumption. It was however useful to use these equations to give a measure of expected error magnitude related to the manufacturing inconsistencies based on the applied manufacturing tolerances. It is acknowledged that the deflection level required in this project takes the beams into realms whereby the equations lose their accuracy and robustness.

Further to this, the Hatheway effects due to the manufacturing tolerance variations have been discounted as insignificant. Observation of the results in Table 3.30 shows that the effect of the allowed manufacturing tolerances is very small. As such, their influence on the output results will be minimal, given the magnitude in the variations of the output results from pure rectilinear motion. As the Hatheway effects relate only to a single small displacement flexure pair in previous studies, the influence of these effects on multiple compound flexures of high displacement will require further investigation using measuring equipment with sufficient accuracy to map the influences. This may form the subject of a future project.

An interesting result was the positive effect on the rectilinear output gained when the working stage drive screw was moved from its original location to a position where it was bearing directly on the end of the working stage (Figure 3.38). This should not have been the case based on Hatheway's findings as the drive was moved away from the geometric and kinetic centres of the flexure blades.

A possible likely explanation was already broached earlier; the working stage structural stiffness was insufficient to resist the applied loads imposed by the more stiff blades.

The section of the working stage on which the drive screws bore was a long thin slender beam at either end of the stage. This beam was loaded transversely at its lengthwise centre. Observation of the results, Figure 3.40 to Figure 3.44 shows a large oscillation on one end of the chart only. The reason it appears on one end only is because the drive screw at a particular end influences the results on one side of centre only. The off end is completely free of any direct influence from the drive screw. To some extent this confirms the hypothesis that the working stage is structurally insufficient to resist the applied loads, an oversight in the switch from titanium to spring steel blades.

- System self compensation

One of the primary reasons for the final design configuration was the desire to use the system itself for possible self compensation of any of the flexure errors. Positioning the flexure assemblies to minimise the effects of assembly on flexure sub assemblies was critical. The behaviour of the individual sub assemblies was unknown specifically, but using a stiff working stage, the notion of self compensation was considered and hence the four subassemblies were positioned in the structure as shown in Figure 3.34.

A higher performance of the working stage at the centroidal position compared to the four corners was realised by the tested design configuration. This was achieved in that the vertical displacement shown by the working stage centroid overall was less than half that shown by the individual flexures. The curved shapes of the data plotted from the four corners of the working stages are shown in Figure 3.40 to Figure 3.44 and the enhanced performance of the working stage centroid can be observed in Figure 3.45, which is distinctly flatter.

The 'hop' in the data where it fails to rejoin at the neutral travel position is at this point unexplainable, although it is suspected to be a compounded or stacked CMM error to some extent.

An interesting observation is the similarity of diagonally opposite pairs in the results (viz. Figure 3.40 and Figure 3.43, viz. Figure 3.42 and Figure 3.44). This suggests there is a measure of cross coupling being played out in the working stage as it is traversed through its travel cycle. The net effect of the cross coupling is to influence

the flexures to partially neutralise each other to give the flat result of Figure 3.45. However, given all of the effects discussed above it is difficult to determine the exact nature of any working stage cross coupling. It may be caused by the flexural function, or by the lack of stiffness of the working stage, or there may influences not yet conceived.

The basis of the comment on cross coupling comes in the main from observations of the similar data band characteristics as discussed above. Though the curves are similar, the various magnitudes vary considerably. For example, comparing the results from Figure 3.40 with Figure 3.43, observation shows that the maximum values are 37μm and 58μm respectively. Another similarity is the mirroring of the data about the x axis, such that the positive end of Figure 3.40 is similar in form to that negative end of Figure 3.43. Similar characteristics can be found on the figures from the other pair, though Figure 3.44 is considerably flatter on the negative side than Figure 3.42 on the positive side of the x axis. Again, the characteristics at the other end are very similar, with a relatively high magnitude widely spaced oscillation shown.

An explanation as to the possible cause of the relatively high magnitude widely spaced oscillation is that there is mechanical interference occurring in the flexure assemblies. This was not observable at the time of the tests and did not appear to be a factor then. The flexures were crudely deflected individually at various times to test for any interference; none was encountered. However, having more fully considered the results of the testing, which has shown the balance between the pairs of flexure blades to be extremely sensitive, some interference or mechanical resistance may have been encountered. Further investigations of the deflected flexures will be required to confirm if this type of interaction has occurred.

- Manufacturability

A major goal of the project was to obviate the requirement for controlled assembly of the flexure components. The components were manufactured according to the design and tolerances required in the drawings, and assembled randomly from the cache of machined components. No attempt was made to select any of the components except in the order required for assembly.

The results attained were very good when the possible conclusions were considered. These possible outcomes were based on the information gleaned from publications such as those by Jones and Hatheway et al, which suggested that random assembly did not produce a good result. Their work was mainly related to displacements that remained within the beam theory parameters, ie small displacements, though Jones has published results relating to displacements up to approximately 10.0mm travel[152]. Published research mainly considered single tandem flexure assemblies (Figure 3.32), rather than multiple assemblies such as this project utilises (Figure 3.34). From the results, especially the centroid result, it is obvious that there is a major interaction and balancing or cross coupling effect exerted on all the flexure assemblies by each other.

In the preceding paragraphs cross coupling has been discussed, but it is the considered opinion of the author that the cross coupling or interaction effects on the flexures has a wider reaching result on the entire system. By this, it appears that the system as a whole will tend to minimise the effects of many of the influences discussed in the above section. This effect is also endorsed by the results shown in Figure 3.45.

Alternatively, it is in fact, the stacked effect of all of the above discussed influences, each having their own input into the system, that produced the measured results. Although outside the scope of this report, a Pareto analysis of the contributing errors and influences could be performed to prioritise those influences that produced the largest affect on the system. Further to this case, additional work is required in the fields of both design and metrology to isolate and minimise these negative influences.

With the metrology, a higher resolution measuring device is required to isolate some of the issues raised above, and thought given to careful redesign is required to remove or minimise the design shortfalls.

3.11 Dynamic considerations:

The work reported herein mainly encompasses the design and prototypical performance for a single axis work stage. The original design and the design requirement specification called for a multi-axis machine table, however in proving the concept use of multiple tandem flexure assemblies, the table was simplified to a single axis. A full dynamic consideration of the table system will be extremely complex and may represent a PhD study of its own at a later point in the design

development. Nevertheless, for the sake of completeness it is pertinent to consider some of the major dynamic issues that may arise when the drive and the second axis are configured into the design.

3.11.1 Leadscrew

The application of a leadscrew to the working stage will be a complex and critical process, as it must be applied in a manner that will reduce any adverse influence on the rectilinearity of the system. As seen from the Hatheway equations discussed in previous sections, application of the leadscrew has dynamic implications that must not be allowed to influence the overall performance of the table. Application of the leadscrew requires that all forces exerted must pass through the kinetic centre of the flexure system. Any force applied other than through the kinetic centre also requires the application of a moment equal to the product of the applied force and the offset distance[200]. These extraneous forces must be minimised to reduce their adverse influence on the rectilinear output of the table system.

A further point to consider at a conceptual level; the leadscrew will form a rigid link between the working stage and the base. This implies that all the forces induced on the working stage and acting parallel to the leadscrew will be transferred to the base directly rather than any other part of the flexure system acting to resist them. In theory this will prevent any system induced vibration in the working stage, providing the overall stage stiffness is also sufficient to transfer the travel induced forces from the flexures to the leadscrew.

3.11.2 Cutter induced forces

The possible effects of the forces induced by the cutting action are at this point to be considered minimal when compared to the likely interaction caused by the acceleration/deceleration of the working stage itself. The orthogonal feed forces (Table 4.19 and Table 4.20) applied by the cutter through the workpiece are all less than 3.5N. For the 3.5N force and assuming a conservative acceleration of 1g, a mass equivalent to this force would be 0.36 kg. It is highly unlikely that the working stages and card holding fixture could be designed such that the total mass in translation is less than or equal to 0.36 kg when the drive components are considered. The table system will have substantially more mass, perhaps 1 – 1.5 kg, giving acceleration forces of approximately 10 – 15N. The bulk of the additional

mass will be added in an effort to ensure the system is stiff and sufficiently robust. This mass would still be substantially less than equivalent conventional dovetail slides suitable for the proposed machine tool.

A second consideration arising from the cutting action is vibration. The cutter is required to operate in excess of 30 000 rpm using a multi-fluted tool. The frequency of the cutter pulse would at a minimum be 60 kHz and up to 120 kHz using a 4 fluted cutter. This frequency range is well beyond what the natural frequency of the system is expected to be.

3.11.3 Second axis

A three axis milling machine by necessity demands that one of the axes is carried by another. The third axis may be independently mounted and used to drive the spindle in the third direction. Therefore, at a conceptual level, the X and Y axes may be grouped together so that the X axis working stage is carried by the Y axis working stage, giving horizontal orthogonal motion relative to the tool, which being carried in the Z axis, is perpendicular to X and Y (Figure 3.2). This combination of axes, then requires the design of the Y axis to be sufficiently substantial to operate beneath and support the combined weight of the X axis working stage and the workpiece fixtures.

Although the single stage design had the traverse direction parallel to the leadscrew, which can be sized sufficiently to form a near rigid link between the working stage and the base, the two axis design will apply loads that are perpendicular (equivalent to force P in Figure 3.30) to the leadscrew and must be resisted by the flexure blades themselves. Section 3.6.1 discusses the complexities of loading the blades parallel to their width. Suffice it to say, that when the second axis is added, the blades carrying the heavier loads will require careful design consideration to achieve a configuration and strength that will support the loads imposed by the machine table acceleration. The dynamic response to the system becomes increasingly complex when the blades are deflected or displaced as shown in Figure 3.31 and may be the basis for a further study outside this PhD research.

At the point to which the prototype was completed, the response of the hinges in this project had only been considered statically in regard to their maximum applied

loads. The design of the multi axis system will require a number of iterations as the mass of the system will be unknown till the design is close to completion.

3.12 Summary and conclusion

A single axis prototype machine table was developed and tested using flexure hinges as the primary means of providing the 'slide' action or table travel for a machine tool. This system comprised of four tandem flexure assemblies, symmetrically placed at the four corners of the machine table to support it on a support base platform (Figure 3.34).

The final prototype design configuration was the result of considerable research and CAD modelling. This prototype design progressed from a monolithic structure to a fabricated structure as various design issues were raised and subsequently solved.

The final fabricated flexure system design allowed the freedom to arrange the flexure assemblies into a configuration that sought to best utilise the advantages of flexure hinges whilst minimising the disadvantages. The main advantages were:

- a frictionless operation equivalent to a traditional machine slide system.
- the ability to orient the blades relative to the machine and process induced forces, to make best use of their inherent geometrical and load carrying properties.
- allowed the selection of suitable materials for both the flexure blades and the support frame components independently.

The main disadvantages were seen as the multiple number components required in the fabricated structure, as opposed to the single part structure of the monolith and the inherent difficulty in alignment when being assembled.

All these fabricated design components were subject to discrete manufacturing errors, which accumulate during assembly. However, by manufacturing the components to geometric tolerances that were tight but inexpensively achievable, the stacking effect of the manufacturing errors was minimised cost effectively.

Manufacturability of the fabricated flexure assembly was a primary consideration for this project. High precision manufacture of the machine tool components was to be avoided if possible as was any form of controlled assembly. Both of these

manufacturing/assembly concerns are expensive and would quickly increase the final cost of any production machine tool being manufactured.

A negative effect of the more relaxed tolerance band was the influence it had on the working stage output precision or accuracy. This was addressed by adding multiple flexure assemblies (four) into the flexure table system. The notion of error distribution or self compensation was the primary factor driving this particular design solution decision. The concluding comments regarding self compensation are presented following the discussion regarding material selection presented below.

The selection of a suitable flexure material was required once a final design concept solution was determined. The range of metals (polymeric materials were discounted early in the design process as unsuitable for this application) available was found to be vast (approximately 1800 in the Cambridge Materials Selector); therefore, a method of isolating the most appropriate metallic material was sought. Selection of the most appropriate material became a major issue in the design solution and as such, published selection processes were reviewed. All were found to involve a lot of tedious algebra or calculation when selecting a material.

The search for a suitable selection process began with a review of the design optimisation process, based on work by Johnson[201], who developed a system of equations to describe the mathematical relationships that exist within a design problem. Further to this optimisation solution, Ashby[202] had taken Johnson's relationships and separated the functional requirements, the geometry, and the material properties into what he defined as the system performance equation. Extracting the material parameters from the performance equation gave a defined set of constraints that were met by an appropriate material from which to fabricate the flexures.

However, defining the material parameter equations from Johnson's relationships proved tedious and complex. In an attempt to minimise the effort required to isolate the material parameters from each of the relevant system equations, the author developed a novel approach using dimensional analysis.

In this approach, all the appropriate relationships and parameters that described the design were listed. These relationships and parameters were then non-

dimensionalised to isolate the unique ψ groups, which are the equation components that remain relevant to the material selection process. Once these equations were isolated, they were rearranged to group the material properties into ratios forming the desired material parameters (M_i). The values of M_i were either maximised or minimised to select appropriate materials from Ashby Diagrams[203]. Using this method of material selection, a titanium alloy was selected for use as the flexure material.

Although none of the steps used in the materials selection process is unique in itself, the author believes that the combination of these steps does produce a new and unique method of material selection.

When selected, the suitable flexure material physical properties were used to finalise dimensions and the flexure table system design could be concluded. That is, the most compact and flexible system had been designed to meet the design specification requirement.

It is to be noted that due to availability, spring steel was substituted for the higher performance titanium alloy. Spring steel was suitable as a flexure material for the prototype, but would not have met the fatigue life requirements for a production machine.

The final design of the flexure table was manufactured using traditional job shop processes, and then carefully assembled, ensuring all components fit together as expected. No 'controlled' assembly process was used during assembly.

Travel tests were conducted on the prototyped design, and its performance measured to gauge any out of plane (vertical) errors in its expected linear travel. Out of plane errors were found to exist at each of the four corners of the working stage. These errors were analysed to determine the system rectilinearity. From this analysis, common characteristics were found to exist amongst the data sets.

The data showed a general trend throughout that could be described as a rocking motion. It is believed that this rocking motion was attributed to an imbalance between the flexure stages due largely to variations in the physical properties of discrete components within the flexure assemblies.

It was also noted, that the flexures that formed diagonally opposite pairs, had data trends that were similar though mirrored about the travel position neutral point (zero on the X axis of Figure 3.40 - Figure 3.45).

The orientation of the flexure assemblies relative to each other as they were mounted into the structure would seriously influence the rectilinear output if any assembly's travel was not parallel to all the others. An attempt was made to align the flexure sub-assemblies parallel to one another during the final structure assembly. If however the stages were not aligned then depending on the level of misalignment, they would tend to drag the working stage in the favoured direction.

Another noticeable common feature of the data was the high frequency oscillation that was superimposed over the general data trend. This oscillation was considered to be caused by the repeatability of the CMM, which was operating very close to the limits of its published capability, ±4.5μm. Also investigated was the possibility of an influence on the results of the working stage data capture zone surface roughness.

Surface roughness was considered and investigated to determine if the oscillation effect was the CMM responding to the working stage surface. Surface roughness tests were performed and compared with the data from the CMM tests. No positive correlation was found to exist. The surface roughness effect on the CMM data was concluded as minimal, once again pointing back to the CMM's capability. This was concluded as the data fell largely within the CMM's repeatability range.

Also noted on the data plots were the large amplitude oscillations, which appeared only on one end of each chart. Further examination as to their source was required and these investigations showed it to be an influence from the working stage drive. The working stage drive is a critical component of the flexure table system. Its effect has been demonstrated clearly within the results attained by the subsequent testing of the prototype.

Early tests showed the negative influence on the linear output quality such that removing the original leadscrew drive improved the output markedly. However, introducing the simplistic screw actuators in place of the leadscrew, the author unwittingly introduced a minor source of 'large' oscillations that were superimposed over the output in one table travel direction only, but dependent on which drive screw

was being used. These 'large' oscillations appeared only in one place on each data plot, and were explained as the influence of the screw actuators operating against the working stage cross member upon which they were bearing.

The improved result that came about by removing the leadscrew and replacing it with the two M8 screw adjusters is unexplainable in terms of Hatheway's equations. According to Hatheway the move away from the kinetic centre of the hinges should have given a worse result. Observation of the results showed that the large oscillations were on the off end away from the drive screw. It is believed that the inadvertent flexible nature of the working stage may have allowed the displacement forces to deflect the screw end of the table also influencing the rectilinear output. However at the off end there was no screw influence and therefore the output did not show the large oscillations.

Results from the two drives indicate the sensitivity of the system to working stage drive influence. Therefore, negating this influence will be a major requirement if the flexure table design is to be applied to a functional machine tool as a machine table. The working stage will require driving through its travel range, to make it into a working tool, and to this end, the position of the drive attachment will impose significant design issues to keep the working platform dynamic mass minimised. Perhaps a design encompassing a fully floating leadscrew and wobble pin would be the next iteration in negating the drive influences. As developments in linear motor technology continue to progress, it may be possible to adapt such technology as a contactless drive.

A point to note was that the data capture zones were not flat in relation to the working stage. The ends of the working stage outboard of the flexure assembly attachment points were shown to be measurably sagging, and thus would influence the CMM output by showing a greater deflection as the probe approached the outer ends of the cut-off length.

Another element of the evolving design philosophy that latterly influenced the final system configuration was a desire to use the system itself to self-compensate for some of the inherent and expected errors. Having researched the likely influence from the Hatheway effects, the notion of using multiple flexure assemblies to self compensate or negate some of these affects was applied. Four assemblies placed symmetrically at

the corners of the working stage were integrated into the design. With a superior understanding of the theoretical function of the flexure assemblies, a symmetrical design was used in an attempt to ensure balanced loading on all of the flexures.

The four individual capture zones were chosen to reflect the position of the flexure assemblies. Data taken from these zones produced results that were somewhat unexpected, in as much as they revealed influences far beyond those predicted by the Hatheway equations. When the data from the capture zones was considered with regard to its spread and trend, an initial response was to assume that the self compensation affect had failed to balance the flexures as desired. However, the CMM derived working stage centroid data plot displayed a remarkable self compensating effect with the very flat data trend (Figure 3.45). It was this flat data trend performance, (19μm) that provided the distinct possibility that the flexure table design was workable in this application.

As with much research, the attained results leave many unanswered questions and this section of this project is no exception. There is room here now to move ahead and research the negative error causing influences with further design refinement to improve the output to be more in line with what was expected.

Many of the errors discovered by testing the prototype flexure table design fall outside this current study and will require further analysis and investigation to have their influence removed or severely reduced.

This in part was due to the CMM working at the limits of its published capability; a number of the errors may in fact be functions of the CMM limitation. Metrology equipment should be operating with accuracy levels at ten times the smallest tolerance requirement to precisely determine errors relating to measurement. As such, performance measurement requires the use of a more highly accurate measuring device (laser interferometer) to determine the exact nature and magnitude of any system discrepancies. Perhaps it should be noted here that at the time of writing, the flexure table system, has not been integrated into a working machine tool.

When test results are considered in light of the preceding report, the only conclusion that can be drawn is one that supports the viability of the flexure table design as a

functional component in a machine tool specifically designed to function in a small working envelope and for use only to machine polymeric materials.

---

[1] Kalpakjian, S., Schmid, SR. *Manufacturing engineering and technology.* 4th edition 2001 Prentice Hall Inc. New Jersey USA. ISBN 0-13-017440-8 Page 962

[2] Smith, ST. Flexures, Elements of Elastic Mechanisms. 2000 Ed, Gordon & Breach Science Publishers. The Netherlands. ISBN: 90-5699-261-9 Page 2

[3] Jones, RV. *Instruments and experiences, Papers on measurement and design.* 1988 edition John Wiley & Sons Ltd Chichester England. ISBN 0 471 91763 X

[4] Smith, ST. Flexures, Elements of Elastic Mechanisms. 2000 Ed, Gordon & Breach Science Publishers. The Netherlands. ISBN: 90-5699-261-9

[5] Smith, ST. Chetwynd, DG. *Foundations of Ultraprecision mechanism design. Developments in nanotechnology volume 2*. 1st Edition 3rd printing 1997. Overseas publishers association, Amsterdam, The Netherlands.

[6] Howell, LL. Compliant Mechanisms. 2001 Ed, John Wiley & Sons Inc. Canada. ISBN: 0-471-38478-X

[7] Lobontiu, N. *Compliant Mechanisms, Design of Flexure Hinges*. 2003 Ed, CRC Press LLC. Florida USA. ISBN 0-8493-1367-8

[8] Smith, ST. Chetwynd, DG. *Foundations of Ultraprecision mechanism design.* Page 99

[9] Smith, ST. *Flexures, Elements of Elastic Mechanisms*. Page 2

[10] ibid Page 1

[11] ibid Page 2

[12] Smith, ST. Chetwynd, DG. *Foundations of Ultraprecision mechanism design. Developments in nanotechnology volume 2*. 1st Edition 3rd printing 1997. Overseas publishers association, Amsterdam, The Netherlands. Page 99

[13] Smith, ST. Chetwynd, DG. *Foundations of Ultraprecision mechanism design.* Page 99

[14] ibid Page 99

[15] Lobontiu, N. *Compliant Mechanisms, Design of Flexure Hinges*. 2003 Ed, CRC Press LLC. Florida USA. ISBN 0-8493-1367-8 Page 2

[16] Smith, ST. Chetwynd, DG. *Foundations of Ultraprecision mechanism design.* Page 99

[17] ibid Page 99

[18] Smith, ST. Flexures, Elements of Elastic Mechanisms. Page 2

[19] Smith, ST. Chetwynd, DG. *Foundations of Ultraprecision mechanism design.* Page 100

[20] ibid Page 100

[21] ibid Page 99

[22] ibid Page 100

[23] ibid Page 99

[24] Smith, ST. *Flexures, Elements of Elastic Mechanisms*. Page 3

[25] Smith, ST. Chetwynd, DG. *Foundations of Ultraprecision mechanism design.* Page 99

[26] ibid Page 100

[27] ibid Page 100

[28] Smith, ST. Flexures, *Elements of Elastic Mechanisms*. Page 3

[29] Lobontiu, N. *Compliant Mechanisms, Design of Flexure Hinges*. Page 3

[30] Slocum, AH. *Precision machine design.* 1992 Prentice Hall Inc. Englewood Cliffs, New Jersey USA. ISBN 0-13-690918-3 Page 58ff

[31] ibid Page 58

[32] ibid Page 58

[33] ibid Page 58

[34] ibid Page 58

[35] ibid Page 58

[36] ibid Page 58

[37] ibid Page 59

[38] Ibid Page 60

[39] ibid Page 60

[40] Smith & Chetwynd *Foundations of ultraprecision mechanism design*. Page 70 - 71

[41] ibid Page 71

[42] ibid Page 71

[43] ibid Page 72

[44] Smith, ST. *Flexures, Elements of Elastic Mechanisms*. 2000 Ed, Gordon & Breach Science Publishers. The Netherlands. ISBN: 90-5699-261-9 Page 10-12

[45] ibid Page 10-12

[46] Smith & Chetwynd. *Foundations of ultraprecision mechanism design*. Page 73

[47] ibid Page 73

[48] ibid Page 73

[49] ibid Page 73

[50] ibid Page 76

[51] Ibid Page 77-78

[52] ibid Page 78

[53] ibid Page 80

[54] Ibid Page 80

[55] Ibid Page 81

[56] Reshetov, DN., Portman, VT. *Accuracy of machine tools.* 1988 Translated edition. The American society of Mechanical Engineers. New York USA ISBN 0-7918-0004-0 Page 193

[57] ibid Page 193

[58] ibid Page 195

[59] ibid Page 195

[60] Smith, ST. *Flexures, Elements of Elastic Mechanisms*. Page 373ff

[61] Smith, ST. Chetwynd, DG. *Foundations of Ultraprecision mechanism design. Developments in nanotechnology volume 2*. 1st Edition 3rd printing 1997. Overseas publishers association, Amsterdam, The Netherlands. Page 95

[62] ibid Page 100

[63] ibid Page 100

[64] ibid Page 103

[65] Kirk, DF. *A Literature Search and Review of the Current Technologies as they would apply to Tolerance Based Reverse Engineering.* 2002 Department of Mechanical Engineering, University of Canterbury, Christchurch, New Zealand.

[66] Smith, ST. *Mechanical systems in nanometre metrology.* PhD Thesis, 1988, University of Warwick Chapter 2

[67] ibid Chapter 2

[68] ibid Chapter 2

[69] Smith, ST. Chetwynd, DG. *Foundations of Ultraprecision mechanism design.* Page 103

[70] Smith, ST. Thesis page 28

[71] ibid page 28

[72] ibid page 29

[73] ibid page 29

[74] Smith, W.F., *Foundations of materials science and engineering.* 2nd edition, International edition 1993. McGraw-Hill Inc Singapore. ISBN 0-07-112843-3

[75] Joseph Edward Shigley, *Mechanical Engineering Design.* 1st metric Ed. International Edition 1986 McGraw-Hill Book Company New York – Chapter 7, Design for Fatigue Strength. Page 227,

[76] ibid Page 241

[77] ibid Page 231

[78] Peterson, JE, Pilkey, WD, Clark, K. *Peterson's Stress Concentration Factors.* 2nd Ed. 1997. John Wiley & Sons Inc. New York. ISBN 0471538493 Page 103 etc

[79] Shigley, J.E., Page 243 – 258

[80] Smith, ST. *Mechanical systems in nanometre metrology.* PhD Thesis, 1988, University of Warwick Chapter 2

[81] Shigley, J.E., Page 233 – 256

[82] Shigley, J.E., Page 674, figure A23-4

[83] ibid Page 254

[84] ibid Page 674, figure A23-4

[85] ibid Page 254

[86] ibid Page 231

[87] Smith, ST. Chetwynd, DG. *Foundations of Ultraprecision mechanism design.* Page 104

[88] Smith, ST. Thesis Chapter 2

[89] ibid page 22

[90] Lobontiu, N. *Compliant Mechanisms, Design of Flexure Hinges*. 2003 Ed, CRC Press LLC. Florida USA. ISBN 0-8493-1367-8 Page 43

[91] Smith, ST. *Flexures, Elements of Elastic Mechanisms.* 2000 Ed, Gordon & Breach Science Publishers. The Netherlands. ISBN: 90-5699-261-9 Page 153

[92] ibid Page 153

[93] Awtar, S., Slocum A. *Analysis and Synthesis of Multiple Degree-of-Freedom Flexure Mechanisms* Doctoral thesis proposal MIT Massachusetts USA Page 5

[94] ibid

[95] Todd, RH., Allen, DK., Alting, L. *Manufacturing processes reference guide* 1st edition 1994 Industrial press Inc. New York NY ISBN 0-8311-3049-0 Page 177

[96] Blake, A. Practical stress analysis in engineering design. 2nd Edition, revised and expanded. 1990 Marcel Dekker Inc. New York ISBN 0-8247-8152-X Page 461

[97] Benham, PP., Crawford, RJ., Armstrong, CG. Mechanics of engineering materials. 2nd Ed. 1999 Addison Wesley Longman Ltd. Harlow, England. ISBN 0 582 25164 8 Page 266 Chapter 10 Buckling Instability.

[98] Deutschman, AD., Michels, WJ., Wilson, CE. Machine design, Theory and practice. Macmillan Publishing Co. Inc. New York USA. 1975 edition ISBN 0 02 329000 5 Page 286

[99] ibid Page 288

[100] ibid Page 288

[101] Smith, ST., Chetwynd, DG. *Foundations of ultraprecision mechanism design.* Page 100

[102] Lobontiu, N. Compliant mechanisms, Design of flexure hinges. CRC Press LLC 2003. Boca Raton USA. ISBN 0-8493-1367-8 Page 354

[103] Blake, A. Practical stress analysis in engineering design. 2nd Edition, revised and expanded. 1990 Marcel Dekker Inc. New York ISBN 0-8247-8152-X Page 461

[104] ibid Page 468

[105] ibid Page 468

[106] Smith, ST. *Flexures, Elements of Elastic Mechanisms.* Page 169

[107] Smith, ST. Chetwynd, DG. *Foundations of Ultraprecision mechanism design.* Page 101

[108] Smith, ST. *Flexures, Elements of Elastic Mechanisms.* Page 387-388

[109] ibid Page 390

[110] ibid Page 390

[111] Jones, RV. Instruments and experiments – papers on measurement and instrument design. 1988 John Wiley & Sons Ltd. Chichester UK. ISBN 0 471 91763 X Page 72ff

[112] ibid Page 73

[113] ibid. Page 73

[114] ibid Page 74

[115] Gooch SD. Design and mathematical modelling of the kinetic sculpture *Blade* Doctor of Philosophy Thesis University of Canterbury 2001 page 36

[116] Ashby, MF. Materials selection in mechanical design. 1st edition 1992. Pergamon Press Ltd. Oxford UK ISBN 0-08-041907-0

[117] Johnson, RC. *Optimum design of mechanical elements.* 1980 John Wiley & Sons Inc. Toronto Canada. ISBN 0-471-03894-6 page 187 -8

[118] ibid page 188

[119] ibid page 188

[120] ibid page 190

[121] ibid page 194

[122] ibid page 193

[123] ibid page 194

[124] ibid page 195-6

[125] ibid page 196

[126] Gooch SD. Design and mathematical modelling of the kinetic sculpture *Blade* Doctor of Philosophy Thesis University of Canterbury 2001 page 36

[127] Johnson 1980 optimum design of mechanical elements page 194

[129] Gooch SD. Design and mathematical modelling of the kinetic sculpture *Blade* Doctor of Philosophy Thesis University of Canterbury 2001 page 36

[130] Ashby, MF. Materials selection in mechanical design. 1st edition 1992. Pergamon Press Ltd. Oxford UK ISBN 0-08-041907-0 page 58

[131] ibid page 24

[132] Gooch SD. Design and mathematical modelling of the kinetic sculpture *Blade* Doctor of Philosophy Thesis University of Canterbury 2001 Page 14

[133] Massey B, and Ward-Smith J. Mechanics of Fluids 7th Edition. Stanley Thornes (Publishers) Ltd. 1998 ISBN 0-7487-4043-0 page 189

[134] Gooch SD. Design and mathematical modelling of the kinetic sculpture *Blade* Doctor of Philosophy Thesis University of Canterbury 2001 Page 14

[135] Massey B, and Ward-Smith J. Mechanics of Fluids 7th Edition. Stanley Thornes (Publishers) Ltd. 1998 ISBN 0-7487-4043-0 page 189

[136] ibid Page 189 -190

[137] Ashby, MF. *Materials selection in mechanical design.* 1st edition 1992. Pergamon Press Ltd. Oxford UK ISBN 0-08-041907-0 Page 91, 162

[138] Blake, A., *Practical stress analysis in engineering design* 1990 Marcel Dekker Inc New York ISBN 0-8247-8152-X Page 137

[139] Young, WC. Budynas, RG. *Roarks formulas for stress and strain.* 7th edition 2002 McGraw-Hill Inc. New York NY ISBN 0-07-072542-X

[140] Massey B, and Ward-Smith J. *Mechanics of Fluids* 7th Edition. Stanley Thornes (Publishers) Ltd. 1998 ISBN 0-7487-4043-0 page 189

[141] Ashby, MF. *Materials selection in mechanical design.* 1st edition 1992. Pergamon Press Ltd. Oxford UK ISBN 0-08-041907-0 Page 91

[142] Walker, JD. *Applied mechanics.* 4th & SI edition 1972 Fletcher & Son Ltd. Norwich UK. ISBN 0-340-11539-4 page 168

[143] Ashby, MF. *Materials selection in mechanical design.* Page 91

[144] ibid Page 18

[145] Benham, PP., Crawford, RJ., Armstrong, CG. *Mechanics of engineering materials.* 2nd Edition. 1996 Addison Wesley Longman Ltd. Harlow, Essex, England. ISBN 0-582-25164-8 Page 237

[146] Blake, A., *Practical stress analysis in engineering design* 1990 Marcel Dekker Inc New York ISBN 0-8247-8152-X Page 137

[147] ibid Page 241

[148] Ashby, MF. *Materials selection in mechanical design.* 1st edition 1992. Pergamon Press Ltd. Oxford UK ISBN 0-08-041907-0 Page 91 and also the CES Selector V4.5 example problem 10 Elastic hinges and couplings

[149] ibid Page 63

[150] Waterman, NA., Ashby, MF. *The Materials Selector.* 2nd Ed Vol 1 1997 Chapman & Hall London UK ISBN 0 412 61550 9 (3 volumes) page 70

[151] ibid page 427

[152] ibid page 427

[153] Ashby, MF. *Materials selection in mechanical design.* Page 24

[154] CES Selector Version 4.5, Copyright© Granta Design Ltd. Build 2004, 3, 16, 1. Granta Design Limited. Rustat House, 62 Clifton Rd., Cambridge, CB1 7EG, United Kingdom

[155] ibid

[156] Timoshenko, SP., Gere, JM. Theory of elastic stability. 2nd edition 1961. McGraw-Hill Book Co. Inc. New York. Library of Congress Catalogue Card Number 59-8568

[157] Gere, JM., Timoshenko, SP., (1878-1972). Mechanics of materials. 4th SI edition 1999. Stanley Thornes (Publishers) Ltd. Cheltenham, UK. ISBN 0 7487 3998 X

[158] Pilkey, WD. Formulas for stress, strain and structural matrices. 1994 edition. John Wiley & Sons Inc. New York NY. ISBN 0-471-52746-7

[159] Smith, ST. *Flexures, Elements of Elastic Mechanisms.* Page 158

[160] Jones, RV. *Instruments and experiences, papers on measurement and instrument design.* Chapters 5 & 9.

[161] Hatheway, AE. *Alignment of flexure stages for best rectilinear performance.* Proceedings of SPIE – The International Society for Optical Engineering. V2542, 1995, pages 70 – 80. ISBN 0-8194-1901-X

[162] Jones, RV. *Instruments and experiences, papers on measurement and instrument design.* Page 72

[163] ibid Page 75

[164] ibid Page 75

[165] ibid Page 76

[166] ibid Page 76

[167] ibid Page 76

[168] ibid Page 77

[169] ibid Page 77

[170] ibid Page 77

[171] ibid Page 78

[172] ibid Page 78

[173] Hatheway, AE. *Alignment of flexure stages for best rectilinear performance.* Proceedings of SPIE – The International Society for Optical Engineering. V2542, 1995, pages 70 – 80. ISBN 0-8194-1901-X Pages 70 – 80

[174] ibid Page 72

[175] ibid Page 72

[176] ibid Page 72

[177] ibid Page 72

[178] ibid Page 73

[179] ibid Page 73

[180] ibid Page 73

[181] ibid Page 73

[182] ibid Page 74

[183] ibid Page 74

[184] ibid Page 74

[185] ibid Page 74

[186] ibid Page 74

[187] ibid Page 75

[188] ibid Page 75

[189] ibid Page 75

[190] Smith, ST. Chetwynd, DG. *Foundations of Ultraprecision mechanism design.* Page 102

[191] ibid Page 104

[192] Jones, RV. Instruments and experiments – papers on measurement and instrument design. Page 74

[193] Hatheway, AE. *Alignment of flexure stages for best rectilinear performance.* Page 78

[194] ibid Page 78

[195] Smith, ST. *Flexures, Elements of Elastic Mechanisms.* 2000 Ed, Gordon & Breach Science Publishers. The Netherlands. ISBN: 90-5699-261-9 Page 390

[196] Hatheway, AE. *Alignment of flexure stages for best rectilinear performance.* Page 78

[197] ibid Page 79

[198] Operators handbook – Tallysurf 10. Taylor Hobson, Leicester, England. Page 6

[199] Hatheway, AE. *Alignment of flexure stages for best rectilinear performance.* Page 79-80

[200] ibid Page 75

[201] Jones, RV. *Instruments and experiences, Papers on measurement and design.* 1988 edition. John Wiley & Sons Ltd Chichester England. ISBN 0 471 91763 X

[202] Ashby, MF. Materials selection in mechanical design. 1st edition 1992. Pergamon Press Ltd. Oxford UK ISBN 0-08-041907-0

[203] ibid Page 24

Table of Contents

Table of Figures

Table of Tables

Chapter 4

Nomenclature

Chapter Four

A comparative list of specific nomenclature relating to the cutting theory comparison is cited on page 233ff.

Symbol	Definition	Units
$\overline{F_x}$, $\overline{F_y}$, $\overline{F_z}$	average orthogonal feed force	N
a	axial depth of cut (Altintas term)	mm
A_s	shear plane area	m^2
b	width of cut	mm
c	feed per tooth	mm
c_s	specific coefficient of heat (Altintas term)	Nm/kg^{o}C
c_t	thermal conductivity of the work material (Altintas term)	W/(m^{o}C)
d	differential	
D	cutter diameter	mm
d	depth of cut (Kobayashi term)	mm
d_c	chip thickness	mm
d_c	deformed chip thickness (Kobayashi term)	mm
F	resultant feed force	N
f	feed/tooth/rev	mm
F	resultant force (Altintas term)	N
F_a	axial feed force	N
f_c	tool feed velocity	m/s
F_c	force component in direction of relative tool travel (feed force)	N
F_f	frictional force between chip & rake face (Kobayashi term)	N
F_{ft}	feed cutting force – perpendicular to tool travel (Altintas term)	N
F_{fm}	normal force on rake face	N

F_n	normal force on shear plane (Altintas term)	N
F_{ns}	force perpendicular to shear plane (Kobayashi term)	N
F_r	radial cutting force – perpendicular to the cutting edge direction of travel (Altintas term)	N
F_s	force component along shear plane	N
F_t	force perpendicular to tool travel (Kobayashi term)	N
F_t	tangential cutting force – in direction of tool travel (Altintas term)	N
F_u	friction force (Altintas term)	N
F_v	normal force (Altintas term)	N
F_x, F_y, F_z	orthogonal feed force	N
h	depth of cut (Altintas term)	mm
h_a	average chip thickness	mm
h_c	deformed depth of cut	mm
h_j	cutting depth for flute j	mm
hp	power consumption	W
i	oblique cutting angle	deg
j	flute designation number	
K	specific cutting force (constant)	kg/mm^2
K_{ac}	cutting constant - axial	N/mm^2
K_{ae}	edge cutting constant - axial	N/mm^2
K_F	Feed specific cutting pressure	N/mm^2
K_f	cutting force ratio	
K_{fc}	cutting constant - feed	N/mm^2
K_{fe}	edge cutting constant - feed	N/mm^2
K_{rc}	cutting constant - radial	N/mm^2
K_{re}	edge cutting constant - radial	N/mm^2
K_T	tangential specific cutting pressure	N/mm^2
K_t	tangential specific cutting pressure	N/mm^2
K_{tc}	cutting constant - tangential	N/mm^2
K_{te}	edge cutting constant – tangential	N/mm^2
l	length of cut	mm
l_c	extend of cutter's initial contact	mm
L_c	shear plane length (Altintas term)	mm
l_t	chip contact length (Altintas term)	mm

m_c	metal removal rate (Altintas term)	kg/sec
N	no. of flutes on cutter	
n	rotation speed	rpm
p, q	experimental cutting force constants	kg/mm^2
P_p, Q_p, R_p, S_p	substitute variables in weighting calculations	
P_s	shear power (Altintas term)	W
P_t	total power (Altintas term)	W
P_u	friction power (Altintas term)	W
Q_c	metal removal rate [m^3/sec] (Altintas term)	m^3/sec
R	resultant cutting force	N
r	chip thickness (or compression) ratio	
r_c	cutter radius	mm
R_c	chip compression ratio (Altintas term)	
rpm	revolutions per minute	min^{-1}
R_T	non dimensional thermal number (Altintas term)	
S_f	roughness of cut surface	
s_t	feed per tooth per rev	mm
T	torque	Nmm
t	cutting time	seconds
t_c	approx undeformed chip thickness	mm
T_{int}	average temp change at rake face – chip interface (Altintas term)	^oC
T_r	ambient temperature (Altintas term)	^oC
T_s	shear plane temperature (Altintas term)	^oC
u	specific cutting force (Kobayashi term)	Ws/mm^3
u_f	friction energy/unit volume (Kobayashi term)	Ws/mm^3
u_s	shear energy/unit volume (Kobayashi term)	Ws/mm^3
V	velocity of tool parallel to F_c	m/s
v	feed rate	mm/min
V_c	chip velocity	m/s
V_m	cut volume per unit time	m^3/s
V_p	peripheral cutting speed	m/min
V_s	shear velocity	m/s
V_w	volume of tool wear/unit time	m^3/s

W	watts	
w	width of cut	mm
z	axial depth of cut	mm
Δd	undeformed shear plane (Altintas term)	
Δs_K	change in chip length parallel to shear plane (Kobayashi term)	mm
Δs_A	deformation in shear plane (Altintas term)	mm
Δt	time increment (Altintas term)	s
ΔT_c	average temperature change in chip (Altintas term)	^oC
ΔT_m	max temp rise of the chip at rake face – chip interface (Altintas term)	^oC
Δy	change in chip thickness perpendicular to shear plane (Kobayashi term)	mm
K_{fe}	average edge force coefficient (Altintas term)	N
K_{te}	average edge force coefficient (Altintas term)	N
α	rake angle (Kobayashi term)	deg
α_n	oblique cutting rake angle	deg
α_r	orthogonal cutting rake angle	deg
α_r	rake angle (Altintas term)	deg
β	friction angle	rads
β	helix angle	deg
β	friction angle (Kobayashi term)	rads
β_a	coefficient of friction	
β_a	average friction angle between rake face and moving chip (Altintas term)	deg
δ	ratio of plastic layer over deformed chip thickness (Altintas term)	
ϕ_i	instantaneous immersion angle	deg
ϕ	shear angle (Kobayashi term)	deg
ϕ_c	orthogonal shear angle	deg
ϕ_c	shear angle (Altintas term)	deg
ϕ_{ex}	cutter exit angle	deg
ϕ_j	immersion angle for flute j	deg
ϕ_n	normal shear angle (oblique cutting)	deg
ϕ_p	tooth spacing (cutter flute pitch)	deg
ϕ_{st}	cutter start angle	deg

γ	shear strain on shear plane (Kobayashi term)	
γ_s	shear strain (Altintas term)	
γ'_s	shear strain rate (Altintas term)	/s
η	chip flow angle	deg
η^1_c	machinability factor (Kobayashi term)	
η^2_c	machinability factor (surface finish neglected) (Kobayashi term)	
η^3_c	machinability factor (tool wear neglected) (Kobayashi term)	
η_c	machinability index	
η_s	machinability (orthogonal cutting) (Kobayashi term)	
η_t	machinability (turning) (Kobayashi term)	
λ_h	factor to consider plastic work done in the thin shear zone (Altintas term)	
λ_s	proportion of heat conducted into work material (Altintas term)	
μ	coefficient of friction (Kobayashi term)	
μ_a	coefficient of friction (Altintas term)	
ρ	specific density (Altintas term)	kg/m^3
σ_c	Specific cutting force (Kobayashi term)	kg/mm^2
σ_s	normal stress (Kobayashi uses kg/mm^2)	MPa
τ_s	shear stress (Kobayashi uses kg/mm^2)	MPa
ω	rotational speed	rads/sec
ψ	flute lag angle	deg

Chapter 4

SPINDLE POWER DETERMINATION

An investigation into cutting R-PVC to determine the power requirements

4.0 Spindle drive

As previously introduced in chapters one and two an approach was made by a local manufacturing company to investigate the design and manufacture of a machine tool for use in the manufacture of a new smart card product commonly used in the banking and other industries requiring identification or secure transactions.

Also introduced earlier was the need for a purpose built machine tool to meet the process requirements of the new card. The production rates called for a machine tool with very short process cycle times. This demand in turn affected the design of the spindle drive and the machine slides. Many of the previously used machine tools were modified from routers or similar machines and maintained their original spindle and slide drive motors which were large by comparison as they were often required to perform much heavier cutting duties. The spindle drive power was investigated with a view to minimising the masses carried by the slides. The intent here was to apply a motor with a more suitable power output and thus reduce its size. Thus, the overall effect was to provide a much smaller motor with a mass that was more easily controllable during the required rapid translations of the process cycle. Smaller slide drives were an added advantage of this reduction in the mass being translated.

This chapter represents one theme from within the overall project though not a core theme. The thrust is an investigation looking to extend the theory of single point to multipoint cutting of polymers by way of comparison of cutting theories. This approach was used to determine the spindle power required by the machining process.

Further to this and to remind the reader, the card design requirement is presented in the following subsections.

4.1 Project summary

4.1.1 Card design requirement specification

The product design requirement specification called for a micro-machining facility to be developed to produce pockets/cavities for integrated circuit chips in rigid polyvinyl chloride sheet. The precision capability of the machine tool demanded repeatable results in the micron range rather than tens of microns.

The desired production rate was approximately 1500 cards per hour using a single cutter spindle and commercially available multi-edge cutters. The single cutter spindle requirement was an attempt to keep the machine relatively simple in design and construction compared with other equipment available in current use.

- Workpiece material characterisation – Rigid Polyvinyl Chloride

The specified production material was rigid polyvinyl chloride (R-PVC) which is a rigid plastic, supplied in sheet form. R-PVC was specified as it is an industry standard for the particular consumer product being manufactured.

The usual material properties published are of significance to component designers and moulding processes invariably and not generally relevant to machining process designers. A search of available machining resources revealed no apparent machining 'bible' for polymers, as there is for metals: The Machining Data[1] handbook is a commonly referred to resource when investigating metal properties with regard to machining metals.

As there were no readily available published references for the machining characteristics of R-PVC, the investigation turned to journal publications as a source of possible information. This research provided two characteristics for R-PVC that were not commonly found in metal cutting processes. They were;

1) R-PVC machines relatively easily except when the depth of cut, cutting speed or positive rake angle of the tool is too large[2].

2) R-PVC is highly abrasive and causes flank and cutting edge wear, which is a phenomenon, not found in metal cutting[3].

4.1.2 Machining process description

- Manufacturing process defined – End milling

The machining operation considered an appropriate process for the project was milling and specifically end milling/slot drilling. During the early project development phases, various other manufacturing processes were assessed, both traditional and non-traditional. Examples of non traditional processes were, laser and chemical machining. However, the milling process was regarded as the most suitable to meet both the component design specification and the desired production rates. It is the standard method commonly used in the industry, which often uses existing machinery modified to suite the new purpose, as previously discussed. This pseudo standard was the process on which the sponsoring company based their machine design requirement. Some further information is now provided with regard to the milling process and its application to the specific card manufacturing requirement.

- Material removal rate

The material removal rate was determined by the production rate demand. This rate was approximately 1500 units per hour or approximately 2.4 seconds per unit. The standard cavity had a material removal volume of approximately 80 mm^3 giving an approximate material removal rate of 40 mm^3/s. This rate gave a product transfer time of approximately 0.4 seconds through the infeed and outfeed sections of the machining process.

- Cutter type, style and size

The cutter was selected from a commercially available solid carbide range suitable for machining aluminium. These cutters were selected on the basis that they would have a high rake angle, consistent with tool design for machining aluminium. The commercially available requirement was essential to keep the cost of the cutters minimised. The use of solid carbide was specified in order to reduce the abrasive effect of the R-PVC material. Cutters suitable for steel were also considered during the practical cutting trials.

The cavity being machined had a designated 2.0 mm radius in the corners to clear the component that was to be fitted into it. As a consequence a 4.0 mm diameter cutter was a suitable diameter choice for the machine tool. However, due to relaxing tool pressures this may have produced oversized corners as the machine changed directions in the cavity corners. Therefore, a 3.0 mm cutter was chosen which allowed

the corners to be interpolated around the change in direction rather than a stop/start change as would have been seen with the 4.0 mm cutter. Cutters with two, three and four flutes were trialled. The three fluted cutter was for ferrous materials, whilst the other two were for aluminium and its alloys. The results of the cutting trials will be discussed in a later subsection of this work.

A commercially available three fluted cutter was initially chosen rather than the custom single edge, 'D' type cutter, as was consistently used by the sponsoring company. An issue that was a problem with the current manufacturing method was the residual rag attached to the machined edges. A multi fluted cutter taking smaller cuts at shorter intervals was considered a means of reducing the possibility of ragging on the edges. This was proven to be the case during the subsequent cutting trials.

- Speeds and feeds

The speeds and feeds are dependent on the material removal rate, which in turn is dependent on the cutter size and style. The cutter feed and rotational speeds were determined by the length of cut and the time taken to form the cavity. The rotational speed of the cutter was also dependent on the allowable feed rate for the particular chosen cutter, and the feed/tooth/rev.

- Cutter forces

The forces generated by the cutter will be dependent on the feed and speed factors given above. The actual forces generated will be a function of the work done during the cavity formation process, and the tool geometry.

As the cutter size and process conditions set the size and type of cutter to be used, it remained only to select a cutter from a particular manufacturer that met these requirements. The various relevant cutter properties are introduced as required in the ensuing text. To this end, they are discussed in more detail from within the relevant sections.

4.2 Determination of the specific cutting force

The specific cutting force is a mandatory requirement for a mathematical analysis of the cutting forces and thus able to give an approximation of the power required.

The determination of the specific cutting force or pressure (the specific energy of cutting) is a complex function of the material properties and the tool geometry. It is

dependent on both of these parameters and as such is unique for each variation of the tool geometry and work piece.

The value of the specific cutting force is usually found by experimental orthogonal cutting trials. The associated experimental work is to determine the cutting forces and in some cases to observe the shape of the chip and its geometry. From these factors it is possible find the shear plane angle, if one is created, and hence the specific cutting force. However, not all plastics form shear planes during cutting[4]. R-PVC, however, does meet this requirement though it is inferred by Kobayashi[5] rather than stated. For those materials that do, determination of the specific cutting force is possible through experimentation and once known may be used to determine the orthogonal cutting power. A limitation to this approach was the fact that the host component was being processed with helical end mills/slot drills, which placed a severe discrepancy between the orthogonal characteristic information and the specific cutting force relevant to the chosen cutters. Further investigation was therefore required to determine the relationships that existed between orthogonal cutters and helical cutters, if indeed there was one in regard to polymeric materials. The investigation formed a major component of the following study to research and report on such a relationship if such exists, particularly with regard to R-PVC.

4.2.1 Determination of the spindle power

The determination of the cutter power was the primary factor that prompted this investigation. The desire to apply a correctly sized electric motor to the cutter spindle was vitally important to the design solution. This was to minimise the mass of the spindle drive and to provide a responsible solution with regard to its energy requirements. The information that was obligatory to determine the power requirements were the force values developed by the working cutter. There were two approaches, which could be made to determine these forces, an analytical approach or an experimental one. A complex and time consuming experimental approach was deemed to be very cost ineffective with regard to the overall project value, and so an analytical solution was sought.

The decision to use an analytical solution was believed to be the most appropriate means to determine the cutting power. This decision was made on the basis that the cutter forces could be calculated, using the specific cutting force data. With this

information available and knowledge of the cutter specification, the cutter torque and power could be readily determined. Therein lay the problem: the specific cutting force information was not readily available with regard to polymeric materials, specifically R-PVC. Thus, the research was instigated to determine what work had been completed with regard to plastics. The following discourse is a description of the processes and investigation undertaken to find a method to determine the cutter power for a helical milling cutter whilst forgoing the expense, time and complication of determining the missing data experimentally.

4.2.2 Introduction to the spindle design

Second only in importance to the bed design, of a milling machine, is the spindle design. Determining the power requirements of the spindle drive is central to such a development and was therefore an area of critical importance in the undertaken work. However, the design of dedicated equipment used to machine plastics is not a common practice, with reports of various pieces of equipment for this purpose frequently being developed from existing metal or wood working machines[6]. Since in these accounts the machines have been developed from machines that are already in use, the determination of the spindle power requirement was usually unnecessary and the existing drive was apparently subsumed into the resultant machine. Within the reported programme of work, developing a new machine with a specific task in mind called for the most economic and feasible design that was practicable. This included determining the spindle power requirements in an effort to conserve resources such as power and weight, furthermore, perhaps most important was a need to minimise mass in order to achieve the high accelerations necessary to obtain the desired production rates.

This study was not commissioned to investigate the behaviour or the mechanics of cutting plastics. Instead, it was a study brought about out of the necessity to uncover a means to find the required spindle power to machine a pocket in rigid polyvinyl chloride (R-PVC) sheet without the need for a colossal experimental programme. Such an experimental approach would result in the determination of the cutting forces crucial to ascertaining the spindle power requirement. Reviews of relevant literature lead to the assumption that the R-PVC behaved in a similar way to a metal when being cut in an orthogonal manner[7]. This theory revolves around the notion of the formation of a shear plane in the cutting zone. Kobayashi's polymer cutting theory was a

surprise in that it mimicked metal cutting. The following treatise does not set out to investigate the cutting process in plastic but merely to compare two procedures that appear to be very similar, namely the orthogonal cutting characteristics of metals and that for R-PVC. The notion then was to extend the assumption from metal cutting theories to encompass the same processes in R-PVC and hence determine the cutting coefficients. From these cutting coefficients, the power required to drive a helical end mill at a rotational velocity and feed rate to achieve the desired manufacturing volume could be determined.

4.2.3 Spindle drive requirements

Table 4.1, below, was developed to define the demands and wishes relating to machining the pockets and so to the design of the spindle itself. However, determining the spindle drive requirements proved to be a major challenge in the development phase of the milling machine mainly due to the lack of associated design information with regard to machining specific polymer types. A Cause and Effect diagram (fishbone diagram) (Figure 4.1) was developed to assist in the further determination of the missing parameters that were required to develop a spindle suitable for the designated purpose of machining the IC chip cavities into R-PVC Smartcards.

4.2.4 Spindle design requirement specification

A demands and wishes list[8] or design requirement specification was developed to define the various requirements and parameters of the cutting process and spindle requirements for the machine tool. A list of these items was created and then each one was defined as a demand or wish. These are summarised in Table 4.1 below.

Table 4.1: Design requirement specification table for pocket machining requirements

Demand	Wish
Low power – high spindle speed motor	
High material removal rate	
Low heat generation	
Dry or air cooled cutting process	
	Use proprietary metal cutting tools
Clean cut edges – no rags remaining	
	No rag removal after machining
Machine Copper and R-PVC together with no ragging and a good surface finish	

	Machine 1500 pockets per hour
Use off the shelf components and technologies	
straightforward, low maintenance design	
	uncomplicated design for spindle bearing lubrication, (not oil mist type)

4.2.5 Steps in determining the required spindle power

A cause and effect (C&E) diagram was developed and is shown in Figure 4.1. This was to assist in determining the power required at the cutter thus achieving the design intent of this aspect of the project. The C&E diagram was used to highlight the unknowns or missing technologies that prevented a complete design from being undertaken. This sub section is limited to determining the spindle power and an analysis of the C&E diagram as it relates to this task is shown in Table 4.2. A thorough approach to each of the entries in the C&E diagram was made and they were classified, shown in Table 4.2 below, according to the design criteria applied from the demands and wishes list and the major headings in the C&E diagram. The solution classification was also driven by the knowledge or technologies available to enable a holistic design of this element of the design. This demonstrated that the items fell into categories depending upon how they interacted with the system in general. The analysis showed that only those items that were affected by the actual properties of the cutting action were unable to be readily satisfied.

This section was limited to an analysis of the design requirements and confirmation of a holistic approach to system development, which in turn identified a significant shortfall in established/published research. Table 4.2 shows an attempt to classify those areas of the spindle design that require further input, outside of this reported work; to enable a solution to be formed. All of the entries below, except four, (cutter friction, power capacity and cutting torque, cutting forces) apparently have workable solutions by way of available knowledge, information and/or technology. The four identified limiting criteria are all related directly to a lack of documented data relating to the cutting processes for polymeric materials. There is comprehensive and significant resource available to those working with metal cutting processes – The Machining Data Handbook[9] for example. The Machining Data Handbook has specific properties that relate to metal cutting but there appears to be no such published data available for machining polymeric materials[10].

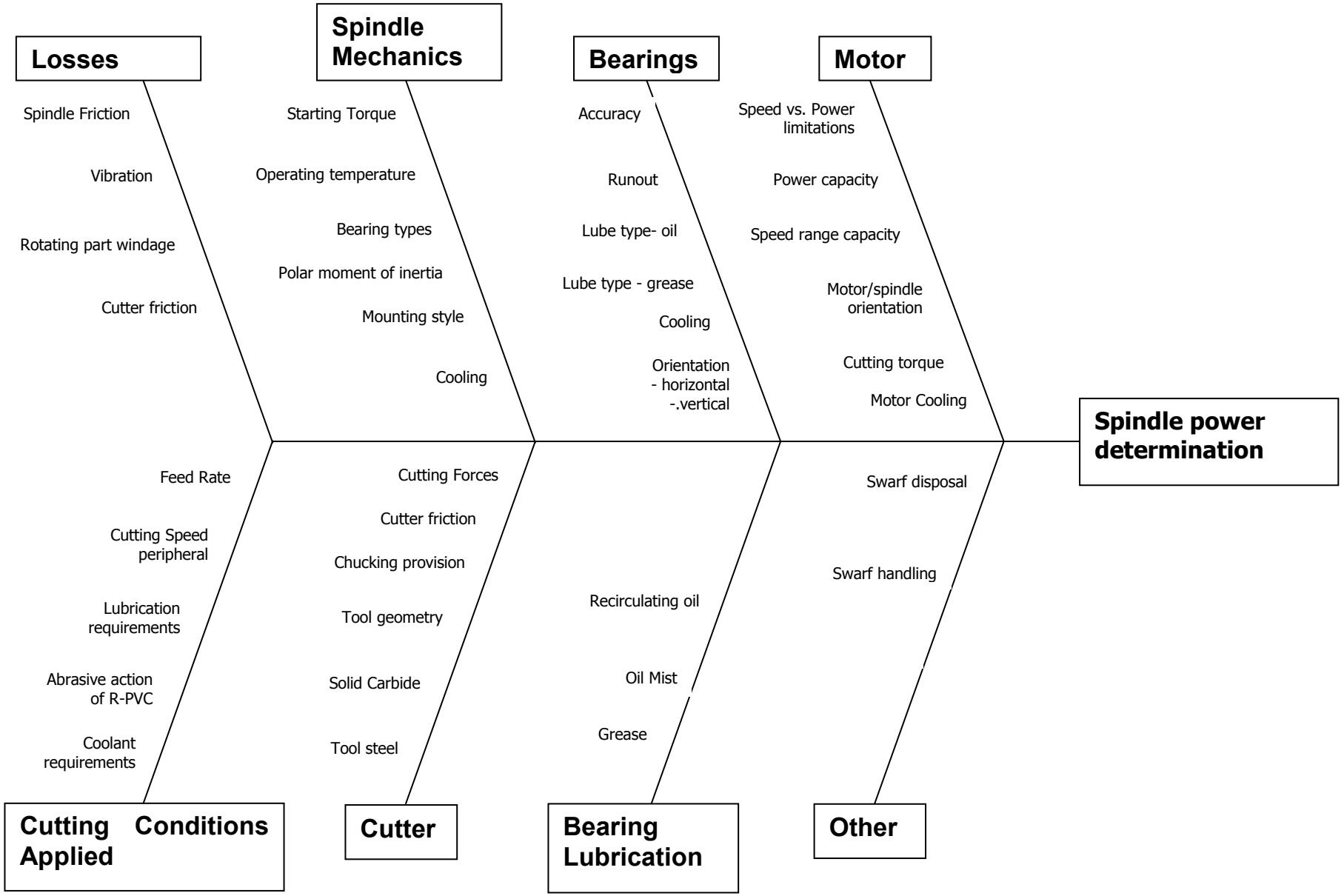

Figure 4.1: Cause and Effect diagram to assist in spindle unit design and development

Table 4.2: Solutions to cause and effect diagram

C&E label	Solution type	Satisfied
Losses		
Spindle friction	component property	
Vibration	configuration and design property	
Rotating component windage	component property	
Cutter Friction	process & component property	**solution not satisfied**
Spindle Mechanics		
Starting torque	component requirements	
Operating temperature	design property	
Bearing designation and type selection	Configuration and design solution	
Polar moment of inertia	component property	
Mounting style	design solution	
Cooling	design solution and component requirements	
Bearings		
Accuracy	component property & design solution	
Runout	component property & design solution	
Lubrication type – oil	Design solution and component selection requirement	
Lubrication type – grease	Design solution and component selection requirement	
Cooling	Component requirements	
Orientation – horizontal - vertical	Design solution	
Motor		
Speed vs. Power limitations	design solution on speed & unknown on power	
Power capacity	Unknown	**solution not satisfied**
Speed range capacity	Design selection	
Motor-spindle orientation	design solution controlled by component selection	
Cutting torque	requires experimental research to determine torque	**solution not satisfied**
Motor cooling	component requirement	

Cutting Conditions Applied	
Abrasive action of R-PVC	material property
Coolant requirements	component selection requirement
Lubrication requirements	Cutting process property requirement
Cutting speed (peripheral)	Design solution – component selection
Feed rate	component selection
Cutter	
Tool steel	component selection based on wear requirements as per R-PVC
Solid carbide	component selection based on wear requirements as per R-PVC
Tool geometry	component selection
Chucking provision	design solution and component selection
Cutter Friction	requires experimental research and trials to determine forces
Cutting forces	requires experimental research and trials to determine forces
Bearing lubrication	
grease	design solution
Oil mist	component requirement – economic considerations
Recirculating oil	component requirement – economic considerations
Other	
Swarf disposal	design solution
Swarf handling	design solution

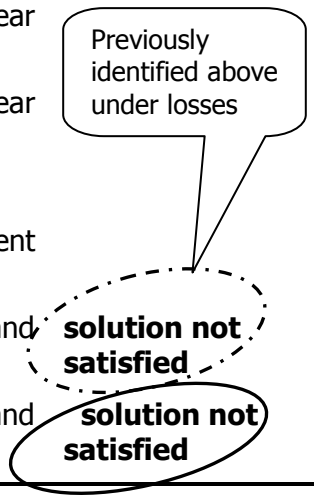

Analysis of the table above indicated there was a need for more data or information regarding the cutting and therefore the milling process in terms of the interaction between the cutting edge and the work piece, when working with homogenous polymeric materials. This conclusive observation therefore gave rise to an investigation into plastic machining. A means of calculating the power requirements of the spindle drive without the need to delve heavily into experimental research was required so as to determine the specific cutting pressure (or specific cutting force) of the R-PVC. (The terms specific cutting force and specific cutting pressure may be used interchangeably throughout this work.) The specific cutting pressure is a

property that allows for the calculation of cutting forces and hence the power consumed in a cutting operation. This property has been reasonably well researched and documented for metals but evidence or lack thereof suggests the same is not true for plastics.

4.2.6 Cutter selection

The selection of a suitable cutter was very much determined by the range of cutters that were available from various suppliers. The main defining parameters were, multi-fluted, bottom cutting and with a high rake angle. Table 4.28 gives the parameters for a suitable three fluted cutter from Prototyp PWZ[11] which, was used for the cutting tests in the physical trials. These trials are discussed fully in a later subsection. The cutter selection is introduced here to offer background information to the reader and as such further information will be included as it is required.

4.3 Introduction to orthogonal plastic (polymer) machining theory

Unlike metal cutting, the machining of plastics has received very little research attention since its introduction, and as a consequence, the topic is poorly supported by technical literature. From this observation, it is clearly evident that plastic machining is not seen as an independent or valued process by industrialists or the vast majority of relevant research personnel. This situation is made blatantly evident from the sparse findings of the author's in depth literature survey on the subject[12] [13] [14]. Therefore when faced with the task of developing a dedicated high speed plastic machining facility numerous design analysis and concept validation shortfalls become apparent. The following commentary expands on these limitations.

Generally, engineers faced with the challenging task of designing a plastic part that requires close dimensional or form tolerancing within a complex shape and in small batch quantities will most likely have to resort to machining processes. However for the designated tolerances and production rates, the plastic host component was to be machined as no other suitable manufacturing or pocketing process existed. The general view that machining plastic is easily done using metal cutting technology is common amongst the manufacturing fraternity[15]. This in turn has lead to many of the dedicated machine tools used in plastics machining being modified from existing metal or woodworking machine tools with varying degrees of success[16]. It was the lack of success of these modifications and the inherent associated problems with existing

plant that has prompted this study to design a purpose built dedicated machine tool to produce the host component.

At the outset of the research undertaking an extensive survey of published research and technologies relevant to machining homogenous polymeric materials, specifically R-PVC, was found to be seriously limited. A considerable volume of research has been documented relating to the machining of metals and ceramics, but very little by comparison has been done with homogenous plastic materials. In support of this finding Kaneeda reported in a 1989 publication that there had been insufficient research performed on these types of cutting processes in general[17]. Naturally it was no surprise to find an associated absence of information related to the goal of this study – high speed machining of plastics.

The Machining Data Handbook[18], contains references for metal machining and in general, any attempt to apply the standard principles of metal machining to plastics would ensnare the designer in some serious problems[19]. Surprisingly, there are however some polymeric materials that can be considered to have some machining properties that are similar to metals and therefore to some extent may be analysed with metal cutting theories or processed with proven metal cutting technologies[20]. The notion that metal cutting theory may be used for various plastics is based on observation of chip formation during cutting, in which a shear plane is apparently observed to form. The formation of the shear plane during cutting is crucial to the application of metal cutting theory. Unfortunately, not all plastics have this property[21], which is affected by the cutting conditions and tool geometry. Not only these properties affect the action of the tool during cutting, there are two others in particular, of the many material properties that apply to R-PVC, that affect cutting and are not readily comparable with cutting metals. These are the abrasiveness of the material on the cutter edges, and the ease of cutting or material removal, with standard metal cutting tooling[22]. The ease of cutting R-PVC allows the use of conventional metal cutting tools usually with high applied rake angles. The abrasiveness is a significant issue because it causes a wear pattern that is very dissimilar to the wear caused by metal machining. The tool edges are rounded off with minimal crater and flank wear occurring[23]. This may require consideration with regard to rubbing of the tool on the cut surface. Furthermore, it may be a problem

when performing extremely shallow cuts with worn tooling at very high spindle speeds. This may mean there are issues to be resolved, such as surface finish and the possible generation of heat due to friction on the rubbing faces of the cutter,[24] though the effect of these is unknown with regard to the power requirements.

A third property of polymeric materials that is exceedingly difficult to locate and in many cases has been investigated only very meagrely, is a property called the specific cutting pressure or specific cutting force. The specific cutting pressure as previously mentioned is a property that allows for the analytical investigation of cutting forces and hence the power consumed in a cutting operation. This property once found, usually by experimental orthogonal single point cutting trials can be used to solve the force system generated by a particular cutter as well as the requisite power absorbed.

The derivation of the specific cutting force is demonstrated by Kobayashi in a detailed extract of his work, covered later in this thesis. A brief explanation of the specific cutting force is introduced here as it plays an immense role in the designer's ability to assess the cutting power without the need to invest time and effort into experimental work. As the specific cutting force is a particular property of a material that makes this possible, a high emphasis was placed on it. The nomenclature used to define specific cutting force throughout this work is first stated on page 233. Kobayashi uses the same symbol as used for energy, u, with units of kg/mm^2. (Kobayashi uses these units which need to be multiplied by gravitation acceleration to become either N/mm^2 or kgf/mm^2.) By way of comparison Altintas tends to use a 'K' with a subscript to define the specific cutting force. A typical example of Altintas' may well be K_t, for the tangential cutting force coefficient (specific cutting force). This nomenclature inconsistency has unnecessarily increased the complexity of the comparison of the various researched approaches that have been investigated herein.

Before proceeding further with the evaluation of the cutting theories, a short search was made for any software that may have been suitable to support this work. A small software package was located and did provide an alternative approach to selecting the cutting process and cutter. The software package published by Prototyp-Werk Gmbh[25] and was initially supplied by a local tooling supplier. This software package was based on metal cutting theory which is very much dependant on the properties of the material being cut. The value in the software for the Elastic Modulus for

thermoplastics appeared to be a very general single value. The package appeared to be more applicable to the cutter selection rather than the power performance analysis of the cutting mechanics. This for most users is more than adequate as the machine in which the cutter is to be applied generally has more than sufficient spindle power. A further more in-depth look at this software was undertaken and described in a later discussion included below.

In a highly reported publication by Yusuf Altintas[26] the mechanics of metal cutting in terms of the forces involved, is very thoroughly analysed. However, this publication was written specifically with regard to the machining of metals. Altintas was contacted directly with regard to cutting plastic, as part of the attempt to find information about machining plastic materials. No redirection to other existing research could be offered from this line of inquiry. The author was advised to do detailed experimental cutting trials to determine the specific cutting pressures, power consumption, and to gain an understanding of the cutting and machining process characteristics for R-PVC.

The mechanics and the mathematics involved in analysing the cutting process was assumed similar to that of metal removal processes for some plastics, - this was based on comments by Kobayashi[27]. The notion that the assumption of similar cutting processes, between metals and particular polymers could be extended to milling processes began to be investigated. As a precursor Metal cutting theory was researched to gain a basic understanding of the cutting process and also to aid in the investigation of cutting plastic. The chronology of the cutting theory development was also of interest to some extent to gain a measure of understanding of the scale of research that has been undertaken on metal cutting in comparison to that for plastic cutting theories.

4.3.1 General material cutting theory

Upon the conclusion of the initial investigation presented above, unanswered questions remained. The first and most obvious was, "Which characteristics are similar to each other, in both plastics and metals, when machined using similar processes?" This lead to a second search based on the notion of metal cutting theory applied to cutting plastic or polymeric materials.

The obvious point of incursion into this investigation would be with a brief overview of metal cutting theory and some of the history to support the theories that are applied by today's researchers.

The mechanics of metal cutting is similar in some respects to the mechanics of plastic cutting[28] and it is therefore good background material as the processes for arriving at results from either type of cutting action are similar.

- History

The history of metal cutting begins circa 1760 when the first major developments began to evolve, as working in brass, bronze, wrought iron and gray cast iron became more popular. These materials were relatively easily worked using carbon steel that had been hardened and shaped for tooling[29]. The advent of metal cutting, as we know it today, began with the invention and implementation of a horizontal boring machine to machine the cylinders for the first steam engines designed and built by Watts (1776)[30]. The hundred years or so from approximately 1760 has seen the development of machine tools designed to specifically produce the component surface geometries required by the demands of developing economies. Along with these new demands for manufactured features, came the demand for better tooling materials. Machine tools and materials evolved, as did the problems associated with working the new materials such that toward the end of the 19th century rapidly escalating labour and capital costs involved in machining were becoming prohibitively expensive. The reduction in production costs was and still is the major driving force behind the progress and developments in the metal cutting industry[31].

From these primitive beginnings, the metal cutting research fraternity has inevitably turned its focus toward the events occurring in the small volumes of material surrounding the cutting edge of the tool. During the cutting process, the action at the cutting edge is largely unobservable, but the indirect evidence of this action has been the focus of attention by many researchers[32].

The search for a theory that relates cutting forces, tool stresses and temperatures, etc., to the cutting conditions, tool geometry, work piece and tool material properties has been the subject of much research on the notion that it should be possible to establish factors such as cutting power and tool life.[33] The use of empirical relations to find these factors were developed by Taylor (1907), Koenigsberger (1964),

Kronenberg (1966) et al and organisations such as Metcut (1980) by researching experimental data and publishing the results as machining information.[34] The main drawback with this is the immense amount of time taken to research and collate the data and develop a viable and robust model. To reduce this effort, work by others has been put into developing more fundamental relationships, other than the purely empirical ones[35].

A brief summary of the basic material (metal) cutting process will be outlined using the well researched and validated publication by Altintas et al[36].

The material removal process using conventional cutting tools is a complex process, such that after the thousands of hours of research and testing, is relatively well understood[37]. There are still some basic assumptions that are made to ensure that the theories are robust. These assumptions are based around the actual mechanics of material removal and the physical processes that are taking place. The cutting action is defined by three deformation zones that form the basis of metal cutting theory. The primary zone is formed as the cutting edge is driven through the work piece parting the material ahead of the tool. The secondary deformation zone is formed as the chip material partially deforms and moves over the rake face and the third or tertiary zone is where the cut surface rubs on the flank or relief face of the tool as it passes over the newly formed surface.[38] Following on from the notion of the three regions formed in the cutting action there are two assumptions used for the analysis of the primary shear zone. The first is based on the assumption that the shear zone is a thin plane[39] and the second is that a thick shear deformation zone is formed and the analysis is based on the laws of plasticity[40] [41]. In the interests of simplicity Altintas has based his publication around the notion of the thin plane theory and as such makes two more assumptions. The first assumption is that the tool is sharp with no cutting edge radius and the second is that all the primary deformation takes place along an infinitely thin plane[42].

These physical processes are still being deeply researched as the manufacturers of metal cutting tooling strive to improve their products[43] and to that end the assumptions are of paramount importance as they are used to determine the forces involved in actually removing the material from the cut zone of the work piece. The forces can be measured by the use of strain gauge dynamometers suitably positioned

with regard to the cutting edge[44]. This however, will only provide best guess approximations as the analysis best suits a stationary orthogonal tool as it is not possible to analyse a rotating tool in the same way. Cutting face forces are not able to be easily determined on a rotating tool, which is the cutting process that will be associated with the machine tool being developed in this project. The forces that are resultant on the machine tool are measurable. That is, the force resisting the tool from moving forward into the material, the force normal to the direction of travel and to some extent the force attempting to drag the tool into the work (conventional milling) or push it out (climb), can be determined as can the torque required to drive the tool through the material[45].

- The Mechanics of Cutting Plastic

As stated earlier the literature available with regard to the mechanics of cutting plastic is minimal. However, an excellent reference was discovered in the form of the 1967 volume, "Machining of Plastic," written by Akira Kobayashi of the electro-technical laboratory in Tokyo, Japan[46]. This book covers extensively, the mechanics of cutting various plastics with a comprehensive chapter on the fundamental considerations of machining plastics. It would appear that this is still the most comprehensive volume available even 39 years later. The book covers a raft of homogenous plastics and machining processes after the initial description of single edge cutting mechanisms, but unfortunately, it excludes milling. The highly relevant chapter concerning cutting mechanisms is reviewed in following sub sections. The mechanics and analysis used by Kobayashi is similar to that used and published by Altintas et al to describe metal cutting as will be seen in the subsequent dissection of Kobayashi's research contribution.

The project nominated milling process required a more complex analysis, based on the multipoint cutters used. Kobayashi's work on plastic cutting does not venture into the multipoint milling process but does instead give excellent cover of the orthogonal cutting process in his publication. When considering the cutting process, the orthogonal process appeared to be the starting point for research published in this field. In continuing the practise and due to a lack of published multipoint cutter research, in relation to plastics, the orthogonal process was considered a good start

point. To that end, the transition to multipoint cutting is discussed in depth at a later stage in this work.

4.3.2 Review of plastic (polymer) cutting theory

As stated above Kobayashi's seminal work is drawn upon heavily in this section due to its relevance and the apparent lack of other available material. In his work, Kobayashi explains that the field of metal cutting has had extensive research carried out over a long period of time. Most of the metal cutting theories are based on the premise that a shear plane is generated in the material upward from the point of the cutting tool, and the assumption that the metal is an ideal plastic body having a homogenous structure which will yield at the point of maximum shear stress. When the thickness of the metal chip is measured, it is always found to be thicker than the depth of cut and shorter than the cut length of the surface being machined. The flow lines within the chip suggest that the cutting action involves a shearing mechanism[47]. Figure 4.2 demonstrates the change in thickness between the deformed chip, d_c and the undeformed chip, d.

In the cutting of plastics, the assumption of a shear plane formed from the tip of the tool does not hold for all types of plastics, and its presence or absence depends on the cutting conditions and properties of the particular plastic. The rheological behaviour of plastics therefore precludes the assumption that metal cutting theories can always be applied to explain the cutting mechanism in plastics[48]. Perhaps the question that now requires raising here is, "Why is this so?" Unfortunately, Kobayashi does not answer this question. Fortunately, the particular plastic concerned within this work, does form a shear plane in the cutting zone, and therefore does fall within the bounds of the above assumption. The material based reasons for this to occur fall beyond the scope of this investigation.

The first step in the investigation was to fully analyse the work in Kobayashi's publication. This analysis was considered critical to understanding the exact nature of the published research, which without such an understanding, any comparisons with other published work would have been impossible. Due to the minimal level of published research in this field, Kobayashi's work has been reproduced here to enable the reader to fully grasp the nature and complexity involved in determining the desired missing parameters required to evaluate the orthogonal cutting power.

As with all mechanics problems, a good diagram is essential to give a clear picture of the actions occurring in the process. The diagram in Figure 4.2 shown below gives a graphical indication of the forces and applicable physical dimensions of the cutter/work piece interaction as they relate to the orthogonal cutting analysis in the following sub sections.

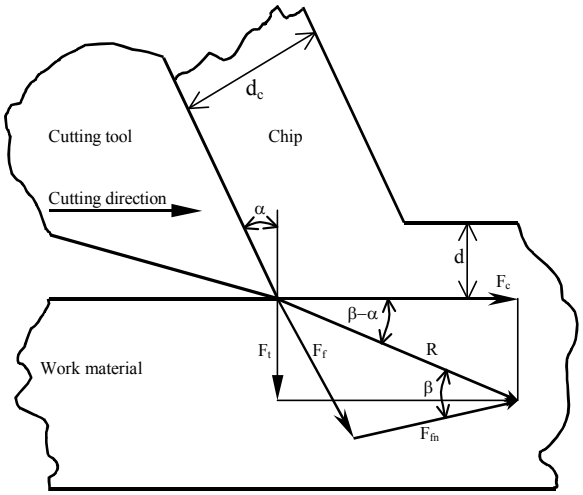

Figure 4.2: Schematic diagram of 2D orthogonal cutting[49].

The following parameters relate to those shown in Figure 4.2 and in Equations [1] – [3],

where;

R = resultant cutting force [kg]
F_c = force component in the direction of relative tool travel [kg]
F_t = force component perpendicular to cutting direction [kg]
F_f = friction force on the rake surface [kg]
F_{fn} = normal force on rake surface [kg]
α = rake angle [deg]
β = friction angle [deg]
d = depth of cut [mm]
d_c = chip thickness [mm]

This entire force system lies in a single plane and from the diagram; the following geometric force relationships can be derived.

$$F_f = F_c \sin\alpha = F_t \cos\alpha \quad [1]$$

$$F_{fn} = F_c \cos\alpha - F_t \sin\alpha \quad [2]$$

$$\mu = \tan\beta = \frac{F_f}{F_{fn}} \quad [3]$$

The analysis of the cutting mechanism developed by Kobayashi is based on six assumptions:

1. The tool's cutting edge is perfectly sharp and straight, cuts perpendicular to the direction of motion, and has a width greater than that of the work-piece.

2. The shear surface is a plane extending upward from the cutting edge.

3. The cutting edge generates a plane surface and a constant depth of cut as the work moves past it with uniform velocity.

4. A continuous chip is produced without a built up edge.

5. The chip does not flow to either side; since it has the same width as the work-piece, (this will not always be true in cutting plastics).

6. There is no contact of the work-piece with the relief surface of the tool (actually, contact between them is often observed in slow speed cutting of plastics, which shows considerable work piece elasticity)[50].

A 2001 publication by Zhang et al raised the issue of relief surface contact when machining plastics. This relief surface contact complicates the theories that Kobayashi puts forward as it considers the cutting zone as three separate regions, one of which is the frictional aspect of the tool relief surface, called the bouncing region[51]. Kobayashi considers this phenomenon as part of a discussion about optimum cutting conditions and the heat generated by the cutting action, and he recognises the most severe situation comes about with materials that possess large elastic recovery modes, where the rake face friction values are highest[52]. The analysis that Kobayashi developed however does not consider the notion of the three zones directly, in that there appears to be no provision made in the breakdown to determine the effects of the separate zones, only the overall friction force shown in Figure 4.2. Zhang et al, however, has indicated that the total cutting forces are the sum of the force components from all three regions[53]. In Kobayashi's work, there was no attempt to quantify the separate effects from any of the zones on the total forces applied during cutting. The experimental verification of Zhang et al showed that the model predicted the major deformation but that there was a maximum error of 37% when predicting the vertical forces and 27% for the horizontal forces[54]. Further interpretation of these results is outside the scope of this work as it involves further experimentation and was based

around a fibre reinforced composite material rather than a homogeneous polymeric material.

Figure 4.3 is given below to show the mechanics of cutting with the forces in equilibrium. This differs from Figure 4.2 in that it shows the force equilibrium when a shear plane is formed.

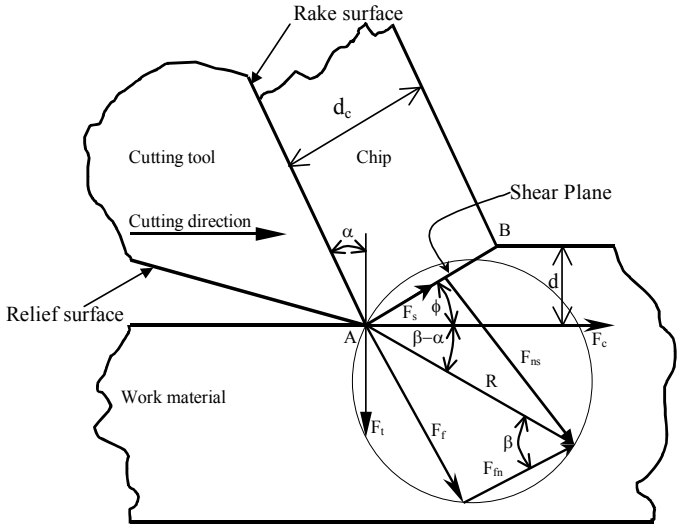

Figure 4.3: Equilibrium of cutting forces when a shear plane is formed.[55]

The parameters applicable to Figure 4.3 are the same in many cases as those in Figure 4.2; however, there are additional parameters that relate to the equilibrium condition. These additional parameters are listed below:

ϕ = shear angle [deg]

F_s = force component along the shear plane [kg]

F_{ns} = force component perpendicular to the shear plane [kg].[56]

The shear angle ϕ is extremely difficult to determine in both plastic and metal cutting and Kobayashi suggests that this may be obtained from direct measurement of micrographs, which is highly inconvenient. A second method is given using the chip thickness ratio, r, which is the ratio of depth of cut, d, to chip thickness, d_c[57]. Again, it is noted that this also is not a good means of determining the shear plane angle, as it is difficult to measure the chip thickness accurately.

Kobayashi's method of determining the forces revolved almost entirely around the knowledge of the chip thickness ratio from which he proceeds to show how the forces may be calculated using the diagram shown in Figure 4.3.

The relationships (extracted from Kobayashi's work) are given in the following equations [4] – [7], where the terms are defined above:

$$\tan\phi = \frac{r\cos\alpha}{1-r\sin\alpha} \quad [4]$$

$$F_s = F_c\cos\phi - F_t\sin\phi \quad [5]$$

$$F_{ns} = F_c\sin\phi + F_t\cos\phi = F_s\tan(\phi+\beta-\alpha) \quad [6]$$

$$A_s = \frac{bd}{\sin\phi} \quad [7]$$

and where;

As = shear plane area [mm2]
b = width of cut [mm]
d = depth of cut [mm]
r = chip thickness ratio

The mean shear, τ_s and normal stresses, σ_s on the shear plane can be calculated from

$$\tau_s = \frac{F_s}{A_s} = \frac{(F_c\cos\phi - F_t\sin\phi)\sin\phi}{bd} \quad [8]$$

$$\sigma_s = \frac{F_{ns}}{A_s} = \frac{(F_c\sin\phi + F_t\cos\phi)\sin\phi}{bd} \quad [9]$$

The shear strain γ is also of interest to the mechanics of the cutting process and is shown in equation 10.[58]

$$\gamma = \tan(\phi - \alpha) + \cot\phi = \frac{\cos\alpha}{\sin\phi\cos(\phi - \alpha)} \quad [10]$$

Of further interest in the cutting process are the various velocities associated with the geometry of the orthogonal cutting action. These are shown in Figure 4.4.

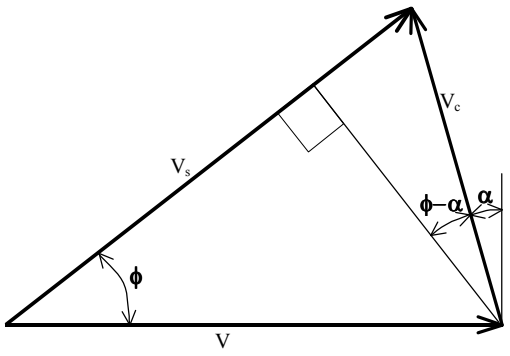

Figure 4.4: Relationship between cutting velocities[56]

The cutting velocity, V is the velocity of the tool parallel to F_c. The chip velocity V_c is the velocity of the chip along the rake surface and the shear velocity, V_s is the velocity of the chip relative to the work piece along the shear plane. In accordance with

kinematic principles, the following relationships, equations [11] – [12], can be shown to exist.

$$V_c = \frac{\sin\phi}{\cos(\phi-\alpha)}V = rV \quad [11]$$

$$V_s = \frac{\cos\alpha}{\cos(\phi-\alpha)}V = \gamma V\sin\phi \quad [12]$$

Another notion put forward by Kobayashi was the energy consideration, which is represented in equations [13] – [15] following. The total energy per unit volume of material removed in an orthogonal cutting process will be:

$$u = \frac{F_c V}{Vbd} = \frac{F_c}{bd} \quad [13]$$

The shear energy per unit volume is given by

$$u_s = \frac{F_s V_s}{Vbd} = t_s\left(\frac{V_s}{Vsinf}\right) \quad [14]$$

The friction energy per unit volume is obtained by

$$u_f = \frac{F_f V_c}{Vbd} = \frac{F_f r}{bd} \quad [15]$$

Kobayashi follows these equations with examples of the orthogonal data obtained from a number of dry cutting trials.[59]

Table 4.3: Typical data obtained in dry orthogonal cutting of R-PVC

d	**α**	**V**	**F_c**	**F_t**	**r**	**φ**	**γ**	**τ_s**	**σ_s**	**σ_c***	**μ**
mm	deg	m/min	kg	kg		deg		kg/mm^2	kg/mm^2	kg/mm^2	
0.05	30	110	2.40	-0.70	0.833	51.1	1.19	7.98	5.55	12.0	0.245
0.05	20	110	3.10	-0.40	0.980	54.2	1.4	8.67	9.24	15.5	0.224
0.05	10	110	3.50	-0.20	0.943	48.0	1.68	9.25	9.17	17.5	0.118
0.05	0	110	4.20	0.60	0.769	37.6	2.07	9.03	9.26	21.0	0.143
0.05	-10	110	4.60	1.5	0.581	27.5	2.69	7.82	7.97	23.0	0.142
0.05	-20	110	4.60	2.2	0.500	21.9	3.39	6.42	6.99	23.0	0.0974

* typically, per unit volume

On the basis that the author's interest is predominately with regard to R-PVC, Kobayashi's results for R-PVC have been reproduced in Table 4.3 above and Table 4.4 below.

Table 4.4: Typical data obtained in dry orthogonal cutting of R-PVC continued[60]

d mm	**u** kg/mm^2	**u_s** kg/mm^2	**u_f** kg/mm^2
0.05	12.0	9.53	2.47
0.05	15.5	12.1	3.35
0.05	17.5	15.6	1.94
0.05	21.0	18.7	2.31
0.05	23.0	21.0	1.97
0.05	23.0	21.8	1.24

The final consideration that Kobayashi comments on is the machinability of plastics. The relevant section of his book begins by asking, "What is machinability?" He defined it as "the ease with which a material can be cut[61]." In this particular case, it refers to plastics specifically, with the result being a defined machinability index. There are three criteria to be considered in measuring machinability: tool life, cut surface finish and the power required to execute the desired cut. Thus 'good machinability' means low power consumption, long tool life and smooth cut surfaces and thus machinability improves as these factors decrease. Machinability, η_c, was defined quantitatively as per equation [16] below.

$$\eta_c{}^1 = \frac{V_m}{V_w.hp.S_f} \qquad [16]$$

where;

V_m = cut volume per unit time [mm^3/min]
V_w = volume of tool wear per unit time [mm^3/min]
hp = net power consumption during cutting [kW]
S_f = roughness of cut surface, [μm]

(Note – Kobayashi does not use the usually recognised symbol for surface roughness, Ra, here.)

The next set of steps that Kobayashi reported were the assumptions underpinning the determination of some of the small values included in the derivation. Also, some of the ratios contained in equation [16] can be expressed in relation to the kinematics of the orthogonal cutting process being investigated. These assumptions are that the surface roughness S_f, and the tool wear V_w may not be considerations, and the fact that the power, hp [kW], is a function of the cutting force F_c [kg] and the cutting speed V [m/min]. This in turn gives the machinability index η_t as:

$$\eta_t = \frac{V_m}{hp} = \frac{2\pi Rdf.6120}{F_c V} = k\frac{df}{F_c n} \quad [17]$$

where;

$V_m = 2\pi Rdf$ (R = radius of work piece [mm],
d = depth of cut [mm],
f = tool feed velocity [mm/min]
$hp = F_c V/6120$ [kW]
n = rotational speed of work piece [rpm]
k = constant

The final conjecture is that the tool feed velocity, f, can be neglected in orthogonal cutting thus giving equation [18].

$$\eta_s = k\frac{d}{F_c} \quad [18]$$

To conclude the analysis the total energy per unit volume of material removed, u, is introduced as per equation [13]: The resulting term being described as the 'specific cutting force' [kg/mm^2]. Thus, the machinability of the material being cut becomes much improved as the value of the specific cutting force decreases. The conventional method of determining the specific cutting force or the machinability of a plastic is to perform experimental single point orthogonal cutting using apparatus that is capable of measuring the applied cutting forces, the tool wear and the surface roughness. A final comment is that the machinability of the material improves as the percentage of continuous chip increases[62].

The formation of continuous flow chips would be the goal of the machinist as this will produce the finest and most accurate surface. In metal cutting, the definition of machinability is defined as the work directed at chip breaking and further definition is in the form of the following four factors:

- Surface finish and integrity of the machined part
- Tool life obtained
- Force and power requirements
- Chip control

Thus, good machinability indicates good surface finish and integrity, long tool life, low force and power requirements[63], and short well defined and curled chips.

Kobayashi's definition appears to differ a little but essentially he has defined a similar regime in that he was looking for a chip type that would meet the four requirements

above and is seeking to use cutting conditions that will produce the 'continuous flow*' type of chip.

4.3.3 Chip formation in plastics

It is perhaps pertinent here to include some information with regard to the type of chip formed during the process of machining plastic. The following table, Table 4.5, presents a summary of the types of chip formed, their probable or major cause and the effect on surface finish. Also included is a brief comparison to the equivalent chip found in metal cutting processes.

Table 4.5: Classification of plastic chip types[64]

Types of chip in plastic cutting	Major cause	Surface finish/ dimensional accuracy	Metal cutting comparison
Continuous			
- Flow*	High elastic deformation	Fine surface, good dimensional accuracy	Not formed in metal cutting
- Shear	Slippage continuously by shear stress	Good surface quality	Continuous flow
Discontinuous			
- Simple shear	Plastic fracture by simple shear stress	excessively rough, very poor dimensional accuracy	
- Complex shear, elastic fracture, brittle fracture	Plastic fracture by shear stress with compressive and/or tensile stress	Both dimensional accuracy and surface finish are very poor	
- Crack	Elastic fracture, brittle fracture	Severe surface marking with poor finish and accuracy	Not formed in metals, except some grades of cast iron

Each of the entries in Table 4.5 is given a little more in depth explanation in the following sub sections.

- Continuous flow chips*

These chips are formed by a smooth and continuous cutting action. Such chips will usually be observed in materials with high elasticity and demonstrate large deformations at fracture. The chips are formed by elastic deformation and not plastic fracture. It is usually seen in slow speed cutting and the deformed chip thickness is nearly equal to the undeformed chip thickness. This type of chip is not observed in metal cutting processes[65]. (The asterisk denotes that this is different from the continuous type chips found in metal cutting[66].)

- Continuous shear chips

This type of chip is formed by shearing action along the formed shear plane. The chip's deformed thickness will be larger than the undeformed thickness. The shear plane will be produced in the direction of minimum work and the chip is formed when the shear strain on the shear plane is less than the limiting rupture strain. This type of chip compares with the continuous flow type found in metal cutting[67].

Both of the previous chip types are formed using tools with positive rake angles. The following types of chip are formed when machining with negative rake angle tools[68].

- Discontinuous simple shear chips

This chip is also produced by shearing along the shear plane, but the shear intervals are large and the chip is discontinuous. These chips occur when the shear strain on the shear plane is greater than the limiting rupture strain[69].

- Discontinuous complex shear chips

This condition is observed as a 'sticky' cutting action. Here the chips are formed by the complex action of a large compressive stress acting with shear stress caused by using a tool with a negative rake angle.

- Discontinuous crack chips

The discontinuous crack type chip is the odd fellow of the lot as it is produced using a highly positively raked tool and a relatively large depth of cut. This tool produces, under certain conditions, a discontinuous chip with cracking around the tool point. This type of chip is formed when cutting brittle materials such as thermosetting plastics and some thermoplastics. During cutting, a crack forms downwards at an oblique angle from the cutting edge into the material, forming a discontinuous 'blocky' chip. The chip is eventually formed when the forming crack is long enough to fail under bending conditions. Thus, this chip formation is a type of brittle fracture. However, the chip is produced by elastic fracture causing 'hackle marks' parallel to the cutting edge in the material. The marking is similar to that seen on hard brittle materials such as glass and is never seen in metal cutting except in some types of cast iron[70].

The brief description of the types of chip formed in plastics was provided to give a little understanding to the reader in a generalised way. The preceding descriptions of the chip types were extracted from Kobayashi's publication, Machining of Plastics. The

specific material about which this project is concerned is R-PVC and the following sub section provides more information extracted from Kobayashi's publication and seeks to inform the reader with regard to some of the characteristics and properties of R-PVC.

4.3.4 Rigid polyvinyl chloride as a work piece material

Rigid-PVC being the material of immediate interest was analysed in depth by Kobayashi and a review of that work follows. Tables 4.3 & 4.4 show the specific orthogonal cutting data published for R-PVC.

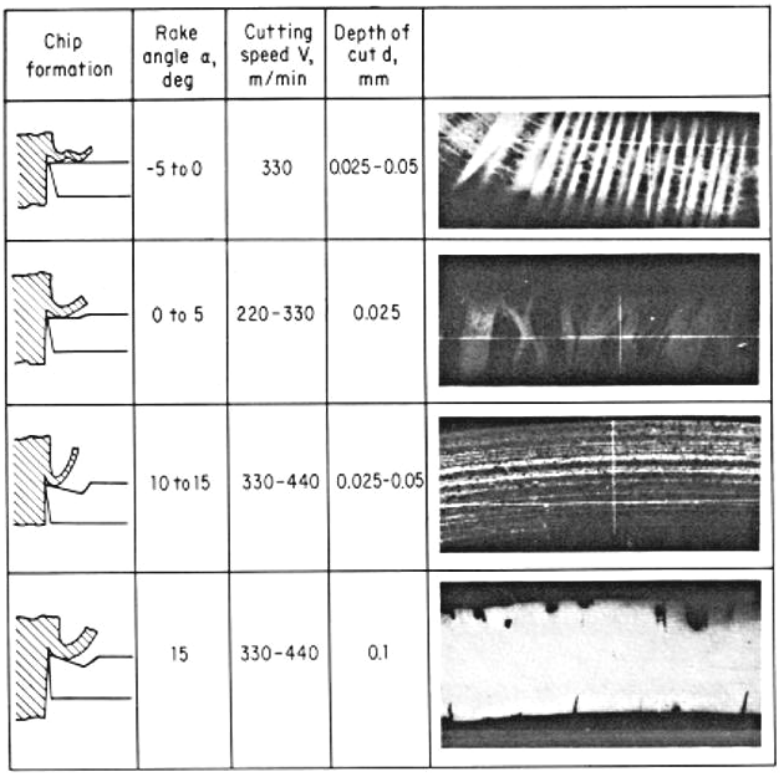

Figure 4.5: Effects of rake angle, cutting speed, and depth of cut on type of chips produced when R-PVC is cut[71].

Rigid PVC is relatively easy to cut with single point tools, except when the depth of cut, the positive rake angle or the cutting speed is too great. The effect of these various parameters is shown in Figure 4.5. The top three types of chips are of the continuous shear type whilst the fourth picture shows a discontinuous shear type, which occurs with deep cutting, high cutting speeds and a steep positive rake angle. Nearly all other types of cutting conditions produce a continuous chip form. The friction of the chip with the rake surface and the heat generated causes the folding and collapsing of the continuous chip into a bunched mass that resembles the discontinuous type of chip formation. The chips do become discontinuous as the depth of cut increases beyond 0.1 mm.[72]

Figure 4.6 presents the charts of Kobayashi's experimental work showing the cutting force component (F_c) relationships as functions of depth of cut (upper charts) and rake angle (lower charts). The cutting force component Fc, relates back to cutting force shown in Figure 4.3 presented previously.

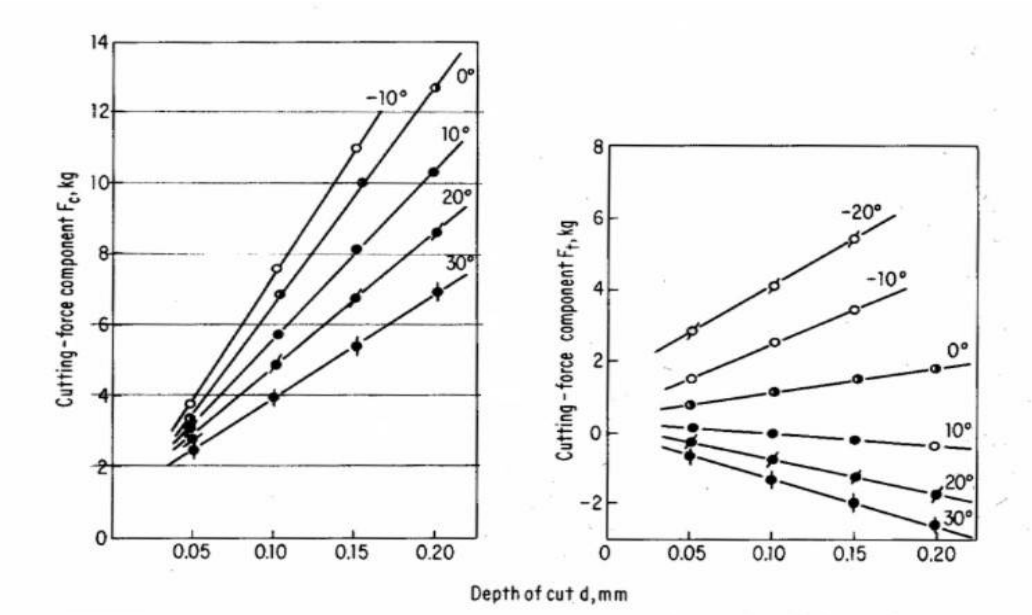

Cutting-force components as a function of depth of cut and tool rake angle when rigid polyvinyl chloride is cut at a cutting speed of 10 m/min.

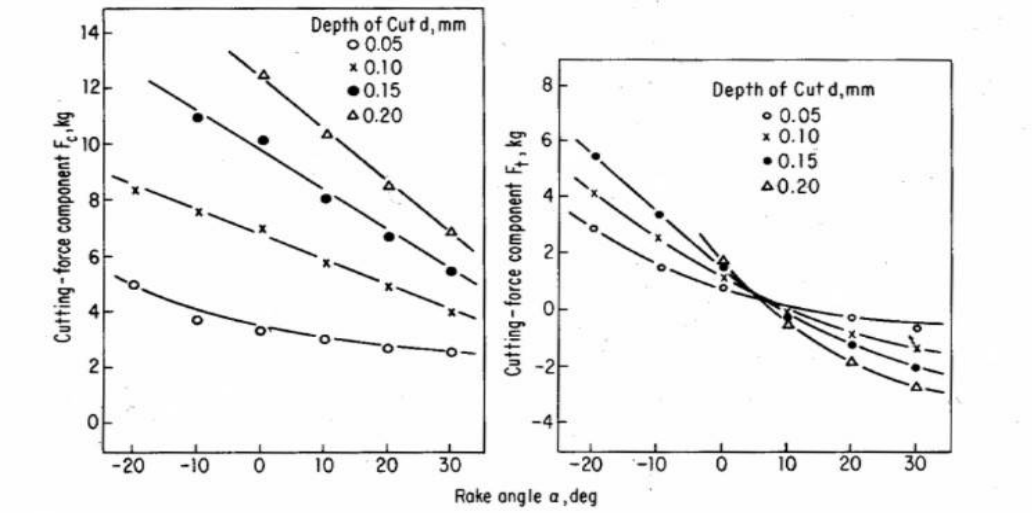

(*a*) Relationship between cutting force parallel to direction of cut F_c, tool rake angle, and depth of cut when rigid polyvinyl chloride is cut at a speed of 10 m/min. (*b*) Relationship between cutting force normal to cutting direction F_t, tool rake angle, and the depth of cut during cutting of rigid polyvinyl chloride.

Figure 4.6: Cutting force relationships[71]

It is unfortunate that the balance of the Kobayashi work concerning cutting R-PVC is predominately based around data collected from trials using a cutting speed of 10 m/min, which is relatively slow, although there are references and data from trials with cutting speeds up to approximately 120 m/min.

There are variations in the cutting forces that come about as the three major parameters concerning the cutting mechanism change: rake, depth of cut and speed. From experimental work, Kobayashi arrived at critical rake angles (Table 4.6) for a cutting speed of 10 m/min. The critical rake angle is defined as the angle at which the cutting force component, F_t, (Figure 4.3) becomes zero.

Table 4.6: Critical rake angles for R-PVC at 10 m/min cutting speed[71]

Depth of cut [mm]	Critical rake angle [deg]
0.05	13
0.10	11
0.15	10

The force component F_c along the direction of cut increases as the depth of cut increases, however the force component F_t, perpendicular to the direction of cut, decreases slightly with a positive rake angle and as the depth of cut increases. Figure 4.7 demonstrates the relationships between the specific cutting forces, the depth of cut and the rake angles.[73]

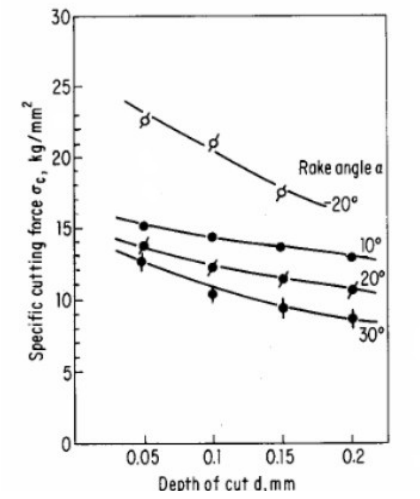

Relationship between specific cutting force, depth of cut, and tool rake angle during cutting of rigid polyvinyl chloride.

Figure 4.7: Specific cutting force relationships[74]

From this data, the specific cutting force can be determined and is shown to be relatively small, but is subject to the same parameters that affect the cutting forces. Thus, Kobayashi recommends that for R-PVC it is better to choose as large a depth of cut as possible and to use a positive rake angle tool to reduce the specific cutting force. However, in selecting the appropriate cutting parameters, the surface finish must also be considered. Cutting speed using carbide tooling affected the surface

finish, but the same was not true with diamond tooling. The surface finish was also dependent on the feed speed. So achieving a smooth surface and an accurate finish was not difficult with R-PVC when the cutting conditions were properly selected.[74]

The tool wear was another area that was investigated by Kobayashi using carbide tooling and at a cutting speed of 100 m/min, a depth of cut of 1.0 mm and a feed rate of 0.6 mm/rev. The tool had a rake angle of 20° and was run for varying periods of time. The tool flank wear with carbide tooling cutting R-PVC was small with K10 type carbide. The flank wear was found to increase with increases in the feed speed, cutting speed and depth of cut. However, in an apparent contradiction Kobayashi found that the higher the cutting speed the smaller the flank wear. Further experimental cutting was made with tool steel, which showed a tendency to wear at the cutting edge: a phenomenon peculiar to plastic cutting, and not observed in metal cutting. The wear characteristic can be seen in Figure 4.8.

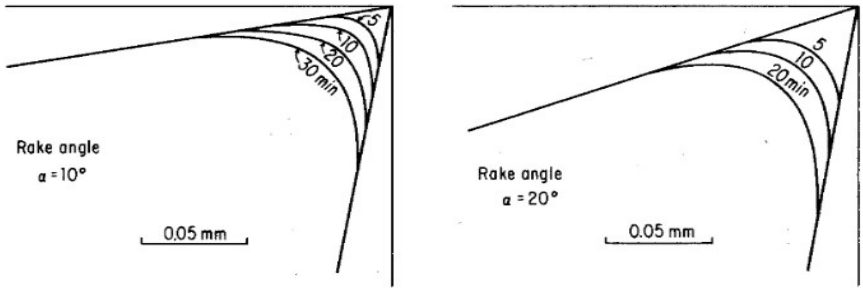

Wear progress on tool's cutting edge when rigid polyvinyl chloride is cut with a high-speed-steel tool (SKH 3) having the rake angle of 10° and 20°, respectively. Cutting speed is 117 m/min and feeding speed is 0.062 mm/rev. Relief angle is 10°. (*Anmi et al.*)

Figure 4.8: Tool edge wear on tool steel cutting edges[75]

An observation was made that if the tool edge radius was larger than the depth of cut then no material removal takes place and the work piece material is merely compressed as the tool passes by with no chip being formed. Conversely when the

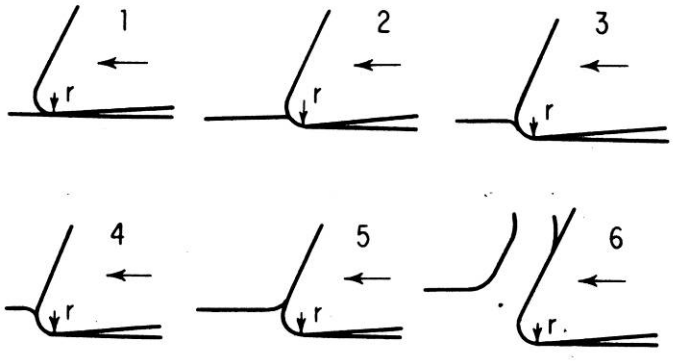

Figure 4.9: Chip formation in relation to tool cutting edge radius[75]

radius of the cutting edge is less than the depth of cut a chip will form. Figure 4.9 demonstrates this from the text by Kobayashi. As the depth of cut increases (Figure 4.9, 1 – 6) chips will only begin to form when the depth of cut exceeds the tip radius[75].

Kobayashi continues in his text with descriptions of cut off methods, drilling and finishing of various plastics. His research contribution is comprehensive but not specific to mill operations and therefore deemed to be only indirectly supportive.

Perhaps the most disappointing result of the published research was the fact that an analytical method does not appear to exist that will provide a solution for determining the cutting forces from the geometry and material properties of the tooling and work piece. Anecdotal evidence suggests that developing such a method has already been the subject of many hours of intense research and as such falls outside the scope of this project. As an alternative solution, comparing established orthogonal metal cutting theory with a similar looking theory relating to polymeric materials was considered and researched. This theory comparison is reported in the following sections.

4.3.5 Comparison of orthogonal cutting theories

Research into the orthogonal plastic and metal cutting theories by Kobayashi and Altintas respectively showed a number of similarities in the documented kinematics and mechanics of the two processes. To test these similarities, the two theories were compared using the Kobayashi's published orthogonal data for R-PVC, which is presented above in Table 4.3. This R-PVC data was data obtained from orthogonal cutting tests, and is comparable to data published for metals in the Machining Data Handbook and assumed to be obtained by similar means. Although Kobayashi doesn't reference any specific historical researcher with regard to the cutting theories he presented, comments made in the opening paragraphs of chapter two of his text[76] suggest that there is a familiarity with established metal cutting theories. In fact, a brief comparison of the published work of M.E. Merchant in the 1944 Journal of Applied Mechanics shows that Kobayashi's theory follows very closely to that of Merchant[77].

The initial comparison was made by comparing the vector force diagrams as they have been published by both Kobayashi (Figure 4.10) and Altintas (Figure 4.11). The similarities were very clear with the only differences coming from the different

nomenclature used by the two authors. In an attempt to clarify the comparison of the theories, the nomenclature used in the equations has been tabulated below each respective figure, with similar variables from each theory being placed in corresponding table cells for ease of cross referencing and comparison. Where there is no direct comparison or no published data from a particular author a space has been left in the relevant column.

-Kobayashi Diagram

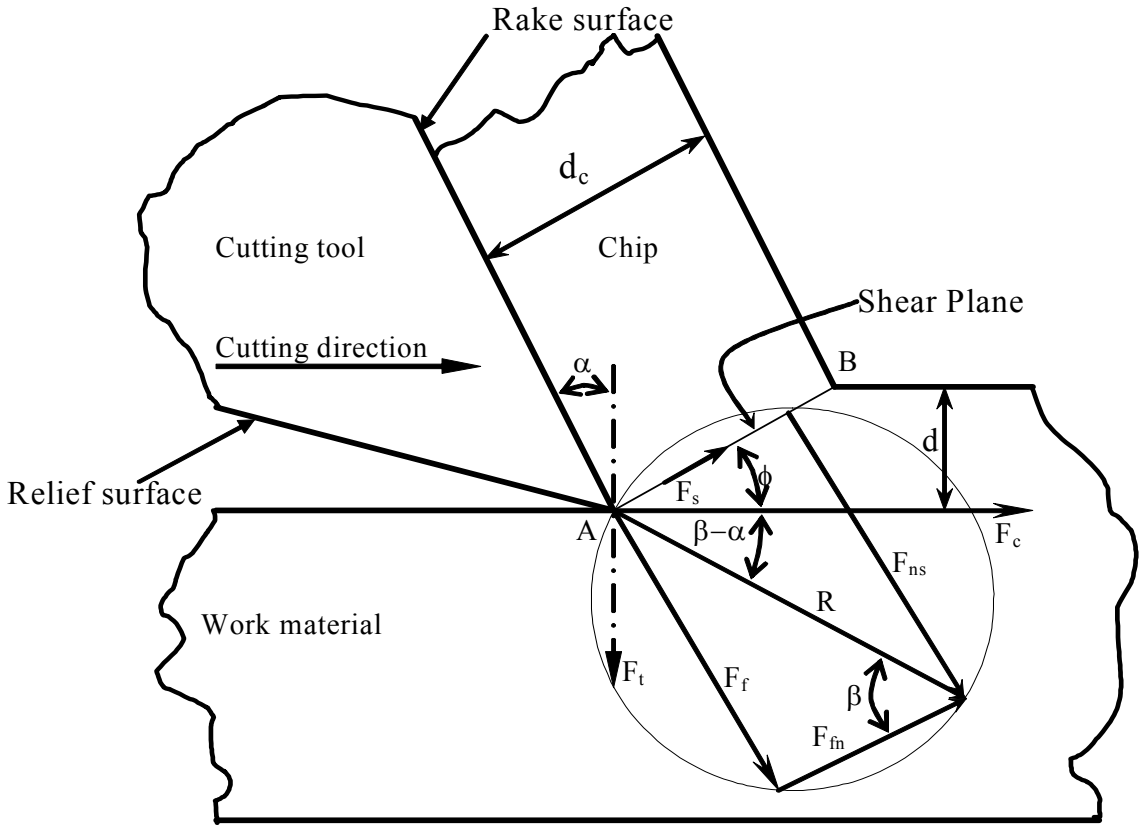

R = resultant cutting force

F_c = force in direction of tool travel

F_t = force perpendicular to tool travel

F_f = friction force on rake face

F_{fn} = normal force on rake face

F_s = force parallel to shear plane

F_{ns} = force perpendicular to shear plane

ϕ = shear plane angle

α = rake angle

β = friction angle

d = depth of cut

d_c deformed chip thickness

Figure 4.10: Cutting force diagram by Kobayashi[54]

-Altintas Diagram

As an aid to assist the reader in understanding and following the detailed theory

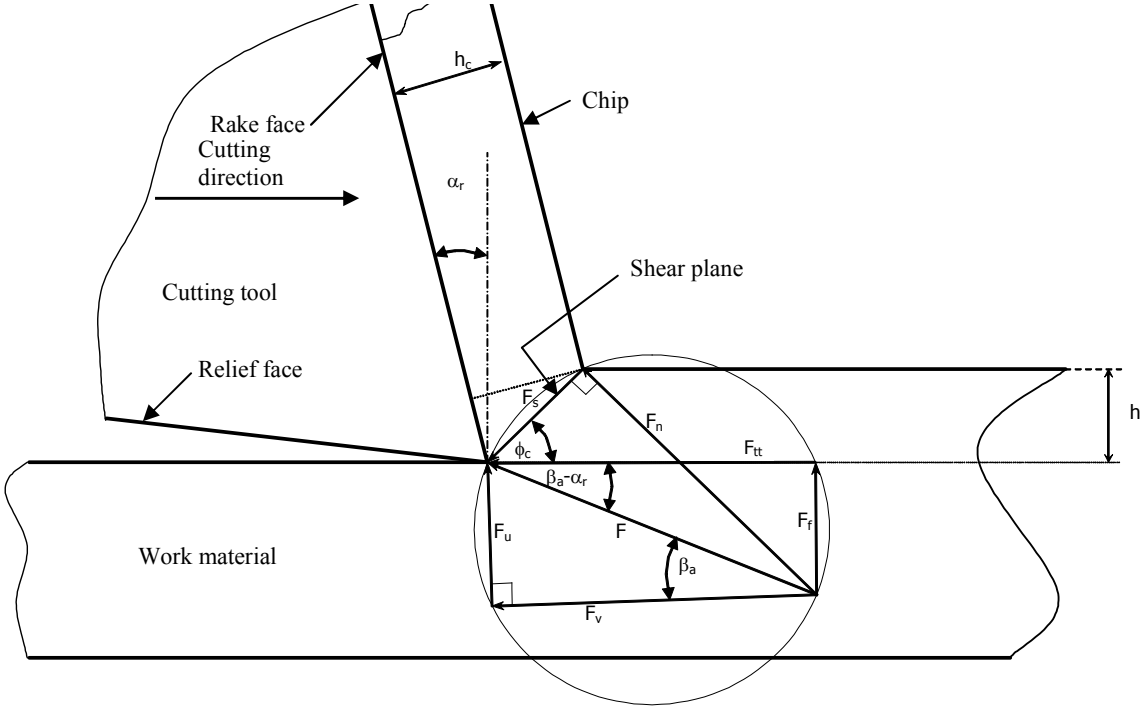

F = resultant force	F_n = force normal to shear plane
F_{tt} = tangential force	ϕ_c = shear plane angle
F_f = feed force	α_r = rake angle
F_u = friction force on rake face	β_a = average friction angle
F_v = normal force on rake face	h = depth of cut
F_s = shear force on shear plane	h_c = deformed depth of cut

Figure 4.11: Cutting force diagram by Altintas[74]

comparison in section 4.3.6, a list of the nomenclature used by the two authors is presented below in two columns. Where there is correlation between the terms they are aligned across the columns, including those terms where the symbol varies. Where there are spaces in either of the two columns there is no direct correlation between the two theories.

Kobayashi analysis terms	*Altintas analysis terms*
<u>Primary Shear Zone</u>	
R – resultant force	F – resultant force
F_c – force in the direction of the tool travel	F_f – feed cutting force – perpendicular to tool travel
F_t – force perpendicular to tool travel	F_{tt} – tangential cutting force – in direction of tool travel

	F_r – radial cutting force – perpendicular to the cutting edge direction of travel
b – width of cut	b – width of cut
d – depth of cut	h – depth of cut
	i – inclination angle – oblique cutting
	F_r – radial force – oblique cutting
ϕ – shear angle	ϕ_c – shear angle – angle between shear plane and direction of cut
V – cutting velocity	V – cutting speed
τ_s – mean shear stress on shear plane	τ_s – shear stress on the shear plane
σ_s – mean normal stress on shear plane	σ_s – normal stress on the shear plane
F_s – force along the shear plane	F_s – shear force on the shear plane
β – friction angle	β_a – average friction angle between rake face and moving chip
μ - coefficient of friction	μ_a - coefficient of friction
α – rake angle	α_r – rake angle
F_{ns} – force perpendicular to shear plane	F_n – normal force on shear plane
A_s – area of shear plane	A_s – area of shear plane
V_s – shear velocity (along shear plane)	V_s – shear velocity
V_c – chip velocity (along rake face)	
	P_s – shear power
	T_s – shear plane temperature
	T_r – ambient temperature
	m_c – metal removal rate [kg/sec] (mass)
	c_s – specific coefficient of heat [Nm/kg^{o}C]
	Q_c – metal removal rate [m^3/sec] (volume)
	ρ – specific density [kg/m^3]
	λ_h – ($0 < \lambda_h \leq 1$) factor to consider plastic work done in the thin shear zone
	λ_s - proportion of heat conducted into work material
	R_T - non dimensional thermal number
	c_t – thermal conductivity of the work material
	L_c – shear plane length
r - chip compression ratio	R_c = chip compression ratio
d_c – deformed chip thickness	h_c – deformed chip thickness
γ – shear strain on shear plane	γ_s – shear strain
	γ'_s - shear strain rate
Δs – change in chip length parallel to shear plane	Δs – deformed plane
Δy – change in chip thickness perpendicular to shear plane	Δd – undeformed plane

Δt – time increment

Secondary Shear Zone

F_v – normal force

F_f – frictional force between chip & rake face

F_u – friction force

P_u – friction power

P_t – total power

ΔT_c – average temperature change in chip

ΔT_m - max temp rise of the chip at rake face – chip interface

l_t – chip contact length

δ – ratio of plastic layer over deformed chip thickness

T_{int} – average temp change at rake face – chip interface

K_{te} – average edge force coefficient (rubbing forces/unit width)

K_{fe} - average edge force coefficient (rubbing forces/unit width)

K_{tc} - cutting constant - tangential

K_{fc} – cutting constant - feed

K_t – tangential cutting force coefficient (specific cutting pressure)

K_f – cutting force ratio[78]

u – total energy/unit volume also specific cutting force

u_s – shear energy/unit volume

u_f – friction energy/unit volume

η^1_c – machinability factor

η^2_c – machinability factor (surface finish neglected)

η^3_c – machinability factor (tool wear neglected)

η_t – machinability (turning)

η_s – machinability (orthogonal cutting)[79]

4.3.6 Formulae comparison for orthogonal cutting theories

- Comparison of two orthogonal single point cutting theories

The following subsection provides a direct comparison between the approaches of the two authors, Kobayashi (polymer) and Altintas (metal). Altintas' formulae align with the widely researched cutting process shear zones and as such, there are equations

that relate to these zones particularly. Whereas Kobayashi does not offer separate considerations of these zones in his calculations.

The comparison is presented as two columns, one for each author. Where there is no line by line corresponding entry, either the respective author has no equivalent approach or the research was not sufficiently developed at the time of publication. It is for this reason and the advances in technological research of this nature that Altintas appears rather more comprehensive. This section presents the comparison of the formulae (two columns), followed by a table with a comparison of the values calculated from typical process data, Table 4.7

Kobayashi	*Altintas*
	Primary Shear Zone
	$F = \sqrt{F_t^2 + F_f^2}$
	where F = resultant force F_f = feed cutting force F_{tt} = tangential cutting force
$F_f = F_c \sin\alpha + F_t \cos\alpha$	$F_s = F\cos(\phi_c + \beta_a - \alpha_r) = F_t \cos\phi_c - F_f \sin\phi_c$
where F_f = tangential or friction force F_c = force in the direction of the tool travel F_t = force perpendicular to tool travel	where F_s = shear force on the shear plane ϕ_c = shear angle – angle between shear plane and direction of cut β_a = average friction angle between rake face and moving chip α_r = tool rake angle
$F_{fn} = F_c \cos\alpha - F_t \sin\alpha$	$F_n = F\sin(\phi_c + \beta_a - \alpha_r) = F_{tt}\sin\phi_c + F_f\cos\phi_c$
where F_{fn} = normal force on rake face α = tool rake angle	where F_n = Normal force on shear plane
$\mu = \tan\beta = \frac{F_f}{F_{fn}}$	
where μ = coefficient of friction β = friction angle	
$r = \frac{d}{d_c} = \frac{AB\sin\phi}{AB\cos(\phi-\alpha)} = \frac{\sin\phi}{\cos(\phi-\alpha)}$	
where r = chip compression ratio ϕ = shear angle d = depth of cut d_c = deformed chip thickness	

AB = length AB in figure 10

$$\tan\phi = \frac{r\cos\alpha}{1 - r\sin\alpha}$$

$$F_s = F_c\cos\phi - F_t\sin\phi$$

where
F_s = force along the shear plane

$$F_{ns} = F_c\sin\phi + F_t\cos\phi = F_s\tan(\phi + \beta - \alpha)$$

where
F_{ns} = force perpendicular to shear plane

$$A_s = \frac{bd}{\sin\phi}$$

where
A_s = area of the shear plane
b = width of cut

$$\tau_s = \frac{F_s}{A_s} = \frac{(F_c\cos\phi - F_t\sin\phi)\sin\phi}{bd}$$

where
τ_s = mean shear stress

$$\sigma_s = \frac{F_{ns}}{A_s} = \frac{(F_c\sin\phi + F_t\cos\phi)\sin\phi}{bd}$$

where
σ_s = mean normal stress on shear plane

$$A_s = b\frac{h}{\sin\phi_c}$$

where
A_s = area of the shear plane
b = width of cut
h = depth of cut

$$\tau_s = \frac{F_s}{A_s}$$

where
τ_s = shear stress on the shear plane

$$\sigma_s = \frac{F_n}{A_s}$$

where
σ_s = normal stress on shear plane

$$V_s = V\frac{\cos\alpha_r}{\cos(\phi_c - \alpha_r)}$$

where
V_s = shear velocity
V = cutting velocity

$$P_s = F_sV_s = m_cc_s(T_s - T_r)$$

where
P_s = shear power
m_c = metal removal rate [kg/sec]
c_s = specific coefficient of heat [Nm/kg°C]
T_s = shear plane temperature
T_r = ambient temperature

$$m_c = Q_c\rho$$

where
Q_c = metal removal rate [m^3/sec]
ρ = specific density of work material [kg/m^3]

$$Q_c = bhV \quad [m^3/s]$$

$$T_s = T_r + \frac{P_s}{m_cc_s} = T_r + \lambda_h(1 - \lambda_s)\frac{P_s}{m_cc_s}$$

where
λ_h = (0 < λ_h ≤ 1) factor to consider plastic work done in the thin shear zone
λ_s = proportion of heat conducted into work material

$$R_T = \frac{\rho c_s V h}{c_t}$$

where
R_t = non dimensional thermal number
c_t = thermal conductivity of the work material

$$L_c = \frac{h}{\sin\phi_c} = \frac{h_c}{\cos(\phi_c - \alpha_r)}$$

where
L_c = shear plane length
h_c = deformed chip thickness

$$R_c = \frac{h}{h_c}$$

where
R_c = chip compression ratio

$$\phi_c = \tan^{-1}\frac{R_c\cos\alpha_r}{1 - R_c\sin\alpha_r}$$

$$\gamma = \frac{\Delta s}{\Delta y} = \frac{\overline{AB'}}{\overline{CD}} = \frac{\overline{AD}}{\overline{CD}} + \frac{\overline{DB'}}{\overline{CD}} = \tan(\phi - \alpha) + \cot\phi$$

$$\gamma_s = \frac{\Delta s}{\Delta d} = \frac{\overline{A_2A_2'}}{\overline{A_1C}} = \frac{\overline{A_2'C}}{\overline{A_1C}} + \frac{\overline{CA_2}}{\overline{A_1C}} = \cot\phi_c + \tan(\phi_c - \alpha_r)$$

where
γ = shear strain on the shear plane
Δs = change in chip length parallel to shear plane
Δy = change in chip thickness normal to shear plane

where
γ_s = shear strain
Δs = deformed plane
Δd = undeformed plane

$$\gamma = \frac{\cos\alpha}{\sin\phi\cos(\phi - \alpha)}$$

$$\gamma_s = \frac{\cos\alpha_r}{\sin\phi_c\cos(\phi_c - \alpha_r)}$$

$$\gamma'_s = \frac{\gamma_s}{\Delta t} \text{ and } \gamma_s = \frac{\Delta s}{\Delta d} \text{ and } V_s = \frac{\Delta s}{\Delta t}$$

where
γ'_s = shear strain rate
Δt = time increment

$$\therefore \gamma'_s = \frac{V_s}{\Delta d} = \frac{V\cos\alpha_r}{\Delta d\cos(\phi_c - \alpha_r)}$$

<u>Secondary shear zone</u>

$$F_v = F_{tt}\cos\alpha_r - F_f\sin\alpha_r$$

$$F_u = F_{tt}\sin\alpha_r + F_f\cos\alpha_r$$

where
F_u = friction force
F_v = normal force

$$\mu_a = \tan\beta_a = \frac{F_u}{F_v}$$

$$\tan(\beta_a - \alpha_r) = \frac{F_f}{F} \rightarrow \beta_a = \alpha_r + \tan^{-1}\frac{F_f}{F_t}$$

$$V_c = \frac{\sin\phi}{\cos(\phi-\alpha)}V = rV$$

where
V_c = chip velocity along the rake face

$$V_s = \frac{\cos\alpha}{\cos(\phi-\alpha)}V = \gamma\sin\phi V$$

where
V_s = shear velocity along the shear plane

$$u = \frac{F_s V}{Vbd} = \frac{F_c}{bd}$$

$$u_s = \frac{F_s V_s}{Vbd} = \tau_s\left(\frac{V_s}{V\sin\phi}\right) = \tau_s\gamma$$

$$u_f = \frac{F_f V_c}{Vbd} = \frac{F_f r}{bd}$$

where
u = total energy/unit volume (specific cutting force)
u_s = shear energy/unit volume
u_f = frictional energy/unit volume

$$\eta_c^1 = \frac{V_m}{V_w P S_f}$$

$$\eta_c^2 = \frac{V_m}{V_w P}$$

$$\eta_c^3 = \frac{V_m}{P}$$

where
η^1_c = machinability factor
η^2_c = machinability factor (surface finish ignored)
η^3_c = machinability factor (tool wear neglected)

$$V_c = r_c V = \frac{\sin\phi_c}{\cos(\phi_c-\alpha_r)}V$$

where
V_c = chip velocity

$$P_u = F_u V_c$$

$$P_t = P_s + P_u$$

$$P = \frac{F_c V}{6120}$$

where
P = cutting power

$$P_t = F_t V$$

$$P_u = m_c c_s \Delta T_c$$

where
P_u = friction power
P_t = total power
ΔT_c = average temperature change in the chip

$$\log\left(\frac{\Delta T_m}{\Delta T_c}\right)$$

$$= 0.06 - 0.195\delta\sqrt{\frac{R_T h_c}{l_t}} + 0.5\log\left(\frac{R_T h_c}{l_t}\right)$$

$$T_{\text{int}} = T_s + \lambda_{\text{int}} \Delta T_m$$

where
ΔT_m = max temperature increase at the rake face/chip interface
l_t = chip contact length
T_{int} = average temperature increase at the rake face/chip interface
λ_{int} = empirical correction factor- accounts for variations along chip/tool contact zone

$$l_t = \frac{h\sin(\phi_c + \beta_a - \alpha_r)}{\sin\phi_c \cos\beta_a}$$

$$\eta_t = \frac{6120 V_m}{F_c V} = \frac{6120(2\pi R df)}{F_c V} = k\frac{df}{F_c n}$$

(turning)

$$\eta_s = k\frac{d}{F_c}$$ (orthogonal)

where
η_t = machinability factor (turning)
η_s = machinability factor (orthogonal cutting)

It should be noted that the measured forces may include both the forces due to shearing and a tertiary deformation process "ploughing" or "rubbing" at the flank of the cutting edge. Thus the measured forces are expressed.[80]

$$F_{tt} = F_{tc} + F_{te}$$

$$F_f = F_{fc} + F_{fe}$$

where
F_{tt} = tangential cutting force
F_{tc} = tangential cutting or shearing force
F_{te} = tangential edge force

F_f = feed cutting force
F_{fc} = feed cutting or shearing force
F_{fe} = feed edge force

Mechanistic modelling of cutting forces

$$F_s = \tau_s b \frac{h}{\sin \phi_c}$$

$$F = \frac{F_s}{\cos(\phi_c + \beta_a - \alpha_r)}$$

$$= \tau_s bh \frac{1}{\sin \phi_c \cos(\phi_c + \beta_a - \alpha_r)}$$

$$F_{tt} = bh\left[\tau_s \frac{\cos \beta_a - \alpha_r}{\sin \phi_c \cos(\phi_c + \beta_a - \alpha_r)}\right]$$

$$F_f = bh\left[\tau_s \frac{\sin(\beta_a - \alpha_r)}{\sin \phi_c \cos(\phi_c + \beta_a - \alpha_r)}\right]$$

$$K_t = \tau_s \frac{\cos(\beta_a - \alpha_r)}{\sin \phi_c \cos(\phi_c + \beta_a - \alpha_r)} [N/mm^2]$$

$$K_f = \tau_s \frac{\sin(\beta_a - \alpha_r)}{\sin \phi_c \cos(\phi_c + \beta_a - \alpha_r)} [N/mm^2]$$

$u = \frac{F_c}{bd} = K$ (specific cutting force [kg/mm^2])[81]

$$K_f = \frac{F_f}{F_{tt}} = \tan(\beta_a - \alpha_c)$$ (dimensionless)

K_t – tangential cutting force coefficient (specific cutting pressure)
K_f = cutting force ratio

$$F_{tt} = K_{tc} bh + K_{te} b$$

$$F_f = K_{fc} bh + K_{fe} b$$

where
K = specific cutting force [kg/mm^2]

where
K_{tc} = tangential cutting constant
K_{te} = average tangential edge force coefficient (ploughing-rubbing forces/unit width)
K_{fc} = feed cutting constant
K_{fe} = average feed edge force coefficient (ploughing-rubbing/unit width)

It is worth mentioning here that Altintas introduces other coefficients to which Kobayashi makes no reference. These are the edge coefficients and are related to the above mentioned edge forces. The average edge force coefficients K_{te} and K_{fe} represent the rubbing forces per unit width[82].

<u>Non linear function of uncut chip thickness</u>

$$K_t = K_T h^{-p}$$

$$K_f = K_F h^{-q}$$

where
p and q are cutting force constants determined by experiment

K_T = specific cutting pressure (tangential)
K_F = specific cutting pressure (feed)

- Theoretical prediction of shear angle

Knowledge of the shear plane angle allows the power consumed during cutting to be determined, and is therefore considered an important area of research. In Altintas's words, "predicting the shear plane angle theoretically has been a most allusive goal without input from metal cutting experiments[83]," and this was found to be the case for the polymeric cutting work addressed in this project.

As background to the reader, three approaches to determine the shear plane angle that have been widely received and accepted are presented here briefly. These are the maximum shear stress principle, the minimum energy principle, and Slipline Field Theory. For the sake of completeness, these three models are introduced in bulleted form, and then where applicable compared in the tabular comparison further below.

- *Maximum shear stress principle* - Altintas reported the maximum shear stress principle as published by Krystof[84] (1939) whereby the shear angle was based on the premise that shear will occur in the direction of maximum shear stress. The resultant force makes an angle ($\phi_c+\beta_a-\alpha_r$) with the shear plane. See Figure 4.11.
- *Minimum energy theory* - In a valuable and noteworthy contribution (1945), Merchant proposed that the shear plane angle could be predicted from the minimum energy principle. This comes about as a result of partially differentiating the cutting power with respect to the shear plane angle, and the following equation is derived[85] (see the tabular comparison below).
- *Slipline Field Theory* - A third model, based on Slipline Field Theory of metal cutting was reported by Lee and Schafer[86] in a 1951 publication and P.L.B Oxley in 1989. In Oxley's publication, Mechanics of Machining[87], the Slipline Field Theory is described in detail, and although this treatise is thorough in relation to metal cutting there appears to be no further work done with it in relation to polymeric materials. On the basis that this approach derived the same shear angle

relationship as the maximum shear stress principle, the Slipline Theory investigation was taken no further in this work.

The remaining two fundamental approaches attempt to theoretically calculate the shear plane angle by presupposing that the shear plane is thin, that the shear stress in the shear plane equals the material's yield shear stress and that the average friction between the tool and the workpiece is known. This leaves only the shear plane angle as an unknown[88]. Further to this, Altintas also states that some of the most fundamental models have assumed a perfect rigid plastic (not polymeric) workpiece material without any strain hardening[89]. The two models are included here as they can be used to demonstrate the relationship that the cutting forces and power consumed decrease with increasing shear angle[90].

The theory comparison continues here, though is to be noted again, Kobayashi does not appear to have published anything relating to plastics and the maximum shear stress principle.

Kobayashi	*Altintas* (Based on work previously published by other authors)
	<u>Max shear stress principle[83]</u> $(\phi_c + \beta_a - \alpha_r)$ angle between the resultant force, F, and shear plane Shear angle is $\phi_c = \frac{\pi}{4} - (\beta_a - \alpha_r)$
No equivalent analysis	<u>Minimum Energy Principle[84]</u> $\frac{dP_t}{d\phi_c} = \frac{d(VF_t)}{d\phi_c}$ $= \frac{-V\tau_s bh\cos(\beta_a - \alpha_r)\cos(2\phi_c + \beta_a - \alpha_r)}{\sin^2\phi_c \cos^2(\phi_c + \beta_a - \alpha_r)}$ $= 0$ where all the terms are the same as those above and putting $\cos(2\phi_c + \beta_a - \alpha_r) = 0$ $\phi_c = \frac{\pi}{4} - \frac{\beta_a - \alpha_r}{2}$ [91]

Krystof, Merchant, and Lee and Schaffer's proposed shear angle prediction equations do not provide a qualitatively accurate result due to over simplification of some of the assumptions. They do, however provide a very important relationship between the shear angle ϕ and the rake angle α, (which is fundamental to metal cutting tool design), and the friction relationship (tan β_a) between the tool and workpiece.

The brief outline of the above two processes is included in this work for the sake of completeness with regard to the metal cutting analysis. The author was unable to establish if any further research using these theories had been performed for polymeric materials, despite an exhaustive search. On this basis it is assumed that no further research exists that relate these theories specifically to polymeric materials. Certainly, Kobayashi's treatise does not include these two additional analytical approaches.

Also from the complete comparison above (page 218 – 225) it can be seen from the two sets of formulae the Altintas's theory is a much more in-depth study of the cutting process. However, it must be noted that the Kobayashi theory was published in 1967 whereas the Altintas theory was published in the year 2000. The Altintas publication contains much current thinking in relation to metal cutting but also draws on the classical works of Merchant et al. It is surprising then that even though there has been some 33 years of further research to draw on; these two theories are incredibly similar.

4.3.7 Comparison using numerical results – single point cutting

In the following comparison, the numerical results from three cutting parameter data sets are compared. The above equations (pages 218 – 225) were solved using the typical experimental orthogonal R-PVC cutting data presented in Table 4.3[91].

The first set is indicated by the annotation AK_E and is based on the experimental data in table 4.3, which was taken directly from Kobayashi's text[91]. The second set (AK_C) is based on Kobayashi's theoretical analyses as detailed on pages 218 – 225. In order to enumerate the results from the equations, appropriate tool and cutting variables were assumed. These values were again extracted from Kobayashi's text[91] to ensure consistency. The final data set, indicated by YA_C, uses Altintas' theoretical analyses (pages 218 – 225), with the same extracted values from Kobayashi's text as indicated

above, substituted, again to enumerate the results for comparison and guarantee uniformity in the outcome.

The enumerated theory results and the experimental data from Table 4.3 are compared below in Table 4.7. This table relates the derived data to the tool rake angle and uses the same headings in the left column as the header row from Table 4.3. These headings are used to group the results and present the three data sets consecutively as they relate to one another other, for ease of comparison.

By way of explanation as to the nomenclature used in Table 4.7, The 'AK' is reference to Kobayashi's work and 'YA' refers to Altintas' work. The subscripts 'E' and 'C' refer to either experimental or calculated results respectively.

Table 4.7: Theory comparison numerical results

Rake angle [deg]		**30**	**20**	**10**	**0**	**-10**	**-20**
Shear plane angle ϕ [deg]	AK_E	51.10	54.20	48.00	37.60	27.50	21.90
	AK_C	51.03	54.17	47.997	37.56	27.46	21.86
	YA_C	51.03	54.17	47.997	37.56	27.46	21.86
Shear strain γ [kg/mm^2]	AK_E	1.19	1.40	1.68	2.07	2.69	3.39
	AK_C	1.19	1.40	1.68	2.07	2.69	3.39
	YA_C	1.19	1.40	1.68	2.07	2.69	3.39
Plane stress σ_s [kg/mm^2]	AK_E	5.55	9.24	9.17	9.26	7.97	6.99
	AK_C	5.54	9.24	9.17	9.25	7.96	6.99
	YA_C	5.54	9.24	9.16	9.25	7.96	6.99
Shear stress τ_s [kg/mm^2]	AK_E	7.98	8.67	9.25	9.03	7.82	6.42
	AK_C	7.98	8.67	9.25	9.03	7.82	6.42
	YA_C	7.98	8.67	9.25	9.03	7.82	6.42
Friction coefficient μ	AK_E	0.245	0.224	0.118	0.143	0.142	0.0974
	AK_C	0.245	0.224	0.118	0.143	0.142	0.0973
	YA_C	0.245	0.224	0.118	0.143	0.142	0.0973
Specific cutting force u [kg/mm^2]u	AK_E	12.00	15.50	17.50	21.00	23.00	23.00
	AK_C	12.00	15.50	17.50	21.00	23.00	23.00
K_t	YA_C	12.00	15.50	17.50	21.00	23.00	23.00
K_{tc}	YA_C	11.99	15.50	17.49	20.99	22.99	22.97

AK_E = Kobayashi experimental data, AK_C = data calculated from Kobayashi's equations using the experimental data published for R-PVC, YA_C = data calculated from Altintas Theory using Kobayashi's published data.

- Discussion of numerical comparison results

The use of Koyabashi's data[92] and equations, along with the equations from Altintas theory, has produced results showing the theories to be highly comparable. The only variation shown in the results was in the K_{tc} (tangential cutting constant) values, which were derived from a slightly different perspective, and include factors applicable to oblique cutting. Kobayashi does not cover this.

On the basis of the good correlation of results, further investigation into the use of Altintas' oblique cutting rules and the transfer of those rules to helical end mills was considered. Altintas' publication[26] includes a section on the analytical modelling of end milling forces. This analytical model seeks to transform the oblique cutting theory into a theory that will allow the determination of the specific cutting pressure. Hence, with knowledge of the specific cutting pressure, the ability to determine the end milling power requirements from the data acquired by performing orthogonal single point cutting trials becomes possible.

4.4 Application of metal milling theory to polymeric material

In the absence of any analysis with regard to the milling process by Kobayashi, and based on the apparent similarity between the orthogonal cutting processes in metal and plastic, it seems reasonable to pose the following question - Is there any validity in applying metal cutting theory, regarding milling cutters, to plastic cutting where there is evidence of shear plane geometry being formed in the polymeric material?

4.4.1 Transfer of theories to helical milling

In an effort to progress from orthogonal single point cutting and the related data to helical multipoint cutting, a method of converting that data to the helical cutters was required. A further literature review produced two pertinent papers relating the prediction of the cutting force coefficients from experimentally obtained orthogonal single point cutting data[93] [94]. The orthogonal cutting parameters were used to assess the cutting forces for every point on each helical flute by applying the classical oblique cutting transformation[95] [96]. Once again, this demonstrated the importance of knowing the specific cutting force applicable to the material being machined and to the tool/work piece geometry. With the oblique specific cutting forces known, a further assumption was necessary to make the transition to the helical cutter. This

assumption was that the helix angle and the oblique angle were equal. With this, it was possible to analyse the helical cutting process.

The helical milling process is a much more complex analysis than orthogonal cutting processes due to the additional coefficients and constants required to make the transfer from cutting in a single plane to cutting in three dimensions. As already explained previously, Kobayashi's work was limited to single plane orthogonal cutting with no indication of what may be expected from multipoint cutting processes. Gaining perspective and an understanding of the additional factors and complexity in the three dimensional process presented sufficient grounds for including a facsimile of Altintas work on helical cutting, which is detailed in the following subsections.

4.4.2 Analytical study of helical end milling

The mechanics of multipoint milling are somewhat dissimilar to those of orthogonal single point cutting. The principle of material removal remains the same in that the

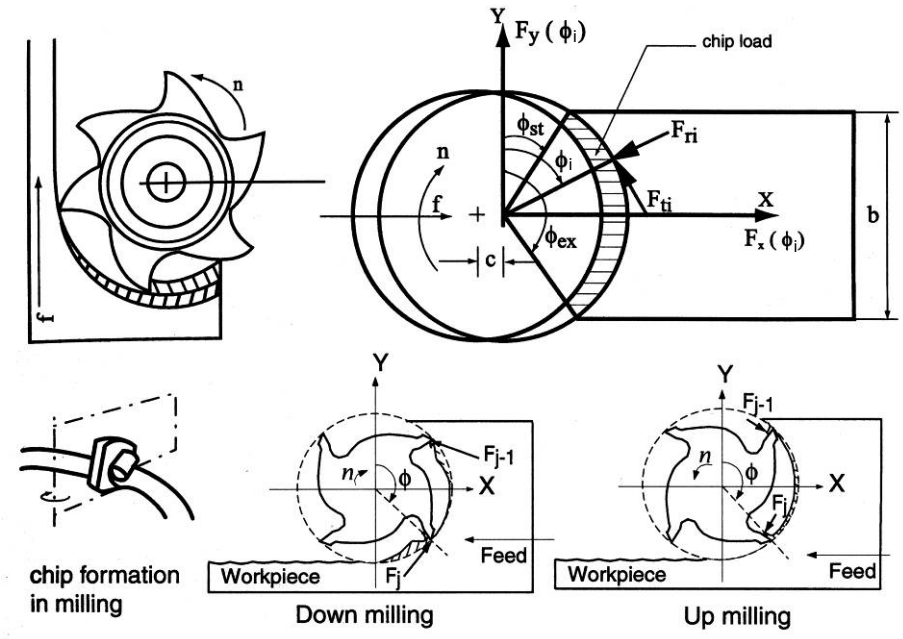

Figure 4.12: Milling cutter geometry[98]

tool moves through the material being machined to remove the unwanted portion. However, there is a major difference in the process. The difference being that the cutting tip experiences two distinct motions. The rotary motion of the rotating cutter and a linear motion caused by the cutter being fed into the work piece. The actual path traced by the cutter tip is a trochoidal form, which produces a swarf chip of varying thickness[97]. Figure 4.12[98] is included to show graphically how the varying chip

thickness is generated. It also gives some further nomenclature required to define the milling process analytically. Figure 4.12[98] shows milling cutter geometry generally whilst Figure 4.13 shows the geometry specific to an end mill.

The following sub section has been extracted from Altintas' publication and is included here to give an appreciation of the added complexity to helical milling and to put perspective on the importance of knowing the specific cutting force values for determining analytical solutions. From the geometry of Figure 4.12

$$h(\phi_i) = c \sin \phi_i \qquad [19]$$

where
c = feed rate [mm/rev-tooth]
ϕ_i = instantaneous immersion angle

- Average chip thickness per revolution h_a

$$h_a = \frac{\int_{\phi_{st}}^{\phi_{ex}} c \sin \phi_i d\phi_i}{\phi_{ex} - \phi_{st}} = \frac{-c \cos \phi_{ex} - \cos \phi_{st}}{\phi_{ex} - \phi_{st}} \qquad [20]$$

ϕ_{st} = cutter starting angle
ϕ_{ex} = cutter exit angle

- Instantaneous cutting torque [Nm]

$$T_c = F_t \frac{D}{2} \qquad [21]$$

where
D = cutter diameter [mm]
F_{tt} = tangential cutting force (parallel to cutting velocity) [N]

- Tooth spacing (cutter flute pitch) ϕ_p

$$\phi_p = \frac{2\pi}{N} \qquad [22]$$

N = number of teeth on cutter

- *Helical End mill Geometry*

Figure 4.13[99] presents typical end mill cutter geometry.

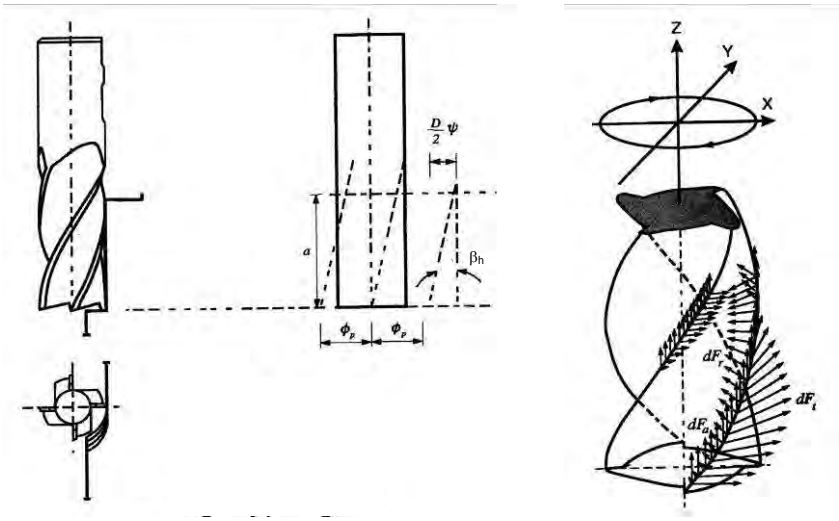

Figure 4.13: Cutter geometry of a helical end mill[98]

$$\tan\beta_h = \frac{D\psi}{2z} \rightarrow \psi = \frac{2z\tan\beta_h}{D} \qquad [23]$$

where
z = axial depth of cut [mm]
ψ = lag angle
β_h = helix angle of cutter
D = cutter diameter[100]

-Analytical modelling of the end milling forces

β_h = helix angle
D = cutter diameter [mm]
N = number of flutes
a = axial depth of cut [mm]
ϕ_i = reference immersion angle
$\phi_j(0) = \phi + j\phi_p; j = 0,1,2,.....,(N-1)$ at axial depth z

lag angle $\psi = k_\beta z$ where $k_\beta = {(2\tan\beta_h)}/{D}$ [101]

$\therefore$ immersion angle for flute *j* at axial depth of cut *z* is

$$\phi_j(z) = \phi + j\phi_p - k_\beta z \qquad [24]$$

Assume helix angle, β_h = i, oblique cutting angle (from Koyabashi's orthogonal cutting model)

The differential forces for differential element *dz* (Figure 4.13) are given by:

$$\begin{aligned} dF_{t,j}(\phi,z) &= \left[K_{tc}h_j(\phi_j(z)) + K_{te}\right]dz \\ dF_{r,j}(\phi,z) &= \left[K_{rc}h_j(\phi_j(z)) + K_{re}\right]dz \\ dF_{a,j}(\phi,z) &= \left[K_{ac}h_j(\phi_j(z)) + K_{ae}\right]dz \end{aligned} \quad [25]$$

where chip thickness is

$$h_j(\phi,z) = c\sin\phi_j(z) \quad [26]$$

The cutting constants can be evaluated from

$$\begin{aligned} K_{tc} &= \frac{\tau_s}{\sin\phi_n}\frac{\cos(\beta_n-\alpha_n)+\tan i\tan\eta\sin\beta_n}{\sqrt{\cos^2(\phi_n+\beta_n-\alpha_n)+\tan^2\eta\sin^2\beta_n}} \\ K_{fc} &= \frac{\tau_s}{\sin\phi_n\cos i}\frac{\sin(\beta_n-\alpha_n)}{\sqrt{\cos^2(\phi_n+\beta_n-\alpha_n)+\tan^2\eta\sin^2\beta_n}} \\ K_{rc} &= \frac{\tau_s}{\sin\phi_n}\frac{\cos(\beta_n-\alpha_n)\tan i-\tan\eta\sin\beta_n}{\sqrt{\cos^2(\phi_n+\beta_n-\alpha_n)+\tan^2\eta\sin^2\beta_n}} \end{aligned} \quad [27]$$

where
K_{tc} = tangential cutting force
K_{fc} = feed cutting force constant
K_{rc} = radial cutting force constant
now assuming:

$\phi_c \equiv \phi_n$ the orthogonal shear angle is equal to the normal shear angle in oblique cutting,

$\alpha_r \equiv \alpha_n$ the rake angle equals the normal rake angle in oblique cutting,

$\eta \equiv i$ the chip flow angle is equal to the oblique angle,

the coefficient of friction β_a and the shear stress τ_s are the same for both orthogonal and oblique cutting[102], which are sound assumptions in this case.

Putting the helix angle β_h = i the oblique angle. The elemental forces can be resolved into feed (x), normal (y) and axial (z) directions using the transformation

$$\begin{aligned} dF_{x,j}(\phi_j(z)) &= -dF_{t,j}\cos\phi_j(z) - dF_{r,j}\sin\phi_j(z) \\ dF_{y,j}(\phi_j(z)) &= dF_{t,j}\sin\phi_j(z) - dF_{r,j}\cos\phi_j(z) \\ dF_{z,j}(\phi_j(z)) &= dF_{a,j} \end{aligned} \quad [28]$$

substituting the differential force and chip thickness equations into the transformation equation leads to

$$dF_{x,j}(\phi_j(z)) = \left\{\frac{c}{2}\left[-K_{tc}\sin 2\phi_j(z) - K_{rc}(1-\cos 2\phi_j(z))\right] + \left[-K_{te}\cos\phi_j(z) - K_{re}\sin\phi_j(z)\right]\right\}dz$$
$$dF_{y,j}(\phi_j(z)) = \left\{\frac{c}{2}\left[K_{tc}(1-\cos 2\phi_j(z)) - K_{rc}\sin 2\phi_j(z)\right] + \left[K_{te}\sin\phi_j(z) - K_{re}\cos\phi_j(z)\right]\right\}dz$$
$$dF_{z,j}(\phi_j(z)) = \left[K_{ac}c\sin\phi_j(z) + K_{ae}\right]dz$$

[29]

integrate the cutting forces along the "in cut" portion of the flute j to obtain total cutting force

$$F_q(\phi_j(z)) = \int_{zj,1}^{zj,2} dF_q(\phi_j(z)) \quad q = x, y, z \qquad [30]$$

where $z_{j,1}(\phi_j(z))$ and $z_{j,2}(\phi_j(z))$ are the axial upper and lower integral limits of the in-cut part of flute j. The integrations are carried by noting [103]

$$\phi_j(z) = \phi + j\phi_p - k_\beta z, \quad d\phi_j(z) = -k_\beta dz \text{ thus} \qquad [31]$$

$$F_{x,j}(\phi_j(z)) = \left\{\frac{c}{4k_\beta}\left[-K_{tc}\cos 2\phi_j(z) + K_{rc}(2\phi_j(z) - \sin 2\phi_j(z)) + \frac{1}{k_\beta}\left[K_{te}\sin\phi_j(z) - K_{re}\cos\phi_j(z)\right]\right]\right\}_{zj,1(\phi_j(z))}^{zj,2(\phi_j(z))}$$
$$F_{y,j}(\phi_j(z)) = \left\{\frac{-c}{4k_\beta}\left[K_{tc}(2\phi_j(z) - \sin 2\phi_j(z) + K_{rc}\cos 2\phi_j(z))\right] + \frac{1}{k_\beta}\left[K_{te}\cos\phi_j(z) + K_{re}\sin\phi_j(z)\right]\right\}_{zj,1(\phi_j(z))}^{zj,2(\phi_j(z))}$$
$$F_{z,j}(\phi_j(z)) = \frac{1}{k_\beta}\left[K_{ac}c\cos\phi_j(z) - K_{ae}\phi_j(z)\right]_{zj,1(\phi_j(z))}^{zj,2(\phi_j(z))}$$

[104][32]

the resultant cutting force acting on the milling cutter is

$$F(\phi_i) = \sqrt{F_x(\phi_j)^2 + F_y(\phi_j)^2 + F_z(\phi_j)^2} \qquad [33]$$

<u>Mechanistic identification of cutting constants</u>

putting

$$dz = a \quad \text{(depth of cut)}$$
$$\phi_j(z) = \phi_i \quad \text{(reference immersion angle)} \qquad [34]$$
$$k_\beta = 0 \quad \text{(lag angle)}$$

and integrating over one revolution

$$\phi_p = \frac{2\pi}{N} \qquad [35]$$

yields average milling forces per tooth period

$$\overline{F}_q = \frac{1}{\phi_p}\int_{\phi_{st}}^{\phi_{ex}} F_q(\phi_i)d\phi_i \quad \sin ce\phi_{st} \le \phi_i \le \phi_{ex} \qquad [36]$$

integrating the instantaneous cutting forces gives

$$\begin{aligned}
\overline{F}_x &= \left\{\frac{Nac}{8\pi}\left[K_{tc}\cos 2\phi_i - K_{rc}\left[2\phi_i - \sin 2\phi_i\right]\right] + \frac{Na}{2\pi}\left[-K_{te}\sin\phi_i + K_{re}\cos\phi_i\right]\right\}_{\phi_{st}}^{\phi_{ex}} \\
\overline{F}_y &= \left\{\frac{Nac}{8\pi}\left[K_{tc}\left[2\phi_i - \sin 2\phi_i\right] + K_{rc}\cos 2\phi_i\right] - \frac{Na}{2\pi}\left[K_{te}\cos\phi_i + K_{re}\sin\phi_i\right]\right\}_{\phi_{st}}^{\phi_{ex}} \qquad [37] \\
\overline{F}_z &= \left\{\frac{Na}{2\pi}\left[-K_{ac}c\cos\phi_i + K_{ae}\phi_i\right]\right\}_{\phi_{st}}^{\phi_{ex}}
\end{aligned}$$

for slot milling where $\phi_{st} = 0 \text{ and } \phi_{ex} = \pi$

$$\begin{aligned}
\overline{F}_x &= -\frac{Na}{4}K_{rc}c - \frac{Na}{\pi}K_{re} \\
\overline{F}_y &= \frac{Na}{4}K_{tc}c + \frac{Na}{\pi}K_{te} \qquad [38] \\
\overline{F}_z &= \frac{Na}{\pi}K_{ac}c + \frac{Na}{2}K_{ae}
\end{aligned}$$

the average cutting forces can be expressed by a linear function of the feed rate (c) and an offset contributed by the edge forces:[105]

$$\overline{F}_q = \overline{F}_{qc}c + \overline{F}_{qe} \quad \text{where} \quad q = x, y, z \qquad [39]$$

Finally cutting force coefficients can be evaluated as follows

$$\text{Tangential cutting constant } K_{tc} = \frac{4\overline{F}_{yc}}{Na}, \quad \text{Tangential edge constant } K_{te} = \frac{\pi\overline{F}_{ye}}{Na}$$

$$\text{Radial cutting constant } K_{rc} = \frac{-4\overline{F}_{xc}}{Na}, \quad \text{Radial edge constant } K_{re} = \frac{-\pi\overline{F}_{xe}}{Na}$$

$$\text{Axial cutting constant } K_{ac} = \frac{\pi\overline{F}_{zc}}{Na}, \quad \text{Axial edge constant } K_{ae} = \frac{2\overline{F}_{ze}}{Na}$$

4.4.3 Effect and determination of the edge coefficients

The edge cutting coefficients, K_{te}, K_{re} and K_{ae} are coefficients that are related to the helical edge length of the cutter.[106]

These coefficients are usually tabulated in an orthogonal cutting data database for the particular tool/work piece geometry and cutting conditions.

The coefficients are represented by the intercept force components per unit cut width of the force-cut thickness functions at zero cut thickness. As such, the K_{ae} value, which is known to be very small in oblique cutting, is usually taken as zero (Armarego and Whitfield, 1985)[107].

Armarego et al states that the method of finding the edge force components involves experimentally measuring the two force components along the cut direction and normal to it and the chip length and thickness ratios. The edge force components are estimated from the intercepts of the measured force-cut thickness functions at zero cut thickness and are subtracted from the measured forces along and normal to the cut direction to estimate the forces due to cutting. These edge force components and basic cutting quantities have to be statistically processed over a number of trials to study the effects of the process variables as well as to establish 'best fit' equations for inclusion in the database (Armarego et al, 1983, 1985)[108].

To gain an appreciation of the edge force component weighting in the equations of the effect a particular set of possible tooling parameters was selected (see below) and the values for P_p, Q_p, S_p and T_p (equation [42]) were calculated. The values for these coefficients were tabulated (Table 4.8) and the database values for a titanium alloy (Ti_6Al_4V) were substituted into the equations. This is further discussed below.

The average milling forces per tooth period can be found from

$$\begin{aligned}
\overline{F}_x &= -K_{te}S_p + K_{re}T_p - \frac{S_t}{4}\left(-K_{tc}P_p + K_{rc}Q_p\right) \\
\overline{F}_y &= -K_{te}T_p - K_{re}S_p + \frac{S_t}{4}\left(K_{tc}Q_p + K_{rc}P_p\right) \quad [109] \\
\overline{F}_z &= -\frac{Na}{2\pi}K_{ae}\left(\phi_{ex} - \phi_{st}\right) + s_t K_{ac}T_p
\end{aligned} \qquad [41]$$

where

$$\begin{aligned}
P_p &= \frac{Na}{2\pi}\left[\cos 2\phi_i\right]_{\phi_{st}}^{\phi_{ex}}; \qquad Q_p = \frac{Na}{2\pi}\left[2\phi_i - \sin 2\phi_i\right]_{\phi_{st}}^{\phi_{ex}} \\
S_p &= \frac{Na}{2\pi}\left[\sin 2\phi_i\right]_{\phi_{st}}^{\phi_{ex}}; \qquad T_p = \frac{Na}{2\pi}\left[\cos 2\phi_i\right]_{\phi_{st}}^{\phi_{ex}}
\end{aligned} \qquad [42]$$

And for the milling application it has been determined that:

N = 3 (no. of flutes on the cutter)

a = 0.65 mm (axial depth of cut)

s_t = 0.03 mm (feed per tooth per rev)

$\phi_i = \pi$ (cutter immersion angle)

$\phi_{ex} = \pi$ (flute exit angle relative to coordinate system)

$\phi_{st} = 0$ (flute entry angle relative to the coordinate system)

The first two equations given in equation [41] can be rearranged so that they can be solved simultaneously to give K_{te} and K_{re}. However, as previously shown, all of the K_{xe} coefficients (where x = t, r or a) are dependent on the tool/workpiece geometry[110]. There was insufficient data about the nominated tool/workpiece pair to derive a solution to these equations. This was because knowledge of the feed and tangential forces is a primary requirement for the material/workpiece pair in order to calculate the K_{xe} coefficients. In order to find a solution for the K_{xe} weightings (P_p, S_p, Q_p, T_p) in the equations [41] and [42], the above cutter parameters (no. of flutes, depth of cut and feed per tooth per rev) were substituted to give numerical values to these weighting coefficients.

Briefly, these cutter parameters were determined by the choice of cutter, which in turn was determined by the design and shape of the cavity in the host component. The selection of the cutter will be discussed in depth in a later sub section of this work.

The cutter parameter values given above are the typical values that were used as parameters for the R-PVC cutting trials described later in this chapter.

By setting the entry angle to $\phi_{ex}=0$ and the exit angle $\phi_{ex}=\pi$, the parameters P_p, Q_p, S_p, and T_p become constants as below, which in turn become the weighting factors for the cutting and edge coefficients.

$$P_p = \frac{Na}{2\pi}(\cos 2\pi) = 0.31 \qquad [43]$$

$$Q_p = \frac{Na}{2\pi}(2\pi - \sin 2\pi) = 1.95 \qquad [44]$$

$$S_p = \frac{Na}{2\pi}(\sin 2\pi) = 0 \qquad [45]$$

$$T_p = \frac{Na}{2\pi}(\cos 2\pi) = 0.31 \quad [46]$$

Substituting the values from equations [43] – [46] into equations [41] and the cutter parameters above give

$$\begin{aligned}
\overline{F}_x &= 0.31K_{re} - \frac{s_t}{4}(-0.31K_{tc} + 1.95K_{rc}) \\
\overline{F}_y &= -0.31K_{te} + \frac{s_t}{4}(1.95K_{tc} + 0.31K_{rc}) \\
\overline{F}_z &= -0.973K_{ae} + 0.31s_tK_{ac}
\end{aligned} \quad [47]$$

substituting in the feed rate per tooth per rev gives the final multipliers for the various coefficients

$$\begin{aligned}
\overline{F}_x &= 0.31K_{re} + 0.00233K_{tc} - 0.0146K_{rc} \\
\overline{F}_y &= -0.31K_{te} + 0.0146K_{tc} + 0.00233K_{rc} \\
\overline{F}_z &= -0.973K_{ae} + 0.0093K_{ac}
\end{aligned} \quad [48]$$

The lack of data available for R-PVC was a major problem and so to gain a better understanding of the coefficient weighting effects, they were investigated using values from Ti_6Al_4V titanium alloy. The associated values below (Table 4.8) were taken from a paper published by Budak et al[111], which described the effects of the edge coefficients during helical milling. An in-depth literature search failed to source any further information with regard to values for the edge coefficients. It was fortuitous that the titanium alloy values were found and able to be utilised as it has properties that are closer to R-PVC than many other metals. The titanium used as a surrogate material was likely to give higher edge coefficient values than actually occurred with R-PVC, thus, erring on the safer side of their effect. Therefore, the values for titanium were assumed suitable and utilised to demonstrate the edge coefficient influence. It is to be noted that Altintas indicates that these coefficients vary with tool wear and any deformation on the cutting edge[112].

Table 4.8: Cutting force and cutting edge coefficients for titanium alloy[113]

Milling Test Ti_6Al_4V						
α_n [deg]	K_{tc} [N/mm^2]	K_{te} [N/mm]	K_{rc} [N/mm^2]	K_{re} [N/mm]	K_{ac} [N/mm^2]	K_{ae} [N/mm]
0	1825	29.7	770	55.7	735	1.8 (neglect)

In the absence of a more suitable data set, the titanium alloy does however; provide details of a suitable nature for comparative purposes because the cutting information related to a shallow depth of cut. The theoretical cutting forces generated due to using the above mentioned titanium alloy were very small (Table 4.9). As a consequence, the assumption was that any error would be proportionally small. For example, an error of up to 30% would still give small erroneous forces.

Table 4.9: Values given as weightings to show the effect of the machining parameters

Force axis	**Weight $K_{\#e}$**	**Value** [N]	**Weight $K_{\#c}$**	**Value** [N]	**Weight K_{rc}**	**Value** [N]
$\mathbf{F}_x$	$0.31K_{re}$	17.27	$0.0023K_{tc}$	4.243	$-0.01463K_{rc}$	-11.26
$\mathbf{F}_y$	$-0.31K_{te}$	-9.21	$0.01463K_{tc}$	27.7	$0.0023K_{rc}$	1.77
$\mathbf{F}_z$	$-0.937K_{ae}$	-0	$0.0093K_{ac}$	6.84		

One thing worth noting with this comparison is the difference between the elastic recovery levels of the two materials. It is likely that the R-PVC will compress to a greater extent during cutting and therefore recover to a higher level than the titanium with regard to the cutting edge. This recovery may adversely influence the clearance face friction power and therefore the rubbing or ploughing action of the cutter, causing the edge forces to have a greater effect in the overall analysis. An experimental investigation of this phenomenon would be required and may be the subject of future research.

Using the constants given by the assumed tool/work piece geometry in equations [48] and the cutting coefficients for titanium given in Table 4.8, the equations give the weighting values shown in Table 4.9. The cutting constants are affected greatly by the parameters of the cut, namely depth of cut and feed per tooth/rev. Whereas the edge constants are not controlled by these same parameters and therefore with very small cuts the edge parameter weightings can be seen to be relatively large compared to the cutting constants. The 'Weight $K_{\#e}$' columns show the magnitude of the effect of the cutter parameters on the $K_{\#e}$ terms (the weighting value and the $K_{\#e}$ value product) and the 'Value' columns show the actual values as they relate to the surrogate material.

Table 4.10 gives and orthogonal force values for cutting titanium alloy based on the data provided in Table 4.8 and the cutter parameters listed above.

Table 4.10: Orthogonal force components for Ti_6Al_4V Titanium alloy

Force axis	Force magnitude [N]	
	All $K_{\#\#}$'s included	$K_{\#e}$'s excluded
F_x	10.25	-7.02
F_y	20.26	29.47
F_z	6.84	6.84

The magnitude of the effect of the edge coefficients when machining with small cuts was shown to have enough effect on the final force values to warrant evaluation. Further research revealed a process that could be utilised to find the edge coefficients from the data on hand that had been published by Altintas et al.

This method was taken from the CutPro User Manual: Machining process modelling, machine tap testing, and chatter vibrations avoidance[114].

The method takes the measured forces (tangential and feed forces) and uses the relationship with the uncut chip thickness. These forces are plotted on a chart and are shown to produce relationships that can be assumed linear. Therefore the relationships can be expressed as equations of the form 'y = mx + c' as below.

Tangential force:

$$F_{tt} = F_{tc} + F_{te} = K_{tc}bh + K_{te}b \qquad [49]$$

Feed force:

$$F_{f} = F_{fc} + F_{fe} = K_{fc}bh + K_{fe}b \qquad [50]$$

where

$K_{tc}b$ and $K_{fc}b$ = slopes of the lines formed by the tangential and feed forces respectively.

$K_{te}b$ and $K_{fe}b$ = edge forces in the tangential and feed directions.

b = width of cut.

The edge forces come about because of the friction between the clearance face of the tool and the finished surface, therefore they are not dependent on the feed rate, nor do they contribute to the shearing action of the cut[115]. Equations [49] & [50] can therefore be expressed as:

Tangential force:

$$F_{tc} = F_{tt} - F_{te} = K_{tc} bh \qquad [51]$$

Feed force:

$$F_{fc} = F_{f} - F_{fe} = K_{fc} bh \qquad [52]$$

to show that the edge forces do not contribute to the shearing. The tangential and feed forces are linearly dependent on the width of cut, b. Therefore the cutting coefficients are:

Shearing coefficients:

$$\begin{aligned} \frac{F_{tc}}{h} &= K_{tc} b, \quad K_{tc} = \frac{F_{tc}}{bh} \\ \frac{F_{fc}}{h} &= K_{fc} b, \quad K_{fc} = \frac{F_{fc}}{bh} \end{aligned} \qquad [53]$$

Edge force coefficients[116]

$$\begin{aligned} F_{te} &= K_{te} b, \quad K_{te} = \frac{F_{te}}{b} \\ F_{fe} &= K_{fe} b, \quad K_{fe} = \frac{F_{fe}}{b} \end{aligned} \qquad [54]$$

Two sets of R-PVC data published by Kobayashi were used for solving the values for the edge coefficients. The data sets were obtained from, i) tabulated data (Table 4.3), and ii) data interpolated from a chart in Figure 4.6 (from Kobayashi's text[117]). The solution involved plotting the data sets and finding the best fit linear regression so that it could be analysed using the "CutPro" method outlined above. Kobayashi's data[118], which is all based on single point orthogonal cutting, is presented in Table 4.11 and was used to provide a line of known slope and y-axis intercept, with depth of cut plotted along the x-axis.

The rake angle was used as the independent variable for the different tool styles, from this data a chart was created using the cutting force and the depth of cut as a starting point. These values are shown in Table 4.11, but have been converted to Newtons. It is the authors understanding that the data used from Kobayashi's publication was obtained by experimental investigation, mainly dry orthogonal cutting.

Table 4.11: Cutting parameters used to determine edge coefficients

Rake Angle a [deg]	**Depth of Cut** d [mm]	**Cutting Force** F_c [N]	**Specific Cutting Pressure** u [N/mm^2] (K_{tc})
30	0.05	23.54	117.72
20	0.05	30.41	152.06
10	0.05	34.34	171.68
0	0.05	41.20	206.01
-10	0.05	45.13	225.63

The specific cutting pressure, u, was used to determine the slope of the line on the graph (Figure 4.14) and the cutting forces were plotted for various values of the depth of cut. These calculated values are shown in Table 4.12. The data values published by Kobayashi, Table 4.11, and converted from kg to N, gives the linear trend equations,

'y = mx +c,' as shown in Figure 4.14.

Table 4.12: Force values F_c based on the line slope and depth of cut increment

Rake angle [deg]	**Depth of Cut** [mm]			
	0.05	0.1	0.15	0.2
-10	45.13	90.25	135.38	-- --
0	41.20	82.40	123.61	164.81
10	34.34	68.67	103.01	137.34
20	30.41	60.82	91.23	121.64
30	23.54	47.09	70.63	94.18

Cut differential		[mm]	0.05
width of cut	b	[mm]	4

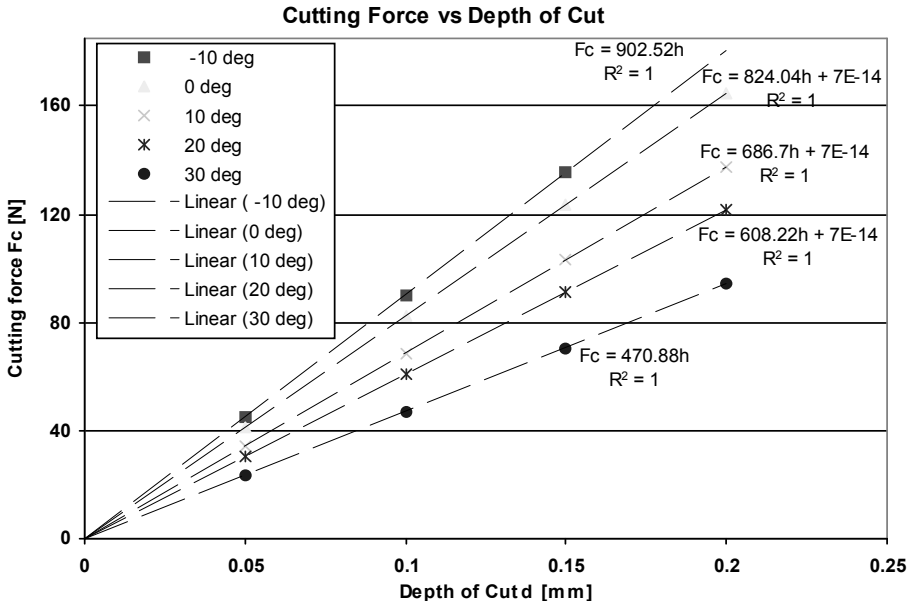

Figure 4.14: Cutting forces vs. depth of cut

The curious thing about this result is the zero y-axis intercept 'c', which means in these cases that there are no edge coefficients: based on Altintas CutPro theories[113] applied to Koyabashi's tabulated data. From the method outlined previously the value on the cutting force, $F_{c,}$ axis (y-axis) at which the trend line intercepts, is representative of the edge coefficient multiplied by the width of cut. This result is concerning when the definition of the edge coefficients is considered. "Edge forces are created by the friction between the clearance face of the tool and the finished surface.[119]" The definition of the edge coefficients necessarily demands that there is some residual force in terms of the tool rubbing on the relief faces. This data may have been published from an analysis without the edge forces included because they were deemed small enough to neglect generally. To test for this condition a second suite of data was extracted from a chart in Kobayashi's text[120], reproduced in Figure 4.6.

4.4.4 Alternative data for finding edge coefficients

A second set of data, interpolated from charts in Figure 4.6[121], was also used to derive the cutting and edge coefficients for R-PVC. The charts were used to extract the force data for the cutting processes. The specific cutting force constant, K_{tc}, relating to the tangential cutting force was given in Kobayashi's tabulated and published data[122], however the K_{fc} values, which relate to the feed force constant, were not published in the same tabulated form. It was published in chart form, therefore making it necessary to interpolate the data from the chart (Figure 4.6, top left). The interpolated data appeared to be the only data available for use in determining the cutting edge coefficients K_{te} and K_{fe} as the author was unable to locate any other reported results. Initially the cutting edge force coefficients will be considered, followed by the feed force coefficients.

4.4.5 Tangential cutting force edge coefficients

Data interpolated from the chart presented in Table 4.13, gives differing values for the forces at the 0.05 mm depth of cut when compared to those shown in the tabulated data (Table 4.3). As such, the line slope values calculated from the tabulated data are also different from the interpolated ones. An explanation as to why the values differ between the two sources could be that the charts[123] are a series of trials where the depth of cut and the rake angle of the tool are varying. However, the tabled data[124] possibly represents data that has been statistically customized to give a more

representative value of all of the trials that were done at the 0.05 mm depth of cut or perhaps more likely, the tabulated data may have been generated from Kobayashi's analytical model.

Table 4.13: Data interpolated from Kobayashi[125]

Force F_c [N]	Depth of Cut [mm]				
Rake angle [deg]	**0.0**	**0.05**	**0.1**	**0.15**	**0.2**
-10	0.0	37.28	74.56	108.40	-- --
0	0.0	32.86	67.69	98.59	125.08
10	0.0	30.41	56.89	80.44	101.53
20	0.0	27.47	48.56	66.71	85.35
30	0.0	24.53	39.24	53.96	68.67

The kilogram (kg) force values given by Kobayashi in his text have been converted to Newtons in Table 4.13. The cutting speed is given in the text as 10 m/min; however, the specific cutting pressure values are independent of the cutting velocity (equation [13]).

Table 4.14: Comparison of data from Kobayashi's published work[124]

F_c [N]	Depth of Cut [mm]		
Rake angle [deg]	**0.05** (see Table 4.11)	**0.05** (**see** Figure 4.6)	**Difference**
-10	37.28	45.13	7.85
0	32.86	41.20	8.34
10	30.41	34.34	3.93
20	27.47	30.41	2.94
30	24.53	23.54	-0.99

The resulting differences shown in Table 4.14 indicated a considerable dissimilarity in the cutting coefficients given by the two methods resulting in the non-zero edge coefficients (Figure 4.15) for the data interpolated from Figure 4.6[126].

The data was plotted and the linear trend lines with their respective equations were added to the chart (Figure 4.15). The equations for the trend lines shown in Figure 4.15, are again of the form 'y = mx + c,' giving the slope of the line (m) and the cutter force, F_c-axis intercepts (c). Table 4.15 tabulates the cutting and edge coefficients results shown in Figure 4.15. The width of cut, b, was set at 4.00 mm as per Kobayashi's data, and this was divided into the slope coefficient (m) and the constant (c) to give the K_{tc} and K_{te} values shown in Table 4.15.

Table 4.15: Comparison of cutting coefficients[127]

Rake angle [deg]	K_{tc} [N/mm^2]	u [K_{tc}] [N/mm^2]	Difference [N/mm^2]
-10	177.81	225.63	47.82
0	153.77	206.01	52.24
10	118.46	171.68	53.22
20	95.89	152.06	57.17
30	73.58	117.72	44.14

The cutting coefficients derived from Kobayashi's graphical data and presented in Table 4.15 show considerably different values to Kobayashi's[128] tabulated data and those that were calculated from the chart using the Altintas' method[129] given above. The differences generated between the edge coefficients are nearly constant at approximately 51N/mm^2 as seen in Table 4.15.

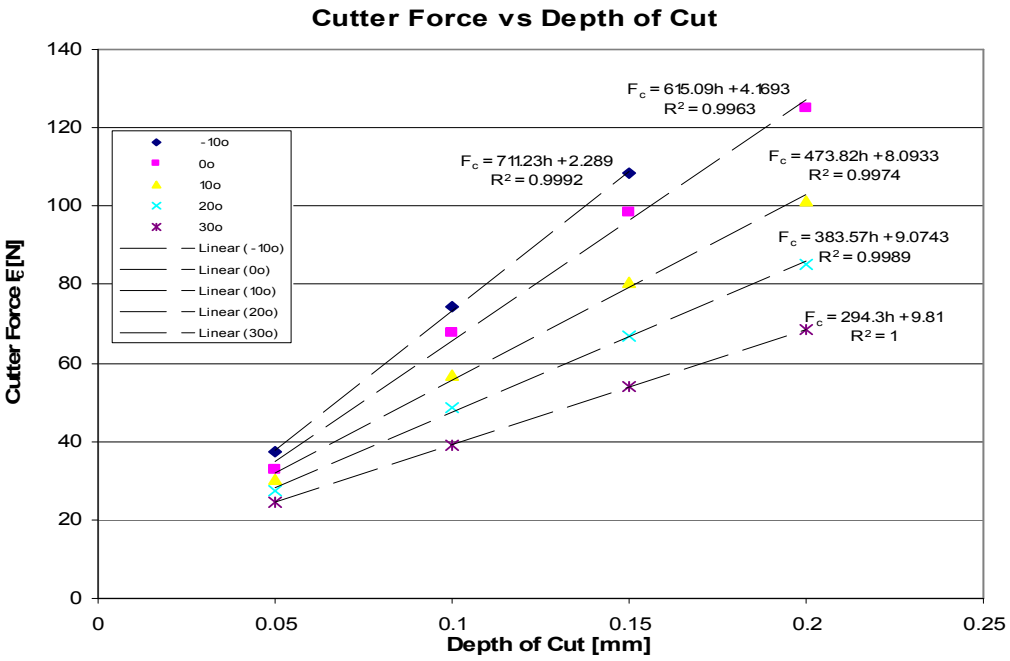

Figure 4.15: Chart showing replotted interpolated data

Table 4.16: Linear equations from Figure 4.15

Rake angle [deg]	Linear Equation	Slope $K_{tc}b$ [N/mm]	K_{tc} [N/mm^2]	F_c axis intercept $K_{te}b$ [N]	K_{te} [N/mm]
-10^o	F_{tc} = 711.23h + 2.29	711.23	177.81	2.29	0.57
0^o	F_{tc} = 615.09h + 4.17	615.09	153.77	4.17	1.04
10^o	F_{tc} = 473.82h + 8.09	473.82	118.46	8.09	2.02
20^o	F_{tc} = 383.57h + 9.07	383.57	95.89	9.07	2.27
30^o	F_{tc} = 294.30h + 9.81	294.30	73.58	9.81	2.45

This is evident from the charted lines in Figure 4.15 when compared to Figure 4.14. The data defining the lines in Figure 4.15 are subsequently summarised in Table 4.16.

4.4.6 Feed force edge coefficients

The data in Table 4.17 was interpolated and simply replotted from the chart published by Kobayashi[130]. Once again, this data was presumed to be the only documented source of feed force data available from which the feed force edge coefficients (these are different to the tangential cutting force edge coefficients) could be determined. This assumption was again based on the difficulty in finding other data relating to orthogonal cutting forces in polymeric materials despite extensive searching and enquiry.

The data tabled by Kobayashi[131] that was used for comparison of the tangential force coefficient, K_{tc}, did not have a value for the specific cutting pressure, u, for the associated feed force and so the same approach as used for the tangential cutting force coefficients could not be utilised. A chart similar to Figure 4.15 was not feasible without the given line slope. Data in Table 4.17 was simply interpolated from Kobayashi's published chart so that it could be accurately reproduced as per Figure 4.16.

Table 4.17: Data interpolated from Kobayashi[132]

F_{tt} [N]		Depth of Cut [mm]			
Rake angle [deg]		0.05	0.10	0.15	0.20
-20		28.45	40.71	54.94	-- --
-10		14.72	25.51	35.32	-- --
0		7.85	11.77	15.70	18.15
10		1.96	0	-1.96	-3.44
20		-2.94	-7.36	-12.75	-16.68
30		-6.38	-13.24	-19.62	-26.00
Width of cut	b [mm]	4.00			

The data plotted in Figure 4.16[133] was interpolated from Koyabashi's data[134] and the trend lines added in accordance with the method described by Altintas.[135] The trend line equations and the coefficients determined from the graphs and equations are given in Table 4.18. A cut width of 4.0mm was used in the calculations.

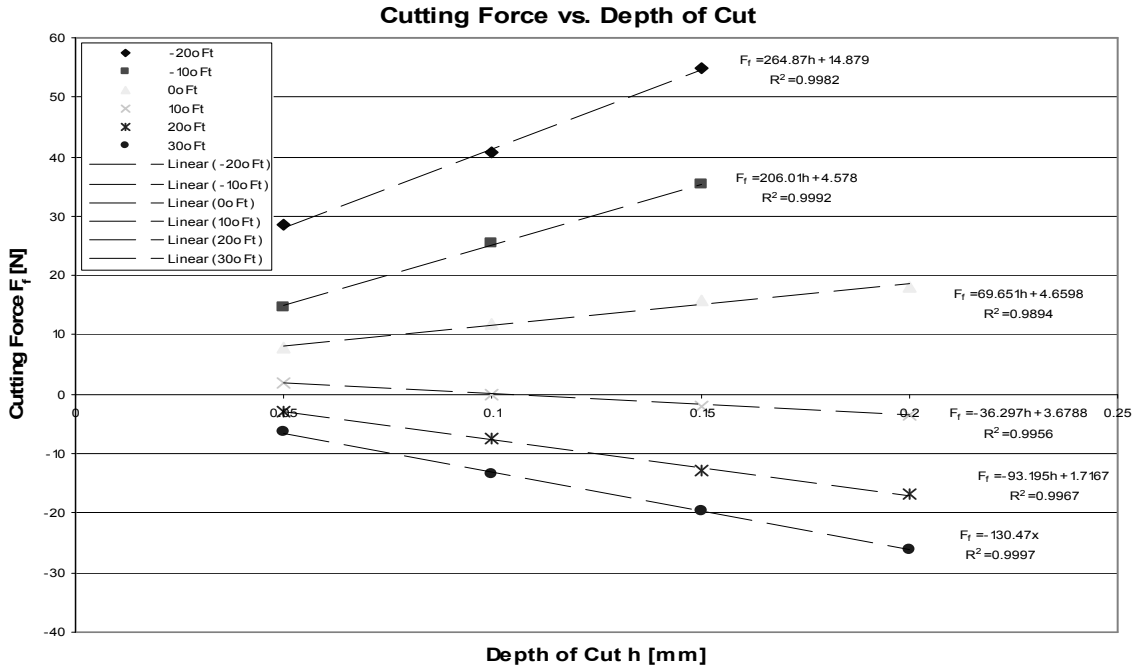

Figure 4.16: Feed cutting force interpolated from Kobayashi[132]

Table 4.18: Linear equations from Figure 4.16

Rake Angle [deg]	**Linear Equation**	**Slope $K_{fc}b$** [N/mm]	**K_{fc}** [N/mm^2]	**F_f axis intercept $K_{fe}b$** [N]	**K_{fe}** [N/mm]
-20	F_{fc} = 264.87h + 14.879	264.87	66.22	14.88	3.72
-10	F_{fc} = 206.01h + 4.578	206.01	51.50	4.58	1.15
0	F_{fc} = 69.651h + 4.6598	69.65	17.41	4.66	1.17
10	F_{fc} = -36.297h + 3.6788	-36.30	-9.08	3.68	0.92
20	F_{fc} = -93.195h + 1.7167	-93.20	-23.30	1.72	0.43
30	F_{fc} = -130.47h	-130.47	-32.62	0.00	0.00

Once a full complement of cutting force and edge coefficients had been determined, the data to calculate the spindle power was available.

4.4.7 Analytical power determination

The focus of this study was to find a link that enabled power consumption requirements of helical milling cutters working in polymeric materials (R-PVC in particular) to be determined without the need to perform expensive and time consuming experimental trials. The preceding analysis confirms that when there is sufficient orthogonal data available and that the polymeric material meets the criteria of forming a shear plane during cutting, it will behave in a manner similar to metals. Therefore, metal cutting theory may be utilised, provided there is sufficient orthogonal cutting data available, or that the cutting coefficients have been published.

The power consumption values ascertained from the previous analytical investigation are shown below in Table 4.19 and Table 4.20. A comparison of the relevant power consumption data from these two tables is presented in Table 4.21.

Table 4.19 gives the calculated power consumption results derived by using Altintas' theory converting orthogonal cutting data to helical milling data, having neglected the edge coefficients.

Table 4.19: Calculated Results - edge coefficients neglected

		Rake angle [deg]						
Description	Symbol	-20	-10	0	10	20	30	Units
Cutting constant	K_{tc}	232.59	235.20	214.28	177.51	160.46	125.68	N/mm^2
	K_{fc}	124.02	84.51	33.77	-11.27	-22.34	-39.03	N/mm^2
	K_{rc}	115.71	110.28	101.20	87.05	67.28	50.41	N/mm^2
Number of flutes	N	3	3	3	3	3	3	
Depth of cut	a	0.65	0.65	0.65	0.65	0.65	0.65	mm
Feed/tooth	c	0.03	0.03	0.03	0.03	0.03	0.03	mm
Cutter radius	r	1.5	1.5	1.5	1.5	1.5	1.5	mm
Cutter speed	n	35000	35000	35000	35000	35000	35000	rpm
Orthogonal Feed Forces	$\mathbf{F}_x$	-1.69	-1.61	-1.48	-1.27	-0.98	-0.74	N
	$\mathbf{F}_y$	3.40	3.44	3.13	2.59	2.35	1.84	N
	$\mathbf{F}_z$	2.31	1.58	0.63	-0.21	-0.42	-0.73	N
Resultant Feed Force	**F**	4.45	4.11	3.52	2.90	2.58	2.11	N
Torque	**T**	6.67	6.17	5.28	4.35	3.87	3.16	Nmm
Power	**P**	**24.44**	**22.61**	**19.36**	**15.94**	**14.18**	**11.60**	**W**

The results presented in Table 4.19 are derived from the tool/work piece geometry using equations [38] to calculate the average orthogonal forces F_x, F_y, and F_z. The edge coefficients in this case were set to zero on the basis that they are generally very small. A review of the weighting effect of the edge coefficients prompted a further investigation of possible methods of determining them. Such a method was found and used in conjunction with published orthogonal cutting data allowing the edge coefficients to be determined. These coefficients were then used to form a comparison of the power consumption, both with and without being applied. The cutting coefficients were derived using equation [27]. The results were tabled below in Table 4.20 and the comparison Table 4.21.

Table 4.20: Calculated Results - edge coefficients included, axial force excluded

Description		Rake Angle [deg]						Units
		-20	-10	0	10	20	30	
Cutting constant	K_{tc}		177.81	153.78	118.46	95.90	73.58	N/mm^2
	K_{fc}	66.22	51.50	17.42	-9.07	-23.30	-32.62	N/mm^2
Edge constants	K_{te}		0.57	1.04	2.02	2.27	2.45	N/mm
	K_{fe}	3.72	1.15	1.16	0.92	0.43	0	N/mm
Number of flutes	n	3	3	3	3	3	3	
Depth of cut	d	0.65	0.65	0.65	0.65	0.65	0.65	mm
Feed/tooth	c	0.03	0.03	0.03	0.03	0.03	0.03	mm
Cutter radius	r_c	1.5	1.5	1.5	1.5	1.5	1.5	mm
Cutter speed	n	35000	35000	35000	35000	35000	35000	rpm
Orthogonal feed forces	F_x	-3.28	-1.468	-0.98	-0.44	0.074	0.48	N
	F_y		2.96	2.90	3.00	2.81	2.60	N
Resultant feed force	F	3.28	3.30	3.06	3.02	2.81	2.64	N
Torque	T	4.92	4.95	4.58	4.53	4.22	3.96	Nmm
Power	**P**	**18.02**	**18.13**	**16.80**	**16.60**	**15.46**	**14.52**	**W**

The axial forces were unable to be included in the data presented in Table 4.21 because there was no source data available. The power values for the two approaches shown in Table 4.19 and Table 4.20 are similar at the ten degree rake angle but tend to diverge in opposite directions toward the extremities. This may be caused by the influence of the axial forces. However, both data sets provide a relatively close spread result in terms of power use.

Table 4.21: Power data summary with differences

Description		Rake Angle [deg]						
		-20	-10	0	10	20	30	units
Spindle power from Table 4.19	P	24.44	22.61	19.36	15.94	14.18	11.60	W
Spindle power from Table 4.20	P	18.02	18.13	16.80	16.60	15.46	14.52	W
Difference		6.42	4.48	2.56	-0.66	-1.28	-2.92	W
Percentage difference [%]		26.26	19.81	13.22	-4.14	-9.03	-25.17	

To confirm that the derived power values presented above in Table 4.21 were similar to those of the machine tool requirement, a sampling of simple cutting trials were performed. The methods and results are described in subsequent sections.

4.4.8 Review of alternative power determination methods

The following subsection briefly researches the possibility of any other means by which the consumed cutter power could be determined. Two alternate methods were explored; one was software based and the other an empirical analytical process.

- Software review

A review of available and appropriate cutter power consumption software was undertaken and only a single software package was deemed appropriate for assessment. This was a package named Computer Cutting-data Service 6.1, a product published by Prototyp – Werke GmbH[136].

The Computer Cutting-data Service (CCS) software suite provides cutting tool management and selection support. Included in the suite was a small software package named Milling Force Optimizer© (MFO)[137]. MFO is a package designed to assist in determining the cutting parameters and effects of a milling processes by specifying the inputs and having the software calculate the outputs. It also shows graphically the fluctuation and magnitude in the cutting forces ultimately to assist with the design of work piece fixtures.

The input parameter table in the programme was completed with values as shown in Table 4.22, which in this case reflect those expected values relating to the cutter for the cutting process under discussion. For the most, many of the software input values are self explanatory and relate directly to the cutting process constraints (such as tool size and feed rate). When selecting the thermoplastic option for the specific cutting force, the programme gives a generic value (150 N/mm^2) for all thermoplastics; however, no value is automatically entered for the specific cutting normal force. Entering a reasonable value for the specific cutting normal force has very little effect on the output results in terms of the power however; the value does affect the output values for the mean cutting normal force, mean feeding force and the mean normal feeding force. Clearly a drawback of this software is the need to have some knowledge of the specific cutting forces of the material being machined and although the specific cutting force is given generically, the specific cutting normal force is not given and left to the user to apply a likely value. Table 4.24 gives some insight into the variation on the affected output parameters when the specific cutting normal force is altered. All other parameters remain unchanged. The specific cutting force value

used below (170 N/mm^2) in Table 4.22, is closer to the value for R-PVC as determined by Kobayashi[138], than the auto supplied value of 150 N/mm^2.

Table 4.22: Mill Force Optimizer (MFO) parameters - Inputs

MFO Machining Parameters	Units	
Cutter diameter	mm	3.0
Number of flutes		3
Radial depth of cut	mm	3.0
Axial depth of cut	mm	0.65
Helix angle	deg	30
Material		Thermoplastic
Specific cutting force (kc1.1)	N/mm^2	170
Increase value (1-cc)		0.9
Specific cutting normal force (kcN1.1)	N/mm^2	17
Increase value (1-ccN)		0.9
Feed rate per tooth	mm/tooth	0.03
Cutting speed (rotational)	m/min	330
Speed (rotational)	1/min	35014
Climb milling		yes
conventional milling		no

Table 4.22 reproduces the parameters used by the Mill Force Optimizer© to calculate the cutting power amongst other factors applicable to the milling process. One small problem that existed with the MFO output, when small cutters were applied in soft materials, was the small number of significant figures it used. For example, the diameter was given as 3.0 mm in the parameter list but was shown as a radius of 2.0 mm in the results list, also the resultant torque level was very low due to the low power input and so the results show zero torque.

Table 4.23: MFO results

MFO results	Value	units
Radius	2 (actual = 1.5)	mm
Axial depth of cut for uniform milling	5	mm
Feed rate	4202	mm/min
cutting angle	180	deg
Mean chip thickness	25	£gm (μm?)
Mean cutting angle	40	deg
Maximum cutting force	6	N

Minimal cutting force	5	N
Mean cutting force (working covered)	6	N
Maximum cutting force fluctuation	1	N
Mean cutting normal force (working covered)	0	N
Mean feeding force	7	N
Mean normal feeding force	9	N
Cutting volume	8	cm^3/min
Specific cutting volume	4953	cm^3/Ws
Torque	0	Nm
Cutting power	33	W
Cutting force fluctuation factor	17	%

Table 4.23 gives the results of the MFO calculations. The labels are given in the table exactly as they are given by the MFO, which has been translated from German. It can be seen that the various resultant forces are given as well as the average forces as they relate to each active cutting flute. Some attempt has been made to give the forces direction with regard to the cut as the normal force is given as well. The last item of information given by this software tool is the percentage fluctuation of the cutting force, which it states, should have a goal of zero. A further screen provides the user with an opportunity to vary parameters in an attempt to achieve a zero goal. From this optimisation process, it was revealed for this project, the depth of cut was required to be 5.0 mm to reach the desired point of zero force fluctuations. Alternatively, a cutter with a helix angle of approximately 78^o would give the same effect, however the axial force is not accounted for here and a helix angle so great

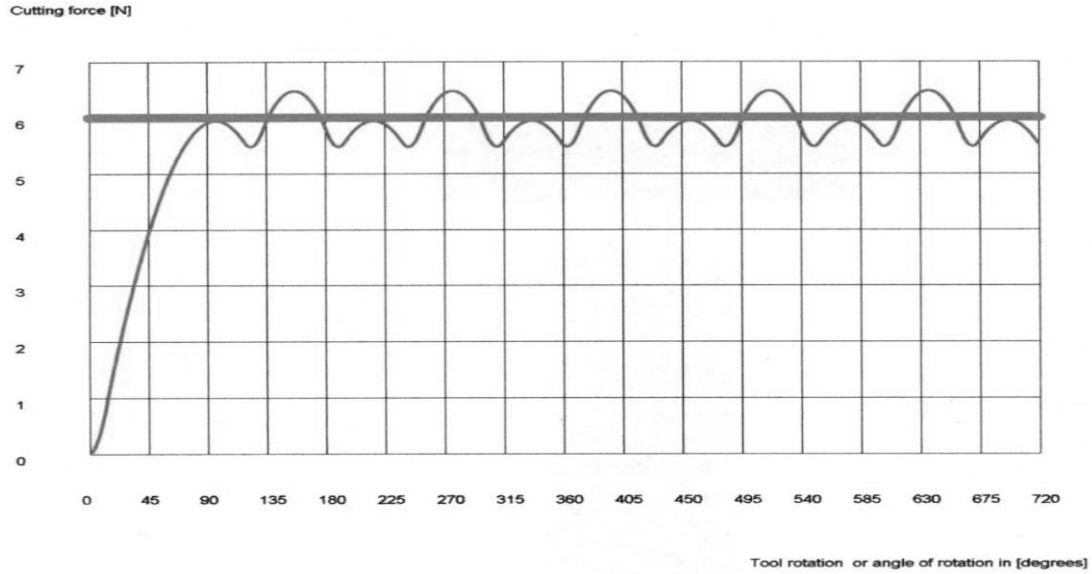

Figure 4.17: Cutting force during tool rotation

would add considerable magnitude to the axial forces on the tool and work piece.

Figure 4.17[139] is a graphic representation of the fluctuating forces that occur during two rotations of the three fluted cutter. The thick horizontal line represents the average applied force (called middle [mean] force in MFO). This figure was taken directly from the software output.

Table 4.24 demonstrates the differences in the forces that are affected by the variation in the specific cutting normal force. Although the forces in themselves are not large and the differences are even smaller, these may have a bearing on the design of the work piece fixtures.

Table 4.24: Differences caused by variations in the specific cutting normal force values

Specific cutting normal force [N/mm^2]	**Mean cutting normal force [N]**	**Mean feeding force [N]**	**Mean normal feeding force [N]**
17	0	7	9
100	3	3	13
170	5	-1	15

The basic information available in the help file was minimal and some description of each of the input and output parameters would be of great assistance to the user. It was the lack of descriptive information about the parameters that contributed to a measure of unease with the interpretation of these results. The terms in themselves were not given adequate description to allow the user to feel confident about applying the software, particularly where the specific cutting forces were required. In addition, the rounding problem discussed earlier provided concern about the inherent inaccuracy of the results when using small tooling and soft work piece materials.

- Analysis of cutting power using the material removal rate

As another possible alternative to determining the power requirement of the spindle, the material removal rate (MRR) method was explored. However, again due to the lack of published data, in particular the specific energy (cutting pressure) values[140] for polymeric materials, this line of investigation was cut short.

The method of power evaluation for which the equation set is reproduced in equations [55] – [63]. This method gave a similar power figure to that of the other methods used above when the specific cutting pressure published by Kobayashi[141] was

substituted in for the specific energy value. The MRR formulae are presented in the follow equations[142].

$$V_p = \pi D n \quad [55]$$

where
V_p = peripheral cutting speed [mm/s]

D = cutter diameter [mm]

n = rotational speed of the cutter [rpm]

$$t_c = \frac{2fd}{D} \quad [56]$$

where
t_c = undeformed chip thickness [mm]

f_c = feed per tooth of the cutter [mm]

d = depth of cut [mm]

$$f_c = \frac{v}{Nn} \quad [57]$$

where
v = linear speed (feed rate) [mm/min]

N = number of teeth on the cutter

$$t = \frac{(l + l_c)}{v} \quad [58]$$

where
t = cutting time [s]
l = length of work piece [mm]

l_c = extent of the cutters first contact with the work piece assuming $l_c << l$ [mm]

$$MRR = \frac{lwd}{t} = wdv \quad [59]$$

where
MRR = material removal rate [mm^3/s]

w = width of cut [mm]

$$T = F_c \frac{D}{2} \quad [60]$$

where
T = torque [Nm]

F_c = cutting force [N]

$$hp = F_c V = MRRu \quad [61]$$

where
hp = power [kW]

V = cutting velocity [mm/sec][143]
u = specific cutting energy [Ws/mm^3]

$$hp = T\omega \quad [62]$$

$$\omega = \frac{2\pi n}{60} \quad [63]$$

ω = rotation speed [rads/sec]

The MRR method is a valid means of analysing the power requirement for a particular process if all the relevant data is available. However, it may only be used when the material specific energy value is known. Once again, these values are not well researched or published for polymeric materials. To calculate the power using the MRR method, Kobayashi's specific cutting pressure value was used in this example. The power consumption determined using the MRR method is given in Table 4.25.

Table 4.25: Numerical results from MRR calculation for milling

Equation	Nomenclature	Value	Units
	D = Cutter diameter	3	mm
	N = Rotational speed	35000	rpm
$V_p = \pi DN$	V_p = cutting speed	329.87	m/min
	f_c = feed/tooth/rev	0.03	mm
	d = depth of cut	0.65	mm
$t_c = 2fd/D$	t_c = approx undeformed chip thickness	0.013	mm
$f_c = v/Nn$	v = feed-rate	3150	mm/min
	n = no. of flutes on cutter	3	
	t = cutting time	2.31	sec/ pocket
$t = (l+l_c)/v$	l = length of cut	120	mm
	l_c = extent of cutters initial contact	1.5	mm
MRR = lwd/t = wdv	MRR = material removal rate	102.38	mm^3/s
	w = width of cut	3	
hp = uMRR	**hp = power**	**17.58**	**W**
	u = specific energy of cutting [Ws/mm^3][144]	171.68	N/mm^2
hp = Tω	T = cutting torque	4.80	Nmm

	ω = rotational speed	3665.19	rads/sec
$T = F_cD/2$	F_c = average cutting force	3.20	N

Table 4.25 gives the numerical results of the MRR investigation using the design parameters for the milling machine project. It is interesting to note that the power calculation gives a result at the high end of the range as defined by the previous two methods above. The values with any significance are shown with double underlines, and the power value, which is also significant, has been boldfaced.

The necessity of knowing the forces applied to the cutter by the process of machining a work piece is of primary importance in the machine design. The magnitude of the orthogonal forces cannot be predicted, nor can they be calculated using the MRR method due to the many unknowns[145]. It was for this reason that the Kobayashi and Altintas theories were researched in depth (the earlier part of chapter four), because they were able to be used to predict the cutting and edge coefficients in helical milling from the tabled orthogonal data as well as the applied forces in the orthogonal axes.

4.5 Experimental cutting trials

4.5.1 Introduction

The uncertainty in calculating the cutter spindle power was alleviated by performing a number of basic cutting trials with readily available equipment, namely the departments' Okuma CNC machining centre in conjunction with a custom mounted high rpm rotary cutting system. During the trials, the rotational speed and power consumption were measured and used to validate the derived results as discussed in the previous sections. Initially the hand tool was chosen because its performance characteristics met the power/speed relationship as well as the ability to chuck a small diameter endmill or slotting drill. The hand-tool performance was advertised as being in the region required by the spindle design demands.

Manufacturing the cards required that they be machined at 1500 cards per hour, giving a process time per card of 2.4 seconds. The use of commercially available 3.0 mm cutters dictated a feed rate of approximately 0.03mm/flute/rev for a three fluted cutter; implying a spindle speed of approximately 35 000 rpm to meet the production rate. It was with these parameters in mind that a hand-tool was selected and adapted to fit into the machining centre in an attempt to confirm the power absorption.

These tests were to serve a twofold purpose; the first was to confirm the spindle power requirement and the second was to observe how the commercially available carbide cutter performed at the speeds and feed rates required to meet the desired production rate in R-PVC.

- Mechanical Requirements of the Cutter Spindle

The following specification (detail) was amassed in order to identify a suitable test facility. Initially, the workpiece tool path was determined for a standard two level pocket and from this the tool total travel length was calculated and an average cutter feed rate velocity was estimated. From the feed rate and cutter style, it was possible to establish a desirable spindle speed range.

The cutter spindle speed required was approximately 35000 rpm, so a Dremel™ MultiPro Model No. 395 (Dremel) was adapted to fit onto the university's three axis CNC milling machine head stock. This allowed controlled and known feed-rates to be used, up to the maximum allowable for the chosen cutter at the selected cutting velocity. The Dremel had a collet chuck that would accept the 3.0 mm diameter solid carbide cutters. Furthermore, it was powered by a 95 watt 230 volt AC motor, and had an advertised maximum speed of 37 000 rpm.

The cutting factors were selected to suit standard cutters provided by various tooling suppliers. A final selection was aided by a software package called Prototyp CCS 6.1™. This allowed the primary requirement constraints for the cutting operation to be analysed following the selection of suitable cutters from the Prototyp™ or SGS™ range of slot drills and plunge cutting end mills. The cutter to be used was a 3.0mm diameter solid carbide 3 fluted tool with a rake angle of 12^{o}, which most closely matched the conditions (parameters) used in the analysis section of this chapter. The selected cutter parameters are given in Table 4.26.

Table 4.26: Cutter Parameters

Primary Cutting Parameters	
Cutter Diameter	3.0 mm
Maximum Cut Width	3.0 mm
Maximum Cut Depth	0.65 mm
Coolant Type	Compressed Air
Bottom Cutting	Yes

Maximum Spindle Speed		35000 rpm
Maximum cutting edge velocity		330 m/min
Number of Flutes		3 or 4
Milling Procedure		Conventional
Short Series Cutter		Yes
Machined Material	R– PVC	Tensile strength – ~50 MPa

4.5.2 Proprietary equipment evaluation

This subsection is mainly concerned with the initial evaluation and testing of proprietary equipment that was available and fit for purpose. Suitable equipment was sourced, evaluated and used for testing. The testing very quickly uncovered deficiencies in the equipment on hand, making it highly unsuitable.

- Preparation for workpiece machining

The initial R-PVC samples for the trial machining were prepared by mounting the plastic card samples onto a 100mm wide x 12mm thick aluminium base plate using isocyanate adhesive. One card was mounted onto either side of the base plate. This initial trial was to investigate the power consumption of the 3.0 mm diameter cutter machining a full width track (3.00mm) in the R-PVC at a depth of 0.65 mm.

The trials were to ensure that the type of cutter selected would actually cut through the R-PVC at the predetermined speeds and feed-rates, to meet the production rate of the card manufacturing process. Initial concerns were that at the 30 000 plus rpm speeds may cause the R-PVC to melt or burn causing the cutter to clog during extended cutting runs. Initial tests using a Dremel Multipro™ indicated that there should be no problems with the selected cutter. The power absorbed during no load running was conveniently determined in these initial tests. The Dremel's published power performance was 95 watts, which was considered sufficient on the basis of the CCS MFO Milling software. However, these tests concluded that the hand-tool failed to meet its published performance, not in power output but in rpm capability running under no load conditions. Due to this shortfall, the hand tool was tested for it's range of speed performance under no-load conditions to decide it's ongoing suitability for the project. This was not a new tool.

- Dremel Multipro performance

The Dremel Multipro (Dremel) was tested for variations in the speed and an attempt was made to measure the rotational speed of the chuck at the various speed settings marked on the speed range control switch. A Pioneer Electric & Research Corporation analogue photo tachometer, model 1030, serial number 3474, speed range 0 – 30 000 rpm, was used to measure the speed of the Dremel's output spindle. The top speed of 37 000 rpm was assumed as this was stated on the appliance's label and was beyond the capacity of the photo tachometer. The following table (Table 4.27) gives the approximate speeds that were measured at the various speed control settings with the photo tachometer at no load.

Table 4.27: Measured speed of the Dremel Multipro and the corresponding maximum cutter feed rates.

Speed Control Position	Published speed [rpm]	Measured Speed [rpm] (approx)	Max Cutter Feed Rate [mm/min]
1	5 000	13 500	1443
2	not published	16 500	1776
3	ditto	22 500	2442
4	ditto	29 500	3219
5	30 000	37 000 (assumed)	4107

Based on the speeds in Table 4.27 above, four short runs were performed using the department's Okuma CNC milling machine.

An AC power meter was used to determine the power absorbed by the Dremel. With the speed setting set to maximum, the power absorbed was approximately 61 watts. At this stage, no other spindle speed settings were tested.

- End mill specification

The specific cutter used for the above test, was selected from the SGS range of tools and supplied by Trade Tools Ltd, New Zealand. The cutter specifications are given in Table 4.28

Table 4.28: End mill data

End Mill Data	
Model No.	
Diameter [mm]	3
No. of flutes	3

Material	Micrograin solid carbide
Cutting direction	Right hand
Bottom cutting	yes
Cooling	Air
Rake angle [deg]	12 – 15
Clearance angle [deg]	6 – 8
Helix angle [deg]	30
Flute length [mm]	$7^{+0.5}$
Overall length [mm]	$38^{+2.0}$

- Preliminary proprietary equipment cutting test results and discussion

Table 4.29: Parameters and results for the primary R-PVC cutting trial

Test Run No.	Speed Setting	Feed-rate [mm/min]	Depth of Cut [mm]
1	5	4000	0.183*
2	5	4000	0.183
3	5	4000	0.665
4	5	3000	0.672

*Verified with a Coordinate Measuring Machine.

Table 4.29 summarises the data retrieved from the primary cutting trials performed with the Dremel Multipro. These results are discussed in the following the paragraphs.

Test run No.1: - The first test cut was performed at a depth of 0.183 mm and at a feed speed of 4000 mm/min along the length of a standard card (approximately 80 mm). The power consumption was measured at approximately 61 watts at no load and approximately 65 watts during the cut. A visual inspection showed the cut was extremely clean with no apparent ragging along the cut edges. The cutter flutes were observed to remain clear and the air-cooling kept the swarf away from the cutter path. There was some slowing of the cutter but not by a significant degree. The slowing speed was only noted as a change in the pitch of the sound of the Dremel as there was no provision for dynamic speed measurement.

Test run No.2: - This test was carried out as a repeat of test run no. 1, and gave similar results.

Test run No.3: - The depth of cut was increased to the maximum considered possible (0.65 mm) for use when machining the IC pockets in the R-PVC card. The power consumption was observed to increase from approximately 61 watts at no load to

approximately 81 watts at full load. The feed-rate was again set to 4000 mm/min. This caused the cutter to plough slightly as the Dremel spindle speed dropped significantly, causing an observed overfeeding (choking) of the cutter. At 37 000 rpm and a feed-rate of 4107 mm/min gave a feed of 0.037mm per tooth: the maximum recommended for the cutter. As the spindle speed fell, the CNC mill maintained the applied feed-rate. The resulting cut was poor in finish particularly along the edges of the cut, which can be explained by the exceptionally 'loose' nose bearings on the Dremel spindle. The surface finish in the bottom of the cut was still very smooth and easily met the quality of finish that the existing machining processes were achieving. It is believed that the 'loose' spindle bearings allowed the cutter to "walk around" the material being removed and caused an oversized cut approximately 3.5 mm wide.

Test run No.4: - The feed-rate was slowed to 3000 mm/min for this run, which improved the Dremel's performance considerably. The spindle speed did not reduce as significantly (again noted as a change in sound pitch) although sufficient to cause over feeding again. The finish in the groove was notably improved suggesting that the overfeeding issue was much less of a problem. The 13-micron difference in depth cannot be readily explained despite the depth of cut being set to the same as the previous test but a best guess would be the poor spindle bearings in the Dremel allowing axial float. The power consumption of 20 watts during cutting was the same as for test run no.3 during the cut.

The primary reason for performing this initial trial was to determine the power consumption required to perform a maximum performance cut in the R-PVC material. To some extent the value of 20 watts confirms the calculated results. The CCS v6.1 software discussed previously showed a power consumption of 33 watts, and these cutting trials have shown that the actual power requirement was approximately 20 watts based on the Dremel hand-tool. The two test runs 3 & 4 showed a similar result for both tests but the actual cutting parameters varied considerably. It will be assumed here that these results corroborate the software results obtained previously although there is an error of greater than 50% and nearly 100% greater than the initial calculated results (16 watts).

- Overcoming the problems

The tests provided a number of interesting points that required further investigation. The first of these was the need to monitor the spindle speed of the Dremel. This was achieved by mounting an electronic opto-switch in close proximity to the spindle chuck to count the rotational frequency. This proved to be more accurate and reliable than the photo tachometer that was initially used and also provided dynamic output. With the capacity to measure the spindle speed, the feed-rate could be varied on the CNC mill to optimise the Dremel's available power and thus minimise the spindle speed loss and reduce the possibility of overfeeding (choking) the cutter. Table 4.30 presents a summary of the results from measuring the spindle speed at no load when the opto switch tachometer was used. The maximum cutting edge speed was calculated as the peripheral speed of the cutting edge of the 3.00 mm diameter cutter at the measured rotational speed. The maximum cutter feed rate was based on 0.03 mm cut per flute per rev also at the measured rotational speed. This feed rate was the maximum recommended feed rate for the cutter whilst working in metallic materials, and in the absence of any other information with regard to polymeric materials was utilised as the maximum rate in the R-PVC. Future investigation may prove that the cutter could be worked at a higher rate in polymeric materials.

Table 4.30: Spindle speed results using the Opto-Switch
All maximum feed rates relate to a 3 mm diameter three-fluted cutter.

Speed control position	Measured speed [Hz]	Measured speed [rpm]	Max cutting edge speed [m/min]	Max cutter feed rate [mm/min]
1	220	13200	124.41	1465
2	285	17100	161.16	1898
3	382	22920	216.02	2544
4	473	28380	267.48	3150
5	539	32340	304.80	3590

- Redesigning the test process

When the results in Table 4.30 are compared with those in Table 4.27, it is easy to see how the initial tests lead to overfeeding and choking of the cutter. The maximum attainable speed of the Dremel proved to be significantly slower, at 32340 rpm, than the published maximum speed of 37 000 rpm. The initial approach for subsequent cutting trials was to introduce the cutter to the work piece at a feed-rate well below

the maximum with the cutting runs significantly longer, of the order of 400 – 500 mm (approximately 10 cards beside one another). Also the longer runs allowed some manual variation of the feed-rate to avoid any detrimental lose of spindle speed. The long runs were to give a more even power consumption reading and an appraisal of the cutter tip condition when working at or near to the maximum feed-rate conditions. The extended runs would also give a measure of the effectiveness of a commercial cutter when working in R-PVC. R-PVC is known to be highly abrasive; therefore, the life of the commercial cutters is of the utmost importance. If ragging or signs of the cutter overheating had appeared during these extended second stage high material removal rate tests, the type of commercial cutter being utilised would have had to be reappraised and an attempt made to find a more suitable cutter. These initial investigations did not pursue the results of having the cutters resharpened.

- Confirming the Dremel performance

The spindle speed variations noted above were the cause of further investigation regarding the reliability of the published data about the Dremel's performance. In the process of testing the equipment, the Dremel showed some remarkable variations in its running speed with respect to the length of time it was running. As commented earlier the speeds were nowhere near the published speeds presented in Table 4.27, with the slowest speed being approximately 13000 rpm. However, this was not stable and with time, it tended to increase and appeared to stabilise at approximately 15000 rpm after 5 – 10 minutes of running time. At the other end of the scale, the published top speed was 37000 rpm. This in reality was never achieved with the tachometer registering a maximum speed of approximately 33500 rpm. Again, this was not a stable speed and it tended to drift down with time, finally appearing to stabilise at approximately 28500 rpm. This tendency for the speed to drift with time was of major concern and required to be remedied in some way if possible. It is worth noting that one of the bearings in the Dremel was particularly noisy, indicating that it was likely to have been badly worn. There was no significant temperature rise in the case of the tool during the tests, which were carried out under no load conditions. One means of attempting to discover the effect of temperature rise in the tool was to apply a source of warm air to the fan intake. This gave a small variation in speed but nothing remarkable.

In an endeavour to find a more stable speed a newer hand-tool, a Mini Drill Q1K-3A was fitted in place of the Dremel and further speed stability tests were carried out.

This newer tool was fitted with a slightly larger prime mover with a published power output of 130 watts and a speed range of 12000 – 33000 rpm.

Testing the tool speed range (12 000 - 33 000 rpm) showed that it also did not perform to the published speeds, and gave poor speed stability under extended running conditions. After approximately 15 minutes continuous running at no load, the speed at the '1' setting had risen from approximately 15 000 rpm to semi stabilise at approximately 20 500 rpm. On the highest setting of '6,' the speed was initially measured at approximately 28 000 rpm and rose over a similar 15 minute period to approximately 30 400 rpm.

Unfortunately, these results were similar to the Dremel and the speed variations just as dismal. However, the decision was made to perform the trials with the newer tool as the nose bearings were in better condition and it was labelled with a higher power output. The maximum loaded spindle speed attainable was approximately 25 000 rpm well below that published, throwing the labelled power value into doubt.

- Conclusion of preliminary cutting trials

A brief series of cutting tests confirmed the inadequacy of this replacement spindle drive, the results of which are shown below. Note that the feed rate and spindle speed are less than required, as under load this unit also failed to perform as labelled.

Table 4.31: Cutting trial results with Mini Drill Q1K-3A

Trial No.		**1**	**2**	**3**	**4**	**5**	**6**
Cutter diameter	mm	3.0	3.0	3.0	3.0	3.0	3.0
No. flutes		3	3	3	3	3	3
Measured cut width	mm	0.34	0.34	0.34	0.34	0.34	0.34
Spindle speed	rpm	24000	23400	23500	24000	24100	24800
Speed setting		6	6	6	6	6	6
Cut depth	mm	~0.55	~0.55	~0.55	~0.55	~0.55	~0.55
Feed rate	mm/min	2886	2650	2550	2220	2220	2000
No load power	watts	82	82	82	82	76	76
Full load power	watts	94	92	92	95	89	87
Working power	watts	12	10	10	13	13	11
Voltage [AC]	volts	234	234	234	234	234	234

Table 4.31 presents the results of this set of cutting trials showing lower power consumption, which can be explained by the lower material removal rates. The 2nd hand-tool proved as inadequate as the first, evident in the shown results. Therefore, due to this lack of spindle drive integrity in both the Dremel and Mini Drill, the power performance analysis was abandoned until a higher specification cutter spindle could be arranged.

Initial thoughts were to purchase an off the shelf item that met the cutter drive requirements, given that an indication of the power consumption was now available. However, finding a suitable "off the shelf" drive with an appropriately powered bearing spindle unit manufactured by a single manufacturer proved to be very illusive. This lead to the decision to develop a custom spindle unit and hence, a unit was designed and assembled with several custom manufactured components for the project's specific task.

4.5.3 Custom designed precision spindle

The two primary considerations in the design requirements of the spindle were the power output and the rotational speed capacity: these two parameters being 50 – 100 watts for the power and 35 – 40 000 rpm for the speed. As previously indicated the cutting power consumption was approximately 20 watts. The system also had additional losses, which were mainly due to the unknown effects from within the spindle bearing housing, hence the increased power specification.

Sourcing a motor with a power output in the specified range proved to be an arduous task. However, a 50 watt, 50 000 rpm brushless DC motor was eventually selected as the prime mover. This selection was made due to the lack of availability of a more suitable motor of greater continuous output than 50 watts and that would run to 40 000 rpm. This was of major concern as a more suitably sized motor would have been 80 to 100 watts but a long search for such a motor proved fruitless. The physical trials would prove that the 50 watt spindle was somewhat underpowered.

A grease lubricated internal grinding spindle assembly with a maximum rotational speed of 40 000 rpm was selected to conjoin the motor. Apart from meeting the speed specification, a grease lubricated unit was deemed to be easily integrated into the test facility design.

Once the selection of the components was complete, the challenge of connecting the two components together to form a powered high speed precision spindle capable of reaching 35 – 40 000 rpm was addressed. To connect the two components, a small high performance shaft coupling was utilised. The drive spindle assembly comprised finally of a brushless DC electric motor, a high performance bearing housing and spindle, a shaft coupling, a tool holding collet chuck and several custom manufactured items. The specifications of all these components can be found in Table 4.32 to Table 4.36 and the adjoining paragraphs.

The new precision spindle assembly was then required to mount into the departments' CNC machining centre.

-Spindle specification

The spindle, an SA Type Internal Grinding Spindle, was manufactured by NSK Nippon Seiko KK International Division in Japan and supplied by NSK Bearings in New Zealand. The spindle specification data is given in Table 4.32.

Table 4.32: Precision spindle specification

Spindle Designation	**Max speed [rpm]**	**Lubrication**	**Shaft orientation**	**Standard output**	**Standard input**
Manufacturer	NSK Nippon Seiko KK International Division, Japan				
NSK SA500	40 000	Grease	Horizontal	Tapered quill shaft	Flat belt drive
Max recommended operating temperature				70^{o} C	

- Motor specification

The motor, EC22 Maxonmotor, manufactured by Maxon Motors of Switzerland and supplied via Rutty in Australia. The DC motor specification data is given in Table 4.33.

Table 4.33: Spindle motor specification

Motor Data		**Controller**	
Manufacturer	Maxon Motor Ag, Switzerland		
Motor model no.	EC22	Amplifier model no.	1-Q-EC Amplifier DEC 50/5
Assigned power rating [W]	50	Supply Voltage V_{cc} [VDC]	10 - 50
Stall torque [mNm]	575	Max output voltage	0.95 x V_{cc}
Max permissible speed [rpm]	50 000	Max permissible speed [rpm]	120 000
Rotor inertia [gcm^2]	3.1	Max output current [A]	10
Speed/torque grad [rpm/mNm]	81	Continuous output current [A]	5
Max efficiency	90	Switching frequency [kHz]	39

- Shaft coupling specification

The shaft coupling between the motor and spindle input was a bellows type manufactured by R+W Coupling Technology, Germany and supplied by Motor Technology Ltd. from the United Kingdom. The coupling was supplied as balanced to 40 000 rpm. The coupling specification data is given in Table 4.34.

Table 4.34: Coupling data

Coupling data	
Manufacturer	R+W Coupling Technology, Germany
Model no.	MK1/1/1/5/3/balanced
Rated torque [Nm]	0.1
Max speed [rpm]	>20 000 balanced
Required speed [rpm]	40 000
Outer diameter [mm]	10
Coupling length [mm]	20
Standard bore H7 [mm]	3
Inertia [gcm^2]	0.4
Clamping screws	2 x M2.5
Axial compression [mm]	0.4
Lateral misalignment [mm]	0.15
Angular misalignment [deg]	1

- Collet chuck

The collet chuck selected to hold the milling cutter was selected from the ISCAR tooling system as the CDP ER11 M10 Mini and was supplied by Frank Myers Tools, Christchurch, New Zealand. The tool chuck was adapted to fit onto the input end of the NSK spindle where the pulley was usually fitted using a custom adapter sleeve. The collet chuck specification data is given in Table 4.35.

Table 4.35: Collet chuck data

Tool chuck data	
Manufacturer	ISCAR Ltd. Israel
Collet holder model no.	CPD ER11 M10 Mini
Collet model no.	ER11 Norm 2-3 DIN 6499
Max run out	0.01 mm

- Custom components

Several components were necessarily manufactured in the department's mechanical engineering workshop. The custom manufactured components are tabled in Table 4.36 and are shown in Figure 4.18.

Table 4.36: Custom components

Component	Material
Manufacturer	University of Canterbury, Dept. of Mech. Eng., Mechanical Workshop
Bellhousing	Aluminium alloy
Spindle mounting clamps	Aluminium alloy
Motor quill shaft	SAE 4140 alloy steel
Spindle shaft/chuck adapter	SAE 4140 alloy steel
Spindle Housing offset mount plate	20 mm mild steel plate
Okuma CNC Mill Adapter plate	25 mm mild steel plate

Refer to Appendix C12 ff for detailed engineering drawings.

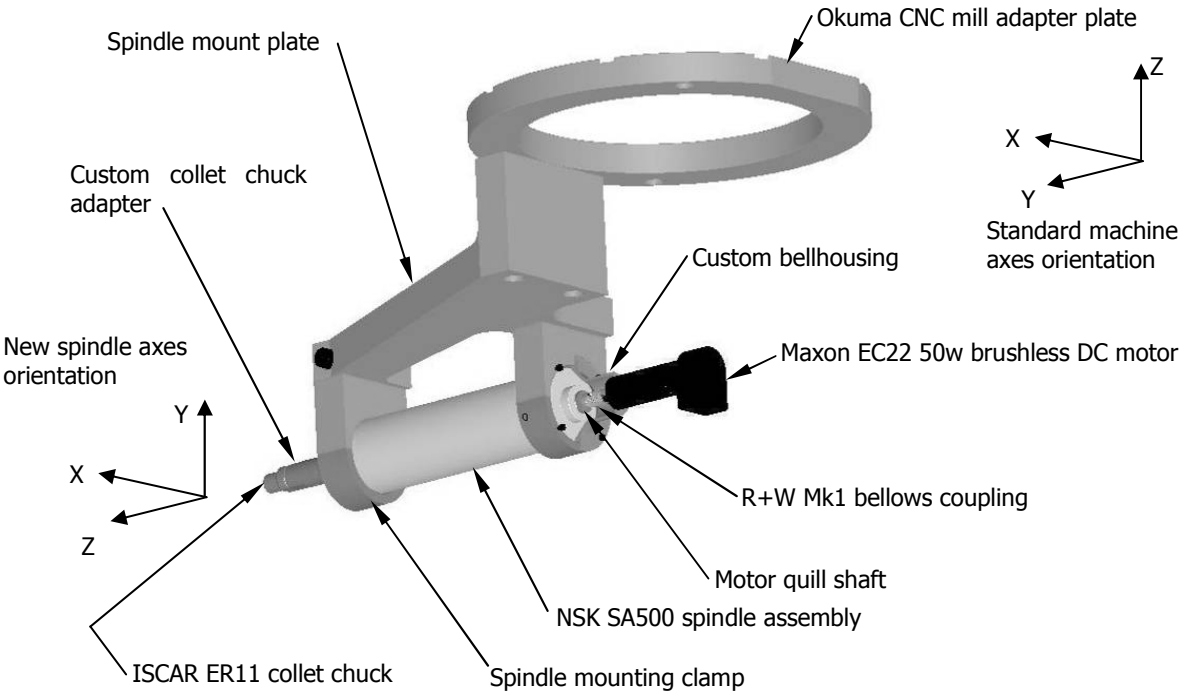

Figure 4.18: General assembly of spindle

Figure 4.18 presents the general assembly of the assembled precision spindle and the adapter frame used to adapt the unit to the Mechanical Engineering Department's CNC machining centre (mill). A number of small problems were encountered as the NSK spindle was necessarily oriented horizontally which was 90^{o} to the usual spindle axis in the machining centre. However, the machining scope only called for movement in a

single axis at a time, therefore the orthogonal axis system in the mill had the axes transposed to suit the new application. The existing Y-axis became the new Z-axis and the existing Z-axis became the new Y-axis (see Figure 4.18). The machining centre was a 2½D machine, which meant the standard Z-axis was not able to be interpolated as rapidly as the standard X and Y-axes during normal operations. However, this did not present any initial difficulties, as the machining runs were all straight parallel cuts across the R-PVC samples in the standard X-axis direction. The area in which problems were mainly encountered was where the operator had to get used to using the cutting tool in a different working orientation.

In addition to the spindle drive assembly, a workpiece holding device was required. For ease of use and as a trial for the proposed card holding system a pneumatic vacuum chuck was developed. The details of this device are introduced below.

- Pneumatic vacuum chuck

The additional fixture took the form of a pneumatically actuated vacuum chuck that was mounted to an angle plate to support the cards for machining in the required vertical orientation (Figure 4.19). The chuck was designed with a pocket to support the card and prevent any movement due to the applied cutting forces. The base of the pocket was flat with 1.0 mm holes drilled at 5.00 mm centres. The holes covered the entire area and were drilled through into a plenum chamber onto which was connected a vacuum generator. A Bosch Rexroth 735 series E060 model ejector was selected as the pneumatically operated vacuum generator. It was capable of drawing a 90% vacuum at an inlet pressure of 4 bar. This equated to a holding force of approximately 13 N, which was considered sufficient to hold the card. Table 4.19 and Table 4.20 give a theoretical indication of the magnitude of the expected forces. At 13 N, the holding force was more than three times the highest expected horizontal forces. However to ensure the card did not move horizontally, the pocket in which it rested was 2.0 mm deep. There were other issues that required addressing before machining the pockets, the main one being the

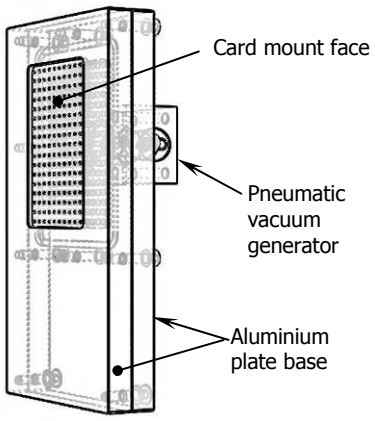

Figure 4.19: Diagram of vacuum chuck

reorientation of the machines axes. With the spindle axis of the machine turned 90^{o} from its standard configuration by the addition of the high speed spindle some careful CAM programming was required to rotate the machine coordinate system. The second issue was that the CNC machining centre was only a 2½D machine. The significance of this limitation did not become apparent until the feed speed was raised to significant levels.

4.5.4 Cutting trial procedure and spindle performance

- Precision spindle performance

The spindle assembly was first bench run to provide the initial 'running in' period and to check its performance. A considerable time was involved in 'running in' the spindle assembly by ramping it up and down through its speed range whilst carefully monitoring the bearing running temperatures. The suppliers of the NSK bearing housing recommended that the bearing temperature should not rise above 70^{o} C. Electrical thermocouples were used to monitor the bearing operating temperature. These thermocouples were placed against the side of the bearing housing and were clamped in place using the aluminium mountings.

Early trials proved very promising with the power absorbed at low speeds being minimal. However as the speed was raised towards the target value of 35 000 rpm the power usage increased till the full 50 watts was being absorbed at approximately 31000 rpm. During operation, the rising bearing temperature, throughout the warm up period, had the effect of reducing the power requirement. This effect stabilised as the operating temperature was reached, such that the maximum speed attainable was still only approximately 32000 rpm. A likely explanation for the unanticipated spindle power consumption was the bearing lubricant. The bearing seals were discounted as having any detrimental effects as they were a non-contact labyrinth type.

The spindle was initially chosen because it was grease lubricated and labyrinth sealed, which simplified its integration into the system. However, the viscous grease proved to absorb more power than initially thought. Even with the rising temperature and the grease's viscosity reducing there was still sufficient drag in the bearings to absorb all available continuous power at a point before the target speed was reached. Beyond this speed, the motor was working in the intermittent section of the power envelope.

The alternatives, oil mist lubrication and pneumatic bearings were considered, both of which were dismissed, on the basis of cost and complexity.

The decision was made to perform the trials at the maximum attainable speed without the idle speed power going beyond the available 50 watts. This in effect reduced the maximum speed to approximately 32000 rpm with a corresponding effect on the maximum feed speed of the cutter.

- Cutting trial procedure

Power determination cutting trials were performed using the high speed spindle described previously and mounted into the Department of Mechanical Engineering's CNC machining centre. These were carried out on R-PVC material in the form of blank cards, which had been attached to a 25 mm thick aluminium backing plate using an isocyanate adhesive. Laying out the cards in this manner allowed cuts approximately 0.65 mm deep to be cut across their faces. Cutting runs of the order of 300 mm in length were performed which allowed the cutter to 'settle down' to a constant working speed along the traverse of the cut. The cutter was the selected 3.0 mm diameter cutter suitable for machining ferrous materials. A clamp-on power meter, an LEM Analyst® 2050[146], and an oscilloscope, a Tektronix TDS 220[147], were connected to the motor controller, to capture a power consumption reading in watts and the speed output in hertz (simply multiplying the frequency reading by 60 gave rpm. A constant speed (rpm) setting was chosen on the motor controller, rather than constant torque, which were the optional motor controller settings. A spindle speed of approximately 520 Hz (31 000 rpm) was used for all the cutting trials though this varied a little (Table 4.37). This was the preferred operating speed for extended periods as the grease lubricated bearings absorbed the total available continuous drive motor power (50 watts). The CNC machining centre was programmed manually to machine the required cutting traverses. The manufacturer's maximum cutter feed recommendations formed the basis of the cutter feed rate selection, which were for machining metals, not polymers. To ensure that cutter choking did not occur, the feed rates were kept below the recommended maximum of 0.1 mm/rev.

4.5.5 Cutting trial performance results – precision spindle

- High feedrate high spindle speed linear traverse results

The overall results from the trials are presented in Table 4.37, which shows the power data in the last three columns and also presents two columns showing the frequency reading and the converted rpm value. As can be seen at this speed the power absorbed by the spindle system while idling was above the 50w continuous rated output of the motor. An assumption was made that all the extra power absorbed during cutting was due to the cutting action, as the rpm of the cutter remained constant. The cutting power is given in the last column which compares well with the expected values as calculated (16.6 w) from Table 4.20.

Table 4.37: High speed spindle cutting trial results – straight traversal cutting

Trial no.	Motor speed	Motor speed setting	Cutter feed speed	Nominal cut depth	No-load power	Working power	Cutting power
	rpm	Hz	mm/min	mm	w	w	w
1	29640	494	2400	0.6	49	68	19
2	31200	520	2400	0.6	53	70	17
3	31200	520	3000	0.65	50	72	22
4	31920	532	3000	0.65	54	75	21
5	31860	531	3000	0.65	53	75	22
6	31920	532	3000	0.65	56	80	24
7	31920	532	3000	0.65	55	75	20
			Average	0.65	52.86	73.57	20.71

Visual examination of the completed cuts indicated that the cutting depth was deeper than 0.65 mm. This was evident from the point of view that the cutter had contacted the backing plate in a number of places having machined through the R-PVC. The increased depth of cut may account for some of the extra power absorbed above the expected value (16.6 w).

For the sake of completeness, a final set of cutting trials were proposed that were based around machining a representative pocket into a card. This required an additional fixture, the pneumatic chuck (introduced in section 4.5.3), to support the card during the machining process.

- Pocket machining results

The profile of the pockets was rectangular but with two separate cutting depths. The inner or deepest of the two was approximately 9.0 x 9.0 x 0.62 mm deep and the outer or shallow pocket was approximately 13.0 x 12.0 x 0.2 mm deep, both measured from the top surface of the card. This was representative of a standard pocket form.

Table 4.38 presents the recorded data showing the actual parameters used for twelve pocket machining trials. This data was collected electronically during each trial, at a frequency of 1 kHz, using an in-house custom designed and built data logging system. It was then filtered to 10 Hz and the resulting data was plotted to obtain a graphical form for the power consumption. Sections of data were interpolated to give four shorter data series. The four regions of interest were; the start idle power (data recorded before cutting), the deep pocket power (data collected during the deep pocket machining), the shallow pocket power (similar to the deep pocket but for the shallow pocket) and the finish idle power. The four 'Average Power' columns shown in Table 4.38 represent the filtered and averaged data for each of the four regions. The data in parentheses gives actual power consumed in machining each pocket.

Table 4.38: Pocket machining test parameters and results

Test no.	spindle speed - actual	Feed speed	Cutter type[#]	Average start idle power	Average total deep pocket power	Average total shallow pocket power	Average finish idle power	Maximum peak cutting power
	rpm	mm/min		w	w	w	w	w
1	24000	1000	S	31.9	39.0 (6.7)	37.6 (5.4)	32.5	8.5
2	24000	1000	S	35.2	37.3 (3.8)	36.5 (3.0)	31.9	5.8
3	24000	1000	S	30.9	37.3 (6.1)	36.6 (5.4)	31.4	8.3
4	30000	1500	S	50.0	62.3 (12.4)	57.8 (8.0)	49.7	14.3
5	30000	300	S	50.6	55.4 (5.0)	54.5 (1.4)	50.2	9.5
6	30000	3000	S	49.2	63.5 (13.2)	58.8 (8.5)	51.5	18.6
7	30900	3000	S	58.9	75.0 (15.6)	69.3 (9.9)	60.0	22.4
8	30900	3000	S	59.2	74.5 (14.8)	70.2 (10.5)	60.2	20.5
9	30900	3000	A	53.3	67.9 (14.9)	58.8 (5.8)	52.7	20.0
10	30900	2100	A	52.3	63.7 (11.2)	56.4 (3.8)	52.7	15.5
11	30900	1200	A	56.2	63.9 (8.6)	57.0 (1.7)	54.3	10.9
12	30900	900	A	59.4	66.0 (6.5)	63.5 (4.1)	59.4	14.0

[#] Note: S = machining suitability for steel, A = machining suitability for aluminium

It is worth noting that during these trials the cutter feed speed was very close to the maximum recommended for ferrous materials. The maximum possible feed speeds were not included in this research and remain outside the scope of this study.

The data in Table 4.38 presents the average cutting power and maximum peak power required to perform the machining tasks for a deep pocket. Comparison shows it matches closely with the cutting power data given in Table 4.37. The match is closer than expected but as the commercial power meter, used to record the data in Table 4.37, only outputs an average value based on a relatively slow sampling rate and the pocket data is averaged; the results are acceptable.

4.5.6 Result summary and discussion

- Results summary

The following table (Table 4.39) presents the data from all the methods of determining the cutting power consumption that were investigated during the course of this study. The calculated power values shown in Table 4.39 differ from those shown in Table 4.19 and Table 4.20 due to the fact that they have been recalculated using a speed of 32000 rpm instead of the original and desired 35000 rpm. Reducing the nominal cutter speed had the effect of reducing the absorbed power values, but it brought the results into line such that a direct comparison of all the values could be made.

Table 4.39: Mechanical cutting power comparison

	Cutter rake angle [deg]						
Analytical methods	-20	-10	0	10	20	30	
Calculated power(K_{te} and K_{fe} excluded)	22.35	20.67	17.71	14.57	12.96	10.60	w
Calculated power (K_{te} and K_{fe} included)	16.47	16.58	15.36	15.18	14.13	13.28	w
Cutting power (MFO software)				25.00	27.00	33.00	w
MRR power			17.58				w
Experimental methods							
Mini Drill working power						13.00	w
High speed spindle (steel cutter type)*				18.42			w
High speed spindle (steel cutter type)**				18.25			w
High speed spindle (Aluminium cutter type)**						17.84	w

*Average power absorbed during straight run trials and including motor efficiency
**Average power absorbed during pocketing trials and including motor efficiency

- Discussion of results

The results indicate that the analytical method was sufficiently accurate to quantify the spindle drive power. However, a major drawback was the power absorbed by the grease lubricated spindle. This was not considered in depth, as it was not thought to be an overriding issue in the design of the high speed spindle. However, as can be seen from the results, the power absorption by the idling spindle dominated the system power consumption. Obviously, this situation would need to be resolved in any production machine environment. However, the excursions into the intermittent operating zone was of very short duration and therefore deemed acceptable to enable completion of the research. In this, there was no obvious compromise to the system performance. The 50 watt motor was rated by Maxon™ at an efficiency of 89%[148]. As the electrical motor power was being measured and not the mechanical power output the efficiency figure must be considered as it will affect the overall result. Recalculating the experimental power values with regard to the efficiency brought the mechanical power values more into line with the analytical values that are shown in Table 4.39. At the time the work was being performed, no motor in the 50 – 100 watt range was available. The nearest available size was an 80 watt motor but its maximum permissible speed (25 000) fell short of the design requirements.

The power consumption range (Table 4.39) shows the extreme values to be given by the MFO software calculation (upper bound value, row three of Table 4.39) and the 'Calculated power without edge constants included' (lower bound value, row one of Table 4.39). This is a useful observation as the bulk of the results fall into a range of 14 - 18 watts. Each power determination method is discussed below.

The result from the Mini Drill gave the lowest power value but this can largely be attributed to the lighter machining duty to which it was subjected. By referring to Table 4.31 the depth of cut, and the feed and cutter speeds are seen to be considerably reduced. This was in keeping with the power and spindle speed available from the Mini Drill. The bearings supporting the spindle were very loose and as such, the accuracy of the cuts was compromised severely. Suffice it to say that this tool did not prove suitable for the duty to which it was subjected and therefore was discarded in favour of a more suitable apparatus.

The MRR method of determining the power makes no reference to the rake angle of the cutter; however, the method proved to predict the power requirement surprisingly consistently with the other methods' results, shown in Table 4.39. Inspection shows it to be slightly above the norm at 17.58 watts. However, a point to note is that the MRR method relies completely on knowledge of the value of the specific cutting energy property of the polymeric material being machined. This property is rarely published for polymeric materials and therefore the usefulness of the MRR method is limited to those materials for which there is published data: generally only metals.

In the author's opinion, the MFO software solution was not designed to give a power consumption output for polymeric materials. The specific cutting pressure required is unique to each material and as such, the generic offering presented by the MFO software gives a wholly unsuitable result. In terms of the power consumption values, they were the highest presented in Table 4.39. The specific cutting pressure used as the generic value for thermoplastics tended to give a lower power requirement value than the value for R-PVC published by Kobayashi[143]. There is still some discrepancy as the values shown by the MFO software remain very high compared to the other results. The author was unable to obtain any details of the analytical approach used within the MFO software to enable any reason to be put forward as to why the power values were so much greater. One possible reason could be rounding error caused by the software increasing the cutter size to 2.0 mm radius from 1.5 mm. Certainly, by using the MFO software, a motor of suitable power output could be selected.

The analytical solution for the calculated power requirements proved to give values that were lower than those the actual testing produced. A summary of the differences between the calculated results was presented previously in Table 4.21. This table shows the difference between the calculated values at the 10^{o} tool rake angle as 4.14%. The calculated values and the experimental values are now compared below in Table 4.40, which shows the percentage differences from the two different analytical approaches. The first with the edge cutting constants excluded and the second with them included.

Table 4.40: Differences between calculated and experimental values

		Rake angle [deg]				Edge coefficient
		10		30		
Calculated power	W	14.57		10.6		Edges excluded
Experimental power			Percentage difference		Percentage difference	
straight run cuts	W	18.42	20.90%			
pockets (steel cutter)	W	18.24	20.12%			
pockets (aluminium cutter)	W			17.84	40.58%	
Calculated power	W	15.18		13.28		Edges included
Experimental power						
straight run cuts	W	18.42	17.59%			
pockets (steel cutter)	W	18.24	16.78%			
pockets (aluminium cutter)	W			17.84	25.56%	

The power values with the edge constants included are higher and therefore closer in value to the experimental results. This indicates that the edge constants are important and their effect should not be ignored. From Table 4.39, there was 0.6 watt (4%) difference in the power requirement in the calculated results at 10^{o} rake angle but this increased to 2.68 watts (20.2%) for the 30^{o} rake angle. There appears to be no immediate explanation for the divergence with the increasing rake angle. It is possible the interpolated data[148] used to determine the edge coefficients was erroneous, however this would not completely account for the larger difference. The rheological behaviour of the R-PVC during cutting was not included in the scope of this research and therefore may form the subject of future work.

The calculated results that included the edge cutting coefficients are sufficiently consistent with the experimental data to be used to determine the power requirements in any future design applications.

The experimental results from the two test approaches gave consistent results when they were compared. However, two different approaches were used in determining the power usage. The power consumption for the straight traversal cuts (Table 4.37) was read directly from a commercial meter that averaged the power data over a relatively slow sample period (of the order of once a second). The second method (Table 4.38) sampled the data at 1 kHz, which was then filtered to 10 Hz and charted

graphically. Due to the very short machining legs, when machining the pockets, the commercial power meter would not have provided an accurate data output, due to the low sampling rate and hence the implementation of the high speed sampling system.

The two different approaches to determining the experimental power gave consistent results. Both approaches were open to a number of errors. Poor 'depth of cut' control due to the method of fixing the card blanks to the backing plate was a problem with the straight traverses. It proved very difficult to spread the adhesive evenly and to have all the cards laying completely flat. This unevenness in the cards gave rise to variations in the actual thickness of material exposed to the cutter. At various points, the cuts penetrated the solidified adhesive and contact was made with the aluminium back plate in small areas, as it was not ideally flat. Contact with the back plate would have been avoided, had it first been machined before fixing the cards in place. Under close scrutiny, the contact spots showed that the depth of cut into the aluminium was minimal and therefore the effects on the result were regarded as negligible.

The second approach, that of interpolating the power from the filtered data was open to discrepancies at the points where the data overlapped. Careful judgment was required to ensure that the correct sections of data were grouped accurately before any averaging took place.

By grouping, the start and finish idle periods together an inherent comparison was made. The difference in the two values was very small with most being less than one watt and the greatest being approximately 3 watts. The three watt difference is difficult to reconcile as the test run on either side had approximately 0.5 watt differences. On average the difference between start and finish idle power was approximately 1 watt.

By considering the average power consumption for the deep pockets, for which the process parameters were similar to the long straight traversals, the values for power consumed was similar. The fact that these values were consistent gave credibility to the methods by which the data was captured and analysed. The 16 - 18% (approximately 3 Watt) difference between the calculated values and the experimental values is not surprising, given that the data being used in the calculations was published in 1967[149] and advances in process understanding, measurement and data acquisition have improved immensely since then. This advance in technology has

allowed additional factors and coefficients, such as the edge coefficients, to be included. The grade of R-PVC being tested at that time was not specified and so there may well be material property differences in the grades used. The current cards are manufactured from four laminated layers of R-PVC material, which may also account for some property differences. However, in the overall picture the experimental and analytical values are sufficiently consistent to give the designer the confidence to specify a suitable motor and spindle speed. Generally, a designer would allow a factor of safety in the power requirement for the choice of a prime mover.

4.6 Conclusion and future direction

In today's ecologically conscious world, the conservation of resources has become major concern to many people and companies in the world alike. It was this notion, to some extent, that lead to the preceding investigation. Many machines in the plastics machining industry were found to be modified from other equipment, usually metal machining tools. As such, the machine's dynamic components (spindle, table slides and slide drives) are required to be much heavier to withstand the forces imposed when machining (milling) metals. These same forces induced by equivalent operations are also present whilst milling polymeric materials; however, they are usually much reduced. Also, the majority of these modified machine tools reuse the existing prime movers, which are usually rated at many times the actual power requirement in the case of R-PVC machining.

The past methods of modifying other equipment is fast becoming untenable as the world moves towards greener and more energy conscious manufacturing methods. The manufacture of components in machined plastic operations is now a multi-million dollar industry and as such call for dedicated machinery to be designed and built. Thus the design of a purpose built spindle and drive to suit the proposed new milling machine considered the above issues and set out to develop a design solution specifically tailored to not only machine plastic materials but also to be somewhat energy conscious. This energy conscious focus was limited to minimising the mass of the dynamic components and applying a more appropriately powered spindle drive solution.

Previous milling machines had been multi-spindle devices with cutters simultaneously operating at relatively low speeds (6 – 7000 rpm) on multiple cards. Such machines

were complicated to set up and the maintenance of production tolerances was difficult. Consequently, the design specification requirement called for a single spindle production facility. Added to the single spindle requirement, a move away from the traditionally used custom 'D' cutters to commercially available multi-fluted carbide cutters was called for because the increasing cost of the custom cutters was becoming unsustainable.

At the project outset, component manufacture production rates were investigated to determine the spindle and cutter performance requirements. In the choice of a multi-fluted cutter, a primary concern was the choking (over feeding) of the cutter when achieving the required production rates (approximately 1500 cards/hour). This was because the tool path length, combined with the required production rate and using a single tool dictated a spindle design speed of approximately 35000 rpm.

With the spindle speed requirement known, the next problem became that of determining the cutting power requirement to meet production demands. This became a challenging task as research showed that there was very little published information about machining polymeric materials.

On the basis that conventional carbide cutters were to be used with the new facility, an expansive review of the behaviour and cutting properties of rigid polyvinylchloride plastic (R-PVC) was undertaken. Early work published by Japanese author Akira Kobayashi[150] proved invaluable to this portion of the research as it was one of the few publications located with material of any relevance to investigating power requirements.

Kobayashi's published research was based on orthogonal cutting of plastics and very little material with any relevance to helical milling in polymeric materials was discovered. To this end, Kobayashi's work with orthogonal cutting was extensively drawn upon as the basis of this chapter's investigation: the determination of cutting power.

A careful and extensive comparison between the orthogonal cutting theories of plastics (Koyabashi) and metals (Altintas) at a mathematical level showed that providing the polymeric material met certain physical characteristics, one being that the polymeric material must form a shear plane, the theories were interchangeable. This similarity

between theories was a useful discovery as it allowed the assumption that the transfer of cutting theory to helical milling cutters was robust providing the formation of a shear plane requirement was met by the polymer.

A major drawback to analytically determining the cutting power was the lack of knowledge of the specific cutting force or pressure for the material being machined. Without this particular information, the resulting power equations were unable to be solved. Neither the Altintas equations nor the often used MRR equations can be solved without this particular piece of information.

Generally, the specific cutting force must be determined from extensive experimental work for each particular material. Yet, in the case of many metallic materials, the cutting coefficients have been published in the Machining Data Handbook[151] and they are able to be referenced when new tooling designs are being executed. However, this information is rare for polymeric materials and what is known is relatively difficult to locate. There does not appear to be a compilation for polymeric materials as there is for metals.

For this reason, the plastics machining data (published by Kobayashi in 1967) was used in the investigation. Data published at a later date could not be located.

A numerical comparison was performed using property values for R-PVC published by Kobayashi and implemented in Altintas' orthogonal metal theory. The results from the metal theory correlated well with the previous work by Kobayashi and on that basis, a further investigation into the transfer of Altintas' helical cutting theory was considered.

Analytical results where determined for the helical power requirement by applying Kobayashi's R-PVC properties to Altintas' helical cutting theory. These results were then compared with experimental results gained from a spindle facility designed and built to test the transfer of the theories. The experimental and analytical results correlated well and confirmed that the transfer of theories was robust.

During the course of the investigation and transfer of theories to milling of polymeric materials, it was discovered that Altintas had included significant research with regard to the cutting edge coefficients relating to the cutter. Kobayashi on the other hand, had not included any comment regarding these coefficient effects in his text. He had however, tabulated data that could be applied to Altintas' theory (as used in the

'CutPro' software) to determine the edge coefficient effect on power consumption. The tabulated data provided a curious result, all the plotted data lines converged to zero, indicating no edge coefficients, an impossibility given the edge coefficient definition. A second set of data interpolated from a chart in Kobayashi's text did return viable non zero values for the edge coefficients. To explain this, two possibilities exist for this apparent inconsistency. The first is that the tabled data represents information that was statistically modified to give a general or average representative view of all the experimental trial data, or perhaps more likely, the tabulated results were generated from Kobayashi's analytical model, which did not include any edge coefficient influence.

The analytical results were tested experimentally by a purpose built milling cutter spindle. This spindle facility was designed to be representative of that which would be applied to the new machining centre. To that end, an "off the shelf" high rpm capable spindle/bearing assembly was sought and integrated into a design used to test machine the R-PVC card components. The bearing assembly selected for the main shaft was a readily available grinding spindle nominally used for carrying the grinding wheel of a small grinding machine.

The analytical power investigation indicated that only 15 – 20 watts was required to meet the cutting power demand to machine the cards as required, therefore, a small high performance electric motor (50 – 100 watts at 50000 rpm) was sought. A motor capable of a 50 watt output and a maximum speed of 50 000 rpm was selected and incorporated into the test facility. Although the components selected were well matched for size and function, the grease filled bearing assembly absorbed much more power than was anticipated at the working rpm. (It absorbed the full 50 watts at 32 000 rpm). This power consumption would not have caused any concern when the spindle was used for its designed application (internal grinding), as the electric motor powering it would have been anything in size up to approximately 3 kW. To limit the loss affect the experimental trial spindle speed was limited to 32 000 rpm which kept the power being absorbed at idle to approximately 50 watts. This ensured that the idle power remained within the manufacturer's continuous output zone. The cutting trials were of fairly short duration, during which the power demand rose into the manufacturer's intermittent power output zone. Use of the motor in the intermittent

zone appeared to have no detrimental effects on the measured results. The 50 watt motor was selected as despite an extensive search, a higher power motor with the same maximum speed capacity was not available.

Trials were performed and a set of results that gave excellent correlation with the analytical values was obtained. This confirmed that the power requirement for machining the pockets into the R-PVC cards was approximately 20 watts, thus confirming the assumption of transferring the metal cutting theory to plastics providing the plastic in question does indeed form a shear plane during the cutting operation.

Also confirmed by the research was the requirement to have in hand knowledge of the specific cutting pressure values for any polymeric materials where a machining power requirement is desired. Further research using orthogonal methods of cutting will be necessary to develop specific cutting pressure tables, for polymeric materials for which that property is unknown, to be used specifically for designing machine tools to work in the plastics arena.

The analysis presented in this work showed that future designers will be able to design drives for polymeric material milling processes using the orthogonal cutting data gained experimentally. Whilst this was not the original intent of this research, which was to determine a method of ascertaining the cutter power consumption without expensive experimental trials, it does show the shortfall in published material and the necessity to know the specific cutting pressures of the particular material being machined. Certainly simple orthogonal trials are less involved than those required in the complex 3D world in which a standard helical milling cutter operates. However, there is still a requirement for these trials, as to date this specific cutting pressure information for polymeric materials appears not to have been sought, as machining plastics as a major manufacturing process is limited.

---

[1] Machinability Data Centre. Metcut Research Associates. *Machining data handbook.* 2d ed. / Compiled by the technical staff of the Machinability Data Centre. Cincinnati, 1972. Original ed. published in 1966 compiled by the technical staff of Metcut Research Associates, Inc. Bib#: 387399

[2] Kobayashi, Akira. *Machining of Plastics.* 1967 McGraw-Hill Inc. 35266 New York. Library of Congress Catalogue Card Number 66-16772. Page 50

[3] ibid Page 54

[4] ibid Page 38

[5] Ibid pages 50 - 56

[6] ibid Page 1

[7] Ibid pages 50 - 56

[8] Hales, C., Gooch, SD. *Managing engineering design.* 2nd Edition 2004. Springer-Verlag London Limited, London, England. ISBN 1-85233-803-2. Pages 110 – 115.

[9] Machining Data Handbook. Metcut Research Associates Inc., Cincinnati, Oh. USA. 3rd Edition

[10] Rohlfs, T. *Understanding the art of machining plastics.* White paper published on internet by Connecticut Plastics Inc. Sales/Technical Support/Quoting Tom Rohlfs tom@connecticutplastics.com http://www.connecticutplastics.com/resour/articles.htm Publish date 22/07/02

[11] Prototyp-Werk GmbH Fabrik für Präzisionswerkzeuge Franz-Disch-Straße 10 D-77736 Zell am Harmersbach Germany. Internet www.prototyp.de

[12] Rohlfs, T. *Understanding the art of machining plastics.*

[13] Kobayashi, Akira. *Machining of Plastics.* 1967 McGraw-Hill Inc. 35266 New York. Library of Congress Catalogue Card Number 66-16772

[14] Kaneeda, T. *Cutting mechanism of rigid polyvinyl chloride.* Bulletin – Japan Society of Precision Engineering. 1989 vol.23 part 4 pages 304-309

[15] ibid page 306

[16] Kobayashi, A. *Machining of Plastics.* Page 1

[17] Kaneeda, T. *Cutting mechanism of rigid polyvinyl chloride.* pages 304-309

[18] Machining Data Handbook. Metcut Research Associates Inc., Cincinnati, Oh. USA. 3rd Edition

[19] Rohlfs, T. *Understanding the art of machining plastics.*

[20] Kobayashi, A. Machining Plastics. Page 38

[21] Kobayashi, A. Machining Plastics. Page 38

[22] Kaneeda, T. *Cutting mechanism of rigid polyvinyl chloride.* Bulletin – Japan Society of Precision Engineering. 1989 vol.23 part 4 page 306

[23] ibid page 304

[24] ibid pages 306-307

[25] Prototyp-Werk GmbH Fabrik für Präzisionswerkzeuge Franz-Disch-Straße 10 D-77736 Zell am Harmersbach Germany. Internet www.prototyp.de

[26] Altintas, Yusuf. *Manufacturing Automation, Metal cutting Mechanics, Machine Tool Vibration, and CNC design*. Cambridge University Press 2000. ISBN 0 521 65973 6

[27] Kobayashi, A. *Machining Plastics.* Page 37-38

[28] ibid Page 38

[29] Trent, EM., Wright, PK. *Metal Cutting.* 4th Edition 2000 Publisher: Butterworth-Heinemann. ISBN 0-7506-7069-X page 2

[30] Boothroyd, G., Knight, WA. *Fundamentals of machining and machine tools.* 2nd Ed. 1989 Published by Marcel Dekker, Inc. New York ISBN 0-8247-7852-9

[31] Trent, EM., Wright, PK. *Metal Cutting.* page 3

[32] Trent, EM., Wright, PK. *Metal Cutting.* page 7

[33] Oxley PLB., *Mechanics of Machining an analytical approach to assessing machinability.* Ellis Horwood limited publishers , Chichester England. 1989 ISBN 0-7458-0007-6 page 18

[34] Metcut (1980) Machining Data Handbook Metcut Research associates Inc., Cincinnati, OH 3rd ed.

[35] Oxley PLB., *Mechanics of Machining an analytical approach to assessing machinability.* page 18

[36] Altintas, Yusuf. *Manufacturing Automation, Metal cutting Mechanics, Machine Tool Vibration, and CNC design.* Chapter 2

[37] Trent, EM., Wright, PK. *Metal Cutting.* page 7-8

[38] Altintas, Y. *Manufacturing Automation, Metal cutting Mechanics, Machine Tool Vibration, and CNC design.* Page 5

[39] Mechant, ME. *Mechanics of the metal cutting process. ii. Plasticity conditions in orthogonal cutting.* Journal of Applied Physics, vol 16:318-324 1945

[40] Lee, EH., Shaffer, BW. *Theory of plasticity applied to the problem of machining.* Journal of applied mechanics, vol 18:405-413 1951.

[41] Palmer, WB., Oxley, PLB. *Mechanics of orthogonal machining.* Proceedings Institution of Mechanical Engineers, vol. 173(no. 24):623-654, 1959.

[42] Altintas, Y. *Manufacturing Automation, Metal cutting Mechanics, Machine Tool Vibration, and CNC design.* Page 6

[43] *Modern Metal Cutting – A practical handbook.* AB Sandvik Coromant 1994 Sandvik Coromant. ISBN 91-972299-0-3 Page I-2 – I-3

[44] Saglam, H., Unuvar, A. *Three component, strain gauge based milling dynamometer design and manufacturing.* Trans. - Society for Design and Process Science. June 2001 vol.5 no.2 pages 95-109.

[45] ibid pages 95-109.

[46] Kobayashi, Akira. *Machining of Plastics.* 1967 McGraw-Hill Inc. 35266 New York. Library of Congress Catalogue Card Number 66-16772

[47] ibid Page 38-39

[48] ibid Page 39

[49] ibid Page 40

[50] ibid Page 40

[51] Zhang, L.C., Zhang, H.J., Wang, X.M. *A force prediction model for cutting unidirectional fibre-reinforced plastics.* Machining Science and Technology, 5(3), p293 – 305 (2001)

[52] Kobayashi, A. *Machining Plastics.* Pages 31-33

[53] Zhang, L.C., Zhang, H.J., Wang, X.M. *A force prediction model for cutting unidirectional fibre-reinforced plastics.* Page 303

[54] ibid page 303

[55] Kobayashi, A. *Machining Plastics.* Page 40 figure 2.4

[56] ibid Page 40

[57] ibid Page 40

[58] ibid Page 41

[59] ibid Page 42

[60] ibid Page 44

[61] ibid Page 42

[62] ibid Page 43

[63] Kalpakjian, S. Schmid, S.R. *Manufacturing Engineering and Technology* 4th Edition Prentice Hall International Upper Saddle River New Jersey USA ISBN 0-13-017440-8 page 560

[64] Kobayashi, A. *Machining Plastics.* Page 17

[65] ibid Page 12

[66] ibid Page 12

[67] ibid Page 14

[68] ibid Page 12 & 14

[69] ibid Page 14 & 15

[70] ibid Page 15

[71] ibid Page 50

[72] ibid Page 51

[73] ibid Page 25

[74] ibid Page 54-55

[75] ibid Page 56

[76] ibid Page 37

[77] Merchant, ME., *Basic mechanics of the metal cutting process.* Journal of Applied Mechanics. Vol. 11:A168-A175, September 1944

[78] Altintas, Yusuf. *Manufacturing Automation, Metal cutting Mechanics, Machine Tool Vibration, and CNC design.* Page 6-46.

[79] Kobayashi, A. *Machining Plastics.* Page 37-47

[80] Altintas, Yusuf. *Manufacturing Automation, Metal cutting Mechanics, Machine Tool Vibration, and CNC design.* Page 13.

[81] Kobayashi, A. *Machining Plastics.* Page 37-47

[82] Altintas, Y. *Manufacturing Automation.* Page 13

[83] ibid Page 17

[84] Krystof, J. *Berichte uber Betriebswissenschaftliche Arbeiten*, Bd., 12 VDI Verlag, 1939

[85] Altintas, Y. *Manufacturing Automation.* Page 18

[86] Lee, EH., Shaffer, BW. *Theory of plasticity applied to the problem of machining.* Journal of Applied Mechanics. Vol. 18:405-413, 1951.

[87] Oxley PLB., *Mechanics of Machining an analytical approach to assessing machinability.* Ellis Horwood limited publishers , Chichester England. 1989 ISBN 0-7458-0007-6

[88] ibid Page 17

[89] Altintas, Y. *Manufacturing Automation.* Page 17

[90] ibid Page 18

[91] ibid Page 6-46.

[92] Kobayashi, A. *Machining Plastics.* Page 44

[93] Budak, E., Altintas, Y., Armarego, EJA. *Prediction of milling force coefficients from orthogonal data.* Journal of Manufacturing Science and Engineering. May 1996 Vol.118 pages 216-224

[94] Altintas, Y. Lee, P. *A general mechanics and dynamics model for helical end mills*. Annals of CIRP Vol.45 no.1 1996 pages 59-64

[95] ibid Page 63

[96] Altintas, Y. *Manufacturing automation.* Page 43

[97] ibid Page 33

[98] ibid Page 37

[99] ibid Page 40

[100] ibid Page 41

[101] ibid Page 43

[102] ibid Page 25

[103] ibid Page 44

[104] ibid Page 44

[105] ibid Page 64

[106] Engin, S., Altintas, Y. *Generalised modelling of milling mechanics: Part I – helical end mills.* The University of British Columbia, Dept of Mechanical Engineering. Vancouver BC Canada

[107] Budak, E., Altintas, Y., Armarego, EJA. *Prediction of milling force coefficients from orthogonal data.* Journal of Manufacturing Science and Engineering. May 1996 Vol.118 page 220

[108] ibid Page 220

[109] ibid Page 219

[110] Altintas, Y. *Manufacturing Automation.* Page 16

[111] Budak, E., Altintas, Y., Armarego, EJA. *Prediction of milling force coefficients from orthogonal data.* Page 220

[112] Altintas, Y. *Manufacturing Automation.* Page 16

[113] Budak, E., Altintas, Y., Armarego, EJA. *Prediction of milling force coefficients from orthogonal data.* Pages 220 - 221

[114] Altintas, Y. *CutPro User Manual: Machining process modelling, machine tap testing, and chatter vibrations avoidance.* Manufacturing Automation Laboratory, University of British Columbia, Vancouver, British Columbia. October 2000

[115] ibid Page 8

[116] ibid Pages 7 -9

[117] Kobayashi, A. *Machining of plastics.* Page 44 and 52

[118] ibid Page 44

[119] Altintas, Y. *CutPro User Manual: Machining process modelling, machine tap testing, and chatter vibrations avoidance.* Page 8

[120] Kobayashi, A. *Machining of plastics.* Page 52

[121] ibid Page 52

[122] ibid Page 44

[123] ibid Page 52

[124] ibid Page 44

[125] ibid Page 52

[126] ibid Page 52

[127] ibid Page 44

[128] ibid Page 44

[129] Altintas, Y. *CutPro User Manual: Machining process modelling, machine tap testing, and chatter vibrations avoidance.* Pages 7 - 9

[130] Kobayashi, A. *Machining of plastics.* Page 52

[131] ibid Page 44

[132] ibid Page 52

[133] ibid Page 52

[134] ibid Page 52

[135] Altintas, Y. *CutPro User Manual: Machining process modelling, machine tap testing, and chatter vibrations avoidance.* Pages 7 - 9

[136] Prototyp-Werk GmbH Fabrik für Präzisionswerkzeuge Franz-Disch-Straße 10 D-77736 Zell am Harmersbach Germany. Internet www.prototyp.de

[137] Kaufeld Dr.-Ing. Michael. *Mill-Force Optimizer 3.0/10.98 Virtual Manufacturing Software*, Am Wachberg 24/D-86497 Horgau Germany. www.hsc-forum.de Dr.Michael.Kaufeld@t-online.de

Nova Software Ltd. Technologiepark – In der Spöck 10 D-77656 Offenburg Germany www.novasoftware.de Email - info@novasoftware.de

[138] Kobayashi, A. *Machining of plastics.* Page 44

[139] Kaufeld, Prof. dr.-Ing M. *A development of virtual manufacturing software.*

[140] Kalpakjian, S. Schmid, S.R. *Manufacturing Engineering and Technology* 4th Edition Prentice Hall International. Upper Saddle River New Jersey USA ISBN 0-13-017440-8 Page 547 - 548

[141] Kobayashi, A., *Machining of plastics* Page 44

[142] Kalpakjian, S. Schmid, S.R. *Manufacturing Engineering and Technology* Page 649 - 650

[143] Ibid Page 547

[144] Kobayashi, A., *Machining of plastics* Page 44

[145] Kalpakjian, S. Schmid, S.R. *Manufacturing Engineering and Technology* Page 649

[146] LEM HEME LTD. *LEM Clamp-on Power meter. Model Analyst 2050.* 1 Penketh place, West Pimbo, Skelmersdale, Lancashire UK WN8 9QX

[147] Tektronics Inc. *Tektronix TDS 220 oscilloscope.* PO Box 1000 Wilsonville, Oregon. 97070-1000

[148] Maxon Motor Ag *Maxon Motor catalogue.* Brünigstrasse 220 Ch-6072 Sachsein 2000 Ed page 126

[149] Kobayashi, Akira. *Machining of Plastics.* Page 50

[150] Ibid

[151] Machining Data Handbook. Metcut Research Associates Inc., Cincinnati, Oh. USA. 3rd Edition

Table of Contents

Table of Figures

Table of Tables

Nomenclature

Chapter Five

Symbol	Definition	Units
A	area of plates	m^2

C	capacitance	pF
C_i	capacitor number	
d	distance between plates	m
DC	direct current	amp
f_a	actual feed speed	mm/s
f_c	feed speed	mm/s
F_p	measured cutting force	N
F_r	reference force	N
P_D	residual signal strength	pF
R_i	resistor number	
S	sensitivity	pF/mm
V_{ac}	alternating voltage	V
V_{out}	output voltage	mV
x	change in distance between plates	mm
%	percentage	
α	distance between cutter and aerial	mm
β	distance between platen and aerial	mm
δV_{out}	change in output voltage	mV
ε	permittivity of the dielectric material	F/m
γ	distance between platen and cutter	mm
μm	micron or micrometer	

Chapter 5

SENSING SYSTEM FOR ADAPTIVE CONTROL

5.1 Adaptive control overview

5.1.1 Introduction

An adaptive control (AC) system is designed to automatically and continuously check various system bounds and constantly vary the machine response to ensure the process remains consistently within those bounding conditions. Control of this nature was first conceived in the 1950's when it was predominantly concerned with autopilot controlling of high performance aircraft, which operate over a wide range of altitude and speed parameters. Although adaptive control has since been widely used in continuous processes throughout the chemical industry, its transfer to the successful control of manufacturing machine processes has been relatively recent[1]. This control strategy can be applied to many different end uses as noted above but in the context of this research, the following general definition is appropriate.

In his book, "*Manufacturing and engineering technology,"* Kalpakjian et al states: "The parameters in a manufacturing process are adjusted automatically to optimise the production rate, product quality and to minimise cost. Parameters such as forces, temperatures, surface finish, and dimensions of the part are monitored constantly. If they move outside an acceptable range, the system adjusts the variables until the parameters again fall within the acceptable range[2]."

The application of adaptive control systems to machining facilities can best be illustrated by an example such as the machining of components (workpieces) with inconsistent condition – typically sand castings. If during the machining of a casting, the cutter encounters a 'hard' spot, the cutter torque may increase dramatically. The system will reassign acceptable feeds and speeds to lower the cutting force to within particular constraints. Without this direct intervention of the controller, or the operator in a manual system, severe/catastrophic damage may occur to the cutter and/or the workpiece. The result without the AC controllers influence would be compromised dimensional accuracy and surface finish.

5.1.2 Adaptive control system – common architecture

A major component of an AC system is the means by which the system monitors information as to the state of the process. This is done using sensors of various types to collect the necessary data. In a manual system, the operator's hearing and sight provide the sources of feedback upon which a response to the process condition can be made. Due to the need for such a system to provide continuous and unabated attention, it is natural to conceive that the manual operator controls the system sub optimally when engaged in continuous manufacturing processes. By using AC systems with built in sensors the machine tool can provide a near instantaneous response to any change in the process state one hundred percent of the time.

Figure 5.1[3] below illustrates the basic componentry and the sensor links in a typical adaptive control system for a turning operation. This particular system monitors the cutting force, spindle torque and vibration during the machining process. If any of

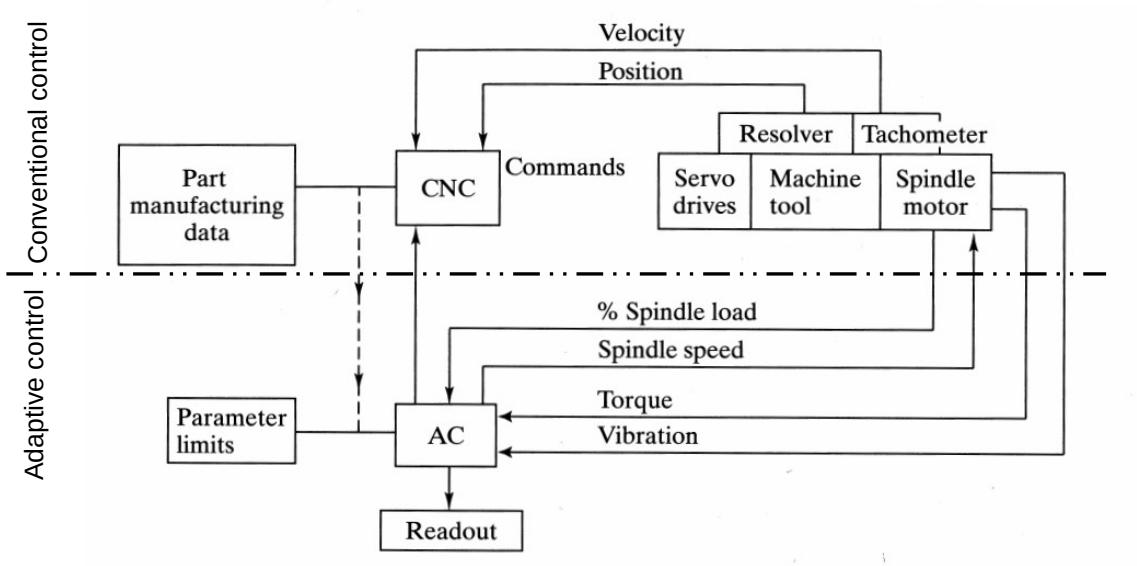

Figure 5.1: Schematic illustration of adaptive control for a turning operation[5]

these parameters fall outside the predetermined constraints, then the system modifies the feed rate and depth of cut in a predefined way, so as to return to acceptable levels[4]. Figure 5.1 also clarifies the additional components necessary to convert a conventional CNC control system (above the chain line) into one with adaptive control capabilities (below the line). One may observe that the AC unit processes information from the parameter limits, torque, vibration and percentage spindle load. From these it outputs data to the CNC module and overrides the normal spindle speed control in real time. The AC system also provides feedback to the operator.

Altintas presented a chapter about 'Sensor assisted machining' in his book entitled "Manufacturing Automation"[5]. In this, he discusses the basics of adaptive control and

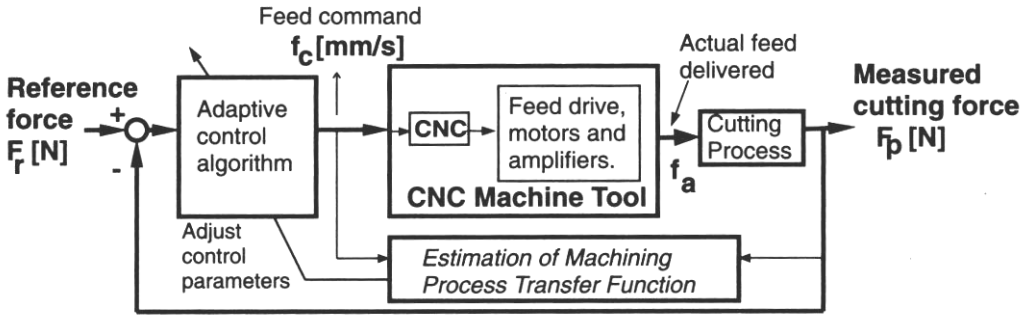

Figure 5.2: Control system block diagram of a general machining adaptive control system[8]

then elaborates briefly about the system sensors required. Figure 5.2[6] presented by Altintas, represents a typical control system block diagram showing the essential elements, and how they relate to each other. Here can be seen that the reference input is the desired cutting force F_r. The actual cutting force F_p is measured on the machine tool by embedded sensors and fed back to the machine process transfer function and the AC system. The adaptive control system outputs back to the CNC controller to adjust the machine rates to comply with the reference force. The design and style of appropriate sensors are the insurance that an adaptive system will work well and provide the system with the relevant reliable and robust information.

On the basis that the above generic AC system describes adaptive control in very broad terms, it was necessary to tailor it to the very specific requirements encompassed within this research. Critical control was required on the tool plunge rate to optimise the material removal above the IC (integrated circuit) contact points. To perform optimally it was necessary to determine the position of the contacts vertically within the card and relevant to the cutter end.

5.1.3 Specific adaptive control system architecture

The primary scope of this section of the work reported here was to develop and conceptually prove a sensor design that would consistently and reliably relay the difference in vertical cutter position compared with the aerial core or IC contact point depth.

Up to this point, only adaptive control and its sensor requirement has been discussed. This is mainly to give the reader a very brief insight into these subjects. The research was primarily focused on a sensory device that could be used in conjunction with a

closed loop feed back control to locate the copper contact points within the card's core. Ultimately, this will form the foundation of an integrated AC system. Using the analogy of the hard spots in a casting, whereby the AC system responds near instantaneously to protect the workpiece and tooling, a similar response was sought for control of the plunge cut into the card. As discussed in a previous chapter, the copper contact pads are very thin and the depth of the pocket is controlled by a particularly tight tolerance. Arresting the plunge and avoiding overshoot was critical to the success of this manufacturing process. Another major concern was the consideration of the inconsistency in the depth of the IC contact points within the core of the smart cards (of the order of microns). Variation in the contact depth is caused by the tolerance bands allowed by the card core manufacturing standards. The contact pad depth was considered relatively consistent across a card batch, but known to vary in depth from batch to batch. A further advantage of AC systems is the ability to record and reuse information with regard to pocket machining operations across subsequent cards. This was important so that the machining process time could be optimised for each batch of cards as well as regaining optimal performance after a card batch change. Achievement of such a function could be performed by using the immediately previous copper contact pad depth as a reference point as well as using the sensor to dynamically measure the depth during machining. The comparison between the two, the previously recorded and the current dynamically measured values, will allow a maximum possible feed rate velocity at the start of the cut but slowing to a rate where no overshoot occurred at the desired depth. Thus forming a notional controlled approach at an optimal performance level during the plunge cut into the card.

5.2 Aerial detection concept development

5.2.1 Design requirement specification

The design specification requirement for a concept sensor was drawn from the above perspective and is presented in Table 5.1 below. It is perhaps pertinent here to remind the reader of some of the background reasons as to why there is a need for the implementation of technology, a sensor such as this will realise.

As the cash transaction card manufacturing industry moves toward developing cards that are capable of more than just being cash, debit, credit or identification cards, the applied technology becomes increasingly complex. This increased sophistication has occurred at a time when advanced new technology is being incorporated into the card systems. Specifically, there is a move towards 'smart' cards with a capability to interact with a parent system in a non-constant way. For such developments, the parent system may be the security system in a building, an ATM, or even the lock system in a vehicle that sends out a pulse of radio frequency that can be sensed by the card. As a consequence of this electro-magnetic interaction, the card is 'powered up' and it is able to respond to allow the carrier to gain access to the building, or vehicle, or service. To make the interaction possible the card must have its own tuned aerial that absorbs and uses the radio frequency. Due to space restrictions, cards are manufactured with the aerials embedded in the PVC core but there are various known manufacturing difficulties in exposing the contacts on the aerial to allow the Integrated Circuit (IC) chip to be connected. As the cores are manufactured in sheet form, the aerial has a tendency to be deposited within a specific zone or tolerance range contained within the core. The object of this study, as previously indicated, was to discover a method of locating the aerial terminals within the PVC core during conventional milling processes and have the machine tool record the depth position at which the copper aerial contact pads were exposed as explained earlier. If adopted, the recorded depth value would form a z axis positional reference to be used in a feed-forward mode to allow high speed aerial location in subsequent cards.

This notion will be implemented in the following way. As the cutter approaches the recorded depth, the machine will dynamically change the velocity profile for the vertical plunge cut while it is in process. Thus, the plunge velocity will be dependent on the position of the cutter relative to the aerial contacts or the plunge cut aerial strike point. This is so that the IC terminals on the aerials can be machined to a specific depth, controlled within a tight tolerance band and as such will minimise the risk of cutter overshoot. The thickness of the aerials is approximately 10 - 100 μm and within this thickness, the top land of the IC pocket is to be maintained within a very tight tolerance band also. This means that there will be small quantities of copper material being machined from the terminal contact pads as the pocket is produced in the PVC card, thus ensuring a clean contact between the aerial and IC.

Table 5.1: Design specification requirement table for the z-axis adaptive tool control system

Demand or Wish [D or W]	Description
D	Detect the aerial circuits in the cards.
W	Provide a measure of vertical tool position (z axis) feedback during machining
D	Maintain the positional 'knowledge' of the aerial circuit terminals z axis position
D	Locate accurately the z axis position of the aerial circuit dynamically
W	Dynamically create distance, velocity and acceleration profiles for the cutter along the z axis
D	Very tight z axis repeatable accuracy band (1 – 5 μm)
D	Minimise the cutter overshoot in the z axis direction whilst meeting production targets
W	Dynamically 'zero' the cutter with non aerial cards
D	Easily and convenient tool change after sharpening or replacement
W	Dynamic tool realignment during the cutting cycle and after tool change or replacement

5.2.2 Conceptual design

A number of models were considered at a conceptual design level using the design specification requirement given in Table 5.1. The outcome from the conceptual design yielded two possible solutions that met the specification.

Use of the carbide milling cutter in conjunction with an appropriate electrical circuit, to provide a measurable electrical spike in the aerial's response to being grounded (when the cutter contacts/strikes the aerial) was the initial notion. Crude testing indicated the presence of the spike, which was found to be almost a step change of an order of magnitude above the baseline signal when strike was made. A major drawback with this method of aerial sensing came by way of the mechanical leadscrew drive, which would not be responsive enough to respond instantaneously to arrest the high speed vertical plunge cut. At the time of testing the aerial/cutter strike response, the cutter's vertical feed speed was assumed to be approximately 3.0 m/min. With an aerial thickness of only 10 μm, any overrun/overshoot of the cutter could cause a significant proportion of the IC/aerial contact pad material to be removed and the top land of the IC pocket to be machined beyond the required depth. Hence, it was mandatory to minimise any overshoot.

The direct grounding approach above simply provides a (on/off) step signal which does not allow for plunge feed velocity ramp-down. As indicated, this introduces initial over travel problems. By contrast, an analogue signal would allow the system to sense the approach distance of the embedded wire and respond accordingly. In support of this solution, a comparison based sensing system was investigated.

Equation [1] shows that the achievable capacitance in a system is directly proportional to the area of the capacitor plates as well as being inversely proportional to their separation distance. Figure 5.3 illustrates the huge difference in relative diameters of the cutter and the aerial wire. The overlap in area between the 3.0mm diameter

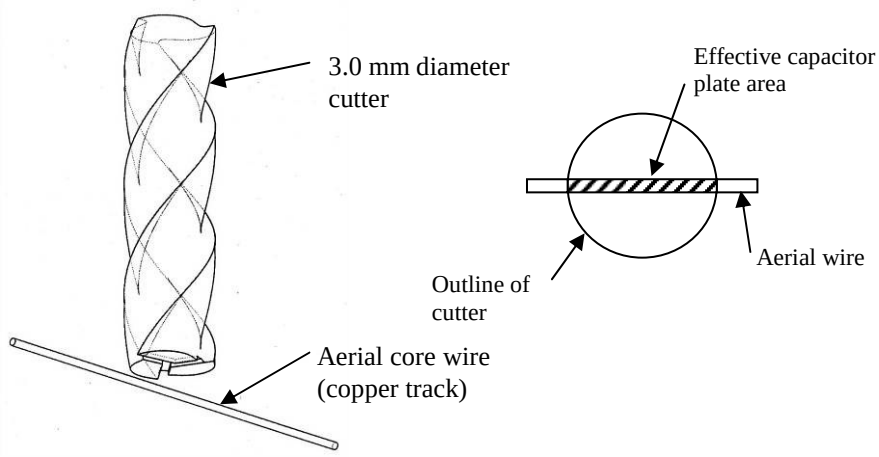

Figure 5.3: Aerial wire diameter compared with cutter

cutter and the longitudinal sectional area of the aerial wire is very small. This intersection is illustrated in Figure 5.3 (right) and indicates the effective capacitor platen area. The face of the cutter was considered as the ideal mobile plate as it was always present due to the machining operation and the notion to implement it in this way would have given a very straightforward and elegant design solution. However, with such a small working juncture, there was insufficient area to generate a useful or reliable return signal until the cutter contacted the wire, which is effectively the unacceptable situation described previously. An increase in sensor capacitance was required in order to produce a robust and reliable signal.

As a result of the poor quality of electrical signal, an ensuing development was to consider exciting the aerial at very high frequencies, of the order of 5 – 10 MHz and then attempt to measure the capacitance change between the aerial and an exciter terminal plate (Figure 5.4 below). This proved fruitless as the higher frequencies failed to improve the signal strength. As it happened, subsequent tests revealed that

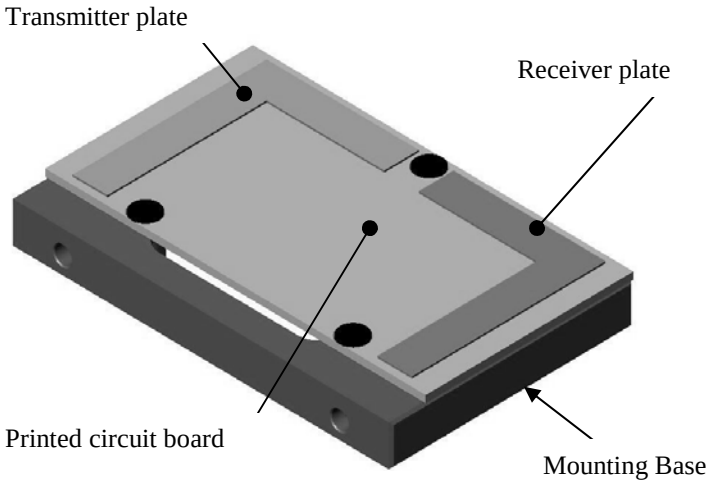

Figure 5.4: Proposed card aerial exciter/receiver

using the higher frequencies or the aerial tuned frequency was unnecessary as the aerial proved to excite to varying degrees at any frequency. So an easily achieved frequency of 105 kHz was selected, a frequency that was away from the natural frequencies to be found in the machining centre.

In a further development, the cutter was replaced, as the active platen, with a steel strip positioned above the aerial core. With this rethink, the plain and elegant design solution of using the cutter as the movable plate became a multifarious issue, as the new platen required very accurate positioning vertically in relation to the end face of the cutter. The major benefit was a dramatic increase in the platen working area followed, with a vastly improved signal to noise ratio, to the point where it became a strong reliable signal. The step change in the receiver signal at the strike point (as described above) was retained and was to be utilised as feedback for the contact point thus giving the measured depth of the aerial within the card. With this progression to

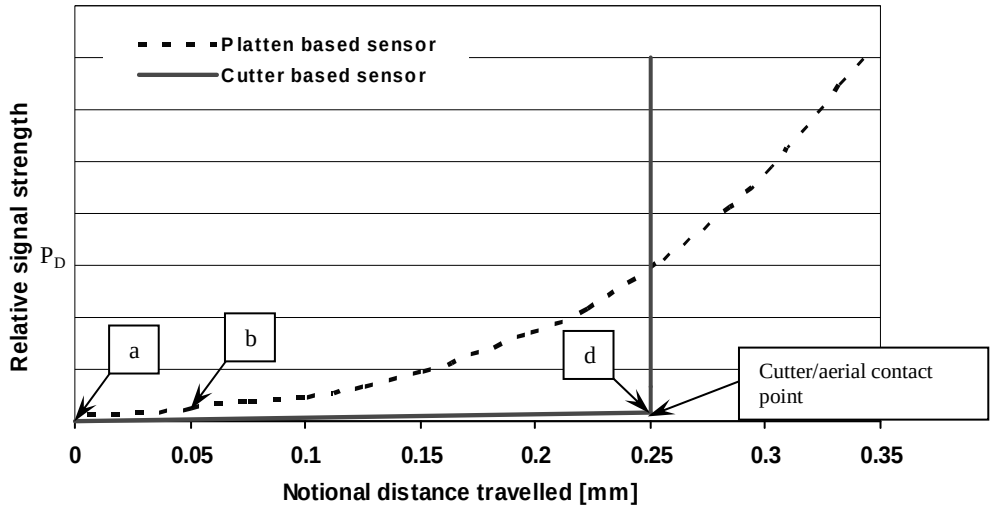

Figure 5.5: Signal strength versus depth of cut approaching the card aerial (schematic for dual sensor array)

a sensor 'array', the notion of 'tracking' the cutter's vertical approach was considered viable.

Figure 5.5 illustrates the signal to depth-of-cut characteristic for the sensor array showing the two signals independently. As the cutter approaches the aerial wire, the platen signal (dotted line) strengthens as the cutter moves towards the strike point, 'd,' shown at 0.25 mm in this case. Also the influence of the cutter approach is shown as the solid line below the dotted line, its influence being significantly less than the platen based sensor (see earlier discussion). At the strike point, the circuit is electrically shorted by the cutter physically contacting the aerial and the signal increases instantaneously to a maximum signal value. Figure 5.5 illustrates the signal spike at cutter contact but also shows the residual capacitance level, P_D, present between the platen and the aerial, at the same instant, where the notional distance travelled equals 0.25 mm. This residual signal, P_D, would equate to the effective distance, γ, between the end face of the cutter and the platen (see Figure 5.6d below). Inspection of Equation [1] shows that the curve in Figure 5.5 follows the capacitance law, which is hyperbolic in nature, where the capacitance of a parallel plate capacitor is given by

$$C = \frac{\varepsilon A}{d} \qquad [1]$$

where

C = capacitance [pF]

A = area of the plates [m^2]

d = distance between the plates [m]

ε = permittivity of the dielectric material [F/m][7]

Equation [2] shows that the sensitivity also increases as the depth-of-cut increases (the cutter to wire distance decreases).

$$S = \frac{dC}{dx} = \frac{\varepsilon A}{2x^2} \qquad [2]$$

where

S = sensitivity [pF/mm]

x = displacement or change in distance between the plates [mm][8]

Equations [1] & [2] show that the capacitance is also proportional to the area of the capacitor's plates, denoted by 'A' in equation [1] above. This capacitance characteristic will be heavily drawn upon to provide the basis of the sensors described herein.

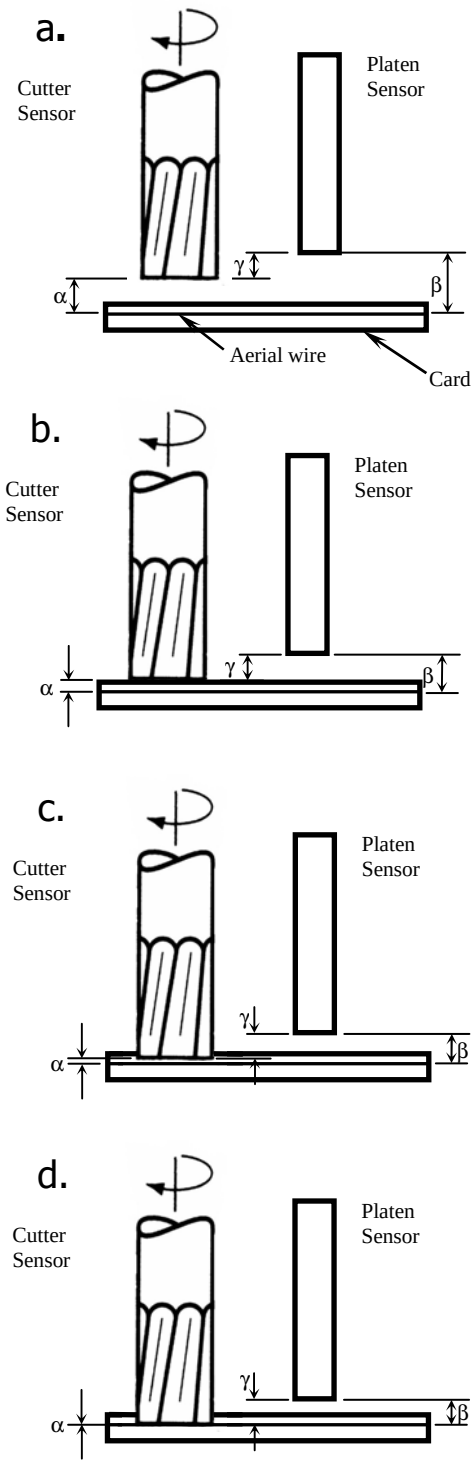

Figure 5.6 (a - d) Plunge cut sensing sequence

The mode of operation visualised with the sensor array arrangement to be adopted is portrayed below.

Figure 5.6 (a - d) below presents a series of schematic illustrations outlining the function of the proposed capacitive sensor array. The two sensors are fixed in position relative to one another, separated by distance, γ; however, once the cutter has made contact with the aerial, the platen sensor must withdraw vertically away from the card to give clearance from the card surface for the deeper section (0.65mm) of the standard IC pocket being machined.

Figure 5.6a represents the starting position of the cutter and hence the array relative to the card. The cutter is shown at distance α from the aerial wire, which is known to be approximately 0.2 mm below the surface of the card in this case. The distance γ is the difference value between α and β, where β is the distance from the aerial wire to the underside of the platen. There is a very small signal strength from both the cutter and the platen based sensors at this point: represented by point 'a' in Figure 5.5

Figure 5.6b illustrates the cutter commencing a plunge cut but at the instant when it is in contact with the card's surface. The

separation α has now been reduced to the value of the distance of the aerial wire below the card surface. Figure 5.5 indicates the relative signal strength of this arrangement: see point 'b'.

Figure 5.6c shows the cutter penetrating the card with a corresponding decrease in the platen to aerial wire distance, β. The signal strengths are represented by the section of the chart in Figure 5.5 between points b and d.

Figure 5.6d represents the situation when the cutter makes contact with the aerial wire. Point 'd' in Figure 5.5 shows the instantaneous signal spike at the strike point within the card. The value P_D also shown in Figure 5.5 is the residual signal strength representing the distance β shown in Figure 5.6d.

A major drawback, that of precisely determining a value for γ, which was critical in providing accurate machining results, was eliminated with this system. Knowing the values of P_D and γ, allows the exact depth of the aerial contact pads to be measured based on the value of P_D and the measured plunge cut depth.

The proposed sequence of events used to 'teach' the machine as to where the exact position of the aerial contact pads are, is as follows. The value of P_D is known at the strike point of the cutter (see Figure 5.5) with the aerial and is recorded by the system. The depth of the plunge cut (z axis travel) is also known at the same point and the position recorded. As a new plunge cut proceeds in a new card, the machine can compare the z axis position with the last known position from within the previous card. At the same time, the last known P_D value is compared with the current signal strength being generated as the new pocket is machined. In this way, the necessity to know the platen to cutter offset is removed as the machine control system can compare the two last known values from the previous card. If the aerial wire is in a shallower position, greater signal strength will be measured for the same relative cutter position than with the previous card. This will in effect warn the machining centre that the aerial wire is shallower in the card and appropriate responses can be initiated by the control system.

Success of this concept would give the capability of designing and utilising dynamic control of the cutter travel distance, velocity and acceleration. Further development of the concept will allow greater control of the cutter as it approaches its final depth and the dynamic means of recalibrating the machine after a cutter change. Systems with

dynamic feedback enable the potential for a very rapid or course feedrate approach for the initial plunge cut, followed by a maximum deceleration rate that is controllable by the mechanical feed system, and so maintain the required final precision, whilst optimising the production rate. Determining and 'remembering' where the target depth is in the core of the card will be possible because the dynamic system provides the machine with this capability. 'Knowledge' of the aerial strike point depth position enables the cutter velocity and distance profiles to be dynamically altered to suit the remaining distance between the cutter and the target (aerial contact pads). Calibration of the changing capacitance value can gauge the theoretical space between the capacitor plates (platen and aerial), translating the space into the remaining travel before coming into contact with the aerial.

Using the sensor array would allow the machine to determine where the terminals should be, and the cutter's vertical plunge speed could be optimised to minimise and control any overshoot during the reaction time following the occurrence of the electrical contact or strike point spike. Minimising the cutter overrun and giving enough control to allow prediction of the magnitude of the overshoot within a very narrow tolerance band would be a principal feature of this hybrid system. Employing this manufacturing method would ensure the position of the contact pads within the cards would always be known to within a pre-determinable toleranced depth. The vertical accuracy of the plunge cut feed system was a prime consideration in the overall machine design. (See the specific entry in Table 5.1: 1 – 5 μm). Now, as a consequence of the above development, the accuracy demand was considered achievable and a feasible solution has been presented. This approach to adaptive machining has hitherto been unavailable. This solution forms the functional core of the proposed machining centre, without which such control would not be easily achievable with existing card machining systems.

- The sensor circuit design

The sensor circuitry used in the above development is included here for the sake of completeness. A comparative capacitive electronic circuit was designed and built to provide an output voltage signal to display on an oscilloscope. A comparative circuit was chosen on the basis that the signal to noise ratio was low and therefore the noise required reducing significantly. Reducing the noise did not prove to be a significant

problem. The introduction of a second card based aerial, excited at the same frequency as the first, was used to improve the signal to noise ratio. The usable variation in voltage that was output could then be used to find a distance relationship between the aerial core and the cutter face.

The concept circuit is given in Figure 5.7, where the power input was 12 volts at a frequency of 105 kHz. The reason a power supply of this type was used was because

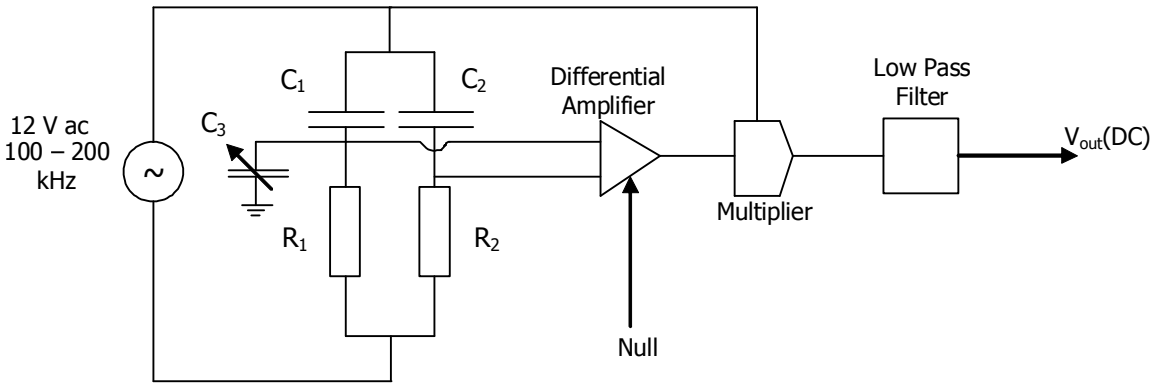

Figure 5.7: Electrical circuit for testing the aerial detection capability

capacitance is known to be a function of alternating current (ac). R_1 and R_2 are resistances chosen to suit the circuit requirements. C1 and C2 are the effective capacitances gained through the coupling of two excited aerials. The two card based aerials were mounted side by side in a holder (refer Figure 5.9). This provided a comparative signal value across the two cards with the added advantage of eliminating much of the noise from the electrical output. One card was used as a baseline signal, which was subtracted from the signal from the card under the cutter. C_3 was the effective capacitance created by the cutter or cutter/platen combination and the card being machined. A differential amplifier was used to set the null point or the point at

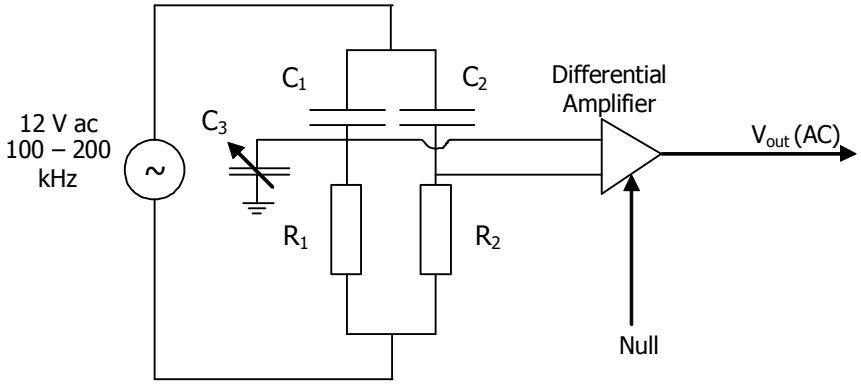

Figure 5.8: Electrical circuit as trialled in the aerial detection testing

which the V_{out} (see Figure 5.7) value was lowest relative to the cutter position. A multiplier was to be used to multiply the output from the 'diff amp' by the excitation

frequency (105 kHz), from there the signal passed through a low pass filter to remove unwanted elements, to give an analogue V_{out} DC signal suitable for processing by computer.

The actual test circuit used is presented in Figure 5.8. This circuit did not include the multiplier or the low pass filter as the output from the differential amplifier was an AC analogue signal suitable for measurement with an oscilloscope, which was used to display the output signal. Initial tests were actually performed using the oscilloscope in a differential mode, which prompted the decision that further testing would be valuable. The test circuit was built with a view to minimising any possible phase shifting caused by the use of the oscilloscope circuitry when in differential mode, and to improve the definition of the results. Good results were achieved and these are discussed section 5.3.2 below.

5.2.3 Concept refinements applicable to multiple card types

The design specification requirement for the manufacturing process calls for the ability to manufacture both 'Smart' cards and conventional cards. The concepts outlined above were designed primarily for use in the smart card manufacturing process whereby use was made of the inbuilt aerial feature of the cards. Conventional cards by design do not have this feature available. Due to this product difference the dynamic control system cannot be operated on the conventional cards as there is no aerial present with which to create any electromagnetic interaction.

To meet the requirement for machining conventional cards a method of determining the tool offset was necessary. The cutter position for machining both card types could be dynamically 'zeroed' at a gauge point, some known distance from the machine's zero point (z axis = 0), at the beginning of each pocketing operation. It is proposed that this may be achieved by using existing laser scanning or shadowgraph technology (a technology already applied to automatic tool length offset detection) to locate the position of the end of the cutter, thus putting it at a known position above the zero point. By keeping the distance between the zero point and the gauge point, as short as practicable the parasitic errors inherent in the leadscrews and general construction of the machine would be minimised (Abbe offset errors[9] etc).

The top surface of the card will be clamped by a vacuum chucking plate, similar to that described on page 268. This card chucking system ensures that the datum surfaces of

the card chuck plate and the top surface of the card were at a common 'zero point' (z axis = 0) or as close as can be achieved within practical limits and a known tolerance band. A window through the chucking plate enables cutter access to the top surface of the card for machining purposes. Chucking the cards in this manner ensures that the pocket depth is measured consistently from the top surface. This is necessary because the cards vary in thickness from card to card, but also vary sometimes across the card as well.

The dynamic zero checking of the tool offset will be performed on a regular basis. The main reason for checking the tool offset frequently is to minimise the post machining quality control time. With the tool being dynamically set at a known offset regularly, the machining centre must machine the products within the tolerance specification. Dynamically measuring the tool offset will also minimise the complexity of tool replacement after either sharpening or completely replacing.

From the above outline of operation, it is clearly evident that the sensor system previously described would be suitable to both smart and conventional cards. A basic experimental investigation was performed on the system to confirm its viability. This investigation is described in detail in the following section.

5.3 Experimental investigation

So that a prototypical experimental investigation could be carried out, a straightforward test system was built to determine the feasibility of the proposed concepts. The test apparatus (Figure 5.9) was designed in a manner that kept it simple and met the installation requirements imposed by the sensor. It was tested and produced a result, however, these were very erratic. In an attempt to improve the sensor test results, an additional means of approaching the aerial wire in a finely controlled manner was required and to that end, a simple fine adjustment device was added (Figure 5.9). The probe was fixed into the capacitance testing apparatus (Figure 5.9) and the sensors were tested. A series of tests were performed under varying conditions and these are discussed below. The results were similar for each of the tests but with varying magnitudes in δV_{out} and the conclusion was drawn that the output signal δV_{out} was of sufficient quality to be useable.

5.3.1 The test apparatus

To ensure that the test equipment was kept simple a small commercially available drill stand was adapted to suit the purpose. This facility had an integrated table and the

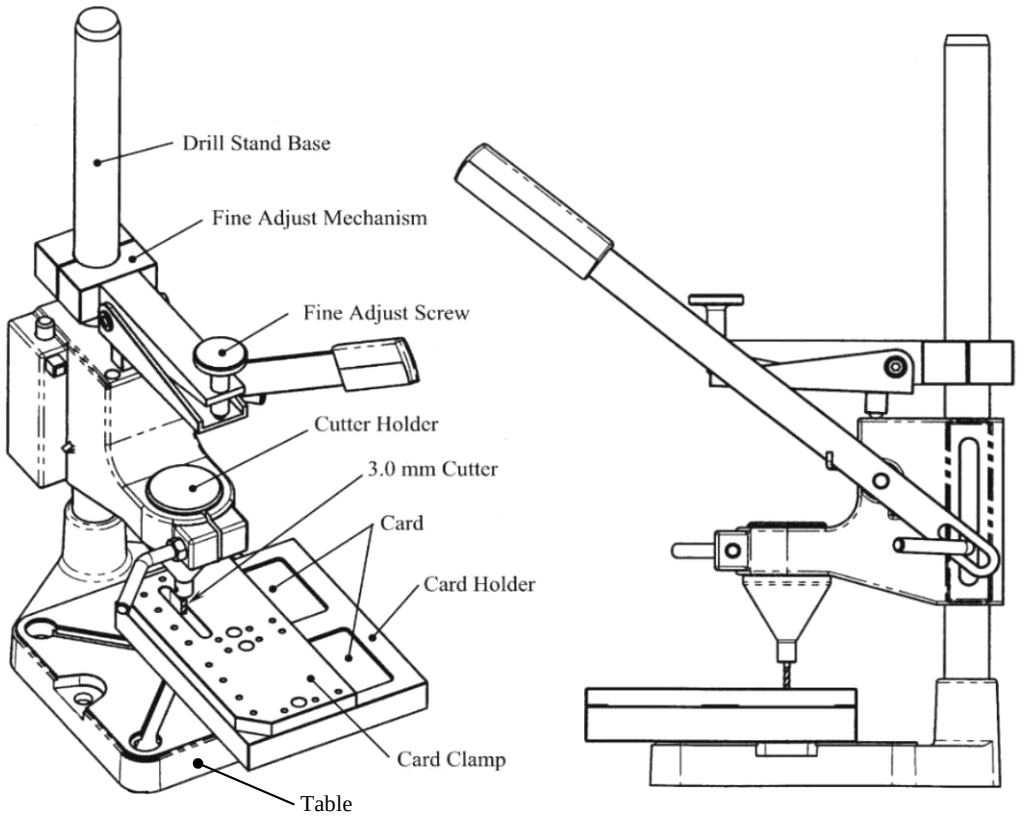

Figure 5.9: Capacitance testing apparatus

necessary support frame, see Figure 5.9. It required the addition of adapters to hold the machine tool cutter, the cards and a fine adjustment mechanism. Fine adjustment of the tool to work-piece distance was required to further enhance the process of capturing the data relating to the capacitance levels at the various tool to work-piece distances. This was an attempt to simulate the actual machining process. Figure 5.9 shows the fine adjust mechanism, as it was developed to assist in precisely controlling the gap. It consisted of a holder, for a 3 mm carbide cutter of the type likely to be found in the final machining process, mounted vertically above the card. The cutter holder was clamped into the main attachment bracket. A screw adjust system giving a fine regulation in the approach of the cutter was attached above the main bracket. The fine adjuster was designed to give a varying feed depending on the position of the linkage arrangement relative to the adjusting screw. This allowed the adjuster to be

positioned such that a full turn of the adjusting screw gave ~0.1 millimetres or significantly less, if the anvil was close to the bottom of its arc. See Figure 5.9.

Additionally a new base block of nonconductive material was manufactured with provision for two aerial exciter plates, (exciter plate as shown in Figure 5.4), to be embedded in it (see card holder in Figure 5.9). This design allowed two aerial cards to be placed over two separate exciter plates in a fully supported and known orientation. The cards were used simultaneously; one as the base signal source and the other was the target. The latter card was extensively modified by stripping some of the PVC covering from above the aerial. However, during testing, the PVC covering was replaced with layers of polyester tape in an attempt to gauge the effect and strength of the coupled capacitance.

This trial was somewhat thwarted when after a period of time the 'stripped' card began to 'curl up'. The curling was suspected to have been caused by further action of the acetone on the PVC. Acetone was used to strip away the material covering from over the aerial wires. A replacement card was sourced and the chemical stripping process was substituted by lightly and carefully sanding the R-PVC covering from above the embedded copper wiring. The sanding process was much more successful and controllable in that the remaining R-PVC was graduated approximately linearly from a full thickness cover of approximately 0.2mm to having the copper wire exposed.

To test the viability of the sensor array concept, a steel platen was made from 1.6 mm thick sheet and attached to the earthed connection as per the circuit diagram in Figure 5.7. This was in addition to the connection to the cutter and effectively formed C_3 (see Figure 5.8). The platen was spaced off the surface of the card at various distances using strip spacers cut from polycarbonate polymer sheet and polyester tape; the thicknesses of each item are given in Table 5.2.

Table 5.2: Materials and thicknesses used for spacers

Spacer material	**Thickness [mm]**
polycarbonate	0.5
polyester tape	0.13

These spacers were stacked to give the platen to card surface distances shown in Table 5.3 to Table 5.5.

Essentially three tests were performed with the signal null point (zero output) set with the probe in different locations. The first test was a test more to check the function of the concept rather than to produce any usable results. The second was with the cutter positioned at nominal distance of 0.5mm from the aerial core. The third was set with the probe on the card's surface (nominally 0.2mm above the aerial strike point). In all of these instances, the null point was preset prior to commencement of the associated trial, such that the generated signal was effectively zero. Any movement of the probe relative to these points was then recorded as an output signal.

As explained above, setting the null point of the system effectively zeroed the output signal with the probe in a particular position. This then set the circuit to generate a signal when the probe/cutter was moved vertically from the particular null point position. Tables 5.3 to 5.5 table the results from the three test series. The signal was set to zero (nulled), then the probe/cutter was moved to the known value 0.065mm shown in Table 5.3. The signal value was recorded and the subsequent distance values were tested. In Table 5.4, the percentage change in the signal values are shown as compared to the initial value recorded at 0.5mm. The third test of the series was performed with the null point set at a different initial vertical position, i.e. on the card's surface, and the same series of spacers was used as for the second test. During these tests, no contact with the aerial wire was made with the probe.

5.3.2 Experimental results and discussion

The aerial was excited with a range of frequencies from ~ 10 kHz to ~1 MHz. However, the excitation response showed a slightly raised characteristic curve that centred approximately at 105 kHz. The lower frequencies did not give high excitation values whilst the higher frequencies tended to produce a slightly better but nevertheless degraded signal. The excitation frequency of 105 kHz was chosen as it appeared to best suit the aerial producing the cleanest output signal, although it would produce a V_{out} value at almost any frequency. 105 kHz was also an easily attained common frequency that could be reproduced without difficulty in the final system design.

Table 5.3 to Table 5.5 below give the measured signal strength V_{out}, in millivolts [mV] for each relative probe position. They also show the variation in signal strength dependent on the chosen position of the null point. The percentage change in signal

strength between the various stacked spacer thicknesses is furthermore presented. All changes, except 0.63 to 0.76mm in Table 5.5, are shown to be above the 10% change threshold, which was considered the level required for a reliable signal. It was recognised that these were step changes using finite thickness spacers (polyester tape) and will give a slightly increased effect over the use of an air gap as proposed in the final design. It should be noted that the 0.065 mm value given in Table 5.3 was an air gap rather than a distance spaced by the tape.

- Experimental results

Table 5.3: Platen to card separation signal strength - null point nominally at 0.065 mm above card surface

Platen to card separation distance [mm]	**V_{out} [mV]**	**Signal change [%]**
0.065 (1 end only of platen propped)	12	
0.13	16	33.33
0.26	22	37.5

Table 5.3 was an initial test primarily performed to gauge the success of the conceptual design. It was also done to provide a notional minimum separation value and to give an indication of the maximum anticipated signal strength (V_{out}). To gain the 0.065 mm spacing shown in Table 5.3, one end only of the platen was propped on the polyester tape giving an average spacing as shown.

Table 5.4: Platen to card separation signal strength - null point nominally at 0.5 mm above card surface

Platen to card separation distance nominally 0.5 mm above card surface [mm]	**V_{out} [mV]**	**Signal change [%]**
0.5	10	
0.63	12	20
0.76	14	16.667

Tables 5.4 and 5.5 present the nominal separation distances used during two of the trials. These values were achieved by 'stacking' the spacer materials as noted in Table 5.2 to sum to the values shown in column one of tables 5.4 and 5.5. The first value, 0.5mm, was used as the initial value from which the later δV_{out} values were determined. The use of the various positions for the null points was to examine the signal strengths and to gain some insight as to where the null point should be positioned to obtain the most effective result. Obviously, the results show the

strongest signal strength when the null point is closest to the card surface; however, the percentage change in signal strength was reduced.

Table 5.5: Platen to card separation signal strength - null point on the card surface

Platen to card separation distance – null point =0 (on the surface) [mm]	V_{out} [mV]	Signal change [%]
0.5	25	
0.63	28	12
0.76	30	7.143

The above results were achieved by using two cards electrically connected as shown in Figure 5.8 with the platen arranged as indicated in Figure 5.10. The function of the second card was to provide a reference signal that could be used to remove the unwanted noise from the system as previously discussed.

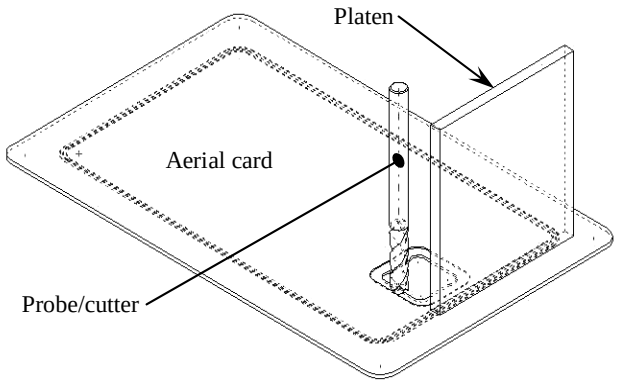

Figure 5.10: Diagram of card and cutter showing the added plate

The results presented above were sufficiently strong to consider the proposed sensor array design being implemented into the machine. A particular issue that may cause some concern will be the snagging or collection of the swarf on the platen, but this was not foreseen as a major problem as it could be overcome by careful placement of the platen into the machining centre and the use of an effective swarf management system. Also, by redesigning the machining process to avoid long strings of swarf, this may be avoidable.

5.4 Conclusion and future direction

The results of this research show that a viable solution was attained and that it is possible to measure the depth of the aerial core relative to the cutter end. The system showed sufficient integrity to ensure the signal strength was at a useable and reliable level.

- Future work

An attempt to quantify the most appropriate separation distance for the platen above the aerial core will need further research with a more advanced test apparatus.

Integrating the sensor into the proposed machine tool will require careful consideration and design so as not to 'clutter' the tool area. This will be a major consideration in the final machine design.

One of the design specification requirements was for a quick change and offset re-alignment of the cutter after sharpening or replacing. This alignment problem has the potential to render the system difficult to use by the operator, by removing the offset simplicity demanded in the design requirement specification.

- Concluding comment

In conclusion, a robust reliable solution to the tool offset reassessment problem was found and a successful and workable outcome has resulted. The dynamic alignment of the tool tip and the working edge of the platen in conjunction with the adaptive control for the plunge cut depth management will create an advanced machine tool configuration that will revolutionise machine control systems in this manufacturing arena.

Special acknowledgement

The author wishes to acknowledge the work and design done on this portion of the project by Julian Phillips, from the Mechanical Engineering Department's electrical workshop.

---

[1] Kalpakjian, S. Schmid, S.R. Manufacturing and engineering technology. 4th edition 2001 Prentice Hall Inc. New Jersey USA. ISBN 0-13-017440-8 Page24

[2] ibid Page 1038

[3] ibid Page 1039

[4] ibid Page 1039

[5] Altintas, Yusuf. Manufacturing Automation, Metal cutting Mechanics, Machine Tool Vibration, and CNC design. Cambridge University Press 2000. ISBN 0 521 65973 6 Page 234ff

[6] ibid Page 234

[7] Rizzoni, G. Principles and applications of electrical engineering. 3rd Edition International edition 2000 McGraw-Hill Inc New York New York ISBN 0-7-117727-2 Page 132

[8] ibid Page 132

[9] Smith, ST. Chetwynd, DG. Foundations of ultraprecision mechanism design. Gordon and Breach Science Publishers, Amsterdam, The Netherlands. 1st Ed 1992 3rd printing 1997 ISBN 2-88124-840-3 Page 72

Table of Contents

Table of Figures

Table of Tables

Nomenclature

Chapter Six

Symbol	Definition	Units
rpm	revolutions per minute	min^{-1}

Chapter 6

CONCLUSIONS AND RECOMMENDATIONS

6.1 Introduction

This project began as an industry inquiry to develop a small "working envelope" milling machine for specific use in the Smart card manufacturing industry. From the original enquiry and the beginnings of the machine design, three major components (a flexure hinge rectilinear machine table, the power requirement when machining plastics at high rpm, and an adaptive control sensing system) were investigated with a view to creating a new design or developing major improvements to existing systems. Although the requirement was for a complete machine tool, only the three topics were investigated and reported in this work (it will be shown in the future work section of this report that the integration of these components will require completing).

The following sections of this chapter summarise the research activities, the results of each part of the study, the conclusions drawn and recommendations for future work.

6.1.1 Investigation and design of a flexure hinge axis

The major reason to pursue this novel design for a machine table using high displacement flexure hinges was based on difficulties encountered using conventional dovetail slides or as an alternative, linear bearings. Dovetail slides by their very design and nature, are required to be large and heavy to meet their design requirements. Linear bearings on the other hand aid in reducing the weight of the slide system, however due to the very short travel and high directional reversal rates required by the production process cycle, these have tended to wear quickly in localised zones, thus compromising the machine accuracy.

Flexure hinges were seen as a possible means to produce a light stiff structure without imposing the restrictions found with traditional dovetail slides or with linear bearings. A system of flexure hinges was investigated and a novel prototype design was constructed and tested.

6.1.2 Power requirement when machining plastic (R-PVC) at high spindle speeds

Issues with current multi-spindle manufacturing techniques were the reason this section of the project was initiated. Setting up machine tools with multiple spindles and expecting all the spindles to meet the required accuracy limits proved to be a slow and tedious process, requiring operator skill levels to be high to achieve an accurate and consistent set-up. A single spindle with a single commercial grade solid carbide cutter was seen as a possible solution. However, to meet the production rate demand of the design specification requirement, the spindle rotational speed was required to be in the 30 – 40 000 rpm range. Issues that quickly came to light were the need to know the power absorbed by the cutter when machining the pocket into the card material and how the card material would respond when machined at very high rpm.

The power requirement was investigated using a mathematical approach and verified experimentally. Cutting trials were completed and the cut and swarf characteristics were observed.

6.1.3 Sensing system for adaptive control

The design of the new generation of smart card calls for an embedded aerial in the card to be electrically connected to an integrated circuit (IC) chip implanted in a small pocket machined into the card's top face. The aerial is embedded in the card core at the time of manufacture and IC pockets are machined into the cards in a later and separate operation. It was necessary to know the depth of the aerial contact points as they varied from card to card due to the stacked tolerances of the card manufacturing lamination process. A sensor was designed to detect the aerial and measure the variable depth. Thus allowing the cutters' velocity and positional trajectory to be controlled with more precision as it arrived in the target zone, both in depth and position.

6.2 Summary of the work conducted

The following sections summarise the work conducted within each of the three major segments of this project.

6.2.1 Investigation and design of a flexure hinge axis

An initial review of current flexure usage and technology was carried out and showed the research level with regard to multi-millimetre displacement metal flexures to be

limited. The review revealed that many flexure applications had been utilised in the past, however these were mainly in the high technology "nano" or "micro" regions. Polymeric materials made up a further high use group where their peculiar properties were used to gain very large displacements, mostly angular or radial applications (eg plastic lunchbox lid) but also a few bending types (eg archery bows and trampolines).

Applications using multiple compound flexure hinges were found to be even more limited than those with single flexures, and those with flexures applied in machine table applications were non-existent as per the authors investigation. Having investigated the notion of applying flexure hinges to a machine table, other issues, such as metrology and 'design for manufacture,' were considered as these influenced the development and design of a rectilinear machine tool table.

Of these concerns was the influence of the machine tool metrology on the design and performance of the proposed new machine. Publications concerning the metrology of machine tools were researched and reviewed in light of the problems likely to be encountered in developing a precision machine tool. There were significant issues, Abbe offset and cosine error possibilities that required careful consideration to minimise any negative effects on the mill's performance.

A subsequent investigation of rectilinear motion using flexures was conducted and a novel and viable concept design was developed that met the design specification requirement. This investigation considered major aspects of the use of flexures in the proposed application. For example, stress regimes, material grain size, and the form of the flexures, a notched thick beam in a monolithic structure or a similar beam in a fabricated structure were all considered.

The use of flexures provides a wear free mechanism generally with only possible fretting or corrosion at bolted or otherwise connected joints. Connected with the characteristic lack of wear there is also no sliding friction between the working stages but hinge blade material hysteresis will exist to some degree due to dislocation movement within the thin material in the hinge.

The design encompassed by the reported research was a symmetrical design where many of the usual issues relating to the bending relationships of the hinges are balanced and therefore their influence was neutralised by varying levels. Symmetrical

tandem flexure designs are naturally compensated and balanced within each assembly due to the nature of the design configuration. However, these types of design require careful consideration of the frame/support structure stiffness to ensure the flexure assemblies translate identically.

As with all beams in bending the forces produced by the bending action of the flexure blades are predictable and can be determined using the traditional and well known beam bending theories and rules. The prediction of forces is complicated by the fact that axial loading applied to the blades, loads aligned along the length, causes changes in the hinge stiffness. This change is to be expected, and is dependent on the magnitude of the tension or compression characteristics of the applied loads. A blade subjected to a compressive load will be less stiff than a similar blade subjected to a tensile load of a similar magnitude and as such they will displace at different rates.

A further drawback of metal flexure hinges is their inability to withstand large angular displacements, which means they are only capable of low levels of rotation if their stress levels are to remain within the elastic deformation limits. Added to the low levels of rotation, the rotation is not pure and the in-situ deformation and load response of each flexure blade is highly complex. Due to the impure rotation, the rotation centre is not fixed and will displace under the action of combined loads. As there are four blades per tandem flexure assembly, it is possible to have a difference in rotation centre displacement for each of the blades which negatively affects the rectilinearity of the system. The table design was based on very small working loads when compared to conventional milling machines, and thus making the assumption that a satisfactorily stiff frame design would help reduce or equalise these negative effects.

As an additional consequence of the low levels of rotation attainable, the notched hinges also made it very difficult to achieve the required table travel and minimise the system footprint/envelope, when fatigue stress levels were considered as governing factors to determine hinge properties. Moreover, the notched beam design causes stress concentrations in the flex zone, adding further to the difficulty in determining the exact level of stress in the already complex nature of the hinge.

From a stress viewpoint it was obvious that the incurred notch stress levels could to some extent be alleviated by increasing the notch radius. This is true, however, increasing the notch radius presented additional difficulties to the manufacturability of

the system. The larger the notch radius, the further apart adjacent beams were required to be spaced to allow tool access for machining. The possibility of machining holes, with a suitable surface finish, other than circular was considered but discarded as impractical. Therefore to achieve the lower bending stress levels the circular notches would be impossibly large, thus reducing further the ability to use the notch design for a compact machine table.

Progressing the design through the various stages of development showed that notched design flexures were inadequate for the task due to being unable to reduce the overall machine table size, whilst maintaining acceptable fatigue stress levels. The decision to switch to a leaf blade hinge was made and an in-depth analysis performed. Analytical considerations of the flexure blades were, their strength in various loading directions and configurations, their orientation, and their geometric and physical properties.

Already mentioned above was the inherent characteristic of impure rotation of notched flexure hinges, added to this, the bent blade style of hinge is naturally less accurate due to the greater bending zone and manufacturing variations in material thickness and stiffness. This was not considered deeply at this point in the design due to the short blade length, but will require an in-depth investigation in any future developments of the table.

Local buckling or tin canning of the flexures was a further consideration investigated as it becomes a problem with the application of large loads along the length of thin sections, in this case the slender blade hinge. To prevent this type of failure occurring, the lengthwise load has to be minimised along the hinge. Use of a fabricated system as opposed to a monolithic structure was one means of achieving optimal load carrying performance in the blades. The choice of orientation of the flexure blades allowed them to be tuned to make best use of their load carrying properties and characteristics.

Monolithic structures provide a set of positive characteristics that are difficult to emulate in a fabricated design (for example there is only one component and the absence of bolted connections is obvious). However, it was manufacturing process shortcomings and load directions on the blades that were the main negative issues with a monolithic design . Nevertheless, the subsequent change from a monolithic structure brought about a new set of problems. Initially, the main points against using a fabricated

assembly were the five fold increase in component parts, and the known associated manufacturing issues concerning the production of multiple similar parts.

With the decision to use leaf blades, also came the decision to use a fully fabricated structure. This was essentially due to the many complications encountered in fabricating a monolithic leaf blade structure that would function within the bounds of the design specification and fatigue life requirements. The manufacturing difficulty encountered using multiple components was considered a lesser problem, than those that were present in constructing a viable functional monolithic structure. The advantages of using a multi-component structure are briefly outlined in the following paragraphs.

Scope to use dissimilar materials for the blades and supporting structure was a significant advantage to be had from the changed approach to the design. A relatively early decision to build the prototype support structure from tooling grade aluminium plate was made; the main reason for this was its excellent machinability, weight and availability.

However, resolving a material for the flexures was a much more arduous process. Research showed that there were more than eighteen hundred metals to consider, though not all were suitable for the flexure blades. A flexure may be seen as a spring, however, springs traditionally store energy and the ideal flexure hinge will store very little energy, yet maintain its flexibility and resistance to plastic deformation. These are major property requirements for flexure hinges, when the bending force is to be minimised, as in this design. To quickly eliminate unsuitable materials, a method of materials selection using a dimensional analysis approach was developed and assessed. This approach combined the work of several authors in a unique way to provide a fast efficient method of selecting a material whose physical properties were maximised or minimised to meet the design requirements. This was principally achieved using traditional beam bending theories and rules to extract material parameters from the appropriately arranged equations.

Manufacturability of the final design solution and the associated manufacturing issues were final considerations in the prototype design. To this end, specific concerns and their influences as they related to the fabricated system were considered. These concerns were issues such as unequal blade lengths, unequal span lengths, the

leadscrew drive and its affect, assembly influences and manufacturing and assembly tolerances. These influences, considered by Hatheway[1], have been well documented for a single pair of flexures giving parallel translation. Their affect on the multiple tandem pairs of flexures found in the reported design configuration has still to be considered in any depth. This will require Hatheway's equations to be expanded or extended to consider the wider scope of the multi-flexure system. Many of these concerns were minimised at the time of design by selecting tight manufacturing tolerances. The tolerance levels where chosen based on the typical capability of a well maintained job shop.

Other influences that will play a major role in translational discrepancies were the variation in material properties as they changed within the billet from which the components were being manufactured. For example, the blade thickness will vary within a particular tolerance range (the rolling margin, usually 5% of thickness) across the sheet, giving thicker and thinner regions that will respond differently to the same loads. Additionally the material composition and heat treatment levels will also vary, again giving different responses to the same loading in different regions of the sheet stock.

A point that became apparent during testing was the flexibility of the supporting structure. The original design was based on the use of a much less stiff titanium blade material, whereas the final tested configuration used spring steel which was nearly twice as stiff as the titanium should have been. Future developments of the table design will be much more focused on the supporting structure stiffness to reduce the structural bending caused by the spring force of the blades.

The prototyped design was tested using a CMM with a method that mimicked the action of the cutter travel in relation to the machine table.

The results were reported and discussed extensively in section 3.10.

6.2.2 Spindle power requirement

The design specification requirement for this section of the project called for a high performance single cutter spindle to meet a production rate of 1500 cards per hour. Of primary concern in meeting this specification, was the power requirement of the spindle drive system, which was considered in light of the demands that would be placed upon

it by the production process. As a part of the investigation the peripheral components were considered: the cutter, a chucking system for the cutter, a bearing system to support the spindle shaft, a high performance coupling and an electric motor, as well as a card holding fixture system.

Coupled with the need for knowledge of the spindle drive motor power, selecting the drive components proved an onerous task. The required components were not widely available "off the shelf" technology for prototyping applications. Historically, many existing machines had been modified from metal or wood working machinery and as such usually continued to utilise the legacy components. These components were designed into the original machine capable of producing much more power than that required for machining the pockets into the R-PVC workpiece.

As the investigation proceeded, it became obvious from the lack of in-print information that machining plastics was not a widely researched or published field. To this end, locating appropriate data regarding the cutting of plastics became a major task. A thorough investigation and review of the limited research material presented information pertaining to orthogonal cutting of polymeric materials, however there was no similar information regarding helical milling of the same materials. A 1967 publication by A Kobayashi[2] became the basis for the analysis relating directly to cutting R-PVC. The orthogonal cutting information proved invaluable and ensured that a solution could be found without the need for expensive and time consuming cutting trials.

Kobayashi's orthogonal cutting theories were applicable to polymeric materials and fortunately extensive data relating to the topic was published in his excellent monograph. From an exhaustive review of the Kobayashi orthogonal theory, there appeared a great many similarities to metal cutting theory. The two orthogonal theories (Kobayashi's plastic cutting and Altintas Metal cutting) were compared and found to give near identical results for R-PVC. The correlation between the two theories was dependent on the polymeric material forming a shear plane within the cutting zone, which R-PVC does, as implied by Kobayashi.

The comparative analysis proved satisfactory giving results of both power output and the direction and magnitude of the cutter generated forces. Alternative methods were researched and although in most cases gave the power absorbed; they all failed to give

the force information. The tested software proved to be unsatisfactory as it was designed for much larger power requirements.

A major shortfall generally, was that all methods of finding the absorbed power require the use of the specific cutting force. This generally, is not a published property of polymers as it is with metals. Kobayashi had completed a significant level of research using various plastics and fortuitously had published his in-depth findings. His publication included the specific cutting force values for a small sample of materials, of which R-PVC was one of them. Unfortunately the information related wholly to orthogonal cutting with no information published that related to cutting using milling processes.

Given the strong correlation between the plastic and metal cutting orthogonal theories, an investigation of milling processes ensued, and the application of helical metal cutting theories to polymeric materials was completed. The helical metal cutting theory was taken from work published by Altintas[3] in 2000 and included a number of additional coefficients not included in Kobayashi's earlier publication. These additional edge and shearing coefficients increased the accuracy of the power absorption predicted, however they are all experimentally determined as they change with cutter geometry.

A series of cutting trials were performed with the results being reported and compared with those gained from the mathematical analysis. This comparison showed the theory transfer to be robust, as the experimental and the derived analytical results correlated strongly. There was however, an approximate difference of 20%, with the trials giving the higher value. Given that a design safety factor of 2 would not be unreasonable, the result can be used with confidence in applying a motor to a new system.

The helical cutting theories gave calculated power consumption values of approximately 15 watts. This power requirement contrasted heavily with the legacy motor found on the sponsoring company's original machine, which was three kilowatts. Even given the losses found in the bearings, it was extremely difficult to justify the size of the legacy motor, and as such, this difference in motor size and power requirement gave the justification for this investigation.

A prototype spindle was fully researched, designed and built, using the calculated design power of approximately 15 watts plus an estimate of the power required to drive

the grease filled precision spindle bearings up to speeds of forty thousand rpm. A suitable motor was sought that would produce sufficient power to meet the cutting requirement and overcome the grease lubrication and frictional losses in the selected bearing assembly. It became apparent early in the search that finding a suitable motor would be a challenge. Originally an 80 watt motor was wanted, but none could be sourced that met the speed requirement of forty thousand rpm. The 80 watt motor was limited to approximately twenty thousand rpm. In light of the restricted speed of the larger motor a smaller 50 watt motor was selected. This motor would produce sufficient power in excess of 50 watts by running it up into the intermittent zone for short operational periods to meet the speed requirements. This proved satisfactory and allowed tests with the spindle idle speed of approximately 31 000 rpm, which absorbed the full 50 watts. The test cuts were limited in duration to a few seconds to ensure the motor did not overheat, whilst working in the intermittent operation zone of the motor's performance curve producing approximately 70 watts. This solution whilst satisfactory for a prototype and the associated testing was a highly unsuitable solution for the final design.

A brushless DC motor was selected because of its high efficiency, high speed and reasonably high power output per motor size. When difficulty was incurred in sourcing an appropriate motor, alternate solutions were sought. These alternate solutions included, step up drives (both gear and belt) and the use of two 50 watt motors with their shafts direct coupled to form a single unit. All of the alternate solutions were discarded in favour of the single motor capable of brief incursions into the intermittent operating zone.

The original concept for the prototype machine was to use a high rpm hand tool supported in a special holder. This proved unsatisfactory as the tool selected failed to meet its published performance. In place of the hand tool a precision grinding spindle was selected and adapted into a functional system. Minimising tool run-out, both concentrically and axially, was the main reason for the choice of the precision grinding spindle.

Choosing this bearing housing unit proved to be a good choice as the unit was robust and easily adapted into a useable system. The loading conditions were well below those expected from a typical grinding application and therefore a long bearing life

could be expected. There a concern that having 'greased for life bearings' would give the system sufficient operating life. However, the particular unit was chosen for its service capacity, 40 000 rpm speed limit, grease filled and belt driven, indicating that the bearings would have sufficient integrity to give a long service life in this application.

A major drawback was the power loss incurred in the bearings of the selected precision bearing housing. This loss (50 watts) was huge when compared with the experimental power absorbed in cutting (18 watts) and was significantly underestimated due to the lack of information available from the manufacturer. The grinding spindle was probably not considered as ever operating with such a low power input. The grease lubricated bearings were protected by labyrinth seals, which were selected to minimise the energy lost by using traditional lip seals. Lip seals also have a tendency to wear the shaft in abrasive climates, such as was the case with the abrasive R-PVC particles.

Cutting R-PVC is relatively easy, but very abrasive to the cutter. R-PVC wears the cutting edge off cutters unlike anything in metal cutting. The sharp leading edge of the cutter is worn/rubbed off till its "roundedness" is equal to the depth of cut, then it rides over the material rather than cutting through it. Solid carbide is the material of choice for cutters and traditionally the industry has used custom carbide "D" cutters to do the machining work.

Part of this project was to investigate the use of commonly available standard metal cutting solid carbide cutters. Initially it was not known what the response of the R-PVC would be to a cutter operating at 30 - 40 000 rpm. First thoughts were that maybe clogging of the cutter or burning and melting of workpiece material would arise. The cutting trials proved that these were not issues and there was no evidence of any of them having occurred. Compressed air was used as a coolant during the cutting operation as the R-PVC must be machined dry.

The cutter, ultimately a 3 fluted 12^{o} rake cutter, produced clean sharp edges, with no rags, in the R-PVC. Small cuts per flute at high rpm and the subsequent high feed rates (3 m/min) produced a well defined chip that cleared the cutter cleanly and left no residue adhering to the flutes.

Workpiece holding was supplied by a custom designed vacuum chuck, which supported the card blanks well during all cutting trials. Testing a chuck of this nature was of

benefit to the project as the final design will incorporate this type of workpiece holding facility. The operation of the chuck was successful, however, a higher density of holes will be required immediately beneath the active machining area to better support the very thin material remaining in the bottom of the pocket.

Swarf management on the machine will be of vital importance. R-PVC is highly electrostatically susceptible and the swarf that was produced adhered electrostatically to just about everything it came into contact with. The air blast from the cutter cooling system dispersed the swarf well during the cutting trials, but it was uncontrolled generally, and blew about the inside of the machining centre safety enclosure. The swarf is very light and easily broken down into small lumps/powder as it appears to be quite brittle. However, as mentioned earlier, R-PVC is also highly abrasive. This combination has the potential to severely scratch the newly machined cards if it is not controlled adequately, making the cards unserviceable. Considerable attention to a suitable swarf management design will be required if potential damage to cards is to be minimised.

Finally an adapter was designed and manufactured that allowed the newly built high speed spindle assembly to be fitted into the department's three axis CNC machining centre for cutting and performance trials. Adapting the spindle to the machining centre in this way avoided the need to develop the balance of the proposed new machine tool into which the spindle was to have been implemented. Successful cutting and power trials to performed and reported.

6.2.3 Sensing system for adaptive control

The sensing system was introduced in chapter 5 with a brief overview of adaptive control. Discussion was presented as to how the common architecture for adaptive control systems fitted into the project. From here, the common architecture was developed into the specific architecture for the sensor system as it related to the project.

Having briefly considered adaptive control system architecture, both generally and specifically relating to the sensory system configuration, a concept design specification requirement was formulated. A design specification table was presented (Table 5.1) and conceptual designs were developed.

One of these conceptual designs was sufficiently developed to allow an initial prototype sensor to be constructed and tested. The results from the initial prototype testing required further development of the device to refine both its application and output signal. Also, concept refinements were applied and further testing completed. These refinements were directed at ensuring the sensor was suitable for the multiple card types being currently manufactured as well as any foreseeable new types yet to be introduced in the immediate future.

A prototype sensor was built, tested and assessed for potential integration into the proposed new machine tool. The results were reported and discussed.

Conclusions drawn regarding the sensor are reported in the conclusions section below.

6.3 Concluding remarks

The following sections report the concluding remarks from this project. These remarks essentially summarise in a general way the detailed findings and conclusions of the previous three chapters.

6.3.1 Investigation and design of a flexure hinge axis – concluding remarks

Research of flexure hinges is well advanced in many areas of today's technological world. However, the use of high performance, high displacement metal hinges in a machine table application was found not to be one of these areas. Dovetail slides and linear bearings are used exclusively, but are problematic in short traversal high cycle process regimes. Therefore, a design solution seeking to find an alternative table support system was sought.

Investigations showed the viability of a fabricated compound flexure hinge system in a small working envelope machine table application. The application employed multiple flexure assemblies to provide the symmetry and support required for the working stage.

Design solutions were sought to overcome the various issues that arose in the course of meeting the design specification requirements. One such issue was the selection of a suitable material for the flexure blades. Polymeric materials were discounted early in the development of the flexures, as they were considered too unstable for the intended application.

A combinatorial process was developed utilising dimensional analysis, Johnson's optimisation and Ashby diagrams to assist in the selection of a suitable blade material. Although the steps used in the process were not unique in themselves, the combination of steps used to select the material is believed by the author to be exclusive. This selection process allowed the most suitable materials to be isolated from the pool of metals quickly and efficiently.

Material selection of the blades allowed the final design solution to be completed; the concept system was prototyped and tested to determine its suitability for the application.

Testing, to some extent, was hampered by the CMM operating at its published repeatability limits. As a rule of thumb, the accuracy of a measuring device should be ten times more accurate than the tightest tolerance being measured. Discussion of the results concluded that some of the erroneous results could be directly attributed to the lack of capability of the CMM.

Results gained from testing of the prototype provided an outcome that proved the concept viable. There were some unexpected results in terms of the individual flexure assemblies at data capture zones, however the centroid of the table proved to show results confirming the self compensating effect of the system and a region of the working stage that would provide planar rectilinear movement.

In considering the reported results, the only conclusion that may be drawn relates to the viability and suitability of the flexure table design to meet the design specification requirement. This specification outlined the machine requirements for a small working envelope milling machine to mill the shallow pockets into credit cards manufactured from polymeric materials. This research has been successful in laying down the ground work for a workable and viable machine table built around the use of flexure hinges and rectilinear translation. Other factors, which were considered to be outside the scope of this thesis, but will nevertheless, require further work are presented in section 6.4.1.

6.3.2 Power requirement - concluding remarks

This investigation sought to extend the theory of single point to multipoint cutting of plastic hereto unreported. Furthermore, a comparison of metal/polymer cutting

theories was undertaken. This new comparison of theories was then used to determine the spindle power required by the machining process.

The power requirement in the case of this project was shown to be approximately 15 watts by both an experimental and analytical processes.

The strong correlation between the theoretical and experimental power usage data showed that future power analysis for helical milling could be determined from the results gained by performing basic orthogonal cutting trials. Orthogonal cutting trials will be required for any material that doesn't have a published specific cutting pressure. Also, for this approach to be valid, a primary requirement for the particular polymer was the formation of a shear plane during the cutting process. Without the development of a shear plane in the cutting zone, it is doubtful that the correlation found to exist between the metal cutting theory and that for polymers would remain robust.

The analysis presented in this work showed that future designers will be able to design drives for milling processes using the orthogonal cutting data gained experimentally. Whilst this was not the original intent of this research, it does show a shortfall in published material and the necessity to know the specific cutting pressures of the particular material being machined. Certainly, simple orthogonal cutting trials are less involved than those required in the complex 3D world in which a standard helical milling cutter operates. However, there is still a requirement for these trials. To date the specific cutting pressure information for polymeric materials has not been seen as important in that it has not been quantified for most plastics. This may be because the field of machining plastic, as a major manufacturing process, has up till now been limited in scope.

6.3.3 Sensing system for adaptive control – concluding remarks

A result was achieved that demonstrated that it is possible to measure the depth of the aerial tracks in the core of the card. The signal strength gained from the prototype indicated that a viable solution with sufficient integrity could be developed and integrated into the proposed machine tool in a useable and reliable system.

In conclusion, a robust reliable sensor array solution to the tool offset reassessment problem was found and a successful and workable outcome has resulted. However, to

fully implement the sensor array into the machine tool further research and design is required. This further work has been outlined in section 6.4.3

6.4 Future work

As with all research projects many questions are posed and answered, but often a great many more questions are asked that have answers outside the scope of the current work brief. This project has been no exception, and the following sections seek to pose some of the questions that have been asked, but have fallen outside the present project scope.

6.4.1 Flexure hinges

There are several areas relating to the flexure hinge system that will require further work and design to alleviate their negative influence on the rectilinearity of the working stage travel.

- A higher resolution metrology device (laser interferometer) is required to retest the flexure table system to isolate the CMM errors.
- The yaw characteristics of the working stage have at this point been ignored. Early indications show that yaw may not be a major problem with this system but insufficient work has been completed to allow any reporting or conclusions.
- Investigation into linking the intermediate platforms on adjacent flexure assemblies and what the effect of doing so would have on the overall system rectilinearity performance.
- What effect would occur by adding of more or having less flexure blade assemblies between the base and working stages.
- The influences that effect a single tandem system, the Hatheway effects, may effect multiple flexure systems in a similar way. However at this point the relationship of Hatheway's' equations in relation to multiple tandem flexure assemblies is largely unknown. This will require further in-depth analysis in conjunction with higher resolution measuring equipment to minimise the influence of measurement errors and direct the analysis toward the influence of errors inherently present due to the manufacturing process shortcomings.

- Investigate the proportion of Hatheway effect errors that can be successfully compensated for by the design configuration itself? This will require a further consideration of the self compensation effects.
- A full and complete vibration and natural frequency analysis will be required to research their influence on the machine's dynamics.
- Vibration and its effect on the rectilinear performance of the working stage. This will encompass the situation where the intermediate stages vibrate independently from each other.
- Fatigue life of the hinges will require further work to ensure the blade life is sufficient in this very high cycle application.
- Use of strain gauges with high displacement capability applied to the flexure blades in a novel new method of measuring the table travel.
- Investigation of drive method alternatives; traditional leadscrew styles, leadscrews with backlash control, linear motors isolated from the working stages so their mass is not carried by the stages.
- Drive positions relative to the geometric and kinetic centres of the flexure blades, when there are multiple tandem pair blade assemblies influencing the performance of the rectilinear movement.

This list is by no means exhaustive but provides a starting point for further work to be performed in perfecting this table system for machine tools, processing small components in polymeric materials.

6.4.2 Power requirements

The requirement for purpose built machine tools to work with polymeric materials is increasing as these materials move into higher technologies. More advanced plastics are being used for applications where injection moulding as a production process may no longer be suitable. This project is a prime example, whereby machining small IC pockets into credit cards is the industry recognised method because moulding the cards is not viable,. This said, anecdotal evidence suggests that polymeric materials other than the commonly used R-PVC are being considered for a new generation of cards. These cards will require machining and therefore their physical properties will be required in the course of designing machine tools to work them. The Machinability

Data Centre[4] publishes the Machining Data Handbook for metals; there is an increasing need for such a reference volume of polymeric materials for the plastics machining industry. However, the only means of collating data such as the specific cutting pressure, and the tool edge coefficients is from physical orthogonal cutting trials – a future project.

6.4.3 Sensing system for adaptive control

The prototype sensor array highlighted areas where further development is required to ensure a completely integrated system. On the sensor system, the most appropriate separation distance between the sensor and the aerial core will require determining to optimise the sensor operation. This is a development requirement of the sensor itself.

Other areas that require future consideration are:

- Integration of the sensing system into the proposed machine tool
- Cutter sensor alignment methodology and tools
- Quick change and tool offset re-evaluation techniques after sharpening or tool change operations

The dynamic alignment of the tool tip and the working edge of the platen in conjunction with the adaptive control for the plunge cut depth management will create an advanced machine tool configuration that will revolutionise machine control systems in this manufacturing arena.

6.4.4 System integration

The work reported in this thesis concludes the research, design, prototyping and testing of three essential elements of a purpose built small working envelope machine tool for machining polymeric materials. The overall design requires that these constituents be integrated into a final shape that fully meets the design specification requirement.

Other areas that will require major consideration are;

- The CNC programming language – the sponsoring company wished to avoid the standard G-code language.
- A graphical user interface to simplify programming of alternative pocket configurations.
- Product infeed and outfeed conveyor systems.

- Dynamic quality control of the finished product as it leaves the milling machine.
- A high efficiency swarf removal and handling system (R-PVC is affected severely by electrostatic interactions)

This list is not exhaustive, but gives a level of understanding to the reader as to the research and development required to produce the full machine tool to meet the perceived need for a machine of this calibre in the market.

---

[1] Hatheway, AE. *Alignment of flexure stages for best rectilinear performance.* Proceedings of SPIE – The International Society for Optical Engineering. V2542, 1995, pages 70 – 80. ISBN 0-8194-1901-X

[2] Kobayashi, Akira. Machining of Plastics. 1967 McGraw-Hill Inc. 35266 New York. Library of Congress Catalogue Card Number 66-16772.

[3] Altintas, Yusuf. *Manufacturing Automation, Metal cutting Mechanics, Machine Tool Vibration, and CNC design*. Cambridge University Press 2000. ISBN 0 521 65973 6

[4] Machinability Data Centre., Metcut Research Associates. Machining data handbook. 2d ed. / Compiled by the technical staff of the Machinability Data Centre. Cincinnati, 1972. Original ed. published in 1966 compiled by the technical staff of Metcut Research Associates, inc. Bib#: 387399

BIBLIOGRAPHY AND APPENDICES

Bibliography

AB Sandvik Coromant. *Modern metal cutting – a practical handbook.* 1st English edition 1994. Sandvik Technical Editorial dept. Sandviken, Sweden. ISBN 91-972299-0-3

Alauddin, M., Choudury, I.A., El Baradie, M.A., Hashmi, M.S.J. *Plastics and their machining: a review* Journal of materials processing technology 54 (1995) p40-46

Altintas, Y. *Manufacturing automation, metal cutting, machine tool vibrations, and CNC design.* 1st edition 2000 Cambridge University Press, Cambridge UK. ISBN 0 521 65973 6

Altintas, Y. *CutPro User Manual: machining process modelling, machine tap testing and chatter vibration avoidance.* 2001 Manufacturing Automation Laboratory, University of British Columbia, Vancouver, Canada.

Amiguet, Bill. *Machining Non-metals* American Machinist November 1982

Ashby, MF. *Materials selection in mechanical design.* 1st Edition 2nd printing 1993 Pergamon Press Ltd. Oxford England. ISBN 0 08 041907 0

Astrom, K.J., Wittenmark, B. *Computer controlled systems, theory and design.* 3rd edition, Prentice Hall, Englewood Cliffs, NJ. 1997

Beer, FP., Johnston, ER, Jr. Dewolf, JT. *Mechanics of materials.* 3rd Edition, International edition. McGraw-Hill Co. New York New York. ISBN 0-07-112167-6

Benham, PP., Crawford, RJ., Armstrong, CG. *Mechanics of engineering materials.* 2nd Edition. Addison Wesley Longman Ltd. Harlow England. ISBN 0-582-25164-8

Blake, A. *Practical stress analysis in engineering design.* 2nd Edition, revised and expanded. 1990 Marcel Dekker Inc. New York ISBN 0-8247-8152-X

Boothroyd, G., Knight, W.A. *Fundamentals of Machining and Machine Tools.* 2nd Edition 1989. Marcel Dekker Inc. New York USA. ISBN 0 8247 7852 9

Brändlein, J., Eschmann, P., Hasbargen, L., Weigand, K. *Ball and Roller Bearings, Theory, Design and Application.* 3rd Edition 1995. John Wiley & Sons Ltd. West Sussex England. ISBN 0 471 98452 3

Chen, G., Yuan, J., Ni, J. *A displacement measurement approach for machine geometric error assessment.* International Jounrnal of Machine Tools & Manufacture. Page 149 Vol. 41 No. 1 Jan 2001.

Dieter, George E. *Engineering Design, a materials and processing approach.* Second International Edition. 1991. McGraw Hill Book Co. Singapore. ISBN 0-07-100829-2

Erkorkmaz, K., Altintas, Y. *High speed CNC system design. Part 1: jerk limited trajectory generation and quintic spline interpolation.* International Jounrnal of Machine Tools & Manufacture. Page 1323 Vol. 41 No. 9 July 2001.

Erkorkmaz, K., Altintas, Y. *High speed CNC system design. Part II: modelling and identification of feed drives.* International Jounrnal of Machine Tools & Manufacture. Page 1487 Vol. 41 No. 10 August 2001.

Erkorkmaz, K. Altintas, Y. *High speed CNC system design. Part III: High-speed tracking and contouring control of feed drives.* International Jounrnal of Machine Tools & Manufacture. Page 1573 Vol. 41 No. 11 September 2001.

Gere, JM. *Mechanics of materials.* 5th edition 2001 Brookes/Cole Thomas Learning Pacific Grove CA USA ISBN 0 534-37133-7

Gere, JM., Timoshenko, SP. *Mechanics of materials.* 4th edition 1999 Stanley Thornes Ltd. Cheltenham UK ISBN 0 7487 3998 X

Gooch, SD. *Design and mathematical modelling of the kinetic sculpture blade.* 2001 Phd Thesis, University of Canterbury, Christchurch New Zealand.

Gooch, SD. *ENME440, Mechanical system design, Course notes 2001.* Dept of Mechanical Engineering, University of Canterbury, Christchurch New Zealand.

Grabchenko, A.I., Verezub, N.V., Lavrinenko, S.N., Ferenov, A.M., Getmanov, A.A., Horvath, M., Mamalis, A.G. *Precision machining of optical products made from polymeric materials.* International Journal of Advanced Manufacturing. Page 93 Vol 17 No. 2 2001.

Grabchenko, A.I., Verezub, N.V., Lavrynenko, S.N., Horvath, M., Mamalis, A.G. *Precision cutting of optical polymer components for bioengineering applications* Journal of Materials Processing Technology 97 (2000) 126–131 June 1998

Granta Design Ltd. *CES Selector Version 4.5* © Build 2004, 3, 16, 1. Granta Design Limited. Rustat House, 62 Clifton Rd., Cambridge, CB1 7EG, United Kingdom

Hales, C., Gooch, SD. *Managing engineering design.* 2nd Edition 2004. Springer-Verlag London Limited, London, England. ISBN 1-85233-803-2

Hamrock, BJ., Jacobson, B., Schmid, SR. *Fundamentals of machine elements.* Internation editions 1999. WCB/McGraw-Hill Singapore. ISBN 0-07-116374-3

Harris, T.A. *Rolling Bearing Anaysis.* 4th Edition 2001. John Wiley & Sons Inc. New York USA. ISBN 0 471 35457 0

Hatheway, AE. *Alignment of flexure stages for best rectilinear performance.* Proceedings of SPIE – The International Society for Optical Engineering. V2542, 1995, pages 70 – 80. ISBN 0-8194-1901-X

Hinduja, S., Roaydi, A., Philimis, P. & Barrow, G. *Determination of optimum cutter diameter for machining 2½-D pockets.* International Jounrnal of Machine Tools & Manufacture. Page 687 Vol. 41 No. 5 May 2001.

Hocheng, H., Puw, H.Y., Huang, Y. *Preliminary study on milling of unidirectional carbon reinforced plastics* Composites Manufacturing Vol.4 No.2 (1993) p103-108

Howell, LL. *Compliant Mechanisms.* 2001 Ed, John Wiley & Sons Inc. Canada. ISBN: 0-471-38478-X

Howell, LL., Midha, A. *A method for the design of compliant mechanisms with small length flexural pivots.* ASME Journal of Mechanical Design, 116, 280, 1994

Ilanko S. *ENME 222, Mechanics of materials A, Course notes 1999*. Dept of Mechanical Engineering, University of Canterbury, Christchurch New Zealand.

Jones, RV. *Instruments and experiences, Papers on measurement and design.* 1988 edition John Wiley & Sons Ltd Chichester England. ISBN 0 471 91763 X

Johnson, RC. *Optimum design of mechanical elements.* 1980 John Wiley & Sons Inc. Toronto Canada. ISBN 0-471-03894-6

Kalpakjian, S. Schmid, SR. *Manufacturing engineering and technology.* 4th Edition, 2001 Prentice Hall, Inc. New Jersey, USA. ISBN 0-13-017440-8

Kaneeda, T. *Cutting Mechanism of Rigid-Polyvinylchloride* Bulletin – Japan Society of Precision Engineering, 1989 Vol. 23 pt4 p304 – 309

Karri, V. *Machining of Filled Polymers Using Single-Edge Tools,* Journal of Composites Technology & Research, JCTRER, Vol. 19, No. 2, 1997, p72-76

Kaufeld M. Professor Dr. –Ing. *Mill-Force Optimizer 3.0 / 10.98* © Virtual Manufacturing Software Am Wachberg 24 / D-86497 Horgau Germany

Kazanskii, Y. *Machining of Polymeric Materials by Cutting.* Soviet C/C of Plasticheskie Massy 1971 Pt N5 pp 78 – 85 (0425.500000) (Translated by R. J. Moseley)

Kim S.M. & Lee S.K. *Prediction of thermo-elastic behaviour in a spindle system considering bearing surroundings.* International Jounrnal of Machine Tools & Manufacture. Page 809 Vol. 41 No. 6 May 2001.

Kobayashi, A. *Machining of Plastics*. 1967. Publisher: McGraw-Hill, Inc., New York USA. Library of Congress Catalogue Card No. 66-16772

Kobayashi, A. *Ultra-precision machining of plastics* SPIE Vol.508 Production aspects of single point machined optics (1984) p31-36

Kopac, J., Korosec, M. & Kuzman, K. *Determination of flow stress properties with help of simple compression and orthogonal machining test.* International Jounrnal of Machine Tools & Manufacture. Page 1275 Vol. 41 No. 9 July 2001.

Lee, H.S., Tomizuka, M. *Robust motion controller design for high accuracy positioning systems.* IEEE Transactions on Industrial Electronics 43 (1) (1996) 48-55.

Lin, Z. -C., Chow, J. –J. *Integration planning model of IDEFO & STEP product data representation methods in a CMM measuring System.* International Journal of Advanced Manufacturing. Page 39 Vol 17 No. 1 2001.

Lobontiu, N. *Compliant mechanisms, Design of flexure hinges.* CRC Press LLC 2003. Boca Raton USA. ISBN 0-8493-1367-8

Machining Data Handbook. 3rd Edition Vol. 1. Machinability Data Centre, Cincinnati Ohio USA.

Machining data handbook. Machinability Data Center., Metcut Research Associates. 2d ed. / Compiled by the technical staff of the Machinability Data Center Cincinnati, 1972. Original ed. published in 1966 compiled by the technical staff of Metcut Research Associates, inc. Bib#: 387399

Massey, B. Revised by Ward-Smith, J. *Mechanics of fluids.* 7th edition 1998. Stanley Thornes (Publishers) Ltd. Cheltenham UK. ISBN 0 412 34280 4

Mei, X., Tsutumi, M. Yamazaki, T., Sun, N. *Study of the friction error for a high-speed precision table.* International Jounrnal of Machine Tools & Manufacture. Page 1405 Vol. 41 No. 10 August 2001.

Oxley, PLB. *Mechanics of machining, an analytical approach to assessing machinability.* 1989 Ellis horwood Ltd. Chichester, England. ISBN 0-7458-0007-6

Pahk, H.J., Lee, D.S., Park, J.H. *Ultra precision positioning system for servomotor – piezo actuator using dual servo loop and digital filter implementation.* International Jounrnal of Machine Tools & Manufacture. Page 51 Vol. 41 No. 1 Jan 2001.

Pahl, G., Beitz, W., Wallace, K. *Engineering design.* London : Design Council ; Berlin : Springer, 1984 ISBN 0850721245

Paros, J.M., Weisbord, L. *How to design Flexure Hinges.* Machine Design. Pages 151-165. Nov 25 1965.

Pilkey, WD. *Formulas for stress, strain, and structural matrices.* 1994 edition John Wiley & Sons, Inc. New York NY ISBN 0-471-52746-7

Portman, &V.T., Sandler, B.Z. *High stiffness precision actuator for small displacements.* International Journal of Machine Tools & Manufacture. Page 1229 Vol. 39 No. 5 1999.

Portman, V.T., Sandler, B.Z., & Zahavi, E. *Rigid 6-DOF parallel platform for precision 3-D micromanipulation.* International Jounrnal of Machine Tools & Manufacture. Page 1229 Vol. 41 No. 9 July 2001.

Press, W.H., Flannery, B.P., Teukolsky, S.A., Vetterling, W.T. *Numerical Recipes in C.* Cambridge University Press, New York 1988.

Puw, H.Y., and Hocheng, H. *Milling of Polymer Composites* Machining of Ceramics and Composites, edited by Jahanmir, S., Ramulu, M., and Koshy, P. 1999 p267-294 Marcel Dekker Inc New York.

Renton, D. Elbestawi, M.A. *Motion control for linear motor feed drives in advanced machine tools.* International Jounrnal of Machine Tools & Manufacture. Page 479 Vol. 41 No. 4 March 2001.

Reshtov, DN., Portman, VT. Accuracy of machine tools. The American Society of Mechanical Engineers, New York, New York 1988 ISBN 0-7918-0004-0

Rizzoni, G. *Principles and applications of electrical engineering.* 3rd Edition International edition 2000 McGraw-Hill Inc New York New York ISBN 0-7-117727-2

Rohlfs, T. *Understanding the art of machining plastics.* White paper published on internet by Connecticut Plastics Inc. Sales/Technical Support/Quoting - Tom Rohlfs. tom@connecticutplastics.com http://www.connecticutplastics.com/resour/articles.htm

Sclater, N., Chironis, N.P. *Mechanisms and Mechanical Devices Sourcebook.* 3rd Edition 2001. McGraw-Hill New York USA. ISBN 0 07 136169 3

Segonds, S., Lagarrigue, P., Redonnet, J.M., Rubio, W. *Compensation for machining defects due to spindle dilatation.* . International Jounrnal of Machine Tools & Manufacture. Page 1439 Vol. 41 No. 10 August 2001.

Shah JJ., Mantyla, M. *Parametric and feature based CAD/CAM, concepts, techniques, applications.* 1995 John Wiley & Sons, Inc. New York, New York. ISBN 0-471-00214-3

Shigley, JE. *Mechanical engineering design.* 1st metric edition. International edition 1986. McGraw-Hill Book Co. Singapore. ISBN 0-07-056898-7

Sines, G. *Elasticity and strength.* Allyn & Bacon, Inc. 1969 Boston USA

SKF Catalogue *3055 E/GB 680 Precision Bearings.* Copyright SKF 1978. Reg.47.8000.1981-07

Slocum, A.H. *Precision Machine Design.* 1992 Prentice Hall Inc. Englewood Cliffs, New Jersey USA. ISBN 0 13 690 918 3

Smith, G. *Advanced machining – The handbook of cutting technology*. 1st edition 1989. IFS Publications Ltd. Bedford UK. ISBN 1-85423-022-0

Smith, ST. Chetwynd, DG. *Foundations of Ultraprecision mechanism design. Developments in nanotechnology volume 2.* 1st Edition 3rd printing 1997. Overseas publishers association, Amsterdam, The Netherlands. ISBN 2-88124-840-3

Smith, ST. *Flexures, Elements of Elastic Mechanisms.* 2000 Ed, Gordon & Breach Science Publishers. The Netherlands. ISBN: 90-5699-261-9

Smith, ST. *Flexures, elements of elastic design.* Gordon & Breach 2000. Reprinted 2003 Taylor & Francis, London, England. ISNB 90-5699-261-9

Smith, ST. *Mechanical systems in nanometer metrology.* PhD Thesis, 1988, University of Warwick

Spiewak, S.A., Nickel, J. *Vibration based preload estimation in machine tool spindles.* International Jounrnal of Machine Tools & Manufacture. Page 567 Vol. 41 No. 4 March 2001.

Stabler, G.V. *The fundamental geometry of machine tools.* Proc. Inst. Mech. Engrs 165 (1951)

Stabler, G.V. *The chip flow law and its consequences, in: Advances in machine tool des.* Res. Pergamon, Oxford, 1964.

Tam S.M., Cheung, K.C. *A new approach for machined parts inspection.* International Journal of Advanced Manufacturing. Page 54 Vol 17 No. 1 2001.

Taylor, J.B., Carrano, A.L., Fathi, Y. *Parametric design and optimisation for a nonlinear precision X-Y microstage.* Journal of manufacturing systems. Page 229. Vol. 19 (4) 2000.

The Technical Staff of Measurements Group, Inc. *Strain Gage Based Transducers: Their Design and Construction.* 1988 Measurements Group Inc, North Carolina, USA. ISBN 0 9619057 0 0

Timoshenko, SP., Goodier, JN. *Theory of elasticity.* 3rd edition 1970 McGraw-Hill, Inc. New York, NY Library of Congress Catalogue Card Number 69-13617

Timoshenko, SP., Young, DH. *Elements of strength of materials.* 4th edition 1964 reprinting. D. van Nostrand Company Inc. publisher. New York NY

Trent, EM., Wright, PK. *Metal cutting*. 4th Edition 2000. Butterworth – Heinemann, Woburn Ma USA. ISBN 0-7506-7069-X

Tryliński, W. *Fine Mechanisms and Precision Instruments, Principles of Design.* 1971 Pergamon Press Ltd. Oxford England. Library of Congress Card No. 72-127320

Tung, E.D., Tomizuka, M. *Feed forward tracking controller design based on the identification of low frequency dynamics.* Journal of Dynamic Systems, Measurement and Control. 115 (3) (1993) 348 – 356.

Van Houten, E. *ENME 332, Mechanics of materials B, Course notes 2004*. Dept of Mechanical Engineering, University of Canterbury, Christchurch New Zealand.

Walker, JD. *Applied mechanics.* 4th SI edition 1972. The English Universities Press Ltd. London UK. ISBN 0 340 11539 4

Wang, F.-C., Wright, P.K. *Open architecture controllers for machine tools Part 2. A real time interpolator.* Journal of Manufacturing Science and Engineering. 120 (2) (1998) 425- 432.

Wang J. *Development of a chip flow model for turning operations.* International Jounrnal of Machine Tools & Manufacture. Page 1265 Vol. 41 No. 9 July 2001.

Ward, IM., Sweeney, J. *An introduction to the mechanical properties of solid polymers* 2nd edition John Wiley & Sons, Ltd, West Sussex, England, UK ISBN 0471 49626 X

Weck, M., Krüger, P., Brecher, C. *Limits for controller setting with electric linear drives.* International Jounrnal of Machine Tools & Manufacture. Page 65 Vol. 41 No. 1 Jan 2001.

Wern, C.W., Ramulu, M., Shukla, A. *Investigation of Stresses in the orthogonal cutting of Fibre-reinforced plastics* Experimental Mechanics, March 1996 p33-41

White, FM. *Fluid mechanics.* 4th Edition International editions 1999. WCB/McGraw-Hill Book Co. Singapore. ISBN 0-07-069716-7

Whybrew, K. *ENME 226 Manufacturing Technology – an introduction to manufacturing processes.* 1999 Dept of Mechanical Engineering, University of Canterbury, Christchurch. New Zealand

Yang, M., -Y., Hong, W., -P. *A PC-NC milling machine with new simultaneous 3-axis control algorithm.* International Jounrnal of Machine Tools & Manufacture. Page 555 Vol. 41 No. 4 March 2001.

Yang, M., -Y., Lee, T., -M. *Hybrid adaptive control based on characteristic of CNC end milling.* International Jounrnal of Machine Tools & Manufacture. Page 489 Vol. 42 No. 4 March 2002.

You, C. –F., Sheen, B. -T., Lin, T. –K. *Robust Spiral Toolpath Generation for Arbitrary Pockets.* International Journal of Advanced Manufacturing. Page 181 Vol 17 No. 3 2001.

Young, WC., Budynas, RG. *Roarks formulas for stress and strain.* 7th edition 2002 McGraw-Hill Inc. New York NY ISBN 0-07-072542-X

Zhang, L.C., Zhang, H.J., Wang, X.M. *A force prediction model for cutting unidirectional fibre-reinforced plastics* Machining Science and Technology, 5(3), p293-305 (2001)

Appendices

Appendix A1

Design requirement specification Checklist

Table A.1 gives the complete Design Specification Requirement checklist as it was presented by Hales et al[5].

Table A.9: Reproduction of Design Specification Checklist

Design Specification Checklist		
Requirements	Contributing Factors	Points to Consider
Functional	Overall geometry	Size, height width, length, diameter, space, number, arrangement
	Motion of parts	Type, direction of motion, velocities, acceleration, kinematics
	Forces involved	Load direction, magnitude, weight, load, impact, stiffness, inertia
	Energy needed	Heating, cooling, conversion, efficiency, pressure, temperature, storage
	Materials to be used	Flow, transport, properties, implications, regulation, lifecycle
	Control system	Electrical, electronic, hydraulic, pneumatic, mechanical
	Information flow	Inputs, outputs, form, display, computer
Safety	Operational	Direct, indirect, hazard elimination, safeguarding
	Human	Warnings, training, instruction, personal protection
	Environmental	Land, sea, air, noise, light, radiation, reaction, transport, emergencies
Quality	Quality assurance	Regulations, standards, codes, accreditation
	Quality control	Inspection, testing, measuring tolerances, labelling
	Reliability	Design life, failures, statistics
Manufacturing	Production of components	Factory limitations, maximum dimensions, means of production, wastage
	Purchase of components	Supplier quality and reliability, inspection
	Assembly	Special regulations, installation, siting, foundations, bolting, welding
	Transport	Material handling, clearance, packaging
Timing	Design schedule	Project planning, project control
	Development schedule	Design detailing, in-house tests, compliance tests
	Production schedule	Manufacture, assembly, quality assurance, packing, transport
	Delivery schedule	Delivery date, distribution network
Economic	Marketing analysis	Size of market, strength of market, distribution, servicing
	Design costs	Design team, computing, information retrieval, reproduction
	Development costs	Design detailing, supplier costs, testing costs
	Manufacturing costs	Tooling, labour, overhead, assembly, inspection, cost to customer
	Distribution costs	Packing, transport, service centres, spare parts, warranty
Ergonomic	User needs	Type of operation, instructions, warnings
	Ergonomic design	Human interface relationships, operation, height, layout, comfort, lighting
	Cybernetic design	Controls, layout, clarity, interactions
Ecological	Material selection	Solid, liquid, gas, stability, protection, toxicity, safety
	Working fluid selection	Liquid, gas, flammability, toxicity
Aesthetic	Customer appeal	Shape, colour, texture, form, feel , smell
	Fashion	Culture, history, trends
	Future expectations	Rate of change, trends
Life cycle	Distribution	Means of transport, nature and conditions of dispatch, rules, regulations
	Operational	Quietness, wear, special uses, working environments, foreseeable misuse
	Maintenance	Servicing intervals, inspection, exchange and repair, painting, cleaning
	Disposal	Recycle, scrap

Appendix A2

1.0.1. Design requirement specification worksheets

The following tables, Table A.2 to Table A.8 give the machine design requirement specification details as they were presented for the project by the sponsoring company's staff. They are reproduced here as formative information and to give the reader an outline of the entire project. Some of the items have been included under group headings that don't seem appropriate. The author has not adjusted these; they are reproduced here as they were presented by the sponsoring company.

The functional requirements of the machine design (see Table A.2) are the fundamental points of consideration and therefore represent the main reasons as to why the project exists.

Table A.10: Functional requirement specification

Functional requirements	
Demands	**Wishes**
Overall Geometry	
	1 m^2 machine footprint
Convenient operator machine height	
Serviceable parts to be easily removed to a work bench	
	Spare drive components for all axes
Full technical specification to be provided for all serviceable parts	
Machine to be of modular construction	
Optimal accuracy capability	
	Minimise noise
X & Y axis dimensional accuracy to ISO standards for a laminated card	
Dimensional accuracy of pocket to manufacturer's standard	
Depth of pocket 0 – ~0.65 mm	
	Weight of machine to be minimised
Allow facility for future laminated card design developments	
Adaptive control system – to suit the milling of the pockets and detecting the embedded	

aerial array connections	
Moving slides – minimum mass for high speed operation	
Card must be held secure during milling	
Precise alignment of the card axis with the machine axis (see **Error! Reference source not found.**)	
	Easy access to all parts of the machine
Energy requirements	
	Fully air-conditioned housing/machine enclosure (temperature stabilised)
Adequately cooled rotating components (e.g. bearings etc)	
In process cutter cooling	
Swarf removal – no rags or loose swarf on the product when machining completed – this will require a dedicated removal system	
Material requirements	
Light materials for moving parts in the card positioning system	
Materials with good damping characteristics to minimise vibration and sound	
Materials should be forgiving to card surfaces (surfaces easily scratched) – dominant card surfaces must remain scratch free throughout handling and machining operations	
	Anti-electrostatic materials or design (R-PVC electrostatically charges very easily)
	Use tooling grade aluminium – or substitute other appropriate materials
Optimise all electrical, electronic, pneumatic and mechanical systems	
	Full PC control – possibly through PLC's
Ease of operator use – access to machine control functions – tool pathing etc.	
Parameterised programming for generic IC pocket forms	
Operators required to enter new machining parameters for new products	
Clear cover over the machine	
Graphical display for CAM type graphics – required for checking tool paths and	

adjustments
Graphics display must show card extremities and depth to which the cutter is programmed simultaneously – tool path
Real time graphics
Software back up system
Single spindle manufacture of 1500 units/hr
Steel parts – electroless nickel aluminium parts – anodised
Product infeed
Thickness measurement
Mill pocket in both 'Smart' and conventional cards
Clean away swarf from card and pocket
Measure pocket depth
Product outfeed
Conveyor outfeed to aid operator inspection
Spindle rotation confirmation before XY axis move
Graphic fault display and fault diagnosis
Programme to be able to perform in jog mode - test card pocket depths only - clear pocket only - check/sort cards by dimensions

Table A.11: Safety requirement specification

Safety requirements	
Demands	**Wishes**
Operational safety	
Completely covered operation with transport covers	
Immediate shutdown when cover opened	
Restart requires PC/PLC reset	
	Authorised personnel only override
System to resume on cover closure from point of interruption	System to resume on cover closure from point of interruption
System must have manual override to allow table movement	
All process swarf to be contained at all times	

Human	
Operators manual – operational instruction	
Danger labels (Industry standard)	
Fail safe design and features	
	Graphical warnings as to system disturbances
Clear indication of cycle state	
Environmental (Low noise – sound proofing)	
Total compliance – relevant electrical regulations	

Table A.12: Quality requirement specification

Quality requirements	
Demands	**Wishes**
Compliance and adherence to the relevant ISO standards throughout card production	
Special requirement to improve tolerance values to meet or exceed relevant ISO standard	
Special consideration to pocket depth control and quality	
Quality Control	
	Dynamic z-axis zeroing of the tool
	Monitoring pocket depth and error feedback for depth control
	May require initial thickness measure prior to milling
	Overall dynamic product gauging with auto discharge for non compliance in product size

Table A.13: Manufacturing requirement specification

Manufacturing requirements	
Demands	**Wishes**
Design for manufacture of the machine tool	
Due regard for standard sizes and components	
Ensure components are applied correctly to manufacturers recommendations	
Ensure manufacturers are confident their products will perform to the required standards	

	Use supplier representatives when practical to sight the application of the component
	All manufactured parts to be trial fitted before surface coating
	Early ordering of items in difficult supply
Machine tool to be fully metric	
	Transparent safety covers where possible
Design for access to all machine components	
	Easy operator set up and operational adjustments

Table A.14: Economic requirement specification

Economic requirements	
Demands	**Wishes**
Keep full record of all material and labour costs	
	Patent/protect design of all major components or sub assemblies
	Seek markets for any incidental developments

Table A.15: Ergonomic requirement specification

Ergonomic requirements	
Demands	**Wishes**
	Machine to be optimised for operator operation
	Position Graphics monitor and any warning lights conveniently
	Intuitive controls and operation
	Cycle position in cycle to be retained to enable cycle resumption and/or restart

Table A.16: Life cycle requirement specification

Life cycle requirements	
Demands	**Wishes**
Cutter life to be at least 50k cavities	
	5 year machine life
	Proprietary components to be applied within their design limits
	Good engineering practice to be applied at all times

[5] Hales, C., Gooch, SD. *Managing engineering design.* 2nd Edition 2004. Springer-Verlag London ltd. London England. ISBN 1-85233-803-2

Appendix B

Figure B.1 is a plot of the data captured from the right front capture zone when using the leadscrew drive in it original design position. This chart is included here as information for the reader to compare the significant changes that took place with the redesign of the leadscrew drive. The data shown is normalised data.

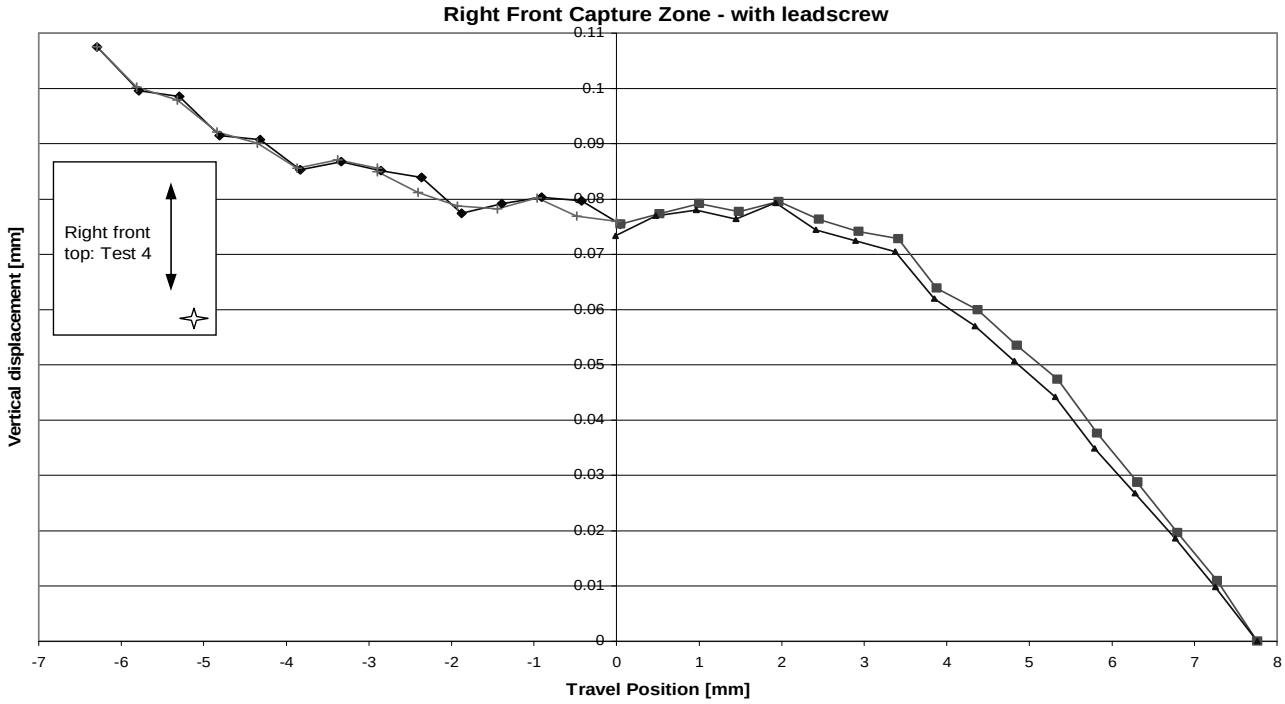

Figure B.16: Complete data plot for Test 4a using original leadscrew drive

DO NOT SCALE

BREAK ALL SHARP EDGES

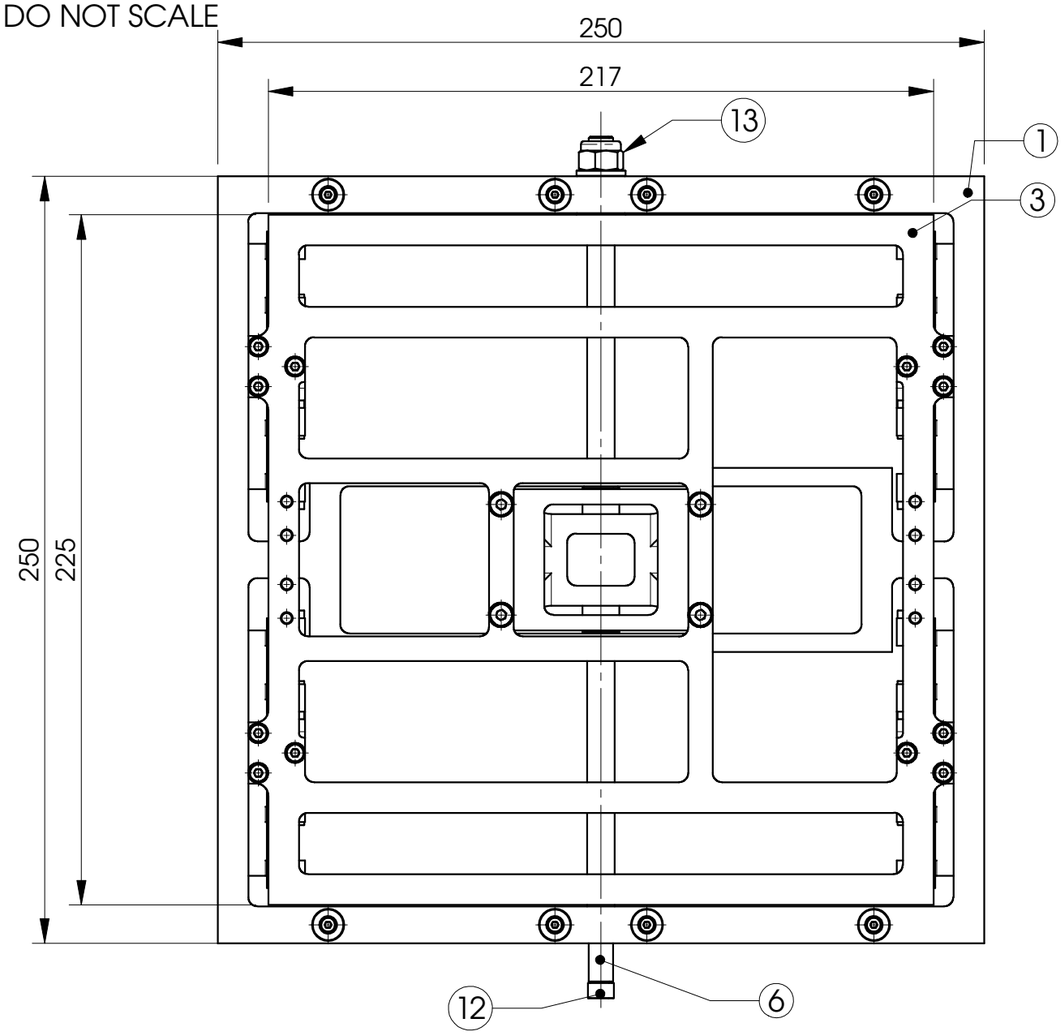

PLAN

ITEM NO.	QTY.	PART NO.	MATERIAL	DESCRIPTION
1	1	BasePlatform	Aluminium alloy tool plate	Base platform
2	4	FabricatedFlexure_Hor	Various	Outer Flexure Stage Assembly
	4	FlexureHinge	Titanium Alloy	Flexure Element
	1	FlexureHinge_Hor	Aluminium alloy tool plate	Outer Flexure Final Stage
	1	FlexureHingeClamp_Hor	Aluminium alloy tool plate	Outer Base Stage
	1	FlexureHingeClamp_Hor	Aluminium alloy tool plate	Intermediate Flexure Stage
	8	FlexureHingeClamp	Aluminium alloy tool plate	Flexure Clamp Plate
	4	ISO 4762 M2.5 x 10 --- 10N		M2.5x10SocketHeadCapScrew
	12	ISO 4762 M2.5 x 8 --- 8N		M2.5x8CapScrew
	8	ISO 4762 M2 x 8 --- 8N		M2.5x10SocketHeadCapScrew
3	1	SecondaryPlatform	Aluminium alloy tool plate	Intermediate Platform
4	28	ISO 4762 M3 x 12 --- 12N		M2.5x10SocketHeadCapScrew
5	2	BasePlatformSupport	Aluminium alloy tool plate	Support for base platform
6	1	Y_AxisLeadScrew	Bright 4140 shaft	Axis lead Screw
7	2	ThrustWasher	Bright 4140 shaft	Lead screw thrust washer
8	1	Y_LeadScrewNut	Aluminium alloy tool plate	Lead screw nut
9	1	X_LeadScrewNutSupport	Aluminium alloy tool plate	Lead screw nut support
10	8	ISO 4762 M4 x 12 --- 12N		
11	8	ISO 4762 M2.5 x 10 --- 10N		M2.5x10SocketHeadCapScrew
12	1	ISO 4762 M5 x 8 --- 8N		
13	1	ISO 7040-M8-N		

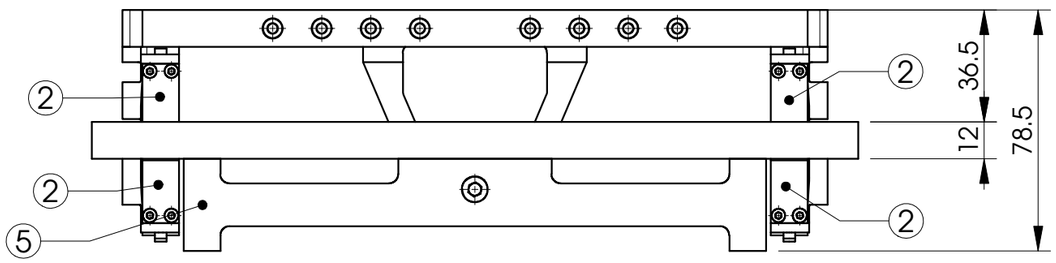

ELEVATION

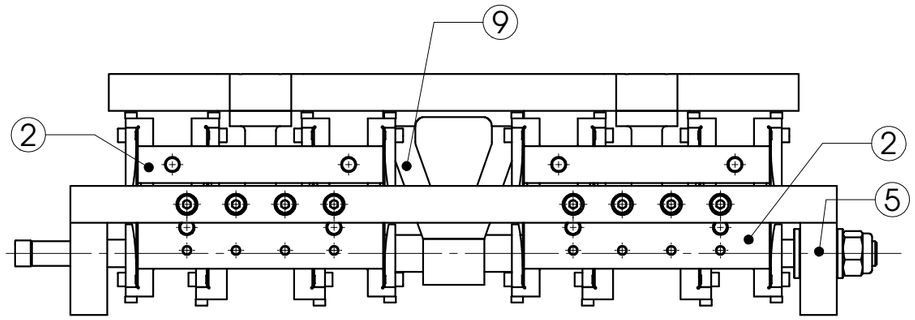

END ELEVATION

Fabricated Flexure X Axis Table		UNIVERSITY of CANTERBURY MECHANICAL ENGINEERING DEPT. CH.CH. N. Z.	
General Assembly	Part No.:00	DRAWN : D Kirk	DATE : January 05
	No. Req'd: 1	CHECKED :	DRG. No : 000105
SCALE : 1:2 -- (A3)	ALL DIMENSIONS IN mm	APPROVED :	

DO NOT SCALE

BREAK ALL SHARP EDGES

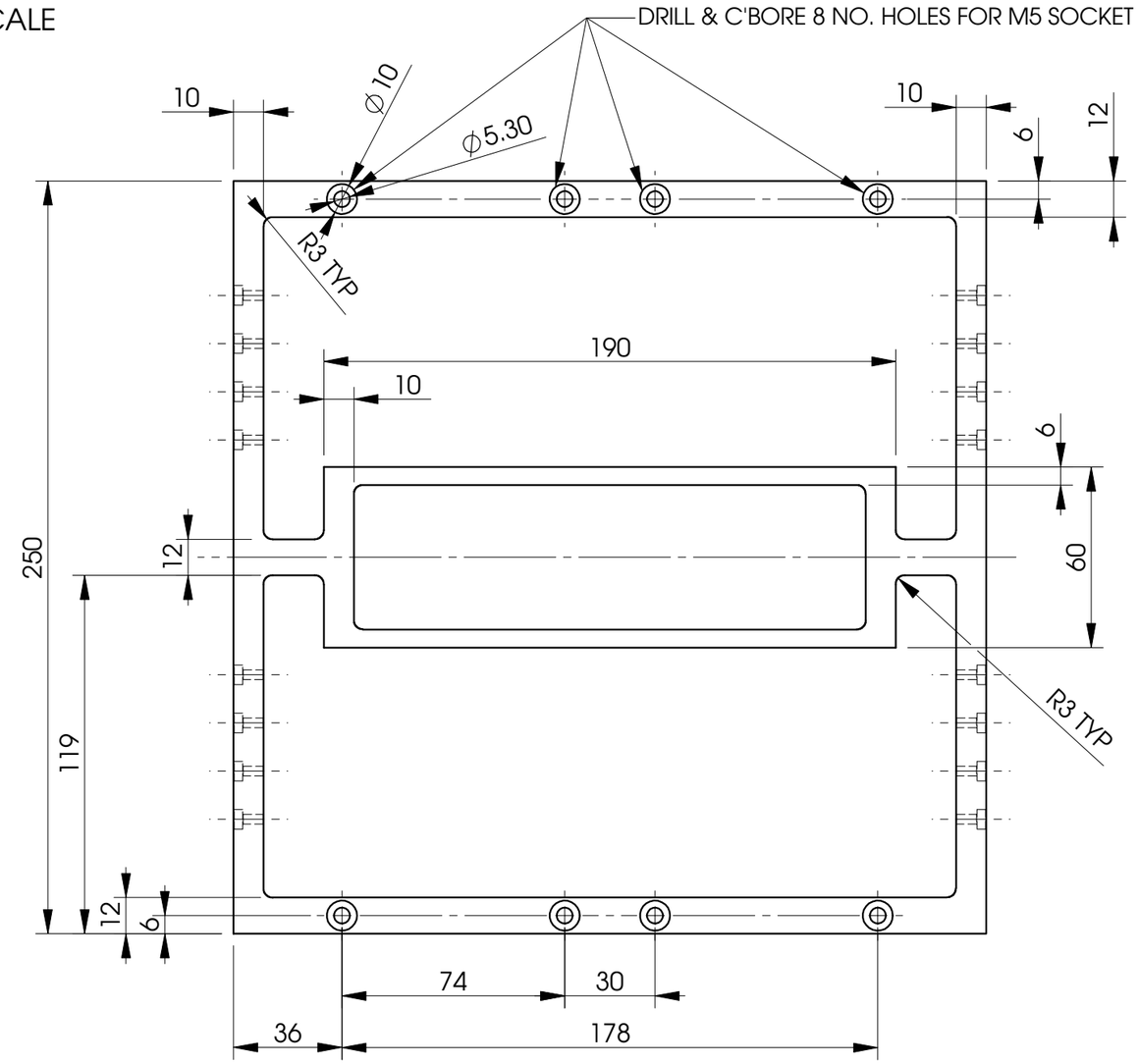

PLAN

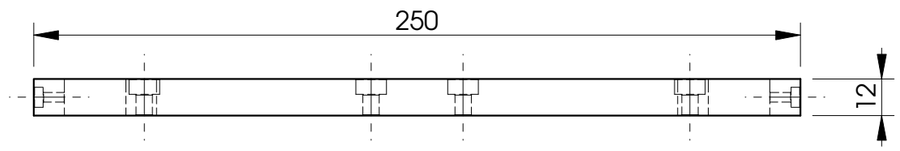

ELEVATION

NOTE:
MAT'L: ALUMINIUM ALLOY TOOL PLATE
QTY: 1 NO.
ALL DIMENSIONS ±0.1MM UNLESS OTHERWISE STATED
PROCESS: EDM WIRECUT OK

DXF fILE NAME:- BasePlatform.DXF

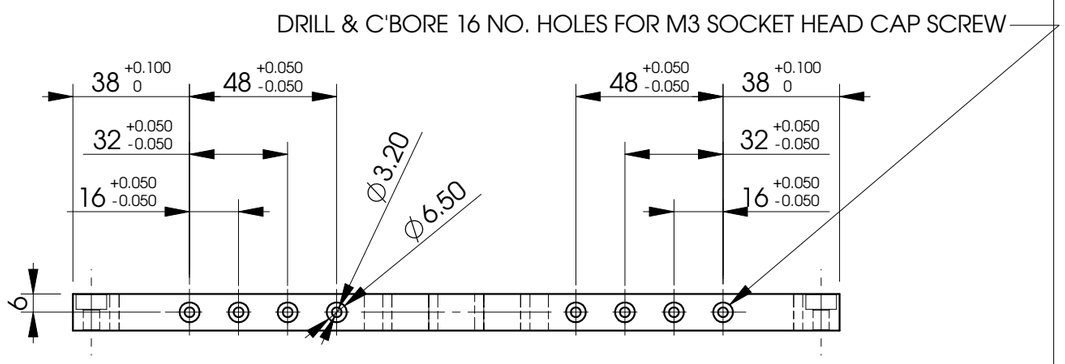

END ELEVATION

Fabricated Flexure X Axis Table		UNIVERSITY of CANTERBURY MECHANICAL ENGINEERING DEPT. CH.CH. N. Z.	
Table Base	Part No.:00	DRAWN : D Kirk	DATE : January 05
	No. Req'd: 1	CHECKED :	DRG. No : 070105
SCALE : 1:2 -- (A3)	ALL DIMENSIONS IN mm	APPROVED :	

FabricatedFlexure40mmMkIII.SLDDRW

11/07/2007

DO NOT SCALE

BREAK ALL SHARP EDGES

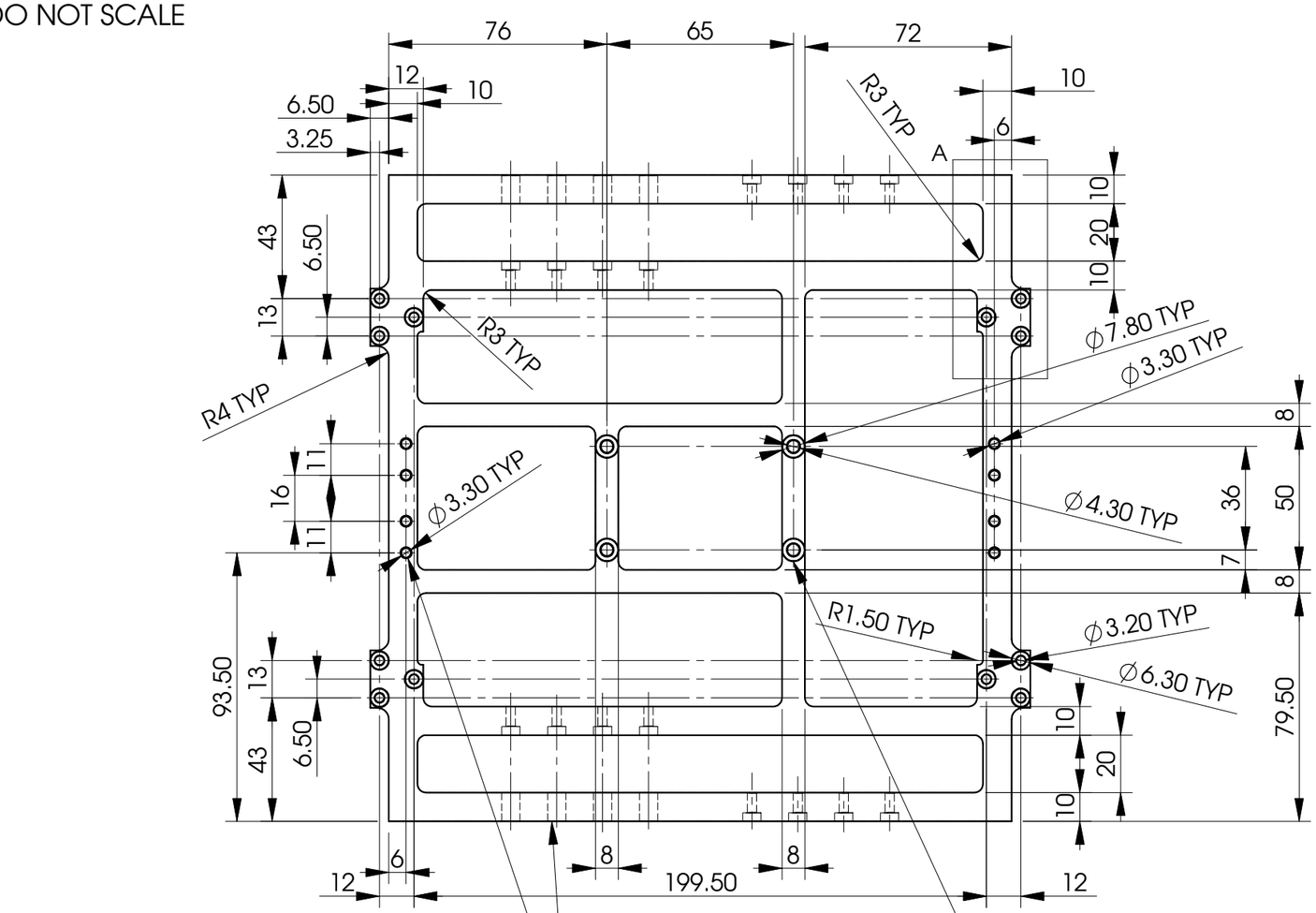

PLAN

DRILL & TAP 8 NO. HOLES M4X8↧ AS SHOWN

DRILL & C'BORE 8 NO. HOLES FOR
M4 SOCKET HEAD CAP SCREWS

DRILL & C'BORE 4 NO. HOLES FOR
M4 SOCKET HEAD CAP SCREWS

DRILL & C'BORE 16 NO. HOLES FOR
M3 SOCKET HEAD CAP SCREWS AS SHOWN

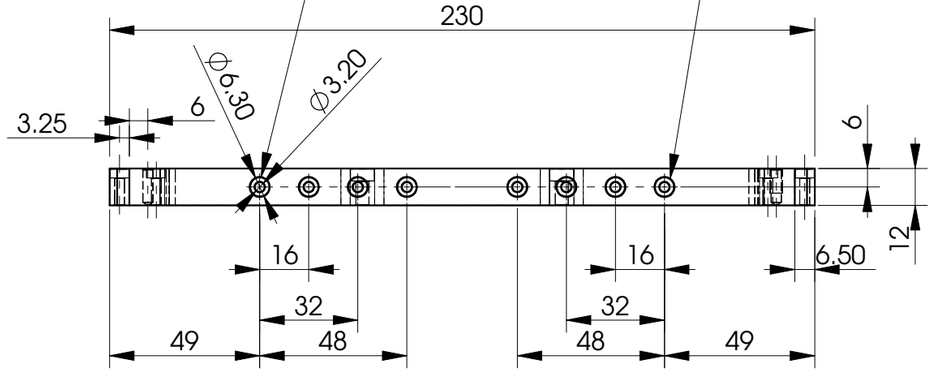

ELEVATION

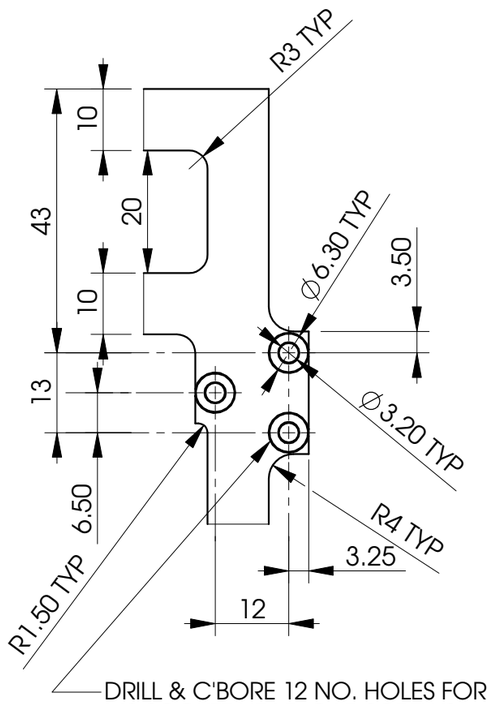

DRILL & C'BORE 12 NO. HOLES FOR
M3 SOCKET HEAD CAP SCREWS

DETAIL A

NOTE:
MAT'L: ALUMINIUM ALLOY TOOL PLATE
QTY: 1 NO.
ALL DIMENSIONS ±0.1MM UNLESS OTHERWISE STATED
PROCESS: EDM WIRECUT OK
DXF FILE NAME:- SecondaryPlatform.DXF

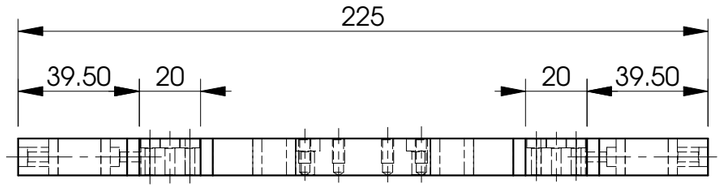

END ELEVATION

Fabricated Flexure X Axis Table		UNIVERSITY of CANTERBURY MECHANICAL ENGINEERING DEPT. CH.CH. N.Z.	
Intermediate Table Stage	Part No.:00	DRAWN : D Kirk	DATE : January 05
	No. Req'd: 1	CHECKED :	DRG. No : 080105
SCALE : 1:2 -- (A3)	ALL DIMENSIONS IN mm	APPROVED :	

DO NOT SCALE

BREAK ALL SHARP EDGES

NOTE:
REFER SHEET NO. 000105 AND 020105
FOR PARTS LIST

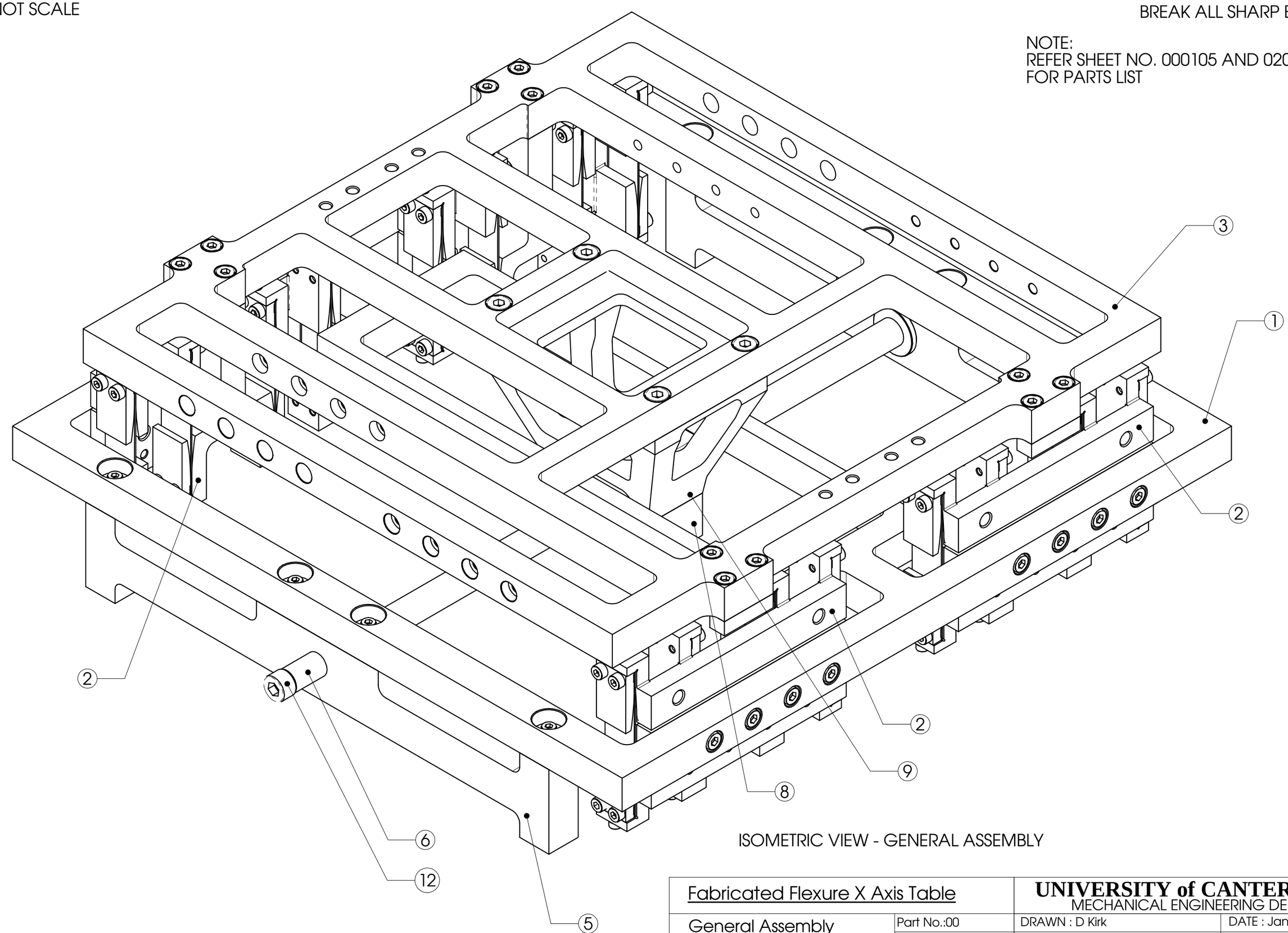

ISOMETRIC VIEW - GENERAL ASSEMBLY

Fabricated Flexure X Axis Table		UNIVERSITY of CANTERBURY MECHANICAL ENGINEERING DEPT. CH.CH. N. Z.	
General Assembly - Isometric View	Part No.:00	DRAWN : D Kirk	DATE : January 05
	No. Req'd: 1	CHECKED :	DRG. No : 010105
SCALE : 1:1 -- (A3)	ALL DIMENSIONS IN mm	APPROVED :	

DO NOT SCALE

BREAK ALL SHARP EDGES

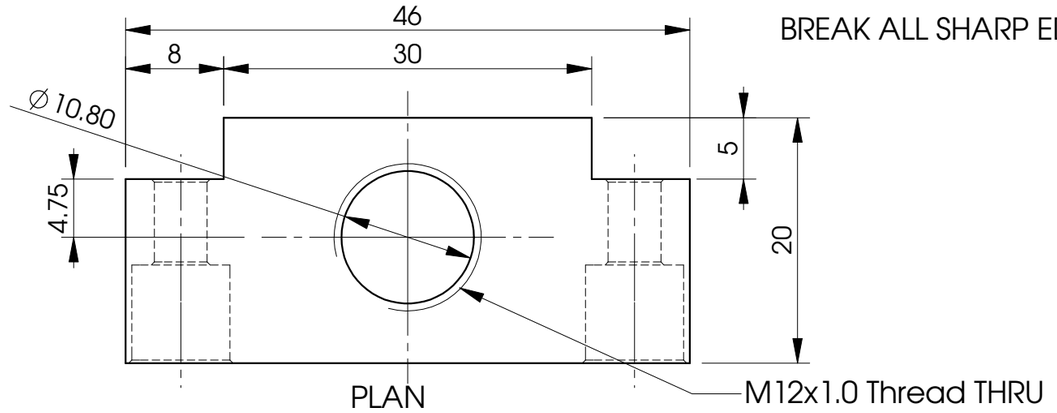

PLAN

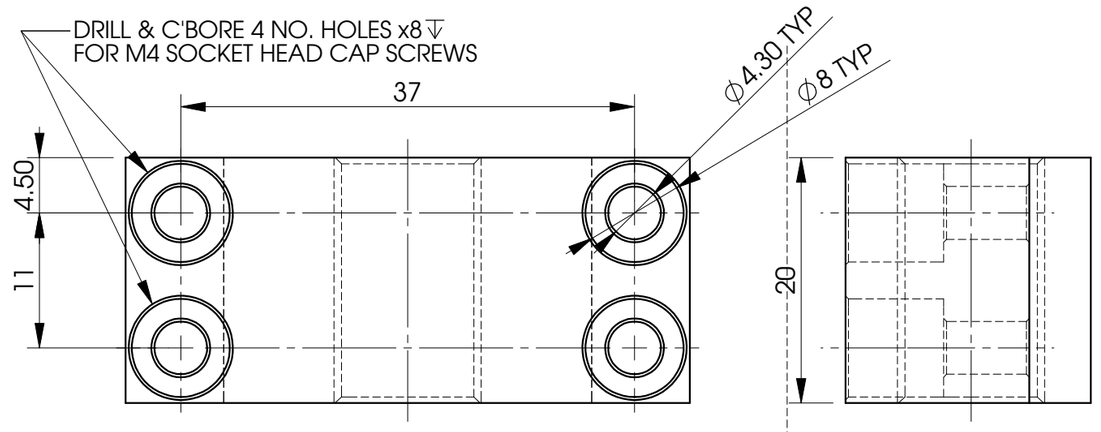

ELEVATION

END ELEVATION

LEADSCREW NUT

NOTE:
QTY: 1 NO. REQ"D
MAT'L: ALUMINIUM ALLOY TOOL PLATE
ALL DIMENSIONS ±0.1MM UNLESS
OTHERWISE STATED

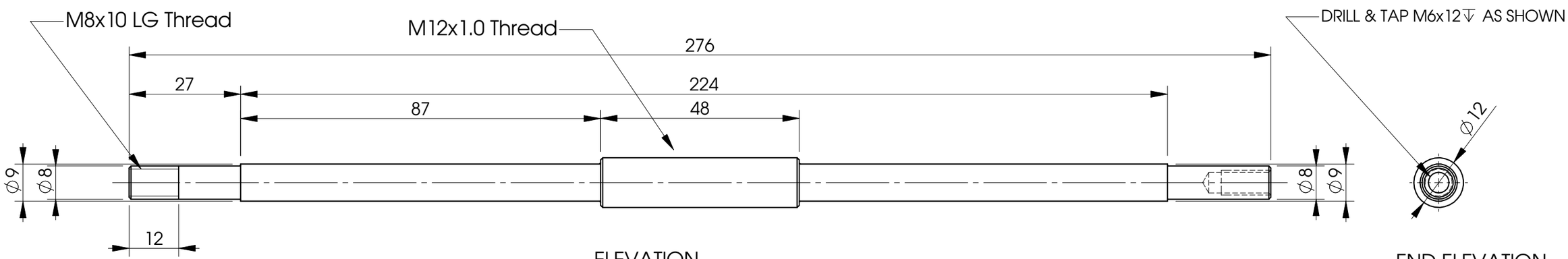

ELEVATION

END ELEVATION

NOTE:
QTY: 1 NO. REQ"D AS SHOWN
MAT'L: BRIGHT 4140 SHAFT
ALL DIMENSIONS ±0.1MM UNLESS
OTHERWISE STATED

Fabricated Flexure X Axis Table		UNIVERSITY of CANTERBURY MECHANICAL ENGINEERING DEPT. CH.CH. N. Z.	
X-Axis Leadscrew & Components	Part No.:00	DRAWN : D Kirk	DATE : January 05
	No. Req'd: 1	CHECKED :	DRG. No : 090105
SCALE : 1:1 -- (A3)	ALL DIMENSIONS IN mm	APPROVED :	

DO NOT SCALE

DRILL & TAP 4 NO. HOLES M5x10↧ AS SHOWN

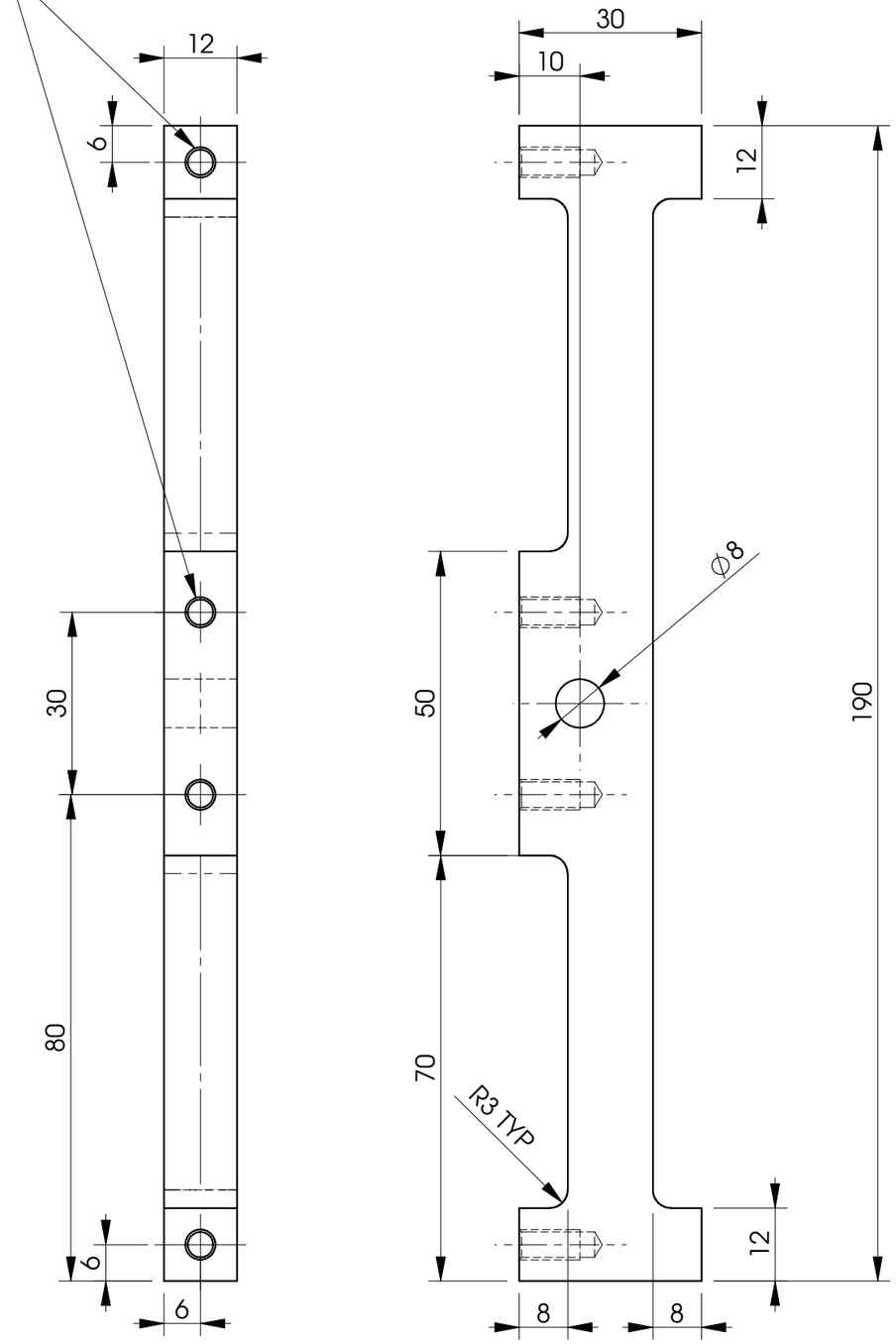

END ELEVATION ELEVATION

FLAXURE BASE SUPPORT

NOTE:
QTY: 2 NO. AS SHOWN
MAT'L: ALUMINIUM ALLOY TOOL PLATE
ALL DIMENSIONS ± 0.1MM UNLESS
OTHERWISE STATED

DXF FILE NAME:- BasePlatformSupport.DXF

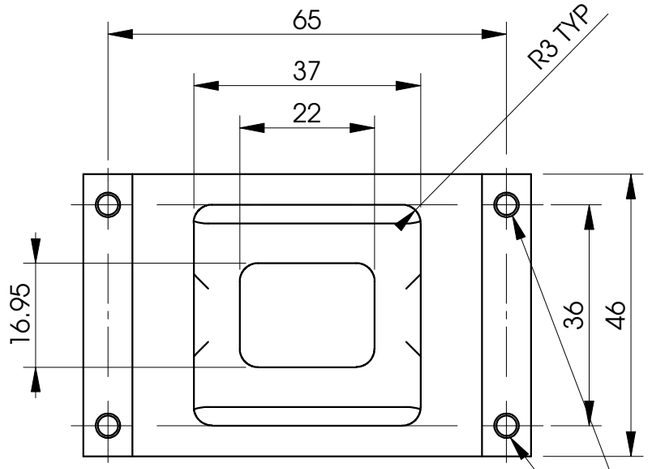

PLAN

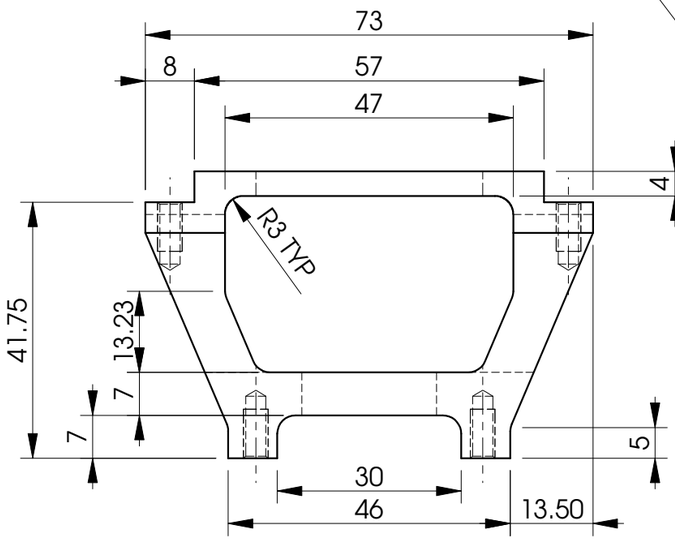

ELEVATION

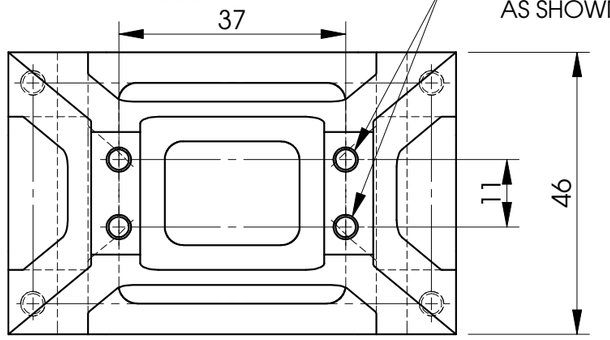

PLAN ON UNDERSIDE

BREAK ALL SHARP EDGES

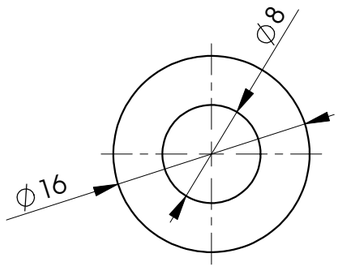

PLAN

NOTE:
QTY: 2 NO. AS SHOWN
MAT'L: EX Ø 16 4140 SHAFT

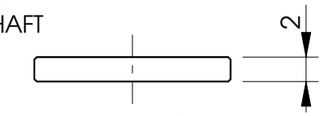

ELEVATION

LEAD SCREW THRUST WASHER
SCALE 2:1

DRILL & TAP 4 NO. HOLES M4x8↧ AS SHOWN

DRILL & TAP 4 NO. HOLES M4x8↧ AS SHOWN

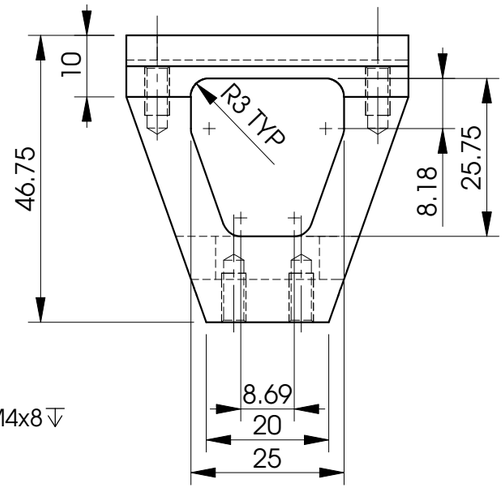

END ELEVATION

NOTE:
QTY: 1 NO. AS SHOWN
MAT'L: ALUMINIUM ALLOY TOOL PLATE
ALL DIMENSIONS ± 0.1MM UNLESS
OTHERWISE STATED

X AXIS LEAD SCREW NUT SUPPORT

Fabricated Flexure X Axis Table		UNIVERSITY of CANTERBURY MECHANICAL ENGINEERING DEPT. CH.CH. N. Z.	
Lead Screw Components	Part No.:00	DRAWN : D Kirk	DATE : January 05
	No. Req'd: 1	CHECKED :	DRG. No : 100105
SCALE : 1:1 -- (A3)	ALL DIMENSIONS IN mm	APPROVED :	

DO NOT SCALE

BREAK ALL SHARP EDGES

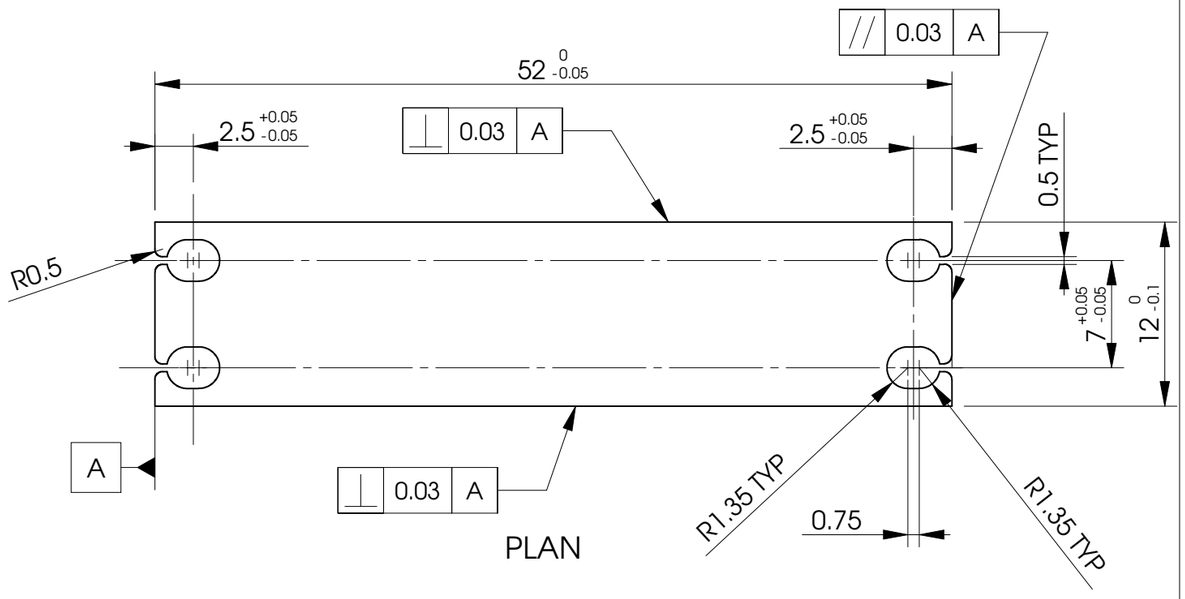

PLAN

ELEVATION

FLEXURE SPRING LEAF

SCALE: 2.5:1
MAT'L: 0.5 THICK TITANIUM ALLOY OR SPRING STEEL SHEET
NO. REQ'D: 4 PER SUB ASSEMBLY

ALL SPRINGS TO BE STACK CUT USING EDM WIRECUT
ALL DIMENSIONS ±0.1MM UNLESS OTHERWISE STATED

DXF FILE NAME:- FlexureHingeBlade2.DXF

ITEM NO.	Description	Material	QTY.
1	Flexure Element	Titanium Alloy or Spring Steel	4

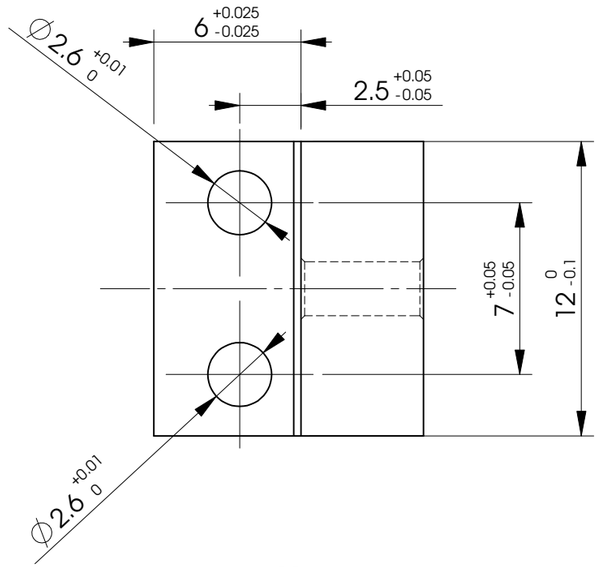

PLAN

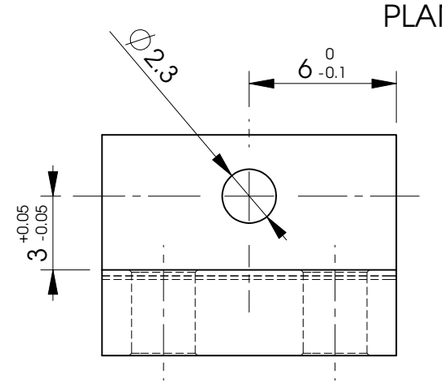

END ELEVATION

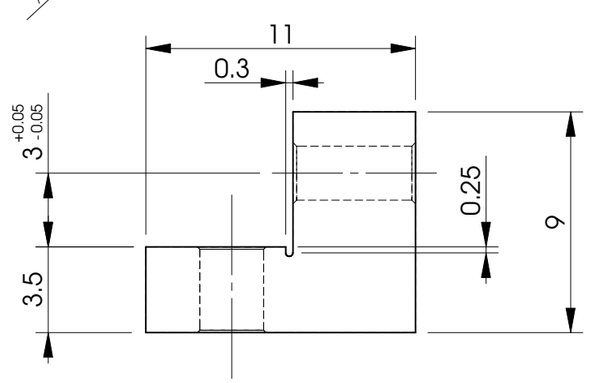

ELEVATION

FLEXURE SPRING CLAMP

NOTE:
MAT'L: 12 THICK ALUMINIUM ALLOY PLATE
NO. REQ'D: 8 PER SUB ASSEMBLY
ALL DIMENSIONS ±0.1MM UNLESS
OTHERWISE STATED

DXF FILE NAME:- FlexureHingeClamp2.DXF

ITEM NO.	Description	Material	QTY.
1	Flexure Blade Clamp	Aluminium Alloy Tool Plate	8

Fabricated Flexure X Axis Table		UNIVERSITY of CANTERBURY MECHANICAL ENGINEERING DEPT. CH.CH. N. Z.	
Components	Part No.:00	DRAWN : D Kirk	DATE : December 05
	No. Req'd: 1	CHECKED :	DRG. No : 031205
SCALE : 4:1 -- (A3)	ALL DIMENSIONS IN mm	APPROVED :	

DO NOT SCALE

BREAK ALL SHARP EDGES

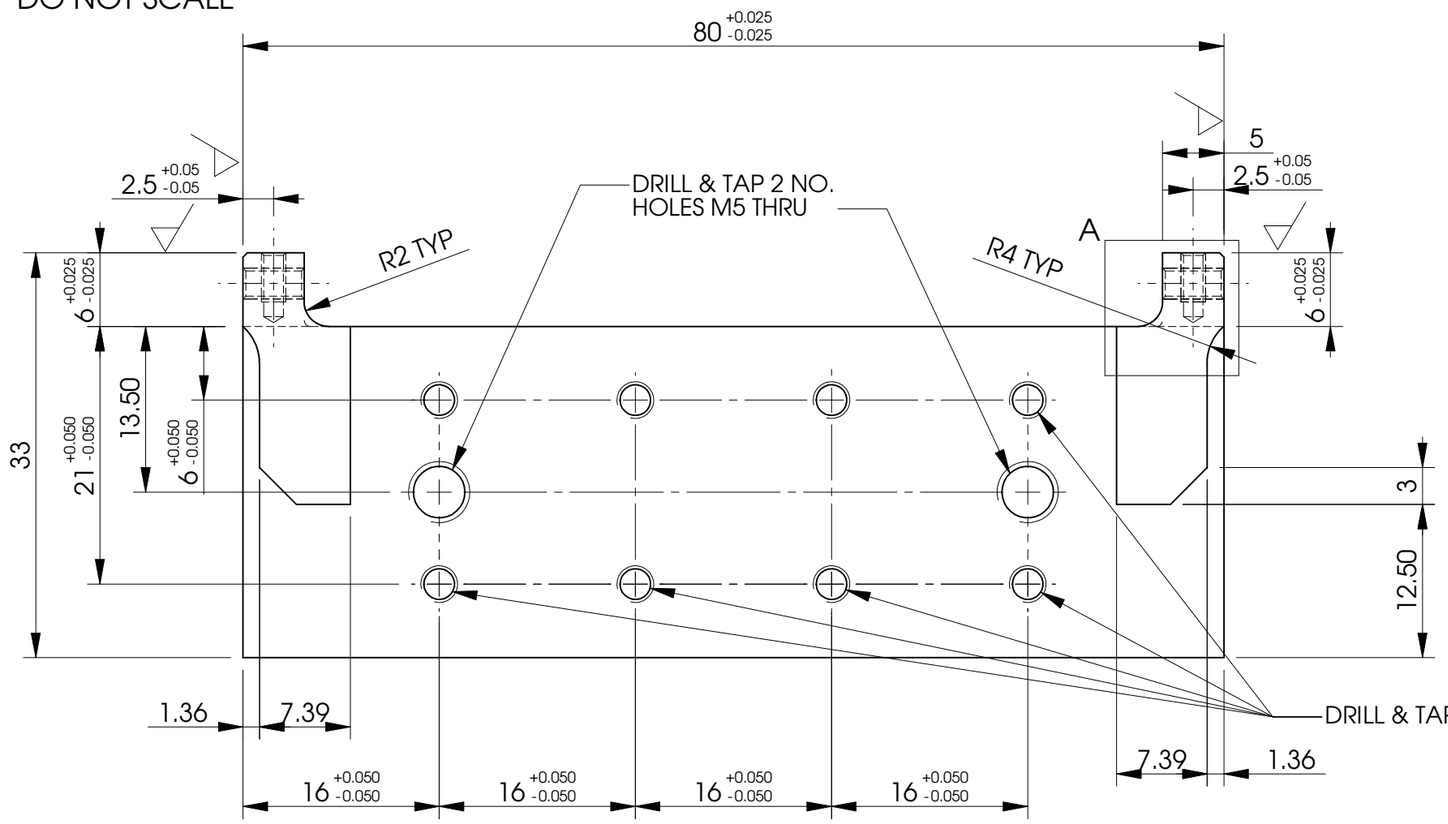

PLAN

TYPICAL CORNER DETAIL

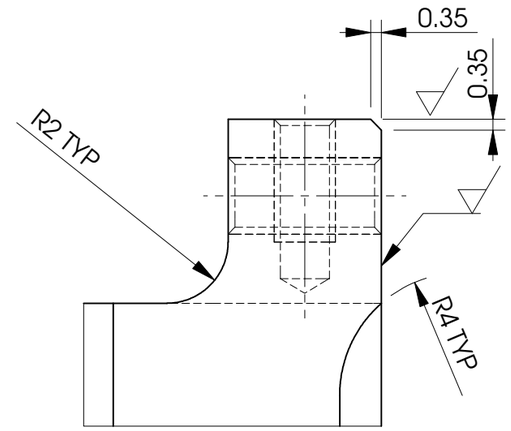

DETAIL A
SCALE 5:1

NOTE:
MAT'L: ALUMINIUM ALLOY TOOL PLATE
NO. REQ'D: 1 NO. PER SUBASSEMBLY
ALL DIMENSIONS ± 0.1MM UNLESS OTHERWISE STATED
DXF FILE NAME:- FlexureBase2.DXF

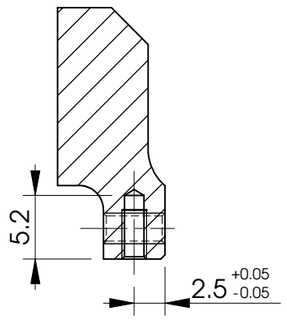

SECTION A A

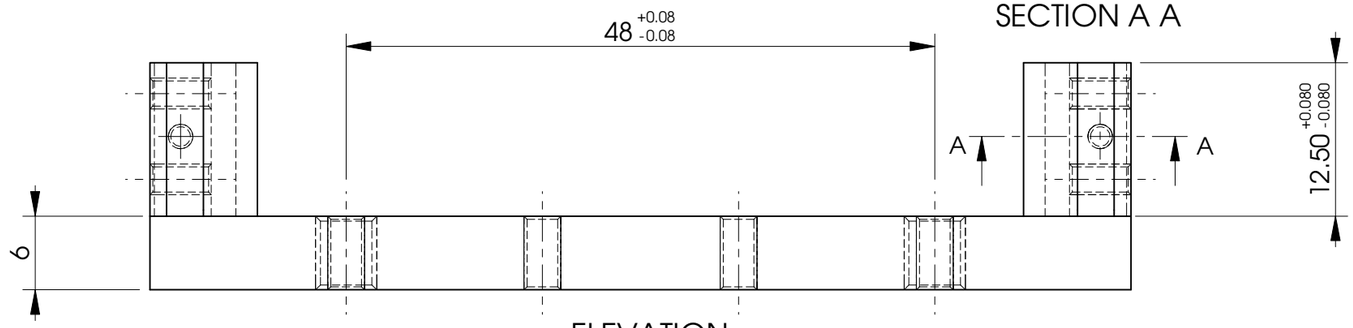

ELEVATION

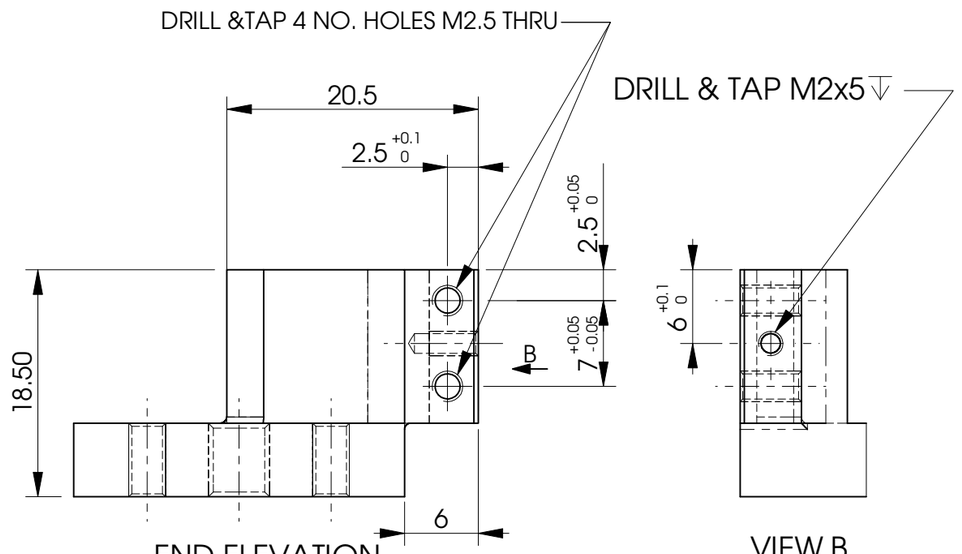

END ELEVATION

VIEW B

ITEM NO.	Description	Material	QTY.
1	Outer Base Stage	Aluminium Alloy Tool Plate	1

Fabricated Flexure X Axis Table		UNIVERSITY of CANTERBURY MECHANICAL ENGINEERING DEPT. CH.CH. N. Z.	
Flexure Base	Part No.:00	DRAWN : D Kirk	DATE : December 05
	No. Req'd: 1	CHECKED :	DRG. No : 051205
SCALE : 2:1 -- (A3)	ALL DIMENSIONS IN mm	APPROVED :	

DO NOT SCALE

BREAK ALL SHARP EDGES

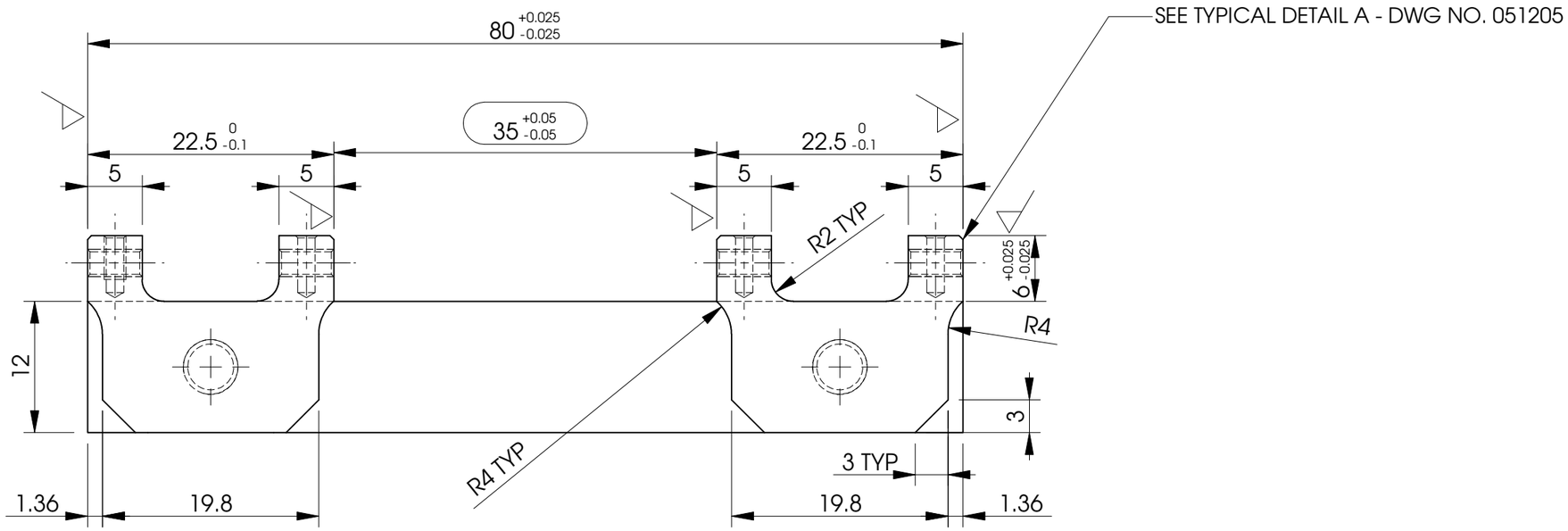

PLAN

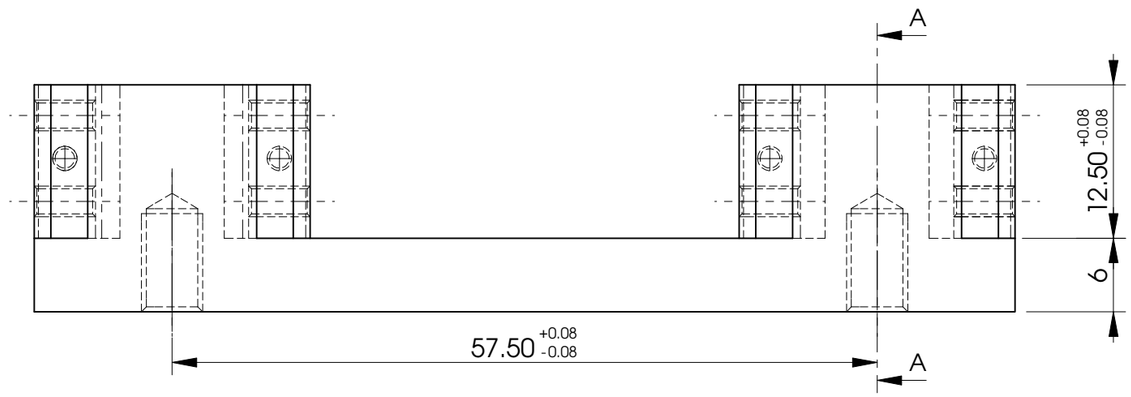

ELEVATION

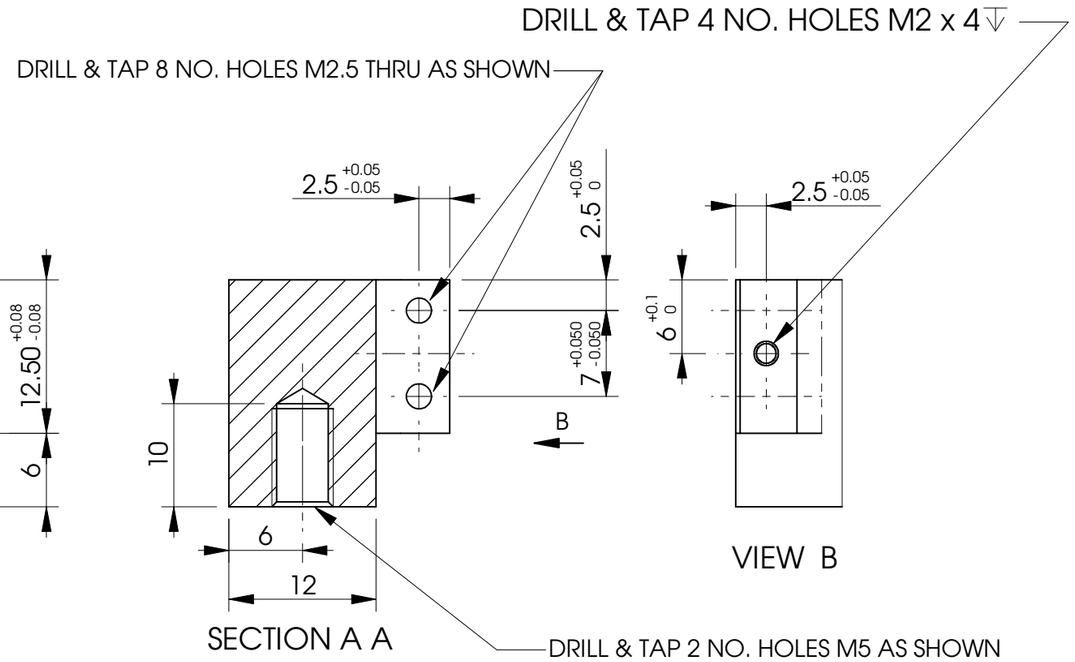

SECTION A A

VIEW B

NOTE:
MAT'L: ALUMINIUM ALLOY TOOL PLATE
NO. REQ'D: 1 NO. PER SUBASSEMBLY
ALL DIMENSIONS ± 0.1MM UNLESS OTHERWISE STATED
DXF FILE NAME:- FlexureIntermediateStage2.DXF

ITEM NO.	Description	Material	QTY.
1	Intermediate Flexure Stage	Aluminium Alloy Tool Plate	1

Fabricated Flexure X Axis Table		UNIVERSITY of CANTERBURY MECHANICAL ENGINEERING DEPT. CH.CH. N. Z.	
Intermediate Flexure Platform	Part No.:00	DRAWN : D Kirk	DATE : December 05
	No. Req'd: 1	CHECKED :	DRG. No : 041205
SCALE : 2:1 -- (A3)	ALL DIMENSIONS IN mm	APPROVED :	

FabricatedFlexure40mmMkIINoCurves.SLDDRW

9/09/2006

DO NOT SCALE

BREAK ALL SHARP EDGES

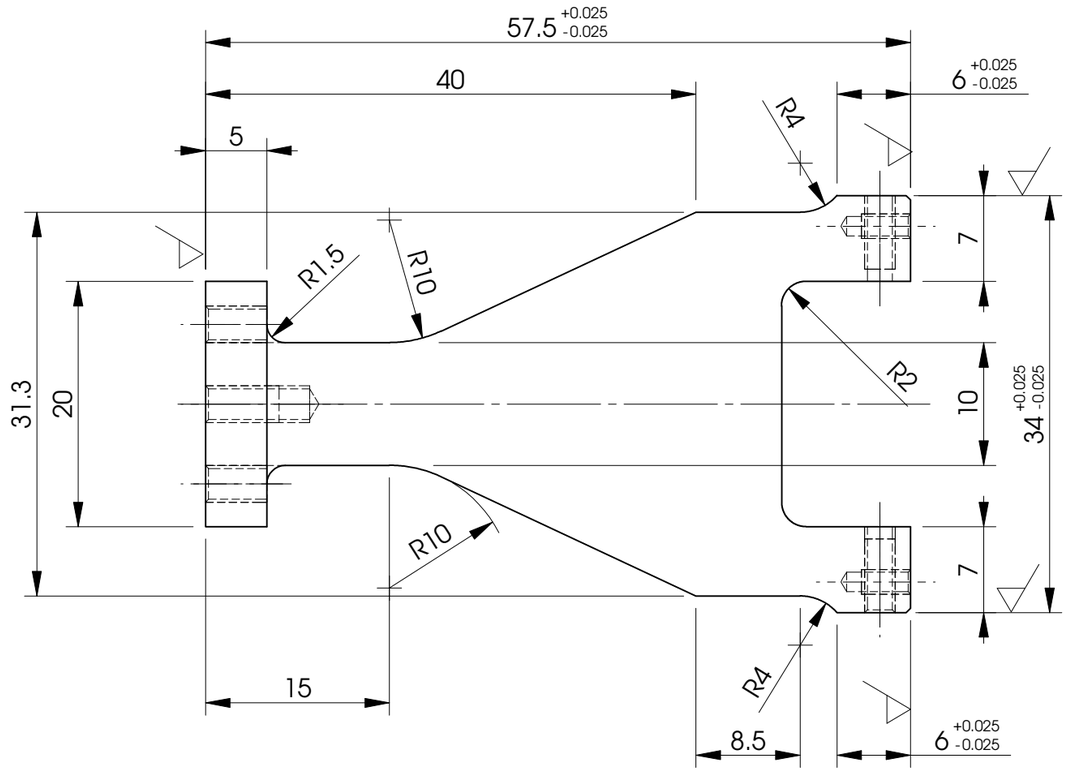

PLAN

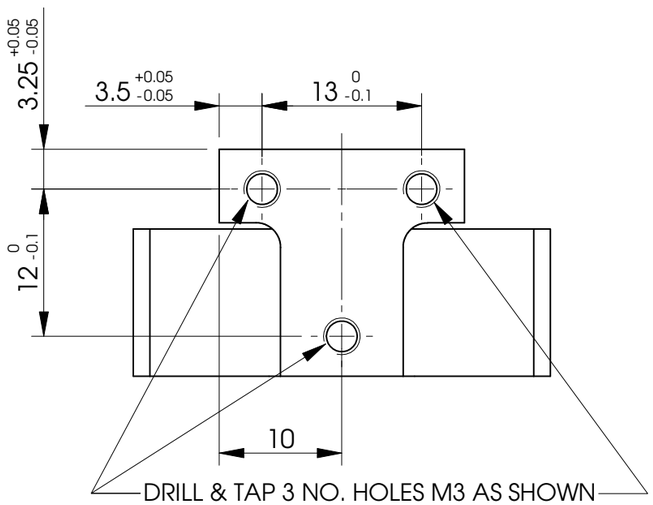

END ELEVATION

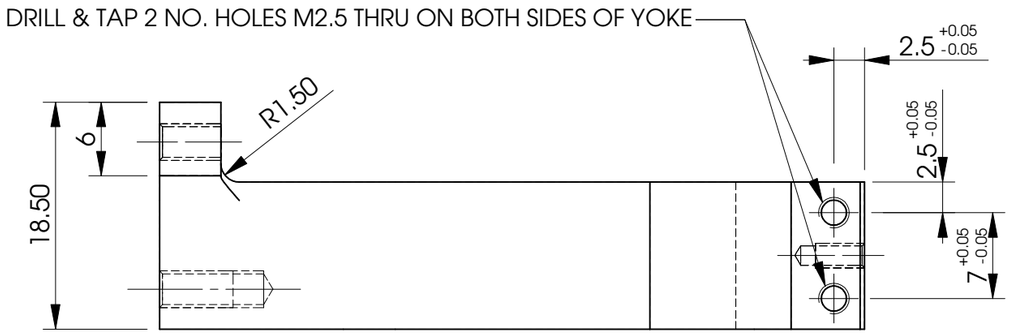

ELEVATION

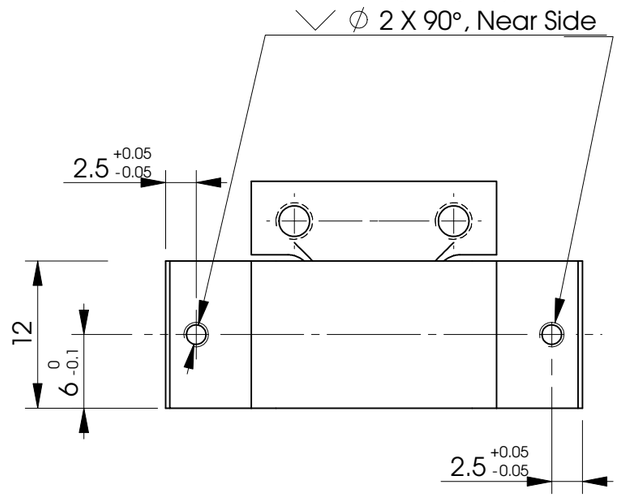

END ELEVATION

ITEM NO.	Description	Material	QTY.
1	Flexure Platform	Aluminium Alloy Tool Plate	1

NOTE:

MAT'L: ALUMINIUM ALLOY TOOL PLATE
QTY: 1 NO. PER OUTER FLEXURE ASSEMBLY
ALL DIMENSIONS ±0.1MM UNLESS OTHERWISE STATED
PROCESS: EDM WIRECUT OK

DXF FILE NAME:- FlexurePlatform2.DXF

Fabricated Flexure X Axis Table		UNIVERSITY of CANTERBURY MECHANICAL ENGINEERING DEPT. CH.CH. N. Z.	
Flexure Platform	Part No.:00	DRAWN : D Kirk	DATE : December 05
	No. Req'd: 1	CHECKED :	DRG. No : 061205
SCALE : 2:1 -- (A3)	ALL DIMENSIONS IN mm	APPROVED :	

FabricatedFlexure40mmMkIINoCurves.SLDDRW

9/09/2006

DO NOT SCALE

BREAK ALL SHARP EDGES

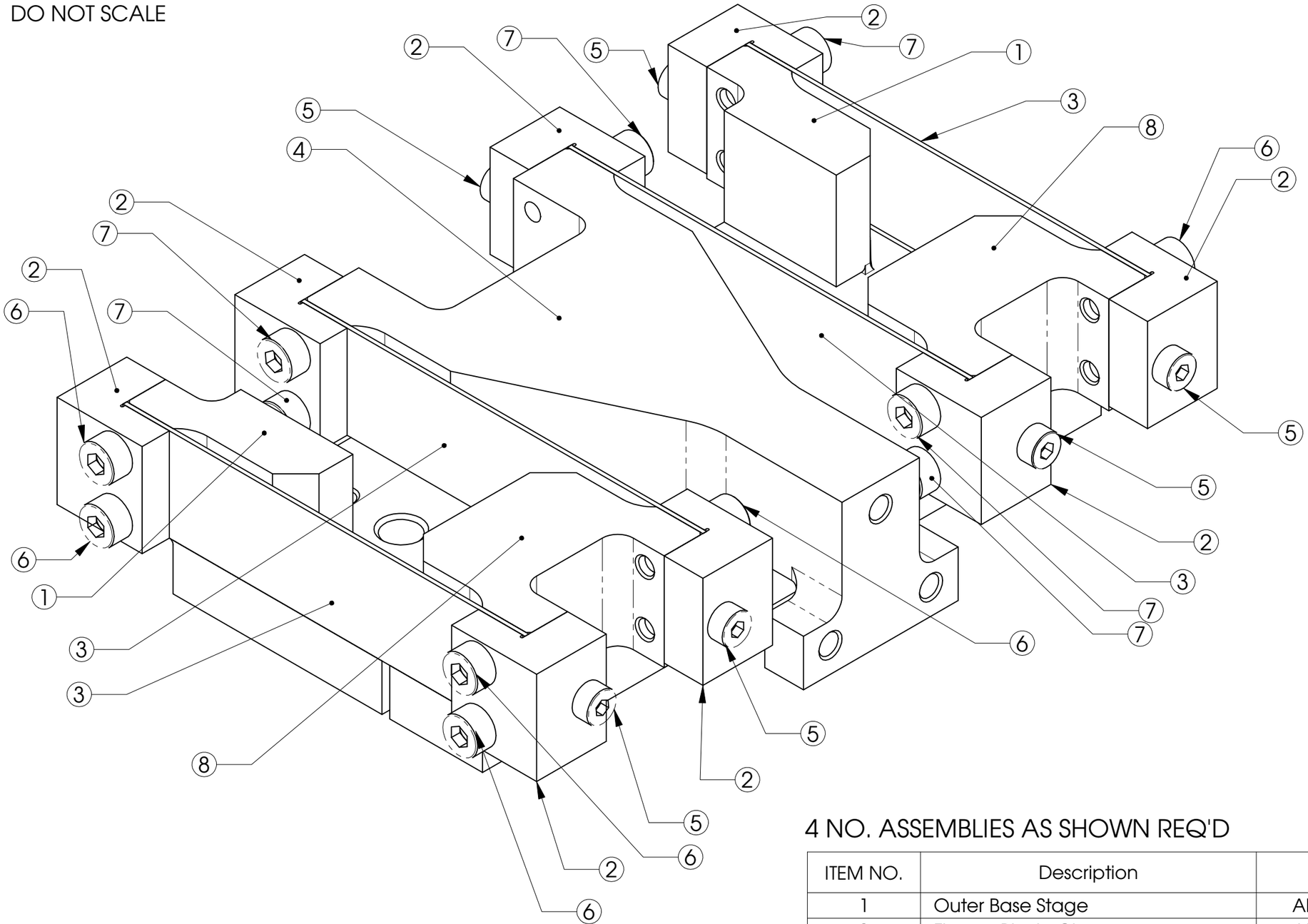

ISOMETRIC VIEW OF FLEXURE ASSEMBLY

4 NO. ASSEMBLIES AS SHOWN REQ'D

ITEM NO.	Description	Material	Qty.	Sheet No.
1	Outer Base Stage	Aluminium Alloy Tool Plate	1	5
2	Flexure Blade Clamp	Aluminium Alloy Tool Plate	8	3
3	Flexure Blade	Titanium Alloy or Spring Steel	4	3
4	Flexure Platform	Aluminium Alloy Tool Plate	1	6
5	M2 x 10 Socket Head Cap Screw		8	
6	M2.5x8 Socket Head Cap Screw		12	
7	M2.5x10 Socket Head Cap Screw		4	
8	Intermediate Flexure Stage	Aluminium Alloy Tool Plate	1	

Fabricated Flexure X Axis Table		UNIVERSITY of CANTERBURY MECHANICAL ENGINEERING DEPT. CH.CH. N. Z.	
General Assembly Inner & Outer Flexures	Part No.:00	DRAWN : D Kirk	DATE : December 05
	No. Req'd: 4 Each	CHECKED :	DRG. No : 021205
SCALE : 2.5:1 -- (A3) ALL DIMENSIONS IN mm		APPROVED :	

DO NOT SCALE

BREAK ALL SHARP EDGES

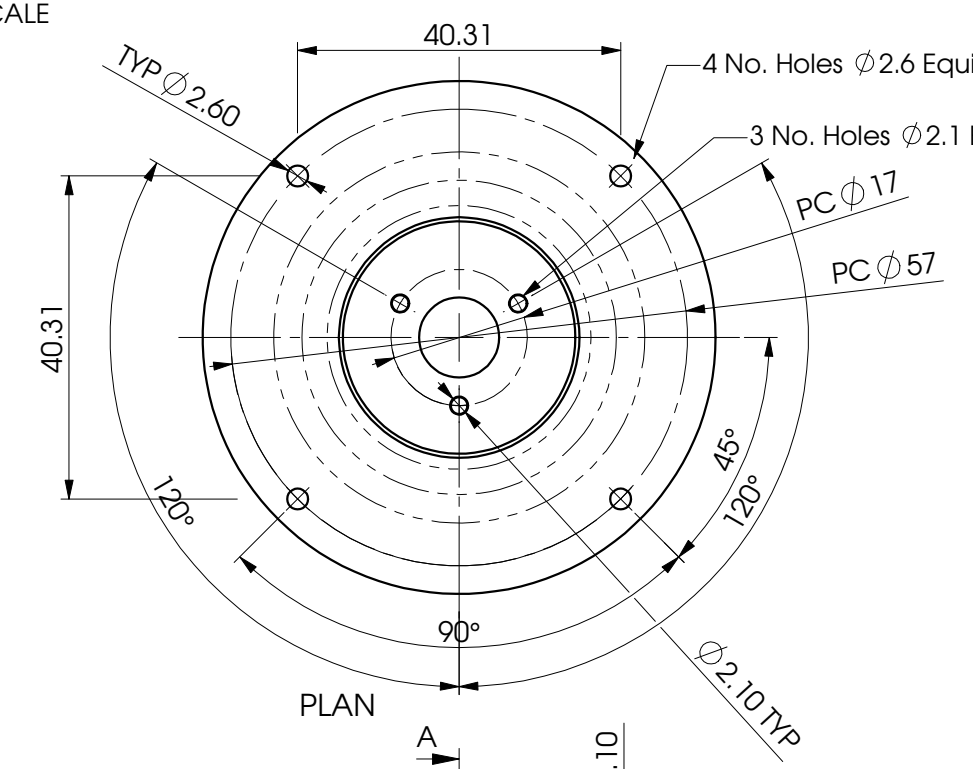

PLAN

NOTE:

MAT'L: Aluminium Tool Plate
QTY: 1 No. Req'd as Shown

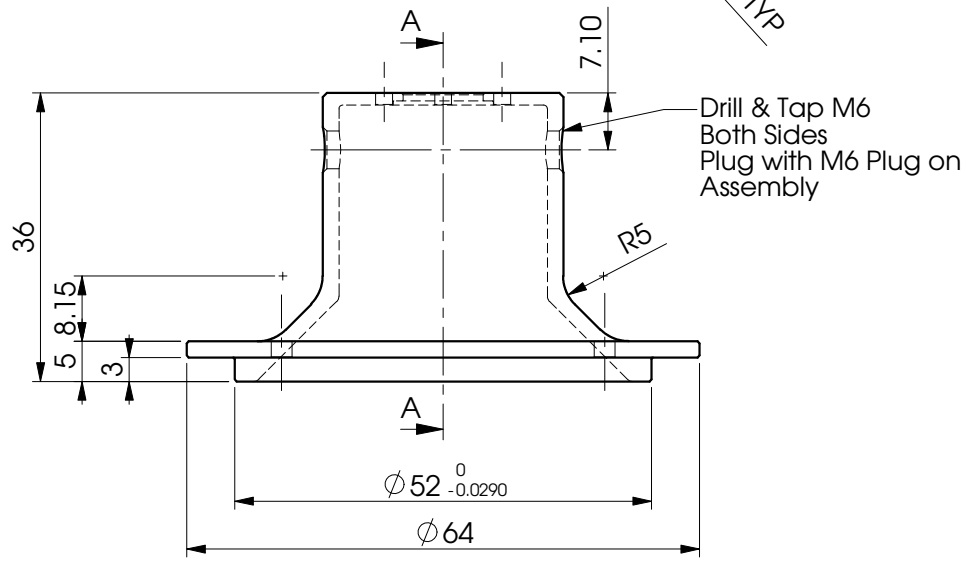

ELEVATION

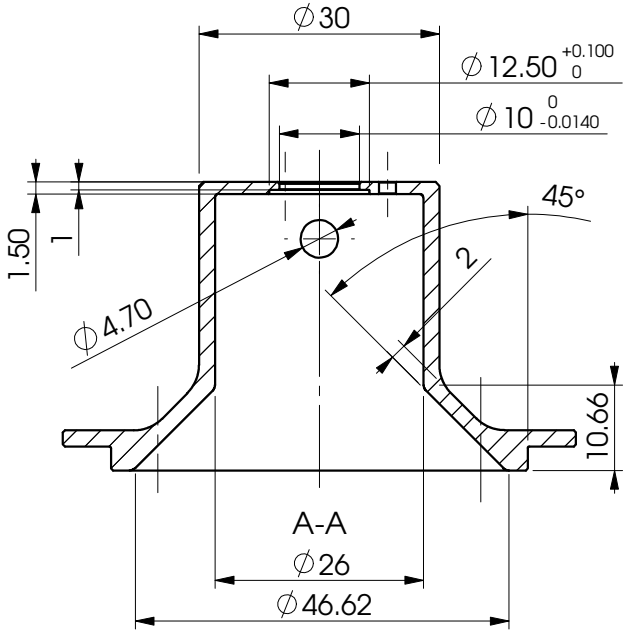

END ELEVATION

SHEET No. 1 of 1

MAXON EC22 BELLHOUSE		UNIVERSITY of CANTERBURY MECHANICAL ENGINEERING DEPT. CH.CH. N.Z.	
BELLHOUSE	Part No.:00	DRAWN : D Kirk	DATE : January 04
	No. Req'd: 1	CHECKED :	DRG. No : 080204
SCALE : 1.5:1 -- (A3)	ALL DIMENSIONS IN mm	APPROVED : DRA	

DO NOT SCALE

BREAK ALL SHARP EDGES

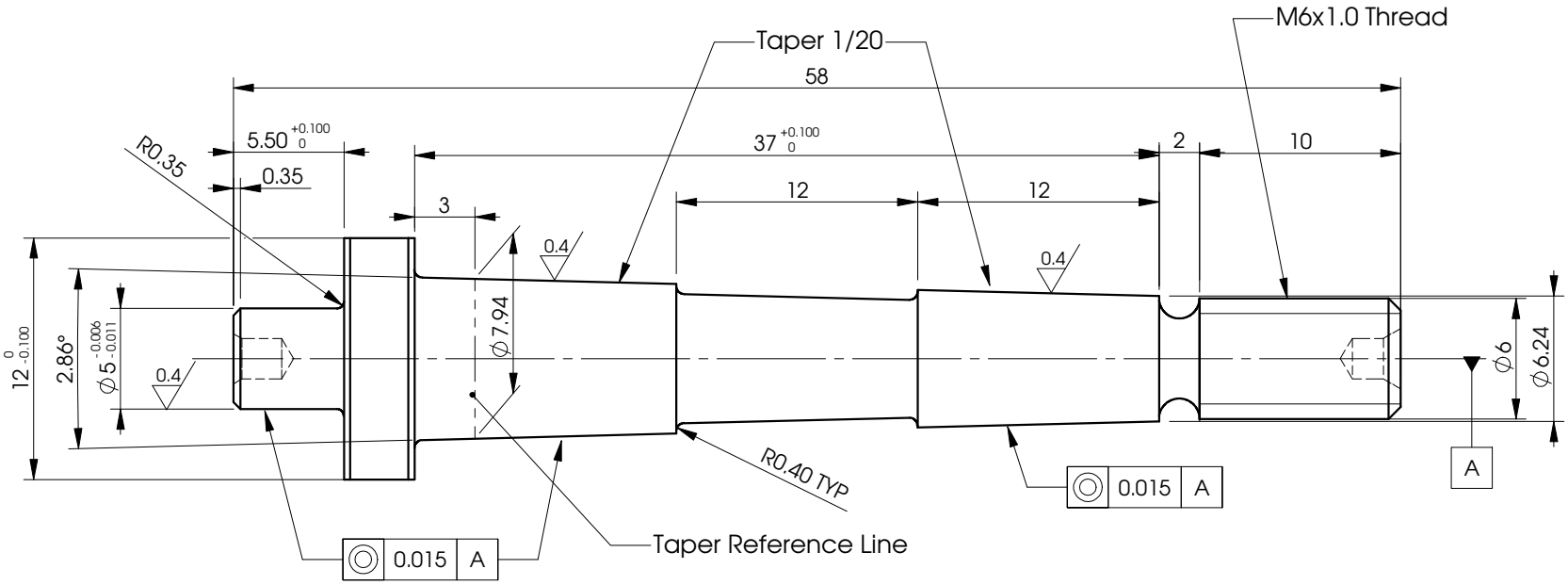

ELEVATION

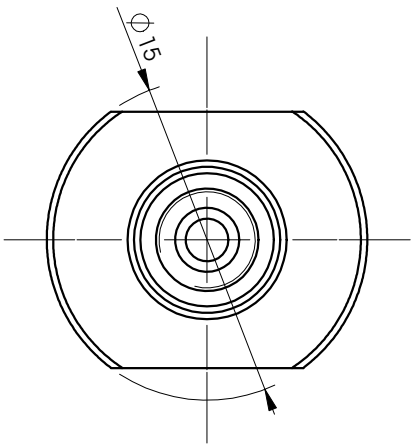

END ELEVATION

NSK SA500 DRIVE SHAFT		**UNIVERSITY of CANTERBURY** MECHANICAL ENGINEERING DEPT. CH.CH. N.Z.	
QUILL SHAFT	Part No.:00	DRAWN : D Kirk	DATE : January 04
	No. Req'd: 1	CHECKED :	DRG. No : 090204
SCALE : 4:1 -- (A3)	ALL DIMENSIONS IN mm	APPROVED : DRA	

DO NOT SCALE

BREAK ALL SHARP EDGES

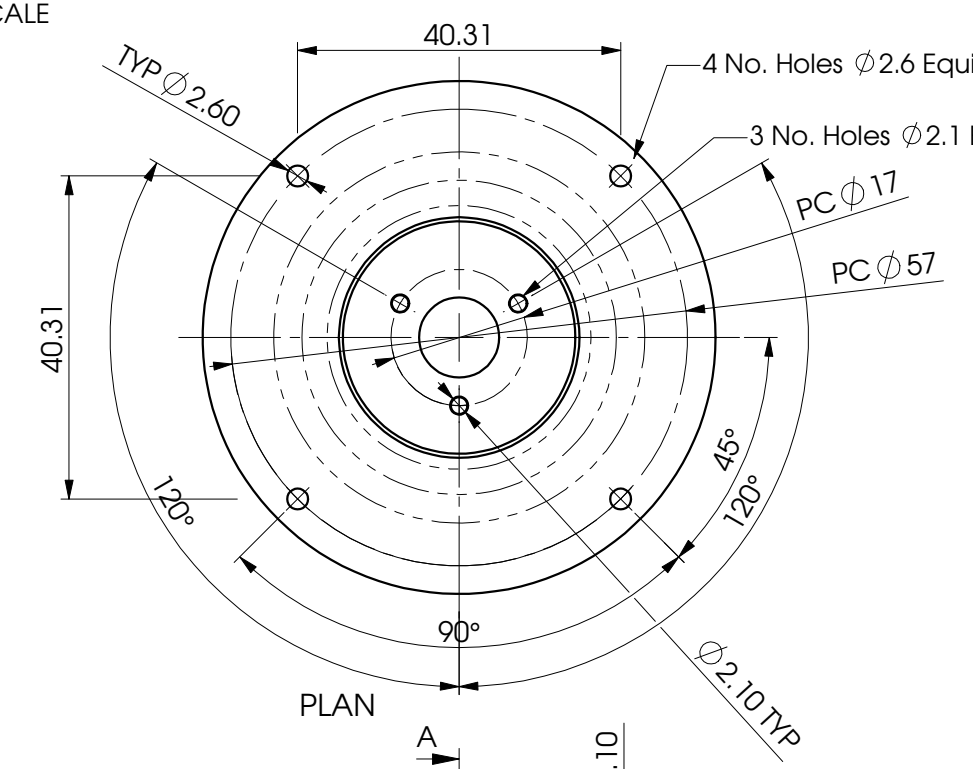

PLAN

NOTE:

MAT'L: Aluminium Tool Plate
QTY: 1 No. Req'd as Shown

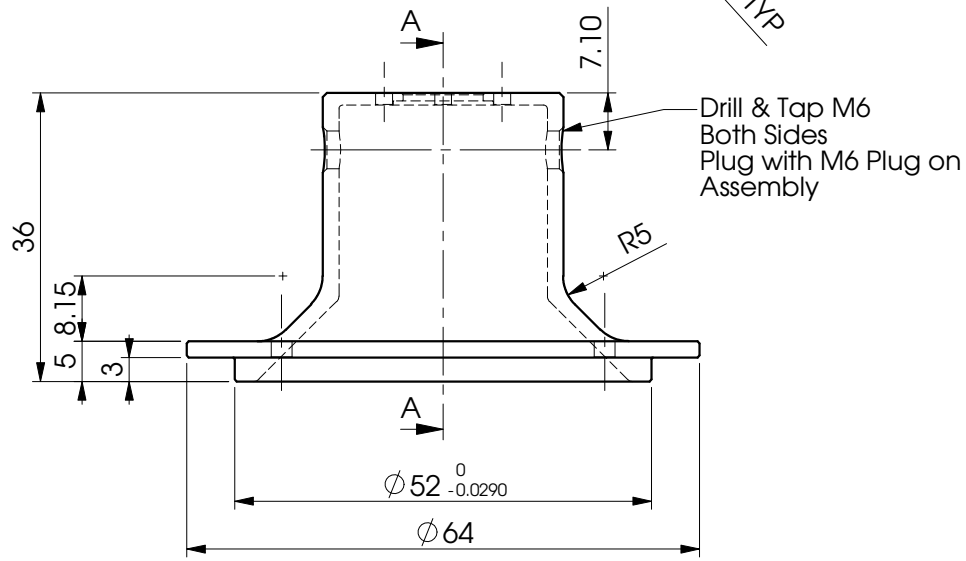

ELEVATION

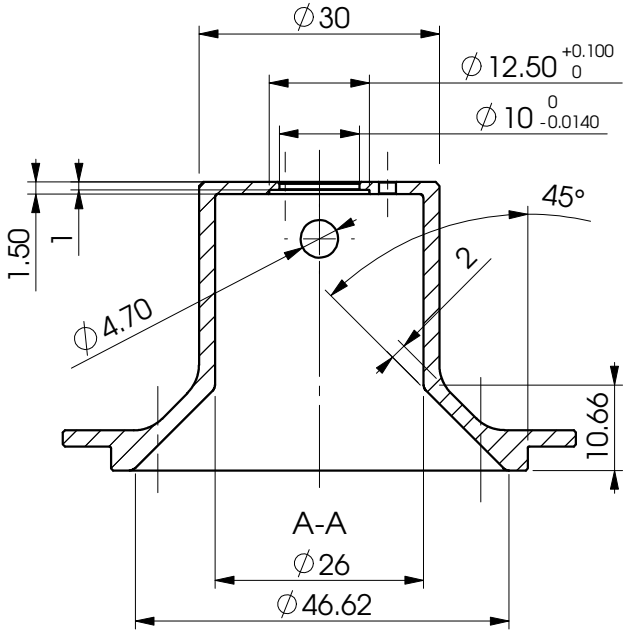

END ELEVATION

SHEET No. 1 of 1

MAXON EC22 BELLHOUSE		UNIVERSITY of CANTERBURY MECHANICAL ENGINEERING DEPT. CH.CH. N.Z.	
BELLHOUSE	Part No.:00	DRAWN : D Kirk	DATE : January 04
	No. Req'd: 1	CHECKED :	DRG. No : 080204
SCALE : 1.5:1 -- (A3)	ALL DIMENSIONS IN mm	APPROVED : DRA	

DO NOT SCALE

BREAK ALL SHARP EDGES

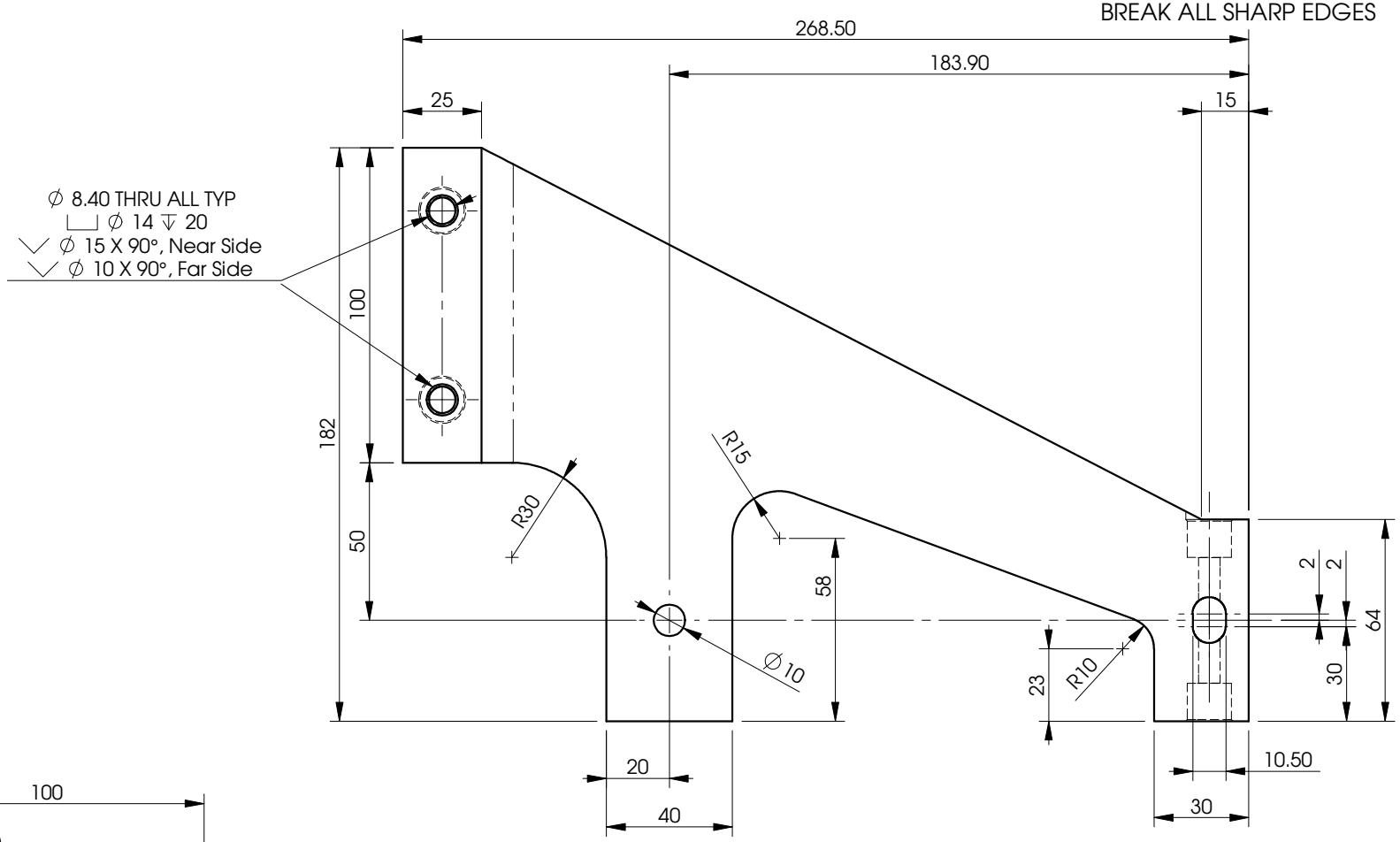

PLAN

Spacer to be Welded to Base Plate
Use Excess Cut from Plate Blank as
Shown on Sheet No.2 of 2 140204

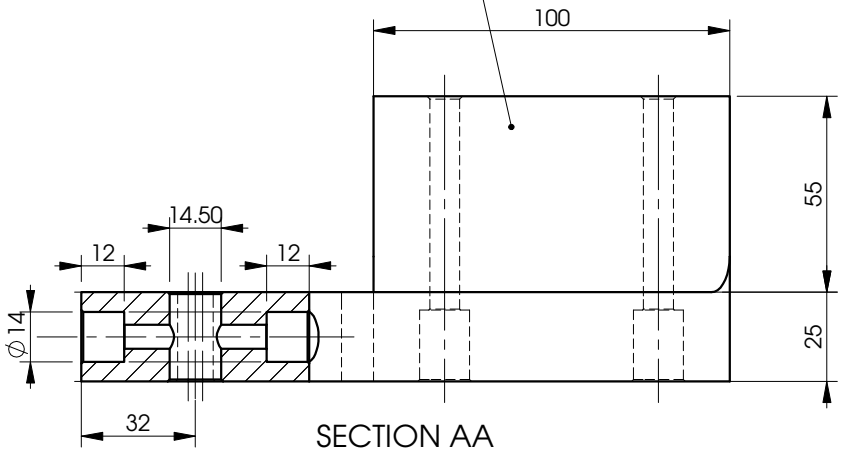

SECTION AA

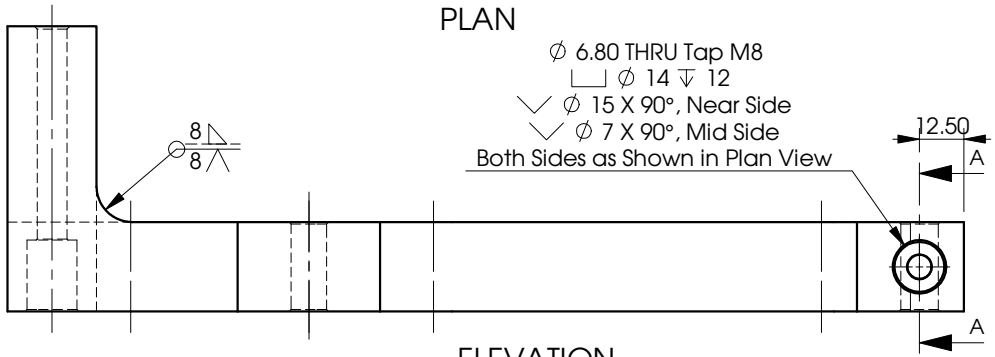

ELEVATION

SHEET No. 1 of 2

OKUMA HIGH SPEED SPINDLE MOUNT		**UNIVERSITY of CANTERBURY** MECHANICAL ENGINEERING DEPT. CH.CH. N.Z.	
SPINDLE MOUNT PLATE	Part No.:00	DRAWN : D Kirk	DATE : January 04
	No. Req'd: 1	CHECKED :	DRG. No : 130204
SCALE : 1:1.5 -- (A3)	ALL DIMENSIONS IN mm	APPROVED : DRA	

DO NOT SCALE

BREAK ALL SHARP EDGES

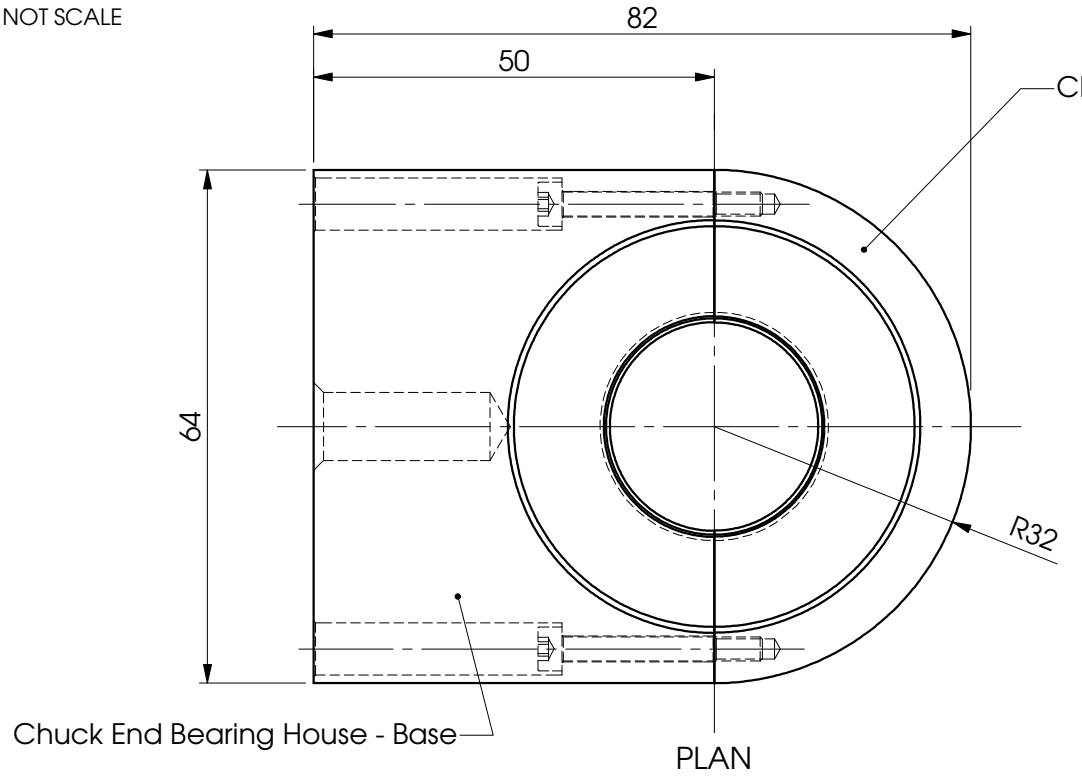

PLAN

NOTE:

See Sheets 1 & 2 of 3 for Base &Cap Detail
Qty; 1 No. Req'd Each
Mat'l; Aluminium Tool Plate

Bearing House to be Machined Assembled
Fit to be a Location Fit H7-h6
(The Housing must not allow the Bearing to move when clamped tight or over crimp the SA500)

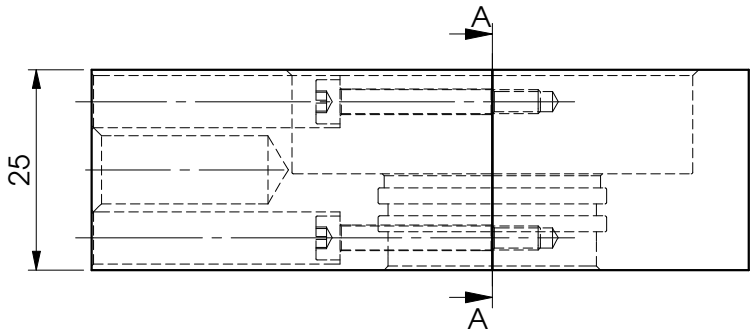

ELEVATION

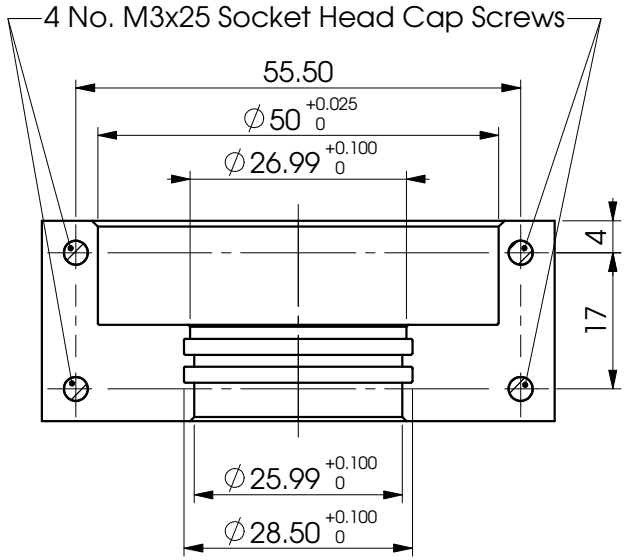

SECTION AA

SHEET 3 of 3

CHUCK END BEARING HOUSE		UNIVERSITY of CANTERBURY MECHANICAL ENGINEERING DEPT. CH.CH. N.Z.	
HOUSING ASSEMBLY	Part No.:00	DRAWN : D Kirk	DATE : Jan 04
	No. Req'd: 1	CHECKED :	DRG. No : 070204
SCALE : 1.5:1 -- (A3)	ALL DIMENSIONS IN mm	APPROVED : DRA	

DO NOT SCALE

BREAK ALL SHARP EDGES

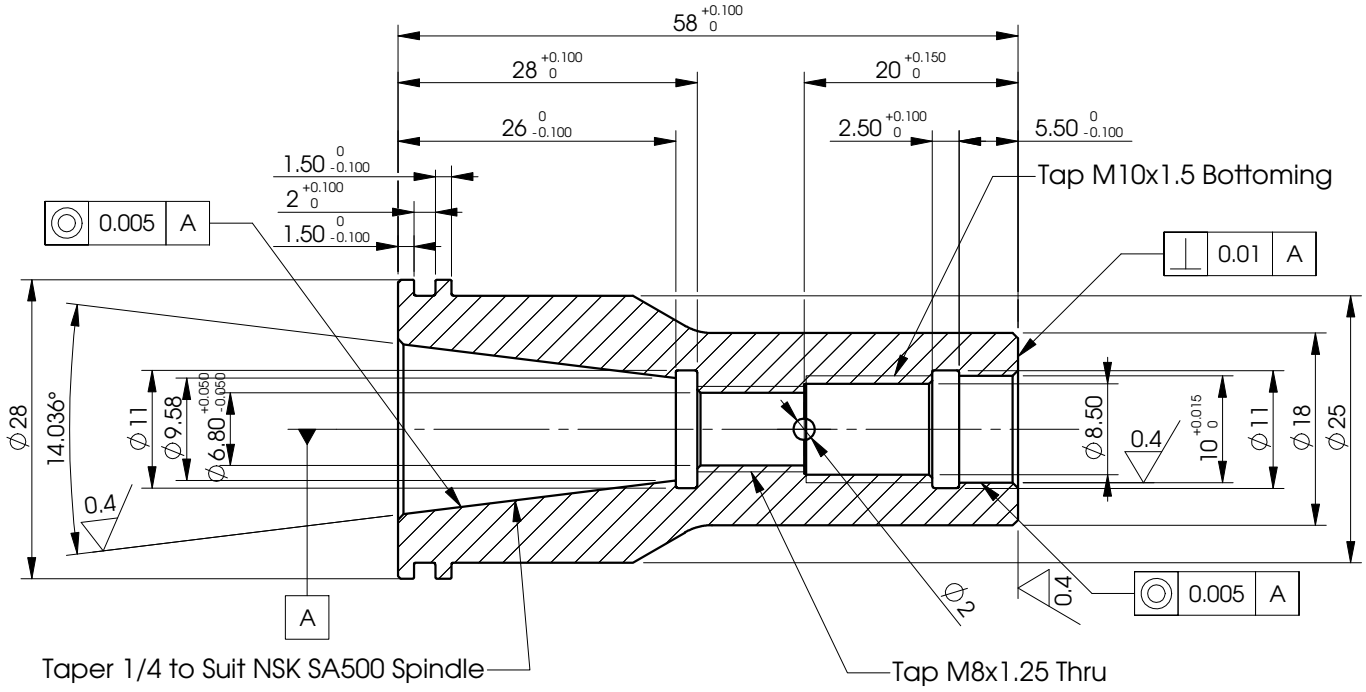

SECTION AA

NOTE:

QTY: 1 No. Req'd as Shown
MAT'L: 4140 Shaft
Finish Grind Indicated Surfaces

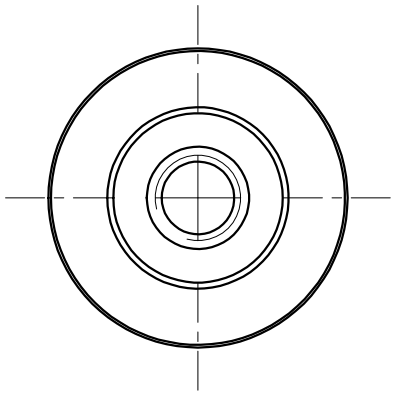

LEFT ELEVATION

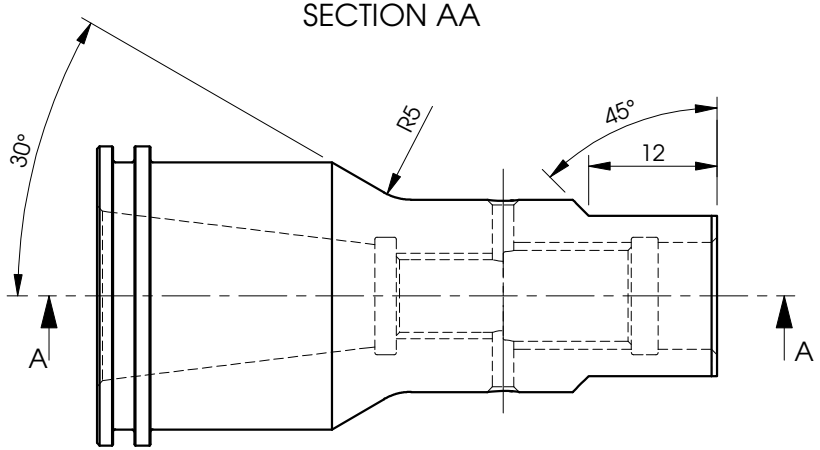

ELEVATION

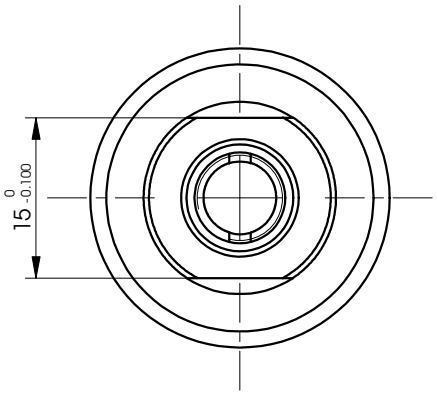

RIGHT ELEVATION

SHEET No. 1 of 1

MILLING SPINDLE		UNIVERSITY of CANTERBURY MECHANICAL ENGINEERING DEPT. CH.CH. N.Z.	
ISCAR ER11 CHUCK ADAPTER	Part No.:00	DRAWN : D Kirk	DATE : January 04
	No. Req'd: 1	CHECKED :	DRG. No : 040204
SCALE : 2:1 -- (A3)	ALL DIMENSIONS IN mm	APPROVED : DRA	

DO NOT SCALE

BREAK ALL SHARP EDGES

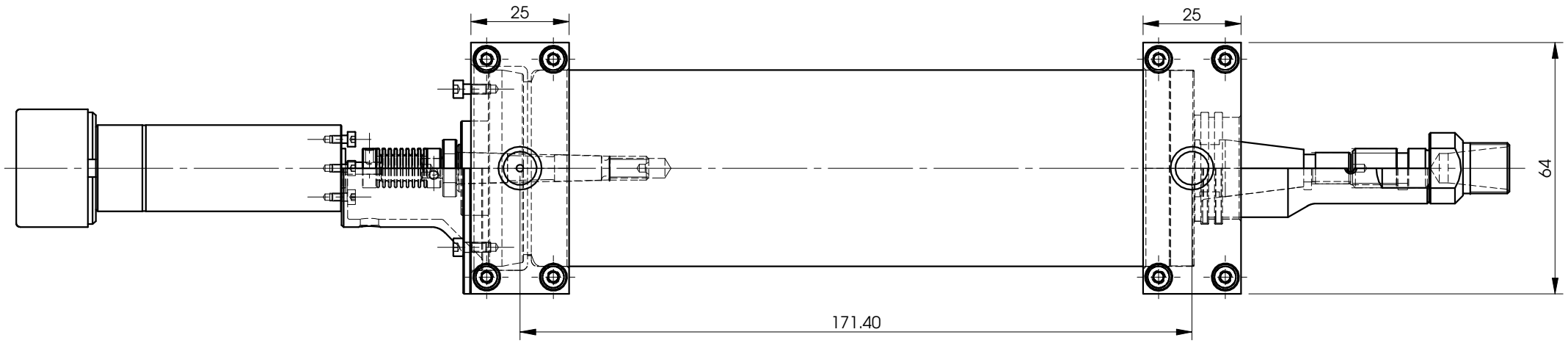

PLAN

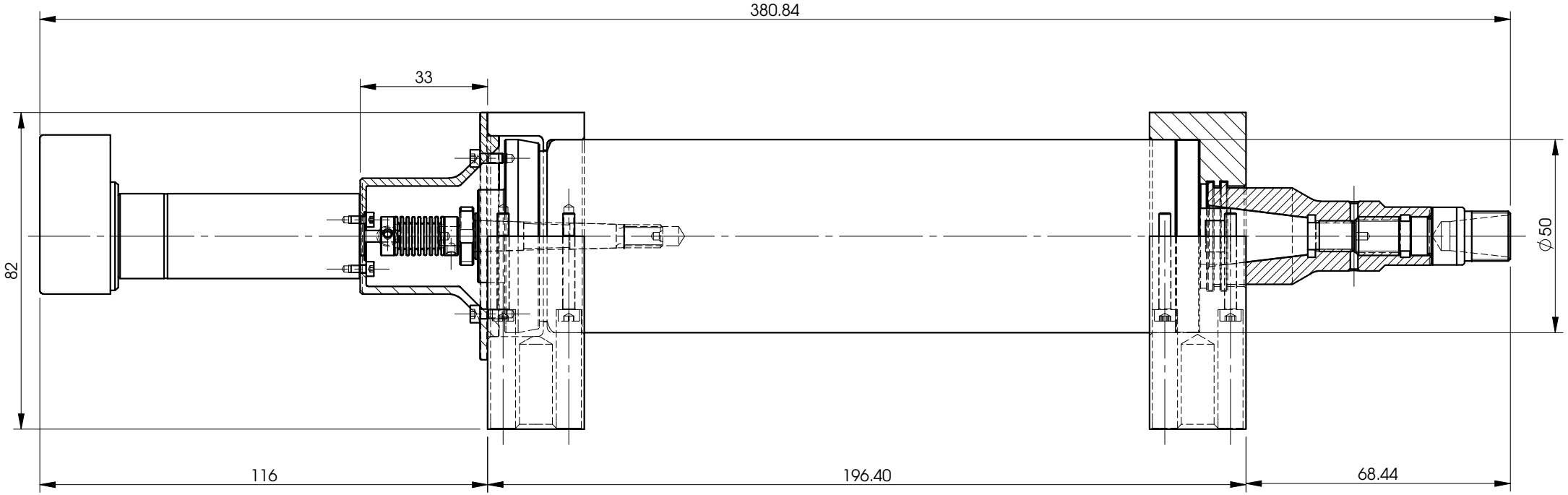

ELEVATION

SEE DETAIL A & B ON SHEET NO. 100204

SHEET No. 1 of 2

MILLING SPINDLE		**UNIVERSITY of CANTERBURY** MECHANICAL ENGINEERING DEPT. CH.CH. N.Z.	
ASSEMBLY	Part No.:00	DRAWN : D Kirk	DATE : January 04
	No. Req'd: 1	CHECKED :	DRG. No : 000204
SCALE : 1:1 -- (A3)	ALL DIMENSIONS IN mm	APPROVED : DRA	

DO NOT SCALE

BREAK ALL SHARP EDGES

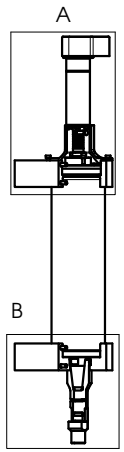

ELEVATION

PICTORIAL DETAIL A (1.5 : 1)

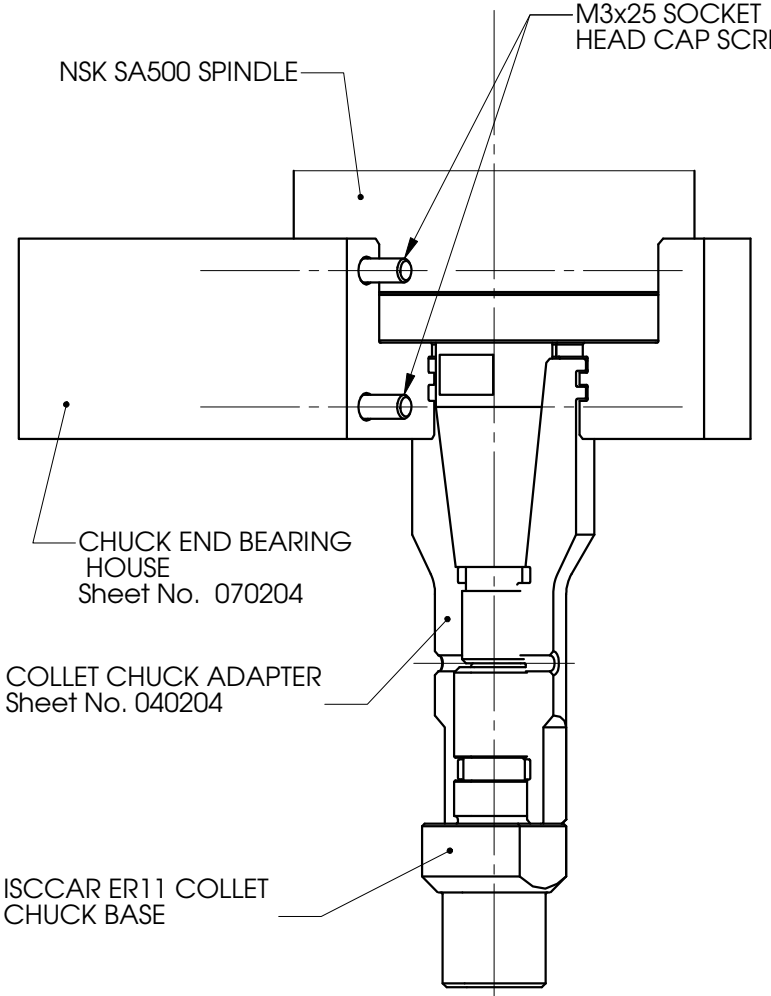

PICTORIAL DETAIL B (1.5 : 1)

SHEET No. 2 of 2

MILLING SPINDLE		**UNIVERSITY of CANTERBURY** MECHANICAL ENGINEERING DEPT. CH.CH. N.Z.	
ASSEMBLY DETAIL	Part No.:00	DRAWN : D Kirk	DATE : January 04
	No. Req'd: 1	CHECKED :	DRG. No : 100204
SCALE : 1.5:1 -- (A3)	ALL DIMENSIONS IN mm	APPROVED : DRA	

DO NOT SCALE

BREAK ALL SHARP EDGES

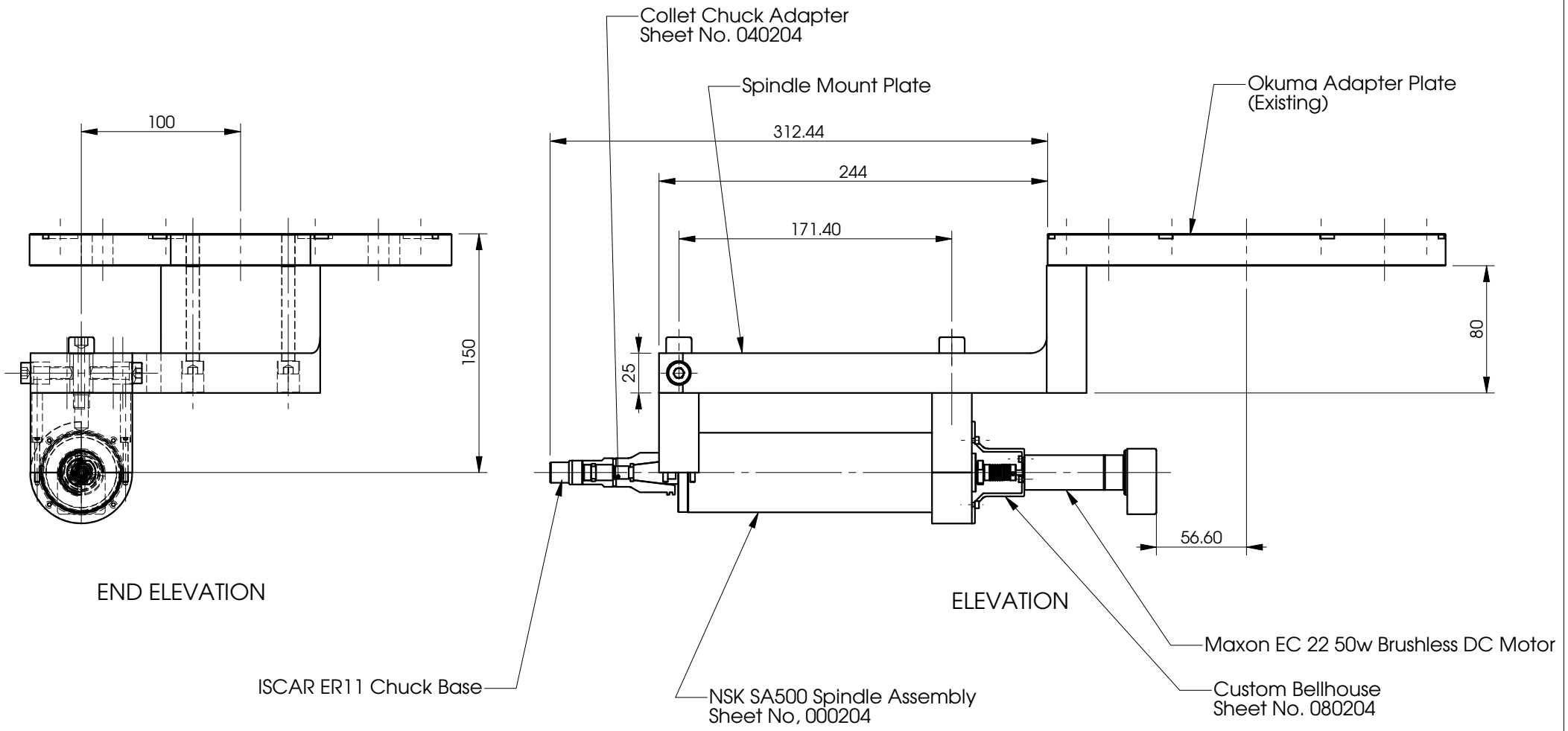

SHEET No.1 of 2

OKUMA HIGH SPEED SPINDLE MOUNT		UNIVERSITY of CANTERBURY MECHANICAL ENGINEERING DEPT. CH.CH. N.Z.	
ASSEMBLY	Part No.:00	DRAWN : D Kirk	DATE : January 04
	No. Req'd: 1	CHECKED :	DRG. No : 110204
SCALE : 1:2.5 -- (A3)	ALL DIMENSIONS IN mm	APPROVED : DRA	

DO NOT SCALE

BREAK ALL SHARP EDGES

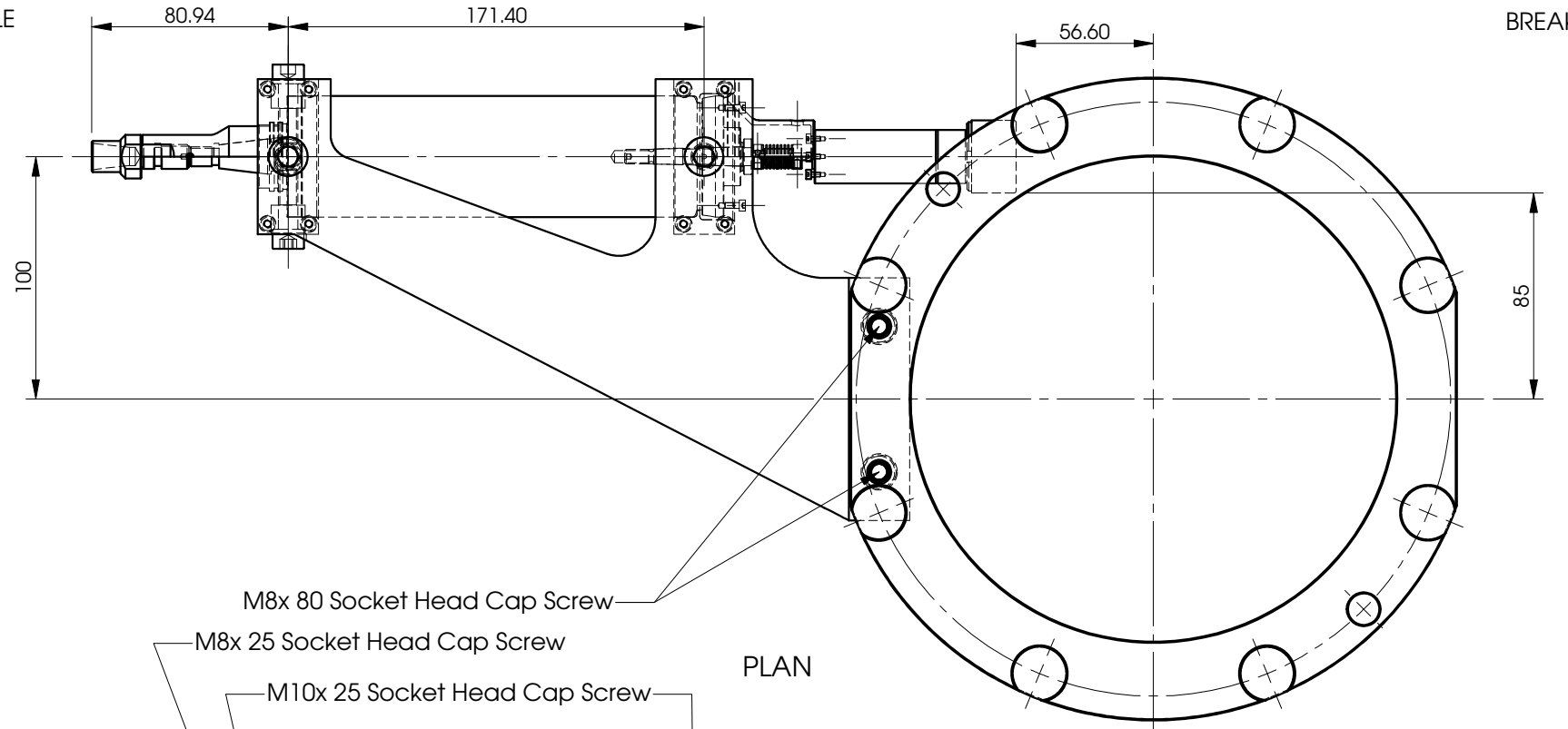

PLAN

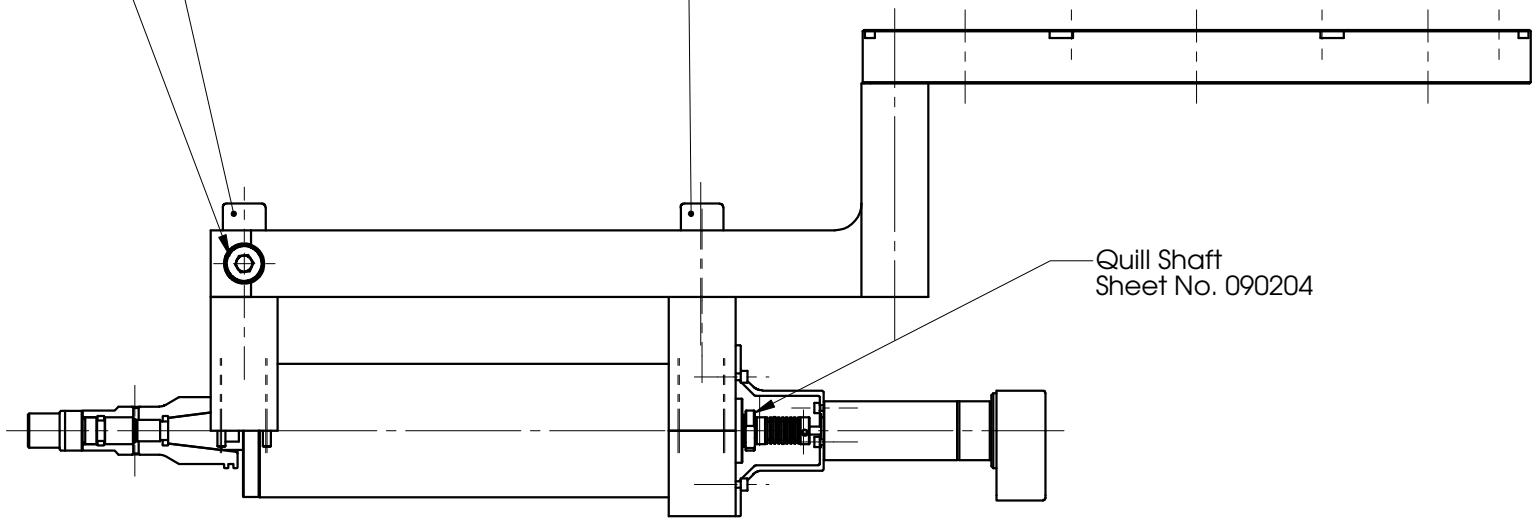

ELEVATION

SHEET No. 2 of 2

OKUMA HIGH SPEED SPINDLE MOUNT		**UNIVERSITY of CANTERBURY** MECHANICAL ENGINEERING DEPT. CH.CH. N.Z.	
ASSEMBLY - PLAN	Part No.:00	DRAWN : D Kirk	DATE : January 04
	No. Req'd: 1	CHECKED :	DRG. No : 120204
SCALE : 1:2 -- (A3)	ALL DIMENSIONS IN mm	APPROVED : DRA	